

# **Handbook on the Physics and Chemistry of Rare Earths, volume 29**

**The Role of Rare Earths in Catalysis**

Elsevier, 2000

Edited by: Karl A. Gschneidner, Jr. and LeRoy Eyring  
ISBN: 978-0-444-50472-2

## PREFACE

Karl A. GSCHNEIDNER, Jr., and LeRoy EYRING

---

*These elements perplex us in our rearches [sic], baffle us in our speculations, and haunt us in our very dreams. They stretch like an unknown sea before us – mocking, mystifying, and murmuring strange revelations and possibilities.*

Sir William Crookes (February 16, 1887)

---

Chapters devoted primarily to catalysis have been published in earlier volumes of the *Handbook*. Note especially chapter 43 on absorption and catalysis on surfaces, chapter 57 on catalysis in organic synthesis, and chapter 61 on coordination catalysts. In this volume we add several chapters that will continue our coverage of these important applications of the rare earths.

Patrick Maestro, in his trenchant foreword, has provided a background of the science and technology for understanding the importance and the basis of the detailed offerings that follow.

Paul-Boncour, Hilaire and Percheron-Guégan have extended the earlier chapter 43, on interactions at surfaces of metals and alloys, to reactions such as hydrogenation, methanation, ammonia synthesis, saturated hydrocarbon reactions, dehydrogenation of hydrogenated materials, hydrodesulfurization, and carbon monoxide oxidation.

Imamura has reported on the wide variety of catalyzed reactions involving metals and alloys in the innovated form of metal overlayers or bimetallic compounds with some transition metals produced from ammonia solutions. These are sometimes deposited on nonmetallic substrates.

Ulla and Lombardo have focused their attention on catalysis with mixed oxides usually having perovskite or perovskite-related structures, but other structures are also considered. Information on the preparation, characterization, and redox reactions of these oxides are considered. Attention is then given to many physico-chemical applications of these materials.

Kašpar, Graziani and Fornasiero present a comprehensive discussion on the background and current role of cerium oxide and associated materials for post-treatment of exhaust gases for pollution control. These three-way catalysts (TWC) are designed to render harmless the CO, NO<sub>x</sub>, and unburned hydrocarbons from internal combustion engines.

Corma and López Nieto consider the wide field of zeolite catalysts containing rare earths from their historic use in petroleum refining in the 1960s to other petrochemical and fine chemical applications today. Application is also found as abatement catalysts for pollutants like  $\text{NO}_x$  and  $\text{SO}_x$ .

Kobayashi documents the use of the triflates (the trifluoromethanesulfonyl group which is a hard Lewis acid in both aqueous and organic solutions) as versatile catalysts in carbon–carbon bond-forming reactions. Their stability in the presence of water, in spite of their being hard Lewis acids, enhances their growing usefulness.

We acknowledge the help of Serafin Bernal in the early stages of shaping the contents and inviting most of the authors to contribute to this volume.

## CONTENTS

Preface v

Contents vii

Contents of Volumes 1–28 ix

Patrick Maestro  
*Foreword* 1

181. V. Paul-Boncour, L. Hilaire and A. Percheron-Guégan  
*The metals and alloys in catalysis* 5

182. Hayao Imamura  
*The metals and alloys (prepared utilizing liquid ammonia solutions) in catalysis II*  
45

183. M.A. Ulla and E.A. Lombardo  
*The mixed oxides* 75

184. Jan Kašpar, Mauro Graziani and Paolo Fornasiero  
*Ceria-containing three-way catalysts* 159

185. A. Corma and J.M. López Nieto  
*The use of rare-earth-containing zeolite catalysts* 269

186. Shū Kobayashi  
*Triflates* 315

*Author index* 377

*Subject index* 409



## CONTENTS OF VOLUMES 1–28

### VOLUME 1: Metals

1978, 1st repr. 1982, 2nd repr. 1991; ISBN 0-444-85020-1

1. Z.B. Goldschmidt, *Atomic properties (free atom)* 1
2. B.J. Beaudry and K.A. Gschneidner Jr, *Preparation and basic properties of the rare earth metals* 173
3. S.H. Liu, *Electronic structure of rare earth metals* 233
4. D.C. Koskenmaki and K.A. Gschneidner Jr, *Cerium* 337
5. L.J. Sundström, *Low temperature heat capacity of the rare earth metals* 379
6. K.A. McEwen, *Magnetic and transport properties of the rare earths* 411
7. S.K. Sinha, *Magnetic structures and inelastic neutron scattering: metals, alloys and compounds* 489
8. T.E. Scott, *Elastic and mechanical properties* 591
9. A. Jayaraman, *High pressure studies: metals, alloys and compounds* 707
10. C. Probst and J. Wittig, *Superconductivity: metals, alloys and compounds* 749
11. M.B. Maple, L.E. DeLong and B.C. Sales, *Kondo effect: alloys and compounds* 797
12. M.P. Dariel, *Diffusion in rare earth metals* 847
- Subject index 877

### VOLUME 2: Alloys and intermetallics

1979, 1st repr. 1982, 2nd repr. 1991; ISBN 0-444-85021-X

13. A. Iandelli and A. Palenzona, *Crystal chemistry of intermetallic compounds* 1
14. H.R. Kirchmayr and C.A. Poldy, *Magnetic properties of intermetallic compounds of rare earth metals* 55
15. A.E. Clark, *Magnetostrictive  $RFe_2$  intermetallic compounds* 231
16. J.J. Rhyne, *Amorphous magnetic rare earth alloys* 259
17. P. Fulde, *Crystal fields* 295
18. R.G. Barnes, *NMR, EPR and Mössbauer effect: metals, alloys and compounds* 387
19. P. Wachter, *Europium chalcogenides: EuO, EuS, EuSe and EuTe* 507
20. A. Jayaraman, *Valence changes in compounds* 575
- Subject index 613

### VOLUME 3: Non-metallic compounds – I

1979, 1st repr. 1984; ISBN 0-444-85215-8

21. L.A. Haskin and T.P. Paster, *Geochemistry and mineralogy of the rare earths* 1
22. J.E. Powell, *Separation chemistry* 81
23. C.K. Jørgensen, *Theoretical chemistry of rare earths* 111
24. W.T. Carnall, *The absorption and fluorescence spectra of rare earth ions in solution* 171
25. L.C. Thompson, *Complexes* 209
26. G.G. Libowitz and A.J. Maeland, *Hydrides* 299
27. L. Eyring, *The binary rare earth oxides* 337
28. D.J.M. Bevan and E. Summerville, *Mixed rare earth oxides* 401
29. C.P. Khattak and F.F.Y. Wang, *Perovskites and garnets* 525
30. L.H. Brixner, J.R. Barkley and W. Jeitschko, *Rare earth molybdates (VI)* 609
- Subject index 655

**VOLUME 4: Non-metallic compounds – II**

1979, 1st repr. 1984; ISBN 0-444-85216-6

31. J. Flahaut, *Sulfides, selenides and tellurides* 1
32. J.M. Haschke, *Halides* 89
33. F. Hulliger, *Rare earth pnictides* 153
34. G. Blasse, *Chemistry and physics of R-activated phosphors* 237
35. M.J. Weber, *Rare earth lasers* 275
36. F.K. Fong, *Nonradiative processes of rare-earth ions in crystals* 317
- 37A. J.W. O'Laughlin, *Chemical spectrophotometric and polarographic methods* 341
- 37B. S.R. Taylor, *Trace element analysis of rare earth elements by spark source mass spectroscopy* 359
- 37C. R.J. Conzemius, *Analysis of rare earth matrices by spark source mass spectrometry* 377
- 37D. E.L. DeKalb and V.A. Fassel, *Optical atomic emission and absorption methods* 405
- 37E. A.P. D'Silva and V.A. Fassel, *X-ray excited optical luminescence of the rare earths* 441
- 37F. F.W.V. Boynton, *Neutron activation analysis* 457
- 37G. S. Schuhmann and J.A. Philpotts, *Mass-spectrometric stable-isotope dilution analysis for lanthanides in geochemical materials* 471
38. J. Reuben and G.A. Elgavish, *Shift reagents and NMR of paramagnetic lanthanide complexes* 483
39. J. Reuben, *Bioinorganic chemistry: lanthanides as probes in systems of biological interest* 515
40. T.J. Haley, *Toxicity* 553
- Subject index 587

**VOLUME 5**

1982, 1st repr. 1984; ISBN 0-444-86375-3

41. M. Gasgnier, *Rare earth alloys and compounds as thin films* 1
42. E. Gratz and M.J. Zuckermann, *Transport properties (electrical resistivity, thermoelectric power and thermal conductivity) of rare earth intermetallic compounds* 117
43. F.P. Netzer and E. Bertel, *Adsorption and catalysis on rare earth surfaces* 217
44. C. Boulesteix, *Defects and phase transformation near room temperature in rare earth sesquioxides* 321
45. O. Greis and J.M. Haschke, *Rare earth fluorides* 387
46. C.A. Morrison and R.P. Leavitt, *Spectroscopic properties of triply ionized lanthanides in transparent host crystals* 461
- Subject index 693

**VOLUME 6**

1984; ISBN 0-444-86592-6

47. K.H.J. Buschow, *Hydrogen absorption in intermetallic compounds* 1
48. E. Parthé and B. Chabot, *Crystal structures and crystal chemistry of ternary rare earth–transition metal borides, silicides and homologues* 113
49. P. Rogl, *Phase equilibria in ternary and higher order systems with rare earth elements and boron* 335
50. H.B. Kagan and J.L. Namy, *Preparation of divalent ytterbium and samarium derivatives and their use in organic chemistry* 525
- Subject index 567

**VOLUME 7**

1984; ISBN 0-444-86851-8

51. P. Rogl, *Phase equilibria in ternary and higher order systems with rare earth elements and silicon* 1
52. K.H.J. Buschow, *Amorphous alloys* 265
53. H. Schumann and W. Genthe, *Organometallic compounds of the rare earths* 446
- Subject index 573

**VOLUME 8**

1986; ISBN 0-444-86971-9

- 54. K.A. Gschneidner Jr and F.W. Calderwood, *Intra rare earth binary alloys: phase relationships, lattice parameters and systematics* 1
- 55. X. Gao, *Polarographic analysis of the rare earths* 163
- 56. M. Leskelä and L. Niinistö, *Inorganic complex compounds I* 203
- 57. J.R. Long, *Implications in organic synthesis* 335
- Errata 375
- Subject index 379

**VOLUME 9**

1987; ISBN 0-444-87045-8

- 58. R. Reisfeld and C.K. Jørgensen, *Excited state phenomena in vitreous materials* 1
- 59. L. Niinistö and M. Leskelä, *Inorganic complex compounds II* 91
- 60. J.-C.G. Bünzli, *Complexes with synthetic ionophores* 321
- 61. Zhiquan Shen and Jun Ouyang, *Rare earth coordination catalysis in stereospecific polymerization* 395
- Errata 429
- Subject index 431

**VOLUME 10: High energy spectroscopy**

1988; ISBN 0-444-87063-6

- 62. Y. Baer and W.-D. Schneider, *High-energy spectroscopy of lanthanide materials – An overview* 1
- 63. M. Campagna and F.U. Hillebrecht, *f-electron hybridization and dynamical screening of core holes in intermetallic compounds* 75
- 64. O. Gunnarsson and K. Schönhammer, *Many-body formulation of spectra of mixed valence systems* 103
- 65. A.J. Freeman, B.I. Min and M.R. Norman, *Local density supercell theory of photoemission and inverse photoemission spectra* 165
- 66. D.W. Lynch and J.H. Weaver, *Photoemission of Ce and its compounds* 231
- 67. S. Hüfner, *Photoemission in chalcogenides* 301
- 68. J.F. Herbst and J.W. Wilkins, *Calculation of 4f excitation energies in the metals and relevance to mixed valence systems* 321
- 69. B. Johansson and N. Mårtensson, *Thermodynamic aspects of 4f levels in metals and compounds* 361
- 70. F.U. Hillebrecht and M. Campagna, *Bremsstrahlung isochromat spectroscopy of alloys and mixed valent compounds* 425
- 71. J. Röhrler, *X-ray absorption and emission spectra* 453
- 72. F.P. Netzer and J.A.D. Matthew, *Inelastic electron scattering measurements* 547
- Subject index 601

**VOLUME 11: Two-hundred-year impact of rare earths on science**

1988; ISBN 0-444-87080-6

- H.J. Svec, *Prologue* 1
- 73. F. Szabadváry, *The history of the discovery and separation of the rare earths* 33
- 74. B.R. Judd, *Atomic theory and optical spectroscopy* 81
- 75. C.K. Jørgensen, *Influence of rare earths on chemical understanding and classification* 197
- 76. J.J. Rhyne, *Highlights from the exotic phenomena of lanthanide magnetism* 293
- 77. B. Bleaney, *Magnetic resonance spectroscopy and hyperfine interactions* 323
- 78. K.A. Gschneidner Jr and A.H. Daane, *Physical metallurgy* 409
- 79. S.R. Taylor and S.M. McLennan, *The significance of the rare earths in geochemistry and cosmochemistry* 485
- Errata 579
- Subject index 581

**VOLUME 12**

1989; ISBN 0-444-87105-5

- 80. J.S. Abell, *Preparation and crystal growth of rare earth elements and intermetallic compounds* 1
- 81. Z. Fisk and J.P. Remeika, *Growth of single crystals from molten metal fluxes* 53
- 82. E. Burzo and H.R. Kirchmayr, *Physical properties of  $R_2Fe_{14}B$ -based alloys* 71
- 83. A. Szytuła and J. Leciejewicz, *Magnetic properties of ternary intermetallic compounds of the  $RT_2X_2$  type* 133
- 84. H. Maletta and W. Zinn, *Spin glasses* 213
- 85. J. van Zytveld, *Liquid metals and alloys* 357
- 86. M.S. Chandrasekharaiah and K.A. Gingerich, *Thermodynamic properties of gaseous species* 409
- 87. W.M. Yen, *Laser spectroscopy* 433
- Subject index 479

**VOLUME 13**

1990; ISBN 0-444-88547-1

- 88. E.I. Gladyshevsky, O.I. Bodak and V.K. Pecharsky, *Phase equilibria and crystal chemistry in ternary rare earth systems with metallic elements* 1
- 89. A.A. Eliseev and G.M. Kuzmichyeva, *Phase equilibrium and crystal chemistry in ternary rare earth systems with chalcogenide elements* 191
- 90. N. Kimizuka, E. Takayama-Muromachi and K. Siratori, *The systems  $R_2O_3$ – $M_2O_3$ – $M'O$*  283
- 91. R.S. Houk, *Elemental analysis by atomic emission and mass spectrometry with inductively coupled plasmas* 385
- 92. P.H. Brown, A.H. Rathjen, R.D. Graham and D.E. Tribe, *Rare earth elements in biological systems* 423
- Errata 453
- Subject index 455

**VOLUME 14**

1991; ISBN 0-444-88743-1

- 93. R. Osborn, S.W. Lovesey, A.D. Taylor and E. Balcar, *Intermultiplet transitions using neutron spectroscopy* 1
- 94. E. Dormann, *NMR in intermetallic compounds* 63
- 95. E. Zirngiebl and G. Güntherodt, *Light scattering in intermetallic compounds* 163
- 96. P. Thalmeier and B. Lüthi, *The electron–phonon interaction in intermetallic compounds* 225
- 97. N. Grewe and F. Steglich, *Heavy fermions* 343
- Subject index 475

**VOLUME 15**

1991; ISBN 0-444-88966-3

- 98. J.G. Sereni, *Low-temperature behaviour of cerium compounds* 1
- 99. G.-y. Adachi, N. Imanaka and Zhang Fuzhong, *Rare earth carbides* 61
- 100. A. Simon, H.J. Mattausch, G.J. Miller, W. Bauhofer and R.K. Kremer, *Metal-rich halides* 191
- 101. R.M. Almeida, *Fluoride glasses* 287
- 102. K.L. Nash and J.C. Sullivan, *Kinetics of complexation and redox reactions of the lanthanides in aqueous solutions* 347
- 103. E.N. Rizkalla and G.R. Choppin, *Hydration and hydrolysis of lanthanides* 393
- 104. L.M. Vallarino, *Macrocyclic complexes of the lanthanide(III) yttrium(III) and dioxouranium(VI) ions from metal-templated syntheses* 443
- Errata 513
- Subject index 515

**MASTER INDEX, Vols. 1–15**

1993; ISBN 0-444-89965-0

**VOLUME 16**

1993; ISBN 0-444-89782-8

- 105. M. Loewenhaupt and K.H. Fischer, *Valence-fluctuation and heavy-fermion 4f systems* 1
- 106. I.A. Smirnov and V.S. Oskotski, *Thermal conductivity of rare earth compounds* 107
- 107. M.A. Subramanian and A.W. Sleight, *Rare earths pyrochlores* 225
- 108. R. Miyawaki and I. Nakai, *Crystal structures of rare earth minerals* 249
- 109. D.R. Chopra, *Appearance potential spectroscopy of lanthanides and their intermetallics* 519
- Author index 547
- Subject index 579

**VOLUME 17: Lanthanides/Actinides: Physics – I**

1993; ISBN 0-444-81502-3

- 110. M.R. Norman and D.D. Koelling, *Electronic structure, Fermi surfaces, and superconductivity in f electron metals* 1
- 111. S.H. Liu, *Phenomenological approach to heavy-fermion systems* 87
- 112. B. Johansson and M.S.S. Brooks, *Theory of cohesion in rare earths and actinides* 149
- 113. U. Benedict and W.B. Holzapfel, *High-pressure studies – Structural aspects* 245
- 114. O. Vogt and K. Mattenberger, *Magnetic measurements on rare earth and actinide mononictides and monochalcogenides* 301
- 115. J.M. Fournier and E. Gratz, *Transport properties of rare earth and actinide intermetallics* 409
- 116. W. Potzel, G.M. Kalvius and J. Gal, *Mössbauer studies on electronic structure of intermetallic compounds* 539
- 117. G.H. Lander, *Neutron elastic scattering from actinides and anomalous lanthanides* 635
- Author index 711
- Subject index 753

**VOLUME 18: Lanthanides/Actinides: Chemistry**

1994; ISBN 0-444-81724-7

- 118. G.T. Seaborg, *Origin of the actinide concept* 1
- 119. K. Balasubramanian, *Relativistic effects and electronic structure of lanthanide and actinide molecules* 29
- 120. J.V. Beitz, *Similarities and differences in trivalent lanthanide- and actinide-ion solution absorption spectra and luminescence studies* 159
- 121. K.L. Nash, *Separation chemistry for lanthanides and trivalent actinides* 197
- 122. L.R. Morss, *Comparative thermochemical and oxidation–reduction properties of lanthanides and actinides* 239
- 123. J.W. Ward and J.M. Haschke, *Comparison of 4f and 5f element hydride properties* 293
- 124. H.A. Eick, *Lanthanide and actinide halides* 365
- 125. R.G. Haire and L. Eyring, *Comparisons of the binary oxides* 413
- 126. S.A. Kinkad, K.D. Abney and T.A. O'Donnell, *f-element speciation in strongly acidic media: lanthanide and mid-actinide metals, oxides, fluorides and oxide fluorides in superacids* 507
- 127. E.N. Rizkalla and G.R. Choppin, *Lanthanides and actinides hydration and hydrolysis* 529
- 128. G.R. Choppin and E.N. Rizkalla, *Solution chemistry of actinides and lanthanides* 559
- 129. J.R. Duffield, D.M. Taylor and D.R. Williams, *The biochemistry of the f-elements* 591
- Author index 623
- Subject index 659

**VOLUME 19: Lanthanides/Actinides: Physics – II**

1994; ISBN 0-444-82015-9

- 130. E. Holland-Moritz and G.H. Lander, *Neutron inelastic scattering from actinides and anomalous lanthanides* 1
- 131. G. Aeppli and C. Broholm, *Magnetic correlations in heavy-fermion systems: neutron scattering from single crystals* 123
- 132. P. Wachter, *Intermediate valence and heavy fermions* 177
- 133. J.D. Thompson and J.M. Lawrence, *High pressure studies – Physical properties of anomalous Ce, Yb and U compounds* 383
- 134. C. Colinet and A. Pasturel, *Thermodynamic properties of metallic systems* 479
- Author index 649
- Subject index 693

**VOLUME 20**

1995; ISBN 0-444-82014-0

- 135. Y. Ōnuki and A. Hasegawa, *Fermi surfaces of intermetallic compounds* 1
- 136. M. Gasgnier, *The intricate world of rare earth thin films: metals, alloys, intermetallics, chemical compounds, ...* 105
- 137. P. Vajda, *Hydrogen in rare-earth metals, including  $RH_{2+x}$  phases* 207
- 138. D. Gignoux and D. Schmitt, *Magnetic properties of intermetallic compounds* 293
- Author index 425
- Subject index 457

**VOLUME 21**

1995; ISBN 0-444-82178-3

- 139. R.G. Bautista, *Separation chemistry* 1
- 140. B.W. Hinton, *Corrosion prevention and control* 29
- 141. N.E. Ryan, *High-temperature corrosion protection* 93
- 142. T. Sakai, M. Matsuoka and C. Iwakura, *Rare earth intermetallics for metal–hydrogen batteries* 133
- 143. G.-y. Adachi and N. Imanaka, *Chemical sensors* 179
- 144. D. Garcia and M. Faucher, *Crystal field in non-metallic (rare earth) compounds* 263
- 145. J.-C.G. Bünzli and A. Milicic-Tang, *Solvation and anion interaction in organic solvents* 305
- 146. V. Bhagavathy, T. Prasada Rao and A.D. Damodaran, *Trace determination of lanthanides in high-purity rare-earth oxides* 367
- Author index 385
- Subject index 411

**VOLUME 22**

1996; ISBN 0-444-82288-7

- 147. C.P. Flynn and M.B. Salamon, *Synthesis and properties of single-crystal nanostructures* 1
- 148. Z.S. Shan and D.J. Sellmyer, *Nanoscale rare earth–transition metal multilayers: magnetic structure and properties* 81
- 149. W. Suski, *The  $ThMn_{12}$ -type compounds of rare earths and actinides: structure, magnetic and related properties* 143
- 150. L.K. Aminov, B.Z. Malkin and M.A. Teplov, *Magnetic properties of nonmetallic lanthanide compounds* 295
- 151. F. Auzel, *Coherent emission in rare-earth materials* 507
- 152. M. Dolg and H. Stoll, *Electronic structure calculations for molecules containing lanthanide atoms* 607
- Author index 731
- Subject index 777

**VOLUME 23**

1996; ISBN 0-444-82507-X

- 153. J.H. Forsberg, *NMR studies of paramagnetic lanthanide complexes and shift reagents* 1
- 154. N. Sabbatini, M. Guardigli and I. Manet, *Antenna effect in encapsulation complexes of lanthanide ions* 69
- 155. C. Görller-Walrand and K. Binnemans, *Rationalization of crystal-field parametrization* 121
- 156. Yu. Kuz'ma and S. Chykhrij, *Phosphides* 285
- 157. S. Boghosian and G.N. Papatheodorou, *Halide vapors and vapor complexes* 435
- 158. R.H. Byrne and E.R. Sholkovitz, *Marine chemistry and geochemistry of the lanthanides* 497
- Author index 595
- Subject index 631

**VOLUME 24**

1997; ISBN 0-444-82607-6

- 159. P.A. Dowben, D.N. McIlroy and Dongqi Li, *Surface magnetism of the lanthanides* 1
- 160. P.G. McCormick, *Mechanical alloying and mechanically induced chemical reactions* 47
- 161. A. Inoue, *Amorphous, quasicrystalline and nanocrystalline alloys in Al- and Mg-based systems* 83
- 162. B. Elschner and A. Loidl, *Electron-spin resonance on localized magnetic moments in metals* 221
- 163. N.H. Duc, *Intersublattice exchange coupling in the lanthanide–transition metal intermetallics* 339
- 164. R.V. Skolozdra, *Stannides of rare-earth and transition metals* 399
- Author index 519
- Subject index 559

**VOLUME 25**

1998; ISBN 0-444-82871-0

- 165. H. Nagai, *Rare earths in steels* 1
- 166. R. Marchand, *Ternary and higher order nitride materials* 51
- 167. C. Görller-Walrand and K. Binnemans, *Spectral intensities of  $f$ - $f$  transitions* 101
- 168. G. Bombieri and G. Paolucci, *Organometallic  $\pi$  complexes of the  $f$ -elements* 265
- Author Index 415
- Subject Index 459

**VOLUME 26**

1999; ISBN 0-444-50815-1

- 169. D.F. McMorro, D. Gibbs and J. Bohr, *X-ray scattering studies of lanthanide magnetism* 1
- 170. A.M. Tishin, Yu.I. Spichkin and J. Bohr, *Static and dynamic stresses* 87
- 171. N.H. Duc and T. Goto, *Itinerant electron metamagnetism of Co sublattice in the lanthanide–cobalt intermetallics* 177
- 172. A.J. Arko, P.S. Riseborough, A.B. Andrews, J.J. Joyce, A.N. Tahvildar-Zadeh and M. Jarrell, *Photoelectron spectroscopy in heavy fermion systems: Emphasis on single crystals* 265
- Author index 383
- Subject index 405

**VOLUME 27**

1999; ISBN 0-444-50342-0

- 173. P.S. Salamakha, O.L. Sologub and O.I. Bodak, *Ternary rare-earth–germanium systems* 1
- 174. P.S. Salamakha, *Crystal structures and crystal chemistry of ternary rare-earth germanides* 225
- 175. B.Ya. Kotur and E. Gratz, *Scandium alloy systems and intermetallics* 339
- Author index 535
- Subject index 553

**VOLUME 28**

2000; ISBN 0-444-50346-3

- 176. J.-P. Connerade and R.C. Karnatak, *Electronic excitation in atomic species* 1
- 177. G. Meyer and M.S. Wickleder, *Simple and complex halides* 53
- 178. R.V. Kumar and H. Iwahara, *Solid electrolytes* 131
- 179. A. Halperin, *Activated thermoluminescence (TL) dosimeters and related radiation detectors* 187
- 180. K.L. Nash and M.P. Jensen, *Analytical separations of the lanthanides: basic chemistry and methods* 311
- Author index 373
- Subject index 401



## Chapter 181

### THE METALS AND ALLOYS IN CATALYSIS

V. PAUL-BONCOUR<sup>1</sup>, L. HILAIRE<sup>2</sup> and A. PERCHERON-GUÉGAN<sup>1</sup>

<sup>1</sup> Laboratoire de Chimie Métallurgique des Terres Rares,  
 UPR209, CNRS, 2–8 rue Henri Dunant, 94320 Thiais, France;

<sup>2</sup> Laboratoire d'Etudes de la Réactivité Catalytique, des Surfaces et Interfaces,  
 UMR 7515, 25, rue Becquerel, 67087 Strasbourg cedex 2, France

#### Contents

Symbols and abbreviations	5	3.3. Hydrogenation of various organic molecules	19
Introduction	6	3.4. Carbon monoxide hydrogenation	22
1. Sample preparation	7	3.4.1. Methanation reaction	22
1.1. Rare-earth alloys: intermetallic compounds and amorphous alloys	7	3.4.2. Methanol synthesis	26
1.2. Supported bimetallic alloys	9	3.5. Ammonia synthesis	31
1.3. Thin films	9	3.6. Reactions of saturated hydrocarbons	34
2. Characterization methods	11	3.7. Hydrocarbon and alcohol dehydrogenation	37
2.1. X-ray diffraction	11	3.8. Hydrodesulfurization	38
2.2. X-ray absorption	12	3.9. Carbon monoxide oxidation	39
2.3. Magnetic measurements	12	4. Discussion and conclusion	39
3. Catalytic reactions	13	References	42
3.1. Hydrogenation of olefins	13		
3.2. Hydrogenation of dienes and alkynes	17		

#### Symbols and abbreviations

AES	Auger electron spectroscopy	FWHM	Full width at half maximum
BET	Brunauer–Emmett–Teller	HREM	High resolution electron microscopy
DSC	Differential scanning calorimetry	LEED	Low energy electron diffraction
$\Delta G_0$	Standard Gibbs free energy	MM	Mischmetal
$\Delta H$	Enthalpy of reaction	$n$	number of moles
$\Delta S$	Entropy of reaction	$P$	pressure
EDAX	Energy dispersive analysis of X-ray	PCT	Pressure composition temperature
EELS	Electron energy loss spectroscopy	$R$	Gas constant, $8.314 \text{ J mol}^{-1} \text{ K}^{-1}$
EPMA	Electron probe microanalysis	SEM	Scanning electron microscopy
ESCA	Electron spectroscopy for chemical analysis	$T$	Temperature
EXAFS	Extended X-ray absorption fine structure	T.O.F.	Turnover frequency
		$T_c$	Curie temperature

$T_E$	Equilibrium temperature	XANES	X-ray absorption near edge structure
$T_S$	Critical temperature	XAS	X-ray absorption spectroscopy
THF	Tetrahydrofuran	XPS	X-ray photoelectron spectroscopy
UPS	Ultraviolet photoelectron spectroscopy	XRD	X-ray diffraction
$V$	Volume		

---

## Introduction

The use of rare earths in catalysis has been the subject of a large number of studies due to their unique electronic properties and their high chemical reactivity. In their review paper Netzer and Bertel (1982) have described the surface chemistry on rare-earth-related materials dealing with the interaction between the rare-earth surface and the reactant gas. They have distinguished reactions of the gas reactant *on* and *with* the rare-earth surface. The studies of the reactions on the surface are performed for a better understanding of the catalytic processes at the surface and can be regarded as model studies. But the reactivity of the rare earth with the reactant can also lead to its transformation into oxide or hydride. Rare-earth oxides have been found to be very good catalysts in many reactions. Another possible way of using rare earths is as alloys with d transition metals which are known to be active in catalysis. Few studies on such intermetallic compounds were presented in the review chapter of Netzer and Bertel (1982), but several new works have been published in the meantime. In this chapter we will therefore mainly present the properties of rare earths alloyed with transition metals. Alloying transition metals with a rare earth is known to modify their electronic properties and therefore their reactivity with surface reactants. In addition, several intermetallic compounds of rare earths and transition metals have the property to absorb hydrogen reversibly, a property which can be used in many hydrogenation or dehydrogenation reactions. However, it was observed that during several catalytic reactions (methanation, alcohol or ammonia synthesis) the intermetallic compounds decompose into transition-metal particles and rare-earth oxide or hydride to form more active catalysts. This catalytic activity can be improved by an appropriate pretreatment under hydrogen or oxidizing reactants at high temperature. Intermetallic compounds were therefore used as precursors of new active catalysts which have been in some cases compared to transition metals supported on rare-earth oxides or classical supports like  $\text{SiO}_2$  or  $\text{Al}_2\text{O}_3$ .

The first section of this chapter will deal with the sample preparation, including alloys, supported metal catalysts and thin films and the activation of the samples before catalytic reaction through various pretreatments. Concerning the characterization methods, Netzer and Bertel (1982) have described methods used in surface science under high vacuum including photoelectron spectroscopy (UPS and XPS), Auger electron spectroscopy (AES), Electron energy loss spectroscopy (EELS), Bremsstrahlung isochromat spectroscopy (BIS), also known as inverse photoemission, Low energy electron diffraction (LEED), work function measurements and thermal desorption. But to characterize the intermetallic compounds and their transformations, bulk characterization

methods are also required. Such methods, like in-situ X-ray diffraction (XRD), X-ray absorption (XAS) and magnetism which have been used in different works, will be described in sect. 2. In the third section the catalytic properties of the rare-earth alloys, thin films and bimetallics will be reviewed by type of reaction, starting with hydrogenation reactions of molecules like olefins, dienes, alkynes, carbon monoxide and nitrogen, then reactions of saturated hydrocarbons involving skeletal rearrangements. The ability of intermetallic compounds to absorb hydrogen can also be used for dehydrogenation reactions. Finally some compounds were also studied in hydrodesulfuration reactions and carbon monoxide oxidation. Section 4 concerns the discussion about the use of rare-earth alloys in catalysis, in particular, what is the role played by the rare earth and what are the perspectives in using such compounds?

## 1. Sample preparation

### 1.1. *Rare-earth alloys: intermetallic compounds and amorphous alloys*

Intermetallic compounds of rare earths and transition metals were prepared by induction, arc or electron beam melting of the pure components under argon or vacuum. In order to obtain single phase and homogeneous samples a subsequent annealing treatment varying from a few hours to several days at appropriate temperatures determined from the phase diagram was applied. The composition and the homogeneity of the samples were analyzed using XRD and in a few cases by electron probe microanalysis (EPMA) or energy dispersive analysis of X-rays (EDAX). Additional surface characterization by XPS were also mentioned.

Amorphous alloys were prepared by a melt-spinning technique under argon (Bryan et al. 1988). The inner and outer surface of the glassy alloys were characterized by XRD analysis. The influence of an annealing treatment was also studied by differential scanning calorimetry (DSC).

The ability of several rare-earth and transition-metal alloys (M) to absorb large amounts of hydrogen reversibly was used to perform hydrogenation or dehydrogenation reactions. The hydrogenation reaction is exothermic and can be schematized as



The hydrides are generally characterized by measuring their pressure–composition isotherms (PCT diagrams) (fig. 1) which allow one to determine the domain of existence of hydrogen solid solution ( $\alpha$  phase) and hydride ( $\beta$  phase), the maximum amount of stored hydrogen (capacity) and their thermodynamic parameters ( $\Delta H$  is the enthalpy and  $\Delta S$  the entropy of the reaction). The PCT diagrams can be obtained using volumetric or thermogravimetric methods. In the first case the amount of absorbed or desorbed hydrogen in moles ( $n$ ) is calculated by measuring the pressure ( $P$ ) in calibrated and thermostated volumes ( $V$ ,  $T$ ) and applying the perfect gas rule ( $PV = nRT$ ). In the second

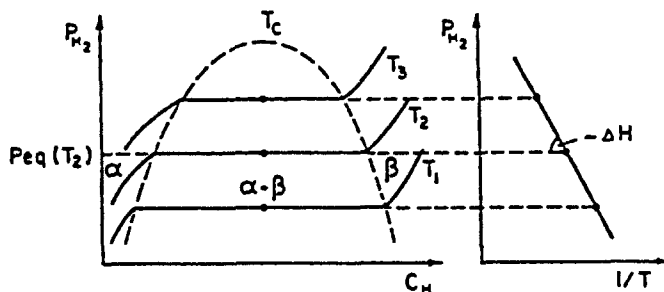


Fig. 1. Schematic representation of pressure-composition isotherms (PCT diagram) of M-H<sub>2</sub> compounds and corresponding Van 't Hoff plot.

case the gain or loss of hydrogen is measured through mass change of the compound. The thermodynamic parameters are calculated using Van 't Hoff's law:

$$\ln P = \frac{\Delta H}{RT} - \frac{\Delta S}{R} \quad (\Delta H < 0, \quad \Delta S < 0). \quad (2)$$

More details concerning the intermetallic compounds and hydrides preparation have been published in the review paper of Percheron-Guégan and Welter (1988).

Before performing the catalytic tests the samples were crushed into fine powders under argon or air and then activated by different kinds of pretreatments. The cleaning or the activation of the surface can be obtained by hydrogen pretreatments at room or low temperature. Siegmann et al. (1978) showed that after several hydrogen absorption-desorption cycles the LaNi<sub>5</sub> surface was decomposed into La oxide or hydroxide and small Ni particles. These activation cycles allow one also to obtain more finely divided powders (5–10 μm) than by mechanical crushing (20–30 μm).

Complexation of the alloys with organic molecules can improve the hydrogen storage capacity and therefore the catalytic activity in hydrogenation reactions (Imamura and Tsuchiya 1981a,b, Imamura et al. 1982). SmMg<sub>3</sub> and NiMg<sub>2</sub> hardly show any indication of hydrogen uptake. However, if these compounds were crushed into a fine powder and placed in contact with equimolecular amounts of aromatic molecules (anthracene, perylene, phenanthrene, chrysene) in the presence of traces of C<sub>2</sub>H<sub>5</sub>Br in anhydrous tetrahydrofuran and stirred for one week, a dark-green powder was formed, the structure of which could be identified as a complex between the intermetallic and the condensed-ring compound.

Imamura et al. (1984, 1986a) described a new way of preparing Raney catalysts using intermetallic compounds as starting materials. They found that, when treated with 1,2-diiodoethane (or dibromoethane) the lanthanide could be etched from the alloy to form the iodide (bromide), leaving a spongy, high-surface-area skeleton of the other element (Ni or Co):



Several intermetallic compounds were studied: LaNi<sub>5</sub>, LaNi, LaCo<sub>5</sub>, SmCo<sub>5</sub>, Sm<sub>2</sub>Co<sub>7</sub> and SmCo<sub>2</sub>. It turned out that LaNi and SmCo<sub>2</sub> were by far the most convenient

for the purpose. For example, after leaching with diiodoethane at room temperature in tetrahydrofuran under anhydrous conditions and extraction at room temperature, the decomposed LaNi alloy grains were dispersed in slurry form, and after washing the resulting powder had a  $96 \text{ m}^2/\text{g}$  BET area with a Ni crystallite size of 4 nm and a pore diameter of 6.5 nm.

For the dehydrogenation of alcohols, (Imamura et al. 1987, 1988), the 100-mesh alloy powders were treated with a solution of a dihalogenoethane (dibromoethane or diiodoethane) in tetrahydrofuran (THF) and with aqueous sodium hydroxide solution. The alloys were then washed with distilled water, dried and stored under dry argon.

For other reactions like methane, ammonia or methanol synthesis the intermetallic compounds are used as precursors of new active catalysts. In this case a bulk decomposition of the starting compounds is required. This can be performed either under a synthesis gas reactant or by applying either an oxidation pretreatment under air,  $\text{O}_2$ ,  $\text{CO}_2$ ,  $\text{N}_2\text{O}$  or by hydrogenation at high temperature.

### 1.2. *Supported bimetallic alloys*

Supported bimetallic alloys were generally prepared by impregnation or coprecipitation of salts on the support.

The Pt-R/ $\gamma\text{-Al}_2\text{O}_3$  catalysts were prepared by impregnating  $\gamma\text{-Al}_2\text{O}_3$  in solutions of  $\text{H}_2\text{PtCl}_6$  and rare-earth chloride (Weiqi et al. 1992, Jianhui et al. 1992). The catalysts were then dried at 393 K and calcined in air at 773 K.

Sohier et al. (1992) prepared  $\text{RM}_x$  compounds from nitrate mixtures or by coprecipitation of rare-earth and metal hydroxides. These catalysts were also compared to a Ni/ $\text{CeO}_2$  catalyst and mixtures of pure Ni with rare-earth oxide or hydroxides.

### 1.3. *Thin films*

Thin films of a rare earth on another metal (or the other way round) were investigated by various authors. However, real alloys were rarely formed and most of the time such studies were performed from a purely surface science point of view (electronic structure, spectroscopic properties ...) and with no direct relevance to catalysis. One may quote, for example, the oxidation studies of tantalum and aluminum with thin cerium overlayers, carried out at low temperature, which showed that cerium enhances the oxide growth on both substrates (Braaten et al. 1989). However, the mechanism was not identical. No alloy was formed with tantalum and a catalytic oxidation took place. On aluminum, the formation of an intermetallic Ce-Al-O oxide layer was evidenced.

Surface science studies of thin films may be very helpful for the understanding of the mechanisms of heterogeneous catalysis on intermetallics. This was true in particular for the AES study of the Ru(0001)-Ce- $\text{H}_2$  interface performed by Walker and Lambert (1992) in the context of ammonia synthesis or the growth of cerium films on polycrystalline rhodium (Warren et al. 1993) on top of which carbon monoxide oxidation was performed.

In recent years, Schmidt and his collaborators published a series of very detailed electron-microscopy studies on palladium, platinum and rhodium dispersed on cerium

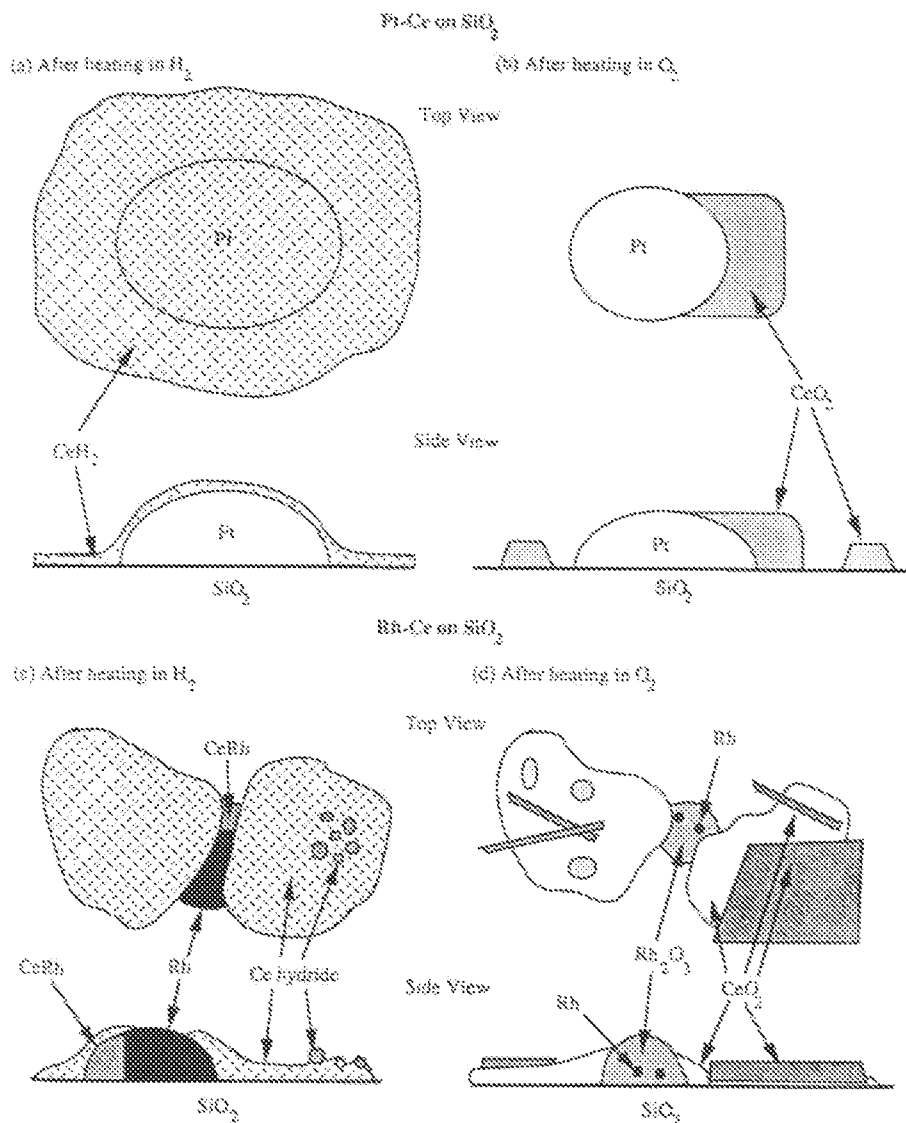


Fig. 2. Illustrations of the idealized morphologies of Pt-Ce and Rh-Ce on  $\text{SiO}_2$  after reducing and oxidizing heat treatments. (a) Treatment of Pt-Ce samples in  $\text{H}_2$  results in the formation of round highly twinned Pt particles. Amorphous  $\text{CeH}_2$  is also formed and covers the surface of the silica as well as the Pt particles. (b) Treatment of Pt-Ce in  $\text{O}_2$  causes the oxidation of Ce to  $\text{CeO}_2$  which forms as rectangular structures adjacent to the Pt particles and as  $\sim 25 \text{ \AA}$  particles distributed over the support. (c) Rh-Ce for high Ce loadings ( $\text{CeRh} \geq 2.5$ ) prepared by addition of Ce from the salt. After heating in  $\text{H}_2$ , CeRh particles are observed in addition to Rh and  $\text{CeH}_2$ . The CeRh intermetallic is not observed at lower Ce loadings or in samples where Ce was added by vacuum evaporation. (d) After heating in  $\text{O}_2$ , the Ce oxidizes to form large  $\text{CeO}_2$  particles and needles, while Rh partially oxidizes to  $\text{Rh}_2\text{O}_3$ . (Chojnacki et al. 1991.)

films deposited on a silica or alumina substrate. The paper by Chojnacki et al. (1991), which deals with the microstructure and reactivity (for ethane hydrogenolysis and carbon monoxide hydrogenation) of Pt–Ce and Rh–Ce particles deposited on silica, is a good example of the difficulties of such studies and, more generally, of the identification of active sites in catalysis. This is because cerium forms many different phases with platinum, rhodium and hydrogen, depending on the experimental conditions (temperature, reducing or oxidizing atmosphere, concentration of cerium). Figure 2 shows very well the complexity of such systems. Intermetallic Ce–Rh was formed under reducing conditions but it was not clear whether it played any role in the catalytic reactivity. Cerium addition was shown to enhance the activity of the catalysts, especially carbon monoxide oxidation, but it was hardly possible to give a simple explanation for the relationship between the microstructure and the catalytic behavior. The picture was even more complicated by the detection in a subsequent study (Krause et al. 1992) of cerium silicate,  $\text{Ce}_2\text{Si}_2\text{O}_7$ , catalyzed by rhodium under reducing atmosphere and stable under oxygen.

## 2. Characterization methods

### 2.1. X-ray diffraction

X-ray diffraction can be used to identify the phases which are present in a catalyst. To follow the evolution of a catalyst during pretreatment or catalytic reaction (ammonia or methanol synthesis), in situ XRD experiments have been performed. For this purpose Nix et al. (1987) have built a high-pressure XRD cell operating up to 50 bar and temperatures up to 700 K. The reactant gases flow over the catalysts sample heated by conduction from a cartridge heater. The temperatures are measured and controlled using a thermocouple fixed into the copper support block (fig. 3).

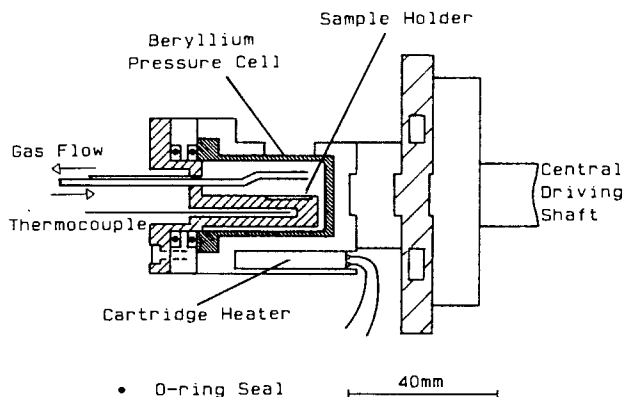


Fig. 3. High-pressure XRD cell (thermal insulation not shown for clarity) (Nix et al. 1987).

The use of appropriate fitting methods, like Rietveld refinements, allows one to obtain the percentage of each phase. Through the line width (FWHM) analysis and Scherrer equation it is possible to estimate the mean crystallite size. However this analysis concerns the size of diffracting domains larger than 30–35 Å.

## 2.2. *X-ray absorption*

X-ray absorption is a powerful technique to obtain local electronic and structural properties and has been widely used to characterize catalysts (Yokoyama 1995). This technique involves the determination of the electronic state through X-ray absorption near edge structure (XANES) analysis and of the local structure through the extended X-ray absorption fine structure (EXAFS). The data can be collected not only in a static but also in dynamic state (in-situ conditions) allowing one to study the catalyst during pretreatment and catalytic reaction.

EXAFS corresponding to the higher energy range of the XAS spectra (60–1000 eV) is an oscillatory structure due to the interaction of the wave emitted by the photoelectron with that backscattered by the neighboring atoms. The EXAFS oscillations can be approximately described as the sum of sinusoidal functions of the closest shells surrounding the central atom. Appropriate analysis involving the knowledge of calculated or experimental amplitudes and phase-shifts of the atoms allows one to obtain local structural parameters such as the nature and the number of neighboring atoms, the interatomic distances and the so-called Debye–Waller factor. The theory of EXAFS has been developed in several reference books (Iwasawa 1995) and will not be detailed here.

In the case of very small metallic particles (a few nm) the coordination number of the shells can be used to determine the size of the metallic particles with an assumption of their shape (Zhang et al. 1995). This analysis is based on the fact that surface atoms have lower coordination numbers than bulk atoms. The mean coordination number can be calculated from the model of metallic particles and compared with the experiment.

XANES corresponds to the excitation of a core electron (1s, 2s, 2p, ...) to empty bound and quasi bound states. This excitation involves multi-electron and multi-scattering processes. Different approaches have been developed to analyze XANES: ab-initio molecular orbital energy, multiple scattering theory, atomic multiplet theory (Vvedensky 1992). However, in many studies empirical edge analyses have been used to determine the valence or the oxidation state of a metal using reference compounds. For example, in the case of mixed-valent or valence-fluctuating lanthanides (Ce, Eu, Yb) the valence can be determined using the ratio of the two white lines observed in the  $L_{III}$  edges (Rohler 1985). For the transition-metal oxides the position and the shape of the edge allow to estimate the oxidation state and even the symmetry of the site (tetrahedral or octahedral) considering molecular orbital models.

## 2.3. *Magnetic measurements*

The study of the magnetic properties of rare-earth and transition-metal elements as well as their alloys concerns a very large field in material science both from a fundamental



and from a technical point of view (Kirchmayr and Poldy 1979). Less magnetic studies are encountered in the frame of catalysis. For example, magnetic measurements have been performed to determine the particle size of small Ni or Fe clusters which display a superparamagnetic behavior below a critical size (Herpin 1968). The composition of bimetallic particles can be estimated by comparing their magnetic properties with those of bulk alloys with known composition. This has been performed by France and Wallace (1988) to characterize decomposed  $\text{CeNi}_{5-x}\text{Co}_x$  intermetallic compounds. According to the Curie temperature variation they were able to estimate the composition of Co–Ni particles on ceria.

On the other hand, in the case of a Pauli paramagnet the magnetic susceptibility is proportional to the density of states at the Fermi level. The change of the electronic properties by alloying leads to a variation of the susceptibility. Weiqi et al. (1992) and Jianhui et al. (1992) have measured the susceptibility to observe changes in the electronic properties of Pd in Pd–R/ $\text{Al}_2\text{O}_3$  catalysts and to correlate them with their catalytic properties.

### 3. Catalytic reactions

#### 3.1. *Hydrogenation of olefins*

The ability of many lanthanide-based intermetallic compounds to absorb hydrogen has attracted a lot of research on the hydrogenation of olefins (Netzer and Bertel 1982). The idea was that a fast diffusion process of absorbed hydrogen from the bulk to the catalyst surface might help to get better activities and selectivities. Indeed a variety of intermetallic compounds proved to be more active by at least one order of magnitude than classical catalysts:  $\text{LaNi}_5$  (Soga et al. 1977),  $\text{PrCo}_5$ ,  $\text{CeCo}_5$ , and  $\text{SmCo}_5$  (Soga et al. 1979); their hydrides were even more active. Kinetic studies (Soga et al. 1979, 1980) and in particular the influence of the hydrogen pressure suggested that the diffusion of hydrogen from the bulk was the rate-determining step, but the influence of the hydrogen pressure and the reaction rates varied largely from one hydride to the other.

Imamura and Wallace (1980) used various intermetallic compounds ( $\text{LaNi}_5$ ,  $\text{CeNi}_5$ ,  $\text{ThNi}_5$ ,  $\text{ThCo}_5$ ) as precursors. After decomposition under oxygen at 350°C they obtained catalysts which were clearly more active than the corresponding classical Ni catalysts. They suggested that geometrical effects were responsible for such a behavior.

$\text{SmMg}_3$  and  $\text{NiMg}_2$  powders complexed with organic molecules (anthracene, perylene, phenanthrene, chrysene) (Imamura and Tsuchiya 1981a,b, Imamura et al. 1982) were able to instantaneously absorb hydrogen at room temperature and exhibited a good activity for the hydrogenation of ethylene at low temperatures. However, the hydrogenation activity could vary noticeably depending on the nature of the aromatic molecule. For example,  $\text{SmMg}_3$ -naphthalene was six times as active as  $\text{SmMg}_3$ -perylene. These differences were interpreted in terms of variations of the electronic interactions between the intermetallic compound and the aromatic molecules.

Imamura et al. (1984, 1986a) described a new way of preparing Raney catalysts using intermetallic compounds as starting materials as reported in sect. 1. The catalytic results

depended very much of the preparation procedure. However, optimized LaNi and SmCo<sub>2</sub> were found to be more active than conventional Ni and Co Raney catalysts for the hydrogenation of ethylene and the dehydrogenation of 2-propanol. These catalysts were stable at room temperature and up to 100°C, but rapid sintering and therefore deactivation occurred at higher temperatures.

Due to its unique capabilities for storing hydrogen, LaNi<sub>5</sub> was certainly the most studied compound in hydrogenation reactions. This can be closely related with the formation of hydrides. When hydrogen is absorbed by LaNi<sub>5</sub>, it dissolves into the lattice to form a solid solution called  $\alpha$  phase. If more hydrogen is added, the  $\alpha$  phase is progressively converted into a  $\beta$  hydride phase following the equation



Depending on the experimental conditions, the occurrence of both phases or of one of them only, will of course change the catalytic behavior.

Barrault et al. (1986c) have studied the hydrogenation of propene on LaNi<sub>5</sub> and LaNi<sub>5</sub>-based intermetallic compounds where one nickel atom was substituted with Co, Fe, Al or Mn. Replacement of Ni by another metal resulted in an important variation of the equilibrium pressure of the corresponding hydride, from 10<sup>-3</sup> (LaNi<sub>4</sub>Mn) to 1.7 atm (LaNi<sub>5</sub>) at room temperature. Hydrogenation of propene exhibited a critical temperature, defined as the temperature corresponding to a sudden increase in activity. This critical temperature was systematically 20–30°C higher than the temperature of the hydride decomposition. For example, on LaNi<sub>5</sub> the conversion of propene was 0.5% at 40°C while the equilibrium temperature of the hydride is 10°C. The conversion increased sharply from 0.5% to 40% as the reaction temperature was increased from 40°C to 100°C. This corresponds to an activation energy of 125–150 kJ/mol, noticeably higher than the ~42 kJ/mol found on classical catalysts. As shown in fig. 4 for LaNi<sub>4</sub>Fe, the same trend was observed with all substituted LaNi<sub>4</sub>M compounds (M = Co, Fe, Al and Mn), but, as indicated in table 1, all the critical temperatures of hydrogenation were higher than with LaNi<sub>5</sub>, which can be related to the fact that LaNi<sub>5</sub> hydride has the lowest equilibrium temperature at 0.9 atm. These results show that the hydrogenation of propene takes place at a marked rate only outside the domain of the  $\beta$  hydride stability and it is likely that the  $\alpha$  phase plays a major part in the reaction. No modifications of the bulk of the catalysts were observed when the samples were analyzed using XRD, but no surface studies were performed.

Johnson et al. (1992) studied the hydrogenation of 1-undecene in the liquid phase at 35°C on LaNi<sub>5</sub> in various experimental conditions of hydrogen pressure, leading therefore to catalysts of different compositions as far as hydride formation was concerned. X-ray photoelectron spectroscopy, AES and magnetic susceptibility measurements showed that a substantial surface segregation of lanthanum occurred so that the surface was mainly composed of La<sub>2</sub>O<sub>3</sub> or La(OH)<sub>3</sub> and Ni particles. However, the underlying  $\alpha$  phase or  $\beta$  hydride phase play an important role, probably acting as a hydrogen reservoir, the hydrogen atoms diffusing to the surface through microcracks and grain boundaries,

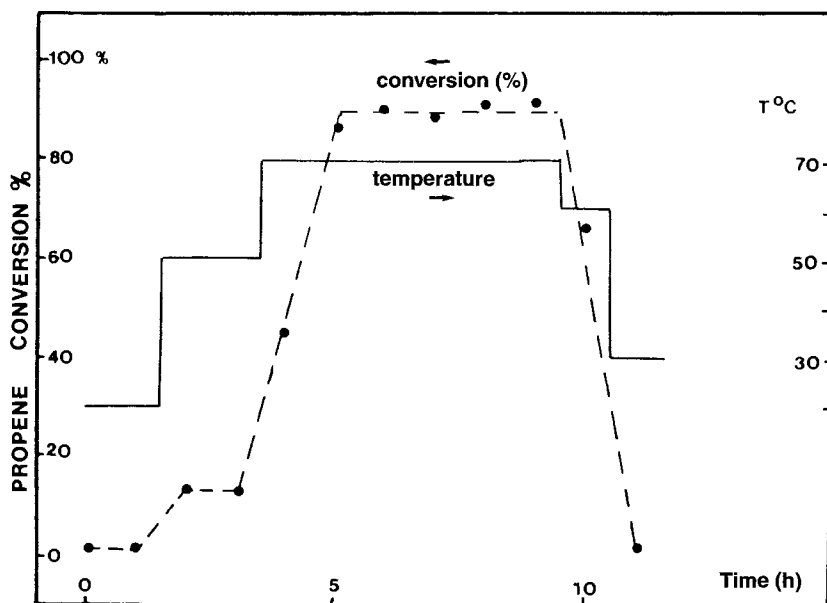


Fig. 4. Hydrogenation of propene in the presence of  $\text{LaNi}_4\text{Fe}$ : time- and temperature-related evolution of the amount of propene hydrogenated (Barrault et al. 1986c).

Table 1  
Results for  $\text{LaNi}_4\text{M}$  compounds in the hydrogenation of propene<sup>a</sup>

Parameter <sup>b,c</sup>	$\text{LaNi}_5$	$\text{LaNi}_4\text{Co}$	$\text{LaNi}_4\text{Fe}$	$\text{LaNi}_4\text{Al}$	$\text{LaNi}_4\text{Mn}$
$T_S$ (K)	313	333	343	373	433
$T_E$ (K)	283	303	308	398	413
$\Delta T = T_S - T_E$	30	30	25	-15	20

<sup>a</sup> Data from Barrault et al. (1986c).

<sup>b</sup>  $T_S$ , critical temperature of hydrogenation of propene ( $P_{\text{H}_2} = 0.9$  atm,  $\text{H}_2/\text{C}_3\text{H}_6 = 9$ ).

<sup>c</sup>  $T_E$ , equilibrium temperature of hydride with  $P = 0.9$  atm.

which is helped by the expansion of the catalyst particle due to the lower density of the hydride phase; indeed, while the  $\alpha$  phase was found to favor the catalytic activity, the conversion was greatly enhanced when the  $\beta$  hydride phase was initially present under the Ni particles. However, even when the hydrogen pressure was maintained above that required for hydride formation, hydrogen was quickly extracted from the  $\beta$  hydride phase, as the alkene was hydrogenated. This is clearly shown in fig. 5, taken from a subsequent paper by Johnson et al. (1994) which deals with the hydrogenation of octene. This figure also shows that, after some time, the system was depleted of octene, the competition for

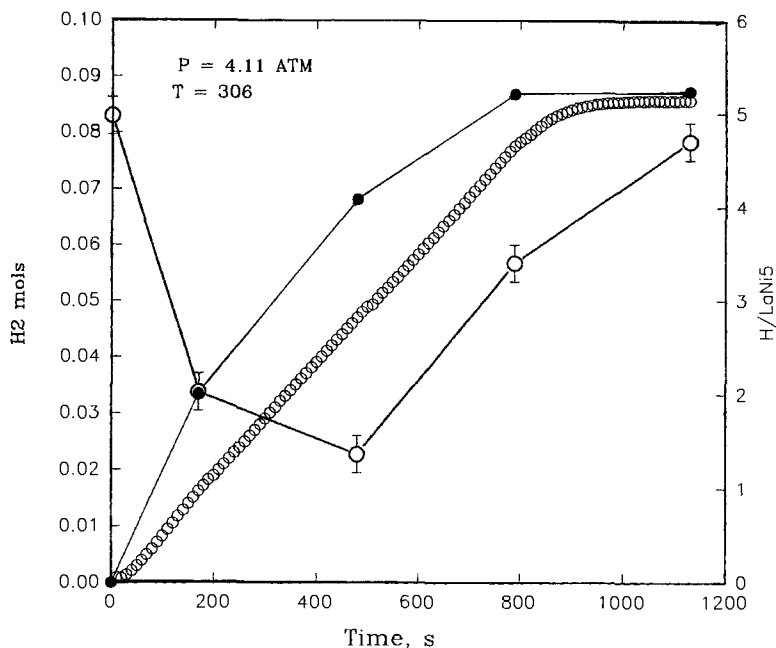


Fig. 5. Octene hydrogenation; initial catalyst is  $\beta$ -LaNi<sub>5</sub>H<sub>5</sub>. Left axis: open circles are mol H<sub>2</sub> introduced from gas reservoir, solid circles are mol H<sub>2</sub> reacted with octene; symbol size exceeds the error in these quantities. Right axis: catalyst composition, H atoms per mol LaNi<sub>5</sub>, open circles (with error bars) (Johnson et al. 1994).

hydrogen on the surface decreased and the hydride phase was regenerated. Consequently, the catalyst composition over most of the reaction period was predominantly  $\alpha$ -LaNi<sub>5</sub>H<sub>x</sub>.

A detailed kinetic study of cyclohexene hydrogenation in a slurry reactor on the metal-hydride-forming alloys LaNi<sub>4.8</sub>Al<sub>0.2</sub>, LaNi<sub>4.9</sub>Al<sub>0.1</sub> and LaNi<sub>5</sub> was performed by Snijder et al. (1993). Such a study is very difficult because, depending on the experimental conditions (hydrogen pressure and temperature which determine the equilibrium curves of the metal hydrides), hydrogen may come from two different sources:

- Hydrogen from the gas phase which diffuses into the solvent and then on the catalyst; in this case we are dealing with a conventional catalyst.
- Hydrogen provided by the hydride, which is therefore both a catalyst and a hydrogen source. The desorption of hydrogen from the hydride must be added in the equation of the reaction rate.

Moreover, as the reaction proceeds, the particles may change from the  $\beta$  phase to the  $\alpha$  phase.

The mechanism of the hydrogenation reaction for hydrogen supplied by the gas phase could be described in terms of a Langmuir–Hinshelwood type of kinetic equation, assuming a fast dissociative adsorption of hydrogen and cyclohexene on two different sites. Following Wallace et al. (1979) and Johnson et al. (1992) it was assumed that these

sites were nickel particles and lanthanum oxide or hydroxide sitting on the intermetallic phase. This implies that the reaction could proceed only at the boundary between these regions. Whatever the state of the catalyst,  $\alpha$  or  $\beta$  phase, the aluminum content or the solvent, the activation energy of the reaction was almost constant, around 37 kJ/mol. Therefore the authors assumed that the nature of the surface where the reaction took place was the same in all cases. Both the reaction rate and the adsorption coefficient of cyclohexene decreased with increasing Al content. This was interpreted in terms of a decrease in the reaction area due to the presence of aluminum atoms at the interface between nickel particles and lanthanum oxide or hydroxide, where the reaction proceeds. Ethanol instead of cyclohexane as a solvent resulted in higher reaction rates, in relation with a lower adsorption coefficient of cyclohexene. Finally, the transformation of the  $\beta$  phase into the  $\alpha$  phase as the reaction proceeds resulted in a continuous decrease in the reaction rate.

Another example of the importance of hydride formation was provided by Zhu et al. (1997) who studied the hydrogenation of oleic acid into stearic acid on a  $\text{LaNi}_{4.8}\text{Fe}_{0.2}$  catalyst at 90°C. In a first experiment, oleic acid was admitted into the reactor before hydrogen. No metal hydride was formed because the acid covered the catalyst powder and hydrogenation was not observed until the mixture was vigorously agitated. In another experiment, hydrogen was admitted first, the hydride was formed almost instantaneously and when the oleic acid was introduced, the hydrogenation started immediately and proceeded quickly. These findings prompted the authors to design a reactor in such a way that the hydride could be continuously regenerated.

Finally a study of the stabilization of the  $\text{LaNi}_5$  hydride by treating the sample under CO or  $\text{SO}_2$  in a gaseous atmosphere or in a liquid phase was performed by Corré et al. (1997). The dehydrogenation of the hydride was followed at 100°C as a function of time. It turned out that the liquid  $\text{SO}_2$  treatment was the most efficient for confining hydrogen in the bulk of the intermetallic. As a consequence no hydrogenation of 1-octene, even at 70°C, was observed. Samples treated under gaseous CO or  $\text{SO}_2$  slowly released hydrogen, and yields of 92–95% of *n*-octane could be obtained in a reasonable time span, but at 40°C, whereas non-treated  $\text{LaNi}_5$  gave 99% conversion at room temperature.

### 3.2. *Hydrogenation of dienes and alkynes*

The design of highly selective catalysts for the hydrogenation of dienes and alkynes is an important problem. Among the transition metals palladium is well known as being the most selective of all for the production of mono-olefins. This selectivity can even be improved when doped, as in the so-called commercial Lindlar catalyst which is composed of palladium and lead supported on calcium carbonate. There is still a need for stable and highly selective catalysts, especially at high conversion.

Sim et al. (1989, 1991) have studied the hydrogenation of but-1-ene, buta-1,3-diene and but-1-yne on a series of  $\text{RPd}_3$  ( $\text{R}=\text{La, Ce, Pr, Nd, Sm}$ ) intermetallic compounds. The reactions were performed at 0°C but all catalysts were submitted to a hydrogen pretreatment at 300°C. They all exhibited a modification of their properties as a function

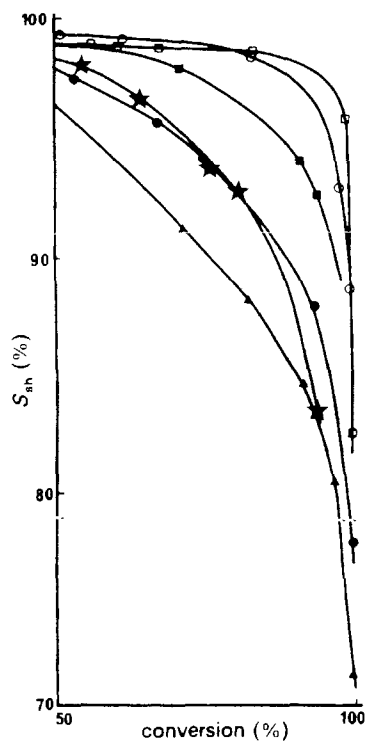


Fig. 6. Hydrogenation of buta-1,3-diene: semi-hydrogenation selectivities ( $S_{sh}$ ) as a function of the conversion (50–100%) on  $RPd_3$  catalysts: triangles,  $CePd_3$ ; solid circles,  $LaPd_3$ ; open squares,  $PrPd_3$ ; open circles,  $NdPd_3$ ; solid squares,  $SmPd_3$ ; stars,  $Pd/pumice$  (H) (Sim et al. 1991).

of time under hydrogen. However, they were all stable after 15 hours under hydrogen and, whatever the hydrocarbon, their order of activity was

$$CePd_3 > LaPd_3 > PrPd_3 > NdPd_3 > SmPd_3. \quad (5)$$

For all reactions,  $CePd_3$  was the most active catalyst, and at the same time the least selective. For the isomerization of but-1-ene into but-2-ene, as compared to the formation of butane, the order of selectivity was

$$CePd_3 < Pd/pumice < LaPd_3 < PrPd_3 = NdPd_3 < SmPd_3. \quad (6)$$

Concerning the semihydrogenation of buta-1,3-diene (fig. 6) and but-1-yne the selectivities, which were all equal to 99% or more at initial conversion, decreased at higher conversion. At 90% conversion they varied between 81 and 97% in the following order:

$$CePd_3 < LaPd_3 \leq Pd/pumice < SmPd_3 < NdPd_3 \leq PrPd_3. \quad (7)$$

XRD and X-ray photoelectron spectroscopy analyses were performed on all the samples, initially and after several hours under hydrogen, in order to study the influence of the pretreatment on the bulk composition and on the surface of the catalysts. These analyses revealed that the intermetallic compounds were decomposed to various extents:

- $\text{PrPd}_3$ ,  $\text{NdPd}_3$  and  $\text{SmPd}_3$  exhibited very small changes even after prolonged exposures under hydrogen; their catalytic properties, low activities, high selectivities for but-1-ene isomerization and the semihydrogenation at high conversion of but-1,3-diene and but-1-yne could therefore be considered as characteristic of palladium intermetallic.
- $\text{CePd}_3$  was more decomposed and the surface could be viewed as palladium atoms surrounded by a catalytically active cerium compound promoting the availability of hydrogen atoms on the palladium site and thus leading to high activity and low selectivity.
- $\text{LaPd}_3$  was very much like  $\text{Pd/La}_2\text{O}_3$  and therefore its properties were very similar to those observed with  $\text{Pd/pumice}$ .

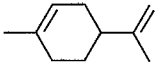
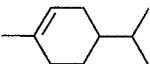
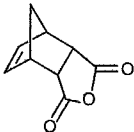
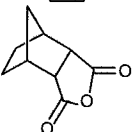
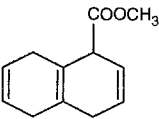
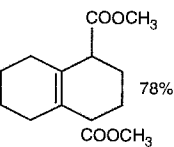
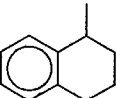
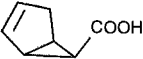
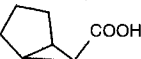
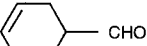
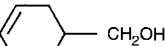
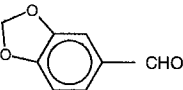
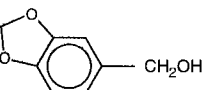
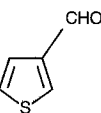
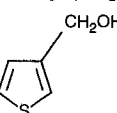
### 3.3. Hydrogenation of various organic molecules

Selective hydrogenation of unsaturated bonds is a very important problem in organic chemistry. Imamoto et al. (1984, 1987) investigated the hydrogenation of over fifty molecules (table 2) with different functional groups on  $\text{LaNi}_5$  and  $\text{LaNi}_{4.5}\text{Al}_{0.5}$  hydrides. All reactions were performed under nitrogen at  $0^\circ\text{C}$  or room temperature and atmospheric pressure. No or very weak reaction was observed with oximes, sulfoxides, sulfones and dithioketals even at higher temperatures, but olefins, alkynes, aldehydes, unsaturated carboxylic acids, nitrocompounds and imines were hydrogenated with very good yields, generally around or above 90%. The alloys could be used repeatedly without significant decrease of activity. Semihydrogenation of alkynes into olefins was not easily performed and, in  $\alpha,\beta$  unsaturated carbonyl compounds,  $\text{C}=\text{C}$  double bonds were hydrogenated before  $\text{C}=\text{O}$  bonds. For example, citral gave 89% of citronellal after 3 h of reaction at  $0^\circ\text{C}$  while 95% of citronellol were obtained after 12 h at room temperature.

Sohier et al. (1992) compared the hydrogenation properties of catalysts derived from  $\text{RM}_x$  ( $\text{M}=\text{Ni}$ ,  $\text{Cu}$  and  $\text{Co}$ ) intermetallic precursors with those prepared from nitrate mixtures or by coprecipitation of rare-earth and metal hydroxides. These catalysts were also compared to a  $\text{Ni/CeO}_2$  catalyst and mixtures of pure  $\text{Ni}$  with rare-earth oxide or hydroxides. The intermetallic compounds were submitted to hydriding-dehydriding cycles, then oxidized by calcination at 293 K (partially oxidized) and at 703 K (fully oxidized). The largest surface areas for oxides were obtained by the coprecipitation route.

The catalysts were tested in isoprene, benzene and naphthalene hydrogenation reactions. The catalysts prepared by oxidation of the intermetallic at 703 K were found to be more active than those oxidized at room temperature. In isoprene hydrogenation the catalyst based on mischmetal has a larger activity than the other alloys and is comparable to the catalysts prepared by other routes. In benzene hydrogenation the  $\text{Ni}$  and  $\text{Ce}$  based catalysts prepared by coprecipitation were found the most active. In naphthalene hydrogenation the fully oxidized intermetallics are four times more active than the partially oxidized ones. In addition they are independent of hydrogen pressure and selective into decaline formation.

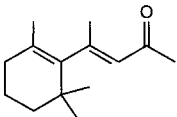
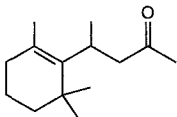
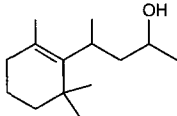
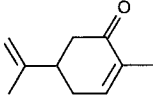
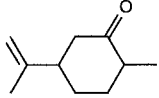
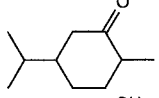
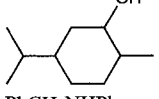
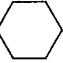
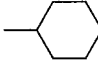
Table 2  
Hydrogenation of organic functional groups with  $\text{LaNi}_5\text{H}_6$  (Imamoto et al., 1987)

Entry	Compound	Cond. <sup>a</sup>	Product	Yield (%) <sup>b</sup>
1	$\text{C}_{10}\text{H}_{21}\text{CH}=\text{CH}_2$	rt <sup>c</sup> , 15 h	$\text{C}_{12}\text{H}_{26}$	86
2	$\text{Ph}_2\text{P}(\text{O})\text{CH}_2\text{CH}=\text{CH}_2$	rt, 11 h	$\text{Ph}_2\text{P}(\text{O})\text{C}_3\text{H}_7$	90
3 <sup>d</sup>		rt, 11 h		88
4 <sup>d</sup>		rt, 18 h		93
5		rt, 4 h	 78%	78
				19
6 <sup>d</sup>		0°C, 3 h		93
7 <sup>d</sup>	$\text{PhC}\equiv\text{CPh}$	rt, 9 h	$\text{Ph}(\text{CH}_2)_2\text{Ph}$	96
8	$\text{PhC}\equiv\text{CC}\equiv\text{CPh}$	rt, 11 h	$\text{Ph}(\text{CH}_2)_4\text{Ph}$	97
9 <sup>d</sup>	$\text{HOCH}_2\text{C}\equiv\text{CCCH}_2\text{OH}$	0°C, 6 h	$(Z)\text{-HOCH}_2\text{CH}=\text{CHCH}_2\text{OH}$ $\text{HO}(\text{CH}_2)_4\text{OH}$	67 10
10 <sup>d</sup>	$\text{C}_{11}\text{H}_{23}\text{CHO}$	rt, 14 h	$\text{C}_{12}\text{H}_{25}\text{OH}$	98
11 <sup>d</sup>		rt, 8 h		91
12 <sup>d</sup>		rt, 9 h		99
13 <sup>d</sup>	$p\text{-ClC}_6\text{H}_4\text{CHO}$	rt, 8 h	$p\text{-ClC}_6\text{H}_4\text{CH}_2\text{OH}$	95
14		rt, 14 h		96
15 <sup>d</sup>	$\text{C}_6\text{H}_{13}\text{COCH}_3$	rt, 37 h	$\text{C}_6\text{H}_{13}\text{CHOHCH}_3$	91
16	2-adamantanone	rt, 16 h	2-adamantanol	92
17 <sup>d</sup>	$p\text{-CH}_3\text{OC}_6\text{H}_4\text{COCH}_3$	rt, 37 h	$p\text{-CH}_3\text{OC}_6\text{H}_4\text{CHOHCH}_3$	85

continued on next page

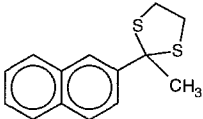


Table 2, *continued*

Entry	Compound	Cond. <sup>a</sup>	Product	Yield (%) <sup>b</sup>
18 <sup>d</sup>	PhCOCOPh	rt, 11 h	PhCOCHOHPH	96
19	PhC≡CCOOH	rt, 15 h	Ph(CH <sub>2</sub> ) <sub>2</sub> COOH	99
20	PhCH=CHCOOC <sub>2</sub> H <sub>5</sub>	rt, 15 h	Ph(CH <sub>2</sub> ) <sub>2</sub> COOC <sub>2</sub> H <sub>5</sub>	93
21 <sup>d</sup>	PhCH <sub>2</sub> OCOC(CH <sub>3</sub> )=CH <sub>2</sub>	0°C, 4 h	PhCH <sub>2</sub> OCOCH(CH <sub>3</sub> ) <sub>2</sub>	91
22 <sup>d</sup>	PhCH=CHCOCH <sub>3</sub>	rt, 17 h	Ph(CH <sub>2</sub> ) <sub>2</sub> CHOHCH <sub>3</sub>	95
23	citral	0°C, 3 h	citronellal	89
24	see entry 23	rt, 12 h	citronellol	95
25 <sup>d</sup>	PhCH=CHCOPh	0°C, 6 h	Ph(CH <sub>2</sub> ) <sub>2</sub> COPh	89
26 <sup>d</sup>	see entry 25	rt, 43 h	Ph(CH <sub>2</sub> ) <sub>2</sub> CHOHPH	99
27 <sup>d</sup>		0°C, 6 h		89
28 <sup>d</sup>	see entry 27	rt, 33 h		95
29		0°C, 3 h		70
				25
30 <sup>d</sup>	see entry 29	rt, 3 h		90
31	PhCH=NPh	rt, 11 h	PhCH <sub>2</sub> NHPh	95
32 <sup>d</sup>	PhCH=N- 	rt, 13 h	PhCH <sub>2</sub> =NH- 	97
33	<i>p</i> -O <sub>2</sub> NC <sub>6</sub> H <sub>4</sub> COOC <sub>2</sub> H <sub>5</sub>	rt, 13 h	<i>p</i> -H <sub>2</sub> NC <sub>6</sub> H <sub>4</sub> COOC <sub>2</sub> H <sub>5</sub>	97
34	PhC(=NOH)CH <sub>2</sub> Ph	rt, 44 h	— <sup>e</sup>	
35	PhC(=NOAc)CH <sub>2</sub> Ph	rt, 50 h	— <sup>e</sup>	
36	PhSCH <sub>2</sub> CH=CH <sub>2</sub>	rt, 28 h	— <sup>e</sup>	
37	PhCOCH <sub>2</sub> S(O)CH <sub>3</sub>	rt, 15 h	— <sup>e</sup>	

*continued on next page*

Table 2, *continued*

Entry	Compound	Cond. <sup>a</sup>	Product	Yield (%) <sup>b</sup>
38	PhCOCH <sub>2</sub> SO <sub>2</sub> CH <sub>3</sub>	rt, 19 h	— <sup>c</sup>	
39	PhSO <sub>2</sub> CH=C(SCH <sub>3</sub> ) <sub>2</sub>	rt, 34 h	— <sup>c</sup>	
40		rt, 38 h	— <sup>c</sup>	
41	PhCH <sub>2</sub> OCONHCH(CH <sub>2</sub> C <sub>6</sub> H <sub>4</sub> OH- <i>p</i> )COOH	rt, 18 h	— <sup>c</sup>	
42	PhCH <sub>2</sub> OCONHCH(CH <sub>2</sub> CH <sub>2</sub> SCH <sub>3</sub> )CONHCH <sub>2</sub> COOCH <sub>3</sub>	rt, 36 h	— <sup>c</sup>	
43 <sup>f</sup>	<i>p</i> -CH <sub>3</sub> OC <sub>6</sub> H <sub>4</sub> COCl	rt, 48 h	— <sup>c</sup>	
44	PhCH=CHCOSC(CH <sub>3</sub> ) <sub>3</sub>	rt, 18 h	— <sup>c</sup>	

<sup>a</sup> Conditions: All reactions were carried out in THF–MeOH(2:3) on a 1-mmol scale using 3 g of LaNi<sub>5</sub>H<sub>6</sub>.

<sup>b</sup> Isolated yield.

<sup>c</sup> rt, Room temperature.

<sup>d</sup> A recovered alloy was used.

<sup>e</sup> No reaction took place.

<sup>f</sup> The reaction was carried out in dry THF.

### 3.4. Carbon monoxide hydrogenation

#### 3.4.1. Methanation reaction

Early work, as reported by Netzer and Bertel (1982), showed that many rare-earth-based intermetallic compounds were active methanation catalysts. Coon et al. (1976, 1978) showed that the most active catalysts contained Fe, Co or Ni, in contrast to Al or Mn. In particular, LaNi<sub>5</sub> and other lanthanide–Ni<sub>5</sub> catalysts gave high conversion into methane and the activity increased with time. This was probably due to a progressive decomposition of the intermetallic into lanthanide oxide during the course of the reaction. Elattar et al. (1978), on the contrary, found a decrease in activity with time on stream for iron containing intermetallics. But several studies showed that this was due to carbon deposition during methanation. Atkinson and Nicks (1977) found very good activities with mischmetal–Ni<sub>5</sub> catalysts. Luengo et al. (1977) observed that in their decomposed states CeCo<sub>2</sub> and CeNi<sub>2</sub> had activities comparable to Co and Ni but were more selective towards the formation of higher hydrocarbons.

Since Netzer and Bertel wrote their chapter in volume 5 of this Handbook (1982), further studies have shown that the best activities are related to more extensive decomposition. This was, for example, the case with a series of Ni-based intermetallic compounds (Paul-Boncour et al. 1986). For LaNi<sub>4</sub>X (X=Ni, Cr, Al and Cu) Ando et al. (1995) observed that only LaNi<sub>5</sub> and LaNi<sub>4</sub>Cr had significant activity in the methanation reaction. XRD analyses revealed their decomposition into metallic nickel

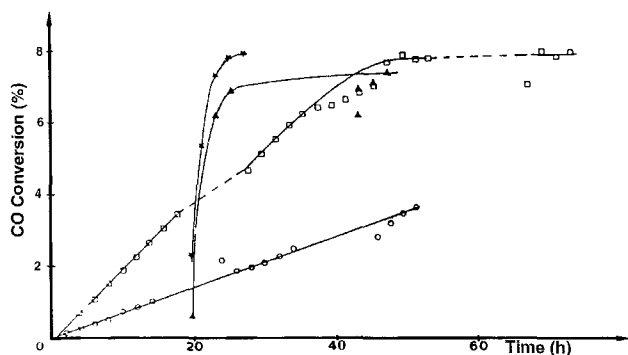


Fig. 7. Influence of the activation procedure on the catalytic activity of  $\text{LaCo}_5$  in the intermetallic in the  $\text{CO}, \text{H}_2$  reaction.  $T = 350^\circ\text{C}$ ,  $P = 0.1$  Mpa,  $\text{H}_2/\text{CO} = 1$ . (a)  $\text{LaCo}_5$  initial; (b)  $\text{LaCo}_5$  reduced by hydrogen for 2 h at  $400^\circ\text{C}$ ; (c)  $\text{LaCo}_5$  oxidized for 3 h at  $350^\circ\text{C}$ ; (d)  $\text{LaCo}_5$  oxidized for 3 h at  $350^\circ\text{C}$  and reduced for 2 h at  $400^\circ\text{C}$ .

and  $\text{La}(\text{CO}_3)(\text{OH})$  and  $\text{La}(\text{OH})_3$ , whereas no metallic nickel was observed for the other two – inactive – compounds.

Barrault et al. (1983a,b) studied the activity of  $\text{LaNi}_5$ ,  $\text{MMNi}_5$  (MM = mischmetal) and  $\text{LaNi}_4\text{Mn}$  with or without activation under hydrogen at  $430^\circ\text{C}$ , which actually did not make much difference. These compounds exhibited activities similar to or even higher than conventional  $\text{Ni}/\text{Al}_2\text{O}_3$  catalysts at comparable reaction temperatures ( $300\text{--}350^\circ\text{C}$ ), and their activity increased with time during the first few hours of the reaction. This was interpreted as due to a progressive transformation of the intermetallic into nickel particles in contact with lanthanide oxide, as shown by X-ray powder diffraction studies. The selectivity towards higher hydrocarbons was very low (2–5% instead of 10–18% with  $\text{Ni}/\text{Al}_2\text{O}_3$ ). The presence of manganese in  $\text{LaNi}_5$  had a detrimental effect on the activity.

Barrault et al. (1986a) have shown that the addition of lanthanum or cerium oxides to cobalt deposited on carbon resulted in a significant enhancement of the catalytic activity, up to two orders of magnitude, and an increase in the selectivity towards higher hydrocarbons (50% instead of a few percent). These results prompted them to study  $\text{LaCo}_5$  (Barrault et al. 1986b). This compound exhibited a good activity, although with a lower selectivity and a higher production of carbon dioxide. The influence of various pretreatments (reduction, oxidation) on the catalytic properties was studied. Figure 7 shows the variation of the activity with time on  $\text{CO} + \text{H}_2$  stream. The main effect of the pretreatment was to reduce the activation period, but the selectivities remained similar in all cases (table 3). After 50 hours the untreated sample (a) had not reached its maximal activity, whereas that of pretreated samples (b–d) had been stabilized. After 2 hours under hydrogen at  $400^\circ\text{C}$  (b) the activation period lasted about 45 hours, whereas it was reduced to one or two hours after 3 hours oxidation at  $350^\circ\text{C}$  (c, d). XRD and EXAFS analyses revealed the decomposition of the intermetallic into Co or CoO and  $\text{La}_2\text{O}_3$ .

A very detailed high resolution electron microscopy (HREM) study, together with X-ray absorption spectroscopy (EXAFS) was performed on  $\text{LaCo}_5$ ,  $\text{Co}/\text{La}_2\text{O}_3$  and

Table 3

Catalytic properties of  $\text{LaCo}_5$  intermetallic compounds and supported cobalt in the  $(\text{CO}, \text{H}_2)$  reaction<sup>a</sup> (Barrault et al. 1986b)

Catalyst	Pre-treatment	Time (h)	Activity ( $\times 10^3$ ) /mol h <sup>-1</sup> g <sup>-1</sup> Co	T.O.F. ( $\times 10^3$ ) (s <sup>-1</sup> )	Selectivity		
					CH <sub>4</sub>	C <sub>2</sub> <sup>+</sup>	CO <sub>2</sub>
$\text{LaCo}_5$	None	40	7.2	200	43	11	46
	Reduced for 2 h at 400°C	40	19	350	44	9	47
	Oxidized for 3 h at 350°C	25	22	225	43	10	47
	Oxidized for 3 h at 350°C, reduced for 2 h at 400°C	45	20	120	44	10	46
$\text{Co } 7.2\%/\text{Al}_2\text{O}_3$ <sup>b</sup>	Oxidized for 3 h at 350°C, reduced for 10 h at 400°C	10	12	20	36	47	17
$\text{Co } 7.2\%/\text{SiO}_2$ <sup>b</sup>	Same	10	15.1	88	51	32	17
$\text{Co } 9.4\%/\text{CeO}_2$	Same	5	1.0	1	<5	7	90
$\text{Co } 8.7\%/\text{La}_2\text{O}_3$	Same	10	17	20	45	16	36

<sup>a</sup>  $T = 350^\circ\text{C}$ ,  $P = 0.1$  Mpa,  $\text{H}_2/\text{CO} = 1$ .<sup>b</sup>  $(\text{CO}, \text{H}_2)$  reaction at  $T = 300^\circ\text{C}$ .

$\text{Co}/\text{CeO}_2$  (Wang et al. 1987). The dispersive role of the carbonaceous deposit was clearly demonstrated on  $\text{LaCo}_5$  and  $\text{Co}/\text{La}_2\text{O}_3$  (fig. 8). Small Co particles (2–12 nm) were fixed at the end of carbon fibers and separated from platelets of  $\text{La}_2\text{O}_3$ . Larger Co particles (50–200 nm) coated with an uneven layer of carbon were also observed. HREM showed that the small Co particles were generally faulted and their surface was oxidized. A similar morphology was observed for  $\text{Co}/\text{La}_2\text{O}_3$  catalyst prepared by impregnation, which displayed catalytic properties similar to the  $\text{LaCo}_5$ -derived catalyst. The growth of carbon in the  $\text{LaCo}_5$  and  $\text{Co}/\text{La}_2\text{O}_3$  specimens can be attributed to an appropriate matching of lattice plane spacing (0.342 nm) of the hexagonal  $\text{La}_2\text{O}_3$  in the (1010) direction with the carbon lattice fringe (0.34–0.35 nm). The catalytic sites on  $\text{Co}/\text{CeO}_2$  were completely different: the cobalt particles were strongly oxidized and were dispersed on cerium dioxide without a carbon deposit. It is not therefore surprising that its catalytic properties are very different from other catalysts: little activity, and very poor selectivity in hydrocarbons, even in methane.

Pseudobinary intermetallic compounds were also studied. Paul-Boncour et al. (1991) compared  $\text{LaNi}_5$  and  $\text{LaNi}_4\text{Fe}$ . The formation of  $\text{Ni}_x\text{Fe}$  particles was evidenced by XRD and Mössbauer spectroscopy. Both the cell parameter ( $a = 0.3544$  nm) and the hyperfine field ( $H_c = 264$  kG) indicated nickel-rich particles with a concentration close to the initial stoichiometry ( $x = 0.15$ ). This alloying effect was observed in the catalytic properties since this sample exhibited a different selectivity from the other  $\text{RNi}_{5-x}\text{M}_x$  activated under the same conditions, with a lower amount of methane and larger amounts of the heavier hydrocarbons ( $\text{C}_2$  and  $\text{C}_3$ ). For  $\text{CeNi}_{5-x}\text{Co}_x$  ( $x = 0, 1, 2, 3, 4, 5$ ) studied by France and Wallace (1988), the oxidation led to the formation of  $\text{Ni}_{5-x}\text{Co}_x$  particles on  $\text{CeO}_2$ . The Curie temperatures of the decomposed alloys were in agreement with those of bulk alloys (fig. 9). The  $T_c$  values, lower after oxidation treatment than after catalytic reaction

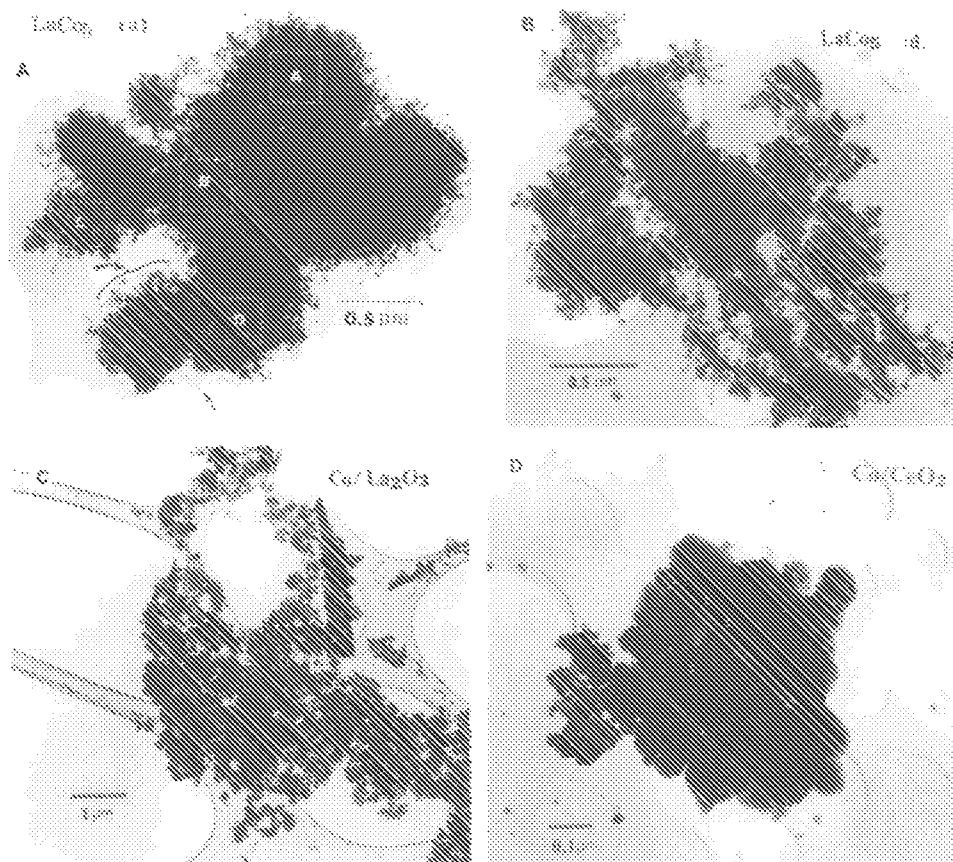


Fig. 8. Typical low-magnification micrographs of the four systems: (A)  $\text{LaCo}_5$ (a), (B)  $\text{LaCo}_5$ (d); (C)  $\text{Co}/\text{La}_2\text{O}_3$ ; (D)  $\text{Co}/\text{CeO}_2$ . Areas in (A) have been selected for X-ray microanalysis analysis, and arrows indicate specific features of interest. (Wang et al. 1987.)

followed by a reducing treatment, were attributed to smaller particle sizes. The surface compositions measured by AES were in agreement with the bulk compositions. The CO conversion and the formation of methane both decreased as the Co:Ni ratio increased, but not linearly. The deviation from linearity was attributed to an alloying effect. Changes of selectivity were also observed with an increase in methane percentage and a decrease in the  $\text{C}_5$  hydrocarbon amount with increasing Co:Ni ratio.

In conclusion, methane and carbon monoxide are not the most desirable products in those reactions. Hydrocarbons of medium ( $\text{C}_4\text{--C}_{10}$ ) or very high (up to  $\text{C}_{40}\text{--C}_{50}$ ) molecular weights have been produced in recent years from synthesis gas on various classical catalysts. Lanthanide-based intermetallic compounds do not seem to be very good candidates for that purpose, if one considers the poor selectivities obtained so far.

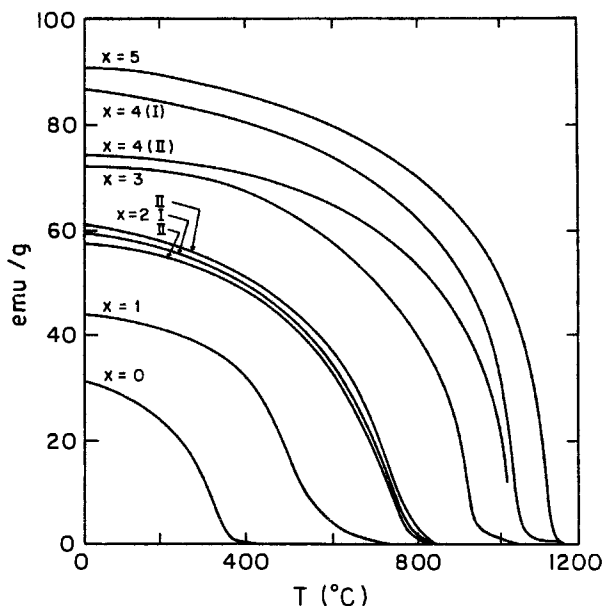
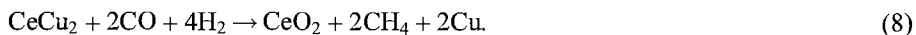


Fig. 9. Thermomagnetograms of the reduced  $\text{CeNi}_{5-x}\text{Co}_x$  (ox) (France and Wallace 1988).

### 3.4.2. Methanol synthesis

The best catalyst for the synthesis of methanol from  $\text{CO} + \text{H}_2$  mixtures is copper/zinc oxide/alumina. Intermetallic compounds of rare earth and copper can be used as precursors for low-temperature methanol synthesis as first reported by Wallace et al. (1982) for  $\text{RCu}_2$  compounds ( $\text{R} = \text{La}, \text{Ce}, \text{Pr}, \text{Ho}$  and  $\text{Th}$ ). The catalytic reaction was performed under 50 bar of  $\text{CO} + \text{H}_2$  at  $300^\circ\text{C}$ , and XRD analyses revealed the decomposition of the intermetallic into lanthanide oxide, 20–30 nm copper particles and copper oxide. Owen et al. (1987) compared the catalytic activity of  $\text{RCu}_x$  compounds, where R stands mainly for cerium in various amounts, but La, Pr, Nd, Gd, Dy and even Ti and Zr were also studied (table 4). The intermetallic compounds were inactive and activation involved oxidation of the alloys using the synthesis gas itself. It started at low pressures (a few bars) and low temperatures (from 353 K upwards). Methane was first produced, then methanol was formed and it is believed that the activation on, for example,  $\text{CeCu}_2$ , involved the following reaction, as already proposed for  $\text{ThCu}_2$  (Baglin et al. 1981):



The activity of several of these catalysts was much higher than that of a commercial copper/zinc oxide/alumina catalyst. In particular they were active at remarkably low temperatures. This was very puzzling because their dispersion was much lower: surface areas of  $1 \text{ m}^2/\text{g}$  instead of 30–40, copper particle size 30–50 nm instead of 10–20.

Table 4  
Methanol synthesis activity of selected copper–lanthanide intermetallic catalysts (Owen et al. 1987)

Alloy precursor	Methanol activity <sup>a</sup> (mole kg <sup>-1</sup> h <sup>-1</sup> )		Activation energy (kJ mole <sup>-1</sup> )	Surface area (m <sup>2</sup> g <sup>-1</sup> )
	Maximum	Steady state		
CeCu <sub>2</sub> <sup>b</sup>	44.5	25.5 <sup>y</sup>	50.4	1.7, <1 <sup>c</sup>
LaCu <sub>2.2</sub> <sup>b</sup>	39	12 <sup>y</sup>		<1 <sup>c</sup>
PrCu <sub>2</sub> <sup>b</sup>	19	13 <sup>y</sup>		
NdCu <sub>2</sub>	13	8.5 <sup>x</sup>	47.4	0.8 <sup>d</sup>
GdCu <sub>2</sub>	12	10 <sup>x</sup>		6.9
GdCu <sub>1.5</sub>	16	9.5 <sup>x</sup>	55.3	
GdCu	19	8 <sup>x</sup>	—	4.0
GdCu <sub>0.5</sub>	<2 <sup>x</sup>			
DyCu <sub>2</sub>	11.5	8 <sup>x</sup>		
ZrCu <sub>2</sub>	6	5 <sup>x</sup>	50	
TiCu <sub>2</sub>	<2 <sup>x</sup>			
CeAg <sub>2</sub>	Inactive <sup>y</sup>			
MM-Cu(1:1) <sup>h</sup>	25	13 <sup>x</sup>		
ThCu <sub>6</sub> <sup>e</sup>		~30		30.5
CeCu <sub>2</sub> <sup>f</sup>		~9		9.9
Cu/ZnO/Al <sub>2</sub> O <sub>3</sub> <sup>c</sup>		<1		42
Cu/ZnO/Al <sub>2</sub> O <sub>3</sub> <sup>g</sup>		44.7		

<sup>a</sup> Reactor conditions: CO/H<sub>2</sub> (0:1), 513 K, 50 bar, space velocity <sup>y</sup>72 000 h<sup>-1</sup>, <sup>x</sup>36 000 h<sup>-1</sup>.

<sup>b</sup> Annealed at 1048 K for 24 hours prior to testing.

<sup>c</sup> Cu surface area by N<sub>2</sub>O decomposition.

<sup>d</sup> Krypton isotherm.

<sup>e</sup> Baglin et al. (1981): CO/H<sub>2</sub> (1:2.4), 523 K, 60 bar, 22 000 h<sup>-1</sup>.

<sup>f</sup> Baglin et al. (1980): CO/H<sub>2</sub> (6:94), 613 K, 60 bar, 31,500 h<sup>-1</sup>.

<sup>g</sup> F.J. Brockner, K.H. Gruendler, L. Morosi, M. Schwarzman, B. Triebkorn and G. Zirkar, South African Patent no. 795 715: CO/CO<sub>2</sub>/H<sub>2</sub>, 503 K, 50 bar, 10 000 h<sup>-1</sup> (mole ℓ<sup>-1</sup> h<sup>-1</sup>).

<sup>h</sup> MM = mischmetal.

Moreover, fig. 10 shows that they were very sensitive to deactivation by carbon dioxide, which is a product of the reaction, although no visible change of the morphology was observed (Owen et al. 1987). This is in contrast with conventional Cu–ZnO/alumina catalysts since it was demonstrated that methanol is generated from carbon dioxide under industrial conditions (Kagan et al. 1975, Chinchén et al. 1987b). Analytical Transmission Electron Microscopy performed on a few catalysts derived from intermetallics suggested that part of the copper was intimately linked with the rare-earth oxide either as very small particles or in an ionic form. Further studies (Shaw et al. 1990a) showed that, at the temperatures where the CeCu<sub>2</sub> catalyst was active for methanol synthesis, only 35–40% of the copper particles were accessible to XRD and most of the cerium was amorphous. EXAFS studies (Shaw et al. 1991) showed that copper was largely present as 2–2.5 nm particles, which would indeed be undetectable by XRD. Generally speaking it seemed that the most active catalysts were the less crystalline materials. It

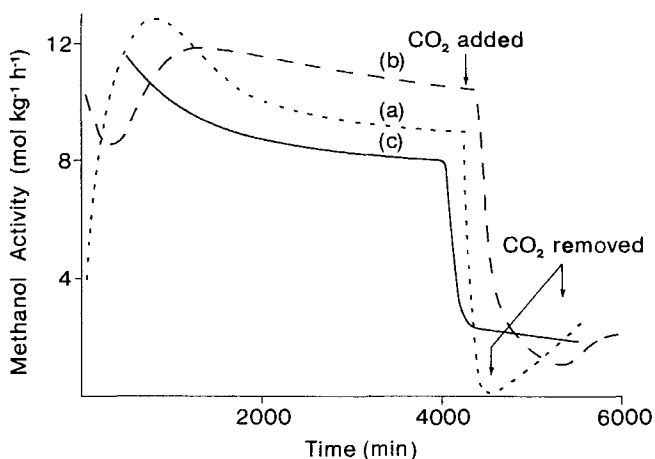


Fig. 10. The deactivation of catalysts for methanol synthesis caused by the addition of  $\text{CO}_2$  to a 1:1  $\text{CO}_2/\text{H}_2$  gas feed at 50 bar, 513 K,  $72000 \text{ h}^{-1}$  speed velocity: (curve a)  $\text{NdCu}_2$  (2%  $\text{CO}_2$ ); (b)  $\text{GdCu}_2$  (1%  $\text{CO}_2$ ); (c)  $\text{DyCu}_2$  (1%  $\text{CO}_2$ ). (Owen et al. 1987.)

was also proposed that the carbon dioxide poisoning was the result of a reaction with lanthanum oxide.

A detailed study of  $\text{NdCu}$ ,  $\text{NdCu}_2$ ,  $\text{NdCu}_5$  and  $\text{CeCu}_2$  by the same group (Nix et al. 1987) using in situ XRD confirmed that there was no correlation between the apparent copper crystallite size and the catalytic activity. Moreover, it showed clearly that the ultimate performance of the catalyst depends very much on the structure and stoichiometry of the precursor and on the conditions (temperature, pressure, flow rates) of the activation process. In particular, several hydride phases were identified which play a necessary part in the formation of the final active catalyst, in which their presence and therefore their possible participation could not be excluded. For example, one can see in fig. 11 that the growth of methanol production correlates very well with the appearance of copper particles and neodymium oxide, and follows the rapid formation and decomposition of an intermetallic hydride phase: hydrogen treatment of the intermetallic compound at low temperature (350–373 K) led to the formation of an hydride; at higher temperatures (423 K) this hydride was transformed into lanthanide hydride which, as the reaction proceeded at the same temperature, was decomposed into lanthanide oxide and copper particles. Omission of the hydrogen treatment to form the hydrides resulted in a relatively inactive catalyst.

Amorphous  $\text{Cu-Ce-Al}$  and  $\text{Cu-MM-Al}$  (MM=mischmetal) were also tried under the same conditions of activation and reaction, and they were also characterized by in situ XRD (Bryan et al. 1988). However, they appeared to be difficult to activate; they required higher temperatures and they were very quickly deactivated. This is in contrast with many reports in the literature, on various materials, where the use of amorphous systems often resulted in substantial improvements of the catalyst performance. A likely explanation was that the formation of hydride phases, which is a necessary step in the



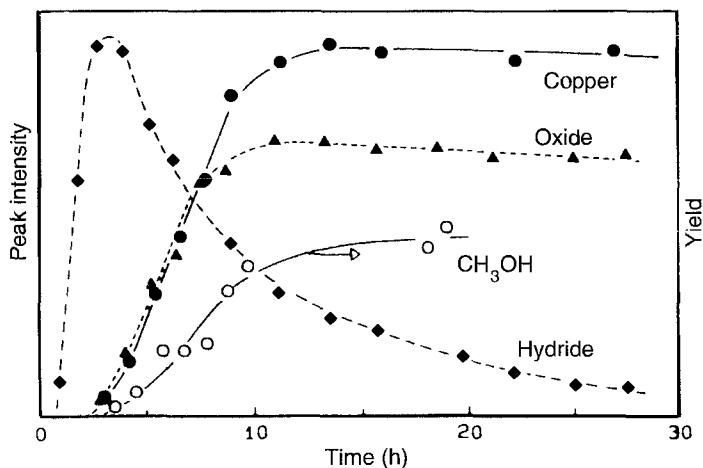


Fig. 11. Structural and activity data (arbitrary units) for synthesis gas activation of NdCu at 15 bar and 423 K showing the correlation between the growth of methanol activity and copper/neodymium oxide peak intensities (Nix et al. 1987).

activation process as shown in the preceding paper (Nix et al. 1987), could not readily take place. This is not in contradiction with the statement (Shaw et al. 1990b) that the most active catalysts are the least crystalline materials (catalyst in their final form), since in those cases the initial catalysts were crystalline and the activation could therefore proceed through a hydride phase.

The importance of the hydride phase was indirectly confirmed by Hay et al. (1988) who performed Temperature Programmed Oxidation experiments on  $\text{CeCu}_2$  and  $\text{CeCu}_6$ . Oxidation profiles in air, nitrous oxide, carbon monoxide and synthesis gas were compared, in relation with XRD observations. Intermetallic compounds activated under air exhibited a markedly reduced activity for methanol synthesis, and again hydrogen exposure was shown to be crucial for the generation of highly active catalysts. The residual activity observed at high temperatures ( $>513\text{ K}$ ) and after exposure to oxygen suggested the existence of two types of sites, the most active sites being also the least stable from both thermal and chemical points of view (Nix et al. 1989). This would imply that activation is best carried out at higher pressures and lower temperatures, as also suggested by the amazingly low temperature activities observed at high pressures (Owen et al. 1987).

The major drawback of these lanthanide-copper alloys is that they are irreversibly poisoned by low concentrations of carbon dioxide, as already indicated above (Owen et al. 1987). The same authors also found that  $\text{ZrCu}_2$  and  $\text{TiCu}_2$  produced catalysts which were active for methanol synthesis, but difficult to activate. In a subsequent paper Owen et al. (1990) studied ternary lanthanide-Zr(or Ti)-Cu alloys with the hope that the addition of the larger lanthanide atom could increase the possibility of hydride formation and therefore the overall properties of these  $\text{Zr}(\text{Ti})\text{-Cu}$  alloys. They prepared a series of

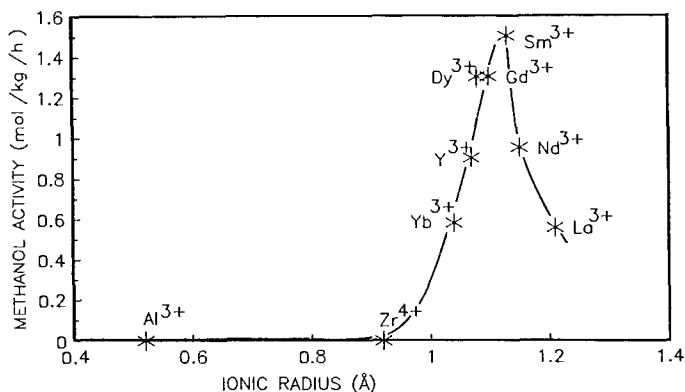


Fig. 12. Variation at maximum methanol activity ( $R_m$ ) with R component for catalysts derived from  $Zr_{0.7}R_{0.3}Cu_{2.0}$  alloys (12 bar, 513 K; also including data for  $Zr_{0.9}Al_{0.1}Cu_{2.0}$  and  $ZrCu_2$ ) (Owen et al. 1990).

Gd, Nd, Dy, La, Sm–Zr–Cu together with several Gd–Ti–Cu alloys. High levels of activity were induced in Zr–Cu and Ti–Cu catalysts by addition of small quantities of lanthanide. They were as active for methanol synthesis as the corresponding lanthanide–copper binary alloys. It was not clear, however, whether the increase in activity, as compared to Zr–Cu and Ti–Cu alloys, resulted from a greater tendency for hydride formation or from the creation of more oxygen vacancies in Zr and Ti oxides. Although this point was not fully developed, it seems that ternary alloys of intermediate composition (for example,  $Zr_{0.7}Gd_{0.3}Cu_{1.5}$ ) had a better long term stability, that is a lesser tendency to carbon dioxide deactivation, than lanthanide–Cu binary alloys. The largest methanol activity for the  $Zr_{0.7}R_{0.3}Cu_{0.2}$ -derived catalyst was found to be strongly dependent of the ionic radius of the R component, with a maximum for the  $Sm^{3+}$  ion as shown in fig. 12.

There has been a lot of controversy about the mechanism of methanol synthesis on industrial Cu/ZnO/alumina catalysts. Chinchén et al. (1986, 1987a) found a linear relationship between the catalytic activity and the copper surface area. They also found that copper deposited on other supports had the same turnover number as on the commercial catalyst. However, Bartley and Burch (1988), Burch and Chappell (1988) and Burch et al. (1988) observed definite support effects. Frost (1988) proposed that the chemistry takes place on a metal-promoted oxide phase, the metal promotion operating through an enhancement of the equilibrium concentration of oxygen vacancies. The fact that Frost (1988) could generate active catalysts based on silver or gold supported on thoria, metals which are normally inactive for methanol synthesis, seemed to confirm his theory. Of course this means that the area of the interface between the metal and the oxide will be crucial for the activity of the catalyst. To check this hypothesis Shaw et al. (1990b) studied the microstructure and the activity for methanol synthesis of Ag–Ce and Ag–Cu–Ce catalysts derived from intermetallic compounds. The activities were very poor and it appeared that the nature of the metal was more important than the oxide phase. The authors soon realized that silver was not a good candidate for such a test.

Oxygen vacancies on an oxide can be formed if two electrons can be raised to the oxide band. Any metal which can form a Schottky junction with an oxide will decrease the enthalpy of formation of a doubly ionized vacancy by allowing electrons to move to the metal Fermi level. To form a Schottky junction, the work function of the metal must be high enough. It happens that silver has a work function 0.4 eV lower than that of copper. For this reason, in a subsequent paper Shaw et al. (1992) reported on the catalytic activity of CeAu<sub>2</sub>, remembering that gold has a work function 0.4 eV above that of copper. Nevertheless no detectable activity could be observed even after activation under CO + H<sub>2</sub> and at much higher reaction temperatures. It appears therefore that the chemical nature of the metal is most important in determining the catalytic properties, although the role of the support was not fully understood. However, it does not seem that these studies were totally conclusive since these catalysts derived from intermetallic compounds are so different from classical Cu/ZnO/alumina: the importance of the hydride phase in the activation process, no correlation of the activity with the apparent surface area, very small copper particles probably responsible for the activity, fast deactivation in the presence of carbon dioxide.

Since classical Cu/ZnO catalysts exhibited a poor stability while the addition of alumina resulted in much better systems, it was tempting to add alumina to Cu–Ce intermetallic compounds. Jennings et al. (1992a), prepared ternary Cu–Ce–Al alloys of various compositions and also tried a variety of other metals (Ca, Cr, Mn, Pd, Zn). Among these ternary alloys aluminum-containing catalysts were the best. In spite of lower initial activities as compared to binary alloys, they exhibited a much better long-term stability. It is believed that the role of aluminum is to stabilize the disperse copper–ceria phases responsible for methanol synthesis activity, although the mechanism for such a process remains unclear.

In conclusion, these investigations have shown that many Cu-based intermetallic compounds, and in particular CeCu<sub>2</sub>, are very active for methanol synthesis, at much lower temperatures than conventional catalysts. It is believed that the active site consists of small copper crystallites in close contact with a CeO<sub>x</sub> phase ( $x < 2$ ). However, the performances of these catalysts are severely deteriorated due to their fast deactivation in the presence of small amounts of carbon dioxide, which is unfortunately a reaction product, and even though it was shown that, initially, CO<sub>2</sub> pulses resulted in an increase in the methanol production (Jennings et al. 1992b, Walker et al. 1992).

### 3.5. Ammonia synthesis

It has long been recognized that lanthanide-based intermetallic precursors can exhibit high specific activities for ammonia synthesis (Takeshita et al. 1976). As also reported by Netzer and Bertel (1982), Takeshita et al. investigated thirty-six intermetallics involving lanthanides and Fe, Co or Ru. Several of them exhibited specific activities exceeding that of the best practical catalyst, which is a standard high-activity Fe catalyst prepared in a more classical way. But the latter, due to its large surface area, was more active on a weight basis. XRD studies showed that the intermetallic compounds were decomposed into

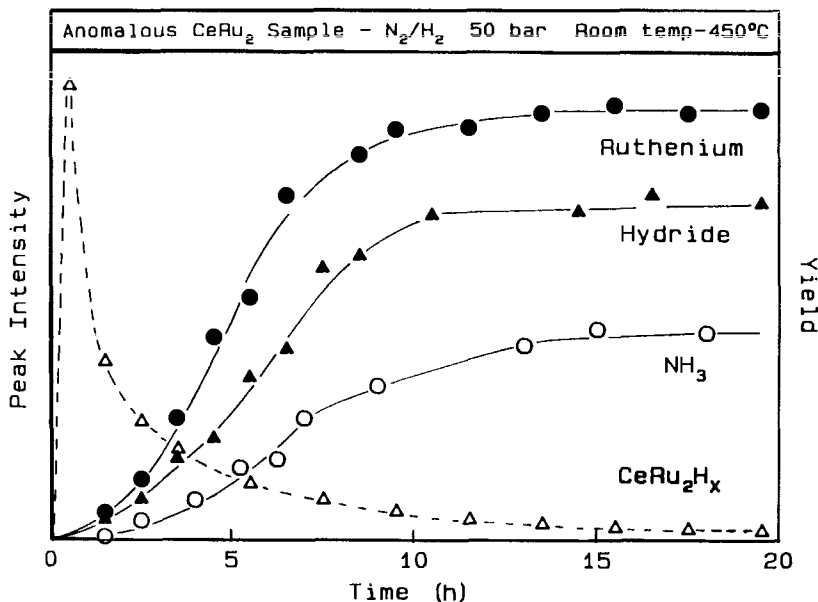


Fig. 13. Structural and activity data for  $\text{N}_2/\text{H}_2$  activation at the anomalous  $\text{CeRu}_2$  sample at 50 bar/450°C showing the correlation between the rise of ammonia activity and the growth of the ruthenium and cerium hydride peak intensities (Walker et al. 1989).

lanthanide nitride and finely divided transition metal which was probably the active phase. Nevertheless the catalytic activity was certainly influenced by the underlying lanthanide compound. In addition, the comparison of the catalytic properties of various  $\text{RCO}_3$ -derived catalysts (Wallace et al. 1977) indicated a decrease in the relative ammonia production as their atomic number increased, but no interpretation was proposed for such an evolution.

More recently Walker et al. (1989, 1990) studied the properties of  $\text{CeRu}_2$ ,  $\text{CeCo}_2$  and  $\text{CeFe}_2$ . Due to the extreme sensitivity of these materials to air, they followed the evolution of their samples in the presence of  $\text{H}_2$  or  $\text{H}_2 + \text{N}_2$  in a controlled atmosphere cell for in situ XRD measurements. Exposure of  $\text{CeRu}_2$  to 20 bar of hydrogen at room temperature resulted in the formation of a ternary hydride phase  $\text{CeRu}_2\text{H}_x$  ( $4 < x < 5$ ) and, more slowly, to another hydride phase of different structure. Raising the temperature up to 450°C led to a progressive transformation of these phases into cerium hydride,  $\text{CeH}_{2+x}$  ( $0 \leq x \leq 1$ ), and ruthenium particles of 3.5–4 nm. A direct exposure of  $\text{CeRu}_2$  to 50 bar of hydrogen at 450°C led to the same result. The  $\text{CeRu}_2$  precursor was then pretreated at 100°C in a  $\text{N}_2/\text{H}_2$  mixture to form the intermetallic hydrides. No ammonia was detected. On increasing the temperature up to 450°C a striking correlation was found between the rise of ammonia production and the formation of ruthenium and cerium hydride particles (fig. 13).

The behavior of  $\text{CeCo}_2$  was roughly the same, except that no ternary hydride but an amorphous phase was formed, and the production of ammonia (table 5) was lower with

Table 5  
Activities of the  $\text{CeH}_{2-x}/\text{M}$  systems at 50 bar in a 1:3 mixture of  $\text{N}_2$  and  $\text{H}_2$  (Walker et al. 1989)

Catalyst system	Temperature ( $^{\circ}\text{C}$ )	Activity $\times 10^5$ (mol $\text{NH}_3$ /(g cat.) $^{-1}$ min $^{-1}$ )
$\text{CeH}_{2-x}/\text{Ru}$	450	4.55
	500	9.17
	550	13.80
$\text{CeH}_{2-x}/\text{Co}$	450	3.25
	500	4.95
	550	6.90
$\text{CeH}_{2-x}/\text{Fe}$	450	2.60
	500	3.81
	550	5.60

a cobalt particle size of approximately 10 nm.  $\text{CeFe}_2$  was even less active, and the size of the iron particles was about 13 nm. In the last two cases CeN was also evidenced but there was no correlation with the ammonia production. Likewise the activity for ammonia synthesis was not related with the amount of exposed metal; this was most striking in the case of  $\text{CeFe}_2$ .

Since the same Cambridge group (Nix et al. 1987) had observed that lanthanide-copper alloys activated in  $\text{CO} + \text{H}_2$  mixtures gave very active methanol-synthesis catalysts containing  $\text{CeO}_2$  and ultradispersed copper, all three samples  $\text{CeRu}_2$ ,  $\text{CeCo}_2$  and  $\text{CeFe}_2$  were submitted to a 40 bar  $\text{CO} + \text{H}_2$  mixture. Above  $250^{\circ}\text{C}$  the three samples decomposed into cerium dioxide and transition-metal particles. However these catalysts were inactive for ammonia synthesis under 50 bar of  $\text{N}_2 + \text{H}_2$  at  $450^{\circ}\text{C}$ , and the Ru- and Co-based compounds displayed a very weak activity at  $550^{\circ}\text{C}$ . Such a deactivation cannot be explained by carbon deposition on the metal particles since the same behavior was observed when the samples were exposed to air at room temperature or after the introduction of 100 ppm of water in a nitrogen stream. The encapsulation of the metal phase by ceria is also unlikely since  $\text{Cu/CeO}_2$  catalysts derived from  $\text{CeCu}_2$  precursors exhibit a very high methanol synthesis activity.

To explain the large difference in activity between the oxide and hydride supports, Walker et al. (1989) invoked a strong metal-support interaction via the oxygen ions of the support. A charge transfer from the metal to the support will result in the formation of  $\text{M}^{\delta+}$  species which can inhibit the dissociation of the nitrogen molecule. Since this is the rate-determining step for ammonia synthesis, this can explain the strong activity decrease with the oxide supports. This interpretation is consistent with EXAFS results on Ru supported on  $\text{MgO}$ ,  $\text{Al}_2\text{O}_3$  and  $\text{SiO}_2$  supports. They indicated that smaller activities were obtained for alumina and silica supports which display a stronger metal-support interaction via the oxygen ions of the support (Bossi et al. 1982).

All these results show that the transition metal is the active phase, but that the support also plays an important role since Ce hydride-based catalysts are active for ammonia

synthesis while  $\text{CeO}_2$ -based systems, obtained by pretreatment of the intermetallics with  $\text{CO} + \text{H}_2$ , are not. The difference was tentatively interpreted by Walker et al. (1989) in terms of differences in hydrogen spillover or electronic transfer, or assuming that the active species consists of very small metal particles, undetected by XRD, and associated with the hydride phase.

The existence of very small particles was indeed evidenced using in situ X-ray absorption spectroscopy (XAS) (Walker et al. 1990) which showed that in the active catalyst  $\text{CeH}_{2+x}$ -Ru the ruthenium particles were a mixture of approximately 3.5 nm crystallites and very low coordination clusters while the inactive catalyst  $\text{CeO}_2$ -Ru contained essentially bulk metallic ruthenium.

The interaction of those very small ruthenium particles with the cerium hydride support may be viewed as electronic or related to a possible spillover of hydrogen from the hydride. A charge transfer from  $\text{CeH}_{2+x}$  to the metal will facilitate the dissociative chemisorption of nitrogen. This is the role already evidenced by alkali metals to promote the activity of ruthenium: the rate of ammonia synthesis increased with decreasing ionization potential of the alkali metal (Aiko et al. 1972). This interpretation received further experimental evidence with the in situ XAS experiments mentioned above (Walker et al. 1990): when  $\text{CeRu}_2$  was decomposed under  $\text{H}_2$  and  $\text{CO} + \text{H}_2$  up to  $450^\circ\text{C}$ , the  $\text{CeH}_{2+x}$  catalyst displayed a very different near-edge structure than  $\text{CeO}_2/\text{Ru}$ , indicating different electronic states for the Ru particles. To provide a deeper understanding of this electronic interaction, Walker and Lambert (1992) performed an Auger electron spectroscopic study of the  $\text{Ru}(0001)$ -Ce- $\text{H}_2$  interface. As cerium was deposited on the ruthenium single crystal, at low coverage ( $<0.5$  monolayer), a significant Ce to Ru charge transfer was observed through the  $\text{N}_{4,5}\text{O}_{2,3}\text{V}$  Coster-Kronig transition. The same electronic behavior was observed when cerium was deposited in the presence of a low pressure of hydrogen. In fact the electron transfer from cerium to hydrogen is very small compared to that of cerium to the ruthenium substrate. As the amount of cerium increased to one or two monolayers the Ce-Ce interaction became important and depolarisation effects occurred. This study also indicated that the deposition of cerium under hydrogen pressure generated a film of bulk hydride with  $\text{CeH}_{2.3}$  stoichiometry.

In addition to this electronic interaction between finely divided ruthenium metal particles and cerium hydride, a hydrogen spillover was also proposed to explain the high activity for ammonia synthesis of these catalysts. Since hydrogen in the octahedral sites of  $\text{CeH}_{2+x}$  is desorbed at  $420^\circ\text{C}$ , atomic hydrogen is certainly present at the temperature of ammonia synthesis ( $450$ – $550^\circ\text{C}$ ). Therefore spillover of atomic hydrogen at the hydride/transition metal interface could occur.

### 3.6. *Reactions of saturated hydrocarbons*

Reports on the isomerization or cracking reactions of saturated hydrocarbons on rare-earth-based intermetallic compounds are very scarce in the literature. Imamura and Tsuchiya (1981b) prepared binary halide catalysts from  $\text{LaAl}_2$ ,  $\text{CeAl}_2$ ,  $\text{PrAl}_2$ ,  $\text{ErAl}_2$  and  $\text{ThAl}_2$  by reaction with methylene halide. They were used for the isomerization of

Table 6  
Activity and selectivity of various alloy-halogen systems<sup>a</sup> (Imamura et al., 1981)

Catalyst system		Conversion <sup>c</sup> (%)	Selectivity <sup>c</sup> (%)
Alloy <sup>b</sup>	Halogen(nmol)		
LaAl <sub>2</sub>	Cl <sub>2</sub>	5.2*	50*
	Br <sub>2</sub> (4.5)	28.8*	73*
CeAl <sub>2</sub>	Cl <sub>2</sub>	15.0*	62*
	Br <sub>2</sub> (5)	31.7*	58*
	I <sub>2</sub> (5)	42.3*	96*
PrAl <sub>2</sub>	Cl <sub>2</sub>	8.3*	56*
	Br <sub>2</sub> (4.5)	39.8*	96*
	I <sub>2</sub> (4.5)	37.1*	97*
ErAl <sub>2</sub>	Cl <sub>2</sub>	25.2*	60*
	Br <sub>2</sub> (4.5)	39.4*	61*
	I <sub>2</sub> (4.5)	35.0*	93*
ThAl <sub>2</sub>	Br <sub>2</sub> (5)	25.5*	60*
	I <sub>2</sub> (5)	39.1*	95*
PrGa <sub>2</sub>	Cl <sub>2</sub>	10.0**	72**
	Br <sub>2</sub> (4.5)	6.0**	77**
ThGa <sub>2</sub>	Cl <sub>2</sub>	24.7***	60***
	Br <sub>2</sub> (5)	46.0*	50***
CeIn <sub>3</sub>	Br <sub>2</sub> (6.5)	trace**	—
	I <sub>2</sub> (6.5)	trace**	—
CeTl <sub>3</sub>	Br <sub>2</sub> (6.5)	—	—

<sup>a</sup> The conversion reaction of *n*-pentane (2 ml) was performed over the above catalysts in CH<sub>2</sub>Cl<sub>2</sub> (8 ml).

<sup>b</sup> The amount of alloy used was 1 mmol.

<sup>c</sup> Asterisks: \*, results obtained at 0°C after 1 h; \*\*, \*\*\*, data measured at 23°C after 20 h and 3 h, respectively.

*n*-pentane. High conversions with good selectivities for the isomerization into isopentane were obtained at room temperature or 0°C (as shown in table 6). The activity increased in the order Cl < Br ≅ I, and iodine also gave the best selectivities. But the addition of halogen in large excess generally led to poor selectivities. An interesting point was that these catalysts were much more active than a simple mixture of aluminum and rare-earth halides. This suggests that the role of the intermetallic was far from negligible, but the nature of the complexes formed by halogenation remained undeciphered.

Skeletal rearrangements of saturated hydrocarbons on CePd<sub>3</sub> were studied by Le Normand et al. (1984). Hydrogenolysis of methylcyclopentane, isomerization of 2-methylpentane and aromatization of 3-methylhexane were performed at 350 or 360°C. The results were compared with those of classical Pd/Al<sub>2</sub>O<sub>3</sub>, Pd/SiO<sub>2</sub> or Pd/CeO<sub>2</sub> catalysts. The activity of CePd<sub>3</sub> itself was very low and palladium atoms seemed to play a minor role. For example, the initial reaction of methylcyclopentane was the selective formation of isopentane, which is not observed on classical palladium catalysts. Air treatment at

Table 7  
Activity in ethane hydrogenolysis (Barrault et al. 1983a)

Catalyst	Time on stream (h)	<i>T</i> (K)	Activity $\times 10^3$ /mol h <sup>-1</sup> (g catal.) <sup>-1</sup>
LaNi <sub>5</sub>	20	669	4.0
MMNi <sub>5</sub>	20	647	8.0
LaNi	20	654	0.2
		693	1.0
La <sub>3</sub> Ni	20	669	2.0
		682	4.0
LaNi <sub>4</sub> Mn	30	700	0.4
Ni-SiO <sub>2</sub> <sup>a</sup>	—	650	2000

<sup>a</sup> Data from Sinfelt (1970).

room temperature or, better, at 120°C, dramatically increased the activity, by two orders of magnitude or more. Quite clearly the behavior was that of a classical palladium catalyst supported for example on alumina, with however an enhanced selectivity towards aromatization and 1–5 ring closure. Obviously a complete rearrangement of the surface had occurred, leading to the formation of active palladium entities on the surface of cerium dioxide, as shown by XPS. Still, the activity remained slightly lower than with a Pd/Al<sub>2</sub>O<sub>3</sub> catalyst at the same temperature of reaction. Apparently the poor activity of the intermetallic compounds for this type of reaction did not encourage further studies in that direction.

In ethane hydrogenolysis (Barrault et al. 1983a,b), the catalytic activity of LaNi<sub>5</sub> increases during 25 hours until saturation. This was attributed to the activation of the catalysts by the intermetallic decomposition into Ni particles and lanthanum hydride leading to an increase of the surface area from a few square meters to 10 m<sup>2</sup>/g. After reaching saturation MMNi<sub>5</sub> (MM=mischmetal) was found to display the larger catalytic activity (table 7) (Barrault et al. 1983a).

The influence of the lanthanide element on the magnetic and catalytic properties of Pt-R (R=Gd, Tb, Dy, Ho and Tm) supported on Al<sub>2</sub>O<sub>3</sub> was investigated by Weiqi et al. (1992) and Jianhui et al. (1992). The heavy rare earths improved the activity and selectivity of the platinum reforming catalysts in the conversion of cyclohexane, *n*-hexane and *n*-heptane. A relationship was established between the evolution of the relative magnetic susceptibility and the catalytic activity as a function of rare-earth content: the increase of the magnetic susceptibility should reflect an increasing number of holes which favors the aromatic reaction of *n*-pentane and cyclohexane. A relationship was also found between the ratio of the susceptibilities  $\chi_{\text{Pt-R}}/\chi_{\text{R}_2\text{O}_3}$  and the aromatization yields of the R element (Gd > Dy > Ho > Tm > Tb). Nevertheless, such a correlation has to be applied with care in the aromatization of *n*-hexane and *n*-heptane where the lanthanide has to be located near the acidic centers, since both metal and acidic sites are necessary to perform isomerization.



### 3.7. Hydrocarbon and alcohol dehydrogenation

The ability of intermetallic compounds to absorb hydrogen reversibly can be used as a driving force in the dehydrogenation reaction of alkanes, alkenes and alcohols, which are thermodynamically unfavorable at moderate temperatures (Chetina and Lunin 1994). For example, the dehydrogenation of alkanes into alkenes at 298 K leads to an increase of the standard Gibbs free energy,



whereas the hydride formation is an exothermic reaction with a negative value of the standard Gibbs free energy:



The introduction of an appropriate metal or intermetallic compound can therefore displace the system towards dehydrogenation. Its absorption capacity can then be restored by appropriate reaction cycles:



The role of the hydride-forming alloy is to absorb the hydrogen evolved from the hydrogenation reaction, to form a stable compound. The same type of reaction can be described for alcohol dehydrogenation. The transformation of propan-2-ol to acetone (Imamura et al. 1987) is accompanied by an increase into a positive standard Gibbs free energy  $\Delta G^\circ = 25 \text{ kJ mol}^{-1}$ , whereas the addition of  $R_2Co_7$  intermetallic compounds shifts it to a negative value  $\Delta G^\circ = -4, -11 \text{ kJ mol}^{-1}$ , for  $R = \text{Pr, Nd and Sm}$  (taking into account the hydride formation).

For the hydrocarbon dehydrogenation the intermetallic compounds as mentioned for  $LaNi_{4.7}Al_{0.3}$  are generally used to remove hydrogen (Imai et al. 1985) and are mixed with an active catalyst like  $Pt/Al_2O_3$ . But  $R_2Co_7$  ( $R = \text{Nd or Sm}$ ) were used simultaneously as catalysts and hydrogen acceptors in the dehydrogenation of cyclohexene to benzene and of *n*-heptane to methylcyclohexane at 398 K (Imamura et al. 1986b). Only traces of the *n*-heptane cyclisation product were observed.

In the presence of  $Zr_2Ni$ ,  $R_2Co_7$  and  $RFe_2$  intermetallic compounds methanol was dehydrogenated in CO and  $H_2$  under mild conditions (356–443 K) (Imamura et al. 1988, 1990). Hydrogen was reabsorbed by the intermetallic to form a hydride and the lanthanides were found more efficient in hydrogen storage than  $Zr_2Ni$ , whereas the activity of the intermetallic compounds varies as  $Zr_2Ni > R_2Co_7 > RFe_2$ . This variation was explained by the possible decrease of catalytic activity of the transition metal  $Ni > Co > Fe$ .

For  $Nd_2Co_7H_{0.1}$ ,  $Nd_2Co_7H_{2.7}$  and  $Nd_2Co_7H_{5.1}$  prepared by hydrogen absorption, the initial rates of dehydrogenation of propan-2-ol at 317 K were  $1.1 \times 10^{-3}$ ,  $6.0 \times 10^{-4}$  and  $3.5 \times 10^{-4} \text{ mmol min}^{-1} (\text{g alloy})^{-1}$ , respectively (Imamura et al. 1987). This activity

decrease with preliminary hydrogen content is a good indication that the formation of the hydride is the driving force for the dehydrogenation reaction. In addition,  $\text{Nd}_2\text{Co}_7$  was found more active than  $\text{Pr}_2\text{Co}_7$  and  $\text{Sm}_2\text{Co}_7$ . The surface of the catalysts was activated by an attack in a solution of dihalogenoethane. The rare-earth element was leached out from the alloy forming a halide leaving a porous high-surface-area cobalt at the surface. The bulk structure of the alloys remained unchanged but the surface analysis by ESCA revealed that after the treatment the Co/Nd ratio was increased by four, whereas it remained almost unchanged for the Pr and Sm alloys. This difference in Co enrichment was used to explain the difference in activity, since Co was supposed to be the active site for the reaction (Imamura et al. 1987). However the catalytic reaction is irreversibly inhibited with time. The observed poisoning in the alcohol dehydrogenation (Imamura et al. 1987, 1988) was attributed to an inhibition of the catalyst by acetone rather than by a reduction of the hydride-forming capacity. In addition the thermal stability of these alloys was not very good since a strong reduction of the activity was observed on heating at 533 K. This deactivation was attributed to a sintering of the surface cobalt particles.

A good way to improve the catalytic properties is to add Pt, Ru or Rh salts at the surface of the alloys (Imamura et al. 1990). The deposition of  $\text{RhCl}_3$  on  $\text{DyFe}_2$  increased its activity in the methanol decomposition by a factor of 18. In the same way the addition of chloroplatinic acid to the alloy suspension of  $\text{Pr}_2\text{Co}_7$  has a promoting effect, increasing 10 times its activity in the propan-2-ol conversion to acetone. The promoter metal provides active sites for the dissociative chemisorption of propan-2-ol and therefore favors a rapid transfer of hydrogen to the hydrogen acceptor by spillover. In addition, the activity of the Pt-promoted system can be reversibly restored by regeneration cycles, the Pt particles having a larger thermal stability than the surface Co particles.

Another way to perform alcohol dehydrogenation using intermetallic compounds as precursors was performed by Ballivet-Tkatchenko et al. (1995). In this case  $\text{RCu}_2$  intermetallics were air oxidized between 423 and 1100 K, leading to  $\text{RCu}_2\text{O}_x$  compounds active in the decomposition of 4-methyl-2-pentanol. XRD analyses show that  $\text{CeCu}_2$  is transformed into  $\text{CeO}_2$  and  $\text{CuO}$ , whereas for  $\text{R}=\text{La}$ , Pr and Nd ternary  $\text{R}_2\text{CuO}_4$  and  $\text{CuO}$  compounds are obtained. The surface areas of the oxidized materials are 5–20 times larger than that of the starting intermetallic compound, and SEM analysis indicates a more porous surface.  $\text{CeCu}_2$ -derived catalysts are active in both dehydrogenation and dehydration of alcohol depending on the reaction temperature (at 473 K there is only dehydrogenation). The other  $\text{R}_2\text{CuO}_4\cdot\text{CuO}$  compounds catalyze only the dehydrogenation reaction with an increase of the activity from La to Nd while the activation energy varies in the opposite order. This change of properties with the lanthanide element shows that  $\text{CuO}$  is not the only active site and that the  $\text{R}_2\text{CuO}_4$  phase plays its role in the catalytic reaction.

### 3.8. Hydrodesulfurization

Moon and Ihm (1996) used  $\text{NdNi}_5$  as an unsupported catalyst in thiophene hydrodesulfurization. But the intermetallic compound itself is not active and activation was

performed by calcination under air at various temperatures from 200 to 700°C followed by sulfurization using a  $\text{H}_2\text{S}/\text{He}$  mixture from 200 to 500°C. The reaction was carried out at 450°C. The best activities were obtained after calcination at 400°C and presulfurization at moderate temperatures (300°C). The activities under various conditions were correlated with changes in the surface area of the catalyst. Calcination at 400°C, sulfurization at 300°C and the reaction itself all contributed to an increase in surface area, with the formation of microcracks, as evidenced by electron microscopy. Nevertheless the activity was not much different from that observed with a Nd–Ni bimetallic catalyst previously studied by the same authors (Moon and Ihm 1993), and the preparation of an intermetallic compound does not seem to bring much advantage.

### 3.9. Carbon monoxide oxidation

As a consequence of the sensitivity to oxygen of these intermetallic compounds, they can only be model systems for all reactions involving oxygen. This is well illustrated by Warren et al. (1993) who studied the oxidation of carbon monoxide on a Rh–Ce surface alloy. Carbon monoxide oxidation is an important reaction because it is one of the three major reactions taking place in the removal of automobile exhaust emissions using the so-called three-way catalysts. It is well known that rhodium is the best transition metal for the reduction of nitrogen oxides, while platinum and palladium are effective for the oxidation of carbon monoxide and unburned hydrocarbons, and ceria, due to its oxygen storage capabilities, is very helpful for the oxidation reactions. In such complex systems a lot of work had to be done to understand all the processes involved.

As part of this project Warren et al. (1993) first studied by AES the growth of a cerium film on polycrystalline rhodium. Annealing the sample between 800 and 1100 K led to the formation of a Ce–Rh alloy, probably  $\text{Ce}_3\text{Rh}_2$ . Oxidation of this surface alloy at room temperature followed by a thermal treatment resulted in the agglomeration of  $\text{CeO}_2$  crystallites on an essentially bare rhodium surface. Chemisorption of CO, in the absence of oxygen, led to a rapid oxidation of CO into  $\text{CO}_2$  in a similar way to that observed with a Rh/ $\text{CeO}_2$  catalyst. After a few adsorption/desorption cycles, no more  $\text{CO}_2$  was produced. It is believed that the  $\text{CeO}_2$  crystallites provide the necessary oxygen by a spillover process. This process had already been suggested on practical catalysts but such a surface science study provided a direct proof for it.

The same reaction was studied by Hardacre et al. (1996) on Pt–Ce alloys ( $\text{PtCe}_2$  and  $\text{Pt}_3\text{Ce}_7$ ). The most active catalyst was produced by  $\text{N}_2\text{O}$  (and not oxygen) pretreatment of  $\text{Pt}_3\text{Ce}_7$  at 720 K. This higher catalytic activity was related with a higher dispersion of both the platinum and ceria phases under these conditions. Such a catalyst was as good as the best classical catalysts prepared by traditional techniques. Ceria spillover of oxygen onto platinum was also invoked, as in the preceding paper, to explain such a high activity.

## 4. Discussion and conclusion

Among all studies on the rare-earth alloys in catalytic reactions, only a few concern thin-film or R–TM bimetallic supported catalysts. In the case of Rh deposited on a thin film

of cerium, the formation of a Ce–Rh intermetallic under reducing conditions has been observed (Chojnacki et al. 1991) but it was not clear whether this intermetallic plays an active role in the catalytic reaction. For the Pt–R/Al<sub>2</sub>O<sub>3</sub> bimetallic catalysts (Weiqi et al. 1992), although the magnetic susceptibility is modified by the addition of the rare earth, the electronic state of the rare-earth element (metal or oxide) was not fully established. On the contrary, a large amount of catalytic studies were performed using rare-earth and transition-metal intermetallic compounds. The fact that most of the catalytic reactions are hydrogenation or dehydrogenation reactions is no coincidence, but can be related to the reversible hydrogenation properties of the intermetallic compound in the conditions of temperature and pressure of the catalytic reactions. This process involves molecular hydrogen dissociation at the surface of the intermetallic compound before diffusion of atomic hydrogen inside the bulk to form a hydride. The first detailed surface and magnetic studies on LaNi<sub>5</sub> (Siegmann et al. 1978) indicated the surface decomposition into Ni or Ni-rich precipitates and La(OH)<sub>3</sub>. The increase of the magnetic susceptibility as a function of the number of hydrogenation cycles showed a progressive decomposition process which is responsible for the decrease in the hydrogen absorption capacity. These Ni particles are expected to be the active sites for the hydrogen dissociation. Since the catalytic reaction takes place at the surface of the catalysts involving adsorption, dissociation and recombination of molecules, the question arises which role is played by the intermetallic itself. In fact, it has been observed in several hydrogenation reactions that the hydride ( $\alpha$  or  $\beta$  phase) should be involved in the reaction. For example, for LaNi<sub>5</sub> and substituted LaNi<sub>4</sub>M compounds (Barrault et al. 1986c) the rise of propene conversion takes place 20–30°C higher than the equilibrium temperature of the corresponding hydride, with an activation energy larger than for classical catalysts. This was interpreted by the active role of the  $\alpha$  phase in this range of temperatures, since no bulk decomposition of the intermetallic compound was observed. In the hydrogenation of 1-undecene (Johnson et al. 1992), it was observed that the catalytic activity was greatly enhanced when the LaNi<sub>5</sub> hydride was present under the Ni and La(OH)<sub>3</sub> surface. This can be related to the high reactivity of the desorbed atomic hydrogen at the surface of the material. In such a reaction the hydride acts as a hydrogen reservoir but its activity decreases when all the hydrogen has been desorbed and the properties of the  $\alpha$  phase are then observed.

The hydrogenation properties of the hydride-forming intermetallic compound was also used as a driving force in alkene, alkane or alcohol dehydrogenation reactions which are thermodynamically unfavorable (Chetina and Lunin 1994). The intermetallic compound can be used both as a catalyst and hydrogen acceptor, but its activity and thermal stability can be enhanced by adding some Rh, Ru or Pt salts at the surface.

Apart from these specific hydrogen absorption and desorption properties, it is clear that the intermetallic compounds are more often used as precursors of new and more active catalysts. The decomposition of intermetallic compounds into transition-metal particles and rare-earth hydride, oxide or hydroxide in the course of the catalytic reaction was evidenced in a large number of catalytic reactions, especially those involving CO dissociation, which produces oxidizing species. The rise of catalytic activity was

related to the large increase in the surface area from a few square meters to  $10\text{--}50\text{ m}^2/\text{g}$ , and to the formation of new active sites. Such catalysts display turnover frequencies comparable to or larger than classical catalysts. An appropriate pretreatment allows one to obtain more rapidly an active catalyst. In the case of  $\text{RCu}_2$  compounds, in the methanol synthesis, their decomposition under hydrogen leads to well-dispersed Cu particles in intimate contact with small rare-earth hydride or oxide particles. It was observed that such catalysts imply different reaction mechanisms than conventional  $\text{Cu/ZnO/Al}_2\text{O}_3$  methanol catalysts where the presence of  $\text{CO}_2$  is essential to maintain a high methanol conversion, whereas it is a poison for catalysts derived from intermetallic compounds (Nix et al. 1989). This was attributed to the role of ceria which can adsorb the methanol precursor, whereas  $\text{CO}_2$  forms a strongly bonded carbonate. In ammonia synthesis the cerium hydride formed by the decomposition of the  $\text{CeRu}_2$  was found to have a promoting effect on the transition-metal catalytic properties. This effect was attributed to a charge transfer from cerium hydride to Ru and/or a hydrogen spillover effect at the surface of the catalysts.

In other reactions, like skeletal rearrangements of saturated hydrocarbons, the decomposition of  $\text{CePd}_3$  into Pd and  $\text{CeO}_2$  was also found to increase its activity by two orders of magnitude with an enhanced selectivity towards aromatization and 1–5 ring closure (Le Normand et al. 1984).

In the case of  $\text{LaCo}_5$  starting intermetallic in  $\text{CO} + \text{H}_2$  reaction, not only the oxidation of the rare earth but also the carbon provided by the CO decomposition plays a role to form a new active catalyst composed of Co particles dispersed from the La oxide platelets by carbon filaments (Wang et al. 1987). Its catalytic properties are similar to that of  $\text{Co/La}_2\text{O}_3$  but very different from that of  $\text{Co/CeO}_2$  (Barrault et al. 1986b). In this last case the Co particles are deposited on ceria and an interaction with the support is expected.

It is also interesting to note that the decomposition of pseudobinary intermetallic compounds ( $\text{LaNi}_4\text{Fe}$  and  $\text{CeNi}_{5-x}\text{Co}_x$ ) leads to the formation of bimetallic transition metal particles which display different selectivities than the catalysts derived from the related binary intermetallic compound (Paul-Boncour et al. 1991, France and Wallace 1988). The characterization of the bimetallic particles by XRD, Mössbauer spectroscopy and magnetism indicated that their composition was close to that of the starting alloy.

To conclude, intermetallic compounds can lead to very active catalysts with different selectivities from conventional supported catalysts. But it was observed that their lifetime was generally short, due to poisoning by reaction products. Although these kinds of catalysts are not yet too promising for industrial application, essentially due to rapid deactivation, they remain interesting from a fundamental point of view. However, due to their specific activity and selectivity compared to conventional catalysts in some hydrogenation or dehydrogenation reactions, further investigations should be performed in order to increase their stability.

## References

- Aiko, K.I., H. Hori and A. Osaki, 1972, *J. Catal.* **27**, 424.
- Ando, H., M. Fujiwara, Y. Matsumura, H. Miyamura, H. Tanaka and Y. Souma, 1995, *J. Alloys & Compounds* **223**, 139.
- Atkinson, G.B., and L.J. Nicks, 1977, *J. Catal.* **46**, 417.
- Baglin, E.G., G.B. Atkinson and L.J. Nicks, 1980, US Patent 4,181,630.
- Baglin, E.G., G.B. Atkinson and J.J. Nicks, 1981, *Ind. Eng. Chem. Prod. Res. Dev.* **20**, 87.
- Ballivet-Tkatchenko, D., J. Branco and A. Pires de Matos, 1995, *J. Phys. Chem.* **99**, 5481.
- Barrault, J., D. Duprez, A. Guilleminot, A. Percheron-Guégan and J.C. Achard, 1983a, *Appl. Catal.* **5**, 99.
- Barrault, J., D. Duprez, A. Percheron-Guégan and J.C. Achard, 1983b, *J. Less-Common Met.* **89**, 537.
- Barrault, J., A. Guilleminot, J.C. Achard, V. Paul-Boncour and A. Percheron-Guégan, 1986a, *Appl. Catal.* **21**, 307.
- Barrault, J., A. Guilleminot, J.C. Achard, V. Paul-Boncour, A. Percheron-Guégan, L. Hilaire and M. Coulon, 1986b, *Appl. Catal.* **22**, 273.
- Barrault, J., A. Guilleminot, A. Percheron-Guégan, V. Paul-Boncour and J.C. Achard, 1986c, *Appl. Catal.* **22**, 263.
- Bartley, G.J.J., and R. Burch, 1988, *Appl. Catal.* **43**, 141.
- Bossi, A., F. Garbassi and G. Petrini, 1982, *J. Chem. Soc. Faraday Trans. I* **78**, 10290.
- Braaten, N.A., J.K. Grepstad and S. Raaen, 1989, *Surf. Sci.* **222**, 499.
- Bryan, S.J., J.R. Jennings, S.J. Kipling, G. Owen, R.M. Lambert and R.M. Nix, 1988, *Appl. Catal.* **40**, 173.
- Burch, R., and R.J. Chappell, 1988, *Appl. Catal.* **45**, 131.
- Burch, R., R.J. Chappell and S.E. Golunski, 1988, *Catal. Lett.* **1**, 439.
- Chetina, O.V., and V.V. Lunin, 1994, *Russ. Chem. Rev.* **63**, 483.
- Chinchen, G.C., K.C. Waugh and D.A. Whan, 1986, *Appl. Catal.* **25**, 101.
- Chinchen, G.C., P.J. Denny, D.G. Parker, M.S. Spencer and D.A. Whan, 1987a, *Appl. Catal.* **30**, 333.
- Chinchen, G.C., M.S. Spencer, K.C. Waugh and D.A. Whan, 1987b, *J. Chem. Soc. Faraday Trans.* **83**, 2193.
- Chojnacki, T., K. Krause and L.D. Schmidt, 1991, *J. Catal.* **128**, 161.
- Coon, V.T., T. Takeshita, W.E. Wallace and R.S. Craig, 1976, *J. Phys. Chem.* **80**, 1878.
- Coon, V.T., W.E. Wallace and R.S. Craig, 1978, Methanation by rare earth intermetallic catalysts, in: *The Rare Earths in Modern Science and Technology*, eds G.J. McCarthy and J.J. Rhyne (Plenum, New York) p. 93.
- Corré, S., Y. Gotoh, H. Sakaguchi and G. Adachi, 1997, *Chem. Mater.* **9**, 1893.
- Elattar, A., W.E. Wallace and R.S. Craig, 1978, Inter-metallic compounds as catalysts for hydrogenation of carbon oxides, in: *Rare Earths in Modern Science and Technology*, eds G.J. McCarthy and J.J. Rhyne (Plenum, New York) p. 87.
- France, J.E., and W.E. Wallace, 1988, *Lanthanide & Actinide Res.* **2**, 165.
- Frost, J.C., 1988, *Nature* **334**, 577.
- Hardacre, C., T. Rayment and R.M. Lambert, 1996, *J. Catal.* **158**, 102.
- Hay, C.M., J.R. Jennings, R.M. Lambert, R.M. Nix, G. Owen and T. Rayment, 1988, *Appl. Catal.* **37**, 291.
- Herpin, A., 1968, *Théorie du Magnétisme* (Institut National des Sciences et Techniques Nucléaires, Saclay) p. 766.
- Imai, H., T. Tagawa and M. Kuraishi, 1985, *Mater. Res. Bull.* **20**, 511.
- Imamoto, T., T. Mita and M. Yokoyama, 1984, *J. Chem. Soc. Chem. Comm.*, p. 163.
- Imamoto, T., T. Mita and M. Yokoyama, 1987, *J. Org. Chem.* **52**, 5695.
- Imamura, H., and S. Tsuchiya, 1981a, *Chem. Comm.*, p. 567.
- Imamura, H., and S. Tsuchiya, 1981b, *J. Catal.* **72**, 383.
- Imamura, H., and W.E. Wallace, 1980, *J. Phys. Chem.* **84**, 3145.
- Imamura, H., W.E. Wallace and K. Soga, 1981, *J. Catal.* **67**, 244.
- Imamura, H., T. Takahashi and S. Tsuchiya, 1982, *J. Catal.* **77**, 289.
- Imamura, H., Y. Kato and S. Tsuchiya, 1984, *Z. Phys. Chem.* **141**, 129.
- Imamura, H., Y. Kato, K. Yamada and S. Tsuchiya, 1986a, *Appl. Catal.* **27**, 243.
- Imamura, H., K. Uamada, K. Nukui and S. Tsuchiya, 1986b, *J. Chem. Soc. Chem. Comm.*, p. 367.

- Imamura, H., K. Nukui, K. Yamada, S. Tsuchiya and T. Sakai, 1987, *J. Chem. Soc. Faraday Trans. I* **83**, 743.
- Imamura, H., S. Kasahara, T. Takada and S. Tsuchiya, 1988, *J. Chem. Soc. Faraday Trans. I* **84**, 765.
- Imamura, H., T. Takada, S. Kasahara and S. Tsuchiya, 1990, *Appl. Catal.* **58**, 165.
- Iwasawa, Y., ed., 1995, *X ray Absorption Fine Structure for Catalysts and Surfaces* (World Scientific, Singapore) 393 pp.
- Jennings, J.R., R.M. Lambert, R.M. Nix, G. Owen and M.D. Shannon, 1992a, *Appl. Catal. A* **81**, 257.
- Jennings, J.R., G. Owen, R.M. Nix and R.M. Lambert, 1992b, *Appl. Catal. A* **82**, 65.
- Jianhui, Li, Li Fengyi and Zhang Xingqun, 1992, *J. Alloys & Compounds* **181**, 521.
- Johnson, J.R., Z. Gavra, P. Chyou and J.J. Reilly, 1992, *J. Catal.* **137**, 102.
- Johnson, J.R., Z. Gavra and J.J. Reilly, 1994, *Z. Phys. Chem.* **183**, 391.
- Kagan, Y.B., A.Y. Rozovskii, L.G. Liberov, E.V. Lin, S.M. Loktev and A.N. Bankirov, 1975, *Dokl. Akad. Nauk SSSR* **224**, 1081.
- Kirchmayr, H.R., and C.A. Poldy, 1979, Magnetic properties of intermetallic compounds of rare earth metals, in: *Handbook on the Physics and Chemistry of Rare Earths*, Vol. 2, eds K.A. Gschneidner Jr and L. Eyring (North-Holland, Amsterdam) ch. 14, p. 55.
- Krause, K.R., P. Schabes-Retchiman and L.D. Schmidt, 1992, *J. Catal.* **134**, 204.
- Le Normand, F., P. Girard, L. Hilaire, M.F. Ravet, G. Krill and G. Maire, 1984, *J. Catal.* **89**, 1.
- Luengo, C.A., A.L. Cabrera, H.B. McKay and M.B. Maple, 1977, *J. Catal.* **47**, 1.
- Moon, Y.H., and S.-K. Ihm, 1993, *Catal. Lett.* **22**, 205.
- Moon, Y.H., and S.-K. Ihm, 1996, *Catal. Lett.* **42**, 73.
- Netzer, F., and E. Bertel, 1982, Adsorption and catalysis on rare earth surfaces, in: *Handbook on the Physics and Chemistry of Rare Earths*, Vol. 5, eds K.A. Gschneidner Jr and L. Eyring (North-Holland, Amsterdam) ch. 43, pp. 304–312.
- Nix, R.M., T. Rayment, R.M. Lambert, J.R. Jennings and G. Owen, 1987, *J. Catal.* **106**, 216.
- Nix, R.M., R.W. Judd, R.M. Lambert, J.R. Jennings and G. Owen, 1989, *J. Catal.* **118**, 175.
- Owen, G., C.M. Hawkes, D. Lloyd, J.R. Jennings, R.M. Lambert and R.M. Nix, 1987, *Appl. Catal.* **33**, 405.
- Owen, G., C.M. Hawkes, D. Lloyd, J.R. Jennings, R.M. Lambert and R.M. Nix, 1990, *Appl. Catal.* **58**, 69.
- Paul-Boncour, V., A. Percheron-Guégan, J.C. Achard, J. Barrault, H. Dexpert and R.C. Karnatak, 1986, *J. Phys. Paris* **47**, C8, 305.
- Paul-Boncour, V., A. Percheron-Guégan, J.C. Achard, J. Barrault and G. Jehanno, 1991, *Eur. J. Solid State Inorg. Chem.* **28**, 449.
- Percheron-Guégan, A., and J.M. Welter, 1988, Preparation of intermetallics and hydrides, in: *Hydrogen in Intermetallic Compounds I*, ed. L. Schlapbach, Vol. 63 of *Topics in Applied Physics* (Springer, Berlin) pp. 11–44.
- Rohler, J., 1985, *J. Magn. Magn. Mater.* **47–48**, 175.
- Shaw, E.A., T. Rayment, A.P. Walker, J.R. Jennings and R.M. Lambert, 1990a, *J. Catal.* **126**, 219.
- Shaw, E.A., T. Rayment, A.P. Walker and R.M. Lambert, 1990b, *Appl. Catal.* **67**, 151.
- Shaw, E.A., T. Rayment, A.P. Walker, R.M. Lambert, R.M. Gounlett, R.J. Oldmann and A. Dent, 1991, *Catal. Today* **9**, 197.
- Shaw, E.A., A.P. Walker, T. Rayment and R.M. Lambert, 1992, *J. Catal.* **134**, 747.
- Siegmann, H.C., L. Schlapbach and C.R. Brundle, 1978, *Phys. Rev. Lett.* **40**, 972.
- Sim, K.S., L. Hilaire, F. Le Normand, R. Touroude, V. Paul-Boncour and A. Percheron-Guégan, 1989, in: *Structure and Reactivity of Surfaces*, eds C. Morterra, A. Zecchina and G. Costa (Elsevier, Amsterdam) p. 863.
- Sim, K.S., L. Hilaire, F. Le Normand, R. Touroude, V. Paul-Boncour and A. Percheron-Guégan, 1991, *J. Chem. Soc. Faraday Trans.* **87**, 1453.
- Sinfelt, J.H., 1970, *Catal. Rev.* **3**, 175.
- Snijder, E.D., G.F. Versteeg and W.P.M. Van Swaaij, 1993, *Chem. Eng. Sci.* **48**, 2429.
- Soga, K., H. Imamura and S. Ikeda, 1977, *J. Phys. Chem.* **81**, 1762.
- Soga, K., H. Imamura and S. Ikeda, 1979, *J. Catal.* **56**, 119.
- Soga, K., T. Otsuka, M. Sato, T. Sano and S. Ikeda, 1980, *J. Less-Common Met.* **71**, 259.
- Sohier, M.P., G. Wrobel, J.P. Bonelle and J.P. Marcq, 1992, *Appl. Catal.* **84**, 169.
- Takeshita, T., W.E. Wallace and R.S. Craig, 1976, *J. Catal.* **44**, 236.
- Vvedensky, D.D., 1992, Theory of X-ray absorption fine structure, in: *Unoccupied Electronic states*, eds J.C. Fuggle and J.E. Inglesfield, Vol. 69 of *Topics in Applied Physics* (Springer, Berlin) p. 139.

- Walker, A.P., and R.M. Lambert, 1992, *J. Phys. Chem.* **96**, 2265.
- Walker, A.P., T. Rayment and R.M. Lambert, 1989, *J. Catal.* **117**, 102.
- Walker, A.P., T. Rayment, R.M. Lambert and R.J. Oldman, 1990, *J. Catal.* **125**, 67.
- Walker, A.P., R.M. Lambert, R.M. Nix and J.R. Jennings, 1992, *J. Catal.* **138**, 694.
- Wallace, W.E., A. Elattar, T. Takeshita, V.T. Coon, C.A. Bechman and R.S. Craig, 1977, Rare earth and actinide intermetallics as catalysts, in: *Proc. 2nd Int. Conf. on Electronic Structure of Actinides*, Wroclaw, Poland, p. 93.
- Wallace, W.E., R.F. Karlicek and H. Imamura, 1979, *J. Phys. Chem.* **83**, 1708.
- Wallace, W.E., J. France and A. Shamsi, 1982, in: *Rare Earths in Modern Science and Technology*, Vol. 3, eds G.J. McCarthy, J.J. Rhine and H.B. Silber (Plenum, New York) p. 561.
- Wang, Z.L., C. Colliex, V. Paul-Boncour, A. Percheron-Guegan, J.C. Achard and J. Barrault, 1987, *J. Catal.* **105**, 120.
- Warren, J.P., X. Zhang, J.E.T. Andersen and R.M. Lambert, 1993, *Surf. Sci.* **287/288**, 222.
- Weiqi, Lu, Li Fengyi and Li Jianhui, 1992, *J. Alloys & Compounds* **181**, 527.
- Yokoyama, T., 1995, Theory and parameters of EXAFS, in: *X ray Absorption Fine Structure for Catalysts and Surfaces*, ed. Y. Iwasawa (World Scientific, Singapore) ch. 2, p. 9.
- Zhang, Z.C., G.-D. Lei and W.M.H. Sachtler, 1995, Metal clusters and particles in zeolites, in: *X ray Absorption Fine Structure for Catalysts and Surfaces*, ed. Y. Iwasawa (World Scientific, Singapore) ch. 7.2, p. 173.
- Zhu, G., Y. Lei, Q. Wang and X. Yang, 1997, *J. Alloys & Compounds* **253–254**, 189.



## Chapter 182

# THE METALS AND ALLOYS (PREPARED UTILIZING LIQUID AMMONIA SOLUTIONS) IN CATALYSIS II

Hayao IMAMURA

*Yamaguchi University, Department of Advanced Materials Science  
 and Engineering, Tokiwadai, Ube 755-8611, Japan*

## Contents

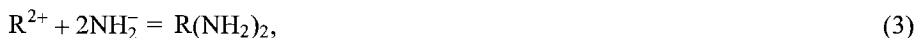
List of symbols	45	3.1.1. Hydrogenolysis of alkanes	56
1. Introduction	46	3.1.2. Hydrogenation of alkenes	57
2. Catalysis of rare earths deposited on silica, active carbon and zeolite from liquid ammonia solutions	47	3.1.3. H <sub>2</sub> adsorption, TPD, H <sub>2</sub> -D <sub>2</sub> isotopic exchange, and IR of adsorbed CO	59
2.1. R/SiO <sub>2</sub>	47	3.1.4. Surface features	61
2.1.1. Catalysis of R/SiO <sub>2</sub> with low loading	49	3.2. Dehydrogenation of cyclohexane	65
2.1.2. Catalysis of R/SiO <sub>2</sub> with high loading	51	3.3. Catalysis of R-Pd/SiO <sub>2</sub> with considerable hydrogen uptake	68
2.2. R/C	53	3.4. Catalytic transfer hydrogenation with ammonia	70
2.3. R/zeolite	54	4. Summary and conclusions	71
3. Catalysis of rare-earth metal overlayers or bimetallic compounds	56	Acknowledgments	72
3.1. Catalysis of R-Co and R-Ni	56	References	72

## List of symbols

C	active carbon	$P_H$	pressure of hydrogen
d <sub>x</sub> , x=1-12	deuteriocyclohexane; e.g. d <sub>1</sub> : C <sub>6</sub> H <sub>11</sub> D	PVA	polyvinyl alcohol
e <sub>am</sub> <sup>-</sup>	ammonia-solvated electron	$q_a$	heat of hydrogen adsorption
$E_a$	apparent activation energy	R	rare earths
$E_t$	true activation energy	TOF	turnover frequency
IR	infrared spectroscopy	TPD	temperature programmed desorption
$k, k', k'', k_1, k_2$	rate constants	XAFS	X-ray absorption fine structure
$k_t$	true rate constant	XANES	X-ray absorption near edge structure
$K$	equilibrium constant of hydrogen	XRD	X-ray diffraction
LEED	low energy electron diffraction	XPS	X-ray photoelectron spectroscopy
$P_c$	pressure of cyclohexane		

## 1. Introduction

Recently there has been a growing interest in catalytic properties of rare earths (R) and related compounds (Edelmann 1996, Hogerheide et al. 1996, Inumaru and Misono 1995, Taube 1995, Yasuda 1995, Imamoto 1994). Since rare-earth elements have specific electron configurations based on 4f orbitals, many intriguing reactions mediated by them which cannot be achieved by d-block transition metal compounds are expected to occur:



where R = Eu or Yb.

It is known that europium and ytterbium among rare-earth elements readily dissolve in liquid ammonia to yield homogeneous solutions with a deep blue color, being characteristic of the ammonia-solvated electrons ( $e_{am}^-$ ) (Thompson 1976). The ammoniated electron is stable at temperatures near 240 K and is a powerful reducing agent. Moreover, the reversibility of eq. (1) is high at low temperatures, and so the reversal is used as a method producing the metallic rare earth in sponge form.<sup>1</sup> The rare-earth metal solutions are known to change through varied steps as shown by Salot and Warf (1968), Juza and Hadenfeldt (1968) and Thompson et al. (1966). The thermal decomposition products of liquid ammonia solutions of Eu and Yb metals finally yield nitride (EuN and YbN) through diamide, triamide or imide.

It has been first shown (Imamura et al. 1989a) that when Fe, Ni, Cu or Ag metal powders are added to this rare-earth metal solution, the dissolved metal in liquid ammonia reacts with the transition metal to form novel rare-earth metal overlayers or rare-earth-containing bimetallic compounds. By using such dissolving power of liquid ammonia, a new preparative method of a novel class of catalytic materials containing rare earths has been developed, and then, their specific catalysis has recently been shown. In the preparation of rare-earth catalysts, the type of matrix substrates which are added to the solutions of Eu or Yb metal in liquid ammonia strongly influences the mode of interactions and the resulting materials. The catalytic properties vary markedly with changes in the way in which the rare-earth species exist on the matrix (Imamura et al. 1991a). Preparation of catalysts composed of Na/Al<sub>2</sub>O<sub>3</sub>

<sup>1</sup> Rockwell Internatl. Co., U.S. Patent 3,770,422 (1973).

has long been carried out using ammonia solutions of alkali metals (Blouri et al. 1968).

In view of these facts, a great deal of attention has been here devoted to understanding how the rare-earth metals exist on the matrix substrate and how this affects the catalytic properties. In sect. 2, rare earths introduced onto (or into) silica, active carbon and zeolite, and their catalysis in connection with changes in their chemical state are characterized. In bimetallic systems, interest in the study of interactions of the rare earth with the d-transition metal has been aimed at unveiling the correlation of the electronic and geometric effects with the catalytic properties for hydrogenolysis, hydrogenation, dehydrogenation, transfer hydrogenation,  $H_2$ - $D_2$  exchange and  $C_6H_{12}$ - $D_2$  exchange. The effects of a rare-earth metal overlayer on such catalytic reactions and related properties over Co and Ni are largely dealt with. These studies are described in sect. 3.

## 2. Catalysis of rare earths deposited on silica, active carbon and zeolite from liquid ammonia solutions

### 2.1. $R/SiO_2$

When  $SiO_2$  is brought into contact with a solution of rare-earth metals dissolved in liquid ammonia, the rare earth reacts readily with  $SiO_2$ , liberating hydrogen gas with simultaneous changes in solution color from blue to colorless (Imamura et al. 1992a,e, 1991b). Figure 1 shows infrared spectra of 15 wt.% Yb/ $SiO_2$  obtained when  $SiO_2$  previously evacuated at 973 K is treated with the ytterbium solutions. The vibration band at  $3744\text{ cm}^{-1}$  of  $SiO_2$  is assigned to free hydroxyl groups (Iler 1979). This band decreases

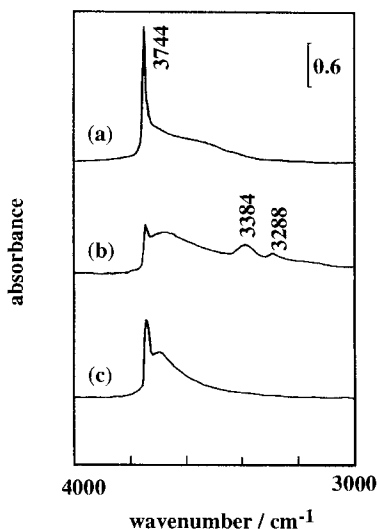


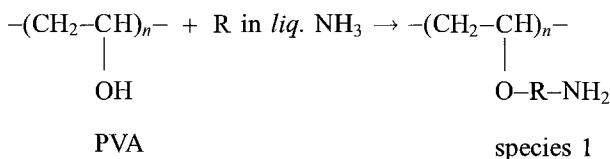
Fig. 1. IR spectra of (a)  $SiO_2$ , (b) 15 wt.% Yb/ $SiO_2$  (as prepared) and (c) 15 wt.% Yb/ $SiO_2$  evacuated at 573 K.

immediately upon contact with the rare earth. Strong absorptions are also observed at 3384, 3288 and 1552  $\text{cm}^{-1}$ , which can be assigned to the  $\text{NH}_2$  species bound to the rare earth by comparison with IR data of amido-metal complexes (Linde and Juza 1974, Warf and Gutmann 1971, Hadenfeldt et al. 1970, Hewkin and Griffith 1966). For  $\text{SiO}_2$  treated with liquid ammonia without rare earth, these bands are not observed and neither is the decrease in absorptions of the hydroxyl groups. Thus, these data give an indication that the rare-earth metals dissolved in liquid ammonia preferentially react with the surface hydroxyl groups of  $\text{SiO}_2$  to form  $\equiv\text{Si}-\text{O}-\text{R}-\text{NH}_2$  (Imamura et al. 1992a,e):



There are different hydroxyl types (free, bridged, vininal and geminal) on silica and their number varies with evacuation temperatures (Voort et al. 1990, Iler 1979). Considering the evacuation temperature (973 K) used here, it seems reasonable to estimate the surface density of OH groups as  $\sim 1.5 \text{ OH nm}^{-2}$  (Voort et al. 1990, Zhuravlev 1987); the total number of OH groups on  $\text{SiO}_2$  ( $380 \text{ m}^2 \text{ g}^{-1}$ ) can be determined. The loading of 13 wt.% Eu or 15 wt.% Yb corresponds roughly to the total amount of OH groups present on the surface of  $\text{SiO}_2$  by assuming a rare-earth metal to OH group ratio of 1:1 in the surface complex. However, the bands of the OH groups unreacted still remain in the IR spectra (fig. 1) of  $\text{SiO}_2$  with loading of 15 wt.% Yb, due to the varied reactivity and distributions of the different hydroxyl groups present on  $\text{SiO}_2$ . Such stoichiometric relationships of the reaction between the rare-earth metal and OH group are almost achieved when polyvinyl alcohol (PVA) with uniform hydroxyl groups is used. As described below, PVA is useful for determining the reaction product and its catalytic properties as a model compound.

PVA, as well as silica, readily reacts with Eu and Yb metal solutions in liquid ammonia, also releasing hydrogen gas. According to IR spectra of R/PVA, the strong, broad OH bands ( $3200\text{--}3500 \text{ cm}^{-1}$ ) of PVA decrease immediately upon reaction with the rare earth. The absorption of OH groups decreases proportionally with increasing levels of the addition of rare earths and finally disappears completely upon the addition of rare earth equivalent to the total amount of OH groups of PVA. The changes in C–O stretching modes are consistent with that alcohol is converted into alkoxide. This agrees with IR data reported for various alkoxides of Gd(III) and Er(III) (Mehrotra and Batwara 1970) and isopropoxides of rare-earth metals (Brown and Mazdiyasi 1970). Vibration bands are also observed at 3354 and 3284  $\text{cm}^{-1}$ ; these are assigned to the  $\text{NH}_2$  species bound at rare earths (Warf and Gutmann 1971, Hadenfeldt et al. 1970). Thus, the rare earths dissolved in liquid ammonia stoichiometrically react with the OH groups of PVA to form PVA-grafted species, following the equation (Imamura et al. 1992a).



This reaction is also consistent with elemental analyses of the product. PVA-grafted rare-earth products by the reaction of PVA with different levels of rare earth are formed, which always incorporate R and N in the atomic ratio 1:0.93–0.95. This suggests that the rare earth can also adopt a trivalent state, which does not hold for this case. However, slight deviations from R/N ratio = 1 indicate the existence of products other than species 1, e.g., bound species in bridged or cross-linked form in which a rare earth reacts with a set of adjacent hydroxyl groups in a polymer or astride two polymers. The PVA-grafted products obtained when the rare earths equivalent to the total number of OH groups present on PVA are introduced has an R:N:C atomic ratio of ~1:0.95:2. Thus, the IR studies and elemental analyses indicate that the OH groups of PVA exhibit highly quantitative reactivity toward the rare earth to form the PVA-grafted rare-earth (II) amide species compared with those of SiO<sub>2</sub>. This is also confirmed by the catalytic reactions (sect. 2.1.1).

The absorption intensity of NH<sub>2</sub> groups gradually decreases as Yb/SiO<sub>2</sub> is treated with elevated temperatures under evacuation. The absorption bands almost disappear upon heating around 573 K (fig. 1). Decomposition of the rare-earth species bound to the surface hydroxyl groups occurs, simultaneously leading to an inactivation of Eu/SiO<sub>2</sub> and Yb/SiO<sub>2</sub> for the catalytic reactions (see sect. 2.1.1). Instead, new absorptions appear at 2180–2230 cm<sup>-1</sup> upon this thermal treatment in the range 573–773 K. These bands are assigned to azides, which show absorptions in a wavenumber region similar to those reported by Ross (1972). For adsorbed ammonia on Cu/Al<sub>2</sub>O<sub>3</sub>, Kritzenberger et al. (1990) have shown that the bands in the region 1950–2350 cm<sup>-1</sup> are identified as surface-bound azides, which are predicted to be possible precursors in the copper nitride formation. This might suggest the possibility of rare-earth nitride formation *via* azide intermediates.

For the rare-earth loading in the range 0–15 wt.% on SiO<sub>2</sub>, it seems quite certain that the rare earth combines chemically through the surface hydroxyl groups of SiO<sub>2</sub>. However, for R/SiO<sub>2</sub> with high loading of rare earth (>13–15 wt.%), details on the states of the excess rare earth present on SiO<sub>2</sub> have not been obtained. This is further discussed in sect. 2.1.2.

#### 2.1.1. *Catalysis of R/SiO<sub>2</sub> with low loading*

The catalytic behavior of R/SiO<sub>2</sub> varies markedly with the level of rare-earth loading. Rare-earth catalysts immobilized on SiO<sub>2</sub>, formed by preferential reaction of rare earth with the OH groups on SiO<sub>2</sub>, exhibit specificity for selective hydrogenation (table 1). These hydrogenations show interesting features, of use for catalytic reactions (Konishi et al. 1995, Imamura et al. 1992a, 1991b). First, the rare earth on SiO<sub>2</sub> can discriminate between conjugated and non-conjugated C=C double bonds. Thus, buta-1,3-diene, isoprene, penta-1,3-diene and cyclohexa-1,3-diene are readily reduced to the corresponding monoenes at 298 K, with almost 100% selectivity, whereas penta-1,4-diene and hexa-1,4-diene remain unchanged. A further useful property of R/SiO<sub>2</sub> is that it shows negligible or very low reducing power for monoenes (propene and but-1-ene), in marked contrast to its reactivity with conjugated compounds. The reactivity of buta-1,3-diene is higher by

Table 1  
Various hydrogenations at 298 K over 13 wt.% Eu/SiO<sub>2</sub> and 15 wt.% Yb/SiO<sub>2</sub>

Catalyst	Reactant	Activity (mmol min <sup>-1</sup> g <sup>-1</sup> )	Product <sup>a</sup>
13 wt.% Eu/SiO <sub>2</sub>	but-1-ene	— <sup>b</sup>	
	buta-1,3-diene	5.9 × 10 <sup>-4</sup>	but-1-ene (51), <i>cis</i> -but-2-ene (49)
	penta-1,4-diene	— <sup>b</sup>	
	benzene	— <sup>b</sup>	
15 wt.% Yb/SiO <sub>2</sub>	propene	5.5 × 10 <sup>-5</sup>	propane (100)
	but-1-ene	4.4 × 10 <sup>-5</sup>	butane (100)
	buta-1,3-diene	6.5 × 10 <sup>-2</sup>	but-1-ene (24), <i>cis</i> -but-2-ene (57), <i>trans</i> -but-2-ene (19)
	isoprene	4.3 × 10 <sup>-2</sup>	3-methylbut-1-ene (18), 2-methylbut-1-ene (27), 2-methylbut-2-ene (55)
	penta-1,3-diene	8.7 × 10 <sup>-3</sup>	pent-1-ene (17), pent-2-ene (83)
	penta-1,4-diene	— <sup>b</sup>	
	hexa-1,4-diene	— <sup>b</sup>	
	cyclohexene	— <sup>b</sup>	
	cyclohexa-1,3-diene	4.6 × 10 <sup>-3</sup>	cyclohexene (100)
	benzene	6.3 × 10 <sup>-5</sup>	cyclohexene (100)
Sm	ethene	1.6 × 10 <sup>-2</sup>	ethane (100)
Yb	propene	1.1 × 10 <sup>-3</sup> (at 323 K)	propane (100)
	penta-1,4-diene	3.5 × 10 <sup>-5</sup>	pent-1-ene (80), pentane (20)

<sup>a</sup> Selectivity (%) in parentheses.

<sup>b</sup> The activity is almost zero within detection limits.

over three orders of magnitude than that of but-1-ene. The Yb/SiO<sub>2</sub>-catalyzed buta-1,3-diene hydrogenation yields preferential but-2-ene formation with a high *cis*:*trans* ratio. Included in table 1 for comparison are the results on rare-earth metal catalysts prepared by the metal vapour technique (Imamura et al. 1989b, 1985). They are active for the hydrogenation of both monoene and diene, but are not selective for conjugated and non-conjugated dienes. Thus, the immobilization of rare earths on the surface of SiO<sub>2</sub> leads to specific catalytic activity. However, upon thermal treatment of R/SiO<sub>2</sub> above ~573 K, the catalyst is completely deactivated for the hydrogenation, due to the decomposition of the rare-earth amide species as shown in IR spectra. Eu/SiO<sub>2</sub> and Yb/SiO<sub>2</sub> show rather similar catalytic behavior, but the activity of Yb/SiO<sub>2</sub> is much higher than that of Eu/SiO<sub>2</sub>.

R/PVA, regarded as a surface model of R/SiO<sub>2</sub>, shows essentially catalytic behavior similar to R/SiO<sub>2</sub>. R/PVA has high reactivity with the capability to discriminate between conjugated and non-conjugated double bonds for the hydrogenation. For three kinds of Yb/PVA catalysts in which 25, 50 and 100% of the OH groups of PVA are converted into grafting of Yb species, turnover frequencies (TOF) in terms of molecules of products

Table 2  
Comparison between R/SiO<sub>2</sub> and R/PVA for hydrogenation at 298 K

Catalyst <sup>a</sup>	Reactant	TOF × 10 <sup>4</sup> s <sup>-1</sup>	Catalyst <sup>a</sup>	Reactant	TOF × 10 <sup>4</sup> s <sup>-1</sup>
15 wt.% Yb/SiO <sub>2</sub>	buta-1,3-diene	1.9	Yb/PVA (0.5 : 1)	buta-1,3-diene	1.2
	isoprene	1.3		isoprene	0.43
	but-1-ene	0.0013	Yb/PVA (0.25 : 1)	buta-1,3-diene	0.78
Yb/PVA (1 : 1)	buta-1,3-diene	0.76	Eu/PVA (1 : 1)	buta-1,3-diene	0.75
	but-1-ene	0.018			

<sup>a</sup> Ratios of R to OH groups are given in parentheses.

formed per site per second are almost equal to each other and are further comparable to those for Yb/SiO<sub>2</sub> (table 2). It can be concluded that the active species of R/SiO<sub>2</sub> and R/PVA are identical.

Yb/SiO<sub>2</sub> is further characterized by the partial hydrogenation of benzene to cyclohexene with extremely high selectivity of 96–100% (Imamura et al. 1993a). Apart from conventional catalysts centering around Ru (Struijk et al. 1992, Fukuoka and Nagahara 1991, Niwa et al. 1990, Galvagno et al. 1988), a new catalytic material consisting of rare earths for the selective hydrogenation of benzene has been developed (Imamura et al. 1993a, 1987a). In spite of thermodynamic disadvantages ( $\Delta G^\circ$  at 298 K is  $-23 \text{ kJ mol}^{-1}$  for benzene to cyclohexene and  $-98 \text{ kJ mol}^{-1}$  for benzene to cyclohexane), there is a strong tendency for the reaction over the rare-earth catalysts to stop at the partially hydrogenated intermediate, rather than to proceed all the way to cyclohexane. Included in table 1 for comparison are the results on the hydrogenation of cyclohexene and cyclohexa-1,3-diene. Cyclohexadiene is readily reduced to cyclohexene with almost 100% selectivity, whereas cyclohexene is virtually inactive for Yb/SiO<sub>2</sub>. This is a reason why the selectivity of Yb/SiO<sub>2</sub> is extremely high.

Eu/SiO<sub>2</sub> and Yb/SiO<sub>2</sub> also exhibit high activity for the disproportionation of cyclohexa-1,3-diene to benzene and cyclohexene, the rates of which are comparable with those of the metallic nickel catalyst (Sakai et al. 1985), being fairly active for this reaction.

### 2.1.2. Catalysis of R/SiO<sub>2</sub> with high loading

Upon increasing loading of rare earth on SiO<sub>2</sub>, particularly above ~15 wt.%, the hydrogenation activity for monoenes suddenly appears (fig. 2). The fraction of 13–15 wt.% separates the catalysts with low loading from high loading, in which there is a marked difference in their catalytic behavior. Evidently, for R/SiO<sub>2</sub> with high loading the rare earth is in excess compared with the total number of surface hydroxyl groups present on SiO<sub>2</sub>. The first portion of rare earth introduced is consumed for the reaction with the surface hydroxyl groups up to the fraction corresponding to 13–15 wt.% (as described in sect. 2.1), and after all the hydroxyl groups are used up, the further loading results in the existence of the rare earth in an active form for the hydrogenation of ethene. The

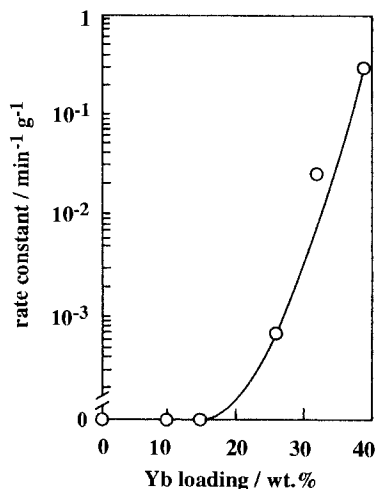


Fig. 2. Rate constant of Yb/SiO<sub>2</sub> for ethene hydrogenation (373 K) vs. Yb loading (wt.%).

Table 3  
Hydrogenation of alkynes at 353 K over 35 wt.% Eu/SiO<sub>2</sub> and 39 wt.% Yb/SiO<sub>2</sub>

Catalyst	Alkyne	Activity (mmol min <sup>-1</sup> g <sup>-1</sup> )	Hydrogenation products (%)
35 wt.% Eu/SiO <sub>2</sub>	acetylene	—	
	propyne	— <sup>a</sup>	
39 wt.% Yb/SiO <sub>2</sub>	acetylene	—	
	propyne	— <sup>a</sup>	
	but-1-yne	— <sup>a</sup>	
	but-2-yne	$2.6 \times 10^{-4}$	<i>cis</i> -but-2-ene (76), but-1-ene (24)
Sm	but-1-yne	— <sup>a</sup>	
	but-2-yne	$3.5 \times 10^{-4}$	<i>cis</i> -but-2-ene (65), but-1-ene (35)
Yb	acetylene	—	
	but-1-yne	— <sup>a</sup>	
	but-2-yne	$1.2 \times 10^{-5}$	<i>cis</i> -but-2-ene (70), but-1-ene (30)

<sup>a</sup> No hydrogenation occurs, but only isomerization is observed.

R/SiO<sub>2</sub> catalysts with high loading are probably those in which an excess of rare earth is present dispersed in almost metallic form on SiO<sub>2</sub>, as described later. Incidentally, the hydrogenation activity of 39 wt.% Yb/SiO<sub>2</sub> is close to that of the rare-earth metals (Imamura et al. 1989b, 1985).

R/SiO<sub>2</sub> with high loading additionally exhibits selective hydrogenation of alkynes. 39 wt.% Yb/SiO<sub>2</sub> discriminates between internal and terminal C≡C triple bonds for the hydrogenation of alkyne (table 3); thus, but-2-yne is readily converted to *cis*-but-2-ene in high selectivity at 353 K, whereas but-1-yne, propyne and acetylene are not



hydrogenated at all under the same conditions. The type of hydrogen addition at terminal and internal  $C\equiv C$  bonds by the rare-earth catalysts is completely contrary to that reported for conventional transition-metal catalysts (Freifelder 1971, Petrov and Forost 1964, Dobson et al. 1961). As shown in table 3, the catalytic behavior of  $R/SiO_2$  with high loading is quite similar to that observed for the rare-earth metal catalysts prepared by metal vaporization (Imamura et al. 1989b,c, 1988a, 1985). The product selectivity for 39 wt.%  $Yb/SiO_2$ -catalyzed but-2-yne hydrogenation is analogous to the results obtained for the  $Yb$  metal catalyst.

In the light of such catalytic properties of  $R/SiO_2$ , some of the rare earth introduced, especially up to the fraction of 0–15 wt.%, is preferentially bound to  $SiO_2$  to form  $\equiv Si-O-R-NH_2$  species, and the rest seems to deposit in active metallic form on  $SiO_2$  with high dispersion. The properties of the latter species largely reflect the hydrogenation of monoenes and alkynes.

## 2.2. $R/C$

The rare earths ( $Eu/C$  and  $Yb/C$ ) introduced onto active carbon ( $C$ ) by impregnation from a liquid ammonia solution of  $Eu$  or  $Yb$  metals are changed through varied steps (metal, amide, imide or nitride) by thermal treatments (Imamura et al. 1999a, 1996a, Konishi et al. 1995), as shown in eqs. (1)–(7) (Salot and Warf 1968, Juza and Hadenfeldt 1968, Thompson et al. 1966). Simultaneously the hydrogenation activity for ethene varies markedly (fig. 3). Upon evacuation of 60 wt.%  $Yb/C$  above 473 K, the hydrogenation activity appears even at 203 K. The activity increases with increasing evacuation temperatures, passes through a maximum around 773 K with an enhancement by over three orders of magnitude and then, the catalyst is completely deactivated upon evacuation at 1373 K. 60 wt.%  $Eu/C$  also exhibits a similar temperature dependence of activity.  $Eu/C$  shows the highest activity when evacuated around 573 K. It is found that

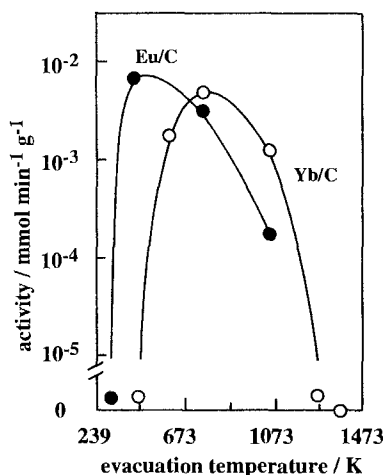
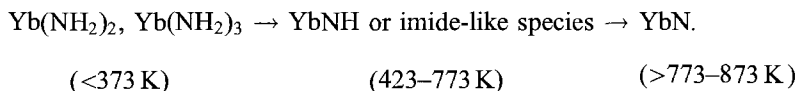


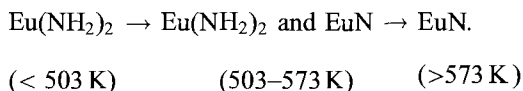
Fig. 3. Effects of evacuation temperatures of  $Eu/C$  and  $Yb/C$  on the hydrogenation of ethene (203 K).

the activity of R/C is comparable to that of conventional Ni/SiO<sub>2</sub> catalysts. The changes in rare earths on active carbon are followed by XRD.

When Yb(II) and Yb(III) amide are treated at 423 K, new diffraction peaks around 31.7, 36.5, 52.8 and 62.0° begin to appear. These peaks observed at 503 K are satisfactorily indexed to a cubic lattice,  $a=4.85 \text{ \AA}$ , being in substantial agreement with the results of ytterbium imide characterized by Hadenfeldt et al. (1970). Upon further treating above 773–873 K, XRD eventually displays the conversion to YbN:



The changes in XRD of europium amide are summarized as follows:



The catalytic properties of rare-earth amide [Eu(NH<sub>2</sub>)<sub>2</sub>, Yb(NH<sub>2</sub>)<sub>2</sub> and Yb(NH<sub>2</sub>)<sub>3</sub>] prepared separately, imide and nitride have been further investigated for comparison. The possibility of rare-earth amide and nitride as active species can be consequently ruled out. Baba et al. (1992, 1993) report that ytterbium introduced into zeolite rapidly lost its hydrogenation activity upon evacuation above 900 K. It is concluded that imide or imide-like species formed on R/C during the thermal decomposition processes of europium and ytterbium amide to nitride at 503–573 K and 423–773 K are active catalysts for the hydrogenation of ethene, respectively. Unlike the ytterbium system, no indications of EuNH formation are recognized, but the possibility that EuNH species generated slightly or fleetingly on the catalyst surface by the thermal treatment catalyze the hydrogenation is high. Juza and Hadenfeldt (1968) find no evidence of EuNH during the thermal decomposition of amide to nitride, but Howell and Pytlewski (1969) report the formation at 503 K. In R/zeolite as described later, the formation of EuNH is suggested (Baba et al. 1995).

Moreover, it has been shown (Imamura et al. 1995a) that such rare-earth imide or imide-like species exhibit oligomerization activity of alkynes. Selective cyclic dimerization and trimerization of propyne and ethyne to cyclohexadiene and benzene occur at 453 K during the oligomerization, respectively, in which the active catalysts are characterized as rare-earth imides induced by the thermal treatment of R/C.

### 2.3. R/zeolite

Europium and ytterbium (R/zeolite) introduced into K<sup>+</sup>-exchanged Y-zeolite by impregnation from liquid ammonia solutions similarly show various catalytic reactivities with changes in evacuation temperatures (Baba et al. 1992). The changes in the chemical state of rare earths with the evacuation temperature are studied by IR and X-ray absorption

Table 4  
Fraction of  $R^{2+}$  and  $R^{3+}$  evaluated from XANES of R/zeolite

Evacuation temperature (K)	Fractions (%)		Evacuation temperature (K)	Fractions (%)	
	$R^{2+}$	$R^{3+}$		$R^{2+}$	$R^{3+}$
<i>Eu/zeolite</i>			<i>Yb/zeolite</i>		
303	53	47	333	16.4	83.6
423	75	25	473	38.6	61.4
473	63	37	573	44.2	55.8
573	53	47	773	22.0	78.0
673	40	60	873	10.2	89.8
773	52	48	973	11.0	89.0
973	88	12			

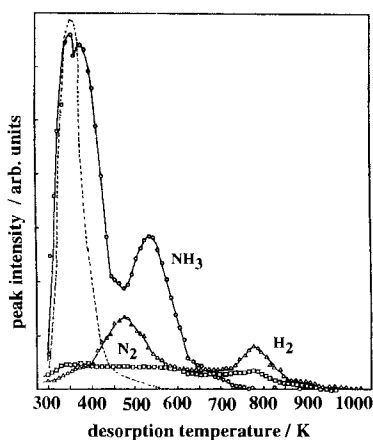
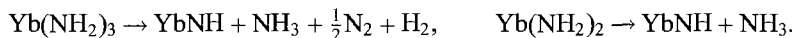


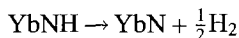
Fig. 4. TPD spectra of gases desorbed from Yb/zeolite. The dashed line expresses  $NH_3$  desorbed from zeolite without rare earth.

fine structure (XAFS), combined with temperature programmed desorption (TPD) measurements. For Yb/zeolite, IR exhibits the presence of Yb amide, which is observed up to 423 K. In XANES spectra, Yb  $L_2$ -edge absorption is observed at 9972 and 9979 eV and the corresponding peaks of  $L_3$ -edge XANES are at 8939 and 8946 eV, respectively. These are very close to energy values attributed to the  $2p \rightarrow 5d$  electron transition of Yb(II) and Yb(III), as reported for  $YbAl_2$  and  $YbAl_3$  (Prabhawalkar and Padalia 1983, Hatwar et al. 1980, Rao et al. 1980). It is evident that Yb/zeolite contains at least two kinds of Yb species. XANES shows that the sample as prepared consists of Yb(III) species mainly and that the Yb species exist as 16.4% Yb(II) and 83.6% Yb(III) upon evacuation at 333 K (Tanaka et al. 1993). As shown in table 4, the fraction of Yb(II) increases with increasing the evacuation temperature and reaches a maximum of 44.2% around 573 K. Then, the fraction of Yb(II) decreased to reach a minimum at 873 K. In TPD (fig. 4) obtained in this temperature range,  $N_2$  is continuously desorbed, while  $H_2$  is desorbed with two maxima at 400 and 780 K. A maximal desorption of  $NH_3$  appears at 540 K.

This  $\text{NH}_3$  desorption corresponds to the decomposition of Yb amides [ $\text{Yb}(\text{NH}_2)_2$  and/or  $\text{Yb}(\text{NH}_2)_3$ ] to the imide species ( $\text{YbNH}$ ):



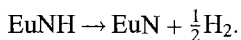
The fraction of Yb(III) species increases at an evacuation temperature  $>600$  K, owing to the decomposition of Yb imide to Yb nitride with evolution of hydrogen:



Eu/zeolite follows similar changes in Eu species with elevating the evacuation temperature: amide  $\rightarrow$  imide  $\rightarrow$  nitride (Tanaka et al. 1995). According to IR, Eu amide decomposes to imide around 420 K and to nitride around 610 K. The fraction of Eu(II) and Eu(III) is summarized in table 4. When the evacuation temperature of Eu/zeolite is elevated from 303 to 423 K, the fraction of Eu(II) increases from 53 to 75% and simultaneously the desorption of  $\text{H}_2$  and  $\text{N}_2$  is observed in TPD. This corresponds to the decomposition of Eu(III) amide to Eu(II) imide:



Subsequently, the fraction of Eu(II) decreases and the Eu(III) species increases about 2.4-fold in the range of 423 to 673 K. This is due to the conversion of Eu(II) imide to Eu(III) nitride:



At evacuation temperatures higher than 673 K, the fraction of Eu(II) increases again to reach 88% at 973 K. Further decomposition of Eu(III) nitride to Eu(II) nitride is presumed.

The changes in catalytic activities of rare earths introduced into zeolite with the evacuation temperature suggest that the Eu(II) and Yb(II) imide species formed exhibit activity for the isomerization and the Michael reaction (Baba et al. 1993, 1995). Unlike the results on R/C (Imamura et al. 1996a), the nitride species obtained by evacuating R/zeolite around 900 K are catalytically active for the hydrogenation of ethene. However, there is a difference in valence state between europium nitride and ytterbium nitride; the former is divalent, while the latter is trivalent.

### 3. Catalysis of rare-earth metal overlayers or bimetallic compounds

#### 3.1. Catalysis of R-Co and R-Ni

##### 3.1.1. Hydrogenolysis of alkanes

Co and Ni are normally active for the hydrogenolysis of alkanes, whereas Eu and Yb metal powders prepared by the metal vapor technique are not active under similar reaction

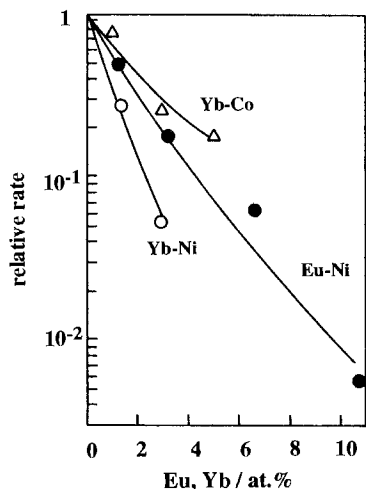


Fig. 5. Relative rates of ethane hydrogenolysis (473 K) *vs.* R content (at.%) in R-Co and R-Ni.

conditions. The hydrogenolysis activity of ethane shows a tendency to decrease with increasing content of rare earths in R-Co (Imamura et al. 1992b) and R-Ni (Imamura et al. 1991d) (fig. 5). Similar kinetic behavior is observed in the hydrogenolysis of cyclohexane. The extent of the decrease in activity is significant even upon addition of small amounts of rare-earth metals. The catalytic activity of 10.6 at.% Eu-Ni is  $\sim 500$  times lower than that seen for pure nickel. The product distribution remains unchanged regardless of alteration in proportion of rare-earth metal introduced; ethane is exclusively decomposed to methane, and cyclohexane undergoes hydrogenolysis to low-molecular-weight alkanes, primarily methane.

As will be discussed later, the continuous decrease in the hydrogenolysis rates is probably due to the rare earth exclusively blocking an active Co and Ni surface atom, resulting in a decrease in the number of specific sites available for structure-sensitive reactions such as alkane rearrangements. If cobalt and nickel are presumed to be active sites for the hydrogenolysis, the behavior is as expected. The Eu- and Yb-containing systems exhibit similar catalytic behavior.

### 3.1.2. Hydrogenation of alkenes

The hydrogenation behavior of the R-Co (Imamura et al. 1992b) and R-Ni (Imamura et al. 1991d) bimetallic catalysts also varies markedly with changes in the content of Eu or Yb (fig. 6). The influence of rare-earth content on the catalytic activity is very different from that observed for the hydrogenolysis reaction described above. Upon the addition of small amounts of rare earths, the hydrogenation activity decreases slightly but it increases conversely for further addition. The dependence of activity on rare-earth content reveals a distinct minimum in the region of 2–4 at.% rare earth and the activity of R-Co and R-Ni increases in the higher-content region. The influence of rare-earth content on the catalytic activity is similarly observed for the hydrogenation of propene and buta-1,3-

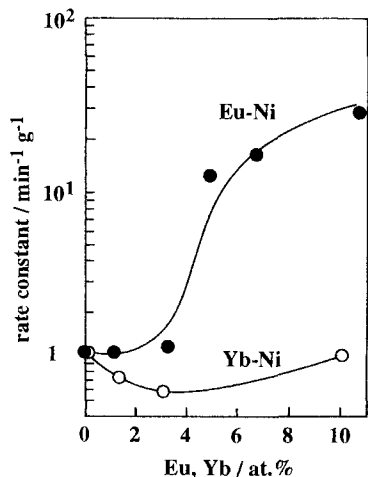


Fig. 6. Rate constant of ethene hydrogenation (213 K) *vs.* R content (at.%) in R-Ni.

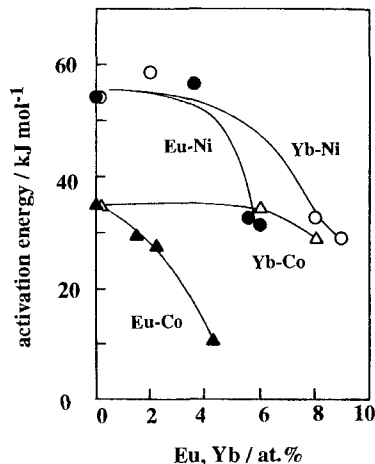


Fig. 7. Effects of rare-earth addition on activation energies for the hydrogenation of ethene.

diene (Imamura et al. 1995c, 1991c). Since rare earths alone shows negligible or very low activity (Imamura et al. 1989b), such a dependence of activity strongly suggests that the existence of some synergetic effects between the rare earth and cobalt (or nickel) metals, rather than the individual component elements, constitutes active sites for the hydrogenation. Comparing both Eu- and Yb-containing systems on the basis of the same atomic fractions of rare-earth metals added, Eu-Co and Eu-Ni show higher activity than Yb-Co and Yb-Ni, respectively.

The rate of hydrogenation is represented by a first-order rate equation with respect to the hydrogen pressure irrespective of the changes of rare-earth content in the catalysts:

$$\text{rate} = r = k \cdot P_{\text{H}}, \quad (8)$$

where  $k$  is the rate constant and  $P_{\text{H}}$  is the pressure of hydrogen. For Eu-Ni and Yb-Ni, the apparent activation energies for ethene hydrogenation vary between 29 and 58 kJ mol<sup>-1</sup> (fig. 7). For the variation in rare-earth content, Arrhenius behavior is observed over the entire temperature range studied (196–253 K). An activation energy of 54 kJ mol<sup>-1</sup> is determined for ethene hydrogenation on Ni. For rare-earth-covered surfaces, the apparent activation energies show a tendency to decrease and fall in the range 29–33 kJ mol<sup>-1</sup> for R-Ni with higher rare-earth content. R-Co shows similar variations in activation energies with varied levels of rare earth (fig. 7). For the Eu-containing system, there is a marked tendency for the activation energy to decrease with increasing rare-earth content.

The rates of hydrogenation increase noticeably with an increase in evacuation temperature of R-Co and R-Ni from 290 to 673 K. For 4.8 at.% Eu-Ni, there is >10<sup>3</sup>-fold increase in activity for changes in temperature between 373 and 673 K.

3.1.3.  $H_2$  adsorption, TPD,  $H_2$ - $D_2$  isotopic exchange, and IR of adsorbed CO

As the rare-earth metals are introduced onto the Co and Ni surface,  $H_2$  chemisorption at first decreases to reach a minimum around 2–4 at.% and increases in the region of higher content (table 5). These results are qualitatively compatible with those obtained for the hydrogenation (fig. 6). The initial decrease in catalytic activity indicates a decrease in the active sites on Co and Ni by surface coverage. This is consistent with the results on the surface composition evaluated by X-ray photoelectron spectroscopy (XPS) (table 6); for Eu–Co and Eu–Ni, the peak intensity ratios of  $Eu_{3d} : Co_{2p}$  (or  $Ni_{2p}$ ) increase proportionally with the addition of Eu to Co (or Ni) (Imamura et al. 1991c,d).

Table 5  
 $H_2$  chemisorption by R–Co and R–Ni

Catalyst	$H_2$ chemisorption ( $\mu\text{mol g}^{-1}$ )	Catalyst	$H_2$ chemisorption ( $\mu\text{mol g}^{-1}$ )
Co	12.9	Ni	37.8
1.2 at.% Eu–Co	10.2	1.2 at.% Eu–Ni	20.0
3.6 at.% Eu–Co	20.7	3.3 at.% Eu–Ni	7.2
8.1 at.% Eu–Co	32.7	6.6 at.% Eu–Ni	25.3
1.3 at.% Yb–Co	6.7	10.6 at.% Eu–Ni	34.5
3.5 at.% Yb–Co	20.0	1.4 at.% Yb–Ni	8.4
7.5 at.% Yb–Co	23.2	3.0 at.% Yb–Ni	8.9
		10.0 at.% Yb–Ni	17.0

Table 6  
Surface composition of Eu–Co and Eu–Ni by XPS

Eu–Co	$Eu_{3d} : Co_{2p}$	Eu–Ni	$Eu_{3d} : Ni_{2p}$
2.8 at.% Eu–Co	3.3	2.0 at.% Eu–Ni	2.0
18.1 at.% Eu–Co	The $Co_{2p}$ peak is not observed within detection limits	3.1 at.% Eu–Ni	5.1
		8.2 at.% Eu–Ni	6.6
		14.8 at.% Eu–Ni	11.2

In TPD for hydrogen, two binding states,  $\beta_1$  and  $\beta_2$  as reported by Christmann et al. (1974) and Volter and Procop (1973), can be discerned on nickel, which occurs at 430 and 510 K, respectively. When small amounts of rare-earth metal are introduced onto Ni, the intensity of the  $H_2$  desorption peak around 430 K decreases (Imamura et al. 1991d). An additional desorption peak at  $\sim 840$  K is observed in the region of high rare-earth content, and this peak increases markedly with increasing proportion of rare earths. The TPD profile of R–Ni with high content shows the alteration in characteristics of hydrogen adsorption.

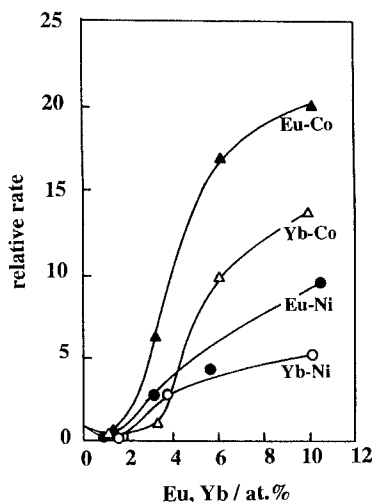


Fig. 8. Relative rates for  $H_2$ - $D_2$  exchange vs. R content (at.%) in R-Co and R-Ni.

The activity of isotopic exchange between  $H_2$  and  $D_2$  as a function of rare-earth content in R-Co and R-Ni (fig. 8) is quite similar to that seen for the hydrogenation of ethene (Imamura et al. 1995b, Imamura and Yoshimura 1994). The apparent activation energies for the exchange reaction also decrease markedly in the high-content region. Certainly the presence of rare-earth metal on Co and Ni strongly influences the state of hydrogen adsorption, resulting in enhanced reactivity to dissociate hydrogen on the surface. Upon the addition of rare-earth metals, the Co and Ni surface is gradually covered and simultaneously certain interactions occur to produce new active centers with improvements of the surface properties, especially in the adsorption characteristics of hydrogen. Thus, R-Co and R-Ni-catalyzed alkene hydrogenation, in which the process involved in the adsorption of hydrogen is a rate-limiting step, is promoted.

CO on Ni/SiO<sub>2</sub> shows two adsorption states, a linear form and a bridge form, which are observed at 2048 and 1972 cm<sup>-1</sup>, respectively (fig. 9). Upon introduction of rare earth onto Ni/SiO<sub>2</sub>, the relative concentration of the bridged CO species decreases much more rapidly than that of the linear ones (Imamura et al. 1992c). The proportions of the linear and bridged forms, the total amount of adsorption and its variations directly reflect changes in the surface composition or structure with changes in the content of rare-earth metals introduced. The decrease in the bridged form also gives an indication that the rare earth covers the active Ni surface, resulting in a relative decrease in the chance of finding an adjacent pair of Ni atoms compared with the chance of finding an isolated Ni atom. The dependence of total absorbance assigned to adsorbed CO on the rare-earth content evidently has a distinct minimum, which is analogous to that observed for the hydrogenation of ethene (fig. 6). In addition, it should be noted that the CO linear bands shift somewhat to higher frequencies with increasing rare-earth content, as shown in fig. 9. IR studies of dinitrogen adsorbed on Eu-Ni/SiO<sub>2</sub> and Yb-Ni/SiO<sub>2</sub> have also been carried out (Imamura et al. 1999b).



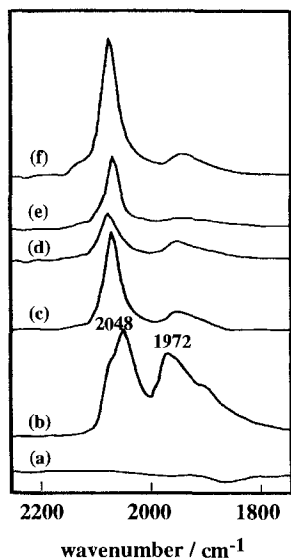


Fig. 9. IR spectra of (a) Eu/SiO<sub>2</sub>, (b) Ni/SiO<sub>2</sub>, (c) Eu-Ni/SiO<sub>2</sub> (Eu/Ni = 0.05), (d) Eu-Ni/SiO<sub>2</sub> (Eu/Ni = 0.11), (e) Eu-Ni/SiO<sub>2</sub> (Eu/Ni = 0.25), and (f) Eu-Ni/SiO<sub>2</sub> (Eu/Ni = 0.67) at room temperature.

#### 3.1.4. Surface features

From the results of H<sub>2</sub> adsorption (Imamura et al. 1992b, 1991d), IR spectra of CO (Imamura et al. 1992c) and XPS (Imamura et al. 1991c,d), inactivation of R-Co and R-Ni in the low-content region is deemed to be a consequence of rare-earth coverage on the catalytically active 3d-transition metal surface. In structure-sensitive reactions, such as alkane rearrangements, a continuous decrease in hydrogenolysis rates is observed (Imamura et al. 1992b, 1991d). In the higher-content region, it is deduced that some synergetic interactions between the rare earth and 3d-transition metals appear; catalytic activation of hydrogen is enhanced, resulting in a marked increase in the specific activity (TOF) of the hydrogenation. Thus the cobalt and nickel metal surface are gradually covered with rare-earth metals and remarkable synergy simultaneously occurs to produce highly active centers for the hydrogenation. For the variation of hydrogenation activity as shown in fig. 6, at least two effects are competitively operative; reduced activity resulting from the coating of catalytically active cobalt or nickel surfaces with rare-earth metals and enhanced activity arising from combined actions of rare-earth and 3d-transition metals. The former effect is pronounced in the low-content region (0–3 at.%) and the latter becomes more prominent than the former in the higher-content region. In particular, the latter effect results in a decrease in activation energies of the hydrogenation with simultaneous drastic changes in the adsorption characteristics of hydrogen, leading to enhanced activity of R-Co (Imamura et al. 1992b) and R-Ni (Imamura et al. 1991d).

The variations in apparent activation energies of hydrogenation from 54 kJ mol<sup>-1</sup> in Ni to 29–33 kJ mol<sup>-1</sup> in 6.0 at.% Eu-Ni or 8.5 at.% Yb-Ni (fig. 7) are discussed in this

connection. If the effect of the adsorption equilibrium on the first-order rate constant  $k$  in eq. (8) is considered,  $k$  is expressed by the following relation:

$$k = k_t \cdot K, \quad (9)$$

where  $k_t$  is the true rate constant and  $K$  is the equilibrium constant of hydrogen. According to the Arrhenius law, the apparent activation energy  $E_a$  associated with  $k$  is expressed as

$$E_a = E_t - q_a, \quad (10)$$

where  $E_t$  denotes the true activation energy and  $q_a$  is the heat of hydrogen adsorption. The rare earth strongly influences the adsorption state of hydrogen with subsequent activation processes and consequently the apparent activation energy  $E_a$  is directly dependent on the magnitude of  $q_a$ . This effect is more pronounced for the catalysts with higher rare-earth content. In comparison between the Eu- and Yb-containing systems, the fact that the hydrogenation activity of the former is usually higher than that of the latter is possibly associated with differences in the decrease of the activation energy. The superiority of Eu-containing systems in activity is similarly observed for the hydrogenation of diene and  $H_2$ - $D_2$  equilibration in which the catalytic activation of hydrogen is important to determine the activity (Imamura et al. 1995b, 1992b, 1991c,d, Imamura and Yoshimura 1994).

If the rare-earth metal exists uniformly on the cobalt and nickel surface, the content of 2–4 at.% rare earth which leads to the minimum activity corresponds to roughly one monolayer coverage of the parent metal particles with Eu or Yb. The more activated R-Co and R-Ni overlayers are those in which the rare earth exists on the cobalt and nickel surface above the amount equivalent to one monolayer. To provide information as to the factors responsible for the dependence of activity on the rare-earth coverage, cobalt and nickel fine particles with different particle sizes (15–28 nm) (produced by a gas-evaporation method; Vacuum Metallurgical Co. Ltd) are used (Imamura et al. 1995c). As shown in the results for R-Ni (fig. 10), the activities ( $k/\text{min}^{-1} \text{ g}^{-1}$ ) increase with decreasing average size of the parent Ni fine particles used, and the level of rare-earth content corresponding to the minimum activity increases with a decrease in the average Ni particle sizes. Eu-Ni with Ni particle size of 19 nm shows promoting effects by introduction of more than ~6 at.% Eu, while for the samples with Ni of 28 nm even introduction above ~2 at.% is sufficient. For R-Co prepared with different particle sizes of Co (15, 21 and 25 nm), similar results are obtained (Imamura et al. 1995c). The content of the rare earth causing the minimum activity also increases with decreasing average size of the Co fine particles as a precursor. An interesting feature is that such variations in activity as a function of proportion of rare earths introduced onto the Co and Ni particles with different average sizes suggest occurrence of nearly uniform coverages of the parent metal surface with Eu or Yb deposited from liquid ammonia solutions. Furthermore, this indicates that the synergy of the R-Co and R-Ni binary systems markedly appears when the surface coverage rises above certain values.

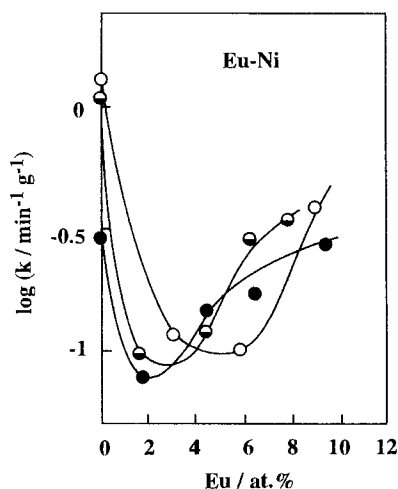


Fig. 10. Effects of particle sizes of Ni precursors on the hydrogenation activity (195 K) of Eu-Ni. Particle sizes: open circles, 19 nm; half-solid circles, 22 nm; solid circles, 28 nm.

It is well known that rare earths combine with the 3d-transition metals to give a large number of alloys and intermetallic compounds, many of which absorb hydrogen copiously (Percheron-Guégan and Welter 1988, Buschow 1984).  $\text{LaNi}_5$  is considered the paradigm among these compounds (van Vucht et al. 1970). Since hydrogen is absorbed dissociatively (Andresen 1978, Kuijpers and Loopstra 1971), the gas must exist, at least fleetingly, as monatomic hydrogen on the surface (Wallace et al. 1978). This indicates that the surfaces of the rare-earth intermetallics are quite active for hydrogen, a feature that has attracted interest in them as active hydrogenation catalysts (Netzer and Bertel 1982, Oyama and Haller 1982, Wallace 1982, Wallace et al. 1980). The remarkable synergy in the region of high rare-earth content may be involved in the formation of a certain surface-alloy layer in analogy with the studies of controlled deposition of rare earths onto single-crystal 3d-substrates reported by Nix et al. (1988) or Andersen et al. (1987, 1988a). To make sure of this, the effect of  $\text{H}_2$  pre-treatment is investigated. It has been shown (Soga et al. 1979, 1977) that for the hydrogenation of alkene over  $\text{RNi}_5$  and  $\text{RCO}_5$ , the catalytic activity of their hydrides is much higher than that seen in the dehydrided state, and that the activity increases with an increase in hydrogen concentration in the hydride. After Eu-Co and Eu-Ni are treated with hydrogen under the same conditions, they are used for the catalytic hydrogenation of propene. As shown in table 7, such a pre-treatment with hydrogen results in an enhancement of activity ( $k'$ ) of Eu-Co and Eu-Ni (Imamura et al. 1995c). When 10.3 at.% Eu-Co and 9.1 at.% Eu-Ni after the  $\text{H}_2$  pre-treatment are subjected to evacuating at 573 K for 1 h, their activities ( $k''$ ) almost return to the original values ( $k$ ) obtained for the untreated catalysts. These facts lead to speculations of the formation of hydrogen-absorbing surface intermetallic phases as a result of interactions between the rare earth and 3d-transition metal, which absorb hydrogen by the  $\text{H}_2$  pre-treatment and desorb the hydrogen by the subsequent evacuation treatment. The effect of the  $\text{H}_2$  pre-treatment on the activity is more pronounced for the R-Co systems

Table 7  
Effects of H<sub>2</sub> pre-treatment on hydrogenation activity of Eu–Co and Eu–Ni<sup>a</sup>

Catalyst	$k/\text{min}^{-1}\text{g}^{-1}$	$k'/\text{min}^{-1}\text{g}^{-1}$ [H <sub>2</sub> treatment <sup>b</sup> ]	$k'/k$	$k''/\text{min}^{-1}\text{g}^{-1}$ [evacuation <sup>c</sup> ]
Co	0.021			
1.3 at.% Eu–Co	0.011	0.45	41	
3.5 at.% Eu–Co	0.0092	0.20	22	
6.5 at.% Eu–Co	0.062	0.78	13	
10.3 at.% Eu–Co	0.078	1.79	23	0.13
Ni	0.13			
3.1 at.% Eu–Ni	0.12	0.25	2.1	
5.9 at.% Eu–Ni	0.090	0.19	2.1	
9.1 at.% Eu–Ni	0.39	3.64	9.3	0.35
12.2 at.% Eu–Ni	0.69	2.65	3.8	

<sup>a</sup> See the text. Reaction temperature: 203 K for Eu–Co and 195 K for Eu–Ni.

<sup>b</sup> Eu–Co and Eu–Ni, previously evacuated at 673 K for 2 h, are exposed to hydrogen (200 Torr) for 1 h at 203 K and at 195 K, respectively.

<sup>c</sup> The catalysts after the H<sub>2</sub> pre-treatment are evacuated at 573 K for 1 h.

than for the R–Ni systems (table 7). This is considered to be due to the fact that R–Co intermetallics has usually lower hydrogen-equilibrium pressures compared with R–Ni intermetallics (Kuijpers 1973) and, hence, under conditions of the same H<sub>2</sub> pre-treatment the concentration of hydrogen taken up by R–Co is probably higher than that of R–Ni.

The remarkable synergy in these binary systems is probably involved in complex effects which consist of electronic and geometric factors. Studies on rare-earth–3d-transition metal intermetallics have made it abundantly clear that there is electron transfer from rare earth to transition metal (Wallace 1973). For Yb/Ni(100), the controlled deposition of rare-earth metal at low coverages can be described as adsorption of Yb on the surface, while at higher coverages a considerable reaction with the Ni substrate is observed (Andersen et al. 1987, 1988a). A  $c(10 \times 2)$  LEED pattern develops, owing to the formation of a specific surface intermetallic compound. Similar behavior has been observed for Nd/Cu(100) with charge transfer from Nd to Cu (Nix et al. 1989, Nix and Lambert 1987). Such interactions are presumed to occur for R–Co and R–Ni with high rare-earth content, which enhances the capacity of this surface to dissociate hydrogen molecules.

R–Co and R–Ni are further characterized by changes in their catalytic properties upon thermal treatment (Imamura et al. 1992b, 1991d). The catalysts are usually used after evacuation at 673 K. The catalytic activity for the hydrogenation and H<sub>2</sub>–D<sub>2</sub> exchange increases  $\sim 10$ – $10^3$  times by treatment between 373 and 673 K (Imamura et al. 1995b, Imamura and Yoshimura 1994). However, this change in evacuation temperature leads to only 1.5-fold increase in H<sub>2</sub> chemisorption of 10.6 at.% Eu–Ni, which does not

correspond to the extent of the increase in activity. The surface areas simultaneously change with evacuation temperature, and then, XPS suggests rearrangement of surface morphology or structure (Imamura et al. 1991e). Thus, it is presumed that the thermal treatment leads to the improvement of catalytic sites with changes in surface structure. For structural studies of Yb/Ni(100) (Andersen et al. 1988a, 1987) and Nd/Cu(100) (Nix and Lambert 1987), rare-earth metal deposition at 300 K leads predominantly to the formation of disordered overlayers, whereas an ordered intermetallic surface compound is formed at elevated temperatures. In addition, the overlayer-to-intermetallic transition has been observed for Nd/Cu(111) (Nix et al. 1988), Sm/Cu(100) (Andersen et al. 1988b), and Sm/Cu(111) (Jaffey et al. 1989). If such a surface reconstruction upon the thermal treatment also occurs in the present systems, this seems to have an effect on increasing the activity of R-Co and R-Ni in view of the catalytic properties of the rare-earth-3d intermetallics.

### 3.2. Dehydrogenation of cyclohexane

The variations in activity for the dehydrogenation as a function of Eu or Yb content in R-Ni (fig. 11) are very similar to those for the hydrogenation; the rates of dehydrogenation decrease upon addition of small amounts of rare earth, pass through a minimum at ~4 at.% rare earth and then increase on further addition (4–14 at.%) (Imamura et al. 1993b, 1992d). Cyclohexane is highly selectively dehydrogenated into benzene (~100%) regardless of alteration in proportion of rare-earth metals added. On the whole, R-Co and R-Ni exhibit a similar behavior in the composition range investigated, but the activity of Yb-containing systems is generally higher than that of Eu-containing systems. The dehydrogenation activity also increases noticeably with increasing evacuation temperature of the catalysts from 373 to 673 K. For 10.0 at.% Yb-Ni, there is a ~500-fold increase in the activity in this temperature range.

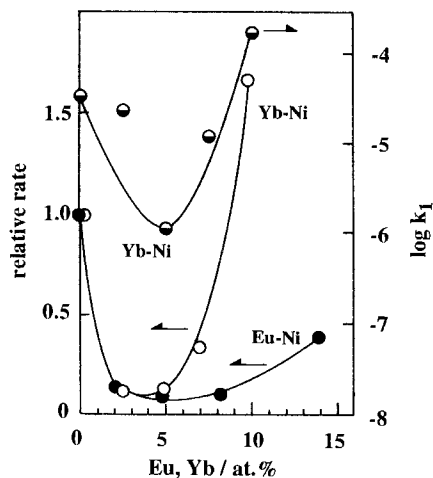
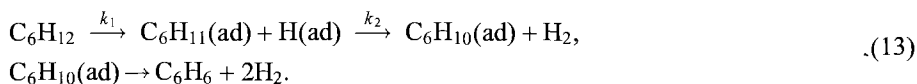


Fig. 11. Relative rates and rate constant ( $k_1$ ) of cyclohexane dehydrogenation (473 K) vs. R content (at.%) in R-Ni.

In a study of the kinetics of the dehydrogenation of cyclohexane over R-Ni, the reaction rates are represented by a rate law of the following form, irrespective of rare-earth content:

$$r = \frac{k_1 P_c}{1 + (k_1/k_2) P_c}, \quad \frac{1}{r} = \frac{1}{k_1 P_c} + \frac{1}{k_2}, \quad (11, 12)$$

where  $P_c$  is the pressure of cyclohexane, and  $k_1$  and  $k_2$  are constants. This rate expression is also found to be applicable for other catalyst systems for cycloalkane dehydrogenation (Hishida et al. 1970), in which  $k_1$  stands for the rate constant of the first hydrogen abstraction and  $k_2$  for that of the second one. A general mechanism of dehydrogenation is indicated by Sinfelt (1970), involving consecutive reaction steps in the reaction sequence



The active catalysts are those in which the first hydrogen atom can be abstracted easily (Fujii et al. 1991, Hishida et al. 1970). The rate constant  $k_1$  obtained from eq. (12) increases with increasing content of rare earths (4–14 at.%) in Yb-Ni (fig. 11) and the surface of Yb-Ni with high rare-earth coverage is found to be more activated.

Apparent activation energies for the dehydrogenation vary between 70 and 83 kJ mol<sup>-1</sup> for R-Ni. An activation energy of 83 kJ mol<sup>-1</sup> is obtained for pure Ni, which is close to that observed for nickel-alumina (Balandin 1958). For rare-earth-covered Ni surfaces, the apparent activation energies decrease to 70–71 kJ mol<sup>-1</sup>, particularly for catalysts with high rare-earth content. The decrease in activation energy is more pronounced for Yb-Ni than for Eu-Ni, which is compatible with the results of dehydrogenation rates (fig. 11). Thus, the presence of rare-earth metals on the Co and Ni surface strongly enhances efficiency of the catalytic activation of the C-H bond [involved in rate constant  $k_1$  in eq. (13)] which controls the dehydrogenation reaction. It has been shown (Imamura et al. 1990, 1988b, 1987b) that the rare-earth-3d intermetallic compounds are active as dehydrogenation catalysts.

The variations in activity of C<sub>6</sub>H<sub>12</sub>-D<sub>2</sub> exchange reaction over Eu-Ni and Yb-Ni (fig. 12) are analogous to those observed for the dehydrogenation of cyclohexane. It can be concluded that both reactions proceed through similar intermediates. Usually the rates of adsorption and desorption of the deuterium and hydrogen deuteride are certainly rapid compared with the corresponding rates for the hydrocarbons; thus, the rates of exchange are limited by the adsorption or subsequent dissociation of cyclohexane. This indicates that the presence of rare earth on the Ni surface leads to acceleration of these processes. Table 8 shows the initial distributions of deuteriocyclohexanes found for Eu-Ni and Yb-Ni with varied levels of rare earths. The effect of rare earths on the isotopic distribution patterns of cyclohexane is evident, in particular at higher content. The isotopic exchange patterns on Ni exhibit a minimum between d<sub>3</sub> and d<sub>7</sub> species and a maximum at d<sub>1</sub>-d<sub>2</sub> and d<sub>8</sub>-d<sub>12</sub> species. R-Ni with low rare-earth content (2.1 and 2.5 at.%) shows

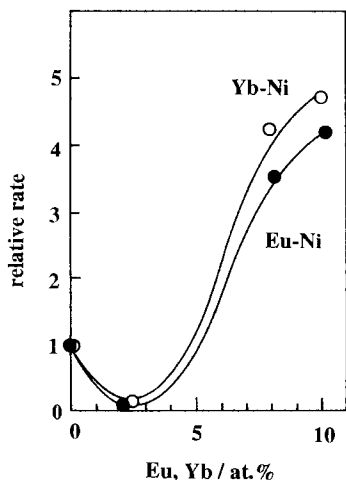


Fig. 12. Relative rates of  $C_6H_{12}-D_2$  exchange (473 K) vs. R content (at.%) in R-Ni.

Table 8  
Initial distribution of deuteriocyclohexane obtained by  $C_6H_{12}-D_2$  exchange reaction

Catalyst	Deuteriocyclohexane (%)											
	d <sub>1</sub>	d <sub>2</sub>	d <sub>3</sub>	d <sub>4</sub>	d <sub>5</sub>	d <sub>6</sub>	d <sub>7</sub>	d <sub>8</sub>	d <sub>9</sub>	d <sub>10</sub>	d <sub>11</sub>	d <sub>12</sub>
Ni	26	1	—	—	—	—	—	2	6	16	25	24
2.1 at.% Eu-Ni	50	—	—	—	—	—	—	—	8	17	17	8
8.2 at.% Eu-Ni	50	34	11	5	—	—	—	—	—	—	—	—
10.2 at.% Eu-Ni	70	23	7	—	—	—	—	—	—	—	—	—
2.5 at.% Yb-Ni	56	7	—	—	—	—	—	—	—	7	15	15
8.0 at.% Yb-Ni	68	24	8	—	—	—	—	—	—	—	—	—
10.0 at.% Yb-Ni	48	37	12	2	1	—	—	—	—	—	—	—

distribution patterns similar to pure Ni (Burwell and Tuxworth 1956, Rowlinson et al. 1955), whereas the catalysts with high content (8.0–10.2 at.%) exhibit different patterns. For 10.2 at.% Eu-Ni and 10.0 at.% Yb-Ni, cyclohexane yields deuteriocyclohexanes characterized by a continuous decrease in concentration from d<sub>1</sub> to d<sub>12</sub> species; thus, increasing content of rare-earth metals on Ni leads to less multiple exchange. Since the multiple exchange requires a free site adjacent to the site or sites by which a hydrocarbon molecule is bound to the surface (Hegarty and Rooney 1989), the geometric discussions of rare earths introduced on the Co and Ni surface (as described in sect. 3.1.4) apply for such variations in isotopic distribution.

### 3.3. *Catalysis of R-Pd/SiO<sub>2</sub> with considerable hydrogen uptake*

Upon introduction of the rare-earth metal onto the Pd surface, the hydrogenation behavior of propene is markedly changed, and the following catalytic features are observed (Imamura et al. 1996b, 1994):

- (1) Considerable hydrogen uptake by the catalyst during the initial step.
- (2) Rapid hydrogenation using hydrogen taken up by the catalyst.
- (3) Supported R-Pd catalysts are effective; unsupported ones are not.
- (4) Hydrogen uptake occurs only in the presence of propene.

When Yb-Pd/SiO<sub>2</sub> (0.042 g; Yb/Pd=0.43) is brought into contact with mixed gases of propene (35 Torr) and hydrogen (35 Torr) at 193 K, the catalyst shows rapid hydrogen uptake over a period of ~10 min at the start of the reaction, followed by the hydrogenation of propene (fig. 13). No reaction of propene with hydrogen is observed during the initial hydrogen uptake; there is an obvious induction period for the hydrogenation. As shown in fig. 13, the catalyst absorbs at least 0.115 mmol of hydrogen and all the hydrogen taken up by the catalyst is consumed to hydrogenate efficiently propene. Thus, the R-Pd/SiO<sub>2</sub> bimetallic system is an interesting example of synergism involved in the enhancement of the ability to take up reactive hydrogen species and to hydrogenate propene using them.

It has been shown that Pd catalysts simultaneously absorb hydrogen during the reactions in which hydrogen participates (Palczewska 1975). However, XRD of Yb-Pd/SiO<sub>2</sub> after the hydrogen uptake shows no indication of PdH. The amounts (0.115 mmol) of hydrogen species taken up by Yb-Pd/SiO<sub>2</sub> exceed those corresponding to stoichiometric palladium hydride (PdH) by about 12-fold. Even if hydrogen is fleetingly absorbed in the Pd metal, the absorbed hydrogen is so stable under these reaction conditions (Lewis 1967) that it cannot thermodynamically desorb to react rapidly with propene as shown in fig. 13. Consequently, no absorption of hydrogen by palladium as an acceptor site is expected. The rare-earth component present on the catalyst can also absorb hydrogen to form more stable metal hydrides (YbH<sub>2</sub> and YbH<sub>3</sub>) (Libowitz and Maeland 1979), but the circumstances are similar for the rare earth. When unsupported Yb-Pd is examined, substantial uptake of hydrogen by the catalyst occurs during the reaction (fig. 14). However, such hydrogen all exists in the form of palladium hydride, and hence is too stable to react with propene, as opposed to the results observed for the supported R-Pd/SiO<sub>2</sub>. Some questions still remain as to which sites accept the hydrogen in (or on) R-Pd/SiO<sub>2</sub>. In supported catalyst systems, the support materials (SiO<sub>2</sub>, Al<sub>2</sub>O<sub>3</sub>, ZrO<sub>2</sub>, MgO and TiO<sub>2</sub>), Pd particle sizes and Pd dispersion have been found to be important factors in determining the hydrogen uptake and the resulting catalytic behavior (Imamura et al. 1996b).

A very important feature of the R-Pd catalyst system is that there is no indication of hydrogen uptake by the catalyst even when R-Pd/SiO<sub>2</sub> is brought into contact with only hydrogen at 193 K. Thus, the hydrogen uptake occurs only in the presence of propene. To determine how the hydrogen uptake is affected by presence of a second gas, two types of reactions differing in sequence of hydrogen and propene addition are carried out. The first reaction consists of exposing Yb-Pd/SiO<sub>2</sub> to hydrogen at 193 K for 30 min, followed by addition of propene (referred to as H<sub>2</sub> → C<sub>3</sub>H<sub>6</sub>). The addition of propene results in



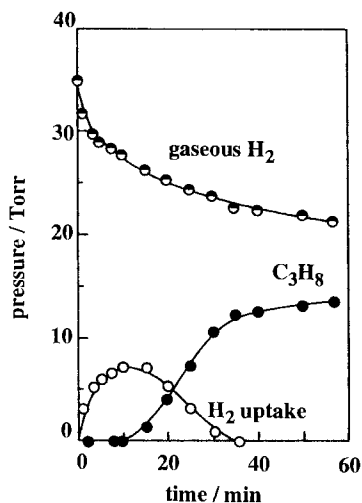


Fig. 13. Hydrogenation of propene (193 K) over Yb-Pd/SiO<sub>2</sub> (Yb/Pd = 0.43).

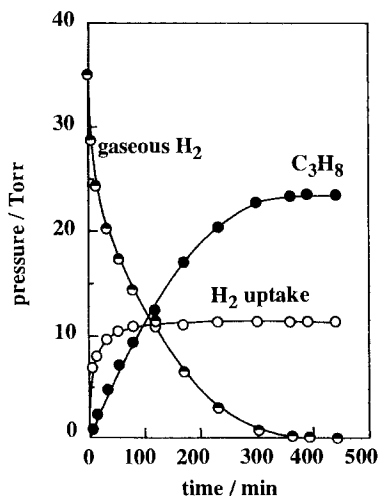


Fig. 14. Hydrogenation of propene (193 K) over unsupported Yb-Pd (Yb/Pd = 0.03).

rapid hydrogen uptake with subsequent hydrogenation, which is very similar to the results shown in fig. 13. It is to be expected that the adsorbed propene plays an important role in the rapid initiation of hydrogen uptake, in which a phenomenon similar to spillover may exist (Conner et al. 1986). Perylene in Pt black/Ce-Y-zeolite is characterized as bridges between the Pt black and zeolite of the catalyst to facilitate hydrogen migration (Neikam and Vannice 1972, Vannice and Neikam 1971). The hydrogenation kinetics shows a negative dependence on the hydrogen pressure and a positive dependence on the propene pressure. In a second reaction, propene is circulated over the catalyst at 193 K for 30 min and then hydrogen is added into the circulating propene ( $C_3H_6 \rightarrow H_2$ ). The induction period almost disappears and immediately the hydrogenation of propene occurs without hydrogen uptake. The kinetic behavior is obviously different from that for the ( $H_2 \rightarrow C_3H_6$ ) run; the rate is approximately proportional to the first power of the pressure of hydrogen and independent of the propene pressure (Bond 1962).

Upon addition of hydrogen and subsequent propene, rapid hydrogen uptake occurs but not in the reverse order; the sites for hydrogen uptake are formed in the presence of both hydrogen and propene. In the ( $H_2 \rightarrow C_3H_6$ ) run, the active sites for hydrogenation are probably formed by the adsorption of propene on vacant sites of the catalyst surface mostly covered with hydrogen; therefore an induction period is required to a certain extent to form such catalytically active sites. Once such active sites are formed, the hydrogen uptake and subsequent hydrogenation process are rapid, in which phenomena similar to spillover may be contained. Similar hydrogenation behavior is observed even when ethene, butene or buta-1,3-diene is used instead of propene. From extensive kinetic studies, it is concluded that the hydrogenation over R-Pd/SiO<sub>2</sub> is by a rate-limited hydrogen uptake

and that the hydrogenation proceeds exclusively using the hydrogen taken up by the catalyst.

### 3.4. Catalytic transfer hydrogenation with ammonia

The use of liquid ammonia solutions of Eu or Yb enables the preparation of active catalysts for transfer hydrogenation in which ammonia is a preferred hydrogen donor. Catalytic transfer hydrogenation using hydrogen donors shows some interesting features which are of potential synthetic importance and use (Johnstone and Wilby 1985, Hartner 1980, Brieger and Nestrick 1974, Furst et al. 1965).

R-Ni/SiO<sub>2</sub>, R-Ru/C, R-Cu/SiO<sub>2</sub> and R-Ag/ZrO<sub>2</sub> are active for catalytic hydrogen transfer from ammonia to organic acceptors (ethene and buta-1,3-diene) (Imamura et al. 1996c). Time courses of the reaction on Eu-Ni/SiO<sub>2</sub> (Eu/Ni=0.72) are shown in fig. 15, where the hydrogenation of ethene occurs effectively with ammonia as a source of hydrogen. As ammonia is consumed during the hydrogenation, nitrogen is stoichiometrically released and hydrogen is scarcely detected in the gas-phase. Thus, the reaction follows the stoichiometrical relationships:  $3\text{C}_2\text{H}_4 + 2\text{NH}_3 \rightarrow 3\text{C}_2\text{H}_6 + \text{N}_2$ . The hydrogenation activity varies markedly with rare-earth content in R-Ni/SiO<sub>2</sub>. Particularly at high levels of europium, Eu-Ni/SiO<sub>2</sub> is activated and its activity increases  $\geq 10$ -fold relative to Ni/SiO<sub>2</sub>. R-Ru/C shows behavior similar to R-Ni/SiO<sub>2</sub>.

Substrate selectivity by catalysts is also observed in this transfer hydrogenation. R-Ni/SiO<sub>2</sub>, R-Ru/C and R-Cu/SiO<sub>2</sub> show activity for the hydrogenation of ethene and buta-1,3-diene, while R-Ag/ZrO<sub>2</sub> is active for buta-1,3-diene but not for ethene. The Eu-Ni/SiO<sub>2</sub> (Eu/Ni = 0.61)-catalyzed buta-1,3-diene hydrogenation yields preferential butene formation with  $\sim 100\%$  selectivity. The yield of but-2-ene is relatively high compared with but-1-ene, and the *trans*:*cis* ratio in the but-2-ene isomer is low ( $\sim 2$ ). This is strikingly different from the results with Ni/SiO<sub>2</sub> or R/SiO<sub>2</sub> alone. Moreover, the product composition differs from that for normal hydrogenation using hydrogen.

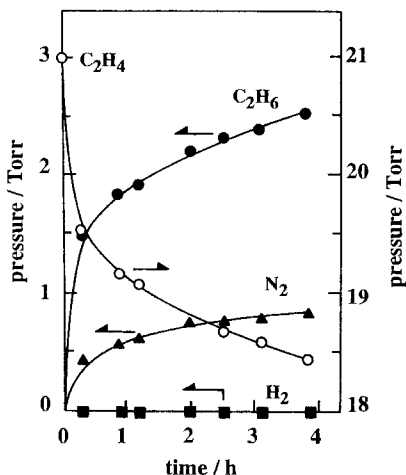


Fig. 15. Transfer hydrogenation of ethene (403 K) from ammonia over Eu-Ni/SiO<sub>2</sub> (Eu/Ni=0.72).

In the transfer hydrogenation on Eu–Ni/SiO<sub>2</sub> (fig. 15), hydrogen is scarcely detected in the gas phase throughout the reaction; thus, the preferential addition processes of hydrogen to the acceptor molecules occur immediately before coupling with subsequent liberation of hydrogen gas. In the absence of acceptors, ammonia remains unchanged at 403 K, and upon introduction of ethene into the reaction system, the transfer hydrogenation from ammonia is initiated. For Eu–Ni/SiO<sub>2</sub> and Yb–Ni/SiO<sub>2</sub>, normal hydrogenation of ethene with molecular hydrogen readily occurs under similar conditions (Imamura et al. 1991d, 1989a). Therefore, the participation of the donor in the hydrogen transfer step rather than the dehydrogenation of the donor and the hydrogen addition to the acceptor is an important factor in determining the activity of the transfer hydrogenation over R–Ni/SiO<sub>2</sub>. In view of isotopic effects observed when NH<sub>3</sub>/C<sub>2</sub>H<sub>4</sub>, ND<sub>3</sub>/C<sub>2</sub>H<sub>4</sub> and NH<sub>3</sub>/C<sub>2</sub>D<sub>4</sub> are used, the transfer hydrogenation proceeds by concerted hydrogen transfer between ethene and ammonia over the catalysts.

#### 4. Summary and conclusions

Utilization of homogeneous liquid ammonia solutions enables the preparation of a novel class of rare-earth-containing catalytic materials, especially in low valent states. The rare earths introduced onto (or into) silica, active carbon and zeolite are changed to nitride through variation in their valence states upon thermal treatments and simultaneously the catalytic properties vary markedly. Eu and Yb metal dissolved in liquid ammonia react readily with reduced transition metal (M: Fe, Co, Ni, Cu, Ru, Pd and Ag) to form various R–M binary catalysts. Basically there are no limitations in the combination of metals used, and R–Co, R–Ni and R–Pd are largely dealt with here. R–Cu and R–Ag have been reported elsewhere (Imamura et al. 1996d, 1991e, 1989a). These rare-earth catalysts have been characterized by various techniques (H<sub>2</sub> adsorption, TPD, IR, XRD, XANES and XPS) and by catalytic reactions (hydrogenation, dehydrogenation, transfer hydrogenation, hydrogenolysis, disproportionation, cyclization, H<sub>2</sub>–D<sub>2</sub> exchange and C<sub>6</sub>H<sub>12</sub>–D<sub>2</sub> exchange).

The behavior of rare earths introduced onto SiO<sub>2</sub> varies with the level of rare-earth loading; for low loading, the rare earth is immobilized on SiO<sub>2</sub> as ≡Si–O–R–NH<sub>2</sub>, while the rare earth for high loading exist in a metallic form with high dispersion. The ≡Si–O–R–NH<sub>2</sub> species show selective hydrogenation, especially for benzene and dienes, and R/SiO<sub>2</sub> with high loading shows the specificity for the hydrogenation of alkynes. For R/C, imide or imide-like species formed during the thermal degradation to nitride show catalytic activity for the hydrogenation of alkene and the selective cyclization of alkyne. The valence variation of rare earths with thermal treatments of R/zeolite is monitored by XANES combined with variations in catalysis.

In the rare-earth metal overlays, the introduction of Eu or Yb onto the Co and Ni surface leads to a continuous decrease in hydrogenolysis activity, whereas the activity of hydrogenation, H<sub>2</sub>–D<sub>2</sub> exchange, C<sub>6</sub>H<sub>12</sub>–D<sub>2</sub> exchange and dehydrogenation shows a tendency to increase. A marked decrease in suitably arranged sites with the fractions of

surface covered by the rare earth is involved in the kinetic behavior of hydrogenolysis as structure-sensitive reactions. The presence of rare-earth metals on Co and Ni strongly enhances the capacity of this surface to activate the H–H and C–H bond, resulting in acceleration of the hydrogenation, isotopic exchange and dehydrogenation in which the activation processes of H–H and C–H are important to determine the activity. It is suggested that the reaction of Co and Ni with rare-earth metals dissolved in liquid ammonia leads to the formation of the intermetallic surface phase. The salient features of rare-earth metal overlayers through additional studies of adsorption property, TPD and isotopic reactions are set forth. R–Pd/SiO<sub>2</sub> shows remarkable synergetic effects involving considerable hydrogen uptake during the hydrogenation of alkenes and dienes. Catalytic transfer hydrogenation using ammonia as a hydrogen source is greatly enhanced by R–Ni/SiO<sub>2</sub>, R–Ru/C, R–Cu/SiO<sub>2</sub> and R–Ag/SiO<sub>2</sub> (Imamura et al. 1999c,d).

### Acknowledgments

The author is grateful for financial support to the Ministry of Education, Science and Culture, Government of Japan.

### References

- Andersen, J.N., J. Onsgaard, A. Nilsson, B. Eriksson, E. Zdansky and N. Martensson, 1987, *Surf. Sci.* **189/190**, 399.
- Andersen, J.N., J. Onsgaard, A. Nilsson, B. Eriksson and N. Martensson, 1988a, *Surf. Sci.* **202**, 183.
- Andersen, J.N., I. Chorkendorff, J. Onsgaard, J. Ghijsen, R.L. Johnson and F. Grey, 1988b, *Phys. Rev. B* **37**, 4809.
- Andresen, A.F., 1978, in: *Hydrides for Energy Storage*, eds A.F. Andresen and A.J. Maeland (Pergamon Press, London) p. 61.
- Baba, T., G.J. Kim and Y. Ono, 1992, *J. Chem. Soc. Faraday Trans.* **88**, 891.
- Baba, T., S. Hikita, R. Koide, Y. Ono, T. Hanada, T. Tanaka and S. Yoshida, 1993, *J. Chem. Soc. Faraday Trans.* **89**, 3177.
- Baba, T., S. Hikita, Y. Ono, T. Yoshida, T. Tanaka and S. Yoshida, 1995, *J. Mol. Catal. A* **98**, 49.
- Balandin, A.A., 1958, *Adv. Catal.* **10**, 96.
- Blouri, B., J.A. Zadeh and P. Rumpf, 1968, *C.R. Acad. Sci. Paris Ser. C* **267**, 170.
- Bond, G.C., 1962, *Catalysis by Metals* (Academic Press, London) p. 229.
- Brieger, G., and T.J. Nestruck, 1974, *Chem. Rev.* **74**, 567.
- Brown, L.M., and K.S. Mazdiyasni, 1970, *Inorg. Chem.* **9**, 2783.
- Burwell Jr, R.L., and R.H. Tuxworth, 1956, *J. Phys. Chem.* **60**, 1043.
- Buschow, K.H.J., 1984, in: *Handbook on the Physics and Chemistry of Rare Earths*, Vol. 6, eds K.A. Gschneidner Jr and L. Eyring (North-Holland, Amsterdam) ch. 47, pp. 1–111.
- Christmann, K., O. Schober, G. Ertl and M. Neumann, 1974, *J. Chem. Phys.* **60**, 4528.
- Conner Jr, W.C., G.M. Pajonk and S.J. Teichner, 1986, *Adv. Catal.* **34**, 1.
- Dobson, N.A., G. Eglinton, M. Krishnamurti, R.A. Raphael and R.G. Willis, 1961, *Tetrahedron* **16**, 16.
- Edelmann, F.T., 1996, *Top. Curr. Chem.* **179**, 247.
- Freifelder, M., 1971, *Practical Catalytic Hydrogenation* (Wiley, New York) p. 86.
- Fujii, T., K. Yukawa and Y. Saito, 1991, *Bull. Chem. Soc. Jpn.* **64**, 938.
- Fukuoka, Y., and H. Nagahara, 1991, *Prepr. Am. Chem. Soc. Div. Pet. Chem.* **36**, 5481.
- Furst, A., R.C. Berlo and S. Hooton, 1965, *Chem. Rev.* **65**, 51.

- Galvagno, S., A. Donato, G. Neri, D. Pietropaolo and P. Staiti, 1988, *React. Kinet. Catal. Lett.* **37**, 443.
- Hadenfeldt, C., H. Jacobs and R. Juza, 1970, *Z. Anorg. Allg. Chem.* **379**, 144.
- Hartner, H., 1980, *Kontakte* **1**, 3.
- Hatwar, T.K., R.M. Nayak, B.D. Padalia, M.N. Ghatikar, E.V. Sampathkumaran, L.C. Gupta and R. Vijayaraghavan, 1980, *Solid State Commun.* **34**, 617.
- Hegarty, B.F., and J.J. Rooney, 1989, *J. Chem. Soc. Faraday Trans. I* **85**, 1861.
- Hewkin, D.J., and W.P. Griffith, 1966, *J. Chem. Soc. (A)*, p. 476.
- Hishida, T., T. Uchijima and Y. Yoneda, 1970, *J. Catal.* **17**, 287.
- Hogerheide, M.P., J. Boersma and V.K. Gerard, 1996, *Coord. Chem. Rev.* **155**, 87.
- Howell, K., and L.L. Pytlewski, 1969, *J. Less-Common Met.* **19**, 399.
- Iler, R.K., 1979, *The Chemistry of Silica Solubility, Polymerisation, Colloid and Surface Properties, and Biochemistry* (Wiley, New York).
- Imamoto, T., 1994, *Lanthanides in Organic Synthesis* (Academic Press, London).
- Imamura, H., and K. Yoshimura, 1994, *Z. Phys. Chem.* **183**, 407.
- Imamura, H., A. Ohmura and S. Tsuchiya, 1985, *J. Catal.* **96**, 139.
- Imamura, H., E. Haku and S. Tsuchiya, 1987a, *Lanthanide & Actinide Res.* **2**, 79.
- Imamura, H., K. Nukui, K. Yamada and S. Tsuchiya, 1987b, *J. Chem. Soc. Faraday Trans. I* **83**, 743.
- Imamura, H., K. Kitajima and S. Tsuchiya, 1988a, *Chem. Lett.*, p. 249.
- Imamura, H., S. Kasahara, T. Takada and S. Tsuchiya, 1988b, *J. Chem. Soc. Faraday Trans. I* **84**, 765.
- Imamura, H., T. Mihara, M. Yoshinobu, Y. Sakata and S. Tsuchiya, 1989a, *J. Chem. Soc. Chem. Commun.*, p. 1842.
- Imamura, H., K. Kitajima and S. Tsuchiya, 1989b, *J. Chem. Soc. Faraday Trans. I* **85**, 1647.
- Imamura, H., K. Kitajima, M. Miyoshi and S. Tsuchiya, 1989c, *J. Mol. Catal.* **52**, L25.
- Imamura, H., T. Takada, S. Kasahara and S. Tsuchiya, 1990, *Appl. Catal.* **58**, 165.
- Imamura, H., H. Yoshimochi, Y. Sakata and S. Tsuchiya, 1991a, *J. Mol. Catal.* **66**, L33.
- Imamura, H., T. Konishi, Y. Sakata and S. Tsuchiya, 1991b, *J. Chem. Soc. Chem. Commun.*, p. 1527.
- Imamura, H., M. Yoshinobu and T. Mihara, 1991c, in: *Catalytic Science and Technology*, Vol. 1, eds S. Yoshida, N. Takezawa and T. Ono (Kodansha, Tokyo) pp. 279–284.
- Imamura, H., K. Yoshimura, S. Hiranaka, Y. Sakata and S. Tsuchiya, 1991d, *J. Chem. Soc. Faraday Trans.* **87**, 2805.
- Imamura, H., M. Yoshinobu, T. Mihara, Y. Sakata and S. Tsuchiya, 1991e, *J. Mol. Catal.* **69**, 271.
- Imamura, H., T. Konishi, Y. Sakata and S. Tsuchiya, 1992a, *J. Chem. Soc. Faraday Trans.* **88**, 2251.
- Imamura, H., S. Hiranaka, M. Takamoto, Y. Sakata and S. Tsuchiya, 1992b, *J. Mol. Catal.* **77**, 333.
- Imamura, H., H. Sugimoto, Y. Sakata and S. Tsuchiya, 1992c, *J. Catal.* **136**, 271.
- Imamura, H., S. Hiranaka, Y. Sakata and S. Tsuchiya, 1992d, *J. Chem. Soc. Faraday Trans.* **88**, 1577.
- Imamura, H., T. Konishi, Y. Tokunaga, Y. Sakata and S. Tsuchiya, 1992e, *Bull. Chem. Soc. Jpn.* **65**, 244.
- Imamura, H., T. Konishi, Y. Sakata and S. Tsuchiya, 1993a, *J. Chem. Soc. Chem. Commun.*, p. 1852.
- Imamura, H., S. Hiranaka, Y. Sakata and S. Tsuchiya, 1993b, *Nippon Kagaku Kaishi*, p. 507.
- Imamura, H., K. Igawa, Y. Kasuga, Y. Sakata and S. Tsuchiya, 1994, *J. Chem. Soc. Faraday Trans.* **90**, 2119.
- Imamura, H., E. Suda, T. Konishi, Y. Sakata and S. Tsuchiya, 1995a, *Chem. Lett.*, p. 215.
- Imamura, H., Y. Kasuga and K. Yoshimura, 1995b, *J. Alloys & Compounds* **231**, 824.
- Imamura, H., Y. Kasuga, K. Abe, Y. Sakata and S. Tsuchiya, 1995c, *Catal. Lett.* **32**, 115.
- Imamura, H., T. Konishi, E. Suda, Y. Sakata and S. Tsuchiya, 1996a, *Bull. Chem. Soc. Jpn.* **69**, 77.
- Imamura, H., K. Igawa, Y. Sakata and S. Tsuchiya, 1996b, *Bull. Chem. Soc. Jpn.* **69**, 325.
- Imamura, H., K. Fujita, Y. Miura, K. Mizuno, Y. Sakata and S. Tsuchiya, 1996c, *Chem. Commun.*, p. 1842.
- Imamura, H., K. Fujita, Y. Sakata and S. Tsuchiya, 1996d, *Catal. Today* **28**, 231.
- Imamura, H., T. Sakamoto, T. Matsuoka, Y. Sakata and S. Tsuchiya, 1999a, *Mater. Sci. Forum* **315–317**, 471.
- Imamura, H., Y. Sakata, Y. Kasuga and S. Tsuchiya, 1999b, *Catal. Lett.* **58**, 179.
- Imamura, H., Y. Miura, K. Fujita, Y. Sakata and S. Tsuchiya, 1999c, *J. Mol. Catal. A* **140**, 81.
- Imamura, H., T. Sakamoto, M. Ichikawa, Y. Sakata and S. Tsuchiya, 1999d, *J. Jpn. Pet. Inst.* **42**, 359.
- Inumaru, K., and M. Misono, 1995, *Shokubai (Catalyst)* **37**, 198.

- Jaffey, D.M., A.J. Gellman and R.M. Lambert, 1989, *Surf. Sci.* **214**, 407.
- Johnstone, R.A.W., and A.H. Wilby, 1985, *Chem. Rev.* **85**, 129.
- Juza, R., and C. Hadenfeldt, 1968, *Naturwissenschaften* **55**, 229.
- Konishi, T., E. Suda and H. Imamura, 1995, *J. Alloys & Compounds* **225**, 629.
- Kritzenberger, J., E. Jobson, A. Wokaun and A. Baiker, 1990, *Catal. Lett.* **5**, 73.
- Kuijpers, F.A., 1973, *Philips Res. Rep. Suppl.* **2**.
- Kuijpers, F.A., and B.A. Loopstra, 1971, *J. Phys. Paris Suppl.* **32**, C1-657.
- Lewis, F.A., 1967, *The Palladium Hydrogen System* (Academic Press, London).
- Libowitz, G.G., and A.J. Maeland, 1979, in: *Handbook on the Physics and Chemistry of Rare Earths*, Vol. 3, eds K.A. Gschneidner Jr and L. Eyring (North-Holland, Amsterdam) ch. 26, pp. 299–336.
- Linde, V.G., and R. Juza, 1974, *Z. Anorg. Allg. Chem.* **409**, 199.
- Mehrotra, R.C., and J.M. Batwara, 1970, *Inorg. Chem.* **9**, 2505.
- Neikam, W.C., and M.A. Vannice, 1972, *J. Catal.* **27**, 207.
- Netzer, F.P., and E. Bertel, 1982, in: *Handbook on the Physics and Chemistry of Rare Earths*, Vol. 5, eds K.A. Gschneidner Jr and L. Eyring (North-Holland, Amsterdam) ch. 43, pp. 217–320.
- Niwa, S., F. Mizukami, M. Toba, T. Murakami and M. Ueda, 1990, *Nippon Kagaku Kaishi*, p. 284.
- Nix, R.M., and R.M. Lambert, 1987, *Surf. Sci.* **186**, 163.
- Nix, R.M., R.W. Judd and R.M. Lambert, 1988, *Surf. Sci.* **203**, 307.
- Nix, R.M., R.W. Judd and R.M. Lambert, 1989, *Surf. Sci.* **215**, L316.
- Oyama, S.T., and G.L. Haller, 1982, *Catalysis (Specialist Periodical Report)*, Vol. 5 (The Chemical Society, London) pp. 333–365.
- Palczewska, W., 1975, *Adv. Catal.* **25**, 245.
- Percheron-Guégan, A., and J.-M. Welter, 1988, in: *Topics in Applied Physics*, Vol. 63, ed. L. Schlapbach (Springer, Berlin) pp. 11–48.
- Petrov, A.A., and M.P. Forost, 1964, *J. Gen. Chem. USSR* **34**, 3331.
- Prabhawalkar, V., and B.D. Padalia, 1983, *Curr. Sci.* **52**, 799.
- Rao, C.N.R., D.D. Sarma, P.R. Sarode, E.V. Sam-pathkumaran, L.C. Gupta and R. Vijayaraghavan, 1980, *Chem. Phys. Lett.* **76**, 413.
- Ross, S.D., 1972, *Inorganic Infrared and Raman Spectra* (McGraw-Hill, New York).
- Rowlinson, H.C., R.L. Burwell Jr and R.H. Tuxworth, 1955, *J. Phys. Chem.* **59**, 225.
- Sakai, M., T. Kimura, T. Nakaoka, Y. Sakakibara and N. Uchino, 1985, *Bull. Chem. Soc. Jpn.* **58**, 505.
- Salot, S., and J.C. Warf, 1968, *J. Am. Chem. Soc.* **90**, 1932.
- Sinfelt, J.H., 1970, *Ind. Eng. Chem.* **62**, 66.
- Soga, K., H. Imamura and S. Ikeda, 1977, *J. Phys. Chem.* **81**, 1762.
- Soga, K., H. Imamura and S. Ikeda, 1979, *J. Catal.* **56**, 119.
- Struijk, J., M. D'Angremond, W.J.M. Lucas-De Regt and J.J.F. Scholten, 1992, *Appl. Catal.* **83**, 263.
- Tanaka, T., T. Hanada, S. Yoshida, T. Baba and Y. Ono, 1993, *Jpn. J. Appl. Phys.* **32**, 481.
- Tanaka, T., T. Yoshida, S. Yoshida, T. Baba and Y. Ono, 1995, *Physica B* **208&209**, 687.
- Taube, R., 1995, *Macromol. Symp.* **89**, 393.
- Thompson, D.S., E.E. Hazen and J.S. Waugh, 1966, *J. Chem. Phys.* **44**, 2954.
- Thompson, J.C., 1976, *Electrons in Liquid Ammonia* (Clarendon Press, Oxford).
- van Vucht, J.H.N., F.A. Kuijpers and H.C.A.M. Bruning, 1970, *Philips Res. Rep.* **25**, 133.
- Vannice, M.A., and W.C. Neikam, 1971, *J. Catal.* **20**, 260.
- Volter, J., and M. Procop, 1973, *Z. Phys. Chem. Leipzig* **253**, 33; **249**, 344.
- Voort, P.V.D., I. Gillis-D'Hamers and E.F. Vansant, 1990, *J. Chem. Soc. Faraday Trans.* **86**, 3751.
- Wallace, W.E., 1973, *Rare Earth Intermetallics* (Academic Press, New York).
- Wallace, W.E., 1982, *Chemtech*, p. 752.
- Wallace, W.E., R.F. Karlcek Jr and H. Imamura, 1978, *J. Phys. Chem.* **83**, 972.
- Wallace, W.E., A. Elattar, H. Imamura, R.S. Craig and A.G. Moldvan, 1980, in: *The Science and Technology of Rare Earth Materials*, eds W.E. Wallace and E.C. Subbarao (Academic Press, New York) pp. 329–351.
- Warf, J.C., and V. Gutmann, 1971, *J. Inorg. Nucl. Chem.* **33**, 1583.
- Yasuda, H., 1995, *Shokubai (Catalyst)* **37**, 205.
- Zhuravlev, L.T., 1987, *Langmuir* **3**, 316.

## Chapter 183

### THE MIXED OXIDES

M.A. ULLA and E.A. LOMBARDO

*INCAPE (FIQ, UNL-CONICET), Santiago del Estero 2829,  
 (3000) Santa Fe, Argentina*

---

#### Contents

Introduction	75	2.4. Hydrogenation	106
1. Rare-earth-containing mixed oxides	76	2.4.1. Hydrogenation and hydrogenolysis of hydrocarbons	106
1.1. Structure	76	2.4.2. CO <sub>x</sub> hydrogenation and hydroformylation of ethylene	107
1.1.1. Perovskites (ABO <sub>3</sub> )	76	2.5. Environmental catalysis	114
1.1.2. Perovskite-related structures	77	2.5.1. Catalytic combustion	114
1.1.3. Other structures	77	2.5.1.1. ABO <sub>3</sub> -type perovskites	115
1.2. Preparation and characterization of mixed oxides	77	2.5.1.2. Effect of A-site partial substitution	117
1.2.1. Preparation of massive perovskites	78	2.5.1.3. Effect of A- and B-site partial substitution	119
1.2.2. Preparation of supported mixed oxides	78	2.5.1.4. Surface composition	123
1.2.3. Support stabilization	83	2.5.1.5. High-temperature combustion catalysts	124
1.3. Reducibility of perovskite-type mixed oxides	83	2.5.2. CO oxidation	129
1.3.1. Bulk reduction	83	2.5.3. NO and N <sub>2</sub> O decomposition	132
1.3.2. Surface reduction	85	2.5.4. NO reduction	140
1.4. Oxygen sorption	86	2.6. Miscellaneous reactions	145
2. Applications in heterogeneous catalysis	90	2.7. Future trends	150
2.1. Partial oxidation	90	3. Other catalytic applications	151
2.2. partial oxidation of methane to synthesis gas (syngas)	92	3.1. Photocatalysis	151
2.2.1. Membrane reactors	95	3.2. Electrocatalysis	152
2.3. Oxidative coupling of methane	97	3.3. Gas sensors	153
2.3.1. Alkali promotion	101	Acknowledgments	154
2.3.2. Membrane reactors	104	References	154

---

#### Introduction

Rare-earth-containing mixed oxides are widely used in many engineering, electromagnetic and electronic applications. Among these materials, perovskite-type oxides with the general formula ABO<sub>3</sub> are the most widely studied. One important driving force is the

ability of these oxides to accommodate a large variety of A and B cations with basically the same crystalline structure. This series of isomorphous solids exhibits a wide range of electric, magnetic, optic and catalytic properties which are readily applied in various commercial devices.

A concise, illustrative description of the chronological development of perovskite catalysis since 1952 is provided in the review of Tejuca et al. (1989).

The rare-earth-containing mixed oxides commonly used in catalytic applications will be presented in the first section of this chapter. In the second section, the applications to different types of reactions will be described, making cross-references among them. The final section will provide a general overview of other miscellaneous applications connected to their catalytic properties such as photocatalysis, electrocatalysis and gas sensors.

## 1. Rare-earth-containing mixed oxides

The most often found types of mixed oxides are: perovskites ( $\text{RBO}_3$ ),  $\text{K}_2\text{NiF}_4$ -type oxides ( $\text{R}_2\text{BO}_4$ ),  $\text{R}_{n+1}\text{B}_n\text{O}_{2n+1}$  ( $n=2$  or  $3$ ), lamellar perovskites, pyrochlores, spinels, and oxide solid solutions. Perovskite oxides are, by far, the most commonly used oxides. Therefore, this chapter will reflect this situation by putting more emphasis on this type of materials. Within this section the structure, preparation methods and general characteristics of the mixed oxides will be discussed. Note that R stands for rare-earth elements while A includes all types of elements.

### 1.1. Structure

#### 1.1.1. Perovskites ( $\text{ABO}_3$ )

The ideal perovskite structure is cubic, with the B (smaller cation) in six-fold coordination and the A (larger cation) in twelve-fold coordination with the oxygens. Although there are some limits regarding the size of the cations that can fit the structure, they are wide enough as to allow the incorporation of a large variety of elements. Typical A elements are rare earths, alkalines and alkaline earths, while the B sites are usually occupied by transition metals.

The tolerance factor ( $t$ ), introduced by Goldschmidt (1926) is used to define the range of ionic radii of the A, B and X elements allowed by the perovskite structure:

$$t = \frac{r_A + r_X}{\sqrt{2}(r_B + r_X)},$$

where  $r_X \equiv r_o$  in the case of perovskite-type oxides;  $t=1$  for the ideal cubic structure.  $0.75 \leq t < 1.0$  are the allowed limits for obtaining a perovskite structure. As  $t$  becomes smaller within this range, the lattice becomes distorted (rhombohedral, orthorhombic, tetragonal, etc.). For the perovskite structure to exist other constraints apply, such as minimum cation radii, stability of the elements in six- and twelve-fold coordination, etc.



Both anion and cation vacancies occur in perovskite structures. The former are more common than the latter. Vacancies are assimilated into the structure resulting in supercells of the basic network. Anion excess has been reported in several systems. A cation vacancies occur more often than B vacancies. This is due to the inherent stability of the  $\text{BO}_3$  groups that permit the absence of numerous A cations without collapse of the crystalline network. B-site vacancies are not energetically favored, and the few cases of B-cation vacancies reported in the literature occur in hexagonal perovskites. Rao et al. (1984) cover in detail numerous examples of anion vacancies and excess as well as A- and B-cation vacancies. Other reviews, books and book chapters have been published containing valuable structural information on these materials. The reader is referred to Galasso (1969), Goodenough and Longo (1970), Wells (1984) and Baran (1990), among others, for a deeper coverage of this subject.

These mixed oxides allow the introduction of a large variety of cations within the same structure to study their effect upon the catalytic behavior. This feature is particularly useful both in practical and fundamental catalytic studies. This is why many articles and several books have been published on perovskite catalysis.

#### 1.1.2. *Perovskite-related structures*

The  $\text{K}_2\text{NiF}_4$  structure ( $\text{A}_2\text{BO}_4$ ) is favored for some cation combinations, e.g.,  $\text{La}_2\text{NiO}_4$ , or obtained by mild reduction of the  $\text{ABO}_3$  oxide, e.g.,  $\text{La}_2\text{CoO}_4$  from  $\text{LaCoO}_3$ . This structure is made up of perovskite layers separated by AO layers of the rock salt type in a 1:1 ratio. There are other structures in which the proportion is  $n:1$ . With  $n=2$  one obtains  $\text{A}_3\text{B}_2\text{O}_7$ , and  $n=3$  yields  $\text{A}_4\text{B}_3\text{O}_{10}$  (3 perovskite + 1 rock salt layers).

Lamellar perovskites of the general formula  $\text{M}^{\text{I}}(\text{A}_{n-1}\text{B}_n\text{O}_{3n+1})$  are also known and have been tried as catalysts for reactions such as oxidative coupling of methane. [Barrault et al. (1992)]. One example of this type is  $\text{CsCa}_2\text{Nb}_3\text{O}_{10}$  which consists of blocks built up from three perovskite layers interleaved with  $\text{Cs}^+$  cations. Other perovskite-related structures have been discussed by Baran (1990).

#### 1.1.3. *Other structures*

There are a few catalytic applications in which other mixed oxide structures are cited. Among them are pyrochlore compounds such as  $\text{La}_2\text{Zr}_2\text{O}_7$ , spinels such as  $\text{AB}_2\text{O}_4$ , and lanthanum beta aluminates, all of them with well-defined crystalline structures. There are also a few examples of oxide solid solutions made up of a rare-earth oxide and a transition-metal oxide.

#### 1.2. *Preparation and characterization of mixed oxides*

This section will again focus on perovskites with references to the preparation of other mixed oxides. Note, however, that several methods described for perovskite synthesis may be applied to other solids.

### 1.2.1. *Preparation of massive perovskites*

In the last thirty years there has been a permanent search for a synthesis procedure able to yield homogeneous, high-surface-area materials. Moreover, the best method should be economical for large-scale production. Setting aside the traditional solid reaction method (calcination of a mechanical mixture of fine powdered oxides) many preparation procedures have been reported in the patent and open literature. They all start with the preparation of suitable solutions containing the cations in the right proportion to obtain the desired mixed oxide.

Table 1 shows different routes to prepare the required oxides. Starting from one or more solutions containing the required cations, three main steps are identified: precursor synthesis, drying and calcination.

The best precursors are obtained using the sol-gel technique for they require lower calcination temperatures, allow better microstructural and compositional control plus the flexibility to produce a variety of shapes. Chandler et al. (1993) have reviewed the chemical aspects of solution routes to produce mixed oxides. The thermal decomposition of heterobinuclear complexes reported by Skaribas et al. (1991) leads to the production of perovskite oxides. More recently, Moreau et al. (1996) synthesized binuclear complexes of La-Ni, La-Co and La-Cu. Upon calcination at  $\sim 973$  K, the former two complexes yielded  $\text{LaNiO}_3$  and  $\text{LaCoO}_3$  perovskites while the latter yielded  $\text{La}_2\text{CuO}_4$ . The main limitation in this and related methods is the complicated synthesis of the binuclear complexes that makes their application for large scale processing very unlikely.

The precursor is usually oven-dried at  $\sim 373$  K before calcination (table 1). However, it is also attractive to explore other faster, less involved routes to produce the mixed oxides. One option is to avoid the precursor synthesis through dehydration of the starting solution. Freeze-drying has been extensively used for research purposes. The surface areas obtained are in the mid-range  $10\text{--}30\text{ m}^2/\text{g}$  depending on the cations involved.

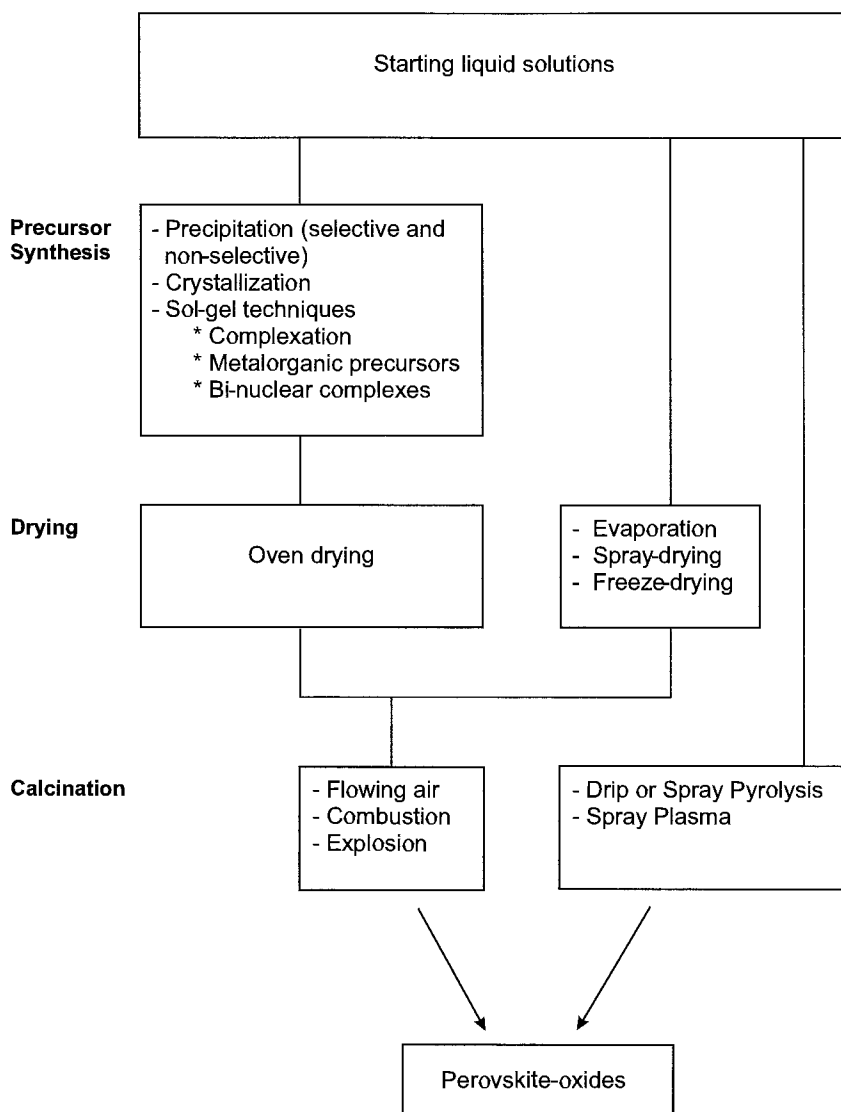
Following either route, a dry solid is obtained which must be calcined (table 1). The traditional calcination procedure is to heat the solid at  $T > 1000$  K under flowing air for several hours and, sometimes, up to one day. Using metalorganic precursors prepared by the sol-gel technique a faster calcination procedure can be used to ignite the solid in air as reported by Merzhanov and Borovinskaya (1972). An even faster calcination is achieved by "exploding" the precursor inside a calorimetric bomb using pure oxygen at high pressure as reported by Milt et al. (1995).

A very attractive route is the direct pyrolysis of the liquid solution (table 1). Recently, Gordes et al. (1995) have reported the successful preparation of several perovskite oxides in large batches using drip pyrolysis. Undoubtedly, when applicable, there is sizeable time saving in comparison to any other known method.

### 1.2.2. *Preparation of supported mixed oxides*

One important limitation of massive mixed oxides is their relatively low surface area. To overcome this limitation, mixed oxides supported on high-surface-area refractory oxides are required. The problem is not easy to tackle due to the strong chemical interaction

Table 1  
Preparation methods of perovskite-oxides<sup>a</sup>



<sup>a</sup> Excludes the traditional solid reaction method starting from a mechanical mixture of fine powdered oxides.

of the components of the mixed oxide and the support which limits the spreading of the oxide on the surface.

The first attempts to prepare supported perovskites by Gallagher et al. (1974) and Chien et al. (1975) started from aqueous slurries containing perovskite particles, cordierite or alumina, and a binding agent. However, after calcination at high temperature the perovskite powder reacted with the support, generating other compounds with low catalytic activity.

The reaction between perovskite components and the support material to form other stable albeit non-catalytic compounds, often takes place. Among others, Nudel et al. (1987) reported that  $\text{LaCoO}_3$  could not be formed on an  $\text{Al}_2\text{O}_3$  support. The only compound detected after impregnation with an equimolar solution of La and Co nitrates was the  $\text{CoAl}_2\text{O}_4$  spinel. To overcome this problem several approaches have been attempted, such as precoating the support with a blocking agent, for example,  $\text{La}(\text{NO}_3)_3$  to impair the Co reaction with  $\text{Al}_2\text{O}_3$ , (Nudel et al. 1987, Mizuno et al. 1986, Collongue et al. 1991). In a similar vein, freeze-drying has been used by Johnson et al. (1976) to obtain a more homogeneous material, while citrate precursors were used by Zhang et al. (1988) to achieve high dispersion. However, in all cases, the dispersions obtained were low even when  $\text{LaCoO}_3$  was formed by reaction of  $\text{Co}(\text{NO}_3)_2$  with  $\text{La}_2\text{O}_3$  as reported by Nudel et al. (1986). In a recent publication Saracco et al. (1996) prepared MgO-supported  $\text{LaCr}_{1-x}\text{Mg}_x\text{O}_3$  ( $x=0-0.5$ ) following an approach somewhat similar to Nudel et al. (1986). In this case, they prepared solid mixtures of  $\text{La}(\text{NO}_3)_3 \cdot 6\text{H}_2\text{O}$ ,  $\text{Cr}(\text{NO}_3)_3 \cdot 9\text{H}_2\text{O}$  and  $\text{Mg}(\text{NO}_3)_2 \cdot 6\text{H}_2\text{O}$  to give a final 17/1 MgO/ $\text{LaCr}_{1-x}\text{Mg}_x\text{O}_3$  molar ratio which were mixed with 30 wt% of citric acid and 40 wt% of water. After reaction-dehydration at 455 K, grinding and calcination at 1373 K for 4 hours the desired material was obtained. It is not clear, however, how much perovskite is supported and which fraction is present as a composite of perovskite and MgO crystals.

A very comprehensive work was undertaken by Misono and his co-workers, as summarized in the publication of Mizuno et al. (1992a). Based on their previous studies they selected  $\text{ZrO}_2$  as the support for  $\text{LaCoO}_3$  and used a variety of adsorption and instrumental techniques to characterize the material prepared. This work illustrates the many difficulties involved in producing a well-dispersed supported perovskite and the tough job of characterizing a thin overlayer of crystalline material. In order to minimize the preferential formation of  $\text{La}_2\text{Zr}_2\text{O}_7$ , the zirconia impregnated with La and Co nitrates cannot be calcined at temperatures beyond 1123 K. If the temperature is too low (<1000 K) the  $\text{LaCoO}_3$  will not be formed. At loadings of ca. 4% the surface of the support should be covered by one layer of  $\text{LaCoO}_3$ . However, if this solid is completely dispersed, it will not show any XRD pattern. No other technique will unambiguously confirm the presence of the perovskite structure. So, the authors resort to probe molecules that are selectively adsorbed on either  $\text{ZrO}_2$  or  $\text{LaCoO}_3$  to trace the formation of the mixed oxide overlayer. This is combined with the use of XPS to follow the evolution of both Co and La surface concentration.

Figure 1 shows the evolution of the pyridine and NO adsorbed with increasing mixed oxide loading. Note that at 5%, pyridine is no longer adsorbed while NO reaches a

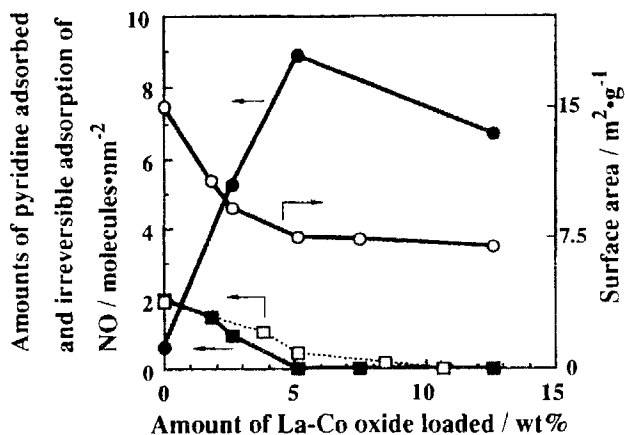


Fig. 1. Changes in the amount of NO adsorbed, surface area, and amount of pyridine adsorbed with the amount of La-Co oxide load: solid circles, amount of NO adsorbed; open circles, specific surface area of La-Co/ZrO<sub>2</sub>; squares, amount of pyridine adsorbed (ZrO<sub>2</sub>, solid squares 15 m<sup>2</sup> g<sup>-1</sup>, open squares 26 m<sup>2</sup> g<sup>-1</sup>). The amount of pyridine adsorbed was estimated by the integrated IR peak intensity of pyridine (1446 cm<sup>-1</sup>). With permission from Mizuno et al. (1992a).

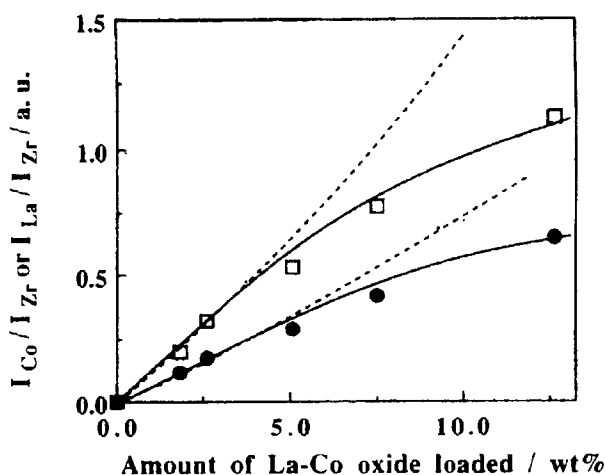


Fig. 2. XPS intensity ratio ( $I_{\text{Co}2p3/2}/I_{\text{Zr}(3d5/2+3d3/2)}$  and  $I_{\text{La}3d5/2}/I_{\text{Zr}(3d5/2+3d3/2)}$ ) as a function of the amount of La-Co oxide loaded: circles,  $I_{\text{Co}2p3/2}/I_{\text{Zr}(3d5/2+3d3/2)}$ ; squares,  $I_{\text{La}3d5/2}/I_{\text{Zr}(3d5/2+3d3/2)}$ . Calculated XPS intensity ratios are shown as dashed lines. With permission from Mizuno et al. (1992a).

constant value of 9 molecules/nm<sup>2</sup>. This is symptomatic of total blocking of the zirconia surface with a LaCoO<sub>3</sub>-like layer. The XPS data shown in fig. 2 are consistent with this picture. Other indirect evidence supporting this overall picture shown by Misono and co-workers is:

- (i) At loadings higher than 5%, first  $\text{LaCoO}_3$  and then  $\text{La}_2\text{Zr}_2\text{O}_7$  reflections become visible in the X-ray patterns.
- (ii) At calcination temperatures over 1123 K, e.g., 1173 K, 5.1 wt%, reflections appeared at  $28.7^\circ$  (shoulder attributed to  $\text{La}_2\text{Zr}_2\text{O}_7$ ),  $32.9^\circ$  and  $33.3^\circ$  ( $\text{LaCoO}_3$  doublet), and  $36.8^\circ$  ( $\text{Co}_3\text{O}_4$ ). The peak intensities of  $\text{La}_2\text{Zr}_2\text{O}_7$  sharply increased at 1373 K.
- (iii) The rate of oxidation of propane per  $\text{m}^2$  of exposed oxide (measured at 548 K) was the same for massive  $\text{LaCoO}_3$  and  $\text{La-Co}(5.1 \text{ wt}\%)/\text{ZrO}_2$  calcined at 1123 K.
- (iv) The EDX composition of individual particles of  $(\text{La-Co})/\text{ZrO}_2$  with loadings between 2.6 and 7.5% gives  $\text{La/Co} \approx 1$ .

More difficult to understand is why the catalytic activity for propane oxidation varies so much with calcination temperatures between ca. 900 and 1400 K. The activity goes through a sharp maximum at 1123 K and becomes negligible at 1373 K.

Is it possible to use the same approach to prepare supported  $\text{La}_{0.8}\text{Sr}_{0.2}\text{CoO}_3$ ? The driving force is the much higher activity of this formulation compared with  $\text{LaCoO}_3$ . Fujii et al. (1987) impregnated twelve different solids with the corresponding nitrates and found that  $\text{ZrO}_2$  was by far the best support. However, the Sr substitution did not increase the catalytic activity of supported perovskite as it does in unsupported ones. The reason for this phenomenon was later found out by the same group and reported by Mizuno (1990): Sr preferentially reacts with the support to form  $\text{SrZrO}_3$ . This illustrates that the preparation method, support, etc., must be tailored for each case.

In a recent publication Marti et al. (1995) reported the preparation of  $\text{La}_{0.8}\text{Sr}_{0.2}\text{MnO}_{3+x}$  (LSM) supported on  $\text{LaAlO}_3$  and  $\text{LaAl}_{11}\text{O}_{18}$ . They used both the citrate and the coprecipitation methods and found no difference in catalytic activity after calcination at 1370 K. The best catalyst for methane combustion was LSM/ $\text{LaAlO}_3$ . No attempt was made to ascertain the extent of dispersion of the perovskite on the supports.  $\text{La}_{0.8}\text{Sr}_{0.2}\text{MnO}_{3+x}$  supported on  $\text{LaAlO}_3$  was found to be thermally more stable than the other catalysts investigated.

Another view of the field of supported perovskites emerges from the work of Moreau et al. (1996). They reported the formation of lamellar silicate/oxide nanocomposites. They exchanged the sodium cations of montmorillonite with heterobinuclear complexes containing La and one of the following transition metals: Ni, Co or Cu. Afterwards, the exchanged silicate was freeze-dried and then heated in air at 673 K, a temperature high enough to form the oxide from the starting complex. The insertion of the X-ray non-visible oxide produced an expansion of the lamellar structure. This spacing between layers does not lead to a straightforward calculation of the thickness of the perovskite (oxide) layers. This is due to the important contraction caused by the thermal treatment that leads to discontinuities in the oxide layer. The X-ray diffraction patterns of  $\text{La-Ni}$  oxide intercalated montmorillonite heated at 673 K clearly show a very well-defined 001 reflection typical of the lamellar structure (fig. 3).

Chemical vapor deposition might be an attractive route to produce supported mixed oxides. To achieve this, suitably volatile precursors are required.

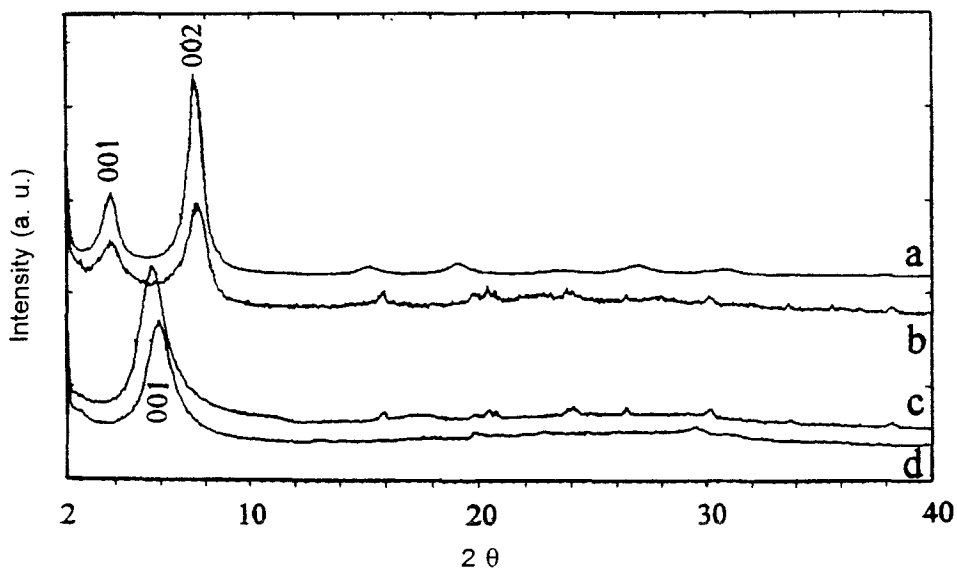


Fig. 3. XRD diffraction patterns of Montmorillonite/La,Ni-bis(3-carboxysalicydene) ethylene diamine heated at: (a) room temperature; (b) 473 K; (c) 573 K; (d) 673 K. With permission from Moreau et al. (1996).

### 1.2.3. Support stabilization

In combustion and exhaust gas treatment applications the reaction temperature is high enough to facilitate the  $\gamma\text{-Al}_2\text{O}_3 \rightarrow \alpha\text{-Al}_2\text{O}_3$  transition with the concomitant surface area reduction. The addition of lanthanum improves the thermal stability of  $\gamma$ -alumina as reported by Schaper et al. (1983, 1984) and Matsuda et al. (1984) among others. The stabilized supports contain two types of mixed oxides:  $\text{LaAlO}_3$  with perovskite structure and  $\text{La}_2\text{O}_3 \cdot 11\text{Al}_2\text{O}_3$  (lanthanum beta aluminate). The role of the latter is controversial. Beguin et al. (1991) reported that the  $\beta$ -aluminate becomes visible at ca. 1500 K and at that point the surface area drastically decreases. They proposed that this phase may be formed by a solid-state reaction between  $\text{Al}_2\text{O}_3$  and  $\text{La}_2\text{O}_3$ .

On the other hand, Kato et al. (1988) studied the addition of different rare-earth oxides to  $\gamma\text{-Al}_2\text{O}_3$  in a 5/95 ratio. They found that in those systems where  $\beta$ -aluminates were detected after firing at 1473 K the surface area was always higher than in those cases where only  $\alpha\text{-Al}_2\text{O}_3$  was detected. They concluded that the common feature of thermally resistant supports is that they have a layered aluminate structure which retards support sintering.

## 1.3. Reducibility of perovskite-type mixed oxides

### 1.3.1. Bulk reduction

Only the B cations are normally reduced in  $\text{RBO}_3$ . Their reducibility is strongly dependent on the type of B cations involved and to a lesser extent on the rare earth. Besides, if

Table 2  
Reducibility of perovskite-type mixed oxides

Mixed oxide	Reducing atmosphere	Extent of reduction (e/molecule)	Temperature (K)	Reference(s)
LaCrO <sub>3</sub>	H <sub>2</sub>	$1.3 \times 10^{-2}$	1273	Fierro and Tejuca (1984)
LaMnO <sub>3</sub>	H <sub>2</sub>	1.0	1073	Fierro et al. (1984)
	H <sub>2</sub> (10%)/N <sub>2</sub>	1.0	1323	Vogel et al. (1977)
LaFeO <sub>3</sub>	H <sub>2</sub>	3.0	1270	Tascón et al. (1985)
	H <sub>2</sub> (19%)He	3.0	1270	Wachowski et al. (1981)
YFeO <sub>3</sub>	H <sub>2</sub> (15%)He	3.0	1013	Carreiro et al. (1985)
LaCoO <sub>3</sub>	H <sub>2</sub>	3.0	773	Crespin and Hall (1981)
	D <sub>2</sub>	3.0	898	Crespin and Hall (1981)
LaNiO <sub>3</sub>	H <sub>2</sub>	3.0	748	Fierro et al. (1985)
LaRhO <sub>3</sub>	H <sub>2</sub>	3.0	703	Gysling et al. (1987)
LaRhO <sub>3</sub>	CO	2.25	850	Tascón et al. (1986b)

the R position is partially occupied by cations in oxidation states  $\leq 2$ , the reducibility increases. The rationale for this behavior is that in order to maintain the electroneutrality, the B cation is oxidized to a higher oxidation state, e.g. Co<sup>IV</sup>, and oxygen vacancies are generated. Usually this oxidation state is highly unstable and easily reduced back to the original +3 oxidation state. This whole process makes the lattice oxygen deficient and consequently easier to be attacked by the reducing agent, making it easier to achieve higher extents of reduction than in the case of A<sup>III</sup>B<sup>III</sup>O<sub>3</sub> oxides.

Under mild reduction conditions B cations with stable lower oxidation states may lead to the formation of other mixed oxide phases. Increasing the reduction severity usually leads to a full reduction of the B cation to the metal state.

Table 2 compiles reducibility data reported in the literature. Note that the reducibility increases going down the table as expected from the increased noble metal character of the B cations involved. At maximum reduction, 3e/molecule, the solid at this point usually shows the reflections corresponding to the rare-earth single oxide while the reduced metal remains invisible due to its small particle size (high dispersion). Only after heating at higher temperature in an inert gas does the metal sinter and become X-ray visible.

Note that the chromate is hardly reduced and the manganate is only reduced to 1e/molecule under extreme reduction conditions. CO is not as effective as H<sub>2</sub> as a reducing agent and leaves carbon residues on the surface of the rhodate. Nakamura et al. (1979) studied the lattice stability at 1273 K at 1 atm total pressure as a function of oxygen partial pressure. The order of stability of the oxides under these conditions is essentially the same as that reported in table 2: LaVO<sub>3</sub>  $\approx$  LaCrO<sub>3</sub> > LaFeO<sub>3</sub> > LaMnO<sub>3</sub> > LaCoO<sub>3</sub> > LaNiO<sub>3</sub>. The order between LaFeO<sub>3</sub> and LaMnO<sub>3</sub> is inverted if the different extents of reduction are considered. When comparing reduction data obtained with samples of different origin, special attention should be paid to the particle size and crystallinity of the

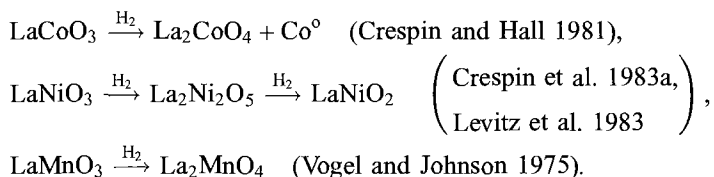


mixed oxides. These are two key factors responsible for the large differences in reduction temperatures reported in the literature for samples of the same composition.

The reduction process can be reversed by careful reoxidation. There are reports in the literature that the following mixed oxides have been reversibly reduced and oxidized:  $\text{LaCoO}_3$  [Crespin and Hall (1981)],  $\text{LaNiO}_3$  [Crespin et al. (1983a)],  $\text{LaRhO}_3$  [Tascón et al. (1986a)] and  $\text{PrCoO}_3$  [Fierro et al. (1988)]. The sintering of the metals in the reduced solid should be avoided to achieve reversibility.

Other general features of the mixed oxide reduction are:

- The reducibility of the mixed oxides increases with decreasing size of the R cation. This is related to the structural stability of the lattice.
- The partial substitution of R by a divalent cation such as alkaline earth facilitates the reduction. This is due to an increase in anion vacancy concentration that facilitates oxygen diffusion and the existence of the transition metal cation in a higher, less stable oxidation state such as  $\text{Co}^{\text{IV}}$  in  $\text{La}_{1-x}\text{Sr}_x\text{CoO}_{3-y}$ .
- In some instances during mild reduction, stable mixed oxide phases have been identified. The following cases have been reported in the literature:



More detailed reviews concerning the stability of perovskites in a reducing atmosphere have been published by Tejuca et al. (1989) and Petunchi and Lombardo (1990).

### 1.3.2. Surface reduction

The surface of the mixed oxide is expected to be reduced at lower temperatures than the bulk. This is particularly important in hydrogenation reactions where finely dispersed metal atoms and/or coordinatively unsaturated sites may be required. Figure 4 dramatically illustrates how much easier it is to reduce the surface than the bulk of  $\text{LaCoO}_3$  and the partially substituted oxides  $\text{La}_{0.6}\text{Sr}_{0.4}\text{CoO}_3$  and  $\text{La}_{0.8}\text{Th}_{0.2}\text{CoO}_3$ . The XPS spectra show that  $\text{Co}^{2+}$  and  $\text{Co}^\circ$  appeared on the perovskite surface at reduction temperatures at least 100 K lower than in the bulk. In the same vein, Gysling et al. (1987) observed a 130 K difference between the reduction temperatures needed to detect  $\text{Rh}^\circ$  on the surface and in the bulk of  $\text{LaRhO}_3$ .

The O1s signal also yields important information concerning the surface reduction processes that occur during the  $\text{H}_2$  treatment. In the case of  $\text{LaCoO}_3$  upon reduction two O1s signals are detected. One corresponds to lattice oxygen and the other one, at higher binding energy (BE), is assigned to terminal OH groups. These are formed using the water produced during reduction with  $\text{H}_2$ . This phenomenon is enhanced when Sr partially substitutes La and is suppressed by Th substitution. This is in line with the basicity of  $\text{Th} < \text{La} < \text{Sr}$ . A higher basicity means a greater tendency to form hydroxyls.

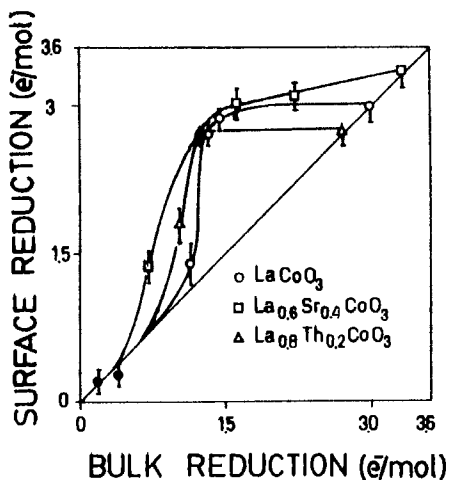


Fig. 4. Correlation between surface reduction, determined by XPS, and bulk reduction, calculated from the hydrogen uptake in a gas recirculating system. Data points with solid circles are from Lombardo et al. (1983). With permission from Marcos et al. (1987).

Further important information obtained from the photoelectron spectra is the change in surface composition that occurs upon exposure to reducing atmosphere at different temperatures. Figure 5 shows this effect on three cobaltates. The migration of metallic cobalt to the surface is expected, as  $\text{Co}^0$  cannot possibly fit into the oxide lattice and is expelled to the grain boundaries.

#### 1.4. Oxygen sorption

As mentioned above, many perovskite structures show oxygen vacancies in their structure and/or admit excess oxygen under certain conditions. Among the most studied systems presenting this feature are the perovskites, having in position A a rare-earth and/or alkaline-earth cation, and on B sites a first-row transition metal. These structural features must be connected with the interaction of the lattice with oxygen gas and strongly influence the adsorption-desorption patterns of oxygen.

The temperature-programmed desorption (TPD) of oxygen has been thoroughly studied by a number of researchers, generally in connection with the catalytic application of mixed oxides. In what follows the general characteristics of TPD studies will be discussed with special emphasis on structural information. Those particular features pertaining to a given type of reaction will be dealt with in the next section.

By far, the most studied perovskite containing excess oxygen is  $\text{LaMnO}_{3.12}$  which was prepared by Tofield and Scott (1974) by reacting the single oxides in oxygen at 1473 K. The degree of oxidative non-stoichiometry strongly depends on the oxygen partial pressure and on both the temperature and duration of the firing as shown by Kamegashira et al. (1984). The non-stoichiometry can also be modified by the partial substitution of the A and B cations.

The non-stoichiometry is much less pronounced in other  $\text{LaMO}_3$  ( $M=\text{Fe}, \text{Co}, \text{Ni}$ ) perovskites. Through the partial substitution of the rare earth by an alkaline earth, the

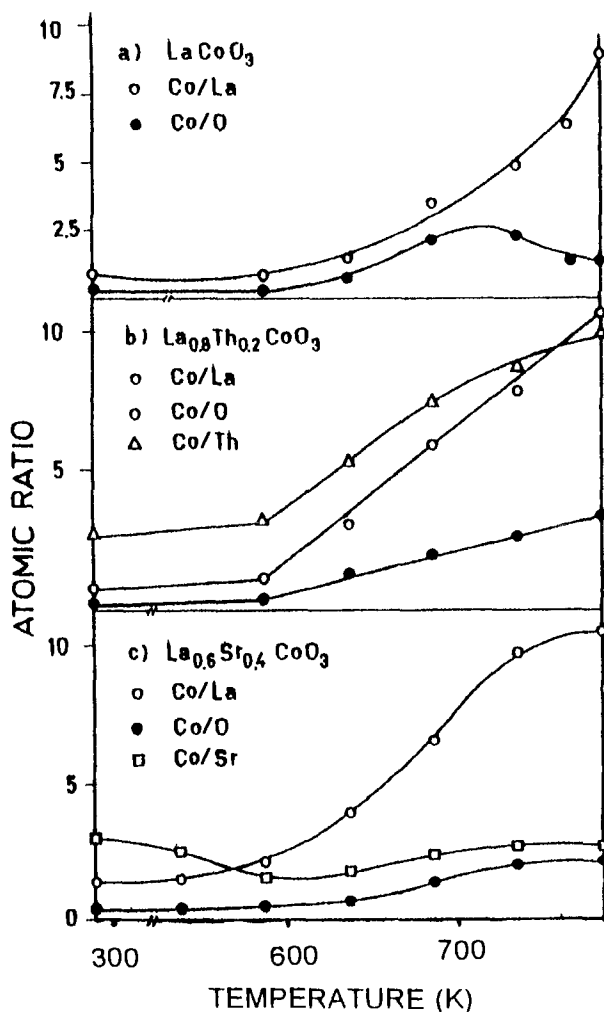


Fig. 5. Effect of reduction temperature on the XPS calculated atomic ratios of the elements. Trap with liquid air,  $p_{\text{H}_2} \approx 1$  atm. With permission from Marcos et al. (1987).

oxygen deficiency becomes apparent and the general formula can then be written as:  $\text{La}_{1-x}\text{Sr}_x\text{MO}_{3-\delta}$ .

The TPD of oxygen of these perovskites directly reflects the non-stoichiometry of the starting mixed oxides and is also influenced by other features of the particular system such as stability of different oxidation states of the transition metal. The thermograms usually show up to three peaks that are named  $\alpha$ ,  $\alpha'$  and  $\beta$  in order of increasing temperature. Figures 6–8 show typical TPDs of  $\text{LaMO}_3$  and  $\text{La}_{1-x}\text{Sr}_x\text{MO}_{3\pm\lambda}$  ( $\text{M}=\text{Cr}, \text{Fe}, \text{Mn}, \text{Co}, \text{Ni}$ ). The lowest-temperature peak ( $\alpha$ ) is assigned to chemisorbed oxygen. The  $\alpha'$  is

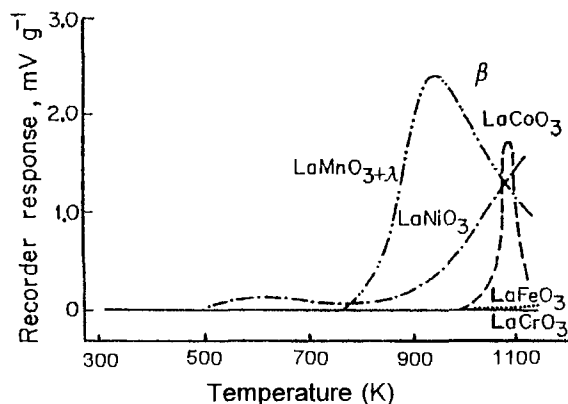


Fig. 6. Temperature-programmed desorption of oxygen from  $\text{LaBO}_{3+\lambda}$  ( $\text{B} = \text{Co}, \text{Fe}, \text{Mn}, \text{Ni}, \text{Cr}$ ). Oxygen preadsorption  $1073 \text{ K} \rightarrow 298 \text{ K}, 1.33 \times 10^4 \text{ Pa}$ . With permission from Seiyama et al. (1985).

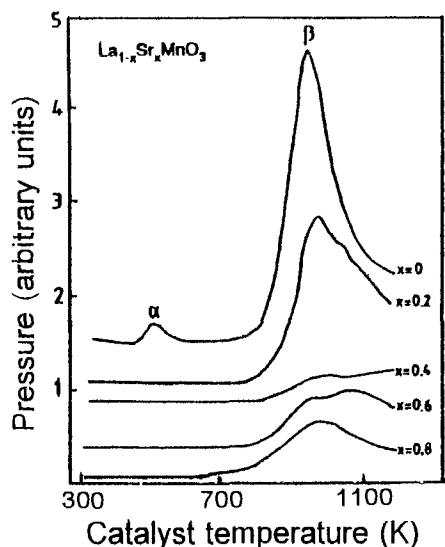


Fig. 7. TPD profile of oxygen from  $\text{La}_{1-x}\text{Sr}_x\text{MnO}_3$ . With permission from Chan et al. (1994).

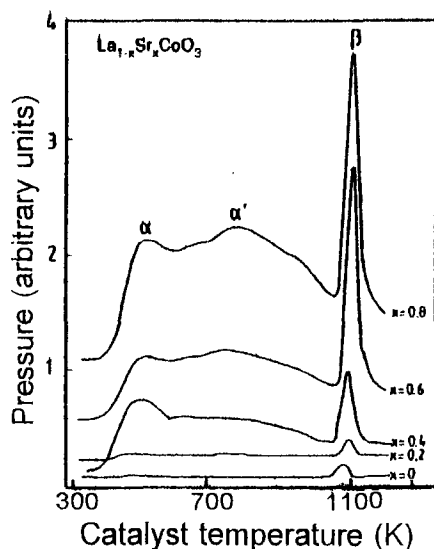


Fig. 8. TPD profile of oxygen from  $\text{La}_{1-x}\text{Sr}_x\text{CoO}_3$ . With permission from Chan et al. (1994).

associated with  $\text{O}_2$  chemisorbed at the oxygen vacancies while the highest-temperature  $\beta$  peak corresponds to lattice oxygen associated with the partial reduction of the B cation. The three peaks have also been reported in  $\text{LaSrNiO}_4$  ( $\text{K}_2\text{NiF}_4$  structure) by Zhao et al. (1996). Chan et al. (1994) have calculated the amount of  $\alpha$ ,  $\alpha'$  and  $\beta$  oxygen desorbed from several lanthanum perovskites partially substituted with either Sr or Ce (table 3). One monolayer of oxygen coverage is estimated to contain ca.  $1 \times 10^{15}$  oxygen atoms/ $\text{cm}^2$ . Hence, the  $\alpha$  desorption is at most equivalent to two layers while the  $\alpha'$  peak goes up

Table 3  
Peak temperatures ( $T_p$ ) and amount of desorbed oxygen from TPD spectra<sup>a</sup>

$x$	$\alpha$ $T_p$ (K)	Desorbed oxygen (atoms/cm <sup>2</sup> )	$\alpha'$ $T_p$ (K)	Desorbed oxygen (atoms/cm <sup>2</sup> )	O/Sr	$\beta$ $T_p$ (K)	Desorbed oxygen (atoms/cm <sup>2</sup> )
<i>La<sub>1-x</sub>Sr<sub>x</sub>MnO<sub>3</sub></i>							
0	514	$2.32 \cdot 10^{14}$	—	—		949	$2.79 \cdot 10^{15}$
0.2	—	—	—	—		987	$2.77 \cdot 10^{15}$
0.4	—	—	—	—		1020	$4.76 \cdot 10^{14}$
0.6	—	—	—	—		1072	$7.63 \cdot 10^{14}$
0.8	—	—	—	—		1072	$9.92 \cdot 10^{14}$
<i>LaMn<sub>1-x</sub>Cu<sub>x</sub>O<sub>3</sub></i>							
0	514	$2.32 \cdot 10^{14}$	—	—		949	$2.79 \cdot 10^{15}$
0.2	—	—	—	—		949	$2.05 \cdot 10^{15}$
0.4	—	—	—	—		1088	$5.75 \cdot 10^{14}$
0.6	589	$2.18 \cdot 10^{15}$	—	—		1124	$2.66 \cdot 10^{15}$
<i>La<sub>1-x</sub>Sr<sub>x</sub>CoO<sub>3</sub></i>							
0	465	$4.03 \cdot 10^{13}$	—	—		1066	$3.07 \cdot 10^{14}$
0.2	466	$1.88 \cdot 10^{14}$	711	$7.74 \cdot 10^{14}$	0.13	1080	$4.58 \cdot 10^{14}$
0.4	485	$2.04 \cdot 10^{15}$	713	$1.09 \cdot 10^{16}$	0.23	1082	$2.32 \cdot 10^{15}$
0.6	499	$1.02 \cdot 10^{15}$	740	$1.04 \cdot 10^{16}$	0.20	1107	$6.79 \cdot 10^{15}$
0.8	506	$1.83 \cdot 10^{15}$	771	$1.78 \cdot 10^{16}$	0.16	1108	$6.11 \cdot 10^{15}$
<i>La<sub>1-x</sub>Ce<sub>x</sub>CoO<sub>3</sub></i>							
0	465	$4.03 \cdot 10^{13}$	—	—		1066	$3.07 \cdot 10^{14}$
0.1	423	$1.19 \cdot 10^{13}$	—	—		1088	$1.45 \cdot 10^{15}$
0.2	451	$2.35 \cdot 10^{13}$	—	—		1096	$1.40 \cdot 10^{15}$
0.4	453	$3.18 \cdot 10^{13}$	—	—		1108	$5.79 \cdot 10^{15}$

<sup>a</sup> With permission from Chan et al. (1994).

to 18 layers of oxygen atoms. These numbers are consistent with the assignments of the  $\alpha$  and  $\alpha'$  peaks.

In manganites and cobaltates the partial substitution of La by Sr has opposite effects (figs. 7 and 8) upon the low temperature oxygens ( $\alpha$  and  $\alpha'$ ). As a matter of fact, the ferrates and cuprates behave as the cobaltates. One possible explanation rests on the different stability of the 4+ oxidation state of the transition elements.  $Mn^{4+}$  is by far more stable in the perovskite structure than any of the other three  $B^{4+}$  cations. This makes the manganites retain an excess oxygen in their structure, a situation not observed in the other three mixed oxides. The introduction of Sr instead of La reduces the concentration of excess oxygen needed to compensate the presence of  $Mn^{4+}$  in the lattice. Note that the O1s spectra of perovskites also indicate that adsorbed oxygen is always present on the perovskite surface together with the intrinsic lattice oxygen.

Oxygen adsorption at 308 K on  $\text{LaMO}_3$  ( $M = \text{Cr, Mn, Fe, Co, Ni}$ ) was reported by Kremeníć et al. (1985). They found two maxima for Mn and Co. The reversibly adsorbed oxygen represents a small fraction of the total adsorption. The double volcano shape of the total oxygen adsorption plot is similar to the activity plot from total oxidation. The role played by the different oxygen vacancies and non-stoichiometry in explaining the catalytic behavior of mixed oxides will be thoroughly discussed in the following section.

## 2. Applications in heterogeneous catalysis

The different applications have been classified by reaction type: oxidation (sect. 2.1–2.3), hydrogenation (sect. 2.4), environmental (sect. 2.5) and miscellaneous (sect. 2.6). The environmental applications have been grouped together in view of the present relevance of this field. It includes total oxidation of organic compounds and CO, redox processes such as  $\text{CO} + \text{NO}$  reaction and  $\text{NO}/\text{N}_2\text{O}$  decomposition.

### 2.1. Partial oxidation

This section includes the selective oxidation of hydrocarbons and oxygenated compounds, oxydehydrogenation and ammoxidation. Partial oxidation to syngas and oxidative coupling of methane will be treated in the following section.

Table 4 summarizes the most relevant applications of mixed oxide catalysts in partial oxidation. Kremeníć et al. (1985) studied the oxidation of  $\text{C}_3\text{H}_6$  and  $i\text{-C}_4\text{H}_8$  over  $\text{LaMO}_3$  ( $M = \text{Cr, Mn, Fe}$ ). These catalysts were effective for the total oxidation of both hydrocarbons. By increasing the  $i\text{-C}_4\text{H}_8/\text{O}_2$  ratio they could obtain acceptable

Table 4  
Mixed oxides in partial oxidation and oxydehydrogenation reactions

Reaction	Catalyst	Reference
$i\text{-C}_4\text{H}_8 \rightarrow \text{CH}_2=\text{C}(\text{CH}_3)\text{-CHO}$	$\text{LaMO}_3$ ( $M = \text{Cr, Mn, Fe}$ )	Kremeníć et al. (1985)
$\text{C}_6\text{H}_5\text{CH}_3 \rightarrow \text{C}_6\text{H}_5\text{CHO}$	$\text{LaCoO}_3$	Madhok (1986)
	$\text{LaMO}_3$ ( $M = \text{Co, Fe, Cr}$ )	Agarwal and Goswami (1994)
$\text{C}_2\text{H}_5\text{OH} \rightarrow \text{CH}_3\text{-CHO}$	$\text{LaMO}_3$ ( $M = \text{Co, Mn, Fe, Ni}$ )	Shimizu (1986)
$i\text{-C}_3\text{H}_7\text{OH} \rightarrow \text{CH}_3\text{-CO-CH}_3$	$\text{La}_{1-x}\text{Sr}_x\text{FeO}_3$	Radha and Swamy (1985)
	$\text{La}_2\text{MnMO}_6$ ( $M = \text{Co, Ni, Cu}$ )	
$\text{C}_2\text{H}_6 \rightarrow \text{C}_2\text{H}_4$	$\text{La}_{1-x}\text{Sr}_x\text{FeO}_3$	Yi et al. (1996)
$i\text{-C}_4\text{H}_8 \rightarrow \text{C}_4\text{H}_6$ ( $2\text{-C}_4\text{H}_8$ )	$\text{La}_{1-x}\text{Sr}_x\text{FeO}_3$	Shimizu (1992)
$i\text{-C}_4\text{H}_{10} - i\text{-C}_4\text{H}_8$	$\text{Ce}_{0.8}\text{Zr}_{0.2}\text{O}_2$ solid solution on fluorite structure)	de Leitenburg et al. (1996)
$\text{C}_6\text{H}_5\text{CH}_3 + \text{NH}_3 \rightarrow \text{C}_6\text{H}_5\text{CN}$	$\text{YBa}_2\text{Cu}_3\text{O}_{6+x}$	Hansen et al. (1988)

yields of methacrolein. The activity for methacrolein formation followed the order  $\text{LaCrO}_3 > \text{LaFeO}_3 > \text{LaMnO}_3 > \text{LaCoO}_3 = \text{LaNiO}_3$ . Note that this order is coincident with the stability of the perovskites (TPD and reducibility data, fig. 6 and table 2).

Toluene has been oxidized to benzaldehyde over  $\text{LaMO}_3$  ( $M = \text{Co}, \text{Fe}, \text{Cr}$ ) with 70% selectivity at 15% conversion. Agarwal and Goswami (1994) reported the formation of benzoic and maleic acids together with benzaldehyde. The three perovskites behave quite similarly, reaching the highest yield to benzaldehyde at 723 K.

Shimizu (1986) studied the oxidation of ethanol to acetaldehyde over  $\text{LaMO}_3$  ( $M = \text{Co}, \text{Mn}, \text{Fe}, \text{Ni}$ ) and  $\text{La}_{1-x}\text{Sr}_x\text{FeO}_3$ . The partial pressure of both the alcohol and oxygen were about the same, 0.11–0.2 atm using He as diluent. The pressure dependency for acetaldehyde formation was 0.5 for both reactants between 573 and 623 K. No  $\text{CO}_2$  was formed in this temperature range. The total oxidation increased sharply above 623 K. The activity for the formation of acetaldehyde decreased in the following order:  $\text{Co} > \text{Mn} > \text{Ni} > \text{Fe}$ . The best catalyst containing Sr was  $\text{La}_{0.8}\text{Sr}_{0.2}\text{FeO}_3$ .

Radha and Swamy (1985) studied the reaction of 2-propanol to acetone and hydrogen over  $\text{La}_2\text{MnMO}_6$  ( $M = \text{Co}, \text{Ni}, \text{Cu}$ ). By monitoring the change in conductivity of the oxides upon acetone adsorption, they concluded that the surface is predominantly covered with acetone under their reaction conditions. In turn, the desorption of acetone is the rate-determining step involving electron transfer from the surface to the adsorbed species.

$\text{La}_{1-x}\text{Sr}_x\text{FeO}_{3-y}$  ( $0 \leq x \leq 1$ ) has been used in oxidative dehydrogenation of ethane and isobutene. Yi et al. (1996) studied the former reaction and further investigated the phase diagram to verify a phase separation between La-rich and Sr-rich perovskites. They explored the 573–1073 K temperature region and reported that the maximum ethylene selectivity occurred at 923 K. At lower temperatures,  $\text{CO}_2$  predominates and at higher temperatures, cracking and synthesis gas formation occur. DTA and XRD indicate that a phase separation occurs between La-rich and Sr-rich perovskites. This separation was reflected in both the conductivity and catalytic activity.

de Leitenburg et al. (1996) studied the oxydehydrogenation of  $i\text{-C}_4\text{H}_{10}$  over  $\text{CeO}_2/\text{ZrO}_2$  solid solutions.  $\text{Ce}_{0.8}\text{Zr}_{0.2}\text{O}_2$  is the best formulation for this reaction. The addition of  $\text{ZrO}_2$  stabilizes the material against the drop in surface area observed in  $\text{CeO}_2$ . Besides, the  $\text{ZrO}_2$  addition significantly increases selectivity towards isobutene formation.

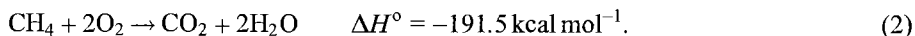
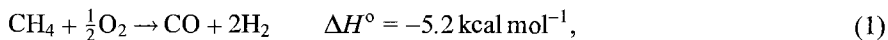
Hansen et al. (1988) reported that  $\text{YBa}_2\text{Cu}_3\text{O}_{6+x}$  catalyzes the ammoxidation of toluene. A sharp change in selectivity occurred in their system at a given partial pressure of oxygen. The bulk composition of the nitrile-selective catalyst was close to  $\text{YBa}_2\text{Cu}_3\text{O}_6$ . When  $x > 0$ , the catalyst became  $\text{CO}_2$ -selective. These results seem to suggest that the oxygen stoichiometry plays a key role in the catalyst selectivity for this reaction.

In brief, the results reviewed here are useful indicators that perovskite oxides are potential catalysts for selective oxidation applications. However, there are not enough data available to elaborate a rational theory able to explain and later predict the behavior of perovskites in the selective oxidation of hydrocarbons and oxygenates to higher valued products.

## 2.2. *partial oxidation of methane to synthesis gas (syngas)*

Over the past several years extensive efforts have been made to find a novel energy-efficient route for the production of syngas with a  $\text{H}_2/\text{CO}$  ratio about 2.0 which is the desirable ratio for methanol and Fischer–Tropsch synthesis processes.

According to Choudhary et al. (1996a) the following reactions are expected to occur simultaneously in the partial oxidation of methane to syngas (POM):



Syngas can be obtained as equilibrium product of reaction (1). The main requirement for a syngas catalyst is therefore to activate methane and oxygen under conditions where the equilibrium composition is favorable, and where the catalyst is not active for total oxidation (reaction 2) or coke formation.

Due to the reducing reaction conditions under which the catalyst is working, it is expected that its surface will be reduced during reaction or during the heating procedure in nitrogen. On the other hand, Rostrup-Nielsen (1984) proposed that the reaction of methane and oxygen to produce syngas, CO and  $\text{H}_2$ , over nickel-based catalyst requires 12 neighboring active sites, and to produce coke the requirement is 16 neighboring active sites. Thus, in order to avoid coke formation, it is important to obtain finely dispersed metal particles. It is well known that R-based perovskites, after treatment under reducing atmosphere, can modify the oxidation state of the element in the B site and in many cases can be reduced to the metallic state, having a highly dispersed  $\text{B}^0$  in the R-oxide matrix. Thus, these mixed oxides are presented as potential catalysts for POM.

Slagtern and Olsbye (1994) studied the catalytic behavior of La–B–O (B = Co, Cr, Ni, Rh) systems for POM. La-based perovskites were obtained in the samples with Co, Cr and Ni. La–Rh–O and La–Rh–Ni–O samples were amorphous phases. Rh-based samples were prepared using  $\text{RhCl}_3 \cdot 4\text{H}_2\text{O}$ . Elementary analyses showed that Cl remained in these solids, probably as LaOCl. This phase was detected by XRD in La–Rh–O catalysts after the catalytic test (table 6). The gas effluent was analyzed on-line by a gas chromatograph. The main by-product was  $\text{CO}_2$ , and small amounts of  $\text{C}_2$  hydrocarbons (<0.3%) were detected.

Table 5 shows the initial methane conversion and CO yield, the latter after 40 h under reaction condition at 1073 K. The results of the X-ray diffraction patterns of different samples before and after the reaction test are shown in table 6.

The systems containing Rh and/or Ni gave the highest initial CO yields at 1073 K. No apparent deactivation was observed on La–Rh–O samples during the 120 h reaction experiment. After this period, the coke content of the catalyst was 0.25 wt%. The CO yield obtained over this catalyst indicated that the reaction reached equilibrium.  $\text{LaNiO}_3$  initially gave a promising activity and selectivity, but deactivation was observed after 17 h on stream, probably due to coke formation (2.98 wt%).

La–Rh–Ni–O samples presented CO yield comparable to La–Rh–O. Some deactivation was observed after 20 h on stream, but no further decrease in activity and CO selectivity



Table 5  
Methane conversion and carbon monoxide yield at 1073 K<sup>a,b</sup>

Catalyst	CH <sub>4</sub> conversion (%) (initial)	CO yield (%)	
		Initial	40 h on stream
LaCrO <sub>3</sub>	26	3	2
LaNiO <sub>3</sub>	89	84	46(17 h)
La-Rh-O	96	90	93
La-(Rh,Ni)-O	81	80	69
LaCoO <sub>3</sub>	25 (89%, 30 h)	0 (87%, 30 h)	76

<sup>a</sup> With permission from Slagtern and Olsbye (1994).

<sup>b</sup> Reaction conditions: CH<sub>4</sub>:O<sub>2</sub>:N<sub>2</sub>=2:1:4;  $F=30\text{ cm}^3\text{ min}^{-1}$ , catalyst 0.5 ml.

Table 6  
XRD analysis of the catalysts before and after the catalytic test<sup>a,b</sup>

Catalyst	XRD before test	XRD after test
LaCrO <sub>3</sub>	LaCrO <sub>3</sub> , one unidentified peak	LaCrO <sub>3</sub> , some unidentified peaks
LaNiO <sub>3</sub>	LaNiO <sub>3</sub> , some NiO	NiO, traces of Ni <sup>o</sup> + unidentified peaks
La-Rh-O	probably LaOCl, traces of Rh <sup>o</sup>	LaOCl, Rh <sup>o</sup>
La-(Rh,Ni)-O	probably LaOCl	probably LaOCl, some La <sub>2</sub> O <sub>3</sub> and La(OH) <sub>3</sub>
LaCoO <sub>3</sub>	LaCoO <sub>3</sub> , some La <sub>2</sub> O <sub>3</sub> , traces of Co <sub>3</sub> O <sub>4</sub> + unidentified peaks	La <sub>2</sub> O <sub>3</sub> , probably some La(OH) <sub>3</sub> , La <sub>2</sub> O <sub>2</sub> CO <sub>3</sub>

<sup>a</sup> With permission from Slagtern and Olsbye (1994).

<sup>b</sup> Reaction conditions: see table 5.

was recorded during the testing period (120 h), suggesting that Rh could prevent the formation of coke over Ni.

LaCrO<sub>3</sub> and LaCoO<sub>3</sub> were active for total oxidation and CO<sub>2</sub> was the main product obtained (table 5). However, after LaCoO<sub>3</sub> had been 30 h on stream at 1073 K, methane conversion rose from 25% to 89% and CO selectivity increased to 98%.

All samples were expected to be reduced during reaction. NiO, probably traces of Ni<sup>o</sup>, and unidentified phases were observed after reaction on LaNiO<sub>3</sub>. NiO might be formed by reoxidation of Ni<sup>o</sup> during the cooling and storing of the samples. Rh<sup>o</sup> was formed during the catalytic test, and was detected in the XRD patterns (table 6).

No reduced metals, Co<sup>o</sup>, Ni<sup>o</sup> or Rh<sup>o</sup>, were observed on LaCoO<sub>3</sub> and La-Rh-Ni-O samples after reaction. However, very small particles with diameters lower than 50 Å could be formed, which would be beyond the detection limit of the XRD instrument. Slagtern and Olsbye (1994) suggested that these metal particles might be on the surface acting as active sites.

The LaNiO<sub>3</sub>, La<sub>0.8</sub>Ca<sub>0.2</sub>NiO<sub>3</sub>, La<sub>0.8</sub>Sr<sub>0.2</sub>NiO<sub>3</sub> and LaNi<sub>1-x</sub>Co<sub>x</sub>O<sub>3</sub> catalytic properties for POM were studied by Choudhary et al. (1996a). Table 7 shows the methane

Table 7

Surface area of perovskite oxide catalysts and their specific activity in oxidative conversion of methane to syngas at 1073 K<sup>a,b</sup>

Perovskite composition	Surface area (m <sup>2</sup> g <sup>-1</sup> )	CH <sub>4</sub> conversion (%)	CO selectivity (%)	H <sub>2</sub> /CO ratio
LaNiO <sub>3</sub>	4.5	77	95	1.91
LaNi <sub>0.8</sub> Co <sub>0.2</sub> O <sub>3</sub>	4.1	64	84	1.70
LaNi <sub>0.6</sub> Co <sub>0.4</sub> O <sub>3</sub>	3.6	54	76	1.40
LaNi <sub>0.4</sub> Co <sub>0.6</sub> O <sub>3</sub>	3.4	54	59	1.34
LaNi <sub>0.2</sub> Co <sub>0.8</sub> O <sub>3</sub>	2.7	27	22	1.00
LaCoO <sub>3</sub>	2.4	12	75	0
La <sub>0.8</sub> Ca <sub>0.2</sub> NiO <sub>3</sub>	4.1	65	86	1.45
La <sub>0.8</sub> Sr <sub>0.2</sub> NiO <sub>3</sub>	3.5	48	60	1.31

<sup>a</sup> With permission from Choudhary et al. (1996a).

<sup>b</sup> Feed = 64.3 mol% CH<sub>4</sub> and 35.7 mol% O<sub>2</sub>, GHSV = 5.2 × 10<sup>5</sup> cm<sup>3</sup> g<sup>-1</sup> h<sup>-1</sup>.

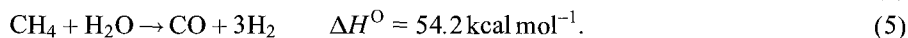
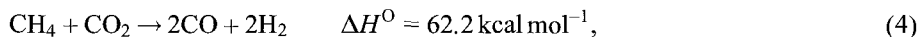
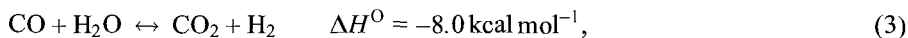
conversion, the CO selectivities and the H<sub>2</sub>/CO ratio for these solids. Conversion of methane and selectivity to CO decreased as the substitution of Ni by Co increased. The H<sub>2</sub>/CO ratio also decreased with increasing substitution.

LaNiO<sub>3</sub> was highly active and selective. The SEM micrograph and the XRD patterns of this solid after the reaction showed drastic structural changes, and only phases of La(OH)<sub>3</sub> and Ni<sup>0</sup> were identified. Due to the reducing atmosphere at high conversion of methane to CO and H<sub>2</sub>, the bulk reduction of LaNiO<sub>3</sub> occurred in agreement with an earlier report by Slagtern and Olsbye (1994).

The activity and selectivity of La<sub>0.8</sub>Ca<sub>0.2</sub>NiO<sub>3</sub> and La<sub>0.8</sub>Sr<sub>0.2</sub>NiO<sub>3</sub> were lower than those of LaNiO<sub>3</sub> and at the same time showed a fast deactivation during the catalytic process. The performance of LaCoO<sub>3</sub> as catalyst for POM to syngas was poor according to Choudhary et al. (1996a), but they did not test the time-on-stream stability. Note that Slagtern and Olsbye (1994) found for the Co perovskite that the CO yield increased after 30 h on stream and its value was comparable to that of LaNiO<sub>3</sub> (See table 5). Lago et al. (1997) reported some interesting clues to understand the behavior of LaCoO<sub>3</sub> for the POM reaction. They prerduced the perovskite in situ, producing Co<sup>0</sup> finely dispersed on La<sub>2</sub>O<sub>3</sub>(La–Co–O). This pretreated catalyst was active for methane combustion and only traces of CO and H<sub>2</sub> were observed during the reaction. The XRD and XPS spectra showed that under reaction conditions Co<sup>0</sup> was completely reoxidized, regenerating the original perovskite structure. The hydroxyl groups of La<sub>2</sub>O<sub>3</sub> might have contributed to the reoxidation of cobalt metal during the reaction via a reverse spillover process. They also tested different cobalt-containing perovskites RCoO<sub>3</sub> (R = Pr, Nd, Sm, and Gd) under the same pretreatment mentioned above. The Gd–Co–O system presented the best performance for CO and H<sub>2</sub> production at 1009 K. The methane conversion was 73% and the selectivities for CO and H<sub>2</sub> were 79 and 81%, respectively. The activity of the other perovskites decreased in the following order: Sm–Co–O ≫ Nd–Co–O > Pr–Co–O.

No reoxidation process to  $\text{RCoO}_3$  under the POM reaction was observed for  $\text{Gd-Co-O}$  and  $\text{Sm-Co-O}$ . However,  $\text{Nd-Co-O}$  was partially reoxidized to  $\text{NdCoO}_3$ . The authors proposed that the catalyst deactivation by reoxidation of  $\text{Co}^0$  dispersed on rare-earth oxides depends strongly on the nature of the rare-earth element and on the thermodynamic stability of the parent perovskite structure.

Interesting results were reported by Choudhary et al. (1996a) concerning the simultaneous partial and total oxidation of methane (reactions 1 and 2), the gas shift reaction (3) and reforming of methane with  $\text{CO}_2$  and steam (reactions 4 and 5) over  $\text{LaNiO}_3$ :



As a result of coupling the exothermic oxidation reactions (1)–(3) and the endothermic  $\text{CO}_2$  (4) and steam (5) reforming reactions over the same catalyst, the overall process could be conducted in a mildly endothermic, almost thermoneutral or slightly exothermic regime by changing the reaction conditions, especially the reaction temperature, and/or  $\text{CH}_4/\text{O}_2$  ratio in the feed. Thus, this process could evolve with little or no external energy requirement.

The results of methane reaction with  $\text{O}_2$ ,  $\text{CO}_2$  and  $\text{H}_2\text{O}$  over  $\text{LaNiO}_3$  are shown in fig. 9 (overleaf). The negative conversion of  $\text{CO}_2$  and  $\text{H}_2\text{O}$  observed at temperatures lower than 1073 K indicates that both compounds were produced during the process. However, when those conversions were positive, the selectivity based on methane to  $\text{CO}$  and  $\text{H}_2$  was close to 100%. The net heat of reaction,  $\Delta H_r$ , for the overall process is estimated by subtracting the heat of formation of the components in the feed at the reaction temperature from that of the components in the product stream.

High methane conversion, almost 100% selectivity to  $\text{CO}$  and  $\text{H}_2$  at 1123 K and  $\text{H}_2/\text{CO}$  ratio of about 2.0 could be obtained in this catalytic process. Since the heat produced by the exothermic reactions is used by the endothermic ones, it is expected that the transformation occurs in a more energy-efficient manner, avoiding the hot spot formation on the catalyst and, consequently, reaction runaway conditions.

### 2.2.1. Membrane reactors

One serious problem of the partial oxidation of methane from an economical point of view is the selection of the oxidant. When air is used as oxidant, a large amount of nitrogen is introduced into the reaction mixture which is not easy to separate from the  $\text{CO}$  and  $\text{H}_2$ . Thus, either recycling with cryogenic separation or pure oxygen are required. As an option, reactors based on dense ceramic membranes are presented as potentially useful for POM to syngas using air as a source of oxygen. In principle, the ceramic membrane can be shaped into a hollow-tube reactor, with air passed over the outside of the membrane and methane through the inside. The membrane is permeable to oxygen at high temperature. Oxygen ions are transported across the ceramic material. According to Teraoka et al. (1985), Mazanec et al. (1992) and Gur et al. (1992), membranes made

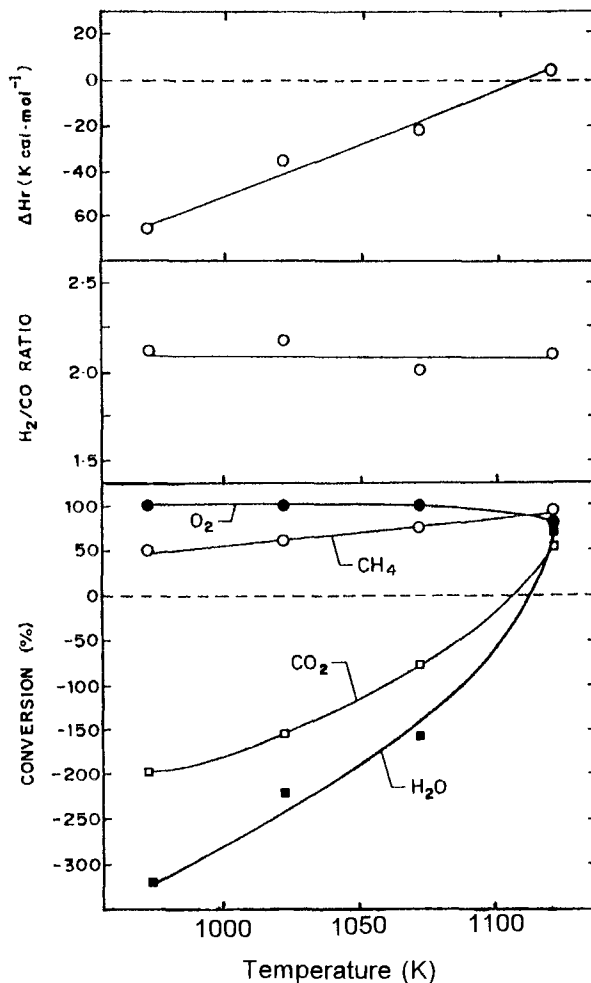


Fig. 9. Influence of temperature on conversion, H<sub>2</sub>/CO ratio and net heat of reaction in oxidative conversion of methane to syngas in presence of steam and CO<sub>2</sub> in the feed. Reaction conditions: CH<sub>4</sub>/O<sub>2</sub> = 2.1, CH<sub>4</sub>/H<sub>2</sub>O = CH<sub>4</sub>/CO<sub>2</sub> = 12.0, GHSV = 43 100 cm<sup>3</sup> g<sup>-1</sup> h<sup>-1</sup>. With permission from Choudhary et al. (1996a).

of mixed oxides can successfully separate oxygen and nitrogen at flux rates that could be considered commercially feasible.

Balachandran et al. (1995) prepared hollow membrane tubes made of SrCo<sub>0.5</sub>FeO<sub>x</sub> and La<sub>0.2</sub>Sr<sub>0.8</sub>Fe<sub>0.2</sub>Co<sub>0.8</sub>O<sub>3±x</sub> and tested them for partial oxidation reaction. To facilitate the catalytic reactions, a Rh-based catalyst was loaded onto the inner tube surface and in order to prevent the solid-state reaction between the catalyst and the ceramic tube, a gold wire mesh was wrapped around the tube.

The hollow tube made of  $\text{La}_{0.2}\text{Sr}_{0.8}\text{Fe}_{0.2}\text{Co}_{0.8}\text{O}_{3\pm x}$ , sintered at 1473 K, had a grain size of  $\sim 10\ \mu\text{m}$  and a density of  $\sim 5\ \text{g cm}^{-3}$ . At the beginning of the test reaction at 1123 K, this tube broke into several pieces. The cause of this behavior was that this material presented different structures depending on the oxygen environment. Cubic perovskite was the structure for the oxygen-rich atmosphere (20%  $\text{O}_2$ ). As the oxygen partial pressure was below 5%, the stable structure was oxygen-vacancy-ordered phase and this material expanded substantially after the phase transition. During the test reaction, high oxygen pressure was maintained outside the tube and low oxygen pressure inside. The material on the inner wall could loose more oxygen than that on the outer one. Thus, a stable oxygen gradient was generated and the material depending on its location in the tube may have different phases. Therefore, the factor responsible for the tube fracture appeared to be the lattice mismatch between the materials on the inner and outer walls of the tube.

$\text{SrCo}_{0.5}\text{FeO}_x$  showed a remarkable structural stability at high temperature and with different oxygen partial pressure. The conversion of methane using this tube was  $>98\%$ , the selectivity to CO was 90%, and the  $\text{H}_2/\text{CO}$  ratio was around 2.0. Some of these reactor tubes have been tested for syngas production up to  $\sim 1000\ \text{h}$ .

Tsai et al. (2000) tested  $\text{La}_{0.2}\text{Ba}_{0.8}\text{Fe}_{0.8}\text{Co}_{0.2}\text{O}_{3-y}$  as membrane material for POM at 1123 K during 1440 h under diluted methane stream. The products without any addition of other catalysts were mainly  $\text{CO}_2$ ,  $\text{H}_2\text{O}$ ,  $\text{CH}_4$  and  $\text{O}_2$ . However, these compounds could be further reformed to CO and  $\text{H}_2$  by packing either 5%  $\text{Ni}/\text{Al}_2\text{O}_3$  or 5%  $\text{Rh}/\text{Al}_2\text{O}_3$  on top of the membrane surface. The methane conversion was 95% and the CO selectivity was close to 100%.

Changes in the surface structure and/or composition of this membrane after long time-on-stream were revealed by the XRD and EDS techniques. Two perovskite phases with close lattice parameters might coexist on the reaction side. Besides, a strong peak of BaO was observed on the air-side surface. The EDS analysis for the membrane cross-sectional area showed that the barium content was significantly increased on the air-side surface, while a slightly higher Co content was found on the reaction-side surface. Note that the composition changes were preferentially located near both surfaces while the structure in the membrane center part remained similar to that of the fresh membrane.

The differences between the  $\text{La}_{0.2}\text{Ba}_{0.8}\text{Fe}_{0.8}\text{Co}_{0.2}\text{O}_{3-y}$  membrane and that prepared by Balachandran et al. (1995),  $\text{La}_{0.2}\text{Sr}_{0.8}\text{Fe}_{0.2}\text{Co}_{0.8}\text{O}_{3\pm x}$ , are the chemical stability and high oxygen permeation rates under reaction conditions for the Ba-based perovskite which prevent lattice mismatch and the subsequent fracture of the membrane during reaction.

### 2.3. Oxidative coupling of methane

The oxidative coupling of methane (OCM) is an attractive process for producing  $\text{C}_2$  (ethane and ethene) and  $\text{C}_{2+}$  hydrocarbons. There have been many studies since Keller and Bhasin (1982) demonstrated the viability of these reactions. It is generally accepted that the initial step in OCM involves methane activation by abstracting a hydrogen atom from methane, producing a methyl radical. The oxygen species on the catalytic surface at high temperature (reaction temperature range 950–1150 K) are responsible for this activation.

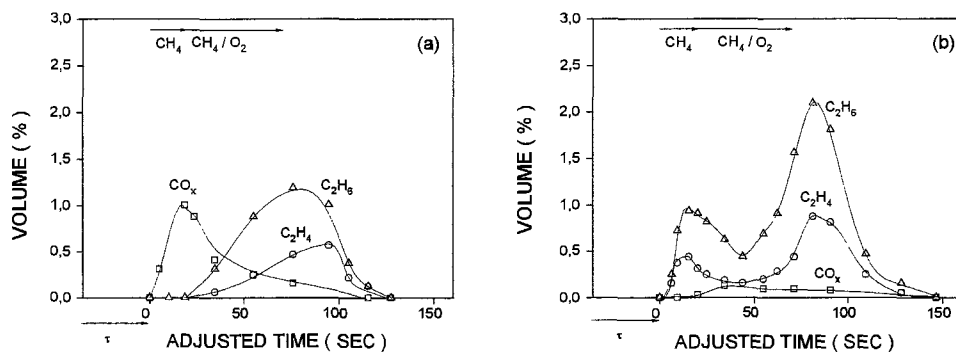


Fig. 10. Transient response to out-of-phase methane and oxygen step at 1023 K. (a)  $\text{Li/TiO}_2$ ; (b)  $\text{Li/La}_2\text{O}_3\text{-2TiO}_2$ . With permission from Miró et al. (1990).

A study of the nature of oxygen species adsorbed on  $\text{LaAlO}_3$  was carried out by Tagawa and Imai (1988) using the delayed pulse technique and TPD method. They reported that the adsorbed oxygen species, strongly attached to the surface, even after outgassing at 823 K, were responsible for the formation of  $\text{C}_2$  hydrocarbons while a weakly adsorbed oxygen species was involved in the formation of  $\text{CO}_2$  (total oxidation). The behavior of oxygen species on the R-based mixed oxide surface can be analyzed by the Temperature Programmed Desorption (TPD) technique, as was mentioned in sect. 1.4. The peak at low temperature is usually produced by adsorbed oxygen located at oxygen vacancies, which is easily removed by heating, whereas that at high temperature is considered to be lattice oxygen, associated to the reduction of B cations to lower valencies, which is stored in the lattice and could migrate to the surface. Thus, the amount and mobility of the lattice oxygen play an important role in the OCM process.

Miró et al. (1990) reported results of transient studies of OCM over different titania-supported alkali-metal catalysts and demonstrated that the role of lattice oxygen strongly depended on the catalyst used. The transient experiments were carried out in a flow system especially designed to minimize dead volume, and a combination of 3-way solenoid valves and a 16-loop valve was used to generate either step or pulse functions in the methane feed. In the step mode, at time zero the He feed to the reactor was switched to pure methane, and after 30 seconds to a mixture of methane and a small (2%) oxygen concentration for 60 seconds. Helium was then used to sweep reactants and products out of the reactor. Figures 10a and b show the transient response for  $\text{Li/TiO}_2$  and  $\text{Li/La}_2\text{O}_3\text{-2TiO}_2$  in the step experiments described above. When pure methane was first passed over  $\text{Li/TiO}_2$ , the main product was  $\text{CO}$ , with only trace amounts of  $\text{C}_2$  hydrocarbons (fig. 10a). As the mixture  $\text{CH}_4 + 2\% \text{O}_2$  was fed to the reactor, the production of  $\text{C}_2$  increased and  $\text{CO}$  decreased. Figure 10b shows the results of the same experiment for  $\text{Li/La}_2\text{O}_3\text{-2TiO}_2$ . When the degassed sample was contacted with pure methane (first step) significant amounts of  $\text{C}_2$  were produced from the reaction of lattice oxygen and methane. The shape of  $\text{C}_2$  vs time curve presents a maximum due to lattice oxygen depletion on the surface. As the mixture of methane and oxygen

Table 8  
Electrical conductivity and catalytic properties of R-mixed oxides<sup>a,b</sup>

Catalyst	Structure	Conduction type	Conversion of CH <sub>4</sub> (%)	Selectivity to C <sub>2</sub>
La <sub>0.8</sub> Sr <sub>0.2</sub> MnO <sub>3-δ</sub>	perovskite	n-type <sup>c</sup>	11.9	18.35
LaFe <sub>0.8</sub> Nb <sub>0.2</sub> O <sub>3-δ</sub>	perovskite	n-type	11.4	18.88
LaYO <sub>3</sub>	bixbyite	Insulator	16.8	45.69
LaYO <sub>3</sub>	perovskite	Insulator	14.4	27.12
La <sub>0.8</sub> Sr <sub>0.2</sub> YO <sub>2.9</sub>	perovskite	Electrolyte <sup>d</sup>	15.4	43.70

<sup>a</sup> Data from Alcock et al. (1993).

<sup>b</sup> Reaction conditions: CH<sub>4</sub>/O<sub>2</sub> = 6, 65% He, *T* = 1068 K.

<sup>c</sup> p-type, but performs as n-type under the conditions of the experiment.

<sup>d</sup> Ionic conductor.

was admitted (second step), the production of C<sub>2</sub> increased due to the interaction of methane with probably both adsorbed and lattice oxygen. These results were confirmed in pulse experiments. It is interesting to note that in pure methane, Li/La<sub>2</sub>O<sub>3</sub>-2TiO<sub>2</sub> yielded selectively C<sub>2</sub> opposed to Li/TiO<sub>2</sub>, which produced only CO. This behavior could be explained by taking into account the presence of lanthanum in the first catalyst. The active oxygen for the OCM reaction probably came from the interaction between lithium and La-based mixed oxides formed during the calcination of the solid.

The electronic properties of the catalyst could be related in some respect with the activated oxygen species involved in the OCM process. In this way, Alcock et al. (1993) studied the catalytic behavior of different mixed oxides exhibiting a wide range of electrical properties, going from superconducting oxides, La<sub>2-x</sub>Sr<sub>x</sub>CuO<sub>3-δ</sub>, through semiconducting p-type oxides, La<sub>0.8</sub>Sr<sub>0.2</sub>BO<sub>3-δ</sub> (B = Co, Cr, Mn), semiconducting n-type oxides, LaFe<sub>0.8</sub>Nd<sub>0.2</sub>O<sub>3-δ</sub>, pure ionic conductor, La<sub>0.8</sub>Sr<sub>0.2</sub>YO<sub>2.9</sub>, to insulators, LaYO<sub>3</sub>. Of all the compounds studied, only LaYO<sub>3</sub> has two crystal structures, bixbyite and perovskite.

The R-based mixed oxides with p-type electronic conductivity as well as the superconducting oxides were found to be inactive for the OCM reaction, and only total combustion of methane was observed. The only exception was La<sub>0.8</sub>Sr<sub>0.2</sub>MnO<sub>3-δ</sub>, which is probably an n-type conductor under the experimental conditions used. This solid is likely to be n-type under reducing atmosphere due to the stability of the Mn<sup>2+</sup> ion. La<sub>0.8</sub>Sr<sub>0.2</sub>MnO<sub>3-δ</sub> and LaFe<sub>0.8</sub>Nd<sub>0.2</sub>O<sub>3-δ</sub>, both considered n-type conductors, had low selectivity to C<sub>2</sub>, whereas La-Sr-Y-O systems, either ionic conductors or insulators, presented a good selectivity to those compounds (table 8).

La<sub>0.8</sub>Sr<sub>0.2</sub>YO<sub>2.9</sub> was more active than the LaYO<sub>3</sub> perovskite (table 8). The partial substitution of La by Sr increased the concentration of the oxygen vacancies and the valency of Y, without making it an electronic conductor. In other strontium-substituted perovskites, like the superconductor La<sub>2-x</sub>Sr<sub>x</sub>CuO<sub>3-δ</sub>, the Sr addition increased not only the vacancies of oxygen and Cu valency but also their electronic conductivities. Therefore,

Table 9  
Oxidative coupling of methane over LaYO<sub>3</sub> mixed oxides

Structure	Ratio CH <sub>4</sub> /O <sub>2</sub>	Reaction temperature (K)	Conversion of CH <sub>4</sub> (%)	Selectivity to C <sub>2</sub>	Reference
Bixbyite	6	1068	16.8	45.69	Alcock et al. (1993)
	2	973	28.6 <sup>a</sup>	14.3	Rehspringer et al. (1991)
	5	973	24.8 <sup>a</sup>	16.2	Rehspringer et al. (1991)
Perovskite	6	1068	14.4	27.12	Alcock et al. (1993)
	2	973	26.9 <sup>a</sup>	0.4	Rehspringer et al. (1991)
	5	973	22.9 <sup>a</sup>	0.5	Rehspringer et al. (1991)

<sup>a</sup> After 8 hours on stream.

a combination of either an insulator or an ionic conductor with the increase of oxygen vacancies and B valency appears to increase the C<sub>2</sub> production.

The differences in selectivity for LaYO<sub>3</sub> bixbyite and LaYO<sub>3</sub> perovskite reported by Alcock et al. (1993) and Rehspringer et al. (1991) are shown in table 9. It is clear from both experiments that the perovskite structure favored total oxidation while the bixbyite structure led to C<sub>2</sub> formation. This change in selectivity would be interpreted in terms of the differences in oxygen environment of lanthanum in both structures, as proposed by Rehspringer et al. (1991). The number of oxygens surrounding the cationic site are (i) in bixbyite 6 for both La and Y and (ii) in perovskite 12 for La and 6 for Y. If it is accepted that the cationic sites are the loci for methane activation, the oxidation rate will depend on the number of oxygens nearest to the active site and the relative distance between the cation and the oxygen. Thus, the (111) face being the most stable one for perovskite structure, La is surrounded by 6 oxygens, and for bixbyite this number drops to 4. This different oxygen environments for the active site could explain the observed reactivity difference.

CaO–CeO<sub>2</sub> form solid solutions with a high mobility of lattice oxygens. Zhang and Baerns (1992) used this solid as a model catalyst to evaluate the influence of oxygen mobility on C<sub>2</sub> formation. A notable advantage of this catalyst is the possibility of varying the oxygen-ion conductivity in a controllable way by changing the CaO content.

A certain amount of Ca is incorporated into the CeO<sub>2</sub> matrix to form a fluorite-type solid solution with a solubility limit around 20%. According to XPS results the surface composition was approximately equal to the bulk. There is a small enrichment of Ca on the surface for solids with low Ca content. The surface area of the catalysts prepared did not differ significantly.

Pure CaO and CeO<sub>2</sub> have rather low oxygen-ion conductivities. However, this conductivity notably increased first and then decreased as the substitution of Ce by Ca increased, having a maximum around the solubility limit. As the Ca content exceeded this limit, the conductivity decreased gradually due to the formation of additional calcium oxide crystallites. The dependence of selectivity to C<sub>2</sub> for OCM reaction on the Ca content



followed a similar pattern to the oxygen-ion conductivity. Thus, the synergistic interaction between Ca and Ce resulting in large  $C_2$  selectivity may be tentatively ascribed to the increasing oxygen-ion conductivity.

### 2.3.1. Alkali promotion

Yamamura et al. (1994) found that although the perovskite oxides alone showed a relatively low catalytic activity for the OCM reaction (table 10), a noticeable increase in activity and selectivity to  $C_2$  was observed when those mixed oxides were promoted by alkali halides. NaCl was the most effective promoter among the alkali halides.

The catalytic activity for OCM over mixed oxides with perovskite structure,  $GdMnO_3$  and  $CaMnO_3$ , and these solids promoted with alkali compounds were reported by Siriwardane and Shamsi (1990). The catalytic performance of these perovskites was compared with that of mechanical mixtures of oxides with similar elementary composition.  $GdMnO_3$  promoted with  $Na_4P_2O_7$  was found to be an active and selective catalyst. A  $C_2$  yield of 20% was obtained over this catalyst at 1100 K. There was no appreciable change in either the methane conversion or  $C_2$  yield after 26 h on stream.  $CaMnO_3$  alone and promoted with either  $Na_4P_2O_7$  or  $Na_2CO_3$  was found to be a poor catalyst for this reaction.

According to the Mn 3s XPS spectra obtained for all the samples, the manganese on the surface was in a mixed oxidation state of 3+ and 4+. The structure of  $GdMnO_3$  demands Mn to be 3+ while in  $CaMnO_3$  it is 4+. However, there was a combination of  $Mn^{3+}$  and  $Mn^{4+}$  on both surfaces and their relative proportion was slightly different on the two samples.

The activity and selectivity for  $GdMnO_3$  and  $GdMnO_3$  promoted with Na-based compounds are shown in table 11. The catalytic behavior of  $GdMnO_3$  and  $Gd_2O_3$ -MnO mixture was similar. XRD patterns show that in both solids the structure did not change during the reaction. Thus, having the Gd and Mn adjacent to each other was the key which contributed to the different catalytic properties on these catalysts compared to those of single oxides.

Table 10  
OCM over perovskite oxides promoted with NaCl<sup>a,b</sup>

Structure	Conversion of $CH_4$ (%)	Selectivity to $C_2$	Yield
BaPrO <sub>3</sub>	20.5	34.3	7.1
NaCl/BaPrO <sub>3</sub>	26.1	53.1	13.9
NaNbO <sub>3</sub>	16.1	38.7	6.2
NaCl/NaNbO <sub>3</sub>	45.5	45.6	20.8
KNbO <sub>3</sub>	8.5	41.2	3.5
NaCl/KNbO <sub>3</sub>	36.8	46.5	17.1
NaCl/LiNbO <sub>3</sub>	16.9	76.0	12.8

<sup>a</sup> Data from Yamamura et al. (1994).

<sup>b</sup> Reaction conditions:  $CH_4:O_2 = 2:1$ ,  $T = 1023$  K.

Table 11  
Catalytic performance of catalysts containing Gd and Mn after 2 hours of OCM reaction at 1101 K<sup>a,b</sup>

Catalyst	Conversion of CH <sub>4</sub> (%)	Selectivity to C <sub>2</sub>	Yield
Mn <sub>3</sub> O <sub>4</sub>	7.4	13.8	1.0
Na <sub>4</sub> P <sub>2</sub> O <sub>7</sub> /Mn <sub>3</sub> O <sub>4</sub> <sup>c</sup>	15.4	50.8	7.8
Gd <sub>2</sub> O <sub>3</sub>	12.2	48.0	5.8
Na <sub>4</sub> P <sub>2</sub> O <sub>7</sub> /Gd <sub>2</sub> O <sub>3</sub> <sup>c</sup>	15.0	21.0	3.1
GdMnO <sub>3</sub>	11.2	1.1	0.2
Na <sub>2</sub> CO <sub>3</sub> /GdMnO <sub>3</sub> <sup>c</sup>	13.2	7.4	1.0
Na <sub>4</sub> P <sub>2</sub> O <sub>7</sub> /GdMnO <sub>3</sub> <sup>c</sup>	16.9	49.7	8.4
Gd <sub>2</sub> O <sub>3</sub> -Mn <sub>3</sub> O <sub>4</sub>	9.1	2.3	0.2
Na <sub>4</sub> P <sub>2</sub> O <sub>7</sub> /Gd <sub>2</sub> O <sub>3</sub> -Mn <sub>3</sub> O <sub>4</sub> <sup>c</sup>	16.2	50.9	8.2

<sup>a</sup> Data from Siriwardane and Shamsi (1990).

<sup>c</sup> Moles of Na-based promoter/moles of solid = 0.1.

<sup>b</sup> Reaction conditions: CH<sub>4</sub>:O<sub>2</sub>:He = 8.8:1.6:6.9.

The elementary composition of the surfaces of these catalysts was analyzed by Auger Electron Spectroscopy (AES). This technique provides information about the elementary composition on the surface up to a depth of about 30 Å. The Na/Gd ratio obtained from AES data for Na<sub>4</sub>P<sub>2</sub>O<sub>7</sub>/GdMnO<sub>3</sub> was 0.48, and that for Na<sub>2</sub>CO<sub>3</sub>/GdMnO<sub>3</sub> was 0.76. Since the latter produced lower C<sub>2</sub> yield than the former, this suggests that phosphorus played a significant role on the catalytic properties of this perovskite. Moreover, the sodium alone did not promote the activity. Thus, the good performance of Na<sub>4</sub>P<sub>2</sub>O<sub>7</sub>/GdMnO<sub>3</sub> could not be related to either Na, P, or Mn on the surface. The active sites might have been formed by a complex interaction involving all the elements on the surface, as suggested by the authors.

High temperature causes the partial loss of the promoter during the reaction resulting in catalysts in which the dispersion and location of the promoter components are not readily controlled. The layered perovskites seem to be an interesting system to fix the alkali close to the lanthanide species in a perovskite environment. The structure of this kind of perovskites is made up of layers of alkali ions dispersed and sandwiched between lanthanide perovskite layers.

Layered perovskites A<sub>2</sub>R<sub>2</sub>Ti<sub>3</sub>O<sub>10</sub> (A=K, Rb, Na; R=La, Nd, Sm, Gd, Dy, Ce) and alkali-carbonate-promoted double perovskite LaCaMnCoO<sub>6</sub> were tested as OCM catalysts by Campbell (1992) using a packed-bed reactor. In the co-fed experiments, a gas stream containing methane, oxygen and nitrogen at a given composition was fed to the reactor. In cyclic or sequential mode experiments methane, nitrogen or oxygen were alternatively fed.

Table 12 shows the conversion of methane and selectivity to C<sub>2</sub> for the layered perovskite-type materials using a co-fed mode. K<sub>2</sub>La<sub>2</sub>Ti<sub>3</sub>O<sub>10</sub> and K<sub>2</sub>Pr<sub>2</sub>Ti<sub>3</sub>O<sub>10</sub> presented the highest C<sub>2</sub> yields, comparable to many of the results reported for active OCM catalysts.

Table 12  
Activity and selectivity for OCM reaction over layered perovskites<sup>a,b</sup>

Catalyst	Conversion of CH <sub>4</sub> (%)	Selectivity to C <sub>2</sub> (%)	Yield (%)	GHSV (h <sup>-1</sup> )
K <sub>2</sub> La <sub>2</sub> Ti <sub>3</sub> O <sub>10</sub>	39	42	16.3	3000
K <sub>2</sub> Nd <sub>2</sub> Ti <sub>3</sub> O <sub>10</sub>	26	24	6.3	3750
K <sub>2</sub> Sm <sub>2</sub> Ti <sub>3</sub> O <sub>10</sub>	25	23	5.8	3000
K <sub>2</sub> Dy <sub>2</sub> Ti <sub>3</sub> O <sub>10</sub>	25	15	3.9	3430
K <sub>2</sub> Gd <sub>2</sub> Ti <sub>3</sub> O <sub>10</sub>	29	20	5.7	1770
Rb <sub>2</sub> La <sub>2</sub> Ti <sub>3</sub> O <sub>10</sub>	21	31	6.6	4500
Na <sub>2</sub> La <sub>2</sub> Ti <sub>3</sub> O <sub>10</sub>	35	28	9.8	4620
K <sub>2</sub> Ce <sub>2</sub> Ti <sub>3</sub> O <sub>10</sub>	29	36	10.4	715
K <sub>2</sub> Pr <sub>2</sub> Ti <sub>3</sub> O <sub>10</sub>	34	40	13.2	3430

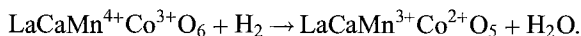
<sup>a</sup> Data from Campbell (1992).

<sup>b</sup> Reaction conditions: CH<sub>4</sub>/O<sub>2</sub> = 2, *T* = 1073 K.

The effect of changing the CH<sub>4</sub>/O<sub>2</sub> ratio (2, 4, 8) and reaction temperature (973, 1023, 1073 K) on the coupling process was determined for K<sub>2</sub>La<sub>2</sub>Ti<sub>3</sub>O<sub>10</sub>, Rb<sub>2</sub>La<sub>2</sub>Ti<sub>3</sub>O<sub>10</sub> and Na<sub>2</sub>La<sub>2</sub>Ti<sub>3</sub>O<sub>10</sub>. The methane conversion, ethene/ethane ratio, and CO<sub>2</sub>/CO ratio decreased while the C<sub>2</sub> selectivity and O<sub>2</sub> conversion increased with the increase of CH<sub>4</sub>/O<sub>2</sub> ratio. Raising the temperature resulted in higher methane and O<sub>2</sub> conversions, ethene/ethane and CO<sub>2</sub>/CO ratios and C<sub>2</sub> selectivity.

The K<sub>2</sub>La<sub>2</sub>Ti<sub>3</sub>O<sub>10</sub> did not show any significant deactivation after 149 h on stream. At the end of the 149 h run, 1.2% CO<sub>2</sub> was introduced into the reactant stream. This resulted in a decrease of methane conversion with constant C<sub>2</sub> selectivity. After that, 10 ppm of ethyl chloride was added to the stream showing an increase of the CO<sub>2</sub>/CO ratio and slow deactivation of the catalyst.

According to Campbell (1992), the double perovskite, LaCaMnCoO<sub>6</sub>, was of interest as a cyclic mode methane coupling catalyst due to its structure and redox properties. This mixed oxide has an ordered perovskite structure showing multiple occupations of both A (La, Ca) and B (Mn, Co) sublattices. The crystalline material presented some ordered domains, while in other areas the cations were distributed at random. For the ordered domains, the most probable structural model was an ABO<sub>3</sub> perovskite-type structure in which Mn<sup>4+</sup> and Co<sup>3+</sup> ions occupy B positions in adjacent ABO<sub>3</sub> units while La<sup>3+</sup> and Ca<sup>2+</sup> ions alternate in A positions. Two ions of this structure can be reduced:



The unpromoted LaCaMnCoO<sub>6</sub> showed a good methane conversion, 18.7%, in the cyclic mode; however the C<sub>2</sub> selectivity was low, <2% at 1123 K. Na<sub>2</sub>CO<sub>3</sub> addition to this material changed its catalytic properties. At 1123 K, Na<sub>2</sub>CO<sub>3</sub>/LaCaMnCoO<sub>6</sub> gave high C<sub>2</sub> selectivity (>80%) but low methane conversion (10%). The XRD patterns of fresh and used catalyst were consistent with the double perovskite. No incorporation of Na in the perovskite structure during the reaction was observed. Other alkali promoters were tested

such as  $\text{K}_2\text{CO}_3$ ,  $\text{Li}_2\text{CO}_3$ ,  $\text{Rb}_2\text{CO}_3$  and  $\text{Cs}_2\text{CO}_3$ , but for this mode of reactant feeding, the best was  $\text{Na}_2\text{CO}_3$ .

The presence of alkali on the surface of mixed oxides, added as a promoter or fixed into the solid structure as in layered perovskites, significantly improved the  $\text{C}_2$  yield, suggesting that these elements influence the oxygen species responsible for the formation of methyl radicals and/or limit the concentration of those oxygen sites associated with the total oxidation of methane.

### 2.3.2. *Membrane reactors*

There seems to be a limit on the  $\text{C}_2$  yield in a fixed-bed reactor around 25%. This limit could arise from the instability of the partial oxidation products which is higher than that of methane. Some alternate reactor configurations have been proposed recently in order to improve this yield; among them, membrane reactors have attracted increasing attention in the scientific community because they offer several advantages for OCM such as simplicity in process design, safety in operation, and the possibility of achieving higher  $\text{C}_2$  selectivity and yield.

The ceramic membrane reactors can be classified into two groups according to the type of membrane used: (i) dense ionic-conducting membrane and (ii) porous ceramic membrane; both kinds of membranes are covered with a catalyst layer. For the first group, methane is brought into contact with one of the membrane surfaces and reacts with oxygen, which is permeating from the other surface. The oxygen is transported across the ceramic material in the form of anions rather than molecules. In principle, this membrane is permeable to the oxygen at high temperature, but not to nitrogen or any other gas. The catalytic properties of membrane surface, oxygen permeability, oxygen-ion conductivity and operating conditions are critical for the performance of dense-membrane reactors. For the second group, the membrane serves as an oxygen distributor and methane reacts with this oxygen in a manner identical to that in conventional fixed-bed reactors. The performance of the porous-membrane reactor strongly depends on the kinetics associated with the catalyst used for the OCM reaction and the distribution of oxygen along the axial direction.

Wang and Lin (1995) proposed the use of a dense ionic-conducting membrane with catalytically active surface, selective for OCM. In this case, the oxygen permeating from the other side of the membrane may directly replace the oxygen in the active sites consumed in the methane activation process. If the oxygen permeability through the membrane could be controlled to be comparable to the oxygen consumption rate on the surface, it could be possible to minimize the methane combustion resulting in an extremely high  $\text{C}_2$  selectivity. However, the calcination of the membrane-catalyst system at high temperature could lead to a complex interfacial structure between the coated catalyst particles and the membrane surface; such membrane composites could not maintain the original catalytic properties. This could be due to the formation of non-conducting phases and/or the generation of catalytically inactive compounds.

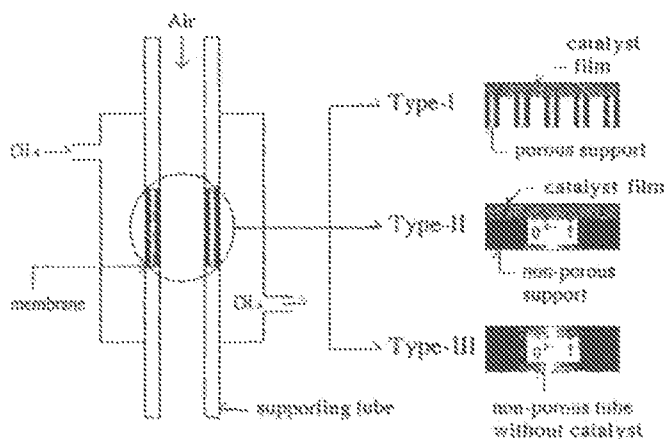


Fig. 11. Diagram of membrane reactor system. With permission from Nozaki et al. (1992).

Table 13  
Composition of different membranes<sup>a</sup>

Support	Catalyst layer	Type
SiO <sub>2</sub> -Al <sub>2</sub> O <sub>3</sub>	Bi <sub>2</sub> O <sub>3</sub> -CeO <sub>2</sub> (MC) <sup>b</sup>	I
YSZ <sup>c</sup>	PbO-K <sub>2</sub> O	II
CSZ <sup>d</sup>	PbO-K <sub>2</sub> O	II
MSZ <sup>e</sup>	PbO-K <sub>2</sub> O	II
Sr(CeYb)O <sub>3</sub>	PbO-K <sub>2</sub> O	II
Sr(CeYb)O <sub>3</sub>	-	III

<sup>a</sup> Data from Nozaki et al. (1992).

<sup>d</sup> MSZ: magnesia-stabilized zirconia.

<sup>b</sup> MC, molten alkali carbonates of K<sub>0.76</sub>Li<sub>1.24</sub>CO<sub>3</sub>.

<sup>e</sup> CSZ: calcia-stabilized zirconia.

<sup>c</sup> YSZ: yttria-stabilized zirconia.

Some of the many different types of catalysts which have good catalytic properties for the OCM reaction qualify as membrane materials. Membrane reactors for OCM were designed and tested by Nozaki et al. (1992). Three kinds of reactors were developed: the first one consisted of a porous membrane covered with a thin film of catalyst (type I); the second one, a dense ionic-conducting membrane (non porous) with catalytic layer (type II); and the third one was a membrane made of perovskite-type mixed oxides which was active for OCM (type III). Figure 11 presents the diagram for the membrane reactor system and table 13 shows the different materials used for supports and coated catalysts.

A Type-I membrane containing Ce (13%) on the surface was tested at 1023 K. The results showed it to be a good catalyst for the total oxidation of methane. On the other hand, the type-II membrane, in which the support was calcia-stabilized zirconia (CSZ) and magnesia-stabilized zirconia (MSZ) showed lower activity than yttria-stabilized zirconia (YSZ). The activation energy of the last membrane (non porous) for the formation

of  $C_2$  was almost the same as that of the type-I membrane (porous). These results suggest that the reaction rate was limited by oxygen transport in CSZ and MSZ type-II membranes and by the surface reaction of methane in the YSZ type-II membrane.

The selectivity to  $C_2$  over the type-III membrane  $SrCe_{0.95}Yb_{0.05}O_3$  (commercially available membrane), was 100% but the conversion of methane was low. This might be symptomatic of the oxide-ion conductivity control since activity is enhanced by the addition of  $PbO-K_2O$  (Type-II membrane).

OCM catalytic properties of R-based mixed oxide ceramic membranes appeared to be determined by the synthesis method, oxygen permeation from one side to the other, surface composition, and the electronic conduction mechanism.

## 2.4. Hydrogenation

Under this heading all the reactions involving  $H_2$  as one of the reactants will be reviewed. They include: hydrocarbon hydrogenation and hydrogenolysis,  $CO_x$  hydrogenation and olefin hydroformylation. The common denominator in all these systems is that the perovskite surface is reduced to varying extents depending on the reactant mixture composition.

### 2.4.1. Hydrogenation and hydrogenolysis of hydrocarbons

Libby (1971) was probably the first author to report that hydrocarbons could be hydrogenated and hydrogenolysed over  $RCoO_3$  ( $R=La, Nd, Py$ ). From then on, for roughly 20 years, a number of papers were published on this subject. Between 1989 and 1992 two reviews touched on this matter (Tejuca et al. 1989, Petunchi and Lombardo 1990) and a specific one was published by Ichimura et al. (1992). No original papers have been published during the 1990s.

Lombardo and co-workers published a series of papers between 1980 and 1986 on the hydrogenation and hydrogenolysis of  $C_2-C_4$  hydrocarbons over reduced  $LaCoO_3$  and  $LaCoO_3$  supported on  $La_2O_3$ . They concluded that these reactions occur over metallic centers ( $Co^0$ ) generated either during reaction or hydrogen pretreatment of the catalyst.

The following experimental facts support the above statement:

- (i) Table 14 reproduced from Petunchi et al. (1981) shows three criteria that support the role of  $Co^0$  on the surface of  $LaCoO_3$ .
- (ii) Lombardo et al. (1983) using XPS detected the onset of surface reduction ( $Co^{3+} \rightarrow Co^0$ ) at a temperature 150 K lower than in the bulk.
- (iii) Nudel et al. (1984) reported that a mild reduction of  $LaCoO_3$  was needed to selectively hydrogenate 1,3-butadiene to linear butenes. Using  $D_2$  and NMR spectroscopy they concluded that the reaction mechanism was consistent with the presence of  $Co^0$  on the catalyst surface.
- (iv) Ulla et al. (1987) reported an induction period when reacting  $CO_2 + H_2$  over unreduced  $LaCoO_3$  at 550 K. This induction period was eliminated when the oxide was prereduced in  $H_2$  at 573 K.

Table 14  
Criteria for differentiation of ethene hydrogenation mechanisms over metals and metal oxides<sup>a</sup>

Criterion	Oxides	Metals	LaCoO <sub>3</sub>
Deactivation <sup>b</sup>	No	Yes	Yes
Self-hydrogenation	No	Yes	Yes
C <sub>2</sub> H <sub>4</sub> + D <sub>2</sub>	C <sub>2</sub> H <sub>4</sub> D <sub>2</sub> <sup>c</sup> C <sub>2</sub> H <sub>4</sub>	C <sub>2</sub> H <sub>6-y</sub> D <sub>y</sub> <sup>d</sup> C <sub>2</sub> H <sub>4-x</sub> D <sub>x</sub>	Multiply-exchanged ethene and ethane

<sup>a</sup> With permission from Petunchi et al. (1981).

<sup>b</sup> Applies to short runs at or below room temperature.

<sup>c</sup> Low-temperature experiments.

<sup>d</sup> Average deuterium exchanged depends on the metal considered.

Ichimura et al. (1980, 1981a,b) studied the hydrogenation and hydrogenolysis of C<sub>2</sub>–C<sub>5</sub> hydrocarbons and concluded that exposed Co<sup>3+</sup> are the loci of catalytic activity. Although ionic cobalt may be active in this kind of reaction, it has been long recognized that coordinatively unsaturated (partially reduced) cations are at the center of active sites. Furthermore, the question is that when metallic centers are present on the surface, they will exhibit a much higher activity than the ionic cobalt.

In this vein, the work of Crespin et al. (1983b) on LaNiO<sub>3</sub> is particularly enlightening. On this solid, it is possible to stabilize Ni<sup>3+</sup>, Ni<sup>2+</sup>, Ni<sup>+</sup> and Ni<sup>0</sup> through the carefully controlled reduction of the oxide with pure H<sub>2</sub>. EXAFS measurements have shown that no mixed states could be detected. The four solids were tried as ethylene hydrogenation catalysts. LaNiO<sub>3</sub> was inactive at 293 K while LaNiO<sub>2</sub> showed negligible activity at 268 K. La<sub>2</sub>Ni<sub>2</sub>O<sub>5</sub> exhibited good activity at 268 K, and by far the most active was Ni/La<sub>2</sub>O<sub>3</sub> at 195 K. In brief, if metal sites are present on the catalyst surface they will dominate over the less active cationic centers.

It is concluded that under very mild reducing conditions, coordinatively unsaturated Co<sup>2+</sup> (very unlikely Co<sup>3+</sup>) may be the loci of hydrogenation activity. However, as soon as metallic centers (Co<sup>0</sup>) appear on the oxide surface, they will become the main actors in the hydrogenation of hydrocarbons. The applicability and limitations of these guidelines to the hydrogenation of CO<sub>x</sub> will be outlined in the following section.

#### 2.4.2. CO<sub>x</sub> hydrogenation and hydroformylation of ethylene

CO and CO<sub>2</sub> may react with H<sub>2</sub> to yield hydrocarbons and oxygenates. Both types of products are thermodynamically favored and therefore, the route selection is catalytically controlled. Other secondary undesirable reactions may occur leading to carbon deposition and CO consumption (water gas shift reaction). Fe and Co are traditional Fischer–Tropsch catalysts while Cu and Rh lead the reaction to alcohol formation.

Watson and Somorjai (1982) and Gysling et al. (1987) found out that LaRhO<sub>3</sub> was a promising catalyst for the synthesis of linear alcohols from CO + H<sub>2</sub>. In the early 1980s the former authors were trying to understand the variable catalytic behavior of Rh-containing formulations. One of the uncontrolled variables might be the reduction of the cations to

Table 15  
XPS data for Rh3d<sub>5/2</sub> signal

Rh compound	Binding energy <sup>a</sup>	Reference
Rh <sup>0</sup> (metal)	307.1	Gysling et al. (1987)
	307.1	Brinen and Malera (1972)
	307.1	Foley et al. (1983)
LaRhO <sub>3</sub>	308.6 (1.25)	Gysling et al. (1987)
	311.0 (2.0)	Watson and Somorjai (1982)
Used LaRhO <sub>3</sub>	307.7 (2.7)	Watson and Somorjai (1982)
Reduced LaRhO <sub>3</sub> <sup>b</sup>	Rh <sup>0</sup> + Rh <sup>3+</sup> <sup>c</sup>	Gysling et al. (1987)
Reduced LaRhO <sub>3</sub> <sup>d</sup>	307.1	Gysling et al. (1987)

<sup>a</sup> Full width at half maximum given in parentheses.

<sup>c</sup> See fig. 9.

<sup>b</sup> Reduction conditions: 573 K 1 hour, 2:1 =H<sub>2</sub>:CO.

<sup>d</sup> Reduction conditions: 573 K, 0.5 hour, pure H<sub>2</sub>.

the metallic state. So, they decided to use LaRhO<sub>3</sub> in their studies. They prepared the perovskite using the classical ceramic method and studied the catalytic behavior using a H<sub>2</sub>:CO=1:1 mixture at 6 atm pressure in the 500–600 K temperature range.

Gysling et al. (1987) prepared the mixed oxide following a more involved procedure. They reported that the best result was obtained using an excess of the La compound and eliminated the La<sub>2</sub>O<sub>3</sub> excess by leaching the calcined solid with a warm diluted acetic acid solution. They operated at the same H<sub>2</sub>/CO=1 ratio, reaction temperature range 500–639 K, but at 50 atm pressure.

Both groups reported good selectivities to oxygenates and agreed that methanol is not an intermediate in the formation of C<sub>2+</sub> oxygenates. The higher oxygenates may be formed by CO insertion into surface alkyl fragments. However, their key point of discrepancy is about the presence of Rh<sup>+</sup> species under reaction conditions. Table 15 summarizes key XPS data reported by both groups. To begin with, there is a significant difference in both binding energy (BE) and peak width reported for Rh<sup>3+</sup> on the fresh catalyst. After use, the Watson and Somorjai catalyst yields a wide Rh 3d<sub>5/2</sub> signal that according to the authors is symptomatic of the presence of Rh<sup>+</sup>. Under similar circumstances (not exactly the same, though) Gysling et al. (1987) found that the Rh 3d<sub>5/2</sub> spectrum could be convoluted by a combination of the Rh<sup>3+</sup> and Rh<sup>0</sup> signal (see fig. 12). To further sustain the key role of the Rh metal, Gysling et al. (1987) ran the same experiments on a Rh/SiO<sub>2</sub> catalyst and reported a very similar product distribution. They also ran C<sub>2</sub>H<sub>4</sub> hydroformylation over LaRhO<sub>3</sub> that has been prereduced in H<sub>2</sub> at temperatures between 473 and 598 K. Since the selectivity to propionaldehyde remained essentially constant they concluded that Rh<sup>+</sup> may not have been present. They based their conclusion on the fact that Rh<sup>+</sup> is known to favor the hydroformylation reaction in the liquid phase. In one point they agreed and this is that Rh<sup>0</sup> is present in used LaRhO<sub>3</sub> and plays a role (key role for Gysling et al.) in the reaction mechanism.



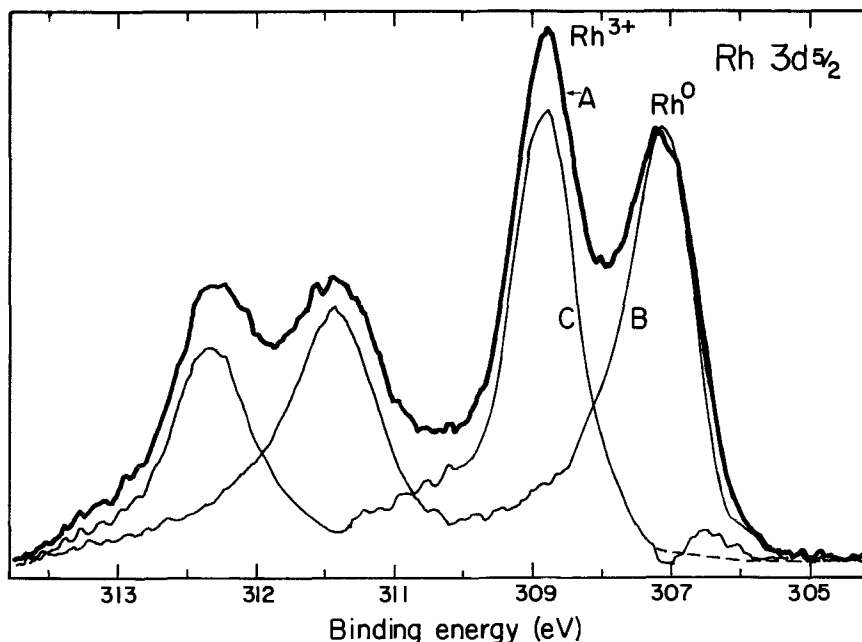


Fig. 12. Deconvolution of the Rh 3d<sub>5/2</sub> spectrum of LaRhO<sub>3</sub> reduced at 573 K in 2:1 H<sub>2</sub>:CO into Rh<sup>0</sup> and Rh<sup>3+</sup> components from fully reduced LaRhO<sub>3</sub> and untreated LaRhO<sub>3</sub>. With permission from Eastman Kodak Company (Gysling et al. 1987).

Cu-based perovskites have also been used to produce oxygenates. Brousard and Wade (1986), Brown Bourzutschky et al. (1990) and Rojas et al. (1990) prepared, characterized and used LaMn<sub>1-x</sub>Cu<sub>x</sub>O<sub>3+y</sub> as catalysts while van Grieken et al. (1991) did the same with LaTi<sub>1-x</sub>Cu<sub>x</sub>O<sub>3</sub>.

LaMn<sub>1-x</sub>Cu<sub>x</sub>O<sub>3+y</sub> maintains the perovskite structure up to  $x=0.6$ . Beyond this level, La<sub>2</sub>CuO<sub>4</sub> and CuO are formed. These are, in fact, the stable phases when  $x=1$ . The LaMnO<sub>3.24</sub> solid was weakly active for the CO hydrogenation and produced only hydrocarbons. With Cu substitution the activity gradually increased and selectivity to alcohol became higher than 90%. Brown Bourzutschky et al. (1990) made these kinetic measurements at 7.5–14 atm, 498–573 K, H<sub>2</sub>/CO ratios 1–3. In all cases, the catalysts were prereduced in H<sub>2</sub> at 523–573 K. This treatment stopped 2 hours after no more water could be detected by gas chromatography downstream of the reactor. For comparison, they also studied under the same conditions: Cu/SiO<sub>2</sub> unpromoted and promoted with La<sub>2</sub>O<sub>3</sub>, Cu/La<sub>2</sub>O<sub>3</sub>, Cu/MnO<sub>2</sub> + La<sub>2</sub>O<sub>3</sub>, and unsupported copper powder. The catalysts were characterized by XRD and XPS before and after use.

Cu<sup>0</sup> is present in all the catalysts studied except LaMnO<sub>3.24</sub>. There is a fair correlation between the Cu molar fraction in perovskites and lanthanum supported catalysts as shown in fig. 13. Table 16 shows the product distribution obtained with all the catalysts assayed.

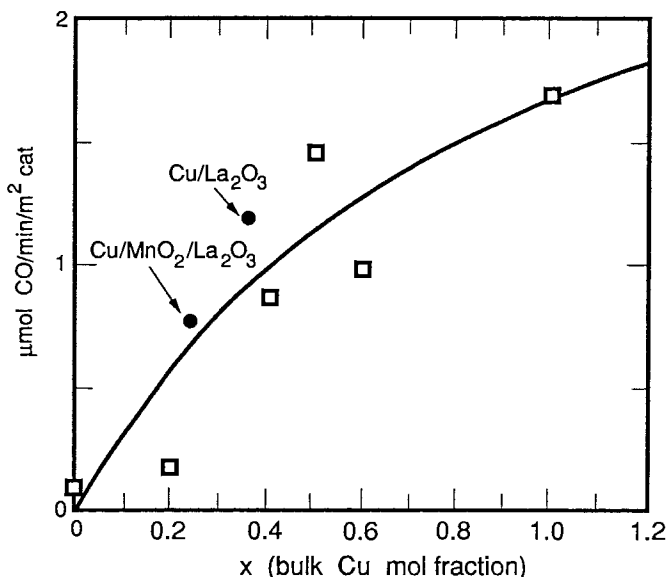


Fig. 13. Correlation of CO hydrogenation activity with bulk Cu mole fraction, for perovskites and lanthana-supported catalysts ( $H_2/CO=2$ ,  $P=10.6$  atm,  $T=573$  K). With permission from Brown Bourzutschky et al. (1990).

Note the similarities in selectivity observed in all the catalysts except those containing only  $Cu^0$  ( $Cu/SiO_2$ ) and without copper ( $LaMnO_{3.24}$ ). The first conclusion that arises from this study is that  $Cu^0$  is needed to obtain high selectivity to alcohols but this is not enough. Promotion of copper with  $La_2O_3$  or  $NaO_x$  is required to reach high selectivities to oxygenates. Following the ideas of Klier et al. (1982) and in line with their own catalytic and characterization results, Brown Bourzutschky et al. (1990) proposed that both  $Cu^0$  and  $Cu^+$  are required for the synthesis of alcohols. It is also proposed that  $Cu^+$  can be stabilized at the adlineation between metallic copper and  $La_2O_3$  or  $NaO_x$ . The presence of manganese together with  $La_2O_3$  does not significantly affect activity but it seems to somewhat suppress the formation of  $C_{2+}$  alcohols.

$LaTi_{1-x}Cu_xO_3$  ( $0 \leq x \leq 1$ ) were studied by van Grieken et al. (1991). For comparison they also included  $Cu/La_2O_3$ . They tested the catalysts at higher pressure and higher  $H_2/CO$  ratio than Brown Bourzutschky et al. (1990). The data are reported in table 17. Note that Cu in this matrix is less selective for alcohol production than  $LaMn_{1-x}Cu_xO_3$  (table 16). Furthermore,  $Cu/La_2O_3$  and  $LaCuO_{2.5}$  ( $La_2CuO_4 + CuO$ ) exhibit very different alcohol selectivities in both studies.

Rojas et al. (1990), based on their Auger measurements, and Fierro (1992) in his review, argue that copper is mainly present as  $Cu^+$  under reaction conditions. They justifiably say that XPS is not a good tool to distinguish  $Cu^0$  from  $Cu^+$  due to the overlapping BE's of these two oxidation states. Instead, they argue, the X-ray-induced Auger spectrum is the right tool to distinguish  $Cu^+$  from  $Cu^0$  at the surface level. They show the Auger

Table 16  
Product distribution for all catalysts: overall selectivities<sup>a,b</sup>

Catalyst <sup>b</sup>	Selectivity (%) <sup>c</sup>		
	HC	MeOH	C <sub>2+</sub> OH <sup>d</sup>
LaMn <sub>1-x</sub> Cu <sub>x</sub> O <sub>3-λ</sub> perovskites			
<i>x</i> = 0.0	100.0	0.0	0.0
<i>x</i> = 0.2	6.3	81.4	11.6
<i>x</i> = 0.4	4.0	84.6	9.9
<i>x</i> = 0.5	7.0	79.9	9.3
<i>x</i> = 0.6	10.2	70.4	18.4
<i>x</i> = 1.0	5.7	81.4	12.7
NaO <sub>x</sub> /Cu powder	9.1	84.5	5.1
Cu/SiO <sub>2</sub>	81.6	4.5	7.2
La <sub>2</sub> O <sub>3</sub> /Cu/SiO <sub>2</sub>	34.0	48.7	1.4
Cu/La <sub>2</sub> O <sub>3</sub>	6.6	78.0	14.4
Cu/MnO/La <sub>2</sub> O <sub>3</sub>	5.2	87.7	6.9

<sup>a</sup> With permission from Brown Bourzutschky et al. (1990).

<sup>b</sup> H<sub>2</sub>/CO = 2, *P* = 10.6 atm, *T* = 573 K, *F*/*W* ≈ 60 cm<sup>3</sup> min<sup>-1</sup> (g catalyst)<sup>-1</sup>.

<sup>c</sup> Number of C atoms in product/total number of C atoms in all organic products.

<sup>d</sup> DME completes the balance in cases where figures do not total 100%.

Table 17  
Methanol from syngas: activity and product distribution for all catalysts<sup>a,b</sup>

Catalyst	<i>x</i> <sub>CO</sub> (%)	Selectivity (%)					
		MeOH	CO <sub>2</sub>	CH <sub>4</sub>	C <sub>2</sub> H <sub>6</sub>	DME	C <sub>2+</sub> OH
LaTiO <sub>3</sub>	0.6	31	31	29	—	9	—
LaTi <sub>0.8</sub> Cu <sub>0.2</sub> O <sub>3</sub>	12.7	39	34	9	6	10	2
LaTi <sub>0.5</sub> Cu <sub>0.5</sub> O <sub>3</sub>	22.4	78	13	5	1	1	2
LaTi <sub>0.4</sub> Cu <sub>0.6</sub> O <sub>3</sub>	21.0	83	10	4	1	1	2
LaCuO <sub>3</sub>	21.3	73	15	7	2	1	1
Cu/La <sub>2</sub> O <sub>3</sub>	7.7	18	38	25	10	9	—

<sup>a</sup> With permission from van Grieken et al. (1991).

<sup>b</sup> Reaction conditions: H<sub>2</sub>/CO = 3, GHSV = 3500 h<sup>-1</sup>, reaction temperature 573 K, *P* = 50 atm. All the catalysts were prerduced at 623 K with H<sub>2</sub> (20%)/He.

spectrum of LaMn<sub>0.5</sub>Cu<sub>0.5</sub>O<sub>3</sub> (not the Ti-containing solid) which gives a single signal usually assigned to Cu<sup>+</sup>.

The main difference between van Grieken et al. (1991) and Brown Bourzutschky et al. (1990) is that the latter conclude that both Cu<sup>0</sup> and Cu<sup>+</sup> play a role in the production of oxygenates while van Grieken et al. (1991) only postulate Cu<sup>+</sup> as the locus of catalytic activity for synthesis of oxygenates. In order to sort out this controversy, it would be

Table 18  
 $\text{CO}_2 + \text{H}_2$  reaction over  $\text{La}_{1-y}\text{M}_y\text{CoO}_3$  ( $\text{M}=\text{Sr}, \text{Th}$ ): catalytic activity, selectivity and  $\text{C}_{2+}$  production at different extents of reduction<sup>a,b</sup>

Perovskite	Reduction temperature (K)	Extent of reduction <sup>c</sup> ( $\text{e}^-/\text{molecule}$ )	$\nu^0 \times 10^3$	$S_x^d$	$\text{C}_{2+}^e$
$\text{LaCoO}_3$	—	0.0	<sup>f</sup>	0.65	0
	573	1.2	10.4	0.52	13
	623	1.3	20.2	0.54	11
	673	1.4	20.7	0.57	6
	723	2.4	13.7	0.58	4
	773	3.0	18	0.67	2
$\text{La}_{0.8}\text{Th}_{0.2}\text{CoO}_3$	—	0.0	<sup>f</sup>	0.70	0
	573	1.1	130	0.89	2
	623	1.4	123	0.92	2
	673	1.6	130	0.87	2
	773	2.9	120	0.82	2
$\text{La}_{0.6}\text{Sr}_{0.4}\text{CoO}_3$	—	0.0	<sup>f</sup>	0.80	0
	573	1.3	40	0.91	3
	623	2.2	14.7	0.67	18
	673	2.4	14.4	0.55	14
	773	3.3	4.2	0.32	30

<sup>a</sup> With permission from Ulla et al. (1987).

<sup>b</sup> Batch gas recirculating system,  $\text{H}_2 : \text{CO}_2 = 4 : 1$ ; reaction temperature 553 K, total pressure 160 Torr; 300 mg of catalyst.

<sup>c</sup> Reduction of  $\text{Co}^{3+}$  to  $\text{Co}^0$  corresponds to  $n$  electrons per formula weight of mixed oxide.

<sup>d</sup> Selectivity to methane at constant  $\text{CO}_2$  conversion  $X_{\text{CO}_2} = 0.20$ .

<sup>e</sup> The  $\text{C}_{2+}$  fraction included hydrocarbons containing two, three and four carbon atoms; at constant  $\text{CO}_2$  conversion  $X_{\text{CO}_2} = 0.20$ .

<sup>f</sup> The reaction showed an induction period.

helpful to study the syngas conversion on a solid only containing  $\text{Cu}^+$  on the surface under reaction conditions, something hard to achieve under rather severe reducing conditions.

Very little work has been reported concerning the hydrogenation of  $\text{CO}_2$  over perovskite oxides. The most comprehensive work to date has been reported by Ulla et al. (1987) and Marcos et al. (1987). They studied the  $\text{CO}_2 + \text{H}_2$  reaction over  $\text{La}_{1-x}\text{M}_x\text{CoO}_3$  ( $\text{M}=\text{Sr}, \text{Th}$ ). This system is expected to yield hydrocarbons and no oxygenates. They used XRD, XPS and  $\text{H}_2$  chemisorption to characterize the different solids that were almost always prereduced in  $\text{H}_2$ . They worked below atmospheric pressure in a recirculation system,  $\text{H}_2 : \text{CO}_2 = 4 : 1$ , and at 553 K. In fact, they used  $\text{CO}_2 + \text{H}_2$  as a test reaction to characterize the evolution of the different solids following hydrogen reduction.

When the oxides were not prereduced in  $\text{H}_2$ , an induction period of over 100 minutes was observed in all cases. To obtain a stable catalyst the oxide should be prereduced in  $\text{H}_2$  at  $T > 553$  K. However, the activity and product distribution were affected by the

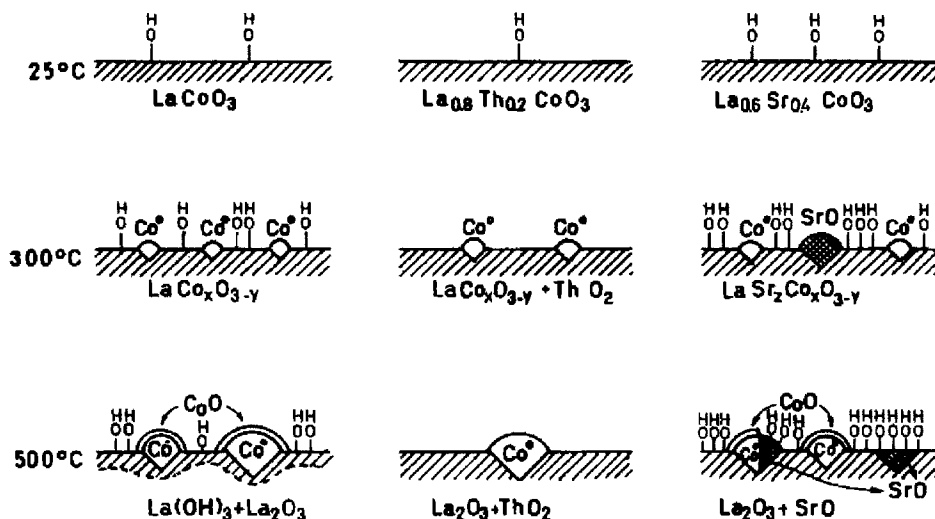


Fig. 14. Reduction model of the three mixed oxides. With permission from Marcos et al. (1987).

pretreatment temperature (extent of reduction). The reduction temperature was varied between 573 and 773 K. The activity and product distribution obtained are shown in table 18.

Marcos et al. (1987) proposed a model of the reduction process of the same set of catalysts basically supported by the XPS studies. The main steps during the reduction at the surface level are schematically presented in fig. 14. The XPS data that support this model are shown in figs. 4 and 5.

$\text{La}_{0.8}\text{Th}_{0.2}\text{CoO}_3$  is the most stable oxide of this triad. This mixed oxide does not adsorb water to such an extent as the others do. The hydroxyl surface concentration is low and therefore the cobalt clusters are not easily reoxidized.  $\text{LaCoO}_3$  and even more so  $\text{La}_{0.6}\text{Sr}_{0.4}\text{CoO}_3$  show increasing reactivity with the water generated during reduction. This generates higher concentrations of surface hydroxyls that in turn increase the driving force to reoxidize the cobalt clusters. This model is consistent with the sharp decrease in both CO chemisorption and ethylene hydrogenation at 253 K reported by Petunchi et al. (1981). This is not the case, however, when a reducing reacting mixture is contacted with the prereduced oxide at reaction temperatures higher than 650 K as reported by Ulla et al. (1987). In such a case the catalyst surface is instantaneously reduced by the reacting mixture. Note that the general characteristics of the surface evolution during the  $\text{H}_2$  treatment may be applicable to other situations such as the previous cases of  $\text{LaMn}_{1-x}\text{Cu}_x\text{O}$ ,  $\text{LaTi}_{1-x}\text{Cu}_x\text{O}_3$  and even  $\text{LaRhO}_3$ . This refers to surface enrichment in the reduced transition metal (Co or Cu) at mild conditions, partial reoxidation and/or decoration of the exposed metal depending upon the basicity and/or spreading tendency of the accompanying oxide(s) (e.g.,  $\text{Mn}_2\text{O}_3$ ,  $\text{La}_2\text{O}_3$ ,  $\text{ThO}_2$ ).

$\text{Co}^0$  is a necessary component of the active site but its specific activity and selectivity are strongly influenced by the accompanying cations. Note:

- The drastic changes in turnover frequencies effected by the different cations.
- The role played by the molecular dispersion of the components in the crystalline starting solid in determining the catalytic properties of the reduced solids (matrix effect).
- The cobalt/other cations ratios which are modified by the hydrogen treatment (fig. 5) and which produce sharp changes in both TOF and product distribution. Another interesting conclusion of their studies is that the  $\text{C}_{2+}$  selectivity, when  $\text{CO}_2$  is hydrogenated, is affected in the same way as in the case of  $\text{CO}$ , i.e.  $\text{Sr} > \text{La} \gg \text{Th}$ . This seems to indicate that both reactions start from the same point,  $\text{CO}$ , in agreement with similar views of other authors.

## 2.5. *Environmental catalysis*

In the last two decades, government regulations that limit the level of pollutants in exhaust gases from stationary and mobile sources have become increasingly severe. This, in turn, has boosted the search for new, less expensive catalysts to eliminate gas contaminants such as  $\text{CO}$ ,  $\text{NO}_x$ , volatile organic compounds (VOCs) including hydrocarbons,  $\text{SO}_2$ , and particulates such as soot from diesel engines. In fact, the production of environmental catalysts is today the largest item in this manufacturing activity.

One way to lower costs is to substitute, totally or partially, noble metals by cheaper materials. In this vein, rare-earth-containing mixed oxides have been assayed to eliminate several pollutants. They are now in use for several commercial applications, mainly for  $\text{CO}$  oxidation and odor elimination. Efforts are being made to develop new uses of these materials in other environmental fields. In what follows, the use of mixed oxides in total oxidation, nitrogen oxides decomposition and  $\text{NO}_x$  reduction will be reviewed.

### 2.5.1. *Catalytic combustion*

The term catalytic combustion generally means a complete oxidation of hydrocarbons to  $\text{CO}_2$  and  $\text{H}_2\text{O}$  over solid catalysts. Catalyst technology for air-pollution control such as exhaust gas treatment, abatement of the emission of VOCs, combustion of diesel soot particles, and high temperature combustion have boosted research in catalytic combustion.

Oxide-supported platinum or Pd catalysts have been used for the complete combustion of hydrocarbons, mainly for the purpose of cleaning exhaust gases. However, the new application of the catalytic combustor to gas turbines or boilers is arousing research interest on catalysts with good thermal stability and combustion activity at high temperatures.

Prasad et al. (1984) have summarized the required properties of suitable combustion catalysts:

- (1) The ignition of fuel/air mixture should be possible at a temperature as low as possible.

- (2) The activity of the catalyst should be sufficiently high to maintain the complete combustion at the lowest inlet temperature and at the highest values of space velocity.
- (3) The support should have a large surface area, low pressure drop, good thermal shock resistance, and it should allow high working temperature.
- (4) The support should maintain moderately high surface area under high-temperature combustion conditions (~1300 K).
- (5) The catalyst system should be stable to allow prolonged use at operating temperatures of up to 1500 K.

According to Zwinkels et al. (1993), of all noble metals, palladium has superior properties but is suitable for high-temperature combustion only if it is strongly attached by the formation of a complex with the support to avoid vaporization and/or sintering of the active metal at working temperature (above 1000 K). Alternative catalyst materials, such as single oxides of transition metals, can be considered because of their high melting point (>1600 K). However, Quinlan et al. (1989) reported that severe sintering may occur in those single oxides at temperatures as low as two thirds of their melting point. On the other hand, R-based mixed oxides containing transition metals are more suitable for this purpose taking into account that they combine good thermal stability and relatively high catalytic activity.

Voorhoeve et al. (1972) were the first to report the high catalytic activity of perovskite-type oxides for heterogeneous oxidation, triggering many studies thereafter, which used these materials as catalysts for hydrocarbon combustion.

**2.5.1.1.  $ABO_3$ -type perovskites.** Nitadori et al. (1988) reported the catalytic activities of R-based perovskite-type oxides,  $RBO_3$  (R=lanthanides, B=Cr, Co, Fe, Mn, Ni) for propane oxidation at 500 K. The activity order was always for any lanthanide  $RCoO_3 > RMnO_3 > RNiO_3 \gg RFeO_3 \approx RCrO_3$  (fig. 15), showing that the R element had a smaller effect on the catalyst than the transition-metal element at the B site. They also found that the activity for methanol oxidation over  $RFeO_3$  calcined at 1100 K (R=La, Sm, Gd) did not change much with R. However, Arakawa et al. (1982) reported for the same reaction over  $RFeO_3$  (R=lanthanides) calcined at 1500 K that the catalytic activity increased remarkably from La to Gd. They suggested that it might be a result of the decrease in the covalency of the Fe–O bond due to the fact that the physical properties of the lanthanides, such as ionic radius, charge density and magnetic moment, changed significantly from La to Gd and that these changes would influence the electronic state of the B site. However, since no surface area were reported, it is not clear how to assign the effective influence of the lanthanide element upon the catalytic activity.

The effect of the rare-earth elements La, Pr, Nd and Gd in  $RMnO_{3+x}$ ,  $RFeO_{3-x}$  and  $RCoO_3$  perovskites on the catalytic activity for the total methane oxidation was studied by Marti and Baiker (1994) and Baiker et al. (1994). These results are shown in table 19. The low reaction rate at 770 K for  $PrCoO_3$ , about 30 times lower than that for the other  $RCoO_3$ , was attributed by Baiker et al. (1994) to the presence of  $Pr^{4+}$  and  $Co^{2+}$ .

The reaction rate data shown in table 19 are in agreement with those of Nitadori et al. (1988). The role of lanthanides at the R site is secondary as long as they are trivalent.

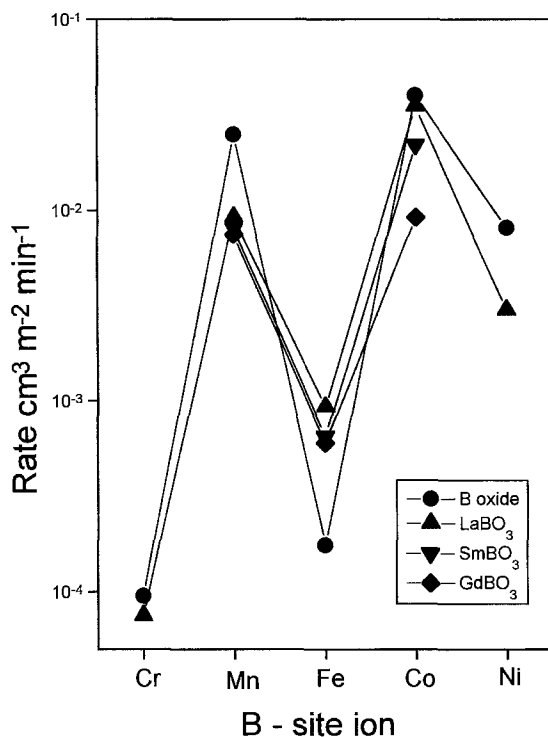


Fig. 15. Catalytic activities of R-based perovskites and B-site oxides for propane oxidation at 500 K: (a) oxides of B-site metals; (b) LaBO<sub>3</sub>; (c) SmBO<sub>3</sub>; (d) GdBO<sub>3</sub>. With permission from Nitadori et al. (1988).

Kremenić et al. (1985) studied C<sub>3</sub>H<sub>6</sub> and C<sub>4</sub>H<sub>8</sub> oxidation over LaBO<sub>3</sub> (B=Cr, Mn, Fe, Co, Ni) perovskite-type oxides, finding remarkable differences among these catalysts. The order of activity for both reactions is Co > Mn > Ni ≫ Cr ≈ Fe. The same study was performed by Nitadori et al. (1988) for C<sub>3</sub>H<sub>8</sub> oxidation and they found the following order: Co > Mn > Ni ≫ Cr ≈ Fe. It is clear from these results that Co and Mn at the B site in a perovskite-type structure are the most active 3d-transition metals, Fe being the least active one.

Moreover, the close parallelism between the reaction rate for C<sub>3</sub> and C<sub>4</sub> oxidation at 570 K and total oxygen adsorption in this series of LaBO<sub>3</sub> oxides obtained by Kremenić et al. (1985) indicates that these hydrocarbon oxidation reactions occur through a mechanism in which adsorbed oxygen is the dominant O species participating in the process.

Arai et al. (1986) reported the temperature at which the conversion level of CH<sub>4</sub> was 50%,  $T_{50\%}$ , for methane combustion over LaBO<sub>3</sub> (B=Co, Mn, Fe, Cu, Ni, Cr) compared to Pt(1%)/Al<sub>2</sub>O<sub>3</sub>. These results are shown in table 20. The activities of LaBO<sub>3</sub> (B=Co, Fe, Mn) catalysts were similar and quite close to that of Pt/Al<sub>2</sub>O<sub>3</sub>, following the same trend as the data reported in table 19 for the same materials, (0.12, 0.11 and 0.14 μmol m<sup>-2</sup> s<sup>-1</sup>, respectively).



Table 19  
Reaction rate for methane oxidation over  $\text{RBO}_{3+x}$

B-site	R-site	Rate ( $\mu\text{mol m}^{-2} \text{s}^{-1}$ )	$T$ (K)	Reference
$\text{Mn}^a$	La	0.14	770	Marti and Baiker (1994)
	Gd	0.16	770	
	Nd	0.29	770	
	Pr	0.23	770	
$\text{Fe}^a$	La	0.11	770	Marti and Baiker (1994)
	Gd	0.16	770	
	Nd	0.11	770	
	Pr	0.15	770	
$\text{Co}^a$	La	0.12	770	Baiker et al. (1994)
	Gd	0.19	770	
	Nd	0.16	770	
	Pr	$\sim 0.005$	770	
$\text{Mn}^b$	La	0.380	822	McCarty and Wise (1990)
$\text{Fe}^b$	La	0.370	913	

<sup>a</sup> 1%  $\text{CH}_4$ ; 4%  $\text{O}_2$ ; GHSV =  $135\,000 \text{ h}^{-1}$ ;  $w = 0.1 \text{ g}$ .

<sup>b</sup> 1.5%  $\text{CH}_4$ ; 4.2%  $\text{O}_2$ ;  $w = 0.040 \text{ g}$ ;  $F = 200 \text{ cm}^3 \text{ min}^{-1}$ .

Table 20  
Methane oxidation activity of  $\text{LaBO}_3$  and  $\text{Pt}/\text{Al}_2\text{O}_3$  catalysts<sup>a,b</sup>

Catalyst	$\text{LaBO}_3$						$\text{Pt}(1\%)/\text{Al}_2\text{O}_3$
	Co	Mn	Fe	Cu	Ni	Cr	
$T_{50\%}$ (K)	800	850	845	945	975	1050	790
Surface area ( $\text{m}^2 \text{ g}^{-1}$ )	3.0	4.0	3.1	0.6	4.8	1.9	146.5

<sup>a</sup> Data from Arai et al. (1986).

<sup>b</sup> Reaction conditions: 2 vol%  $\text{CH}_4$  in air; space velocity  $45\,000\text{--}50\,000 \text{ h}^{-1}$ .

In brief, the effect of the transition metal at the B site in  $\text{LaBO}_3$  for the total oxidation of hydrocarbons depends on the reaction temperatures: (i) Below 500 K, the kind and valency of the 3d-transition metal element are of primary importance. (ii) Above 500 K, the activity is less sensitive to the B-site element.

**2.5.1.2. Effect of A-site partial substitution.** As already mentioned in sect. 1.4, the properties of these mixed oxides can be easily modified by the partial substitution of the A-site cation and the most obvious effect is observed in the oxygen-sorptive properties. The oxidation activity is often improved by this modification.

Nitadori et al. (1988) found that the catalytic activity for  $\text{C}_3\text{H}_8$  oxidation over  $\text{R}_{1-x}\text{Sr}_x\text{CoO}_3$  increased several times upon Sr substitution for R, regardless of the kind of trivalent rare-earth ion. As for the extent of the substitution, a maximum was observed at

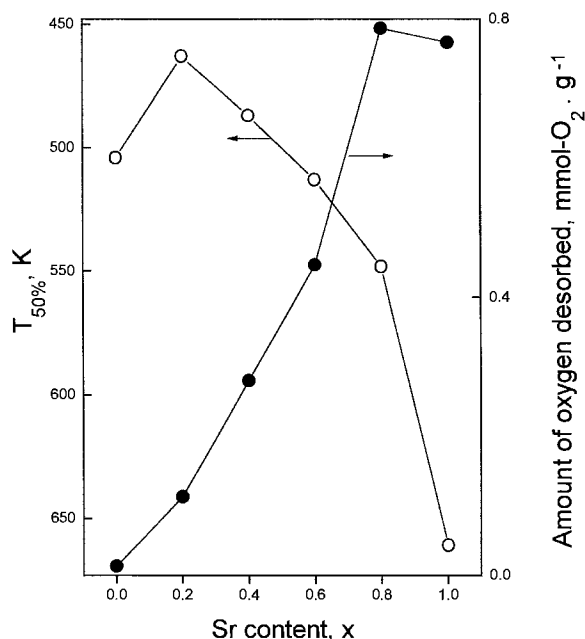


Fig. 16. Catalytic activity for *n*-butane oxidation (squares) and amount of oxygen desorbed below 1123 K (circles) as a function of *x* in  $\text{La}_{1-x}\text{Sr}_x\text{Co}_{0.4}\text{Fe}_{0.6}\text{O}_3$ .  $T_{50\%}$  is the temperature for 50% conversion of *n*-butane. With permission from Zhang et al. (1990).

$x=0.1$  for  $\text{Gd}_{1-x}\text{Sr}_x\text{CoO}_3$  and  $x=0.2$  for  $\text{La}_{1-x}\text{Sr}_x\text{CoO}_3$ . They observed similar results on  $\text{La}_{1-x}\text{Sr}_x\text{MnO}_3$ , and the maximum was at  $x=0.6$ .

According to the TPD patterns, oxygen desorption became easier upon Sr substitution. This means that the oxidizing power of  $\text{R}_{1-x}\text{Sr}_x\text{BO}_3$  is increased, promoting the catalytic activity of these mixed oxides for oxidation. The decrease of this activity at higher extents of substitution may be explained because of both a slower reoxidation step in the redox cycle of the catalysts and a lower reactivity of individual oxygen species.

Yamazoe and Teraoka (1990) summarized the results from several researchers who reported rates for oxidation of hydrocarbons over Co- and Fe-perovskite-type oxides that tend to be maximum at smaller *x* values (0.1–0.4) than Mn perovskites (0.6–0.8). Figure 16 shows the amount of desorbed oxygen and the catalytic activity, expressed in terms of the temperature at which the conversion of  $\text{C}_4\text{H}_{10}$  was 50% ( $T_{50\%}$ ), as a function of the Sr content, *x* in  $\text{La}_{1-x}\text{Sr}_x\text{Co}_{0.4}\text{Fe}_{0.6}\text{O}_3$ . The amount of desorbed  $\text{O}_2$  increased monotonically with La substitution up to  $x=0.8$  while  $T_{50\%}$  had a maximum at  $x=0.2$ , in agreement with the results mentioned above.

Lintz and Wittstock (1996) compared the results obtained for the catalytic combustion of acetone over substituted Mn perovskite containing La and Sr as A cation with those of the  $\text{CuMn}_2\text{O}_4$  catalyst. The latter material, copper manganate, is a well-known oxidation catalyst for VOCs removal and is commercially available.  $\text{La}_{0.8}\text{Sr}_{0.2}\text{MnO}_3$  ( $64 \text{ m}^2 \text{ g}^{-1}$ ) was even more active than the commercial catalyst.

Table 21  
 $T_{50\%}$  for methane combustion over  $\text{La}_{1-x}\text{A}_x\text{BO}_3$

$\text{La}_{1-x}\text{A}_x\text{BO}_3$	Seiyama (1992) <sup>a</sup>		Choudhary et al. (1996b) <sup>b</sup>	
	$x$	$T_{50\%}$	$x$	$T_{50\%}$
$\text{LaMnO}_3$	0	852	0	966
$\text{La}_{1-x}\text{Sr}_x\text{MnO}_3$	0.2	783	0.3	943
$\text{LaCoO}_3$	0	798	0	907
$\text{La}_{1-x}\text{Sr}_x\text{CoO}_3$	0.2	791	0.3	910
$\text{La}_{1-x}\text{Ag}_x\text{CoO}_3$	—	—	0.3	833
$\text{La}_{1-x}\text{Ag}_x\text{MnO}_3$	—	—	0.3	865
$\text{La}_{1-x}\text{Ag}_x\text{NiO}_3$	—	—	0.3	850

<sup>a</sup> 2%  $\text{CH}_4$  in air, space velocity 45 000–50 000  $\text{h}^{-1}$ .

<sup>b</sup> 4%  $\text{CH}_4$  in air, space velocity 51 000  $\text{cm}^3 \text{g}^{-1} \text{h}^{-1}$ .

Seiyama (1992) reported the activities for methane oxidation on the A-site substituted perovskite-type oxides,  $\text{La}_{1-x}\text{A}'_x\text{BO}_3$  ( $\text{A}' = \text{Sr}, \text{Ca}, \text{Ba}, \text{Ce}$ ,  $\text{B} = \text{Co}, \text{Mn}, \text{Fe}$ ). The manganates were more affected and  $\text{La}_{0.6}\text{Sr}_{0.4}\text{MnO}_3$  was the most active for methane oxidation.

An important increase of the methane combustion activity of  $\text{LaBO}_3$  ( $\text{B} = \text{Mn}, \text{Co}, \text{Ni}$ ) perovskites due to the partial substitution of La by Ag instead of Sr was reported by Choudhary et al. (1996b) (table 21). The highest combustion activity corresponded to  $\text{La}_{0.7}\text{Ag}_{0.3}\text{CoO}_3$  perovskites. Table 21 compares the results of Choudhary et al. (1996b) with those of Seiyama (1992). Although the experimental conditions used to obtain the data were different, it is possible to analyze the tendency. The activities for  $\text{La}_{1-x}\text{Sr}_x\text{CoO}_3$  and  $\text{LaCoO}_3$  were almost the same while in the manganates, the presence of Sr at the A site improved the activities.

**2.5.1.3. Effect of A- and B-site partial substitution.** Another interesting partial substitution is B' for the B site. It can produce a defect structure as in the case of the A-site partial substitution. Moreover, a strong synergic effect can be expected mixing two B-site elements which are both catalytically active. Zhang et al. (1990) studied  $\text{La}_{1-x}\text{Sr}_x\text{Co}_{1-y}\text{Fe}_y\text{O}_3$  perovskites as catalyst for  $\text{CH}_4$  and *n*-butane oxidation. The surface areas of all these catalysts were between 4.7 and 3.3  $\text{m}^2 \text{g}^{-1}$  except for  $\text{La}_{0.6}\text{Sr}_{0.4}\text{Co}_{0.4}\text{Fe}_{0.6}\text{O}_3$  (7.5  $\text{m}^2 \text{g}^{-1}$ ). Table 22 shows the amount of desorbed oxygen determined by TPD after a pretreatment with flowing  $\text{O}_2$  at three different temperatures, 1073, 573 and 300 K. Except for  $\text{LaCo}_{0.4}\text{Fe}_{0.6}\text{O}_3$  ( $x=0, y=0.6$ ) and  $\text{La}_{0.6}\text{Sr}_{0.4}\text{CoO}_3$  ( $x=0.4, y=0$ ), the amounts of desorption obtained at 573 K were close to those observed at 1073 K. Moreover, the Sr-containing material for  $0.4 \leq x \leq 0.8$  and  $y \neq 1$ , pretreated at 300 K, desorbed a large amount of oxygen comparable to those observed when samples were pretreated at 773 and 1073 K. These results suggest that oxygen sorption proceeds easily and rapidly even at room temperature on the oxides with such mixed A and B compositions.

Table 22  
Effect of oxygen pretreatment temperature on the amount of desorbed oxygen<sup>a</sup>

$\text{La}_{1-x}\text{Sr}_x\text{Co}_{1-y}\text{Fe}_y\text{O}_3$		Amount of $\text{O}_2$ desorbed ( $\mu\text{mol g}^{-1}$ ) <sup>b</sup>		
$x$	$y$	$T = 1073 \text{ K}^c$	$T = 573 \text{ K}^c$	Room temperature <sup>c</sup>
0.8	1	639.4	643.8	199.4
	0.8	755.9	763.6	745.9
	0.6	756.3	761.0	757.8
	0.4	785.0	792.7	744.8
0.4	0.6	282.9	278.9	275.6
	0	207.3	151.6	78.5
0	0.6	12.1	5.3	1.3

<sup>a</sup> Data from Zhang et al. (1990).

<sup>b</sup> Amount of  $\text{O}_2$  desorbed below 1123 K.

<sup>c</sup> Temperatures at which oxygen pretreatment was started ( $T \rightarrow$  room temperature).

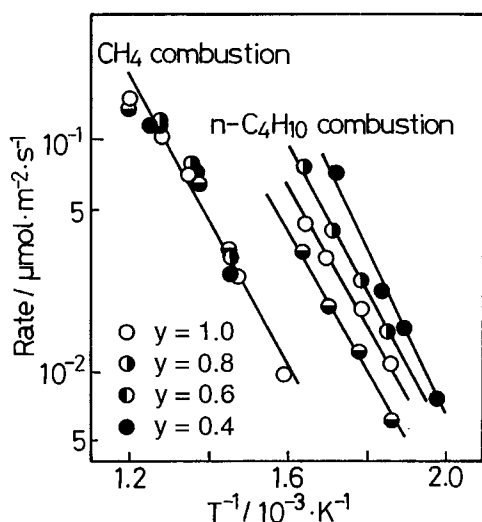


Fig. 17. Arrhenius plots of the rates of *n*-butane and methane combustion over  $\text{La}_{0.2}\text{Sr}_{0.8}\text{Co}_{1-y}\text{Fe}_y\text{O}_3$  for different values of  $y$ . With permission from Zhang et al. (1990).

Figure 17 shows the Arrhenius plots of the reaction rates of *n*-butane and  $\text{CH}_4$  oxidations over  $\text{La}_{0.2}\text{Sr}_{0.8}\text{Co}_{1-y}\text{Fe}_y\text{O}_3$ . The effects of the B-site composition were different depending on the reactants. The *n*-butane combustion activity increased as  $y = 1.0 < 0.6 < 0.8 < 0.4$ , while the methane combustion was hardly affected by this substitution.

The temperature range of these two reactions was different, 473–573 K for *n*-butane combustion and 623–773 K for methane combustion. On the other hand, the partial substitution of Fe for Co enhanced the oxygen desorption below ~573 K,  $\alpha$  desorption. The amount of  $\text{O}_2$  desorbed after a pretreatment at 300 K in  $\text{O}_2$  (table 22) for  $\text{La}_{0.2}\text{Sr}_{0.8}\text{Co}_{1-y}\text{Fe}_y\text{O}_3$  ( $y \neq 1$ ) is clearly higher than that for  $\text{La}_{0.2}\text{Sr}_{0.8}\text{FeO}_3$ . It has turned

out that the changes in combustion activities with the B-site composition could be related to the amount of  $\alpha$  oxygen which remains in the oxides. In fact, the temperatures of *n*-butane combustion are rather close to those of large desorption peaks.

In the temperature range of the methane combustion reaction, on the other hand,  $\alpha$  oxygen has already been desorbed and this may explain the similar catalytic activities observed for these mixed oxides.

As mentioned in sect. 2.5.1.1 the activity of  $\text{ABO}_3$  perovskite-type oxides for  $\text{CH}_4$  combustion is almost not affected by changes in the B-site cations (table 19). The partial substitution of Sr or Ag in the A site (table 21) improved the catalytic activities but not so much as observed for hydrocarbon combustion at low reaction temperatures. (See sect. 2.5.1.2).

As discussed in sect. 1.4, three kinds of oxygen species with different bonding strength coexist at the surface of perovskite-type oxides: the adsorbed oxygens  $\alpha$  and  $\alpha'$  which seem to be more active and available to react with hydrocarbons at low temperature, and the lattice oxygen ( $\beta$ ). As the reaction temperature rises the coverage of adsorbed  $\text{O}_2$  decreases but the  $\beta$  oxygen becomes reactive, and at high reaction temperature operation is predominantly by the lattice oxygen.

At low temperature, the reaction rate can be expressed by a Rideal-Eley mechanism where dissociatively adsorbed oxygen is assumed to be in equilibrium with gas-phase  $\text{O}_2$  and to react with gaseous  $\text{CH}_4$ . The kinetic rate expression is given by Arai et al. (1986) as

$$r = \frac{k_a P_{\text{CH}_4} \sqrt{K_{\text{O}_2} \cdot P_{\text{O}_2}}}{1 + \sqrt{K_{\text{O}_2} \cdot P_{\text{O}_2}}},$$

with kinetic constant  $k_a = A_a^\alpha e^{-E_a/RT}$ , equilibrium constant  $K_{\text{O}_2} = K_{\text{O}_2}^\circ e^{-\Delta H_{\text{O}_2}/RT}$ ,  $P_{\text{CH}_4}$  the partial pressure of  $\text{CH}_4$ ,  $P_{\text{O}_2}$  the partial pressure of  $\text{O}_2$ ,  $E_a$  the activation energy, and  $\Delta H_{\text{O}_2}$  the heat of oxygen adsorption.

At high temperatures, the oxidation rate by the redox mechanism could be considered zero order with respect to the partial pressure of  $\text{O}_2$  owing to the rapid incorporation of  $\text{O}_2$  gas phase to the lattice. Thus, the kinetic expression is

$$r = k_b \cdot P_{\text{CH}_4}$$

with kinetic constant  $k_b = k e^{-E_b/RT}$ .

Within the range of temperatures where all the oxygens associated with the catalyst should be considered, the rate expression becomes

$$r = \frac{k_a \cdot P_{\text{CH}_4} \sqrt{K_{\text{O}_2} \cdot P_{\text{O}_2}}}{1 + \sqrt{K_{\text{O}_2} \cdot P_{\text{O}_2}}} + k_b \cdot P_{\text{CH}_4}.$$

Arai et al. (1986) determined the kinetic parameters for methane combustion over  $\text{La}_{0.6}\text{Sr}_{0.4}\text{MnO}_3$  prepared by decomposition of metal acetates and/or nitrates calcined

Table 23  
Kinetic parameters for methane combustion over  $\text{La}_{1-x}\text{Sr}_x\text{MnO}_3$  calcined at different temperatures<sup>a</sup>

$x$	Calcination temperature (K)	Surface area ( $\text{m}^2 \text{g}^{-1}$ )	$E_a$ (kcal/mol)	$E_b$ (kcal/mol)	$\Delta H_{\text{O}_2}$ (kcal/mol)	$T_{50\%}$ (K)	Reference
0.4	1123	3.3	20.3	25.0	69.6	755	Arai et al. (1986) <sup>b</sup>
0.4	1473	0.3	14.1	39.7	65.6	856	
0.2	973	28	9.16	—	—	823	Gunasekaran et al. (1996) <sup>c</sup>
0.2	1073	20	37.70	—	—	853	
0.2	1173	12.5	14.04	—	—	868	
0.2	1273	8	18.53	—	—	893	

<sup>a</sup> See sect. 2.5.1.3 for symbols.

<sup>b</sup> Reaction conditions: 2%  $\text{CH}_4$  in air, space velocity 45 000–50 000  $\text{h}^{-1}$ .

<sup>c</sup> Reaction conditions: 0.28%  $\text{CH}_4$ , 12%  $\text{O}_2$ , and balance He,  $F = 70 \text{ cm}^3 \text{ min}^{-1}$ .

at 1123 and 1473 K. The 473–1123 K temperature range was explored in the catalytic evaluation. These parameters are shown in table 23. The calcination temperature not only modified the surface area but also the activation energy related to lattice oxygen,  $E_b$ , displacing the contribution of oxygen ( $\beta$ ) at higher temperature which in turn decreased the activities of the catalysts as seen in table 23 comparing the  $T_{50\%}$  values for both samples.

On the other hand, Gunasekaran et al. (1996) prepared  $\text{La}_{0.8}\text{Sr}_{0.2}\text{MnO}_3$  using the Pechini method and calcined the precursor at 973, 1073, 1173 and 1273 K. A shift in the light-off temperature  $T_{50\%}$  to higher values due to the increase of the calcination temperature is shown in table 23. It could be related to the decrease of surface area because of the sintering during the calcination treatment at high temperature. However, changes on the surface composition could also be responsible for the decrease in activity. X-ray photoelectron spectroscopy studies revealed a decrease in the Mn surface concentration for the samples sintered from 973 to 1273 K.

Sri Rahayu et al. (1995) investigated the possibility of lowering the combustion temperature of diesel soot particulates by using perovskite-type oxides.  $\text{La}_{0.2}\text{Sr}_{0.8}\text{MnO}_3$  doped by Pt and Pd were studied using thermogravimetric (TGA) and differential thermal analysis (DTA). The catalysts to be analyzed were prepared by mixing the perovskite-type oxide with simulated diesel soot and then loaded in the analyzer. The soot conversion was calculated from the TGA curves. The DTA curves provide the maximum rates of oxidation corresponding to the top of the exothermic signals. The results are shown in table 24.

$\text{La}_{0.2}\text{Sr}_{0.8}\text{Mn}_{0.91}\square_{0.09}\text{O}_{3+x}$  and  $\text{La}_{0.2}\text{Sr}_{0.8}\text{Mn}_{0.999}\text{Pd}_{0.001}\text{O}_{3+\lambda}$  showed the best performance. The enhancement of the activity in the former case could be assigned to the increase of  $\text{Mn}^{+4}/\text{Mn}^{+3}$  ratio, as Vrieland (1974) suggested:  $\text{Mn}^{+4}$  and  $\text{Mn}^{3+}$  can act as a redox couple on the surface. The differences of the catalytic behavior related to the noble metal, Pt or Pd, could be associated with the different oxidation states of the metal inside the perovskite matrix,  $\text{Pd}^{+2}$  and  $\text{Pt}^{+4}$ , as suggested by Johnson et al. (1977).

Table 24  
Conversion of diesel soot over  $\text{La}_{0.8}\text{Sr}_{0.2}\text{MnO}_{3+\lambda}$  doped with Pt or Pd<sup>a</sup>

$\text{La}_{0.8}\text{Sr}_{0.2}\text{Mn}_{1-y-x}\text{B}_y\Box_x\text{O}_{3+\lambda}$ sample <sup>b</sup>			1st peak		2nd peak	
B	y	x	TGA (% loss <sup>c</sup> )	DTA [T (K)]	TGA (% loss <sup>c</sup> )	DTA [T (K)]
—	0	0	25.0	573	56.7	753
—	0	0.09	20.0	548	60.2	733
Pt	0.001	0	20.0	568	56.7	758
Pt	0.008	0.092	23.3	578	56.7	733
Pd	0.001	0	20.0	533	60.0	723
Pd	0.008	0.092	18.3	563	56.7	763

<sup>a</sup> Data from Sri Rahayu et al. (1995).

<sup>c</sup> Percent of weight loss related to the peak of DTA.

<sup>b</sup>  $\Box$  are B-site vacancies.

Perovskite-type oxides with A and/or B sites partially substituted present properties such as structural defects and reactivity of adsorbed and lattice oxygen that play a central role in catalytic combustion. However, preparation methods as well as temperature of calcination could affect the surface area, and most important, changes on the surface composition that will be reviewed in the following section.

**2.5.1.4. Surface composition.** Kirchnerova et al. (1993) studied methane combustion over  $\text{La}_{1-x}\text{Sr}_x\text{B}_{1-y}\text{B}'_y\text{O}_3$  (B = Co, Ni, Fe, B' = Fe, Ni) prepared by spray-freezing/freeze drying and found an excellent activity for the composition  $\text{La}_{0.66}\text{Sr}_{0.34}\text{Ni}_{0.3}\text{Co}_{0.7}\text{O}_3$  at 823 K of 9.11  $\mu\text{mol/s.g}$ . However, expressing the combustion rate per unit surface area, the activity became 0.55  $\mu\text{mol/m}^2\text{s}$ , comparable to one of the less active perovskites that they prepared,  $\text{La}_{0.4}\text{Sr}_{0.6}\text{Fe}_{0.4}\text{Co}_{0.6}\text{O}_3$ . The surface composition of this mixed oxide often differs from the bulk. According to Yamazoe and Teraoka (1990) the surface tends to be poor in M-site cations and could have segregated phases. This surface heterogeneity might override changes in the bulk composition. Gunasekaran et al. (1994) prepared  $\text{La}_{0.95}\text{Ba}_{0.05}\text{BO}_3$  (B = Co, Fe Mn) oxides and characterized the surface of these solids by XPS. They used methane combustion as test reaction. On the other hand Milt et al. (1996) prepared  $\text{LaBO}_3$  (B = Co, Fe) by the explosion method and used the same reaction test and XPS analysis. The results of both research groups are shown in table 25. Comparing just the activity of different materials, we conclude that the small amount of Ba in the first two perovskites contributed to increasing the activities almost 15 times. However, the XPS data of perovskite samples reported by Milt et al. (1996) showed two XPS peaks for La 3d<sub>5/2</sub> (table 25) which can be assigned to: (i) La-carbonate-type surface compound (835.5 eV), and (ii) La-perovskite bulk oxides (833.6 eV). Since the specific activities for methane combustion are identical to  $\text{La}_2\text{O}_2\text{CO}_3$  and air-exposed  $\text{La}_2\text{O}_3$ , they concluded that La-carbonate species are abundant on the surface of  $\text{LaCoO}_3$  and  $\text{LaFeO}_3$  and define their catalytic behavior.

Table 25  
Catalytic activity for methane oxidation and B/La surface ratio in different perovskite-type oxides

Catalyst	Surface area (m <sup>2</sup> g <sup>-1</sup> )	BE (eV)		Surface ratio (B/La) <sub>sup</sub>	Rate (770 K) (μmol s <sup>-1</sup> m <sup>-2</sup> ) × 10 <sup>2</sup>	Reference
		La3d <sub>5/2</sub>	B2p <sub>3/2</sub>			
La <sub>0.95</sub> Ba <sub>0.05</sub> MnO <sub>3</sub>	2.7	833.3	641.2	1.02	72.0	Gunasekaran et al. (1994) <sup>a</sup>
LaMnO <sub>3</sub>	—	833.1	641.0	0.96	—	
La <sub>0.95</sub> Ba <sub>0.05</sub> CoO <sub>3</sub>	1.2	832.8	779.3	0.74	60.0	
LaCoO <sub>3</sub>	—	832.8	779.3	0.28	—	
La <sub>0.95</sub> Ba <sub>0.05</sub> FeO <sub>3</sub>	1.2	836.2	709.3	1.36	23.0	
LaFeO <sub>3</sub>	—	833.7	710.2	0.99	—	Milt et al. (1996) <sup>b</sup>
LaCoO <sub>3</sub>	5.7	833.6 835.5	779.7	0.7	4.3	
LaFeO <sub>3</sub>	3.0	834.1 835.5	710.4	1.1	4.0	
La <sub>2</sub> O <sub>3</sub>	7.1	835.4	—	—	3.9	
La <sub>2</sub> O <sub>2</sub> CO <sub>3</sub>	3.9	835.4	—	—	3.6	

<sup>a</sup> Reaction conditions: 2% CH<sub>4</sub> in air.

<sup>b</sup> Reaction conditions: 3% CH<sub>4</sub>, 7.2% O<sub>2</sub>, and balance N<sub>2</sub>,  $F = 113 \text{ cm}^3 \text{ min}^{-1}$ .

The surface heterogeneity is also suggested by the XPS results obtained by Gunasekaran et al. (1994) (table 25), especially for La<sub>0.95</sub>Ba<sub>0.05</sub>FeO<sub>3</sub>. The binding energy value of Fe 2p<sub>3/2</sub> at 709.2 eV is low compared with that of LaFeO<sub>3</sub>. The authors suggested that this could be due to the increase in the average charge of Fe resulting from the Ba partial substitution. However, this effect was not observed on the other La<sub>0.95</sub>Ba<sub>0.05</sub>BO<sub>3</sub> (B = Co, Mn). Besides, the surface ratio of Fe/La on the Ba-substituted lanthanum ferrite is larger (1.34) than the bulk ratio (1.05). Thus, the differences in catalytic activities for methane combustion are primarily affected by the surface composition.

Zhong et al. (1996) found that nanometer-particle-size oxides, LaFe<sub>0.9</sub>B'<sub>0.1</sub>O<sub>3-λ</sub> (B' = Mn, Co, Ni) containing high-valent cations exhibited good catalytic activities for the total oxidation of methane. The samples were prepared by the sol-gel method and calcined at 923 K for 4 h and 1173 K for 2 h to obtain nanometer- and large-size particles, respectively. Before the catalytic test and XPS measurements, all samples were treated with oxygen at 923 K for 1 h until no carbonate peak was detected (C 1s spectra). The O 1s spectra were deconvoluted into two peaks: (i) adsorbed oxygen and (ii) lattice oxygen species. The O<sub>lattice</sub>/O<sub>adsorbed</sub> ratio of nanometer particles was 2–4 times greater than for the larger particles. The order of specific activity (μmol s<sup>-1</sup> m<sup>-2</sup>) at 673 K followed the tendency of this ratio in nanometer particles (fig. 18), consistent with the lattice-oxygen contribution to the methane oxidation reaction discussed in sect. 2.5.1.3.

**2.5.1.5. High-temperature combustion catalysts.** New types of catalysts for high-temperature combustion need to be developed with thermochemical stability in atmo-



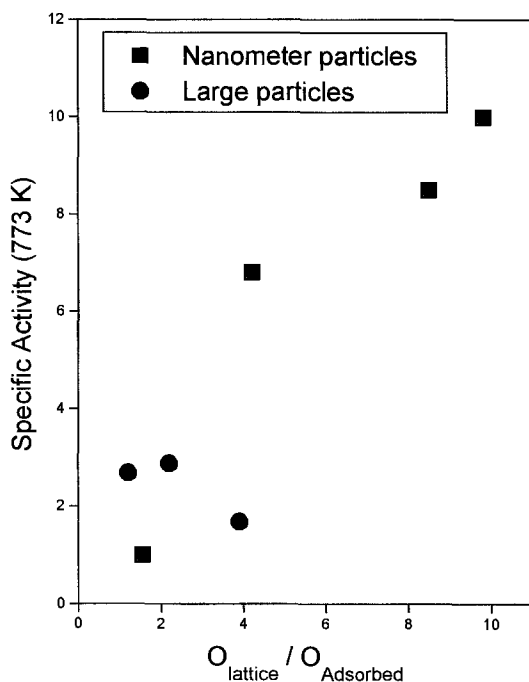


Fig. 18. Relationship between the specific activity and  $O_{\text{lattice}}/O_{\text{adsorbed}}$ . With permission from Zhong et al. (1996).

spheres containing oxygen and steam up to 1500 K. Typical application fields lie in gas turbines or in structured catalytic burners.

As mentioned by Zwinkels et al. (1993) several catalytic materials are being tested in laboratories all over the world. Among them, La-based mixed oxides containing transition metals, stable at high temperature, appear to be some of the most promising candidates, owing to the fact that they guarantee that the combustion process can be initiated at much lower temperatures than in homogeneous burners.

Saracco et al. (1996) prepared a MgO–LaCrO<sub>3</sub> perovskite catalyst by the citrate method. They prepared two series, one using the stoichiometric ratio of the cations to obtain LaCr<sub>1-x</sub>Mg<sub>x</sub>O<sub>3</sub> ( $x=0, 0.1, 0.2, 0.3, 0.4, 0.5$ ), and the other with extra Mg<sup>2+</sup> to produce LaCr<sub>1-x</sub>Mg<sub>x</sub>O<sub>3</sub>:MgO=1:17. In the second series, the perovskite crystals appeared to be randomly dispersed among the MgO crystals according to TEM micrographs. XRD spectra of all the perovskite samples were practically coincident with that of LaCrO<sub>3</sub>. The average surface areas of the two series were  $6 \pm 1 \text{ m}^2 \text{ g}^{-1}$  and  $17 \pm 2.5 \text{ m}^2 \text{ g}^{-1}$ , respectively. Calcination for 5 days in air at 1373 K led to 10% reduction of surface area for the first series and 30% reduction for the second series. However, the differences in catalytic activity for perovskites dispersed among MgO particles before and after being pretreated were not significant, suggesting that the decrease in surface area has to be associated to the sintering of MgO crystals instead of perovskite ones. The presence of MgO in thermodynamic equilibrium with LaCr<sub>1-x</sub>Mg<sub>x</sub>O<sub>3</sub> crystals hampers,

to some extent, the contact between different perovskite particles and the subsequent sintering phenomena. Comparing the conversion of  $\text{CH}_4$  at different temperatures for  $\text{LaCr}_{1-x}\text{Mg}_x\text{O}_3/\text{MgO}$  and  $\text{LaCr}_{1-x}\text{Mg}_x\text{O}_3$  series, the first series performed better than the latter. However, the specific surface area of the first series is almost three times as high as that of the second series, which could be responsible for that difference, since the contribution to the catalytic activity of the  $\text{MgO}$  itself is much lower than that of the perovskite solids.

Saracco et al. (1996) proposed a Rideal–Eley mechanism for  $\text{LaCr}_{1-x}\text{Mg}_x\text{O}_3$  ( $0.2 < x < 0.4$ ) dispersed among  $\text{MgO}$  crystals. They calculated the value of the heat of oxygen adsorption ( $\Delta H_{\text{O}_2} = -43 \pm 2$  kcal/mol) and the activation energies ( $E_a = 24.5 \pm 1.5$  kcal/mol) and found that they are not seriously affected by the level of  $\text{Mg}$  doping. However, as they did not perform any surface characterization, it is not clear how they could assure the real composition of the B site of the perovskite phase.

Collongue et al. (1991) reported the preparation and measurements of catalytic activity of  $\text{LaCrO}_3$  supported on  $\text{Al}_2\text{O}_3$  and  $\text{MgAl}_2\text{O}_4$  (spinel structure). The catalysts were tested for the total oxidation of  $\text{CH}_4$ . The impregnation process on both supports was carried out in two steps. First, the supports were in contact with a  $\text{La}(\text{NO}_3)_3$  solution. After removal of water at 333 K, the solid was calcined at 773 K and cooled down. In a second step, this solid was contacted with a  $\text{Cr}(\text{NO}_3)_3$  solution. After the water was removed, the solid was calcined at 773 K and then at 1273 K for 24 h in flowing  $\text{O}_2$ . The order of impregnation of the cation is critical because of the affinity of the transition metals, such as  $\text{Cr}^{3+}$ , to form a spinel or solid solutions with the supports, especially  $\text{Al}_2\text{O}_3$ . In order to avoid such an interaction,  $\text{La}^{3+}$  must be impregnated first. This precoating of lanthanum has already been discussed in sect. 1.2.2.

The activity of  $\text{LaCrO}_3$  is strongly enhanced by supporting the perovskites on carriers of high specific area like  $\text{Al}_2\text{O}_3$  or  $\text{MgAl}_2\text{O}_4$ . The increase in catalytic activity is due to the higher dispersion of the perovskite phase. Also, supported perovskites were aged at 1340 K under a stoichiometric mixture of air–methane. For the  $\text{LaCrO}_3/\text{Al}_2\text{O}_3$  sample, the loss of activity was assigned to the sintering of the perovskite phase on the alumina surface. The water produced during the reaction at high temperature could attack the perovskite/alumina interphase, then  $\text{LaCrO}_3$  is more likely to sinter, leaving part of the alumina surface free of the mixed oxide. This could explain why the loss of activity ( $135 \cdot 10^{-4} \rightarrow 32 \cdot 10^{-4} \text{ mol h}^{-1} \text{ g}^{-1}$ ) was more pronounced than that resulting from a simple sintering of the support ( $50 \rightarrow 40 \text{ m}^2 \text{ g}^{-1}$ ). For the  $\text{LaCrO}_3/\text{MgAl}_2\text{O}_4$  solid, the loss of specific area ( $32 \rightarrow 18 \text{ m}^2 \text{ g}^{-1}$ ) agreed with the decrease in catalytic activity ( $78 \cdot 10^{-4} \rightarrow 38 \cdot 10^{-4} \text{ mol h}^{-1} \text{ g}^{-1}$ ), suggesting that the coverage of  $\text{MgAl}_2\text{O}_4$  by  $\text{LaCrO}_3$  was preserved although sintering of the solid occurred, showing that  $\text{MgAl}_2\text{O}_4$  spinel seems to be an excellent support for chromium-based perovskite.

In brief, the key issue in high-temperature catalytic combustion is how to develop heat-resistant catalytic materials; in particular, retention of large surface area is one of the main indicators used to rank catalyst quality.

Arai et al. (1989) found that calcination at high temperature (1573 K) of  $\text{La}_{0.6}\text{Sr}_{0.4}\text{MnO}_3$  over  $\text{BaO} \cdot 6\text{Al}_2\text{O}_3$  induced deactivation due to the solid-state reaction between the catalyst

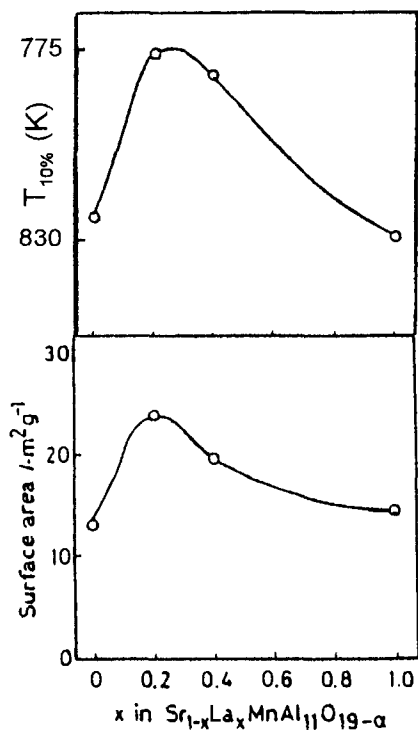


Fig. 19. (a) Catalytic activity for methane combustion ( $T_{10\%}$ ) and (b) surface area after calcination at 1573 K for  $\text{Sr}_{1-x}\text{La}_x\text{MnAl}_{11}\text{O}_{19-\alpha}$ . Reaction conditions:  $\text{CH}_4$  1 vol%, air 99 vol%, space velocity  $48\,000\text{ h}^{-1}$ . With permission from Machida et al. (1990).

phase and the support. Thus, they proposed a combustion catalyst consisting in a single stable phase, such as hexa-aluminate structure.

Machida et al. (1990) prepared  $\text{Sr}_{1-x}\text{La}_x\text{MnAl}_{11}\text{O}_{19-\alpha}$  by hydrolysis of metal alkoxides. All samples were calcined at 1573 K prior to being tested for methane combustion. Figure 19 shows the ignition temperature  $T_{10\%}$  (temperature for 10% of methane conversion) and surface areas for different Sr contents. Both curves have a maximum for  $x=0.2$ . Further studies using TPD, TEM and TGA led to the conclusion that the partial substitution of Sr for La is responsible for the large surface area and low ignition temperature observed after calcination at 1573 K (fig. 19). This superior heat resistance is quite useful for high-temperature combustion. The compositional modification appears to cause both the suppression of crystal growth along the  $c$ -axis that enhances the surface area and the increase in oxidation of Mn ions which promotes active oxygen desorption.

The heat resistance of the hexa-aluminate  $\text{Sr}_{1-x}\text{La}_x\text{MnAl}_{11}\text{O}_{19-\alpha}$  ( $x=0.2$ ) was also evaluated by Arai et al. (1991). The powder sample pressed into a disk underwent isothermal heating at 1573 K for 6400 h in air. No change was observed in the crystal structure or the chemical composition; however, the surface area gradually decreased, staying above  $10\text{ m}^2\text{ g}^{-1}$  after 4200 h of heating.

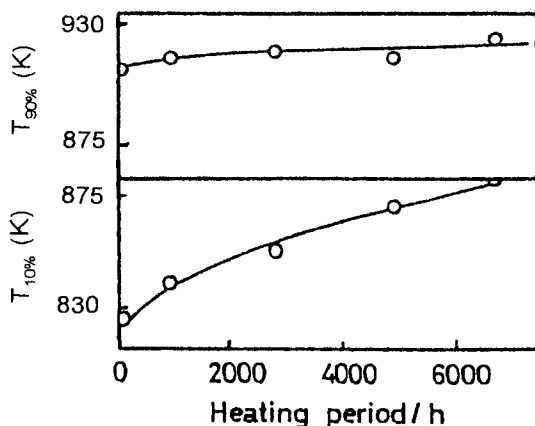


Fig. 20. Methane combustion activity for  $\text{Sr}_{0.8}\text{La}_{0.2}\text{MnAl}_{11}\text{O}_{19-\alpha}$ .  $T_{10\%}$  and  $T_{90\%}$  are the temperatures at which the methane conversion was 10% and 90%. With permission from Arai et al. (1991).

Figure 20 shows the variation of methane combustion activity of  $\text{Sr}_{0.8}\text{La}_{0.2}\text{MnAl}_{11}\text{O}_{19-\alpha}$  after heating at 1570 K for different periods. The activity is expressed as temperatures  $T_{10\%}$  and  $T_{90\%}$ , respectively.  $T_{10\%}$ , related to the combustion-initiation activity, decreased gradually with the decrease in the surface area, whereas  $T_{90\%}$ , complete combustion activity, appeared to be less dependent on the heating period of the catalyst. This is because  $T_{90\%}$  seems to be dependent on the homogeneous gas-phase reaction, which was initiated by radical formation, probably on the catalyst surface at high temperature, and it could not be affected by the lattice oxygen properties of the catalyst.

Industrial catalysts require supports with desirable properties such as resistance to thermal shocks, mechanical strength and chemical stability. For catalytic combustion applications they must be adequately shaped to achieve low pressure drop. The monolithic honeycomb type is the most technologically advanced substrate and successfully satisfies these criteria.

In this way, Isupova et al. (1995) tried to form rings of different perovskite-type oxides, such as  $\text{LaCoO}_3$ ,  $\text{LaMnO}_3$ ,  $\text{La}_{0.7}\text{Sr}_{0.3}\text{CoO}_3$ , without any addition of binders or peptizers; however, after calcination at 773–1173 K, these rings had a rather low mechanical strength. Using alumina as a binder, they found that the surface area was increased and the mechanical strength considerably improved. The alumina seems to suppress sintering, possibly due to the formation of microphase of hexa-aluminate type oxides, which is active and stable at high temperature as mentioned before. Optimized catalysts in the form of honeycomb monoliths were tested in several pilot installations for high-temperature catalytic combustion of gas and liquid fuels. The catalysts worked for two months without loss of activity and monolith integrity.

The incorporation of the catalytic component in the support lattice seems to provide an opportunity to avoid loss of surface area and to keep good catalytic activity even at high temperatures. Such materials can be supported on thermostable substrates or even fabricated as honeycombs.

A number of patents reporting R-mixed oxides to be promising combustion catalysts are summarized by Zwinkels et al. (1993). However, a considerable effort is still needed to develop a generation of catalysts with high combustion activity during extended operation at high temperature.

### 2.5.2. CO oxidation

Oxidation of CO has been used as a test reaction for surface characterization of R-based mixed oxides. Earlier studies reported on this subject have been reviewed by Fierro (1990) and Viswanathan (1992).

The correlation between the activity of  $\text{RMnO}_3$  ( $\text{R}=\text{La, Pr, Nd, Sm, Eu}$ ) for this reaction, tolerance factor and binding energy was analyzed by Viswanathan (1992). The tolerance factor has been introduced in sect. 1.1.1. The element-oxygen binding energy ( $\Delta_{\text{A-O}}$ ) is defined in terms of enthalpy of formation of  $\text{A}_m\text{O}_n$  oxide,  $\Delta H_f$ , metal sublimation energy,  $\Delta H_s$ , and oxygen dissociation energy,  $D_0$ :

$$\Delta_{\text{A-O}} = \frac{\Delta H_f - m\Delta H_s - \frac{1}{2}nD_0}{12m}.$$

The activity increased as the tolerance factor increased, but there were no significant changes in the values of R-O binding energy with the same environment, manganate perovskite, suggesting that the R ion essentially played the role of modifying the B-O bond and was not directly involved as an active site.

In order to evaluate the effect of the B-site element similar studies were performed on  $\text{LaBO}_3$  ( $\text{B}=\text{Co, Mn, Fe, Cr}$ ) by Voorhoeve et al. (1976). The activity for CO oxidation rose as the tolerance factor increased, while it decreased with increasing radius of B ions. The lower B-oxygen binding energy was more favorable for the oxidation of CO, suggesting that the active site involved in the CO oxidation consists of B-O-B clusters. This might imply the participation of surface oxygen in this reaction.

Voorhoeve et al. (1976), Shimizu (1980) and Tascón and Tejuca (1980) have shown an interesting relation between the activity of  $\text{LaBO}_3$  ( $\text{B}=\text{Co, Mn, Ni, Fe, Cr, V}$ ) for the CO oxidation and the electronic state of the transition metal in the B site (fig. 21). As is known, the octahedral environment of  $\text{B}^{3+}$  ions splits the d orbital into two levels and the lower level,  $t_{2g}$ , contains orbitals with higher affinity for  $\text{O}^{2-}$  than the  $e_g$  level. The maximum activities were found for Co, Mn, and Ni, whose  $e_g$  levels have zero or one electron while  $t_{2g}$  levels are half-filled or totally filled. However, Viswanathan (1992) reported that as La was partially substituted by Ce or Sr, their activities could not be related to the electronic state of the B site.

Nakamura et al. (1982) found that the catalytic activity of  $\text{La}_{1-x}\text{Sr}_x\text{CoO}_3$  ( $x=0$  to 0.4) calcined at 1173 K were higher than that of  $\text{LaCoO}_3$  perovskite. The activity presented a maximum for  $x=0.2$ . The reducibility of  $\text{La}_{1-x}\text{Sr}_x\text{CoO}_3$  by CO increased with increasing Sr content, whereas the rate of reoxidation of the reduced catalyst diminished with increasing  $x$ . Therefore, CO oxidation could proceed through a redox mechanism and maximum activity at certain value of  $x$  could be expected due to the competition between

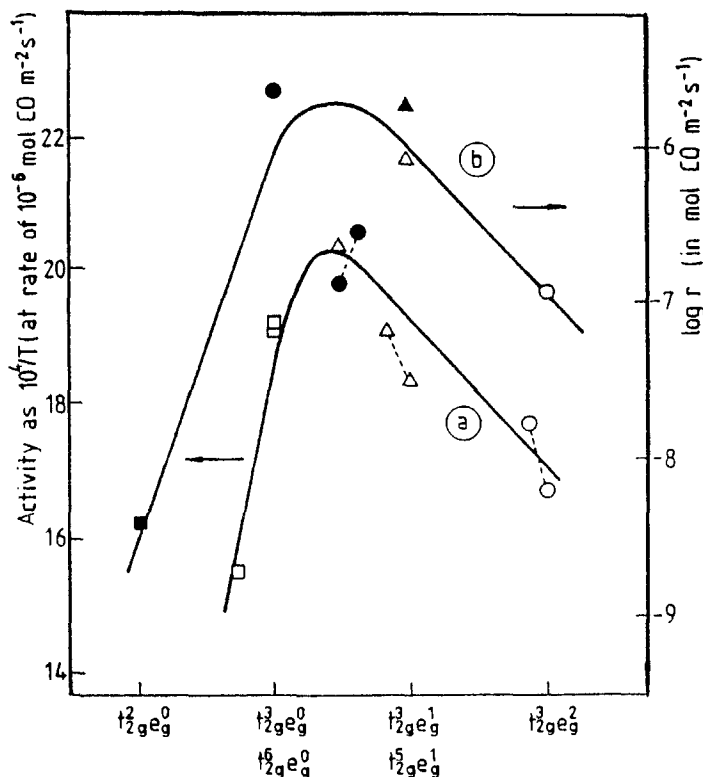


Fig. 21. Activities of  $LaBO_3$  (B, first-row transition element) perovskites for CO oxidation in (a) a 2:1 mixture of CO and  $O_2$  at atmospheric pressure, and (b) a 1:1 mixture of CO and  $O_2$  at atmospheric pressure. Symbols represent the activities of vanadates (solid squares), chromates (open squares), manganates (open triangles), ferrates (open circles), cobaltates (solid circles), and niquelates (solid triangles), plotted at the appropriate d-orbital occupation corresponding to the average valence of the  $B^{3+}$  ion. The activity is given either as (a) the reciprocal of the reaction temperature at which the activity is  $1 \mu\text{mol}$  of CO converted per  $m^2$  of catalyst per second or (b) as the rate of mole CO converted per unit area and unit time. With permission from Fierro (1990).

reduction and reoxidation rate. However, the contribution of adsorbed oxygen should not be overlooked.

Jung et al. (1996) prepared  $Nd_{1-x}Sr_xCoO_{3-\gamma}$  ( $x=0, 0.25, 0.50, 0.75$ ) and studied the effect of Sr substitution on their catalytic activities for CO oxidation. The initial stages of the reaction were investigated using a static reaction system equipped with a differential photoacoustic cell to analyze the products. For the steady-state reaction, a flow reactor system with on-line gas chromatograph was employed. As  $NdCoO_3$  was doped with Sr, part of Co ions were as  $Co^{4+}$  and/or oxygen vacancies were formed. It is well known that the oxygen vacancies can act as an electron donor and become an adsorption site for oxygen molecule. The chemisorbed oxygens on the surface at low temperature can exist

in the form of  $\text{O}_2^-$ ,  $\text{O}_2^{2-}$ ,  $\text{O}^-$  and  $\text{O}_3^-$ , as the temperature increases, according to Kulkarni et al. (1995),  $\text{O}^-$  species are more probable. The kinetic reaction orders obtained for the steady-state reaction were 1 for CO and 0.5 for  $\text{O}_2$ ; this result supports that the molecular oxygen was dissociatively chemisorbed and  $\text{CO}_2$  was produced by the interaction between the adsorbed oxygen and the CO species. However, the kinetic reaction orders obtained for the initial reaction were  $0.85 \pm 0.05$  for CO and 0 for  $\text{O}_2$ . Therefore, the fresh surface of the catalyst was being continuously saturated with oxygen at the beginning of the reaction. But, after this period the adsorption of  $\text{O}_2$  becomes a rate-determining step. Thus, the concentration of the oxygen vacancies in the  $\text{Nd}_{1-x}\text{Sr}_x\text{CoO}_{3-\gamma}$  is the controlling factor for oxidation of CO.

Ramesh and Hegde (1996) reported the oxygen reactivity and the catalytic activity for CO oxidation over cobalt-containing layered defect perovskites,  $\text{YBa}_2\text{Cu}_2\text{CoO}_{7-\gamma}$ ,  $\text{LaBa}_2\text{Cu}_2\text{CoO}_{7-\gamma}$  and  $\text{LaBa}_2\text{Cu}_3\text{O}_{7-\gamma}$ . The orthorhombic  $\text{YBa}_2\text{Cu}_3\text{O}_{7-\gamma}$  structure presents two types of copper atoms, Cu(1) adopting a square planar geometry and Cu(2) in square pyramidal coordination. Pollert et al. (1992) found that the partial substitution of Cu(1) by Co induced an additional oxygen position and the displacement of Co and oxygen ions from their regular sites, suggesting that in the case of  $\text{YBa}_2\text{Cu}_2\text{CoO}_{7-\gamma}$  reactive holes might be located near Cu and Co. Moreover, the oxygen coordination of substituent transition metal cations was also affected by the replacement of Y by La: about 12% of Co ions occupied Cu(2) sites. The larger lanthanum ion and the significant presence of Co at Cu(2) sites resulted in the enrichment of the oxygen content at the rare-earth plane.

TPD patterns of  $\text{LaBa}_2\text{Cu}_3\text{O}_{7-\gamma}$  and  $\text{YBa}_2\text{Cu}_3\text{O}_{7-\gamma}$  were about the same with one peak at 773 K, indicating that the desorbed oxygen came from the same site. However, for  $\text{LaBa}_2\text{Cu}_2\text{CoO}_{7-\gamma}$ , two peaks were observed at 663 and 773 K, consistent with the presence of an additional labile oxygen site. Further interesting evidence for this was that after heating this solid at 723 K, the orthorhombic structure remained, suggesting that the basal plane of oxygen was kept intact.

The activation energies for CO oxidation over  $\text{LaBa}_2\text{Cu}_3\text{O}_{7-\gamma}$ ,  $\text{YBa}_2\text{Cu}_2\text{CoO}_{7-\gamma}$  and  $\text{LaBa}_2\text{Cu}_2\text{CoO}_{7-\gamma}$  were determined as 24.2, 15.9 and 13.6 kcal mol<sup>-1</sup>. Thus, the extra oxygen in the La plane on  $\text{LaBa}_2\text{Cu}_2\text{CoO}_{7-\gamma}$  reacts with CO at temperatures as low as 473 K with substantially low  $E_a$ , comparable with the activity of Pt/ $\text{Al}_2\text{O}_3$  (commercial catalyst).

CO oxidation over  $\text{YBa}_2\text{Cu}_{3-y}\text{B}_y\text{O}_{7-\gamma}$  (B = Co, Al,  $x = 0.12, 0.24, 0.36, 0.48$ ) has been studied by Otamiri et al. (1992). The activity for this reaction decreased with the increasing partial substitution of the B site. It is well known that trivalent cations, such as  $\text{Co}^{3+}$  and  $\text{Al}^{3+}$ , occupy Cu(1) sites. The fresh Al- and Co-substituted oxidized solids were orthorhombic, but after use they shifted to the tetragonal symmetry. This change and the low substitution ( $x = 0.12\text{--}0.48$ ) could explain the differences between these results and those of Ramesh and Hegde (1996).

The kinetics of CO oxidation over  $\text{YBa}_2\text{Cu}_3\text{O}_{6+\gamma}$  and  $\text{PrBa}_2\text{Cu}_3\text{O}_{6+\gamma}$  catalysts was studied in the temperature range 433–473 K by Otamiri and Andersson (1991). The reaction proceeded with an average activation energy of 19.1 kcal mol<sup>-1</sup> for the yttrium

solid and  $17.4 \text{ kcal mol}^{-1}$  for the praseodymium sample. The  $\text{PrBa}_2\text{Cu}_3\text{O}_{6+\gamma}$  exhibited higher activity probably due to its oxidation state. The influence of a central rare-earth ion on the crystal chemistry of  $\text{RBa}_2\text{Cu}_3\text{O}_{7-\gamma}$  series was recently analyzed by Ramesh and Hegde (1994). This study gave the interesting information that larger R ions such as La and Pr in the central cage show a higher oxidation state than the normal value of 3. This could affect the oxygen mobility and copper oxidation state as well as the catalytic activity for oxidation of CO.

$\text{YBa}_2\text{Cu}_3\text{O}_{7-\gamma}$  was tested as a catalyst for oxidation of CO by Jiang et al. (1989), who reported an  $E_a = 27.5 \text{ kcal mol}^{-1}$ . The reduction of this solid caused a decrease of the catalytic activity. This behavior was explained taking into account that the reduction removed the labile oxygen from the lattice. Similar experiments were performed by Halasz et al. (1990) over  $\text{Y}_2\text{BaCuO}_5$ . They found that the  $E_a$  for the oxidized sample was  $24.8 \text{ kcal mol}^{-1}$ , however, as the catalyst was slightly reduced, it dropped to  $11 \text{ kcal mol}^{-1}$ . The exact nature of the change in the surface composition after the slight reduction is not known. However, Noller and Vinek (1980) reported that for the necessary catalytic oxidation reaction two kinds of sites are necessary: (i) electron-pair donor and (ii) electron-pair acceptor. It was further noted that materials with a single oxidation state for the active metal, especially if it was a high oxidation state for the element, have very low or zero catalytic activity. In this respect, it is noticeable that for  $\text{Y}_2\text{BaCuO}_5$ , the Cu is only present as  $\text{Cu}^{2+}$ . Thus, it is probable that during the reduction some  $\text{Cu}^+$  was formed and enhanced the catalytic activity for the oxidation.

The catalytic oxidation of CO to  $\text{CO}_2$  at low temperature is one of the challenging problems in environmental chemistry. The advantage of using R-based mixed oxides as catalysts for CO oxidation is based on the following facts:

- (i) A wide variety of cation substitutions can be made to modify the structure, oxygen vacancies and the activation energy for oxygen adsorption.
- (ii) This type of solids falls into the kind of uniform heterogeneous catalysts where the solid as a whole acts in the catalytic reaction, as proposed by Thomas (1988).

### 2.5.3. NO and $\text{N}_2\text{O}$ decomposition

The decomposition of the thermodynamically unstable nitrogen oxides is in theory the best way to eliminate them from contaminated gas streams.  $\text{N}_2\text{O}$  is relatively easy to decompose catalytically while NO is much harder. In fact, the NO transformation is always limited by the presence of oxygen over all the catalysts assayed so far.

Let us review first the state of the art concerning nitric oxide decomposition. In the last 10 years the search for NO decomposition catalysts sharply increased in an effort to comply with more severe regulations which reduce the allowed emission level of this contaminant. Particularly during the 1990s quite a few papers have been published concerning the use of different rare-earth-containing perovskites and  $\text{K}_2\text{NiF}_4$ -type mixed oxides. Ni, Cu and Co are the most commonly used transition metals.

Teraoka et al. (1990, 1993) systematically tried a large series of perovskite mixed oxides for NO decomposition (table 26). Their ternary and quaternary oxides included in the



Table 26  
Catalytic activity of perovskite-type oxides for the direct decomposition of nitric oxide<sup>a,b</sup>

Catalyst <sup>c</sup>	X[N <sub>2</sub> ] (%)		Catalyst <sup>c</sup>	X[N <sub>2</sub> ] (%)	
	973 K	1073 K		973 K	1093 K
La <sub>1-x</sub> Sr <sub>x</sub> CoO <sub>3</sub>			La <sub>0.8</sub> Sr <sub>0.2</sub> Co <sub>0.8</sub> B' <sub>0.2</sub> O <sub>3</sub>		
<i>x</i> = 0 (3.6)	3.7	7.5	B' = Cr (4.8)	2.7	2.0
<i>x</i> = 0.2 (8.1)	45.0	72.0	Mn (4.6)	30.4	43.4
<i>x</i> = 0.20.2 (5.7)	44.5	67.9	Fe (6.8)	46.8	68.7
<i>x</i> = 0.20.4 (5.1)	31.2	48.7	Co (8.1)	45.0	72.0
La <sub>1-x</sub> Sr <sub>x</sub> Co <sub>0.4</sub> Fe <sub>0.6</sub> O <sub>3</sub>			Ni (5.6)	34.2	70.5
<i>x</i> = 0 (3.3)	9.2	12.8	Cu (4.9)	24.9	35.9
<i>x</i> = 0.20.2 (6.1)	24.9	56.2	La <sub>0.4</sub> Sr <sub>0.6</sub> Mn <sub>0.8</sub> B' <sub>0.2</sub> O <sub>3</sub>		
<i>x</i> = 0.20.4 (7.5)	17.5	37.1	B' = Mn (4.0)	10.8	25.1
<i>x</i> = 0.20.8 (3.8)	8.0	24.7	Fe (11.5)	27.6	57.1
<i>x</i> = 0.21.0 (3.3)	9.8	27.9	Co (10.8)	23.1	55.7
La <sub>1-x</sub> Sr <sub>x</sub> MnO <sub>3</sub>			Ni (12.1)	28.2	62.4
<i>x</i> = 0 (9.1)	7.6	13.5			
<i>x</i> = 0.20.6 (4.0)	10.8	25.1			

<sup>a</sup> With permission from Teraoka et al. (1993).

<sup>b</sup> Reaction conditions: 1.0 vol% NO diluted in He, *W/F* = 4.0 g s cm<sup>-3</sup>.

<sup>c</sup> Figures in parentheses are specific surface areas in units of m<sup>2</sup> g<sup>-1</sup>.

B site either Fe, Co, Ni, Cr, Mn or Cu. The partial substitution of La by Sr was needed to increase the catalytic activity to an acceptable level. The presence of a transition metal able to change oxidation state relatively easy was also required. Although La<sub>0.8</sub>Sr<sub>0.2</sub>CoO<sub>3</sub> seems to be the best one, there is not a great difference among several of the formulations shown in table 26. A more detailed study should be made to justify their conclusion that La<sub>0.8</sub>Sr<sub>0.2</sub>CoO<sub>3</sub> is a promising catalyst. Note that all the formulations become active at ~973 K under the conditions assayed.

These early papers already hint that two essential elements may play important roles in this reaction: (i) oxygen vacancies, and the consequently enhanced oxygen mobility increased by the partial substitution of La by Sr; (ii) the redox ability of the transition-metal cation. This subject was developed in more detail in the papers published afterwards.

In a recent paper Zhao et al. (1996) used Ni-based ABO<sub>3</sub> and A<sub>2</sub>BO<sub>4</sub>-type mixed oxides. They covered a wide range of temperatures (273–1173 K), studied the adsorption–desorption phenomenon and used several instrumental techniques.

The four oxides studied were LaNiO<sub>3</sub>, La<sub>0.1</sub>Sr<sub>0.9</sub>NiO<sub>3</sub>, La<sub>2</sub>NiO<sub>4</sub> and LaSrNiO<sub>4</sub>. The latter was the most active, selective (to N<sub>2</sub>) and stable catalyst. Figure 22 shows the evolution of both conversion and selectivity to N<sub>2</sub> with temperature. Below 773 K the authors reported some transient, non-catalytic activity for the decomposition reaction.

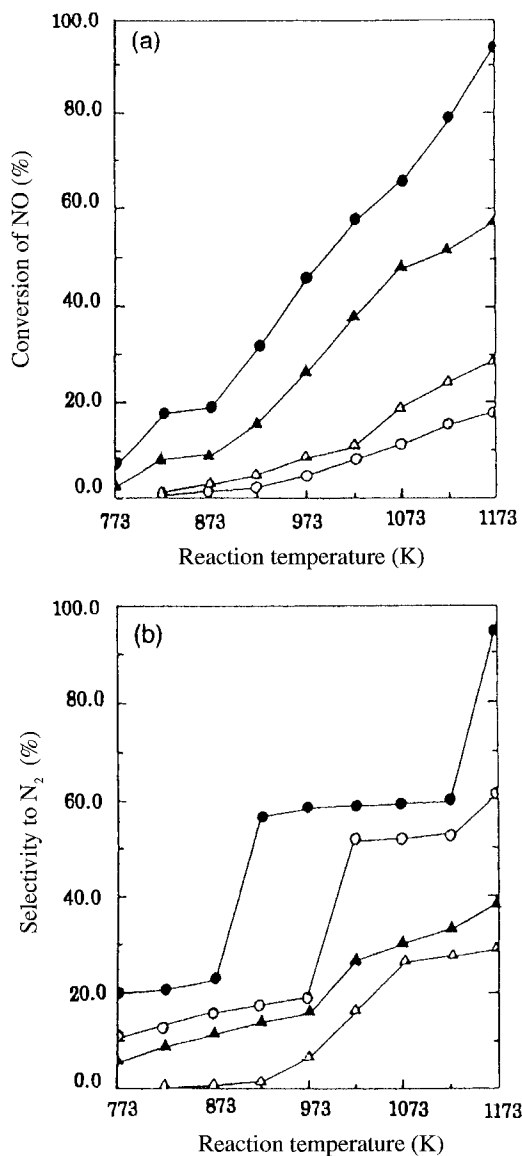


Fig. 22. (a) Conversion of NO and (b) selectivity to  $\text{N}_2$  vs. reaction temperature. Symbols: solid circles,  $\text{SrNiO}_4$ ; open circles,  $\text{La}_2\text{NiO}_4$ ; solid triangles,  $\text{La}_{0.1}\text{Sr}_{0.9}\text{NiO}_3$ ; open triangles,  $\text{LaNiO}_3$ . With permission from Zhao et al. (1996).

They carefully characterized the phases using XRD and concluded that the oxide with  $\text{A}_2\text{BO}_4$  structure is more stable than  $\text{ABO}_3$ .

Temperature-programmed desorption of oxygen and nitric oxide provided some clues to the nature of active sites involved in the reaction. Table 27 collects the characterization data obtained; the last column shows the NO conversion. There is a certain correlation

Table 27

Desorption temperatures, areas of desorption peaks, nonstoichiometric oxygen ( $\lambda$ ) and the activity of NO decomposition<sup>a</sup>

Catalyst	O <sub>2</sub>		N <sub>2</sub>		N <sub>2</sub> O		NO + NO <sub>2</sub>	$\lambda$	NO conversion <sup>a</sup> (%)
	<i>S</i> (cm <sup>2</sup> m <sup>-2</sup> )	<i>T</i> (K)	<i>S</i> (cm <sup>2</sup> m <sup>-2</sup> )	<i>T</i> (K)	<i>S</i> (cm <sup>2</sup> m <sup>-2</sup> )	<i>T</i> (K)			
La <sub>2</sub> NiO <sub>4</sub>	15.09	1145	1.45	385	0.47	480	5.05	+0.068	17.21
LaNiO <sub>3</sub>	1.78	1135			1.83	445	20.87	-0.083	28.81
LaSrNiO <sub>4</sub>	3.01	950	0.50	440	2.01	510	62.11	-0.160	94.20

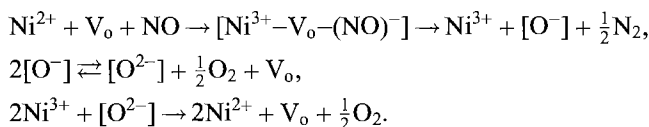
<sup>a</sup> With permission from Zhao et al. (1996). Reaction temperature 1173 K; GHSV = 2800 h<sup>-1</sup>; NO mol % = 1.5, He balance.

between the total amount of NO + NO<sub>2</sub> desorbed during the TPD of NO and conversion. This correlation is much better, however, between the latter and the amount of nonstoichiometric oxygen ( $\lambda$ ). The authors, in agreement with others, assign the active role in the catalytic act to negatively charged adsorbed nitric oxide.

The picture is clarified when the oxygen adsorption behavior of the four samples is analyzed. It was found that the order of the desorption temperature correlates with NO conversion, i.e. the lower the desorption temperature (larger mobility of oxygen is attained at a given temperature), the higher activity is observed.

Zhao et al. (1996) proposed a reasonable tentative mechanism for NO decomposition. Based upon the fact that LaNiO<sub>3</sub> with the lowest content of Ni<sup>2+</sup> shows almost no selectivity to N<sub>2</sub> in the low-temperature regime and the lowest one in the catalytic region, while the contrary occurs with La<sub>2</sub>NiO<sub>4</sub> (fig. 22b), they assigned a central role to the presence of a high concentration of Ni<sup>2+</sup> in the catalyst. Ni<sup>2+</sup> should be oxidized to Ni<sup>3+</sup> and NO reduced to NO<sup>-</sup>. Observing the activity curves, fig. 22a, one sees that the oxides with oxygen vacancies are more active than the almost stoichiometric ones. This points to an important role for vacancies in the reaction mechanism as well. Perhaps the NO<sup>-</sup> is adsorbed at sites neighboring those where NO decomposition occurs.

To complete the catalytic cycle the Ni<sup>3+</sup> must be reduced and the vacancies regenerated. This is tentatively accounted for by the authors in the proposed redox mechanism that follows:



The oxygen mobility in the lattice is needed for this mechanism to be possible. This is consistent again with the correlation observed between vacancy concentration (which facilitates oxygen mobility) and catalytic activity as estimated from NO conversion.

At higher temperatures, e.g.,  $T \geq 1073$  K, the dismutation of oxygen species would be accelerated and the lattice oxygen (O<sup>2-</sup>) would take part in the reproduction of active

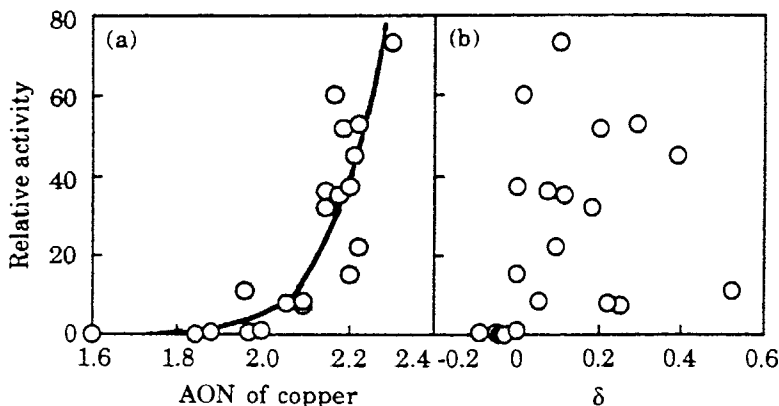
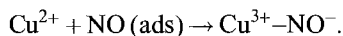


Fig. 23. Correlation between the catalytic activities of NO decomposition (1073 K) in linear scale and (a) AON of copper (a) or (b)  $\delta$  for  $\text{La}_{2-x}\text{A}'_x\text{Cu}_{1-y}\text{B}'_y\text{O}_{4\pm\delta}$ . With permission from Yasuda et al. (1993).

sites. The proposed mechanism requires further work to be proven but is most consistent with the authors' results.

The other important transition metal incorporated into the perovskite lattice is Cu. As a matter of fact, there is an important driving force to try this cation in another matrix after its success to catalyze NO decomposition when exchanged into certain zeolites such as ZSM5 and ferrierites. Yasuda et al. (1990) studied the decomposition of NO over  $\text{La}_{2-x}\text{A}'_x\text{Cu}_{1-y}\text{B}'_y\text{O}_{4\pm\delta}$  ( $\text{A}' = \text{Sr, Ba, Ca}$ ;  $\text{B}' = \text{Zr, Al}$ ) and also concluded that the oxidation of the transition metal cation ( $\text{Cu}^{2+} \rightarrow \text{Cu}^{3+}$ ) plays a key role in the reaction mechanism. They found a certain correlation between the average oxidation number (AON) of copper and the relative activity for NO decomposition (fig. 23a). Contrary to the case of the Ni-containing oxides, no correlation was found with the oxygen non-stoichiometry (fig. 23b). How could the sharp increase in activity be reconciled with increasing AON? The answer was found in the XPS data. Neither the binding energy nor the  $I_{\text{sat}}/I_{\text{main}}$  of the Cu 2p signal changed with the rare-earth substitution that modifies the bulk oxidation state of Cu. Moreover, the  $\text{L}_3\text{VV}$  Auger peak assignable to  $\text{Cu}^{2+}$  (ca. 918 eV) remained unchanged with varying  $x$ . This seems to indicate that on the surface,  $\text{Cu}^{3+}$  cannot exist due to a partial desorption of oxygen from the surface layer.

The authors also studied the  $\text{N}_2\text{O}$  decomposition on the same catalysts and found it to be much faster than NO decomposition. Since both reactions leave  $\text{O}_{\text{ads}}$  on the catalyst surface it was concluded that oxygen desorption is not the rate-determining step of NO decomposition on these solids. On the other hand, the retarding effect of  $\text{O}_2$  gas is consistent with the idea that  $\text{O}_2 \leftrightarrow 2\text{O}(\text{ads})$  is in equilibrium. In brief, all their data are consistent with a mechanism in which the active sites for NO decomposition are coordinatively unsaturated  $\text{Cu}^{2+}$  ions on the surface that can be easily oxidized to  $\text{Cu}^{3+}$  upon NO adsorption:



Note that this step bears resemblance to that proposed by Zhao et al. (1996) over Ni-containing mixed oxides. However, Yasuda et al. (1990) did not assign any role to oxygen vacancies in the lattice. They compared the activity of their catalyst with  $\text{La}_{0.8}\text{Sr}_{0.2}\text{CoO}_3$  and Cu-ZSM5. The latter is active at temperatures between 573 and 773 K. The perovskites are active at higher temperatures, and at  $T > 800$  K  $\text{La}_{1.5}\text{Sr}_{0.5}\text{CuO}_4$  is three times more active than  $\text{La}_{0.8}\text{Sr}_{0.2}\text{CoO}_3$  (per unit surface area). The mixed oxides may be used in high-temperature applications where the zeolite-based formulation may not be durable enough.

Lin et al. (1993) studied the interaction of NO with  $\text{YBa}_2\text{Cu}_3\text{O}_7$  using XPS and FTIR. They covered a wide range of temperatures from 300 to 1200 K. They observed the formation of nitride, nitrate, nitrite and nitrito (FTIR) on the surface and the release of  $\text{N}_2$ ,  $\text{N}_2\text{O}$  and  $\text{NO}_2$ . The nitrite ion ( $\text{NO}_2^-$ ) is by far the most abundant species at  $T \geq 800$  K. Again, the NO interaction with the solid oxidizes less than 24% of the lattice Cu(II) ions. The authors pointed out that the lattice barium atoms can be expelled from the structure and reported a substantial segregation of BaO to the surface of the oxide at  $\sim 900$  K. In brief, again the  $\text{Cu}^{2+} \leftrightarrow \text{Cu}^{3+}$  redox cycle is implicitly proposed here as an important step of the reaction mechanism.  $\text{NO}_2^-$  is the predominant species at high temperature, and the superconducting oxide not only provides the active sites for the adsorption of NO but also contributes to the stabilization of the reaction intermediates.

It was not until recently that  $\text{N}_2\text{O}$  was recognized as an atmospheric pollutant which contributes to stratospheric ozone destruction and greenhouse effects. This gave more emphasis to the search of active catalysts to decompose  $\text{N}_2\text{O}$ .

Even before these findings, the decomposition of  $\text{N}_2\text{O}$  was studied because the oxide is often formed during the decomposition and reduction of NO over many catalysts. Furthermore, on other occasions, it was used as a test reaction to investigate the nature of active sites on metal and metal-oxide catalysts. Thus, there is a wealth of information concerning this reaction on all kinds of solids. The reader is referred to the article by Swamy and Christopher (1992) for a coverage of this reaction occurring on perovskite-related oxides. This review concerns the study of  $\text{N}_2\text{O}$  decomposition as a model reaction. As such it tries to relate catalytic behavior of several perovskites with structural features, thermodynamic oxygen bond energy and orbital occupancy. Double perovskites and  $\text{R}_2\text{A}_2\text{BO}_4$  structures are also covered by Swamy and Christopher (1992) with the same overall goal of finding correlations between catalytic behavior and several physicochemical properties of the solids used.

Misono and co-workers studied the decomposition of  $\text{N}_2\text{O}$ , Wang et al. (1995), over similar solids and using the same tools as in the previously analyzed contribution of Yasuda et al. (1990) (*vide ultra*). More precisely, Wang et al. (1995) carried out the decomposition of  $\text{N}_2\text{O}$  over  $\text{La}_{2-x}\text{Sr}_x\text{CuO}_4$  ( $x=0-1$ ),  $\text{La}_2\text{MO}_4$  ( $\text{M}=\text{Co}, \text{Ni}, \text{Cu}$ ) and  $\text{LaMO}_3$  ( $\text{M}=\text{Cr}, \text{Mn}, \text{Fe}, \text{Co}, \text{Ni}$ ). As was the case with NO the  $\text{N}_2\text{O}$  decomposition is first-order in the nitrogen oxide and of negative order (inhibited) in oxygen partial pressures. In fact, when the solid was pretreated in He at 1073 K the initial reaction rate increased but then gradually diminished due to inhibition by oxygen formed by the reaction.

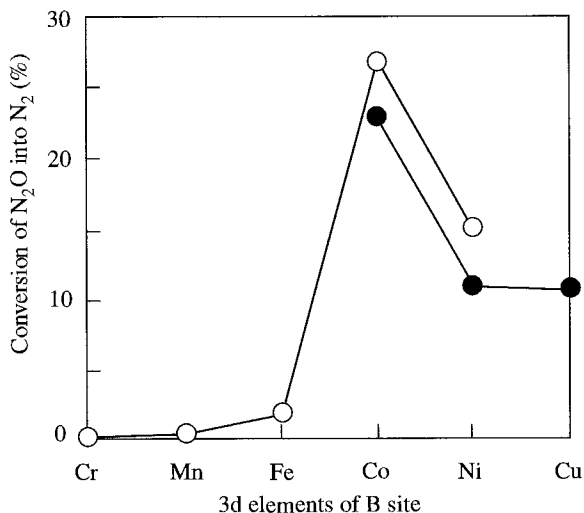


Fig. 24. Activity profiles of N<sub>2</sub>O decomposition over LaMO<sub>3</sub> (open circles) and La<sub>2</sub>MO<sub>4</sub> (solid circles) at 723 K,  $W/F = 0.3 \text{ g s cm}^{-3}$ . With permission from Wang et al. (1995).

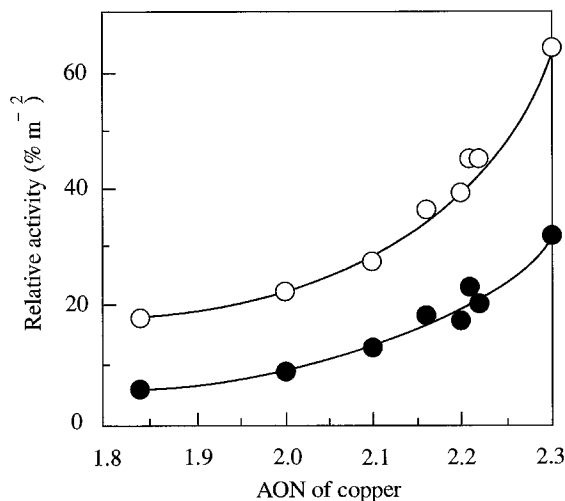


Fig. 25. Correlation between the activity for N<sub>2</sub>O decomposition and the average oxidation number (AON) of copper for La<sub>2-x</sub>Sr<sub>x</sub>CuO<sub>4</sub> at 723 K (solid circles) and 773 K (open circles),  $W/F = 0.3 \text{ g s cm}^{-3}$ . With permission from Wang et al. (1995).

The effect of the transition-metal cation upon catalytic activity for N<sub>2</sub>O decomposition is shown in fig. 24. Note that Co is the best, independent of the matrix used. Also note that in the case of oxidation reactions, a twin-peak pattern with Co and Mn at the peaks is obtained as in the case of simple transition-metal oxides (Yamazoe and Teraoka 1990, Nitadori et al. 1988).

The surface oxidation state of the transition metal and the availability of vacancies and/or adsorbed oxygen play a central role in defining the catalytic behavior of the oxides for this and other reactions. Particularly enlightening is fig. 25 which shows how the catalytic activity increases with the increasing average oxidation number (AON) of copper.

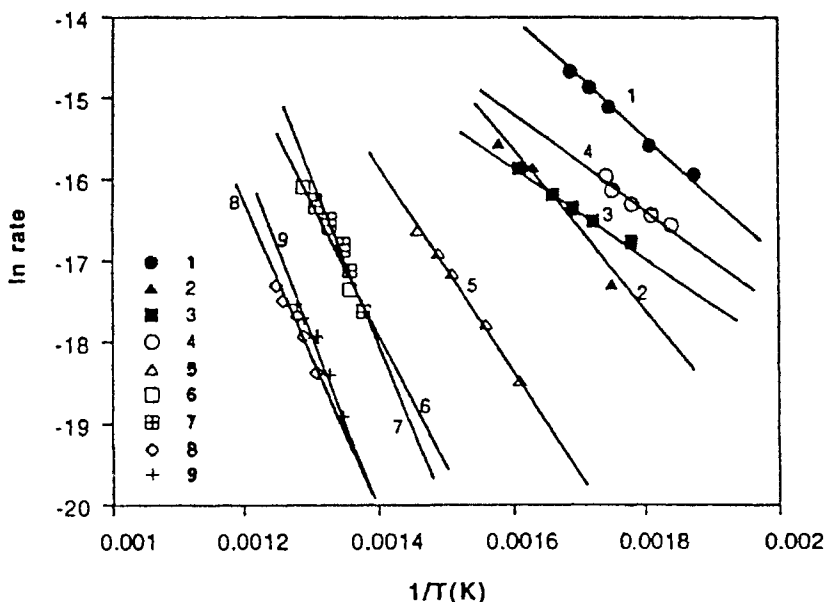


Fig. 26. Comparison of Arrhenius plots for the decomposition of nitrous oxide over different catalysts: (1) Pt/Al<sub>2</sub>O<sub>3</sub>; (2) Pt/Al<sub>2</sub>O<sub>3</sub>; (3) Pd/C; (4) La<sub>0.8</sub>Sr<sub>0.2</sub>CoO<sub>3</sub>; (5) La<sub>0.8</sub>Sr<sub>0.2</sub>FeO<sub>3</sub>; (6) La<sub>0.8</sub>Sr<sub>0.2</sub>MnO<sub>3</sub>; (7) La<sub>1.8</sub>Sr<sub>0.2</sub>CuO<sub>4</sub>; (8) La<sub>0.8</sub>Sr<sub>0.2</sub>CrO<sub>3</sub> and La<sub>0.8</sub>Sr<sub>0.2</sub>YO<sub>3</sub>. With permission from Gunasekaran et al. (1995).

As discussed above, at higher AON of copper the  $\text{Cu}^{2+} \rightarrow \text{Cu}^{3+}$  oxidation becomes more facile and the reaction rate increases because a larger concentration of surface  $\text{N}_2\text{O}$  is generated.

Gunasekaran et al. (1995) also reported kinetic data on the decomposition of  $\text{N}_2\text{O}$  over La<sub>0.8</sub>Sr<sub>0.2</sub>MO<sub>3-δ</sub> (M=Cu, Fe, Mn, Co or Y) and La<sub>1.8</sub>Sr<sub>0.2</sub>CuO<sub>4-δ</sub>. The catalytic performance was compared with that obtained with Pd(0.5%)/Al<sub>2</sub>O<sub>3</sub>, Pd(0.5%)/carbon and Pt(0.5%)/Al<sub>2</sub>O<sub>3</sub>.

Figure 26 shows a good synthesis of the results obtained by Gunasekaran et al. (1995). It is clearly shown that La<sub>0.8</sub>Sr<sub>0.2</sub>CoO<sub>3</sub> has an activity similar to the supported noble metals. Particularly at  $T > 773$  K, its activity becomes comparable to Pd/Al<sub>2</sub>O<sub>3</sub>. However, the latter is not affected by 4.5% O<sub>2</sub> in the gas feed while the former exhibits a significant decrease in rate at 773 K. The light-off temperature is much lower on Pd/Al<sub>2</sub>O<sub>3</sub> although it can be decreased by 80 K on the perovskite material when the surface area is increased from 2 to 11 m<sup>2</sup>/g.

Summing up, there is general agreement that by increasing the oxidation number of the B cations, the catalytic activity for both NO and N<sub>2</sub>O decomposition is enhanced. Many researchers also assign a positive role to the development of oxygen vacancies in the oxide structure. The formation of negatively charged NO<sub>x</sub><sup>-</sup> adsorbed species seems to be a necessary step in nitrogen oxides decomposition.

Generally speaking, Cu-ZSM5 is active at lower temperatures than Cu, Ni or some other metal containing perovskites. Thus, the latter being structurally more resistant, it might be used for applications at  $T \gg 750$  K.

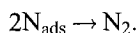
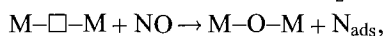
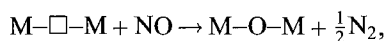
A common negative feature of all these catalysts is the strong inhibition by oxygen of the decomposition reaction. This leads to the use of different reduction agents to abate  $\text{NO}_x$  emissions as discussed in the next section.

#### 2.5.4. NO reduction

Since the early seventies, perovskite oxides have been tried as potential replacement of three-way catalysts for car exhaust gases treatment. In Chapter 184 the ceria-containing three-way catalysts will be thoroughly covered while in this chapter we will refer to all the other formulations used for the reduction of nitric oxide.

Tejuca et al. (1989) provided a brief review about this subject. Before 1989 the most prominent published contributions were those of Voorhoeve et al. (1975, 1976). The main B cations studied were Co and Mn while several cations were inserted in the A position partially substituting lanthanum. The rationale for this approach is found in the role assigned to oxygen vacancies in the dissociation of NO. The substitution of La by lower-valent cations induces the formation of oxygen vacancies.

A mechanism has been proposed by Voorhoeve et al. (1975, 1976) which involves two types of NO adsorption:



In order to find out whether the oxidation of the B cation or the lanthanum vacancies were responsible for the increase in NO reduction activity, Voorhoeve et al. (1975) tested mixed oxides  $(\text{A}_y\text{A}'_{1-y})\text{Mn}_{1-x}^{3+}\text{Mn}_x^{4+}\text{O}_3$ , where A and A' represent La, Bi, Pb, Sr, Na, K or Rb. These solids contained nearly constant proportions of  $\text{Mn}^{3+}/\text{Mn}^{4+}$  but with different A–O binding energies. Their data indicate that the binding energy of surface oxygen plays a central role in defining the catalytic activity for this reaction. Weaker oxygen bonding favors both the formation of oxygen vacancies and the NO reduction.

By the mid 1970s, several groups, industrial and academic, were searching for good three-way catalysts with the hope of eliminating or at least minimizing the use of noble metals. In this vein, Lauder's patent from Dupont was very encouraging. Lauder (1975) supported  $\text{La}_{0.6}\text{Sr}_{0.4}\text{Co}_{0.94}\text{Pt}_{0.03}\text{Ru}_{0.03}\text{O}_3$  on Torvex alumina and used it to treat exhaust gases from a single-cylinder engine. Unleaded gasoline was used and the test was run for 800 hours. Within the slightly oxidizing operating window, the removal of CO, hydrocarbon and  $\text{NO}_x$  was above 80%. However, this and other perovskite catalysts are poisoned by  $\text{SO}_2$ , a fact that has impaired their use in automobile exhausts.

During the last decade the study of NO reduction surged again. Most publications report results on the  $\text{NO} + \text{CO}$  reaction over several complex perovskite and perovskite-related



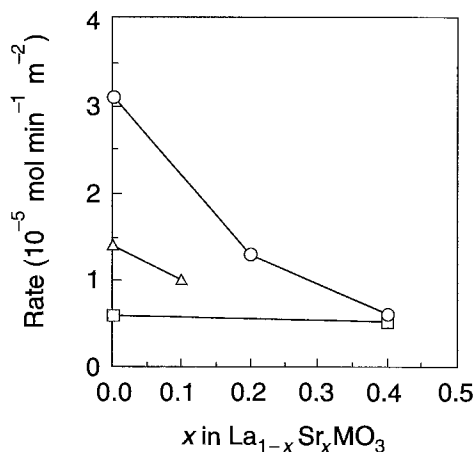


Fig. 27. Changes in the catalytic activity for the CO-NO reaction at 573 K. Activities are given for  $\text{La}_{1-x}\text{Sr}_x\text{CoO}_3$  (circles),  $\text{La}_{1-x}\text{Sr}_x\text{MnO}_3$  (squares) and  $\text{La}_{1-x}\text{Sr}_x\text{FeO}_3$  (triangles). With permission from Mizuno et al. (1992b).

structures containing up to five different cations. Only in a few cases has the effect of excess oxygen been investigated.

Misono and co-workers continued their series of studies on NO and  $\text{N}_2\text{O}$  decomposition and also explored the reduction of NO with CO. Mizuno et al. (1992b) report the data obtained for CO + NO, CO +  $\text{NO}_2$  and CO +  $\text{O}_2$  reactions using as catalysts  $\text{La}_{1-x}\text{Sr}_x\text{MO}_3$  (M = Co, Fe, Mn, Cr, Ni;  $x = 0-0.4$ ). Their main goal was to elucidate the controlling factor for the reduction of NO. The activity order for the CO + NO reaction was  $\text{LaCoO}_3 > \text{LaFeO}_3 > \text{LaMnO}_3 > \text{LaCrO}_3 > \text{LaNiO}_3$ .

A large amount of  $\text{N}_2\text{O}$  was formed from the initial stage over  $\text{LaMO}_3$  (M = Co, Mn, Fe, Cr, Ni) at 573 K. The time course of the NO + CO reaction (performed in a batch recirculation system) reflects this situation. These results support a two-step reaction pathway in which  $\text{N}_2\text{O}$  is an intermediate for nitrogen formation. Öcal et al. (1994) confirm the role of  $\text{N}_2\text{O}$  as intermediate in this reaction over perovskite oxides. They used steady-state isotopic transient kinetic analysis to study the mechanism of NO + CO reaction over  $\text{LaCoO}_3$ . They concluded that  $\text{N}_2\text{O}$  was an intermediate in the formation of  $\text{N}_2$  at  $T < 873$  K. They also concluded that at high temperature  $\text{CO}_2$  desorption became the rate-limiting step of the overall reaction. This is likely due to the rapid formation and slow decomposition of very stable carbonates on the perovskite surface as reported by Milt et al. (1996).

The partial substitution of La by Sr either decreases or has no effect on the catalytic activity for the reaction (fig. 27). This is at variance with the tendency observed by the same group for the oxidation of propane. The decrease in activity with increasing Sr substitution is explained by Mizuno et al. (1992b) in terms of the increased oxidation of the B cation which in turn makes it more difficult to adsorb the nitric oxide as  $\text{NO}^-$ . This view is further supported by the fact that after reduction,  $\text{La}_{0.6}\text{Sr}_{0.4}\text{CoO}_3$  becomes more active.

Lindstedt et al. (1994) studied perovskites similar to those of Mizuno et al. (1992b), although at higher reaction temperatures (873–1223 K). They limited their studies to the best ones screened by Mizuno et al. (1992b), i.e.,  $\text{La}_{1-x}\text{Sr}_x\text{MO}_3$  ( $\text{M}=\text{Co Fe}$ ). They confirmed that prereduced  $\text{LaCoO}_3$  is more active than the oxidized solid. Moreover, they found that the reduced perovskite became  $\text{La}_2\text{CoO}_4$  during the catalytic tests conducted at high temperature. However, the iron perovskite retained its original structure. The  $\text{La}_2\text{CoO}_4$  was reversibly reoxidized to  $\text{LaCoO}_3$ . They also extended the previous studies by introducing excess  $\text{O}_2$  in the reactant mixture. Under these circumstances, the NO reduction decreased to zero. This behavior is qualitatively similar to conventional three-way catalysts that become inefficient for NO reduction under lean-burn conditions (excess oxygen).

Since  $\text{LaCoO}_3$  is a reasonably good catalyst for NO + CO reaction and  $\text{CeO}_2$  is usually incorporated in three-way catalysts as an oxygen reservoir, the logical direction to follow is to explore the partial substitution of La by Ce. This was recently done in a systematic way by Forni et al. (1996). They prepared a series of  $\text{La}_{1-x}\text{Ce}_x\text{CoO}_{3+\delta}$  ( $x=0-0.2$ ) perovskite-type catalysts. They used as a reference for comparison  $\text{La}_{0.9}\text{Sr}_{0.1}\text{CoO}_3$ . Note that no more than 0.05 Ce atoms could be introduced in the perovskite structures. At  $x \approx 0.05$ ,  $\text{CeO}_2$  reflections appeared in the diffraction patterns. Their kinetic results are consistent with a two-step mechanism for the reaction between NO and CO to produce  $\text{N}_2$  and  $\text{CO}_2$ , the intermediate being  $\text{N}_2\text{O}$ . The reaction temperature was varied between 423 and 723 K. Ce ions seem to act as stabilizer of  $\text{O}_2^-$  ions on the catalyst surface.

Ladavos and Pomonis (1992) studied NO reduction with CO over  $\text{La}_{2-x}\text{Sr}_x\text{NiO}_{4-\lambda}$ , with  $0 \leq x \leq 1.50$ . The substitution of La by Sr produces a maximum activity at  $x = 1.0$ . At lower  $x$  values the activity changes very little, but it drops significantly between  $x = 1.0$  and 1.5.

Ladavos and Pomonis (1993) prepared supported  $\text{LaNiO}_3/\text{Al}_2\text{O}_3$  and  $\text{La}_2\text{NiO}_4/\text{ZrO}_2$  and tested them in the NO + CO reaction. They compared the activities of the supported perovskites with massive ones. On a per-gram basis  $\text{La}_2\text{NiO}_4/\text{ZrO}_2$  is about four times more active than massive  $\text{La}_2\text{NiO}_4$ . It is not possible to go much beyond this point because the authors could not find a method to obtain reliable data about the dispersion of the mixed oxide on the  $\text{ZrO}_2$  support. The alumina support was undoubtedly not suitable for this perovskite.

In a series of papers published by Swedish and Japanese researchers, they used supported and massive perovskites of the general formula  $\text{La}_{1-x}\text{Sr}_x\text{M}_{1-2y}\text{Cu}_y\text{Ru}_y\text{O}_3$  ( $\text{M}=\text{Al, Mn, Fe or Co}$ ) as catalysts for the reduction of NO with CO. Skoglundh et al. (1994) prepared nine alumina washcoated mixed oxide catalysts containing La, Sr, Cu and Ru. The solids obtained were thoroughly characterized using several techniques. They were tested in two different reactant streams: (i) NO/CO/ $\text{C}_3\text{H}_6$ / $\text{O}_2$ / $\text{N}_2$  (feed stream A) and (ii) NO/CO/ $\text{N}_2$  (feed stream B).

The electron-microscopic observation of the samples prepared showed the presence of nanosize particles (60–200 nm) which sometimes were accompanied by larger (1–10  $\mu\text{m}$ ) flake-like formations. The smaller particles form agglomerates which almost cover all the surface of the alumina washcoats. The total surface area of the washcoat, impregnated

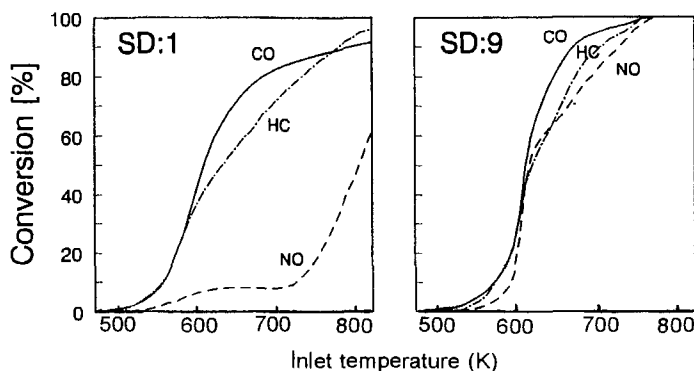


Fig. 28. Degree of conversion of NO, CO and  $C_3H_6$  plotted versus the inlet temperature of the feed stream A, determined under stoichiometric conditions ( $S=1.0$ ), for the catalysts SD:1 and SD:9. With permission from Skoglundh et al. (1994).

Table 28

Light-off temperatures for feed streams A and B determined under stoichiometric conditions ( $S=1.0$ )<sup>a,b</sup>

Catalyst metal composition	Feed stream A <sup>c</sup>			Feed stream B <sup>d</sup>	
	NO	CO	$C_3H_6$	NO	CO
LaCu	534	337	360	488	452
LaCu <sub>0.9</sub> Ru <sub>0.1</sub>	458	351	367	426	418
LaCu <sub>0.8</sub> Ru <sub>0.2</sub>	377	336	342	398	375
La <sub>0.9</sub> Sr <sub>0.1</sub> Cu	561	370	377	447	418
La <sub>0.9</sub> Sr <sub>0.1</sub> Cu <sub>0.9</sub> Ru <sub>0.1</sub>	448	358	366	413	398
La <sub>0.9</sub> Sr <sub>0.1</sub> Cu <sub>0.8</sub> Ru <sub>0.2</sub>	333	331	337	364	360
La <sub>0.8</sub> Sr <sub>0.2</sub> Cu	550	364	372	438	400
La <sub>0.8</sub> Sr <sub>0.2</sub> Cu <sub>0.9</sub> Ru <sub>0.1</sub>	445	350	356	384	370
La <sub>0.8</sub> Sr <sub>0.2</sub> Cu <sub>0.8</sub> Ru <sub>0.2</sub>	343	338	346	357	351

<sup>a</sup> With permission from Skoglundh et al. (1994).

<sup>c</sup> Feed stream A: NO/CO/ $C_3H_6$ /O<sub>2</sub>/N<sub>2</sub>.

$$^b S = \frac{2[O_2] + [NO]}{[CO] + 9[C_3H_6]}$$

<sup>d</sup> Feed stream B: NO/CO/N<sub>2</sub>.

and calcined at 1173 K, varied between 40 and 60 m<sup>2</sup>/g. After analyzing the metal content of more than 50 fragments of each type, it is concluded that the monoparticles exhibit the chemical composition of perovskites. The flakes, on the other hand, show compositions closer to La<sub>2</sub>CuO<sub>4</sub>. Figure 28 shows the evolution of CO, HC and exemplifies the drastic increase in NO reduction obtained when Sr and Ru are introduced in the perovskite lattice. This was confirmed for all the other samples as can be seen in table 28 for feed stream A. The authors have also studied the effect of modifying the composition of the feed stream from overall reducing to overall oxidizing. As expected, the more oxidizing the reacting mixture, the lower NO conversion is achieved under otherwise identical conditions.

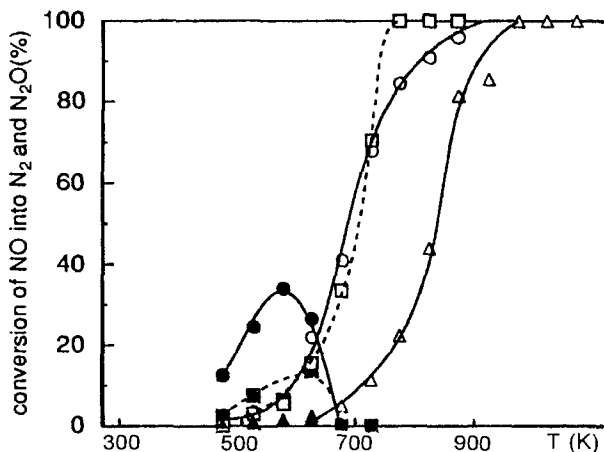


Fig. 29. Temperature dependence of the degree of conversion of NO to  $N_2$  and  $N_2O$  in CO-NO reaction over  $La_{0.8}Sr_{0.2}Co_{1-2y}Cu_yRu_yO_3$ ; circles, CCR0 ( $y=0$ ); squares, CCR5 ( $y=0.05$ ); triangles, CCR10 ( $y=0.10$ ). Open and solid symbols represent conversions to  $N_2$  and  $N_2O$ , respectively. With permission from Teraoka et al. (1996a).

Although the X-ray diffraction patterns clearly show the presence of the perovskite phase in all cases, it is still premature to ascribe a unique catalytic role to this phase. More studies are needed to try to elucidate the possible role of other species that are or might be present in all these formulations.

A year later, the Swedish groups associated with Teraoka and co-workers reported studies made on massive perovskites  $La_{0.8}Sr_{0.2}Co_{1-2y}Cu_yRu_yO_3$ . Teraoka et al. (1996a) reported data obtained for solids with  $0 \leq y \leq 0.2$  and used them to catalyze both CO oxidation and CO+NO reaction. They used Co instead of Al because perovskites containing the former element are generally more active than those containing aluminum.

Figure 29 shows the effect of partial substitution of Co by Cu/Ru over the NO+CO reaction. It is clearly seen that this substitution decreases the rate of reaction but sharply increases the selectivity to  $N_2$ . A similar decrease in oxidation activity was observed for CO+O<sub>2</sub> reaction. Since both reactions have been proposed to occur via an intrafacial mechanism, the negative effect of Co substitution by Cu/Ru may be explained by the decrease in weakly bonded oxygen observed by the authors during TPD experiments. As an additional comment Teraoka et al. (1996a) noted that the solubility of Ru in a K-type framework was very low, i.e. they synthesized  $(La_{0.82}Sr_{0.18})_2Co_{0.46}Cu_{0.51}Ru_{0.03}O_4$ .

In a short communication, Teraoka et al. (1996b) further emphasized the importance of Cu/Ru incorporation in the perovskite matrix. They concluded that for  $y=0.1$   $La_{0.8}Sr_{0.2}Co_{1-2y}Cu_yRu_yO_3$  has an activity similar to both  $La_{0.8}Sr_{0.2}CoO_3$  and 0.5% Pt/Al<sub>2</sub>O<sub>3</sub> for NO+CO reaction.

The state of the art of nitrogen oxides reduction over both massive and supported mixed oxides may be summarized as follows:

- Extensive data using CO as reducing agent have been reported during the 1970 and 1990s.
- Mixed oxides are not active for the CO+NO reaction under lean-burn conditions (excess oxygen). In this regard, they behave in the same way as commercial three-way catalysts (see ch. 184).
- Most researchers have shown convincing evidence of the fact that  $\text{N}_2\text{O}$  is an intermediate in the reduction of NO with CO.
- Opposing views exist regarding the catalytic role of oxygen vacancies in the oxide lattice (*vide ultra*).
- Recent studies using supported mixed oxides show encouraging results. Better characterizations of the solids are needed to ascertain the loci of catalytic activity on the surface of these complex systems.

The effect of  $\text{H}_2\text{O}$  and  $\text{SO}_2$  should be revisited on all these new formulations in order to evaluate their potential application under realistic conditions.

## 2.6. *Miscellaneous reactions*

A variety of reactions have been studied on mixed oxides beyond those described in the previous sections. They may be classified into two main groups: (i) one category is made up of those that are attractive in themselves due to their economical value, and (ii) the other one includes test reactions used to correlate catalytic behavior with the physico-chemical properties of the mixed oxides.

The dehydrogenation of methanol to methyl formate is an example of one important commercial reaction. Rodríguez-Ramos et al. (1991) used  $\text{LaM}_{1-x}\text{Cu}_x\text{O}_3$  ( $\text{M}=\text{Mn}, \text{Ti}$ ) to catalyze this reaction. Figure 30 shows the effect of temperature upon conversion, selectivity and yield when the reaction is carried out over  $\text{LaMn}_{0.5}\text{Cu}_{0.5}\text{O}_3$ . The yield averages 25% and was kept constant after two hours on stream. Note the decrease in selectivity at increasing temperature due to the decomposition of the formate.

Tables 29 and 30 show activity and selectivity data as well as dispersion of copper on both Mn- and Ti-based perovskites. The dispersion of Cu was calculated from CO adsorption at 77 K assuming a CO:Cu = 1:1 stoichiometry. A close look at the data reported in these tables indicate that neither the nature of the B cation nor the prereduction in  $\text{H}_2$  affect the catalytic behavior of the perovskites. Thus, the main conclusion from this work is that the active site is directly associated with the presence of surface copper species. To ascertain the oxidation state of Cu, Rodríguez-Ramos et al. (1991) resorted to the use of X-ray photoelectron spectroscopy. Figure 31 clearly shows that both the prereduced and used catalyst contain either  $\text{Cu}^+$  or  $\text{Cu}^0$  or both types of reduced species. This technique does not allow us to discriminate between  $\text{Cu}^0$  and  $\text{Cu}^+$  but a closer look at the Auger parameter corresponding to the  $\text{L}_{3}\text{M}_{4.5}\text{M}_{4.5}$  transition undoubtedly confirms that only  $\text{Cu}^0$  is present in used catalysts. Furthermore, quantitative XPS measurements indicate that some migration of copper from the subsurface to the topmost layer seems to occur on prereduced catalysts and/or used catalysts.

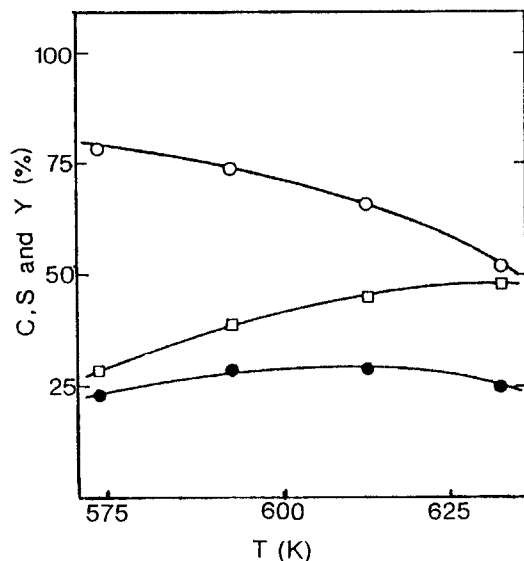


Fig. 30. Dependence of the reaction temperature on the stationary conversion and selectivity of the  $\text{LaMn}_{0.5}\text{Cu}_{0.5}\text{O}_3$  catalyst prereduced at 573 K for 12 h: squares, total conversion; open circles, selectivity to methyl formate; solid circles, yield. With permission from Rodríguez-Ramos et al. (1991).

Liang and Weng (1993) reacted toluene and oxygen over  $\text{La}_{1-x}\text{Sr}_x\text{NiO}_3$ . Quite surprisingly they found a high concentration of rearrangement and disproportionation products as shown in table 31. They studied the same reaction over  $\text{LaMO}_3$  ( $M = \text{Mn, Fe, Co or Ni}$ ) and found that no such reactions occurred. So the authors concluded that  $\text{NiO}$  and  $\text{La}_2\text{NiO}_4$  phases are responsible for the rearrangement and disproportionation reactions. When benzene was used instead of toluene, none of these products were observed. This seems to indicate that rearrangement starts at the methyl group.

Liu et al. (1996) have recently shown that  $\text{La}_{2-x}\text{Sr}_x\text{CuO}_{4 \pm \lambda}$  catalyze the hydroxylation of phenol in the liquid phase. This is one of the few cases in which perovskite oxides have been used to catalyze liquid-phase reactions. Table 32 compares the catalytic behavior of different solids. Among other things, it shows that the mechanical mixture of  $\text{CuO}$ ,  $\text{SrO}$  and  $\text{La}_2\text{O}_3$  is much less active for this reaction than the mixed oxide containing the same cations.

Another article concerning liquid-phase reactions catalyzed by perovskites is that by Sugunan and Meera (1995). They studied the reduction of ketones and oxidation of alcohol using  $\text{RBO}_3$  ( $R = \text{La, Pr or Sr, B = Cr, Mn, Co or Ni}$ ) perovskites. Their goal was, however, to correlate data from these test reactions with surface electron-donor properties of these oxides. The electron-donor properties were investigated by the adsorption of electron acceptors with different electron affinities such as *para*- and *m*-dinitrobenzene, benzoquinone, etc. They adsorbed these electron acceptors on both the mixed and the individual oxides. The results obtained are not conclusive to explain the catalytic behavior of the solids studied on the basis of this single property, as is often the case in many catalytic systems.

Table 29  
Dehydrogenation of methanol to methyl formate over  $\text{LaMn}_{1-x}\text{Cu}_x\text{O}_3$  oxides<sup>a</sup>

Sample	$T_{\text{red}}$ (K) <sup>b</sup>	$D$ (%) <sup>c</sup>	$A^d$ ( $\mu\text{mol/g Cu s}$ )	$\text{TOF} \cdot 10^3$ ( $\text{s}^{-1}$ ) <sup>e</sup>	$S_{\text{MF}}$ <sup>f</sup> (%)	$Y_{\text{MF}}$ <sup>g</sup> (%)
$\text{LaMn}_{0.4}\text{Cu}_{0.6}\text{O}_3$	473	—	13.63	—	63	25
	573	10.5	13.38	8.0	60	26
	723	—	15.30	—	56	25
$\text{LaMn}_{0.5}\text{Cu}_{0.5}\text{O}_3$	573	7.8	17.96	14.3	65	29
$\text{LaMn}_{0.6}\text{Cu}_{0.4}\text{O}_3$	573	13.0	22.54	11.0	63	27
$\text{LaMn}_{0.8}\text{Cu}_{0.2}\text{O}_3$	523	—	7.56	—	73	5
	573	23.0	—	—	—	—
	623	—	15.71	—	60	10
$\text{LaMnO}_3$	573	—	0.02	—	0	0

<sup>a</sup> With permission from Rodríguez-Ramos et al. (1991). Reaction temperature 513 K, time on stream: 5.5 hours.

<sup>b</sup> Reduction in hydrogen for 12 hours.

<sup>c</sup> Dispersion calculated assuming  $\text{CO}:\text{Cu} = 1:1$ .

<sup>d</sup> Reaction rate of methanol disappearance.

<sup>e</sup> Considering those active sites titrated by carbon monoxide chemisorption.

<sup>f</sup> Selectivity to methyl formate.

<sup>g</sup> Yield to methyl formate.

Table 30  
Dehydrogenation of methanol to methyl formate over  $\text{LaTi}_{1-x}\text{Cu}_x\text{O}_3$  oxides<sup>a</sup>

Sample	$T_{\text{red}}$ (K) <sup>b</sup>	$D$ (%)	Reaction conditions		$A$ ( $\mu\text{mol/g Cu s}$ )	$S_{\text{MF}}$ (%)	$Y_{\text{MF}}$ (%)
			$T$ (K)	$t$ (h)			
$\text{LaTi}_{0.2}\text{Cu}_{0.8}\text{O}_3$	473	—	473	1	8.37	77	25
	573	4.8	—	—	—	—	—
	623	—	473	1	8.38	73	25
			513	5.5	10.68	59	27
$\text{LaTi}_{0.7}\text{Cu}_{0.3}\text{O}_3$	573	20.0	—	—	—	—	—
	623	—	473	1	21.65	63	22
			513	5.5	27.64	51	23
$\text{LaTiO}_3$	573	—	473	1	0	0	0
			513	5.5	0.06	0	0

<sup>a</sup> With permission from Rodríguez-Ramos et al. (1991). See the footnotes in table 29.

Another case where the test reaction has been used to correlate catalytic behavior and physicochemical properties, is the interesting vanadium-containing system studied by Trikalitis and Pomonis (1995). They studied the transformation of isopropanol over  $\text{La}_{1-x}\text{Sr}_x\text{VO}_3$ . This solid contains vanadium in at least two oxidation states,  $\text{V}^{\text{III}}$  and  $\text{V}^{\text{IV}}$ . The systematic variation of the Sr content modifies the acid–base balance on the surface

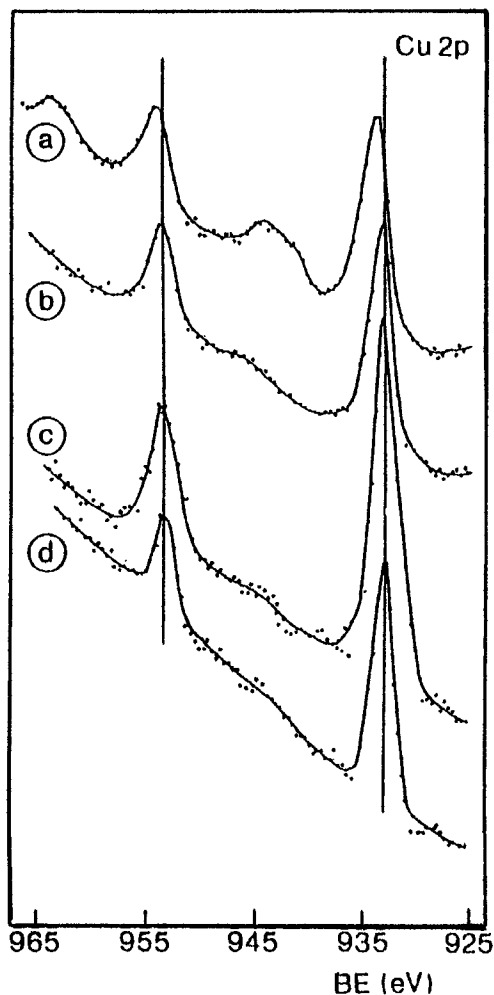


Fig. 31. Copper 2p core level electrons in  $\text{LaMn}_{0.4}\text{Cu}_{0.6}\text{O}_3$  catalyst subjected to various pretreatments; (a) in a flow of nitrogen at 523 K; (b) sample a after 6 h on-stream; (c) reduced in hydrogen at 573 K for 12 h; (d) sample c after 6 h on-stream. With permission from Rodríguez-Ramos et al. (1991).

of the perovskite. One sensitive method to follow this variation is the product distribution obtained from isopropanol. On acid sites, dehydration will occur while on other basic or metallic sites, dehydrogenation is the preferred pathway. The authors observed a good correlation between the acid–base distribution and acetone selectivity. In going from  $\text{LaVO}_3$  to  $\text{SrVO}_3$ , the acetone selectivity increases from 10 to 40%.

Ammonia oxidation was the test reaction chosen by Yu et al. (1992) to investigate connections between structure and catalytic properties in  $\text{La}_{1-x}\text{Sr}_x\text{NiO}_{3-\lambda}$  and  $\text{La}_{1-1.33x}\text{Th}_x\text{NiO}_{3-\lambda}$ . For  $x < 0.3$ , both types of solids only showed the reflections corresponding to the perovskite structure. At  $x \geq 0.3$ , several other phases appeared, i.e.  $\text{NiO}$ ,  $\text{La}_2\text{NiO}_4$  and  $\text{ThO}_2$ . As the Sr concentration increases, the number of oxygen



Table 31  
Percentages of products from toluene disproportionation over  $\text{La}_{1-x}\text{Sr}_x\text{NiO}_3$  ( $x > 0$ )<sup>a</sup>

Product (mol %)	Temperature (K)		
	493	553	613
<i>La<sub>0.7</sub>Sr<sub>0.3</sub>NiO<sub>3</sub></i>			
Ethylbenzene	36.36	32.02	30.51
<i>p</i> -Xylene	25.20	22.26	18.53
<i>m</i> -Xylene	22.34	28.43	33.52
<i>o</i> -Xylene	16.10	17.29	17.44
<i>La<sub>0.5</sub>Sr<sub>0.5</sub>NiO<sub>3</sub></i>			
Ethylbenzene	25.46	19.53	17.85
<i>p</i> -Xylene	23.53	25.18	25.93
<i>m</i> -Xylene	30.96	31.20	31.25
<i>o</i> -Xylene	21.05	24.09	24.97
<i>La<sub>0.3</sub>Sr<sub>0.7</sub>NiO<sub>3</sub></i>			
Ethylbenzene	32.08	25.79	17.09
<i>p</i> -Xylene	21.20	22.80	27.34
<i>m</i> -Xylene	29.54	27.01	33.21
<i>o</i> -Xylene	17.18	24.40	22.36
<i>SrNiO<sub>3</sub></i>			
Ethylbenzene	31.11	22.66	22.24
<i>p</i> -Xylene	22.17	26.33	24.51
<i>m</i> -Xylene	26.52	32.82	28.87
<i>o</i> -Xylene	20.20	19.19	24.38

<sup>a</sup> With permission from Liang and Weng (1993).

vacancies also rises and a decrease in  $\text{Ni}^{3+}$  concentration occurs due to the formation of  $\text{Ni}^{2+}$  to maintain the charge balance. The opposite effect occurs when  $\text{Th}^{4+}$  is inserted in the lattice. Cation vacancies are now generated which tend to stabilize the  $\text{Ni}^{3+}$  and therefore increase its concentration at higher Th substitutional levels. The authors claim that there is a correlation between NO selectivity and  $\text{Ni}^{3+}$  concentration. However, they correlate the  $\text{Ni}^{3+}$  concentration with NO selectivities between 80 and 100%, a too narrow span to justify their conclusion.

A novel system was introduced to the catalytic field by Matsuda et al. (1993). A solid of the general formula  $\text{ALaNb}_2\text{O}_7$  is made up of the layer compound  $\text{LaNb}_2\text{O}_7$  with double perovskite structure interleaved with A atoms. If the interlayer compound is water, they call the compound  $\text{HLa}_2\text{Nb}_2\text{O}_7$  to indicate the acidic character of this system. They report the results obtained when 1- and 2-butanol were reacted over this solid at temperatures between 453 and 623 K. The secondary alcohol was much more reactive, as expected for an acid catalyst. Consistent with this, no dehydrogenation product was formed when

Table 32  
Activity of different catalysts in phenol hydroxylation<sup>a</sup>

Catalyst	Phenol conversion (%)	Product conversion (%)			O <sub>2</sub> evolved (ml)
		CAT	HQ	BQ	
La <sub>2</sub> CuO <sub>4</sub>	50.9	29.6	20.3	1.0	12
La <sub>1.9</sub> Sr <sub>0.1</sub> CuO <sub>4</sub>	40.8	23.2	16.6	1.0	19
La <sub>1.3</sub> Sr <sub>0.7</sub> CuO <sub>4</sub>	10.5	6.4	4.1	0	85
LaSrCuO <sub>4</sub>	2.2	1.4	0.8	0	100
CuO	11.7	7.4	2.3	2.0	78
La <sub>2</sub> O <sub>3</sub>	0	0	0	0	0
SrO	0	0	0	0	0
CuO–La <sub>2</sub> O <sub>3</sub> –SrO	10.5	6.0	3.5	1.0	80

<sup>a</sup> With permission from Liu et al. (1996). CAT=catechol. HQ=hydroquinone, BQ=benzoquinone. Reaction time 2 hours; reaction temperature 343 K; reaction medium water; medium pH=7.0; phenol:H<sub>2</sub>O<sub>2</sub>:H<sub>2</sub>O (molar ratio) = 1:1:60; mass of catalyst used was 0.1 g.

2-butanol was the reactant. When 1-butanol was the reactant, butyraldehyde was formed at temperatures below 573 K and largely predominated at about 473 K.

## 2.7. Future trends

There is a fertile, largely unexplored world of novel catalytic applications of rare-earth-containing mixed oxides.

On the preparation side, the development of more economical synthesis methods apt for the commercial-scale production of high-surface-area solids is required. Methods such as atomic layer epitaxy offer a good route to obtain supported mixed oxides. However, this method in its present version is expensive and restricts the potential applications of these materials. The key factor in these methods is to achieve a good spreading of the active material on the support surface. New characterization procedures are needed to ascertain whether or not the supported nanoparticles of the desired compound are indeed formed.

The preparation of supported mixed oxides is also relevant in the processing of one type of membrane materials in which the active solid is deposited on top of catalytically inactive porous structure such as alumina. However, the synthesis of membranes entirely made of mixed oxides should not be overlooked, although this is a matter that needs further refinement to produce adequate materials.

The use of membrane reactors is still in its infancy. In recent years, these reactors using mixed-oxide catalysts have been used in the oxidative coupling and partial oxidation of methane to syngas. There is ample opportunity to extend these studies to achieve a much better understanding of these systems. Besides, there are other applications such as the selective oxidation of both hydrocarbons and oxygenates that deserve attention. It has

been already said in sect. 2 that there is a lack of data concerning this field even using conventional reactors.

The use of supported mixed oxides in both catalytic combustion and  $\text{NO}_x$  reduction are challenging applications. In the case of high-temperature catalytic combustion there is an unsatisfied need to obtain solids able to maintain high combustion activity during extended operation, i.e., high-surface-area structurally stable solids. Another hot subject that deserves exploration is the use of washcoated highly dispersed mixed oxides for the selective reduction of  $\text{NO}_x$  with CO and hydrocarbons. These studies should be conducted in the presence of both  $\text{SO}_2$  and  $\text{H}_2\text{O}$  to evaluate the potential practical application of these catalysts.

### 3. Other catalytic applications

The other main applications of mixed oxides supported by their catalytic properties may be classified as photocatalysis, electrocatalysis and gas sensors. We will give a brief introduction to these three topics and several references for the reader who may wish to know more about these applications.

#### 3.1. Photocatalysis

It has been known for many years now that several perovskites are active photocatalysts in reactions such as  $\text{H}_2$  and CO oxidation, and decomposition of  $\text{H}_2\text{O}$  and  $\text{N}_2\text{O}$  (see the review by Kutty and Avudaitai 1992).

Van Damme and Hall (1981) tried three perovskites in the oxidations of  $\text{H}_2$  and CO and found that  $\text{SrTiO}_3$  and  $\text{BaTiO}_3$  were good catalysts for the latter reactions while  $\text{LaCoO}_3$  was totally inactive for both reactions. This conclusion is indicative of a more general observation, i.e., the rare-earth-containing mixed oxides  $\text{RBO}_3$  are not particularly suitable for photocatalytic applications.

Very recently, however, a perovskite-related structure has been shown to exhibit fairly good photocatalytic activity. Domen et al. (1996) prepared and characterized a layered perovskite series with the general formula  $\text{K}_{1-x}\text{La}_x\text{Ca}_{2-x}\text{Nb}_3\text{O}_{10}$ . They also retrieved previous data obtained with layered perovskite-type niobates  $\text{AV}_{n-1}\text{Nb}_n\text{O}_{3n+1}$  ( $\text{A}=\text{K}, \text{Rb}$  or  $\text{Cs}$ ;  $\text{B}=\text{La}, \text{Ca}, \text{Pb}$  and others;  $n=2$  or  $3$ ) which were found to possess high photocatalytic activity for  $\text{H}_2$  evolution from aqueous methanol solutions.

Domen et al. (1996) prepared silica-pillared  $\text{K}_{1-x}\text{La}_x\text{Ca}_{2-x}\text{Nb}_3\text{O}_{10}$  using as a precursor an alkylammonium-exchanged niobate which was stirred in tetraethylorthosilicate (TEOS) at 353 K for 72 h. This treatment was repeated twice. The filtered solid was calcined at 773–973 K for 4 h in air. The solids obtained with varying La content were tried for  $\text{H}_2$  evolution from a 10 vol% aqueous alcohol solution using a high-pressure Hg lamp (450 W). Table 33 shows the results obtained for solids containing variable La concentrations. Note the beneficial effect of La incorporation.

Table 33

c-axis length, surface area and photocatalytic activity for decomposition of water of layered perovskite compounds with variable interlayer cation density:  $K_{1-x}La_xCa_{2-x}Nb_3O_{10}$ <sup>a</sup>

Precursor	c-axis length (nm)		BET surface area (m <sup>2</sup> g <sup>-1</sup> )	Rate of H <sub>2</sub> evolution of silica pillared niobates (μmol h <sup>-1</sup> ) <sup>b</sup>
	Before calcination	After calcination		
(C <sub>8</sub> H <sub>17</sub> NH <sub>3</sub> )Ca <sub>2</sub> Nb <sub>3</sub> O <sub>10</sub>	3.26	2.93	200	10 800
(C <sub>8</sub> H <sub>17</sub> NH <sub>3</sub> ) <sub>0.75</sub> La <sub>0.25</sub> Ca <sub>1.75</sub> Nb <sub>3</sub> O <sub>10</sub>	3.31	2.95	320	11 200
(C <sub>8</sub> H <sub>17</sub> NH <sub>3</sub> ) <sub>0.50</sub> La <sub>0.50</sub> Ca <sub>1.50</sub> Nb <sub>3</sub> O <sub>10</sub>	3.29	2.95	110	14 700
(C <sub>8</sub> H <sub>17</sub> NH <sub>3</sub> ) <sub>0.25</sub> La <sub>0.75</sub> Ca <sub>1.25</sub> Nb <sub>3</sub> O <sub>10</sub>	3.33	2.76	48	7900

<sup>a</sup> With permission from Domen et al. (1996).

<sup>b</sup> H<sub>2</sub> evolution from a 10 vol.% aqueous alcohol solution using a high-pressure Hg lamp (450 W).

### 3.2. Electrocatalysis

A whole chapter would be required to review the use of perovskites in the field of electrochemistry as solid electrolytes, electrodes and electrochemical reactors in general. In this section we will limit our incursion in this field to give the reader a brief outlook of recent applications of rare-earth-containing perovskites in electrocatalyzed reactions, and their use as catalyst for bifunctional air electrodes.

Eng and Stoukides (1991) reviewed the many attempts made in the past to convert methane into useful raw materials by using solid oxide electrolytes. Chiang et al. (1993) further explored the solid-electrolyte-aided direct coupling of methane. They chose for their studies a two-electrode one-chamber cell, a design easy to apply to existing catalytic processes since it does not require reactants to be separated. Their electrolytes were SrCe<sub>0.95</sub>Yb<sub>0.05</sub>O<sub>3-α</sub> (SCY) and yttria-stabilized zirconia (YSZ). Figure 32 shows how the rate enhancement ratio ( $\rho$ ) was affected by the cell voltage when the two electrolytes were used. Using SCY at 1023 K  $\rho$  reaches a value of 8. The selectivity to C<sub>2</sub> hydrocarbons is 100% when the current density (cell voltage) is low enough, but at higher levels CO<sub>2</sub> is produced and the C<sub>2</sub> selectivity drops to ~65%. The main limitation for the practical application of this type of processes is the low current density and concomitant low productivity.

An interesting example of the application of perovskites as electrodes was published by Müller et al. (1994). La<sub>0.6</sub>Ca<sub>0.4</sub>CoO<sub>3</sub> has excellent catalytic properties for O<sub>2</sub> reduction and evolution as shown by Shimizu et al. (1990). In order to obtain a more durable electrode material, Müller et al. (1994) used graphitized carbon (70 m<sup>2</sup>/g) as support of the perovskite catalysts. They described in detail the technique used to prepare the electrode which was assayed using an experimental setup adequate for the intended application of this electrode, namely Zn/air batteries. Their main advance over previous formulations was to achieve longer durability of the electrode with some reduction in current density when compared to the previous work of Shimizu et al. (1990). The authors also suggest routes to improve the overall performance of this attractive system.

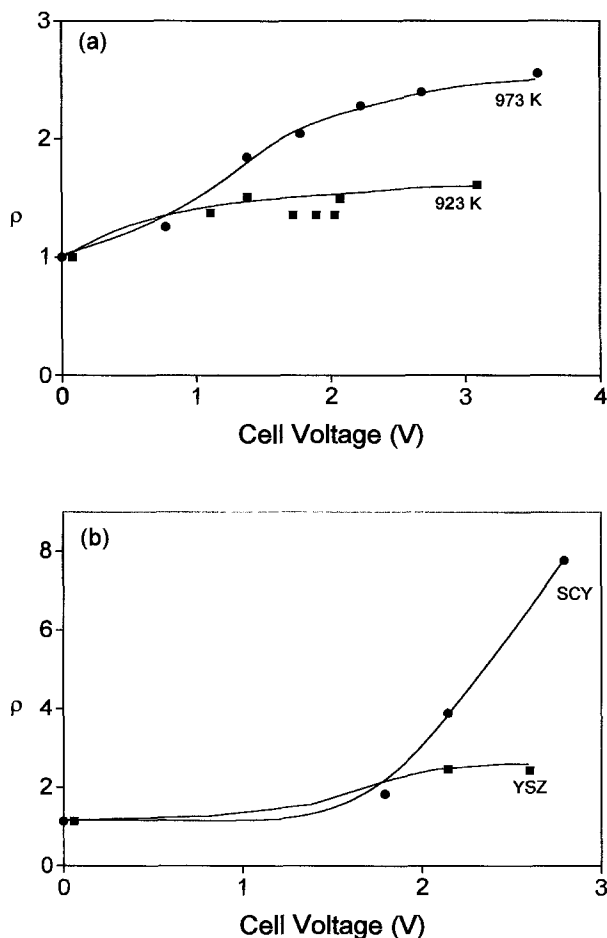


Fig. 32. Cell voltage vs rate enhancement ratio ( $\rho = r/r_0$ ): (a) effect of temperature with SCY electrolyte; (b) effect of electrolyte at 1023 K. With permission from Chiang et al. (1993).

### 3.3. Gas sensors

There are several types of gas sensors in current use. Semiconductor-type sensors are sensitive to either a single gas or group of gases that modify electrical properties of the solids. A classical example is ZnO whose n-type conductivity changes proportionally to  $P_{O_2}^{-1/4}$ , although this effect only becomes measurable at high temperatures due to diffusion limitations.

It is then natural to think that certain perovskite oxides sensitive to the partial pressure of oxygen may be used in the same way as single oxides. One typical example is  $\text{La}_{1-x}\text{Sr}_x\text{CoO}_{3-\delta}$ . These compounds can release oxygen, and as a result  $\text{Co}^{4+}$  is reduced to  $\text{Co}^{3+}$  with an increase in resistivity. This effect is accentuated as the Sr fraction ( $x$ )

increases. Using this property, perovskite-containing sensors have been developed for alcohols.  $\text{LaNiO}_{3-\delta}$  also behaves in the same way and has also been used as alcohol sensor. Kudo (1990) gave a detailed mechanistic explanation of how these sensors work and provided operating data of these devices. In the same review, other sensors with perovskite structure are described. They are used to detect oxygen in combustion exhaust gases and several combustible gas detectors such as CO and  $\text{H}_2$ . In brief, this is another wide field whose coverage goes beyond the scope of this review.

## Acknowledgments

To all our coworkers at INCAPE who have contributed to the field of perovskite catalysis. To CONICET and Universidad Nacional del Litoral for their continuing support to our research. To Elsa Grimaldi for her help in the edition of the English manuscript.

## References

- Agarwal, D.D., and H.S. Goswami, 1994, *React. Kinet. Catal. Lett.* **53**(2), 441.
- Alcock, C.B., J.J. Carberry, R. Doshi and N. Gunasekaran, 1993, *J. Catal.* **143**, 533.
- Arai, H., T. Yamada, K. Eguchi and T. Seiyama, 1986, *Appl. Catal.* **26**, 265.
- Arai, H., K. Eguchi and M. Machida, 1989, Cation substituted layered hexaaluminates for a high-temperature combustion catalyst, in: *Proc. MRS Int. Meeting on Advanced Materials*, Vol. 2, p. 243.
- Arai, H., K. Eguchi, M. Machida and T. Shiomitsu, 1991, *Catal. Sci. Technol.* **1**, 195.
- Arakawa, T., S. Tsuchiya and J. Shiokawa, 1982, *J. Catal.* **74**, 317.
- Baiker, A., P.E. Marti, P. Keusch, E. Fritsch and A. Reller, 1994, *J. Catal.* **146**, 268.
- Balachandran, U., J.T. Dusek, R.L. Mieville, R.B. Poeppel, M.S. Kleefisch, S. Pei, T.P. Kobylinski, C.A. Udovich and A.C. Bose, 1995, *Appl. Catal. A* **133**, 19.
- Baran, J.E., 1990, *Catal. Today* **8**, 133.
- Barrault, J., C. Grosset, M. Dion, M. Ganne and M. Tournoux, 1992, *Applied Catal. A* **88**, 197.
- Beguín, B., E. Garbowski and M. Primet, 1991, *Appl. Catal.* **75**, 119.
- Brinen, J.S., and A. Malera, 1972, *J. Phys. Chem.* **76**, 2525.
- Brousard, J.A., and L.E. Wade, 1986, *Prepr. Am. Chem. Soc. Div. Fuel Chem.* **31**, 75.
- Brown Bourzutschky, J.A., N. Homs and A.T. Bell, 1990, *J. Catal.* **124**, 52.
- Campbell, K.D., 1992, *Catal. Today* **13**, 245.
- Carreiro, L., Y.T. Quian, R. Kershaw, K. Dwight and A. Wold, 1985, *Mater. Res. Bull.* **20**, 619.
- Chan, K.S., J. Ma, S. Jaenicke, G.K. Chuah and J.Y. Lee, 1994, *Appl. Catal. A* **107**, 201.
- Chandler, C.D., C. Roger and M.J. Hampden-Smith, 1993, *Chem. Rev.* **93**, 1205.
- Chiang, P.H., D. Eng and M. Stoukides, 1993, *J. Catal.* **139**, 683.
- Chien, M.W., I.M. Pearson and K. Nobe, 1975, *Ind. Eng. Chem. Prod. Res. Dev.* **14**, 131.
- Choudhary, V.R., B.S. Uphade and A.A. Belhekar, 1996a, *J. Catal.* **163**, 312.
- Choudhary, V.R., B.S. Uphade, S.G. Pataskar and G.A. Thite, 1996b, *Chem. Commun.*, p. 1021.
- Crespin, M., and W.K. Hall, 1981, *J. Catal.* **69**, 359.
- Crespin, M., L. Gatineau, J. Fripiat, H. Nijs, J. Marcos and E.A. Lombardo, 1983a, *Nouv. J. Chim.* **7**, 477.
- Crespin, M., P. Levitz and L. Gatineau, 1983b, *J. Chem. Soc. Faraday Trans.* **79**, 1181.
- de Collongue, B., E. Garbowski and M. Primet, 1991, *J. Chem. Soc. Faraday Trans.* **87**(15), 2493.
- de Leitenburg, C., A. Trovarelli, J. Llorca, F. Cavani and G. Bini, 1996, *Appl. Catal. A* **139**, 161.
- Domen, K., Y. Ebina, S. Ikeda, A. Tanaka, J.N. Kondo and K. Maruya, 1996, *Catal. Today* **28**, 167.
- Eng, D., and M. Stoukides, 1991, *Catal. Rev. Sci. Eng.* **33**, 375.
- Fierro, J.L.G., 1990, *Catal. Today* **8**, 153.
- Fierro, J.L.G., 1992, *Catal. Rev. Sci. Eng.* **34**, 321.
- Fierro, J.L.G., and L.G. Tejuca, 1984, *J. Catal.* **87**, 126.

- Fierro, J.L.G., J.M.D. Tascón and L.G. Tejuca, 1984, *J. Catal.* **89**, 209.
- Fierro, J.L.G., J.M.D. Tascón and L.G. Tejuca, 1985, *J. Catal.* **93**, 83.
- Fierro, J.L.G., M.A. Peña and L.G. Tejuca, 1988, *J. Mater. Sci.* **23**, 1018.
- Foley, H.C., S.J. DeCanio, K.D. Tau, K.J. Chao, J.H. Onuferko, C. Dybowski and B.C. Gates, 1983, *J. Am. Chem. Soc.* **105**, 3074.
- Forni, L., C. Oliva, F.P. Vatti, M.A. Kandala, A.M. Ezerets and A.V. Vishniakov, 1996, *Appl. Catal. B* **7**, 269.
- Fujii, H., N. Mizuno and M. Misono, 1987, *Chem. Lett.*, p. 2147.
- Galasso, F.S., 1969, *Structure, Properties and Preparation of Perovskite-Type Compounds* (Pergamon Press, Oxford).
- Gallagher, P.K., D.W. Johnson Jr and F. Schrey, 1974, *Mater. Res. Bull.* **9**, 1345.
- Goldschmidt, V.M., 1926, *Skr. Nor. Vidensk. Akad. Oslo*, No. 8.
- Goodenough, J.B., and J.M. Longo, 1970, in: *Landolt-Börnstein New Series*, Vol. 4, Part A, eds K.H. Hellwege and A.M. Hellwege (Springer, Berlin) p. 126.
- Gordes, P., N. Christiansen, E.J. Jensen and J. Villadsen, 1995, *J. Mater. Sci.* **30**, 1053.
- Gunasekaran, N., S. Rajadurai, J.J. Carberry, N. Bakshi and C.B. Alcock, 1994, *Solid State Ionics* **73**, 289.
- Gunasekaran, N., S. Rajadurai and J.J. Carberry, 1995, *Catal. Lett.* **35**, 373.
- Gunasekaran, N., S. Saddawi and J.J. Carberry, 1996, *J. Catal.* **159**, 107.
- Gur, T.M., A. Belzner and R.A. Huggins, 1992, *J. Membr. Sci.* **75**, 151.
- Gysling, H.J., J.R. Monnier and G. Apai, 1987, *J. Catal.* **103**, 407.
- Halasz, I., A. Brenner, M. Shelef and K.Y.S. Ng, 1990, *J. Catal.* **126**, 109.
- Hansen, S., J. Otamini, J.O. Bonvin and A. Andersson, 1988, *Nature* **334**, 143.
- Ichimura, K., Y. Inoue and I. Yasumori, 1980, *Bull. Chem. Soc. Jpn.* **53**, 3044.
- Ichimura, K., Y. Inoue and I. Yasumori, 1981a, *Bull. Chem. Soc. Jpn.* **54**, 1787.
- Ichimura, K., Y. Inoue, I. Kojima, E. Miyazaki and I. Yasumori, 1981b, in: *New Horizons in Catalysis*, *Studies in Surf. Sci. Catal. Series*, Vol. 7, part B, eds T. Seiyama and K. Tanabe (Kodansha-Elsevier, Tokyo) p. 1281.
- Ichimura, K., Y. Inoue and I. Yasumori, 1992, *Catal. Rev. Sci. Eng.* **34**(4), 301.
- Isupova, L.A., V.A. Sadykov, L.P. Solovyova, M.P. Andrianova, V.P. Ivanov, G.N. Kryukova, V.N. Kolomiichuk, E.G. Avvakumov, I.A. Pauli, O.V. Andryushkova, V.A. Poluboyarov, A.Ya. Rozovskii and V.F. Tretyakov, 1995, *Preparation of Catalysts VI, Scientific Bases for the Preparation of Heterogeneous Catalysts, Studies in Surf. Sci. Catal. Series*, Vol. 91 (Elsevier, Amsterdam) p. 637.
- Jiang, A.R., Y. Peng, Q.W. Zhong, P.Y. Gao, H.Q. Yuan and J.F. Deng, 1989, *Catal. Lett.* **3**, 235.
- Johnson Jr, D.W., P.K. Gallagher, F. Schrey and W.W. Rhodes, 1976, *Am. Ceram. Soc. Bull.* **55**, 520.
- Johnson Jr, D.W., P.K. Gallagher, G.K. Wertheim and E.M. Vogel, 1977, *J. Catal.* **48**, 87.
- Jung, H.J., J.T. Lim, S.H. Lee, Y.R. Kim and J.G. Choi, 1996, *J. Phys. Chem.* **100**, 10243.
- Kamegashira, N., Y. Miyazaki and H. Yamamoto, 1984, *Mater. Chem. Phys.* **11**, 187.
- Kato, A., H. Yamashita and S. Matsuda, 1988, *Successful Design of Catalysts, Studies in Surf. Sci. Catal. Series*, Vol. 44, ed. T. Inui (Elsevier, Amsterdam) p. 25.
- Keller, G.E., and M.M. Bhasin, 1982, *J. Catal.* **73**, 9.
- Kirchnerova, J., D. Klvana, J. Vaillancourt and J. Chaouki, 1993, *Catal. Lett.* **21**, 77.
- Klier, K., V. Chatikavanij, R.G. German and G.W. Simmons, 1982, *J. Catal.* **74**, 343.
- Kremenić, G., J.M.L. Nieto, J.M.D. Tascón and L.G. Tejuca, 1985, *J. Chem. Soc. Faraday Trans. I* **81**, 939.
- Kudo, T., 1990, *Catal. Today* **8**(2), 263.
- Kulkarni, G.U., C.N.R. Rao and M.W. Roberts, 1995, *J. Phys. Chem.* **99**, 3310.
- Kutty, T.R.N., and M. Avudaitai, 1992, *Catal. Rev. Sci. Eng.* **34**, 373.
- Ladavos, A.K., and P.J. Pomonis, 1992, *Appl. Catal. B* **1**, 101.
- Ladavos, A.K., and P.J. Pomonis, 1993, *Catal. Today* **17**, 181.
- Lago, R., G. Bini, M.A. Peña and J.L.G. Fierro, 1997, *J. Catal.* **167**, 198.
- Lauder, A., 1975, U.S. Patent 3,897,367. E.I. du Pont Petroleum Laboratory Report PLMRG-75.
- Levitz, P., M. Crespin and L. Gatinéau, 1983, *J. Chem. Soc. Faraday Trans.* **79**, 1195.
- Liang, J.J., and H.S. Weng, 1993, *J. Catal.* **140**, 302.
- Libby, W.F., 1971, *Science* **171**, 499.
- Lin, Y., A.T.S. Wee, K.L. Tan, K.G. Neoh and W.K. Teo, 1993, *Inorg. Chem.* **32**, 5522.

- Lindstedt, A., D. Strömberg and M. Abul Milh, 1994, *Appl. Catal. A* **116**, 109.
- Lintz, H.G., and K. Wittstock, 1996, *Catal. Today* **29**, 457.
- Liu, Ch., Z. Zhao, X. Yang, X. Ye and Y. Wu, 1996, *Chem. Commun.*, p. 1019.
- Lombardo, E.A., K. Tanaka and I. Toyoshima, 1983, *J. Catal.* **80**, 340.
- Machida, M., K. Eguchi and H. Arai, 1990, *J. Catal.* **123**(2), 477.
- Madhok, K.L., 1986, *React. Kinet. Catal. Lett.* **30**, 185.
- Marcos, J., R.H. Buitrago and E.A. Lombardo, 1987, *J. Catal.* **105**, 95.
- Marti, P.E., and A. Baiker, 1994, *Catal. Lett.* **26**, 71.
- Marti, P.E., M. Maciejewski and A. Baiker, 1995, *Preparation of Catalysts VI, Scientific Bases for the Preparation of Heterogeneous Catalysts, Studies in Surf. Sci. Catal. Series, Vol. 91* (Elsevier, Amsterdam) p. 617.
- Matsuda, S., A. Kato, M. Mizumoto and H. Yamashita, 1984, in: *Proc. 8th Int. Catalysis Congress, Berlin, Vol. IV*, p. 879.
- Matsuda, T., T. Fujita and N. Miyamae, 1993, *Catal. Today* **16**, 455.
- Mazanec, T.J., T.L. Cable and J.G. Frye Jr, 1992, *Solid State Ionics* **53**, 111.
- McCarty, J.G., and H. Wise, 1990, *Catal. Today* **8**, 231.
- Merzhanov, A.G., and I.P. Borovinskaya, 1972, *Dokl. Acad. Nauk* **204**, 366.
- Milt, V.G., R. Spretz, M.A. Ulla and E.A. Lombardo, 1995, *J. Mater. Sci.* **14**, 428.
- Milt, V.G., R. Spretz, M.A. Ulla, E.A. Lombardo and J.L.G. Fierro, 1996, *Catal. Lett.* **42**, 57.
- Miró, E.E., Z. Kalenik, J. Santamaria and E.E. Wolf, 1990, *Catal. Today* **6**, 511.
- Mizuno, N., 1990, *Catal. Today* **8**, 221.
- Mizuno, N., H. Fujii and M. Misono, 1986, *Chem. Lett.*, p. 1333.
- Mizuno, N., H. Fujii, H. Igarashi and M. Misono, 1992a, *J. Am. Chem. Soc.* **114**(18), 7151.
- Mizuno, N., M. Tanaka and M. Misono, 1992b, *J. Chem. Soc. Faraday Trans.* **88**, 91.
- Moreau, S., J. Choisnet and F. Beguin, 1996, *J. Phys. Chem. Solids* **57**(6-8), 1049.
- Müller, S., J. Striebel and O. Haas, 1994, *Electrochim. Acta* **39**(11/12), 1661.
- Nakamura, T., G. Petzow and L.J. Gauckler, 1979, *Mater. Res. Bull.* **14**, 649.
- Nakamura, T., M. Misono and Y. Yoneda, 1982, *Bull. Chem. Soc. Jpn.* **55**, 394.
- Nitadori, T., T. Ichiki and M. Misono, 1988, *Bull. Chem. Soc. Jpn.* **61**, 621.
- Noller, H., and H. Vinek, 1980, *J. Mol. Catal.* **51**, 285.
- Nozaki, T., O. Yamazaki, K. Omata and K. Fujimoto, 1992, *Chem. Eng. Sci.* **47**, 2945.
- Nudel, J.N., B.S. Umansky, R.O. Piagentini and E.A. Lombardo, 1984, *J. Catal.* **89**, 362.
- Nudel, J.N., B.S. Umansky and E.A. Lombardo, 1986, *Appl. Catal.* **26**, 339.
- Nudel, J.N., B.S. Umansky and E.A. Lombardo, 1987, *Appl. Catal.* **31**, 275.
- Öcal, M., R. Oukaci and G. Marcelin, 1994, *Ind. Eng. Chem. Res.* **33**, 2930.
- Otamiri, J.C., and S.L.T. Andersson, 1991, *Appl. Catal.* **73**, 267.
- Otamiri, J.C., J.E. Crow and S.L.T. Andersson, 1992, *J. Catal.* **138**, 562.
- Petunchi, J.O., and E.A. Lombardo, 1990, *Catal. Today* **8**(2), 201.
- Petunchi, J.O., M.A. Ulla, J.A. Marcos and E.A. Lombardo, 1981, *J. Catal.* **70**, 356.
- Pollert, E., D. Sedmidubsky, K. Knizek, Z. Jirak, P. Vasek and I. Janecek, 1992, *Physica C* **197**, 371.
- Prasad, R., L.A. Kennedy and E. Ruckenstein, 1984, *Catal. Rev. Sci. Eng.* **26**(1), 1.
- Quinlan, M.A., H. Wise and J.G. McCarty, 1989, *Basic Research on Natural Gas Combustion Phenomena – Catalytic Combustion, GRI-89/0141* (SRI International, Menlo Park, CA).
- Radha, R., and C.S. Swamy, 1985, *Surf. Technol.* **24**, 157.
- Ramesh, S., and M. Hegde, 1994, *Physica C* **230**, 135.
- Ramesh, S., and M. Hegde, 1996, *J. Phys. Chem.* **100**, 8443.
- Rao, C.N.R., J. Gopalakrishnan and J.K. Vidyasagar, 1984, *Indian J. Chem. Sect. A* **23A**, 265.
- Rehnspringer, J.L., P. Poix, A. Kaddouri, D. Andriamasinoro and A. Kiennemann, 1991, *Catal. Lett.* **10**, 111.
- Rodríguez-Ramos, I., A. Guerrero-Ruiz, M.L. Rojas and J.L.G. Fierro, 1991, *Appl. Catal.* **68**, 217.
- Rojas, M.L., J.L.G. Fierro, L.G. Tejuca and A.T. Bell, 1990, *J. Catal.* **124**, 41.
- Rostrup-Nielsen, J.R., 1984, *Catalysis Science and Technology, Vol. 5* (Springer, Berlin), p. 1.
- Saracco, G., G. Scibilia, A. Iannibello and G. Baldi, 1996, *Appl. Catal. B* **8**, 229.



- Schaper, H., E.B.M. Doesburg and L.L. Van Reijen, 1983, *Appl. Catal.* **7**, 211.
- Schaper, H., D.J. Amez, E.B.M. Doesburg and L.L. Van Reijen, 1984, *Appl. Catal.* **9**, 129.
- Seyama, T., 1992, *Catal. Rev. Sci. Eng.* **34**(4), 281.
- Seyama, T., N. Yamazoe and K. Eguchi, 1985, *Ind. Eng. Chem. Prod. Res. Dev.* **24**, 19.
- Shimizu, T., 1980, *Chem. Lett.*, p. 1.
- Shimizu, T., 1986, *Appl. Catal.* **28**, 81.
- Shimizu, T., 1992, *Catal. Rev. Sci. Eng.* **34**(4), 355.
- Shimizu, Y., K. Uemura, H. Matsuda, N. Miura and N. Yamazoe, 1990, *J. Electrochem. Soc.* **137**, 3430.
- Siriwardane, R.V., and A. Shamsi, 1990, *Appl. Catal.* **60**, 119.
- Skaribas, S.P., P.J. Pomonis and A.T. Skoudos, 1991, *J. Mater. Chem.* **1**, 781.
- Skoglundh, M., L. Löwendahl, K. Jansson, L. Dahl and M. Nygren, 1994, *Appl. Catal. B* **3**, 259.
- Slagtern, Å., and U. Olsby, 1994, *Appl. Catal. A* **110**, 99.
- Sri Rahayu, W., L. Monceaux, B. Taouk and P. Courtine, 1995, *Stud. Surf. Sci. Catal.* **96**, 563.
- Sugunan, S., and V. Meera, 1995, *Indian J. Chem.* **34A**, 984.
- Swamy, C.S., and J. Christopher, 1992, *Catal. Rev. Sci. Eng.* **34**, 409.
- Tagawa, T., and H. Imai, 1988, *J. Chem. Soc. Faraday Trans. I* **84**, 923.
- Tascón, J.M.D., and L.G. Tejuca, 1980, *React. Kinet. Catal. Lett.* **15**, 185.
- Tascón, J.M.D., J.L.G. Fierro and L.G. Tejuca, 1985, *J. Chem. Soc. Faraday Trans. I* **81**, 2399.
- Tascón, J.M.D., A.M.O. Oliván, L.G. Tejuca and A.T. Bell, 1986a, *J. Phys. Chem.* **90**, 791.
- Tascón, J.M.D., A.M.O. Oliván and L.G. Tejuca, 1986b, *J. Chem. Technol. Biotechnol.* **36**, 136.
- Tejuca, L.G., J.L.G. Fierro and J.M.D. Tascón, 1989, *Adv. Catal.* **36**, 237.
- Teraoka, Y., H.M. Zhang, S. Furukawa and N. Yamazoe, 1985, *Chem. Lett.*, p. 1743.
- Teraoka, Y., H. Fukuda and S. Kagawa, 1990, *Chem. Lett.*, p. 1.
- Teraoka, Y., T. Harada, H. Furukawa and S. Kagawa, 1993, in: *New Frontiers in Catalysis, Proc. 10th Int. Congr. on Catalysis, Budapest, Hungary, Part C*, p. 2649.
- Teraoka, Y., H. Nii, S. Kagawa, K. Jansson and M. Nygren, 1996a, *J. Mat. Chem.* **6**(1), 97.
- Teraoka, Y., H. Nii, S. Kagawa, K. Jansson and M. Nygren, 1996b, *Chem. Lett.*, p. 323.
- Thomas, J.M., 1988, *Angew. Chem. Int. Ed. Engl.* **27**, 1673.
- Tofield, B.C., and W.R. Scott, 1974, *J. Solid State Chem.* **10**, 183.
- Trikalitis, P.N., and P.J. Pomonis, 1995, *Appl. Catal. A* **131**, 309.
- Tsai, C.Y., A.G. Dixon, W.R. Moser and Y.H. Ha, 2000, *AIChE J.*, in press.
- Ulla, M.A., R.A. Migone, J.O. Petunchi and E.A. Lombardo, 1987, *J. Catal.* **105**, 107.
- van Damme, H., and W.K. Hall, 1981, *J. Catal.* **69**, 371.
- van Grieken, R., J.L. Peña, A. Lucas, G. Calleja, M.L. Rojas and J.L.G. Fierro, 1991, *Catal. Lett.* **8**, 335.
- Viswanathan, B., 1992, *Catal. Rev. Sci. Eng.* **34**(4), 337.
- Vogel, E.M., and D.W. Johnson, 1975, *Termochim. Acta* **12**, 49.
- Vogel, E.M., D.W. Johnson Jr and P.K. Gallagher, 1977, *J. Am. Ceram. Soc.* **60**, 31.
- Voorhoeve, R.J.H., J.P. Remeika, P.E. Freeland and B.T. Mathias, 1972, *Science* **177**, 353.
- Voorhoeve, R.J.H., J.P. Remeika, L.E. Trimble, A.S. Cooper, F.J. Disalvo and P.K. Gallagher, 1975, *J. Solid State Chem.* **14**, 395.
- Voorhoeve, R.J.H., J.P. Remeika and L.E. Trimble, 1976, *Ann. New York Acad. Sci.* **272**, 3.
- Vrieland, E.G., 1974, *J. Catal.* **32**, 415.
- Wachowski, L., S. Zielinski and A. Burewicz, 1981, *Acta Chim. Acad. Sci. Hung.* **106**, 217.
- Wang, W., and Y.S. Lin, 1995, *J. Membr. Sci.* **103**, 219.
- Wang, Y., H. Yasuda, K. Inumaru and M. Misono, 1995, *Bull. Chem. Soc. Jpn.* **68**, 1226.
- Watson, P.R., and G.A. Somorjai, 1982, *J. Catal.* **74**, 282.
- Wells, A.F., 1984, *Structural Inorganic Chemistry*, 5th Ed. (Clarendon Press, Oxford).
- Yamamura, M., N. Tsuzuki, H. Okado, T. Wakatsuki and K. Otsuka, 1994, *Appl. Catal. A* **115**, 269.
- Yamazoe, N., and Y. Teraoka, 1990, *Catal. Today* **8**, 175.
- Yasuda, H., N. Mizuno and M. Misono, 1990, *J. Chem. Soc. Chem. Commun.*, p. 1094.
- Yasuda, H., T. Nitadori, N. Mizuno and M. Misono, 1993, *Bull. Chem. Soc. Jpn.* **66**, 3492.
- Yi, G., T. Hayakawa, A.G. Andersen, K. Suzuki, S. Hamakawa, A.P.E. York, M. Shimizu and K. Takehira, 1996, *Catal. Lett.* **38**, 189.
- Yu, Z., L. Gao, S. Yuan and Y. Wu, 1992, *J. Chem. Soc. Faraday Trans.* **88**(21), 3245.

- Zhang, H.M., Y. Teraoka and N. Yamazoe, 1988, *Appl. Catal.* **41**, 137.
- Zhang, H.M., Y. Shimizu, Y. Teraoka, N. Miura and N. Yamazoe, 1990, *J. Catal.* **121**, 432.
- Zhang, Z., and M. Baerns, 1992, *J. Catal.* **135**, 317.
- Zhao, Z., X. Yang and Y. Wu, 1996, *Appl. Catal. B* **8**, 281.
- Zhong, Z., Q. Yan, X. Fu and J. Gong, 1996, *Chem. Commun.*, p. 1745.
- Zwinkels, M.F.M., S.G. Järås, P.G. Menon and T.A. Griffin, 1993, *Catal. Rev. Sci. Eng.* **35**(3), 319.

## Chapter 184

### CERIA-CONTAINING THREE-WAY CATALYSTS

Jan KAŠPAR, Mauro GRAZIANI and Paolo FORNASIERO

*Dipartimento di Scienze Chimiche, Università di Trieste, Via L. Giorgieri, 1,  
 34127 Trieste, Italy*

#### Contents

List of symbols	159	2.3.1.1. CO oxidation	203
List of abbreviations	160	2.3.1.2. NO reduction	212
1. Introduction	160	2.3.2. Water–gas shift reaction	221
1.1. Historical background	161	2.3.3. Steam reforming	226
1.2. Automobile emission regulations	163	2.4. Supported-metal–CeO <sub>2</sub> interactions	229
1.3. The three-way catalyst (TWC)	165	2.4.1. Effects of high-temperature	
1.4. Operation of catalytic converters	167	oxidising atmosphere	230
2. Role of CeO <sub>2</sub> in TWC technology	169	2.4.2. Effects of high-temperature	
2.1. Oxygen storage and release capacity	169	reducing atmosphere	232
2.1.1. Temperature-programmed		3. Advanced TWC technology	235
reduction of CeO <sub>2</sub> using H <sub>2</sub>		3.1. CeO <sub>2</sub> –ZrO <sub>2</sub> mixed oxides	235
(H <sub>2</sub> -TPR) and CO (CO-TPR) as		3.1.1. Synthesis and phase diagram	237
reductants	174	3.1.2. Thermal stability	241
2.1.2. Temperature-programmed		3.1.3. Redox properties: textural and	
reduction of CeO <sub>2</sub> /Al <sub>2</sub> O <sub>3</sub> using		structural dependence	246
H <sub>2</sub> (H <sub>2</sub> -TPR) and CO (CO-TPR)		3.1.4. Catalytic reactions	252
as reductants	188	3.2. Other systems	257
2.1.3. Temperature-programmed		4. Conclusions	258
reduction and OSC of NM/CeO <sub>2</sub>		4.1. Summary of state of art and future	
and NM/CeO <sub>2</sub> /Al <sub>2</sub> O <sub>3</sub>	190	perspectives	258
2.2. Stabilisation of metal dispersion	201	Acknowledgements	259
2.3. Catalytic activity	203	References	259
2.3.1. CO/NO/hydrocarbon reactions	203		

#### List of symbols

<i>c</i>	cubic	$\lambda$	equivalence ratio, ratio of the total
<i>m</i>	monoclinic		oxygen in the air–fuel mixtures burning
<i>t</i> , <i>t</i> <sup>*</sup> , <i>t</i> <sup>′</sup> , <i>t</i> <sup>′′</sup>	tetragonal CeO <sub>2</sub> –ZrO <sub>2</sub> phases		in the engine to the total oxygen required
$\alpha$ -phase,	non stoichiometric CeO <sub>2–x</sub> phases		for the complete combustion of the fuel
$\sigma$ -phase		$\sigma$	electrical conductivity

## List of abbreviations

Å	Ångström	mm	millimeter
A/F	air-to-fuel ratio	mol	mole
BE	binding energy	MT91,	US federal emission regulation
BET	Brunauer–Emmett–Teller, surface area according to BET method	MT 94	
CCC	close-coupled converter	NM	noble metal
c.d.	coordinated defect	nm	nanometer
cm	centimeter	NMR	nuclear magnetic resonance
EGR	exhaust gas recirculation	OBC	oxygen buffering capacity
EU	European Union	OSC	oxygen storage capacity
EUDC	extra-urban driving cycle	<i>p</i>	pressure
EXAFS	extended X-ray absorption fine structure	Pa	pascal
eV	electronvolt	ppm	parts per million (10 <sup>-6</sup> )
FTP	federal test procedure	rt	room temperature
FTIR	Fourier transform infrared	s	second
g	gram	SEM	scanning electron microscopy
GHSV	gas hourly space velocity	SMSI	strong metal support interaction
h	hour	TEM	transmission electron microscopy
HC	hydrocarbons	TLEV	California transitory low emission vehicle
HREM	high resolution electron microscopy	TPD	temperature programmed desorption
HSA	high surface area	TPR	temperature programmed reduction
HTR	high-temperature reduction	TWC	three way catalyst
Hz	hertz	ULEV	California ultra low emission vehicle
K	Kelvin	US	United States
km	kilometer	W/F	weight to flow ratio (time factor)
J	joule	WGS	water gas shift reaction
LEV	California low emission vehicle	wt.	weight
LSA	low surface area	XAS	X-ray absorption spectroscopy
m	meter	XANES	X-ray absorption near edge spectroscopy
min	minute	XRD	X-ray diffraction
ml	milliliter	XPS	X-ray photoelectron spectroscopy

## 1. Introduction

The present chapter is concerned with the main aspects of the role of CeO<sub>2</sub> and CeO<sub>2</sub>-containing materials in three-way catalysis. The aim is to give a critical evaluation of selected aspects related to the role of CeO<sub>2</sub>-based compounds in the exhaust post-treatments rather than an exhaustive review of available literature on automotive pollution control, for which we refer the reader to excellent reviews which have appeared recently (Taylor 1984, 1993, Shelef and Graham 1994, Amiridis et al. 1996, Kummer 1986, McCabe and Kisenyi 1995). For aspects concerning the relationships among automobiles,

pollution and health, we recommend a recent book (Degobert 1995). Purposely, references to technical papers or patent literature have been avoided where possible. The chapter is organised as follows: first the fundamental aspects of the three-way catalysts (TWCs) are described, then the different promotional effects of  $\text{CeO}_2$  are described. The relative importance of these roles is discussed in sect. 4.1. An entire section is devoted to  $\text{CeO}_2$ – $\text{ZrO}_2$  mixed oxides due to their extensive use since 1994, in advanced TWCs. Finally, some conclusion and future perspectives are given in sect. 4.

### 1.1. *Historical background*

The first concern regarding automobile emissions presumably was a German law issued on February 3rd, 1910. It stated that “the vehicles must be safe and built so as to preclude any nuisance for the public, by smoke or odour” (Degobert 1995). (K.E. Ditsch, 1987, *Abgasuntersuchungen von in Verkehr befindlichen Fahrzeugen, Gegenwart und Zukunft*, Bundesrepublik Deutschland, VDI Berichte, No. 639, pp. 75–85.) Since then, the introduction in the USA in 1966 of the Clean Air Act and its subsequent amendments in 1968, 1970, 1971 etc., represented a major development which focused the attention of automotive manufacturers on the problem of limitation of emissions of the pollutants contained in automotive exhausts. As shown in table 1, the automotive exhaust is a

Table 1  
Typical composition of automotive exhausts (Taylor 1993)

Product	Vol. %	Product	Vol. %
$\text{CO}_2$	13.5	HC	750 ppm <sup>a</sup>
$\text{H}_2\text{O}$	12.5	$\text{NO}_x$	1050 ppm
$\text{O}_2$	0.51	CO	0.68
$\text{N}_2$	~72	$\text{H}_2$	0.23

<sup>a</sup> Based on  $\text{C}_3$ .

complex mixture of products with variable proportions, which are conventionally grouped into three major categories:  $\text{NO}_x$ , CO and hydrocarbons (HC). It is worth noting that while  $\text{NO}_x$  can be transformed by a reduction process to the harmless  $\text{N}_2$ , removal of the latter two pollutants requires a simultaneous oxidation to  $\text{CO}_2$ . There are a number of reasons which makes the removal of these pollutants a difficult task. These range from chemical problems such as an extreme variability of reaction temperature, starting from ambient temperature upon the vehicle start-up and reaching temperatures up to 1273 K, which may occur when driving on a motorway; to strong and continuous oscillations in the exhaust composition; to engineering problems such as the need for a high resistance of the catalysts to mechanical and thermal shocks.

The variability of the exhaust emissions with the air/fuel ratio (A/F) is illustrated in fig. 1, where A/F is expressed as the sometimes-used equivalence ratio ( $\lambda$ ). The  $\lambda$  value is defined as the ratio of the total oxygen in the air–fuel mixtures burning in the engine

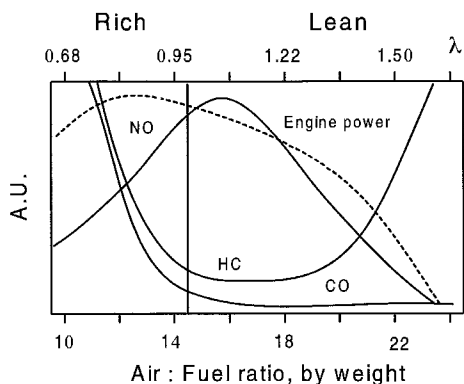


Fig. 1. The effect of the air/fuel (A/F) ratio (w/w) on automotive gasoline engine emissions. (Church et al. 1989.)

to the amount of oxygen required for the complete combustion of the fuel. It can also be conveniently measured as a ratio of the actual A/F to the stoichiometric A/F. An A/F of 14.6 corresponds to an equivalence ratio of  $\lambda = 1$ , which is also referred to as the stoichiometric point. The predominant nitrogen-containing species is NO, which is formed when the combustion temperature in the engine exceeds 1900 K. The production of NO<sub>x</sub> reaches a maximum slightly above the stoichiometric point. Here maximum combustion temperatures are reached in the engine. Increasing  $\lambda$  further results in a decrease of the engine temperature, thereby lowering the NO<sub>x</sub> emissions. The high production rate of CO and unburned/partially burned HC which is observed under fuel-rich conditions ( $\lambda < 1$ ) is associated with a low availability of oxygen. Accordingly, the CO formation decreases at high equivalence ratios. The increase of HC production under lean-burn conditions ( $\lambda \gg 1$ ) is associated with poor combustion in the missed gas-fire region ( $\lambda > 1.15$ ).

The transformation of the undesirable components of the exhausts into harmless gases may occur through a variety of chemical reactions, of which those reported in table 2 are generally considered to contribute to the removal of exhaust pollutants (Barbier and Duprez 1994, Taylor 1984, Maillet et al. 1996).

Historically, four generations of de-pollution catalysts/converters can be distinguished (Heck and Farrauto 1995). The first generation was developed to meet the limits imposed for 1976 by the Clean Air Act. The first car to meet these American emission standards

Table 2  
Reactions occurring on automotive exhaust catalysts, which may contribute to exhaust removal

Description	Reaction(s)	Description	Reaction(s)
Oxidation	$2\text{CO} + \text{O}_2 \rightarrow 2\text{CO}_2$ $\text{HC} + \text{O}_2 \rightarrow \text{CO}_2 + \text{H}_2\text{O}^a$	Water-gas shift	$\text{CO} + \text{H}_2\text{O} \rightarrow \text{CO}_2 + \text{H}_2$
Reduction/ Three-way	$2\text{CO} + 2\text{NO} \rightarrow 2\text{CO}_2 + \text{N}_2$ $\text{HC} + \text{NO} \rightarrow \text{CO}_2 + \text{H}_2\text{O} + \text{N}_2^a$ $2\text{H}_2 + 2\text{NO} \rightarrow 2\text{H}_2\text{O} + \text{N}_2$	Steam reforming	$\text{HC} + \text{H}_2\text{O} \rightarrow \text{CO}_2 + \text{H}_2^a$

<sup>a</sup> Unbalanced reaction.

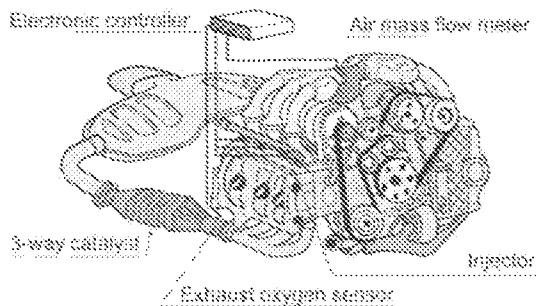


Fig. 2. A modern TWC/engine/oxygen sensor ( $\lambda$ ) control loop for engine exhaust control. (Courtesy of Mr. Crevatin, University of Trieste.)

was a 1975 Chrysler Avenger (Church et al. 1989). At that time, a simple oxidation catalyst could meet the less stringent law restrictions in comparison to today's limits (compare sect. 1.2). Therefore the first generation converter typically contained Pd/Pt supported on  $\text{Al}_2\text{O}_3$  beads, which was provided with an additional air supply. This arrangement was sufficient to meet the initial standards.  $\text{NO}_x$  control was generally achieved by using EGR (Exhaust Gas Recirculation). By recirculating part of the exhaust gases back into the combustion chamber, the combustion temperature was lowered, resulting in reduced  $\text{NO}_x$  emissions. More stringent exhaust emissions standards, including tighter  $\text{NO}_x$  control, had been set in the USA by 1977–1981, which led to an implementation of the control of the exhaust emissions by developing the so-called dual-way catalyst (second generation) and, subsequently, three-way catalyst (TWC, third and fourth generation) (Heck and Farrauto 1995). The former converter usually consisted of a primary bed containing a Rh/Pt-based catalyst for  $\text{NO}_x$  removal, followed by a secondary bed containing an oxidation catalyst equipped with an additional air supply to promote the oxidation reactions (Summers and Monroe 1981). By tuning the engine to run close to stoichiometric conditions, reduction of  $\text{NO}_x$  to  $\text{N}_2$  could be achieved in the first bed, and oxidation of CO/HC to  $\text{CO}_2$  and  $\text{H}_2\text{O}$  was carried out in the second bed (Summers and Monroe 1981). However, such devices could not withstand the progressively tightening demand for exhaust control in the USA in the early 1980s, mainly due to the imperfect A/F control resulting from the use of carburetors. Further,  $\text{NO}_x$  can be easily reduced to  $\text{NH}_3$  under rich conditions, which can then be back-converted over the oxidation catalyst, making  $\text{NO}_x$  removal inefficient. The advent of oxygen sensors (the so-called  $\lambda$  sensor) based on zirconia type ceramics, led to the development of the modern TWC arrangement (fig. 2). In driving conditions, A/F is kept close to the stoichiometric point by a fuel injection device regulated by an electronic feedback system, which uses a signal from the  $\lambda$  sensor. Such integrated exhaust control was first introduced by Volvo in 1979 in commercial vehicles sold in California (Shelef and Graham 1994). Since 1982, these systems have been adopted on most passenger cars in the USA (Taylor 1993).

### 1.2. *Automobile emission regulations*

In the past, exhaust emission standards (limits) have been set in most industrialised countries for passenger cars, light-duty trucks and heavy-duty trucks (gasoline and diesel

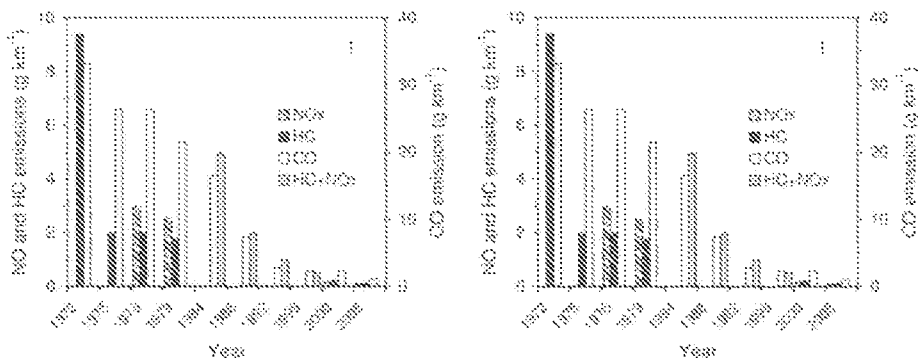


Fig. 3. Evolution of the limits for passenger cars (gasoline-fuelled engine) in (1) Europe and (2) the USA in the period 1972–2005.

engines). For the gasoline engines, nowadays, the requirements are to reduce emissions by about or even more than 95% in comparison to the typical amount of pollutants emitted by late-1960s automobiles with uncontrolled emissions (fig. 3).

As an example, under the European limits the uncontrolled CO emissions in the late sixties were around  $60 \text{ g CO km}^{-1}$ , which should drop, according to an EU proposal, down  $1.0 \text{ g km}^{-1}$  by the year 2005. This is equivalent to a 98% reduction of the CO emissions. Similarly, a very restrictive situation is foreseen for HC emissions. Both lowering of the limits down to  $0.10 \text{ g km}^{-1}$  and the inclusion of the cold start in the vehicle test are important targets which need to be fulfilled. The latter task is a particularly tough one: as shown in fig. 4 (below), depending on the location of the converter, there is a 1–2 minute delay in the conversion of the pollutant which is associated with the initial warming of the catalysts until the so-called light-off temperature is reached. The light-off temperature is conventionally defined as the temperature corresponding to 50% conversion of the pollutants and it corresponds to a switch from kinetically controlled temperature region to temperatures where the conversion is controlled by pore diffusion and/or bulk mass transfer (Heck and Farrauto 1995).

Before the catalyst reaches the light-off temperature, i.e. operating conditions, unconverted exhaust is emitted from the vehicle. This is shown in fig. 4, which illustrates that within the initial 60 s of the federal test procedure (FTP) cycle, the Californian ULEV limits are exceeded in the engine-out emissions. Typically an under-floor converter does not reach the light-off temperature until after 120–180 s. Because of the high efficiency of TWCs, the impact of these uncontrolled emissions represents about 50% or more of the total HC emitted in the whole test procedure. Currently, abatement of the exhaust even in the initial period, immediately after the start-up of the vehicle, represents a major target for the research in three-way catalysis. Generally, the adopted approach consists of the application of the so-called close-coupled converter (CCC). In this arrangement, in addition to the under-floor main converter, a secondary converter is mounted directly on the exhaust pipe, minimising the warm-up of the catalysts. Typically, this results in a decrease of the time lags between the start-up of the engine and the TWC warmed-up



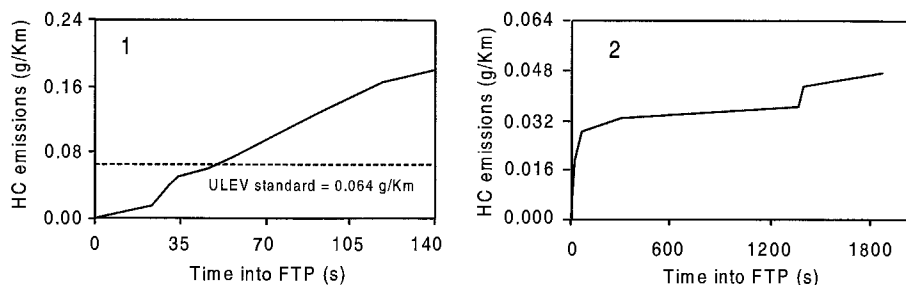


Fig. 4. Cumulative hydrocarbon emissions measured during the federal test procedure (FTP cycle) on a US 1995 car: (1) engine-out emissions; (2) tailpipe emissions with close-coupled catalyst. (Heck and Farrauto 1997.)

operations down to 20–40 s. Bearing in mind the conversion efficiency of the warmed-up TWCs (fig. 5, sect. 1.3), the benefits of such modification are high. With this arrangement tailpipe emissions can withstand even the tight ULEV requirements, due to the fact that the initial period, where the HC emissions are highest, is minimised (fig. 4). However, the CCCs are now exposed to extremely high temperatures, which can reach or even exceed 1273 K under high load/high speed vehicle operations. Consequently, there has been a strong demand for increased thermal stability of TWCs, leading to the so-called advanced TWC technology, which is the subject of sect. 3.

### 1.3. *The three-way catalyst (TWC)*

The TWC represents the state of the art in the catalytic control of exhausts from gasoline engines. It has been extensively employed in the catalytic control of exhausts since 1982. The name is derived from the ability to simultaneously remove all of the three categories of pollutants, i.e.  $\text{NO}_x$ , CO and HC, which are present in the exhausts. Of these,  $\text{NO}_x$  removal/reduction is obviously most efficient under net reducing conditions, in a deficiency of  $\text{O}_2$ . In contrast, both CO and HC are best converted under net oxidising conditions, in excess oxygen. As above noted,  $\text{NO}_x$  removal by using dual-bed catalysts technology is inefficient. However, if one could maintain the A/F ratio close to stoichiometry, then in principle all three pollutants could be converted simultaneously. This is illustrated in fig. 5. There are some features which need comment: as expected, under rich, i.e. net reducing, conditions, the efficiency  $\text{NO}_x$  removal is at a maximum. However, even for relatively slightly oxidising conditions this efficiency drops abruptly. Conversely, in the case of CO and HC conversions, there is a sharp decrease of the removal efficiency as the A/F ratio moves from oxidising to reducing conditions. The vertical lines in fig. 5 delimit the so-called operating A/F window. Within this window all the conversions meet the required levels, nowadays over 95%.

From a technical point of view, the A/F ratio is kept constant in TWC systems by using the closed-loop emission control system depicted in fig. 2, which uses a feedback signal from the  $\lambda$  sensor located upstream of the converter. As discussed in sect. 2.1, the fuelling rate is adjusted according to this feedback, resulting in rapid A/F fluctuation

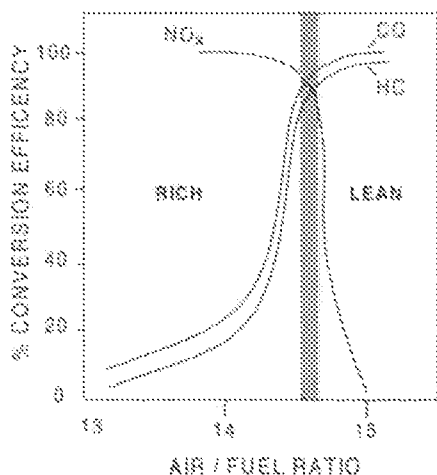


Fig. 5. Dependence of the simultaneous conversions of HC, CO and  $\text{NO}_x$  on the A/F ratio in a three-way catalyst.

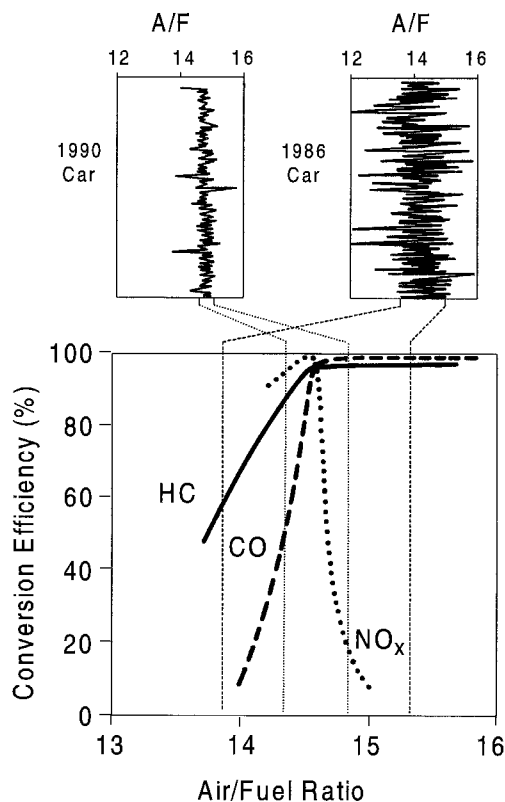


Fig. 6. Relationship between A/F ratio control and  $\text{NO}_x$ , CO and HC conversion efficiencies in 1986 and 1990 vehicles (McCabe and Kisenyi 1995). (Courtesy of Dr. McCabe, Ford Research Laboratory, Dearborn, USA.)

around the stoichiometric point. This results in deviations both on the rich and lean sides. In the early 1980s such systems had intrinsic limitations under driving conditions due to delays in the response of the electromechanical carburetors then employed, slow  $\lambda$ -sensor response etc., which did not allow constant A/F to be maintained in the exhaust. In the 1990s, as the legislation limits became tighter, the efficiency of air-to-fuel control has been significantly improved, as central and multi-point fuel injection substituted carburetors. Nevertheless, there are still significant deviations from the stoichiometric A/F even for 1990s-generation cars (fig. 6).

The impact of such fluctuations on the conversion efficiency is indeed critical. To improve the control of these fluctuations, the OSC component was added, leading to the development of the first TWC catalysts in the early 1980s. Typically such catalysts contained Rh and Pt in 1:5 ratio supported on high-surface-area alumina and a low loading (1–5 wt%) of  $\text{CeO}_2$ . In addition, other base metal oxides<sup>1</sup> such as BaO and  $\text{La}_2\text{O}_3$  were generally added to increase the thermal stability of  $\text{Al}_2\text{O}_3$ . The choice of the noble

<sup>1</sup> The term base metal oxide is widely used in the TWC field and in this chapter to indicate a non-noble-metal oxide promoter; NM indicates a noble metal.

metal (NM) was motivated respectively by the high activity of Rh for CO oxidation, its high selectivity to promote NO reduction to  $N_2$ . Pt was chosen as a good oxidation catalyst to promote HC removal (Taylor 1984, 1993, Taylor and Schlatter 1980).

The selectivity of the TWC is a critical issue. In fact, formation of  $NH_3$  under rich conditions is easily detected on non-selective catalysts (Taylor 1984, Taylor and Schlatter 1980, Otto and Yao 1980). Rh and Ru would be the metals of choice since  $NH_3$  formation is minimised on these catalysts, however the latter shows a high volatility in the oxide form which precludes its use in autocatalysis. Use of Pd was dismissed in the 1980s because of the high  $SO_x$  level in gasoline which greatly inhibits the oxidation activity of this metal (Heck and Farrauto 1995).

The increase of average travelling mileage and operating speed by the late 1980s demanded high thermal stability compared to the early-1980s cars. Particularly the application of TWCs in Europe, where use of catalytic converters became mandatory by 1992/93, was the one requiring high thermal stability, due to the high-speed extra-urban part of the European testing cycle (EUDC cycle). High  $CeO_2$  loaded TWCs were therefore introduced onto the market. These catalysts, which are still employed on some cars, were developed to meet the market requirements of more efficient oxygen storage and higher temperature resistance compared to low-loaded  $CeO_2$  TWCs. The increase of the  $CeO_2$  content was intended to increase the effectiveness of the OSC and hence to provide a large A/F operating window.

Since 1994, advanced TWCs have been introduced onto the market. These catalysts, which were developed to meet the recent EU and US standards (1996/97–1994), employ  $CeO_2$ - $ZrO_2$  mixed oxides as thermally stable OSC systems. In addition, Pd-containing or Pd-only technology has been introduced, owing to the lower  $SO_x$  level in today's gasoline (Heck and Farrauto 1997) (sect. 3).

At present, the research is focussed on the development of year-2005 technology, which as above stated, requires catalysts having remarkably high thermal stability to allow their use in CCCs. Claims have been reported in the literature that suitable systems meeting the EU 2005/Californian ULEV requirements were developed (Heck and Farrauto 1997).

#### 1.4. *Operation of catalytic converters*

As illustrated in fig. 2, the pollution abatement system that is being used in gasoline-fuelled engines is a complex one, consisting of several parts. From a chemical point of view, the catalytic converter is the place where the chemistry occurs. Monolith-type catalysts are now employed in the automotive industry (fig. 7).

Either a metal or a ceramic monolith (honeycomb) is used, the volume of which is approximately equal to the engine cylinder displacement. For a detailed description we refer the reader to the book by Degobert (1995). Due to the relatively high cost, metallic monoliths are typically employed on high-performance automobiles, their main advantage being a fast heating rate due to the small thermal coefficient and mechanical strength. The ceramic monoliths are made of cordierite ( $2MgO \cdot 2Al_2O_3 \cdot 5SiO_2$ ), which is a cheap and readily available material. Its melting point is above 1700 K, which confers sufficient

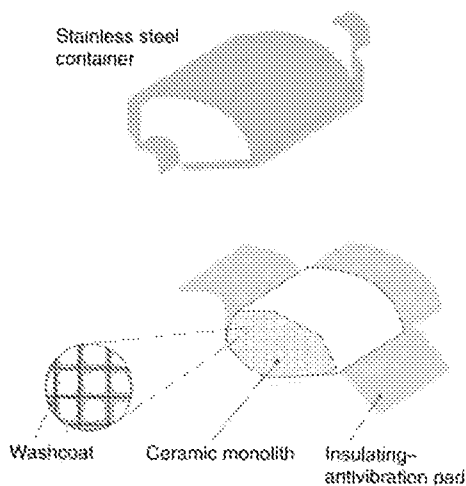


Fig. 7. A typical catalytic exhaust converter. (Degobert 1995.)

thermal resistance under normal engine running conditions. It has also a good thermal shock resistance. Typically a density of 46–62 cells per  $\text{cm}^2$  with a wall thickness of 0.10–0.30 mm is employed. This allows the exhaust gases to pass through the honeycomb with a small pressure drop, keeping a good contact between the active phase and the gas phase.

The active phase (washcoat) is a mixture of noble metals (Rh, Pt and Pd, active catalyst), promoters ( $\text{CeO}_2$  and derived materials, Ni is used in US as sulphur scavenger), surface area stabilisers ( $\text{La}_2\text{O}_3$ , BaO) and high-surface-area  $\text{Al}_2\text{O}_3$ . Of course, proprietary additives, which improve the activity of the TWCs, are also employed. The active phase is supported (washcoated) from slurry onto the monoliths by dipping. Typically it represents about 5–20 wt% of the overall weight of the monolith. The washcoat consists of about 0.15–2.5 wt% of NM and 15–50 wt% of the  $\text{CeO}_2$ -based OSC component, the remaining being  $\text{Al}_2\text{O}_3$  and some proprietary stabilisers. Different strategies may be used for segregation of some components: Rh may be preferentially located on a less reactive carrier such as  $\text{ZrO}_2$ , preventing interactions with  $\text{CeO}_2$ ; the so-called double layer technology protects part of the washcoat from deposition of P- and S-containing poisons, etc. The gas hourly space velocity, i.e. volume of gases passing through a unitary volume of the catalysts, is about 30 000 to 100 000  $\text{h}^{-1}$ , according to the cruising conditions. The operating temperature of the converter is from ambient to over 1273 K. Below the light-off temperature no significant conversion is obtained, while above this temperature conversion higher than 95% is required.

In summary, the operating conditions in the catalytic converters present an extreme variability of the reaction conditions, high conversion of the pollutants being required over a very wide interval of temperatures, space velocities and fluctuating inlet concentrations (compare fig. 8 below).

## 2. Role of CeO<sub>2</sub> in TWC technology

As briefly introduced in sect. 1.3, CeO<sub>2</sub> constitutes the most important promoter of the TWCs. Over the past decade, this application has stimulated extensive research, reported in both the open and the patent literature. For example, a CAS search disclosed that in 1980, when close-loop technology first appeared on the market, 84 scientific articles and 44 patents appeared. In comparison, 10 years later 432 and 357 were respectively reported.

It is an ambitious task to define the role of CeO<sub>2</sub> in three-way catalysis since multiple effects have been attributed to this promoter (Trovarelli 1996). Ceria has been suggested to:

- promote the noble metal dispersion;
- increase the thermal stability of the Al<sub>2</sub>O<sub>3</sub> support;
- promote the water gas shift (WGS) and steam reforming reactions;
- favour catalytic activity at the interfacial metal–support sites;
- promote CO removal through oxidation employing a lattice oxygen;
- store and release oxygen under lean and rich conditions, respectively.

There have been strong discussions on which is the most important promoting effect, and arguments favouring the WGS reaction or OSC have been reported. Whatever is the critical role of CeO<sub>2</sub>, as recently pointed out by Robert McCabe, there is certainly a general agreement that “CeO<sub>2</sub> is good!”<sup>2</sup>.

A perusal of the above listed effects suggests, however, that there is a common point in all of the chemical effects, which is related to the ability of the NM/CeO<sub>2</sub> system to promote the rate of migration/exchange of oxygen species in the reaction. As will be shown in this chapter, we believe that this effect of CeO<sub>2</sub> is a crucial aspect of the CeO<sub>2</sub>-based systems as TWC promoters. The most important of the above listed roles are outlined in the following sections.

### 2.1. *Oxygen storage and release capacity*

The ability of base metals to improve pollutant conversion under exhaust conditions fluctuating between rich (net reducing) and lean (net oxidising) conditions was first pointed out by Gandhi et al. (1976). They suggested that release and adsorption of oxygen, i.e. “oxygen storage”, by base metal oxides such as CeO<sub>2</sub> or NiO under rich and lean conditions, respectively, may be responsible for the improved conversions in cycled feed-streams.

In fact, the electronic control system of the fuel feed, which is back-fed from the  $\lambda$  oxygen sensor, shows a quick oscillating response to A/F fluctuations with a frequency of about 1–4 Hz.

Later investigation showed, however, that such periodic oscillations around the stoichiometric point are generally encountered under constant speed driving. Under

---

<sup>2</sup> Robert McCabe, Plenary Lecture, Third International Conference on f Elements, Paris, France, September 1997.

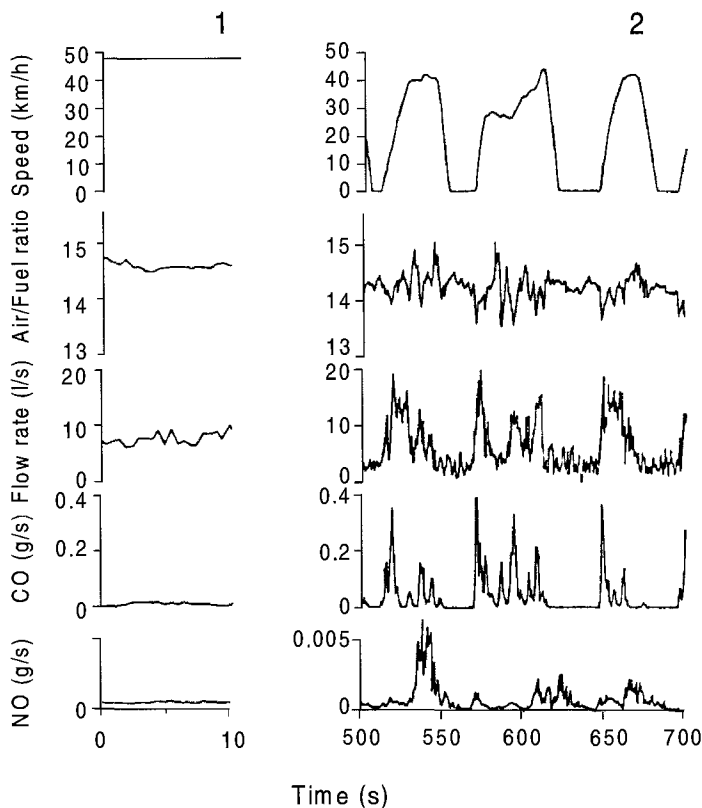
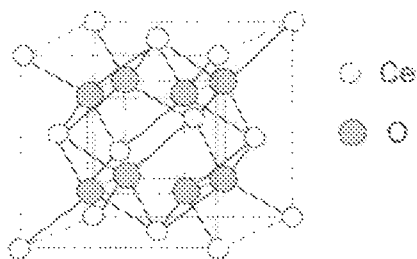


Fig. 8. Comparison of A/F ratio control, exhaust flow-rate and NO-CO emissions in a Buick 1982 model during (1) constant speed and (2) FTP (federal test procedure) variable speed driving. (Hertz and Shinouskis 1985.)

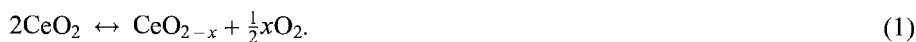
variable vehicle speed, consisting of acceleration-deceleration cycles such as occur in urban driving, the excursion both to the rich and lean side may be quite significant, with a time lag which can be considerable longer than 1 s (Hertz and Shinouskis 1985). This is exemplified in fig. 8 for a Buick 1982 model equipped with an electronic control system. Care should be taken in considering such pictures, since they are obviously concerned with the particular control of A/F employed. However, some qualitative findings reported by Hertz and Shinouskis (1985) appear of general validity: the high load during the acceleration part of cycles leads to high emission flow-rates and prevalently rich A/F excursions. In addition, a Fourier transform power spectrum analysis of the excursion from the stoichiometric point during the warmed part of the FTP cycle, showed peaks at frequency of 0.1-0.2 Hz indicating that the large amplitude deviations in fig. 8 have characteristic periods of several seconds. Several factors may be responsible for such deviation of the A/F ratio, such as, for example, fuel-cut upon releasing the accelerator,

Fig. 9. Fluorite structure of  $\text{CeO}_2$ .

deposition of the fuel during the injection as a film on the pipe wall, which creates transient deviations from correct stoichiometry, etc. (Eyzat 1995).

Even though air-to-fuel control has dramatically improved since these first devices (McCabe and Kisenyi 1995), significant oscillation and deviations from the ideal stoichiometric A/F may occur in driving conditions even with current car technology. This suggests that the general findings reported by Hertz and Shinouskis (1985) should still be taken into account.

The importance of these findings can be understood when the features of the oxygen storage behaviour provided by the  $\text{Ce}^{4+}/\text{Ce}^{3+}$  redox couple are considered. Generally speaking, the oxygen storage can be formally described by the redox reaction of  $\text{CeO}_2$  according to



The amount of oxygen released (left-to-right) or stored (right-to-left) is generally referred to as oxygen storage capacity (OSC). It is worth noting that according to the way of measuring this quantity, both the thermodynamics and kinetics (e.g. rates of cerium-oxide reduction and oxidation) may be the limiting factors for the measured value of the OSC. As a matter of fact, there are a number of underlying phenomena, which should be taken into account when this apparently simple reaction is considered.

From the thermodynamic point of view, the standard potential for reduction of  $\text{Ce}^{4+}$  to  $\text{Ce}^{3+}$  is 1.74 V in solution (Moeller 1982) which indicates that  $\text{Ce(IV)}$  in solution is a strong oxidant. In the solid state, the situation is different.  $\text{CeO}_2$  crystallises in the fluorite structure in which each cerium ion is coordinated by eight oxygen neighbours (fig. 9). This coordination stabilises the  $\text{Ce}^{4+}$  state and makes the reduction of  $\text{CeO}_2$  unfavourable. In fact, the fluorite structure of ceria is a direct result of the ionic nature of ceria and of the charge and size of the ions. Model calculation has shown that it is formed when a sufficiently high number of  $\text{CeO}_2$  units (about 50) are clustered together (Cordatos et al. 1996b).

The ability of  $\text{CeO}_2$  to undergo a relatively easy reduction (*vide infra*) compared to other oxides, can be in principle also related to the general property of fluorite structure/mixed valence oxides to strongly deviate from stoichiometry.

When the oxygen storage capacity, i.e. the amount of oxygen available for the catalytic reactions, is experimentally measured, care must be taken to distinguish whether the

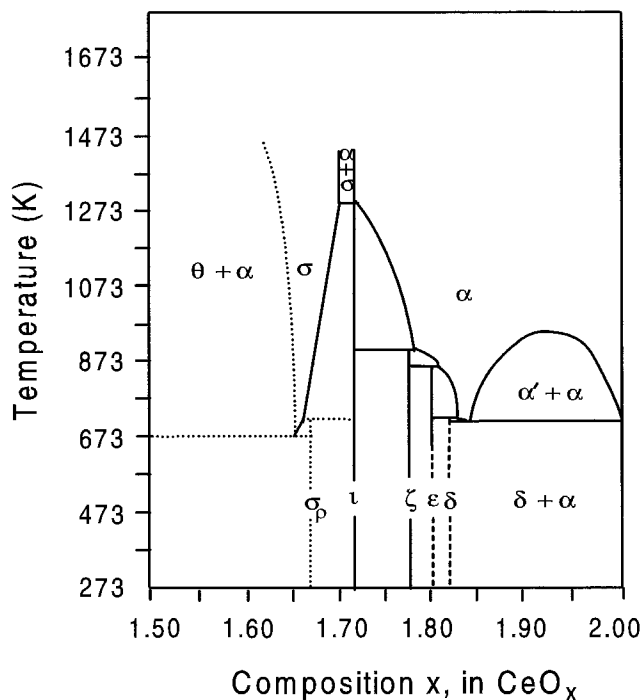


Fig. 10. Phase diagram of the  $\text{CeO}_2$ - $\text{Ce}_2\text{O}_3$  system (courtesy of Prof. Z.H. Kang, University of Arizona, USA).

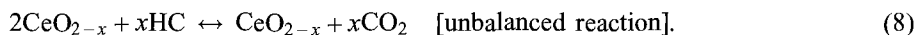
measurements are carried out under a thermodynamic (or quasi-thermodynamic) regime, such as for example by carrying out an isothermal reduction before measuring the oxygen uptake, or under a kinetically controlled regime. In the former case the degree of reduction is generally limited by formation of some non-stoichiometric  $\text{CeO}_{2-x}$  compound (Ricken et al. 1984, Perrichon et al. 1994, Laachir et al. 1991) according to the phase diagram reported in fig. 10. Consistently, isothermal reduction at 973 and 773 K led respectively to  $\text{CeO}_{1.8}$  and  $\text{CeO}_{1.89}$  (Fierro et al. 1987). In the latter case the oxygen storage is measured under kinetic control in order to evaluate those amounts of the oxygen, which can be released/accumulated under the dynamic conditions of an exhaust system.

It is also worth noting that in addition to reaction (1), due to the presence of a variety of reductants and oxidants (compare table 1), other redox reactions may account for the oxygen storage (Schmieg and Belton 1995, Ranga Rao et al. 1996, Herz 1981, Kim 1982, Otsuka et al. 1983):





and for its release:



The relative importance of reactions (2)–(5) should not be disregarded when compared to the oxidation of reduced  $\text{CeO}_{2-x}$  moieties with  $\text{O}_2$ . In fact,  $\text{H}_2\text{O}$ ,  $\text{CO}_2$  and  $\text{NO}$  are good oxidants of  $\text{Ce}^{3+}$ , even if their contribution to ceria oxidation may be different. Consistently, the oxidation with  $\text{NO}$  at 773 K of a  $\text{Pt/Pd/Rh/CeO}_2/\text{Al}_2\text{O}_3$  catalyst appeared to be slower and less effective than the reaction with  $\text{O}_2$  (Herz 1981). In addition, when the above  $\text{Pt/Pd/Rh/CeO}_2/\text{Al}_2\text{O}_3$  catalyst was exposed to lean-exhaust after a rich-exhaust conditioning, within 0.5 s most of the catalyst was oxidised, despite the fact that the  $\text{NO}$  and  $\text{O}_2$  available in the exhaust gases represented only about half of the oxygen atoms stored by the catalyst. This indicates that either  $\text{H}_2\text{O}$  or  $\text{CO}_2$  or both significantly contribute to oxygen storage under real exhaust conditions. Note that both  $\text{H}_2\text{O}$  and  $\text{CO}_2$  are present at relatively high and constant concentration (about 10%) in the exhaust compared to both  $\text{NO}$  and  $\text{O}_2$ . At 773 K, no evidence for significant interaction of  $\text{CeO}_2/\text{Al}_2\text{O}_3$  with propylene was found, suggesting that contribution of the  $\text{HC}$  to the redox activity of the  $\text{Ce}^{4+}/\text{Ce}^{3+}$  redox couple in terms of OSC should be limited (Herz 1981).

Two types of oxygen storage capacity were distinguished by Yao and Yu Yao (1984):

- (i) the so-called complete or ultimate oxygen storage capacity (hereafter this value will be referred to as total-OSC), i.e. an oxygen storage measured under thermodynamic control (*vide infra*);
- (ii) the kinetic oxygen storage, (hereafter referred to as dynamic-OSC), i.e. measured under kinetic control.

The general procedure employed for laboratory determination of the total-OSC is to reduce the catalyst under isothermal conditions using diluted  $\text{H}_2$ - or  $\text{CO}$ -containing mixtures, and the OSC is then measured by  $\text{O}_2$  uptake using a pulse technique (Yao and Yu Yao 1984). Alternatively, the  $\text{H}_2$  consumption, typically measured in a temperature-programmed reduction (TPR) experiment, is given as a measure of the OSC. As will be discussed below, the latter measurement may lead to erroneous values due to contribution of adsorbed/occluded species and  $\text{H}_2$  adsorption/desorption phenomena which are likely to occur during the TPR experiment (Zotin et al. 1993). The total-OSC represents the widest “limiting” amount of oxygen transferable from the catalyst. The dynamic-OSC is typically measured by alternatively injecting pulses of oxidising mixtures, usually  $\text{O}_2$  in inert gas, and reducing mixtures, usually  $\text{CO}$  or  $\text{H}_2$  in inert gas, into a flow of inert carrier passing through the catalysts bed at a fixed temperature. In this way, alternating the oxidising and reducing conditions, as they occur in the real exhaust, may simulate the conditions of A/F fluctuations. Unfortunately, a widely accepted definition and standardisation of the experimental procedure by which dynamic- and total-OSC

Table 3  
Dynamic- and total-OSC measured on CeO<sub>2</sub>

Surface area (m <sup>2</sup> g <sup>-1</sup> )	Reducing agent	Reduction temp. (K)	Oxidation temp. (K)	Technique	Oxygen storage (mol O <sub>2</sub> /mol CeO <sub>2</sub> )		Reference
					Dynamic	Total	
55	H <sub>2</sub> (5%)	800	700	O <sub>2</sub> pulses		0.025	Zamar et al. (1995)
55	H <sub>2</sub> (5%)	1000		TPR		0.095	
55	H <sub>2</sub> (5%)	1300		TPR		0.200	
9.9	CO (2%)	773	773	CO pulses	0.0032	0.005	Yao and Yu Yao (1984)
9.9	CO (1%)	773	773	CO pulses	0.0019	0.004	
194	H <sub>2</sub> (5%)	700	700	O <sub>2</sub> pulses		0.084	Fornasiero et al. (1996a)
10	H <sub>2</sub> (5%)	700	700	O <sub>2</sub> pulses		0.003	
115	H <sub>2</sub> (1%)	700		TPR		0.075	Laachir et al. (1991)
10	H <sub>2</sub> (8.85%)	923		TPR		0.012	Logan and Shelef (1994)
6	H <sub>2</sub> (5%)	700	700	O <sub>2</sub> pulses		0.006	de Leitenburg et al. (1996b)
22	H <sub>2</sub> (1%)	773		TPR		0.028	Tournayan et al. (1991)
2	H <sub>2</sub> (3%)	973		TPR		0.019	Bruce et al. (1996)
54	H <sub>2</sub> (3%)	973		TPR		0.027	
98	H <sub>2</sub> (3%)	973		TPR		0.033	
168	H <sub>2</sub> (3%)	973		TPR		0.043	

should be measured is still missing. A non-exhaustive survey of literature data concerning the OSC measured on CeO<sub>2</sub> is reported in table 3. A perusal of the data reveals that there is a significant scattering of literature data, which does not allow accurate estimation of the “absolute” amount of oxygen which can be stored/released by CeO<sub>2</sub>. The data reported in table 3 reveal that surface area of starting oxide, nature and concentration of the reductants and temperature of reduction heavily affect the total oxygen storage.

To account for the scattering of the literature data, one must consider first the reduction/oxidation processes in pure CeO<sub>2</sub>. For the sake of convenience, we will discuss the redox processes in TWC-related systems in the following order: metal-free CeO<sub>2</sub>, CeO<sub>2</sub>/Al<sub>2</sub>O<sub>3</sub>, and then the noble-metal-supported materials.

#### 2.1.1. *Temperature-programmed reduction of CeO<sub>2</sub> using H<sub>2</sub> (H<sub>2</sub>-TPR) and CO (CO-TPR) as reductants*

In the case of CeO<sub>2</sub>, there is general agreement that the oxidation step (reaction 1) is a fast and exothermic process. At room temperature this reaction proceeds rapidly on the surface and with an appreciable rate in the bulk. In fact, the rate of re-oxidation at room temperature depends also on the nature of the phase formed in the reduction. As long as non-stoichiometric CeO<sub>2-x</sub> are formed during the reduction, the subsequent re-oxidation proceeds even at room temperature, irrespectively of the initial texture of the CeO<sub>2</sub>. Both a low-surface-area (5 m<sup>2</sup> g<sup>-1</sup>) and a high-surface area (115 m<sup>2</sup> g<sup>-1</sup> CeO<sub>2</sub>,

Table 4

Phase designation and formula unit cell content for nonstoichiometric ordered  $\text{Ce}_n\text{O}_{2n-2m}$  phases (Kang and Eyring 1997a,b)

Phase designation	$n$	$m$	Formula	O/Ce ratio
$\iota$	7	1	$\text{Ce}_7\text{O}_{11}$	1.714
$\xi$	9	1	$\text{Ce}_9\text{O}_{16}$	1.778
$\epsilon$	40	4	$\text{Ce}_{40}\text{O}_{72}$	1.800
$\delta$	11	1	$\text{Ce}_{11}\text{O}_{20}$	1.818

reduced at 973 K to give respectively  $\text{CeO}_{1.825}$  and  $\text{CeO}_{1.73}$ , were completely oxidised by dosing with  $\text{O}_2$  at room temperature within 15 h (Perrichon et al. 1994). This indicates that migration of oxygen in the bulk of the reduced  $\text{CeO}_2$  moieties is effective even at room temperature. In fact, when short contact times, e.g. when  $\text{CeO}_{2-x}$  is re-oxidised by a pulse technique (Bernal et al. 1993b, 1998b), or dense ceramic-type  $\text{CeO}_2$ -containing materials are investigated (Sergo and Clarke 1995), a full re-oxidation may not be achieved at room temperature.

When  $\text{CeO}_2$  is reduced at progressively higher reduction temperatures (1073 K, 1173 K, 1273 K), an expanded  $\text{CeO}_{2-x}$  phase (see below) and cubic and hexagonal  $\text{Ce}_2\text{O}_3$  phases are formed (Perrichon et al. 1994). The former two are still easily re-oxidised, while oxidation of the hexagonal  $\text{Ce}_2\text{O}_3$  phase proceeds slowly at room temperature as traces of this phase were detected even after 48 h under air. As shown by HREM studies, oxidation of the hexagonal  $\text{Ce}_2\text{O}_3$  phase leads to formation of an amorphous phase on the surface, which prevents further oxidation in the bulk of the solid at moderate temperatures (Bernal et al. 1998b). According to the phase diagram, transformation of  $\text{CeO}_2$  into the hexagonal  $\text{Ce}_2\text{O}_3$  requires a deep reduction of  $\text{CeO}_2$  above 1673 K in the absence of oxidants (Bevan 1955). However, segregation of  $\text{Ce}_2\text{O}_3$  from  $\text{CeO}_2$  during the reduction was observed even at 1273 K (Bernal et al. 1998b). Also, the hexagonal phase observed by Perrichon et al. (1994) was formed by reduction at 1273 K in  $\text{H}_2$ . Such harsh conditions are never met in a real exhaust, indicating that formation of such phases, whose re-oxidation would be slow, does not occur. The easy oxidation of reduced  $\text{CeO}_2$  moieties may be related to the ability of the fluorite-type oxides to form a variety of non-stoichiometric  $\text{CeO}_{2-x}$  compounds. The phase diagram of  $\text{CeO}_2$  (fig. 10) is quite complex, however, the essential features are that at high temperatures the Ce sesquioxide evolves, according to the oxygen fugacity in the environment and for compositions approximately up to  $\text{CeO}_{1.72}$ , into a  $\sigma$ -phase (related to the C-type sesquioxide structure). Above this composition there is another wide non-stoichiometric region which consists of disordered, fluorite-related  $\alpha$ -phases. The  $\alpha$ -phases transform into a variety of ordered non-stoichiometric phases upon cooling or for reduction temperatures lower than 960 K, which were described by a general formula  $\text{Ce}_n\text{O}_{2n-2m}$ . Some of these phases together with the phase designation are reported in table 4.

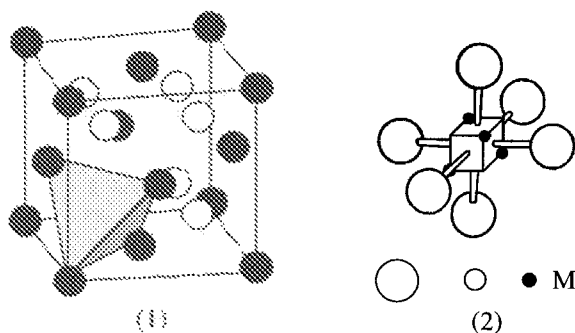


Fig. 11. Fluorite structure composed of eight octants: (1) octant of composition  $\text{Ce}_{1/2}\text{O}$ ; (2) idealised stereo-chemical environment of octahedrally coordinated vacant anion sites (coordinated defect – c.d.). (Martin 1974, Hoskins and Martin 1995, Kang et al. 1996, Kang and Eyring 1997b.)

Formation of non-stoichiometric ordered phases in reduced  $\text{CeO}_2$  is in principle an easy process since anion vacancies are readily mobile in the defective fluorite structures as shown by the above quoted ease of oxidation. A rationale for the non-stoichiometry of the defect fluorite-type structures of the lanthanide oxides and particularly  $\text{CeO}_2$  has long been a matter of extensive studies, and different models have been developed to account for such non-stoichiometric ordered phases (see for example Sorensen 1981, Martin 1974, Kang and Eyring 1997a,b, Hoskins and Martin 1995, Kang et al. 1996). A detailed discussion of these models is outside the scope of this chapter, however it should be observed that in principle, all the models propose a structural unity or defect which is then indefinitely repeated along a specific crystal direction. Martin (1974) suggested that the structure and generation of the above-mentioned ordered phases can be related to the formation of associated vacant oxygen sites which are octahedrally coordinated to the six neighbour oxygens of the formula  $\text{Ce}_4\text{O}_6^{2+}$ , generating a coordination defect (c.d.) such as depicted in fig. 11. This model has been subject to some criticism (Sorensen 1981), however strong evidence for the existence of this c.d. was the observation by neutron diffraction that in both Tb and Pr oxides, the six oxygens nearest to a vacant oxygen site ( $\text{V}_\text{O}^{\bullet\bullet}$ ) move closer to  $\text{V}_\text{O}^{\bullet\bullet}$  which results in an average shortening of the  $\text{V}_\text{O}^{\bullet\bullet}\text{--O}$  distance by about 0.03 nm compared to the average  $\text{O--O}$  bond. Meanwhile, the four nearest cations move away by about 0.02 nm (Kang et al. 1996). These results were taken as an indication that the c.d. is positively charged. The formal electroneutrality is then achieved by assuming that the larger  $\text{Ce}^{3+}$  cation (ionic radii:  $\text{Ce}^{4+}$ , 0.097 nm;  $\text{Ce}^{3+}$ , 0.114 nm; Shannon 1976) occupies a non-defective, negatively charged site  $[\text{Ce}^{3+}\text{O}_2]^-$ . This pattern of charge distribution contradicts the results of calculations of defect formation energies, which suggests that the defect clusters are neutral. However, it should be noted that only very simple defect geometry was generally considered in such studies (Sayle et al. 1992, 1994b, Conesa 1995). Accordingly, a value of  $\Delta E = -1.51$  eV/vacancy ( $-145.7$  kJ mol $^{-1}$ ) was calculated for segregation of an associated anion vacancy  $[\text{Ce}'_\text{Ce} - \text{V}_\text{O}^{\bullet\bullet} - \text{Ce}'_\text{Ce}]^x$  defect to produce separate  $\text{CeO}_2$  and  $\text{Ce}_2\text{O}_3$  phases (Conesa 1995). However, this result contradicts the experimental evidence, which reports the formation of either ordered non-stoichiometric phases or  $\alpha$ -phases, suggesting that inclusion of more complex defect structures should be considered. The assumption

that the large  $\text{Ce}^{3+}$  may occupy a non-defective site has been indirectly confirmed by a systematic study of related fluorite-type oxides (Li et al. 1994). EXAFS characterisation of trivalent-dopant-stabilised  $\text{ZrO}_2$  of fluorite structure showed that oversized cations (e.g. compared to the size of  $\text{Zr}^{4+}$ ) have an eight-fold coordination in the lattice (Li et al. 1994), the oxygen vacancy being associated with the  $\text{Zr}^{4+}$  site. By considering these structural elements, a general structural rationalisation of the whole series of defective Ce, Pr and Tb oxides was recently put forward (Kang and Eyring 1997a,b, Hoskins and Martin 1995, Kang et al. 1996).

The general hypothesis is that all the higher oxides can be described by a sequence of basic modules, each with dimensions of a basic unit fluorite cell. Due to electrostatic repulsion, each module can accommodate no more than two c.d. per cell with different geometric arrangements. These modules are then regularly spaced in the crystal lattice. The relevant observation is that, as also suggested in previous models, the oxygen vacancies show a long-range order in the crystal. The correlation with the  $\alpha$ -phase, which is formed upon heating by a peritectoidal decomposition of these ordered defective phases, can be understood in terms of an order-disorder transition which leaves in the  $\alpha$ -phase only a short-range ordering. These structural features may possibly be related to the efficiency of the oxidation process in the reduced  $\text{CeO}_2$  moieties. In fact, the oxygen motion in the fluorite lattice can be described by a vacancy mechanism. Accordingly, ordering of the vacancies along specific directions and planes makes the oxygen/vacancy motion in the lattice easy, thereby making the oxidation process efficient. This process may be further facilitated by the expansion of the lattice parameter, which is concurrently observed upon reduction. This was shown when the reduction of  $\text{CeO}_2$  by  $\text{H}_2$  was investigated by the XRD technique (Perrichon et al. 1994, Lamonier et al. 1994). Reduction of  $\text{Ce}^{4+}$  (ionic radius 0.097 nm) to give  $\text{Ce}^{3+}$  (ionic radius 0.114 nm) expanded the lattice parameter of the cubic (space group  $\text{Fm}\bar{3}\text{m}$ ) fluorite-type cell of  $\text{CeO}_2$ . This expansion is quite significant and depends on the temperature and the oxygen partial pressure as exemplified in fig. 12, which shows the effect for the  $\alpha$ -phase at 1173 K. Summarising, formation of either ordered or disordered oxygen vacancies upon reduction and the expansion of the lattice parameters are both factors which easily account for the fast oxygen migration even in the bulk of the reduced  $\text{CeO}_2$  moiety, making the oxidation process fast and easy.

In contrast to the observations above, the reduction of  $\text{CeO}_2$  is a relatively slow process. Both the nature of the reductant and the texture of the  $\text{CeO}_2$  strongly influence its kinetics. Reduction under  $\text{H}_2$  has been widely studied using the TPR techniques (Yao and Yu Yao 1984, Bernal et al. 1993b, Perrichon et al. 1994, Padeste et al. 1994, Trovarelli et al. 1992, Zotin et al. 1993, Johnson and Mooi 1987).

Typically, the reduction of  $\text{CeO}_2$  features two peaks at about 770 and 1100 K indicating the presence of respectively labile and strongly held oxygen species. The relative intensity of these peaks appears related to the extent of surface area (fig. 13). This suggested that they can be attributed to removal of surface-capping oxygen and reduction in the bulk of  $\text{CeO}_2$ , respectively (Yao and Yu Yao 1984). This suggestion was further supported by a simple linear correlation between the surface area and the degree of reduction

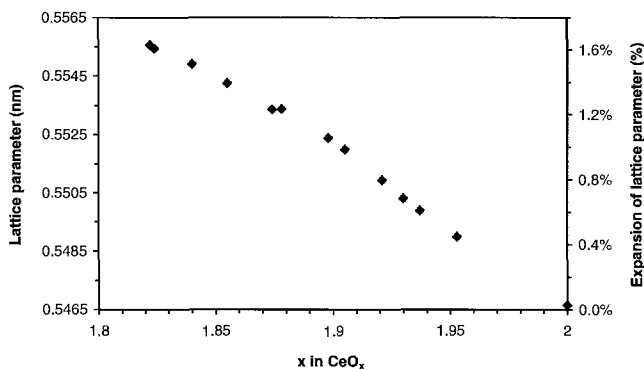
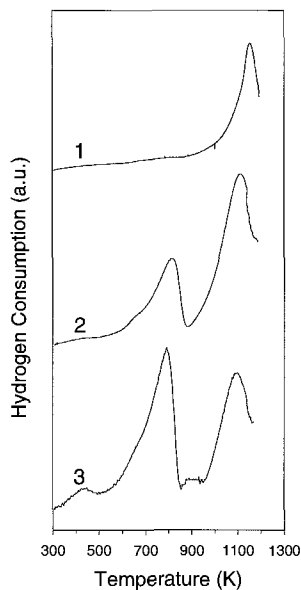


Fig. 12. Expansion of the lattice parameter of the non-stoichiometric cubic  $\alpha$ -CeO<sub>2</sub> phase at 1173 K. (Chiang et al. 1993.)

Fig. 13. Temperature-programmed reduction (H<sub>2</sub>-TPR) profiles of CeO<sub>2</sub> with different surface areas: (1) surface area <2 m<sup>2</sup> g<sup>-1</sup>; (2) 30 m<sup>2</sup> g<sup>-1</sup>; (3) 194 m<sup>2</sup> g<sup>-1</sup>. (Kašpar et al. 1992, unpublished data.)



corresponding to the first peak in the TPR, found by (Johnson and Mooi 1987). The surface model used assumed a cubic morphology for the CeO<sub>2</sub> particles and that the surface is composed of adjacent oxygen anions. On these assumptions, the number of surface-capping oxygens ( $n_{O_c}$ ) can be related to the total number of oxygens ( $n_{O_{tot}}$ ) in a CeO<sub>2</sub> particle of cubic form and size  $a$  by the following equation:

$$\frac{n_{O_c}}{n_{O_{tot}}} = \frac{n^3 - (n-2)^3}{n^3} = \frac{6n^2 - 12n + 8}{n^3}.$$

Using an oxygen ionic radius of 0.14 nm the particle size  $a$  is related to  $n$  by

$$a = 0.28n \text{ (nm)}.$$

If the ceria surface area ( $S_{BET}$ ) is measured in m<sup>2</sup> g<sup>-1</sup> then  $n$  can be expressed as

$$n = \frac{F}{adS_{BET}},$$

where  $F$  is a geometrical factor taking into account the number of faces exposed to the gas environment ( $F=6$  for a cube) and  $d$  is the density of CeO<sub>2</sub> (7.13 g ml<sup>-1</sup>). Substitution of  $n$  and  $a$  into the above expression and use of the appropriate conversion factors leads to the following final equation:

$$H_2^s = 2905k \frac{6(3009/S_{BET})^2 - 12(3009/S_{BET}) + 8}{(3009/S_{BET})^3}.$$

In this equation  $H_2^s$  represents the amount of H<sub>2</sub> (μmol g<sup>-1</sup>) necessary to reduce the surface, and  $k$  is a stoichiometric factor which is equal to 4, 2 or 1 for a reduction

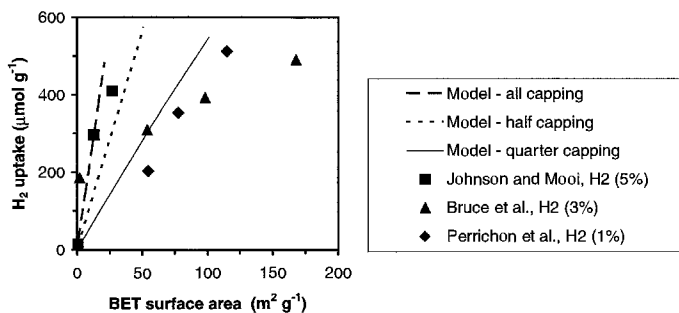


Fig. 14. Johnson and Mooi model for the evaluation of  $\text{CeO}_2$  surface areas: experimental vs. calculated  $\text{H}_2$  consumption. (Johnson and Mooi 1987, Bruce et al. 1996, Perrichon et al. 1994.)

of respectively all, half and a quarter of the capping oxygens (compare below). The estimated  $H_2^s$  are reported in fig. 14 for  $k=1$  and  $k=2$ . For low-surface-area  $\text{CeO}_2$  (surface area  $<15 \text{ m}^2 \text{ g}^{-1}$ ) such as those reported by Johnson and Mooi (1987), a good agreement between the experimental data and calculated values for the reduction of all of the capping oxygens is obtained. Similar models, based on the reduction of the (100) surface of  $\text{CeO}_2$ , have also been derived by other authors (Perrichon et al. 1994, Taha et al. 1998).

This observation suggested that the surface area of  $\text{CeO}_2$  could be measured conveniently by the TPR method (Johnson and Mooi 1987). This, of course, could in principle also represent an important way to estimate the  $\text{CeO}_2$  surface area when dispersed on  $\text{Al}_2\text{O}_3$ . As shown in fig. 14, the model conveniently fitted the authors' data for low-surface-area samples. However, even for a relatively modest surface area of  $23 \text{ m}^2 \text{ g}^{-1}$ , the highest one employed by the authors, the agreement between the experimental and predicted results appears quite poor. Despite this fact, this model has become quite popular among researchers studying the redox behaviour of  $\text{CeO}_2$ -based materials. It was frequently used to establish the contribution of the surface to the total reduction process (see for example Perrichon et al. 1994, El Fallah et al. 1994, Laachir et al. 1991, de Leitenburg et al. 1996b, Bernal et al. 1992b).

As a matter of fact there are a number of limitations intrinsic in the model. First, the assumptions used for the model concerning the particle morphology and surface geometry were derived by considering the (100) or equivalent surfaces of the  $\text{CeO}_2$  particles. A geometric cleavage of the crystal lattice along this plane leads to a solid which can be described as a stacking of parallel, non-coincident planes with respectively (Ce) and ( $\text{O}_2$ ) stoichiometries (Conesa 1995). This surface presents a net electric dipole component perpendicular to the surface, which makes it energetically unfavourable. Model calculations have shown that the energy of the exposed surfaces increases in the following order: (111), (110), (310) and (211) (Sayle et al. 1994b, Conesa 1995). The last surface spontaneously reconstructs into a stepped (111) configuration (Conesa 1995). These calculations suggest that  $\text{CeO}_2$  particles should preferentially expose the (111) plane, which is the one of lowest energy. In agreement, HREM studies of

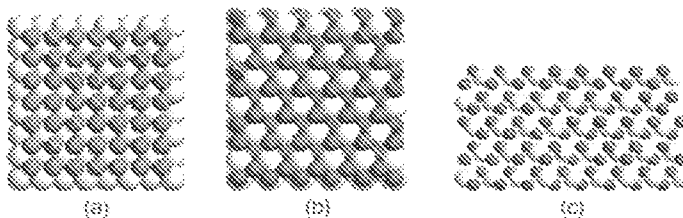


Fig. 15. Model of the (100) and (111)  $\text{CeO}_2$  surfaces: (a) (100) top view; (b) (111) top view, (c) (111) lateral view – (111) is on the top. O–O distances: (100) plane, 2.71 Å, (111) plane, 3.84 Å. (Courtesy of Dr. G. Balducci, University of Trieste.)

$\text{CeO}_2$  revealed that a high-surface-area ( $110 \text{ m}^2 \text{ g}^{-1}$ ) specimen showed small misoriented grains which were principally oriented to expose a predominance of edges which were the (111) planes (Kang and Eyring 1992). This preference for (111) planes became “dramatically apparent” after a mild annealing at 773 K, indicating that any model for the reduction process should take into account that the surface stoichiometry is mainly determined by the (111) surface. Note that this surface can be described as overlaid sandwiches constituted of O–Ce–O planes (Conesa 1995). When the crystal is cleaved along one of these sandwiches, the obtained surface presents a low density of surface oxygens (fig. 15). Oxygens and a subsurface layer of  $\text{Ce}^{4+}$  cations terminate this surface. Both the surface cations and anions are missing one nearest neighbour in their coordination spheres, which is in contrast with the above model. In addition to these considerations, the evaluated surface area is derived by including the  $\text{CeO}_2$  density in the calculation. In samples of low surface area, the  $\text{CeO}_2$  density is close to the value  $7.13 \text{ g cm}^{-3}$ , but this is not the case for non-sintered high-surface-area samples, for which the experimentally measured density is significantly lower. Further, unless an appropriate thermal treatment is applied, the oxide surface is normally populated by surface hydroxyls. In line with all these limitations, subsequent investigations showed that this model is indeed oversimplified. At least two different investigations (Perrichon et al. 1994, Bruce et al. 1996) found a linear relationship between the surface area and the  $\text{H}_2$  consumption in the TPR peak at 770 K, but neither of these followed the prediction of the Johnson and Mooi model (fig. 14). Perrichon et al. (1994) suggested that the surface reduction should be described by a stoichiometric process, e.g. reduction of a quarter of the capping oxygens ( $k=1$ ) which corresponds to the stoichiometry:



rather than by the reduction of half of the capping oxygens ( $k=2$ ) as suggested by Mooi and Johnson (Johnson and Mooi 1987). Nevertheless, even this model gives a non-perfect agreement with the experimental data (fig. 14).

In practice, the TPR profiles of high-surface-area oxides may lead to additional features compared to the low-surface-area samples. In the case of  $\text{CeO}_2$ , when no appropriate pre-treatment of the sample is adopted before the TPR, the reduction profiles are indeed affected both by the presence of reducible surface species and/or bulk carbonates whose



reduction may partially overlap with the peak at 770 K. This may lead even to observation of negative peaks (Perrichon et al. 1994, Laachir et al. 1991, Zotin et al. 1993, Johnson and Mooi 1987, Barbier et al. 1992). Furthermore,  $H_2$  is reversibly chemisorbed on  $CeO_2$  (Bernal et al. 1993b, Trovarelli et al. 1992) and formation of hydrogen bronzes was also inferred on the basis of  $^1H$  NMR studies (Cunningham et al. 1990, Fierro et al. 1987), which may lead to negative desorption peaks in the TPR profiles even for carbonate-free  $CeO_2$  (Bruce et al. 1996). It is worth noting that such artefacts hardly disappeared even after an *in situ* pre-treatment of the  $CeO_2$  in dry air up to 673 K for 2 h. This suggests that the degree of reduction could be evaluated more reliably from oxygen uptakes measured after the reduction (Zotin et al. 1993). Alternatively, some standard procedure for appropriate cleaning of surface from impurities should be employed (Daturi et al. 1998), which generally leads to a better agreement between the two measurements (Fornasiero et al. 1996a).

Even if an alternative model which reliably correlates the surface area with the amount of  $H_2$  consumed in the peak at 770 K is not available at present, the linear type of dependence on the  $H_2$  consumption of the surface area of  $CeO_2$  appears to be a strong argument for attributing this peak mainly to reduction of surface or a near sub-surface region.

Let us now examine the kinetics and the mechanism of the process which has been proposed for the reduction of  $CeO_2$  using  $H_2$  as reductant. At 673–753 K, the kinetics of the reduction of  $CeO_2$  were analysed using the XAS technique (X-ray absorption spectroscopy) in a fast acquisition mode. As shown in fig. 16, the kinetics of the  $CeO_2$  reduction depends on its surface area. For the HSA sample, a relatively fast process occurs initially leading to a 20% reduction after 20 min of reaction, which decreases to 4% in the case of the LSA sample, indicating that the initial reduction process should be related to the extent of surface area. However, this observation seems to be dependent on the temperature of the reduction process. In fact, the extent of reduction after 25 min of the HSA sample was 20, 16 and 8%, respectively at 673, 723 and 753 K. This apparently strange result can be interpreted by considering that above 673 K, the surface area of  $CeO_2$  is unstable (Perrichon et al. 1995) and collapses through extensive sintering. This in turn inhibits the kinetics of the reduction process.

A detailed kinetic analysis of the reduction process, performed by El Fallah et al. (1994), indicated that the reduction kinetics at 673 K can be split into two distinct parts. The first one well agrees with a model where a surface step is rate limiting. The second is consistent with a model where a diffusion of oxygen vacancies in the bulk is rate limiting. The overall reduction process can be described with the mechanism shown in Scheme 1 (El Fallah et al. 1994, Bernal et al. 1993b, 1995b, Laachir et al. 1991, Le Normand et al. 1988). Steps 1–4 in scheme 1 constitute the original scheme proposed by El Fallah et al. (1994): (1) dissociation of chemisorbed  $H_2$  to form hydroxyl groups; (2) formation of anionic vacancies and reduction of  $Ce^{4+}$  sites; (3) desorption of water; and (4) migration of oxygen from the bulk to the surface. However, as argued by Bernal et al. (1995b), chemisorption and dissociation of  $H_2$ , which occur reversibly on  $CeO_2$ , lead to the reduction of  $Ce^{4+}$  in the chemisorption process, as indicated in step 1a. Accordingly,

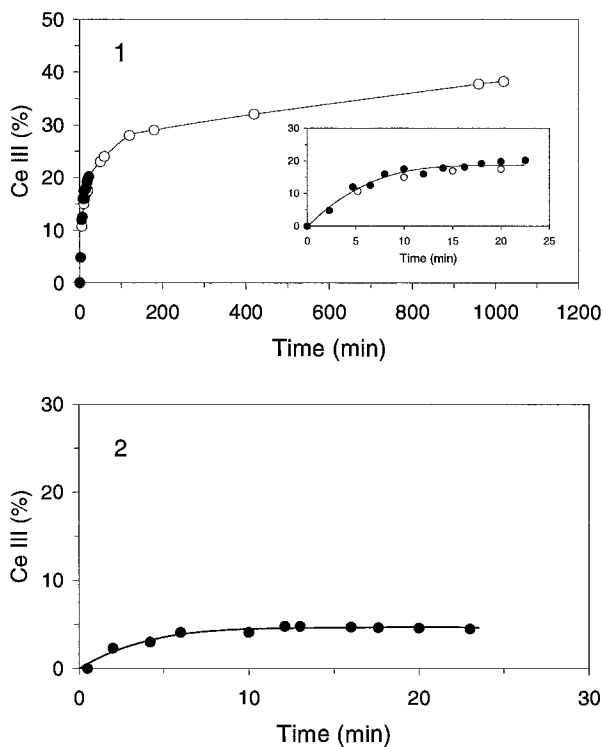
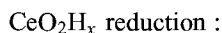
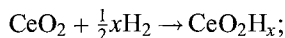


Fig. 16. Dependence of reduction kinetics under  $H_2$  on surface area of  $CeO_2$ : (1) surface area  $125 \text{ m}^2 \text{ g}^{-1}$  (reduction temperature 673 K); (2) surface area  $8 \text{ m}^2 \text{ g}^{-1}$  (reduction temperature 753 K). Data points: solid circles, rates measured by XAS at the  $Ce \text{ L}_{III}$  edge; open circles, rates measured by  $N_2O$  adsorption. (El Fallah et al. 1994.)

magnetic susceptibility measurements showed presence of  $Ce^{3+}$  upon  $H_2$  chemisorption at room temperature on  $Rh/CeO_2$  (Bernal et al. 1992b).

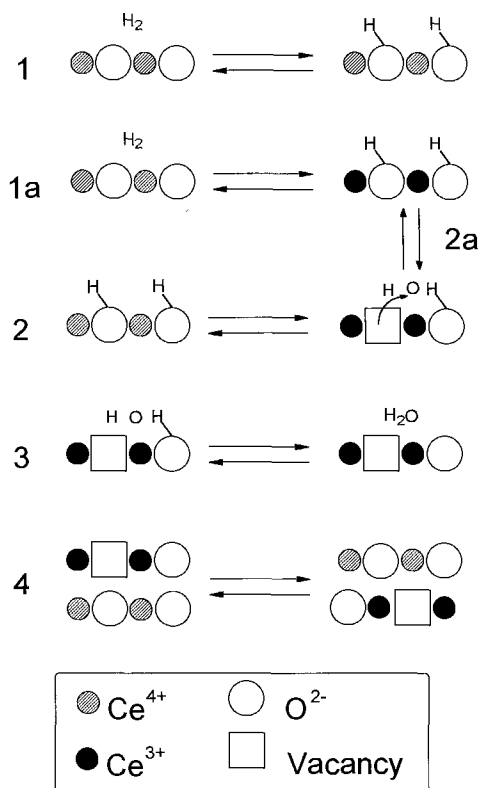
An alternative model for the reduction of  $CeO_2$  was inferred by other authors (Fierro et al. 1987, Cunningham et al. 1990). This model suggests that reduction of  $CeO_2$  occurs via formation of hydrogen bronzes, followed by the reduction step, as follows:



or



This model has been strongly argued by Bernal et al. (1993b) who have suggested that the amount of hydrogen species detected by solid state  $^1H$  NMR after a  $H_2$  treatment at 295–773 K is consistent with a surface process according to step 1a of scheme 1.



Scheme 1. Proposed mechanism for the reduction of  $\text{CeO}_2$ . (El Fallah et al. 1994, Bernal et al. 1993b, 1995b, Laachir et al. 1991, Le Normand et al. 1988.)

Although the linear relationship found for the reduction of carbonate-free  $\text{CeO}_2$  by Bruce et al. (1996) shows a positive intercept for a surface area of  $0 \text{ m}^2 \text{ g}^{-1}$ , consistent with a formation of hydrogen bronzes, it does not provide sufficient evidence for their formation. In fact, this relationship was derived from relatively high-surface-area  $\text{CeO}_2$  and neither was a low-surface-area sample included in the calculations of the linear relationship nor were standard deviations given to ensure the reliability of the extension of the results to low-surface-area samples. It therefore seems reasonable to conclude that at present there is not enough evidence available to discriminate to what extent the formation of hydrogen bronzes may be a predominant pathway for  $\text{CeO}_2$  reduction. This point would certainly be worth of further study.

At this stage we favour the model reported in scheme 1 for the reduction of  $\text{CeO}_2$  using  $\text{H}_2$  as reductant. In this model, steps 1–3 are related to the surface processes, while step 4 represents the migration of oxygen from the bulk to the surface. The latter process is conventionally represented in the opposite way, i.e. it is viewed as a migration of oxygen vacancies to the bulk. The migration of oxygen vacancies is counterbalanced by migration of small polarons (localised electrons) in the opposite direction to maintain the electroneutrality in the solid. An apparent activation energy of  $67 \text{ kJ mol}^{-1}$  was measured

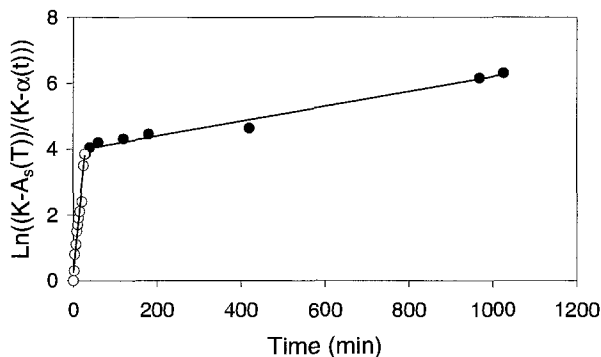


Fig. 17. Isothermal reduction (673 K) of  $\text{CeO}_2$  (surface area  $125 \text{ m}^2 \text{ g}^{-1}$ ): Plot of  $\ln\left(\frac{K-A_s(T)}{K-\alpha(t)}\right)$  vs time; surface adsorption/reduction (open circles) and bulk diffusion (solid circles) as rate-limiting steps. (El Fallah et al. 1994.)

for the initial, i.e. surface-related, part of the reduction process. On the basis of the kinetic data presently available, a rate-determining step cannot be settled. A kinetic equation of the form  $\ln\left(\frac{K-\alpha(t=0)}{K-\alpha(t)}\right) = kt$  was derived from scheme 1 (El Fallah et al. 1994), where  $\alpha$  is the overall degree of reduction defined as the linear combination of the reduced cations (surface  $N_s^C$  and bulk  $N_s^B$ )  $\alpha = (\alpha_s N_s^C) + (\alpha_b N_s^B)$ . Depending on the choice of the rate-limiting step in scheme 1,  $\alpha(t=0)$  is equal to 0 (steps 1 and 2 – surface steps) or to  $A_s(T)$ , the degree of surface reduction at temperature  $T$  (steps 3 or 4 – bulk diffusion).  $K$  is a thermodynamic constant for the overall reduction process at a given ratio of partial pressures ( $P_{\text{H}_2}/P_{\text{H}_2\text{O}}$ ), weighted by a partition factor which accounts for the probability distribution of the reduced cations between the surface and bulk sites. The experimental degree of reduction plotted as  $\ln\left(\frac{K-A_s(T)}{K-\alpha(t)}\right)$  vs. time (fig. 17) clearly reveals that the isothermal reduction of  $\text{CeO}_2$  occurs in two discernible regimes. The initial fast step is associated with a surface reduction while the second, slower process, is associated with the diffusion of oxygen vacancies in the bulk of  $\text{CeO}_2$ .

It should be noted, however, that the  $A_s(T)$  value was evaluated from the initial surface area by employing the Johnson and Mooi relationship which, as above shown, overestimates the actual number of  $V_{\text{O}}^{\bullet}$ . For a complete reduction of the surface layer, a degree of reduction of 23% is calculated for a surface area of  $125 \text{ m}^2 \text{ g}^{-1}$ , which decreases to 11.5% when a stoichiometry of  $\text{Ce}^{4+}:\text{O}^{2-} = 1:4$  is employed for surface reduction, as suggested by Perrichon et al. (1994). Keeping in mind the limitations of the Johnson and Mooi relations and the fact that the breakthrough point (fig. 16) of the reduction process occurs at approximately  $\alpha = 23\%$ , it seems reasonable to assume that apart from a purely surface process, some reduction of a near-subsurface region could occur in the initial part of the reduction. A value of  $D_t = 16 \times 10^{-21} \text{ m}^2 \text{ s}^{-1}$  was reported for the oxygen diffusion coefficient in the bulk of  $\text{CeO}_2$  at 673 K (Martin and Duprez 1996, Rogemond et al. 1996). By using the equation

$$\sqrt{D \cdot t} = a,$$

where  $a$  is the distance covered by the migrating oxygen species in time  $t$ , we calculate that over the time scale employed (1 min), a layer of the  $\text{CeO}_2$  particle about 1.0 nm

thick could be involved in the reduction process. This value is higher than the  $\text{CeO}_2$  lattice parameter (0.541 nm) which further substantiates the suggestion that part of the sub-surface region might be involved even in the initial stage of reduction. This could be consistent with the sandwich type structure of the (111) plane (fig. 15).

An important conclusion is therefore derived from the above considerations: at the usual exhaust temperatures (673–873 K), the ability of pure  $\text{CeO}_2$  to undergo a reduction process is essentially related to the surface or a near-subsurface region on a short time scale such as those found under the oscillating A/F conditions.

However, it has been underlined recently that the redox properties of  $\text{CeO}_2$  can be modified by employing a surfactant route synthesis (Terribile et al. 1997, 1998a,c). The interaction of hydrous cerium oxide with cationic surfactants under basic conditions was employed to prepare  $\text{CeO}_2$  with enhanced textural and redox properties. The obtained samples showed rather high surface area compared to traditional co-precipitation route. Remarkably, the TPR profile of this  $\text{CeO}_2$  showed the appearance of a reduction peak at 700–900 K, whose intensity did not decrease upon redox cycling. The enhanced reduction appeared to be associated with the presence of a new hexagonal  $\text{CeO}_{2-x}$  phase<sup>3</sup>. This contrasts the usual behaviour of high-surface-area  $\text{CeO}_2$  where the peak at 770 K disappears as the surface area collapses upon redox ageing (fig. 13). Apparently, the transition from this new phase to the fluorite one occurs during the redox cycles. This process presumably occurs via a non-topotactic transformation, generating an amorphous  $\text{CeO}_2$  phase on the surface of the crystallites, which seems to be responsible for these enhanced redox properties. Accordingly, ultrafine  $\text{CeO}_2$  particles (2.8–4.0 nm) show enhanced activities in CO oxidation (Masui et al. 1997), but the textural stability is not improved by use of very fine particles (Masui et al. 1998). This point is certainly worth of further studies.

Despite the fact that CO represents the most abundant reductant contained in automotive exhaust, the investigation of the TPR behaviour by using CO as reductant (CO-TPR) has received scarce attention. Generally speaking, the ability of CO to induce the reduction of  $\text{CeO}_2$  has been investigated in connection with the kinetics of CO oxidation rather than addressing this topic specifically. A possible reason for this is that, as shown later, there is a spectacular promotion of the  $\text{CeO}_2$  reduction behaviour in presence of a supported noble metal using  $\text{H}_2$  as reductant. This has not been observed in the CO– $\text{CeO}_2$  and CO–NM/ $\text{CeO}_2$  systems (Laachir et al. 1994). Moreover, the reduction profile is generally measured by detecting the  $\text{CO}_2$  formed and/or the CO consumed. This however can be formed/consumed both by CO oxidation, which leads to creation of oxygen vacancies, and by water gas shift reaction (WGS reaction) of adsorbed CO with surface OH groups leading to a dehydroxylation of the support. In fact, the latter reaction was found to significantly contribute to the overall reduction process for  $\text{Al}_2\text{O}_3$ -supported  $\text{CeO}_2$  (Serre et al. 1993a). Finally the occurrence of a Boudouard-type disproportion of CO to give surface carbon and  $\text{CO}_2$  cannot be discounted under the CO-TPR conditions. The occurrence of the latter reaction can be discriminated by detecting simultaneously both the

<sup>3</sup> Note added in proof: Actually the “ $\text{CeO}_2$ ” phase contained about 0.5–2 wt% Si, which could explain this redox behaviour, compare sect. 3.1.3 (errata corrigé: Terribile et al., 1999, Chem. Commun., p. 477).

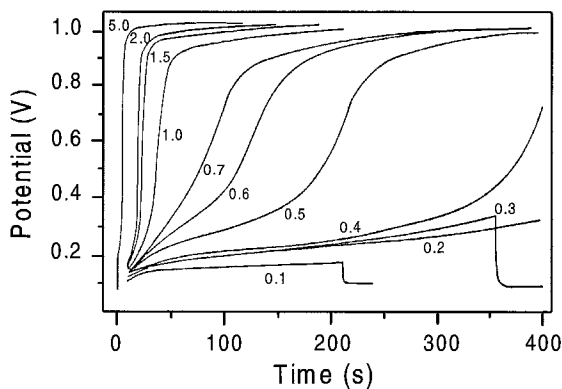


Fig. 18. The potentiometric response for ceria as a function of time in stream of a CO/Ar mixture. (Harrison et al. 1988.)

rates of CO consumption and  $\text{CO}_2$  production. Only a simultaneous quantitative detection of evolved water, together with CO and  $\text{CO}_2$ , permits unambiguous assignment of the reduction process in the CO-TPR, since both the WGS reaction and CO oxidation consume/form respectively CO and  $\text{CO}_2$  at equivalent rates. Unfortunately, the detection of evolved water is not easy due to its extensive adsorption on the surface of  $\text{CeO}_2$ . It is important for the reader to be aware of these limitations when considering the literature data. On the other hand, CO-TPR presents some interesting features due to the fact that CO does not diffuse into the bulk of  $\text{CeO}_2$  particles. Accordingly in this experiment, the reduction may be envisaged as a measure of the oxygen diffusion towards the surface where it is removed by interaction with CO. This may provide useful insights on the rate of oxygen migration in the bulk of the oxide, provided that surface processes are not rate limiting.

In this context, some indications on the kinetics of the CO reduction at 973 K were obtained by Harrison et al. (1988) in an electrochemical reactor. They measured the potentiometric response of a zirconia disc coated with  $\text{CeO}_2$  to the exposure to a CO/Ar mixture. In these experiments, ceria was initially oxidised in a  $\text{O}_2$ (2 mol%)/Ar mixture and then at  $t = 0$ , the gas was switched to a CO(0.1–5 mol%)/Ar mixture (fig. 18). The change in potential is attributed to the removal of lattice oxygen from the ceria, as CO is oxidised to  $\text{CO}_2$ . Although no quantitative data are given, examination of the data reported in fig. 18 suggests that the reduction of  $\text{CeO}_2$  is quite a slow process below a critical concentration of about 0.5 mol% CO. At 973 K, migration of oxygen species in the bulk of  $\text{CeO}_2$  should be fast compared to the time scale reported in fig. 18. Also, most of the  $\text{CO}_2$  desorbs at these temperatures, which suggests that either a limited number of suitable surface sites for CO adsorption are present or the CO adsorption/desorption equilibrium is highly pressure sensitive. In agreement with this idea, the adsorption of CO has been found to be highly sensitive to the nature of the surface and its pre-treatment (Trovarelli 1996). The *autocatalytic* nature of the reduction process, as denoted by the presence of an induction time in the profiles, suggests that the reduction proceeds fast on a partially reduced surface. In agreement, when the potential applied to ceria coated disc was systematically varied to produce oxygen vacancies in the  $\text{CeO}_2$ , the rate of the

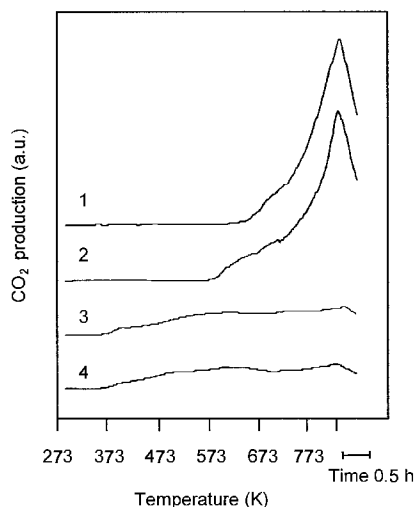


Fig. 19.  $\text{CO}_2$  production during TPR of  $\text{CeO}_2$  in a  $\text{CO}(2 \text{ mol}\%)/\text{He}$  mixture, heating rate  $10 \text{ K min}^{-1}$ : (1)  $\text{CeO}_2$  ( $30 \text{ m}^2 \text{ g}^{-1}$ ) from  $\text{Ce}_2(\text{CO}_3)_3$  (sample a); (2) TPR of sample recycled from run (1); (3)  $\text{CeO}_2$  ( $15 \text{ m}^2 \text{ g}^{-1}$ ) from Aldrich (sample b); (4) TPR of sample recycled from run (3). (Padeste et al. 1993.)

system response to the reaction with CO increased (Harrison et al. 1988). Formation of adsorbed carbonates or carboxylates, i.e. precursors of surface reduction, is hindered on the reduced surface due to the lack of available surface oxygens. However, the strength of linear CO bonding to the cerium cations increases due to retro-donation from  $\text{Ce}^{3+}$  to CO (Li et al. 1989b, Bozon-Verduraz and Bensalem 1994). In summary, these experiments suggest that at low CO pressures, the removal of lattice oxygen from  $\text{CeO}_2$  may be limited by the adsorption kinetics, while at  $p_{\text{CO}} \geq 15$  torr the rate of the oxygen extraction from the bulk is rate limiting.

This interpretation of the reduction of  $\text{CeO}_2$  by CO is substantiated by the CO reduction profiles reported by Padeste et al. (1993) for two  $\text{CeO}_2$  samples of different origin and morphology (fig. 19). Despite the comparable surface areas ( $15$  and  $30 \text{ m}^2 \text{ g}^{-1}$ ), use of a highly disordered, poorly crystalline  $\text{CeO}_2$  leads to a high degree of reduction of 10–15% (fig. 19, trace 1) compared to the value of 1–2% observed over the highly crystalline product (fig. 19, trace 3). The crystal imperfections increase the rate of oxygen extraction from the bulk, thereby accounting for the high reduction rate in the former case. Significantly, the onset of the reduction process is observed at about 373 K for sample b while it is about 700 K for sample a. This contrasts with the usual finding of  $\text{H}_2$ -TPR experiments that an increase of surface area favours the reduction processes occurring at low temperatures, and it indicates that attribution of the different reduction rates to surface processes is unlikely. Since  $\text{Ce}_2(\text{CO}_3)_3$  has been employed as a  $\text{CeO}_2$  precursor for sample a, it is possible that some residual carbonate species remained on the surface after the thermal decomposition of the precursor. Their desorption could hinder the reduction process at the very beginning by diminishing the CO adsorption.

Accordingly, Badri et al. (1991) found that reduction of a highly disordered high-surface-area  $\text{CeO}_2$  ( $115 \text{ m}^2 \text{ g}^{-1}$ ) occurred well below 473 K, while a low-surface-area  $\text{CeO}_2$  ( $5 \text{ m}^2 \text{ g}^{-1}$ ) was reduced to a significant degree only at/above 673 K.

In conclusion, the reduction of  $\text{CeO}_2$  by CO has received relatively scarce attention. Despite this, the comparison of  $\text{H}_2$ -TPR and CO-TPR indicates that low-temperature reduction in the latter case appears to be related to the pre-treatment conditions and degree of crystallinity of the  $\text{CeO}_2$  rather than to the extent of surface area which is the main factor governing the low-temperature reduction processes in  $\text{H}_2$ -TPR.

### 2.1.2. Temperature-programmed reduction of $\text{CeO}_2/\text{Al}_2\text{O}_3$ using $\text{H}_2$ ( $\text{H}_2$ -TPR) and CO (CO-TPR) as reductants

The observation that the low-temperature redox processes may be related to the extent of  $\text{CeO}_2$  surface has highlighted in the past years the necessity of maximising the available surface areas of this component. This can be achieved by supporting  $\text{CeO}_2$  on  $\text{Al}_2\text{O}_3$ , which represents the usual practice of making the TWC washcoat. Generally speaking, in  $\text{CeO}_2/\text{Al}_2\text{O}_3$  systems the redox behaviour is strongly affected by the amount of  $\text{CeO}_2$  deposited (Miki et al. 1988, Shyu et al. 1988b, Yao and Yu Yao 1984). This is exemplified in fig. 20 for  $\text{CeO}_2$  contents varying between 0.8 and 22 wt%.

It appears that despite the broadness of the reduction peaks, some correlations with the reduction behaviour of pure  $\text{CeO}_2$  can be derived: in all the samples a large peak located at about 790–820 K is present which, as above discussed, could be related to the *surface* reduction of  $\text{CeO}_2$ . For high  $\text{CeO}_2$  content a peak at about 1100 K is clearly discernible which can be related to the reduction of  $\text{CeO}_2$  in the bulk. Note that Yao and Yu Yao associated the peak at 900 K (fig. 20, traces 3–5) to this process, suggesting that the easier reduction in the bulk could be related to a down-scale shift of the reduction peak as the  $\text{CeO}_2$  particle size decreases at low  $\text{CeO}_2$  loading. This attribution seems unlikely, since no significant shift of the reduction of  $\text{CeO}_2$  in the bulk is generally observed even for high-surface-area samples. Accordingly, we favour the attribution

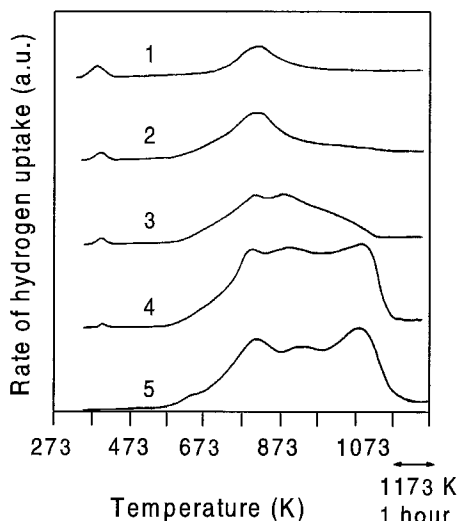


Fig. 20.  $\text{H}_2$ -TPR of  $\text{CeO}_2/\text{Al}_2\text{O}_3$  samples: Curve (1): 0.83 wt%  $\text{CeO}_2/\text{Al}_2\text{O}_3$ ; (2) 2.04 wt%  $\text{CeO}_2/\text{Al}_2\text{O}_3$ ; (3) 6.14 wt%  $\text{CeO}_2/\text{Al}_2\text{O}_3$ ; (4) 11.7 wt%  $\text{CeO}_2/\text{Al}_2\text{O}_3$ ; (5) 21.6 wt%  $\text{CeO}_2/\text{Al}_2\text{O}_3$ . (Yao and Yu Yao 1984.)



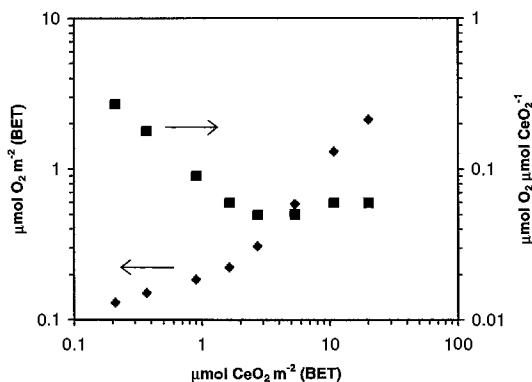


Fig. 21. Irreversible  $\text{O}_2$  uptake at 773 K as a function of  $\text{CeO}_2$  loading. Samples were calcined at 773 K followed by a reduction in  $\text{H}_2$  at 773 K for 2 hours. (Yao and Yu Yao 1984.)

outlined below. Noticeably, the peak at 1100 K is missing for low  $\text{CeO}_2$  loading and it only appears as a shoulder of the broad reduction feature at 770–1100 K at  $\text{CeO}_2$  loadings of and above 6.14 wt%, which corresponds to  $2.7 \mu\text{mol m}^{-2}$  (BET). This indicates that the absence of a peak at 1100 K can be associated with the mechanism by which the  $\text{CeO}_2$  wets the  $\text{Al}_2\text{O}_3$  surface. For low  $\text{CeO}_2$  concentration [ $\leq 2.7 \mu\text{mol m}^{-2}$  (BET)], after the precursor impregnation and calcination, all of the  $\text{CeO}_2$  is present as a dispersed phase. Beyond this saturation point,  $\text{CeO}_2$  tends to aggregate and forms larger crystallites on the  $\text{Al}_2\text{O}_3$  surface, for which the peak at 1100 K is then observed. Such an interpretation is indirectly confirmed by the results of  $\text{O}_2$  chemisorption carried out at 773 K on  $\text{CeO}_2/\text{Al}_2\text{O}_3$  reduced at 773 K for 2 hours (Yao and Yu Yao 1984). As shown in fig. 21, there is an inflection point in the  $\text{O}_2$  chemisorption values at  $2.5 \mu\text{mol m}^{-2}$  (BET) indicating a discontinuity in the  $\text{O}_2$  chemisorption properties. Also, the amount of  $\text{O}_2$  chemisorbed per mol of  $\text{CeO}_2$  decreases from approximately 0.25 mol  $\text{O}_2$  per mol  $\text{CeO}_2$  to reach an almost constant value for  $\text{CeO}_2$  loadings higher than  $2.5 \mu\text{mol CeO}_2/\text{m}^2$  (BET) (fig. 21). A virtually constant particle size of 5.5–6.7 nm was observed for these high loadings. A reasonable interpretation can be put forward for these findings. For a fully developed crystalline structure of the supported  $\text{CeO}_2$  particles, due to the constant particle size, a constant degree of reduction should be expected after a reduction at 773 K. At 773 K the reduction process is limited essentially to surface or near-surface layers. On the other hand, for dispersed particles, a decrease of  $\text{CeO}_2$  loading leads to fine particles, which gradually shows a higher external area. This interpretation reasonably accounts for the observed modifications of the features at 790–820 K and 1100 K. Accordingly, the TPR profiles of  $\text{CeO}_2$  supported on  $\text{SiO}_2$  showed two peaks at 800 K and 1030–1100 K, and the relative intensity of the former peak increased with decreasing  $\text{CeO}_2$  particle size (Trovarelli et al. 1995).

To rationalise the appearance of the features observed at 370 K and 900 K respectively for low and high  $\text{CeO}_2$  loading, Yao and Yu Yao suggested that the peak at 370 K could be associated with labile oxygen species located on  $\text{Al}_2\text{O}_3$  (Yao and Yu Yao 1984). The decrease of the intensity of this peak is associated with an increasing coverage of the  $\text{Al}_2\text{O}_3$  surface. However, while such labile oxygen were detected upon degassing

at 773 K (cf. refs. 21 and 22 in Yao and Yu Yao 1984), we are not aware of their observation in TPR profiles of  $\text{Al}_2\text{O}_3$ .  $\text{H}_2$  adsorption/desorption phenomena such as those observed over high-surface-area  $\text{CeO}_2$  could perhaps better explain the appearance of this peak. The presence of the peak at 900 K is associated with  $\text{CeO}_2$  oxygen species interacting with the  $\text{Al}_2\text{O}_3$ , such as oxygens shared between  $\text{Ce}^{4+}$  and  $\text{Al}^{3+}$ . In fact, no such peak was observed in the TPR profiles of  $\text{CeO}_2/\text{SiO}_2$  samples (Trovarelli et al. 1995). This assignment has been confirmed by careful XRD, XPS, EXAFS and Raman characterisation of  $\text{CeO}_2/\text{Al}_2\text{O}_3$  samples (Miki et al. 1988, Shyu et al. 1988b). The main conclusions from these studies are that upon impregnation of  $\text{Al}_2\text{O}_3$  with  $\text{Ce}(\text{NO}_3)_3$  and subsequent calcination the following features are observed: (i) at low loading [ $\sim 2.5 \mu\text{mol CeO}_2/\text{m}^2$  (BET)],  $\text{CeO}_2$  is highly dispersed over the  $\text{Al}_2\text{O}_3$  surface and it exists partly in the  $\text{Ce}^{3+}$  state as a kind of  $\text{CeO}_{2-x}$  species, denoting a strong interaction with the support; (ii) above this loading the particle size of the deposited  $\text{CeO}_2$  progressively increases, leading to systems whose redox behaviour approaches that of pure  $\text{CeO}_2$ . The interaction of the highly dispersed  $\text{CeO}_{2-x}$  with the  $\text{Al}_2\text{O}_3$  support is indirectly confirmed by detection of a  $\text{CeAlO}_3$  phase formed upon reduction above 1073 K (Shyu et al. 1988b, Miki et al. 1988). Upon oxidation at 1173 K, the dispersed  $\text{CeO}_2/\text{Al}_2\text{O}_3$  is re-formed, indicating a reversibility of the redox process (Miki et al. 1988). The formation of  $\text{CeAlO}_3$  is thermodynamically favoured below 1073 K compared to the reduction to  $\text{CeO}_2$  (Miki et al. 1990). Consequently, when an intimate  $\text{CeO}_2\text{--Al}_2\text{O}_3$  contact is present (highly dispersed samples), the formation of  $\text{CeAlO}_3$  occurs, while for high  $\text{CeO}_2$  loading a significant migration of the cerium cations would be required. This presumably does not occur under transient TPR conditions, making the reduction profiles similar to that of pure  $\text{CeO}_2$ . There is a further point of interest in these observations: formation of  $\text{CeAlO}_3$  was often inferred to be responsible for the decay of the OSC of TWCs upon thermal ageing. Since the oxidation reversibly reforms the starting  $\text{CeO}_2/\text{Al}_2\text{O}_3$ , the inference is that this deactivation pathway may be relatively unimportant.

Similarly to CO-TPR of  $\text{CeO}_2$ , the investigation of  $\text{CeO}_2/\text{Al}_2\text{O}_3$  systems by using CO as reductant has received scarce attention. Serre et al. (1991, 1993a) reported the TPR patterns for a 14.5 wt%  $\text{CeO}_2$  loaded  $\text{Al}_2\text{O}_3$ . Even though these experiments were carried out only up to 973 K, the similarity of the CO-TPR and  $\text{H}_2$ -TPR profiles reported respectively by Serre et al. (1991, 1993a) and Yao and Yu Yao (1984) is remarkable. In both cases the first reduction feature is observed around 770 K and further peaks occur above 920 K.

### 2.1.3. *Temperature-programmed reduction and OSC of NM/CeO<sub>2</sub> and NM/CeO<sub>2</sub>/Al<sub>2</sub>O<sub>3</sub>*

Several authors have investigated the role of the noble metals in the reduction behaviour of  $\text{CeO}_2$ . As a general rule, the presence of the noble metal strongly promotes the reduction of  $\text{CeO}_2$  as the feature at 770–800 K is shifted to low temperatures. This is shown in fig. 22 for a number of NM/ $\text{CeO}_2$  systems. Comparison with the reduction behaviour of  $\text{CeO}_2$  clearly reveals that only the feature which is observed at 770 K in the unsupported sample is significantly affected by the presence of the supported noble metal.

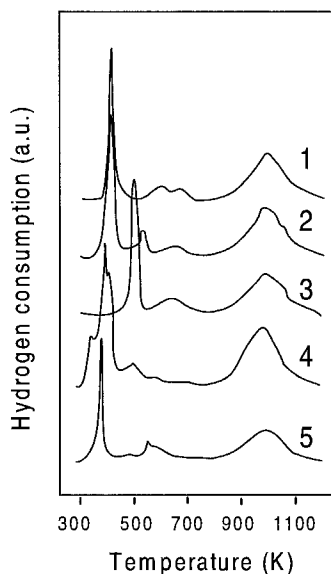


Fig. 22. Temperature-programmed profiles of NM/CeO<sub>2</sub>, with (1) NM=Ir, (2) Pd, (3) Pt, (4) Ru, (5) Rh; NM loading 1 wt%, chloride salts as metal precursors. (Trovarelli et al. 1993.).

An increase of the reduction rate, which can be inferred from the appearance of the H<sub>2</sub>-TPR, was detected using the fast-XAS technique by El Fallah et al. (1994) at 673 K. They compared the reduction of CeO<sub>2</sub> and Rh/CeO<sub>2</sub> samples (surface area 115 m<sup>2</sup> g<sup>-1</sup>): 23% CeO<sub>2</sub> reduction was achieved in the former samples after 20 min in a flow of H<sub>2</sub>, whereas less than 4 s were necessary to achieve the same extent of reduction for the latter one. No further reduction of the Rh/CeO<sub>2</sub> was observed at this temperature even for long reduction times, indicating that at this temperature only the kinetics, rather than thermodynamics, of the CeO<sub>2</sub> reduction are affected.

The H<sub>2</sub>-TPR profiles reported in fig. 22 do not show significant modification of the peak at 1100 K, i.e. the one associated with the reduction in the bulk, while the peak associated with the surface reduction is shifted to low temperatures and split into several components. In the original paper by Yao and Yu Yao (1984), this modification of the low-temperature reduction feature was associated with various types of surface sites. Subsequent investigations have shown that the appearance of the reduction patterns below 770 K is strongly affected by the nature of the metal precursor and the pre-treatment of the sample before TPR (Trovarelli et al. 1992, 1993, Barbier et al. 1992, Harrison et al. 1988). In fact, while several low-temperature reduction features are observed when chlorine-containing precursors are employed, a single reduction feature is obtained when either nitrate precursors (Harrison et al. 1988) or appropriate thermal pre-treatments are employed (Fornasiero et al. 1997). The dependence of TPR profiles of Rh/CeO<sub>2</sub> on the nature of the precursor used was confirmed by using respectively Rh-chlorine and -nitrate precursors to prepare samples which were then thermally pre-treated at 673 K. The low-temperature CeO<sub>2</sub> reduction feature shifted to 430 and 345 K respectively for Cl- and N-containing Rh precursors (Holgado and Munuera 1995). In addition, the presence

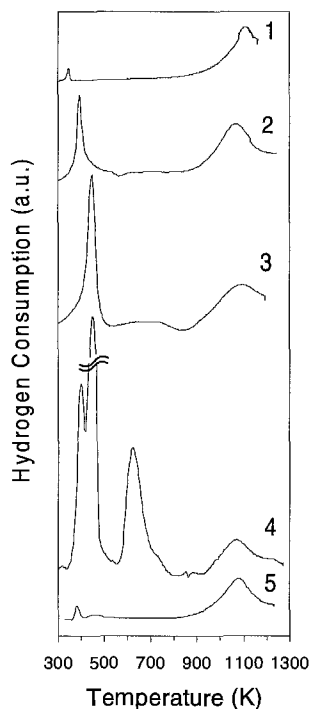


Fig. 23. TPR profiles of 0.5 wt% Rh/CeO<sub>2</sub> from RhCl<sub>3</sub>·*n*H<sub>2</sub>O precursor supported on CeO<sub>2</sub> with different surface areas and pre-treatments: (1) surface area <2 m<sup>2</sup> g<sup>-1</sup>; (2) surface area 38 m<sup>2</sup> g<sup>-1</sup>; (3) surface area 194 m<sup>2</sup> g<sup>-1</sup>; all samples pre-treated at 900 K, 5 h in Ar; (4) surface area 195 m<sup>2</sup> g<sup>-1</sup> (no pre-treatment); (5) surface area <10 m<sup>2</sup> g<sup>-1</sup>, sample recycled from run 3. (Fornasiero et al. 1997; Kašpar et al. 1994, unpublished data.)

of surface carbonates and/or adsorbed nitrates/chlorine further modifies the reduction pattern (Laachir et al. 1991, Zotin et al. 1993, Bernal et al. 1988, Barbier et al. 1992). For example, desorption of carbonates during TPR often leads to the observation of negative peaks around 800–900 K (Laachir et al. 1991). Desorption of such species under inert gas or vacuum is not easy and requires temperatures above 800 K (Laachir et al. 1991). Accordingly, the majority of the pre-treatment procedures employed in the literature appear unable to produce TPR patterns which are free from artefacts. Figure 23 exemplifies the relevance of the contribution of adspecies to the TPR profiles: even in the absence of any pre-treatment there is an additional apparent low-temperature H<sub>2</sub> consumption which cannot be accounted for by any redox process.

In summary, there is a strong variability of the reduction patterns obtained upon doping HSA CeO<sub>2</sub> with the noble metals. However, the following key points appear ascertained: (i) the first peak in the TPR profile, which is generally associated with the reduction of the noble-metal oxide, presents H<sub>2</sub> consumption which lies well above the value required for its reduction. The extra H<sub>2</sub> consumption is attributed to the reduction of easily accessible CeO<sub>2</sub> surface sites (in the absence of adspecies); (ii) the intermediate peaks below 800 K could be easily associated with the effects of reducible adspecies; (iii) the peak at 1100 K appears almost unaffected by the presence of the supported noble metal.

The shift and the split of the reduction feature at 770 K is associated with the ability of the supported noble metal to efficiently dissociate  $H_2$  and then spill active hydrogen species over the support:



where the subscript *s* denotes surface sites. This was directly demonstrated by mixing an aliquot of Rh/CeO<sub>2</sub> with WO<sub>3</sub> followed by a reduction (Cunningham et al. 1992). The powder assumed a blue colour typical of reduced WO<sub>3</sub> bronzes. One could argue that reduction of CeO<sub>2</sub> itself leads to formation of some  $F^+$  centres due to formation of  $Ce^{3+}$  giving a deep blue/black colour. However, spilling of H species over the support was clearly detected by  $H_2$  chemisorption at room temperature (Bernal et al. 1992a,b). Consistently, formation of surface hydroxyls upon  $H_2$  adsorption on Rh/CeO<sub>2</sub> was detected by FTIR (Bernal et al. 1993a). In the presence of chlorine, which is rather difficult to remove (Bernal et al. 1993b, Holgado and Munuera 1995) the spillover phenomena are strongly inhibited, which could result in a splitting of the reduction peaks (Taha et al. 1996, Martin and Duprez 1996).

The magnitude of the reduction peaks below 770 K is also related to the extent of CeO<sub>2</sub> surface area. This is exemplified in fig. 23. Such a finding is consistent with the association of the low-temperature reduction peaks mainly with surface processes. Further, the TPR features reported in fig. 23 point to the critical importance of a high surface area to obtain appreciable reduction of the CeO<sub>2</sub> below 700–800 K, i.e. a significant OSC. Accordingly, when a high-surface-area Rh/CeO<sub>2</sub> ( $194\text{ m}^2\text{ g}^{-1}$ ) was subjected to repetitive TPR/oxidation (at 700 K) experiments, the surface area collapsed to a values  $<10\text{ m}^2\text{ g}^{-1}$ , resulting in no appreciable  $H_2$  uptake below 770 K attributable to CeO<sub>2</sub> reduction (Fornasiero et al. 1997) (fig. 23).

In summary, it seems that on a clean NM/CeO<sub>2</sub> system, reduction of CeO<sub>2</sub> surface/subsurface layers occurs concurrently with that of the metal-oxide precursors as long as contributions from adsorbed species/residual chlorine are absent. This is attributed to the promoting role of the supported noble metal, which spills H species over the support. In contrast, reduction in the bulk is almost unaffected by the supported metal.

Attributing the promotion of the reduction behaviour of CeO<sub>2</sub> only to a spillover of H species could be, however, somewhat restrictive. In fact, the comparison of CO-TPR of metal-free 14.5 wt% CeO<sub>2</sub>/Al<sub>2</sub>O<sub>3</sub> and 2 wt% Pt-loaded support showed a decrease of the initial reduction temperature by about 150 K in the latter case (Serre et al. 1993a). The decrease of the reduction temperature from 770 K to 620 K indicates a significant promotion of the reduction behaviour induced by the supported Pt. If the reduction of CeO<sub>2</sub> by CO is assumed to occur via a chemical pump effect only (i.e. migration of oxygen vacancies to the surface; Trovarelli 1996), then one could expect no significant modification of the TPR behaviour in the presence of the supported metal. On the other hand, if the peak at 770 K observed in the CO-TPR is associated with surface reduction as in the case of  $H_2$ -TPR, then modification of the surface properties upon NM loading is reasonable. Surface  $H_2$  and  $O_2$  oxygen mobility coefficients were measured on Rh/CeO<sub>2</sub>

Table 5  
Dynamic OSC measured over CeO<sub>2</sub> and NM/CeO<sub>2</sub> systems (Yao and Yu Yao 1984)

Run	NM loading (wt%)			Dynamic-OSC <sup>a</sup> measured after ageing at	
	Rh	Pt	Pd	873 K	1073 K
1	—	—	—	0.19	0.14
2	0.04	—	—	0.32	0.19
3	—	0.094	—	0.26	0.21
4	—	—	0.058	0.31	0.25

<sup>a</sup> Measured at 773 K by alternatively pulsing 1% O<sub>2</sub> and 2% CO in He: mol O<sub>2</sub> (100 mol (NM + CeO<sub>2</sub>))<sup>-1</sup>.

by Martin and Duprez (1996, 1997) by an isotopic exchange method, and it turns out that both H<sub>2</sub> and O<sub>2</sub> diffuse very quickly on the CeO<sub>2</sub> surface at 600–800 K.

In accordance with these observations, Gorte et al. found an enhancement of CO<sub>2</sub> evolution from a Rh/CeO<sub>2</sub> model catalyst during the thermal desorption of pre-adsorbed CO (Cordatos et al. 1996a, Zafiridis and Gorte 1993b). It was concluded that Rh promotes the reverse spillover of oxygen species from CeO<sub>2</sub> to the metal particle and thereby favours CO oxidation at lower temperatures compared to the bare CeO<sub>2</sub>. The low-temperature CO oxidation activity appears to be strongly dependent of the particle morphology, since no CO<sub>2</sub> desorption was observed over highly sintered CeO<sub>2</sub> particles (Cordatos et al. 1996a).

In summary, the ultimate oxygen storage which as discussed above can be related to the reduction behaviour of the CeO<sub>2</sub> based systems, is strongly related to the morphology of the CeO<sub>2</sub> particles, the presence of the supported metal and the nature of the reducing agent.

As discussed in sect. 1.3, under real exhaust conditions, the feed-stream quickly oscillates around the stoichiometric point. Accordingly, the OSC measured under dynamic conditions should be more relevant to actual TWC performance. Unfortunately, as already discussed in relation to table 3, the dynamic OSC of CeO<sub>2</sub> systems has been analysed by a minority of authors. Some of the literature data are brought together in table 5.

Generally speaking, dynamic-OSC is considered to be a more useful measurement than total-OSC since the former represents the dynamically adsorbed/desorbed O<sub>2</sub> under transient TWC conditions (Trovarelli 1996). In addition, the total-OSC as measured by TPR is up to 2 orders of magnitude higher than the dynamic-OSC (compare tables 3 and 5), indicating that the dynamic-OSC represents only a fraction of the total-OSC. This is due to the fact that the total-OSC is generally measured up to high temperatures where reduction of CeO<sub>2</sub> becomes significant. In contrast, the dynamic-OSC is generally measured at 500–800 K, i.e. at temperatures where surface redox processes are occurring in the CeO<sub>2</sub> and NM/CeO<sub>2</sub> systems. Accordingly, a perusal of the data reported in tables 3 and 5 reveals that when equal reduction temperatures and comparable surface areas are employed, comparable values are obtained by the two techniques. Thus, on CeO<sub>2</sub> with a surface area of 10 m<sup>2</sup> g<sup>-1</sup>, Yao and Yu Yao (1984) measured a dynamic-OSC of

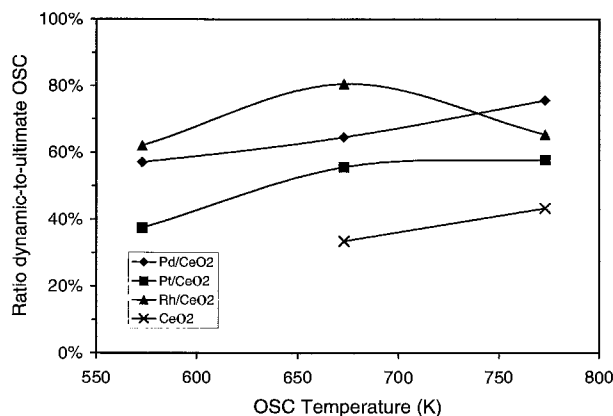


Fig. 24. Ratio of dynamic-to-total-OSC measured over CeO<sub>2</sub> and NM/CeO<sub>2</sub> (surface area 10 m<sup>2</sup> g<sup>-1</sup>). (Yao and Yu Yao 1984.)

0.0006 mol O<sub>2</sub> per mol CeO<sub>2</sub> at 673 K, which is only 5 times lower than the total-OSC of 0.003 mol O<sub>2</sub> per mol CeO<sub>2</sub> measured after an isothermal reduction at 700 K in H<sub>2</sub> (5%) for 2 hours (Fornasiero et al. 1996a). As shown in fig. 24, when both the OSC measurements are performed in the range of temperatures 570–770 K by using pulses of CO as reductant the agreement between the two measurements is rather remarkable. As a general rule, upon increasing the pulsing temperature, more O<sub>2</sub> can be stored under dynamic conditions and the dynamic-OSC approaches the limiting value represented by the total-OSC. The presence of the noble metal increases the dynamic-to-total-OSC from 30–40% to 50–80% with respect to bare CeO<sub>2</sub>. This is perfectly consistent with the above observation that at these temperatures, the reduction rate of CeO<sub>2</sub> is strongly increased in the presence of the noble metal (El Fallah et al. 1994).

The role of the noble metals in modifying the redox properties of CeO<sub>2</sub>/Al<sub>2</sub>O<sub>3</sub> systems under dynamic conditions (dynamic-OSC) was investigated by Su et al. (1985). The data reported in table 6 exemplify the beneficial effect of CeO<sub>2</sub> on the OSC of the NM/Al<sub>2</sub>O<sub>3</sub> catalysts. A perusal of these data reveals that: (i) both Rh and Pt effectively store and release oxygen at 773 K. At this temperature the oxidation/reduction of the supported metal particles occurs easily; (ii) addition of CeO<sub>2</sub> increases the overall amount of O<sub>2</sub> stored/released. Further, as more CeO<sub>2</sub> is added more OSC is obtained.

There are some further considerations to be made. Rh appears a more effective OSC component on a mol basis than Pt (table 6, runs 2 and 6) which could be related to the more noble character of this metal. However, after the more severe ageing at 1173 K, both NM/Al<sub>2</sub>O<sub>3</sub> catalysts show comparable OSC on a mol basis. Remarkably, the OSC of mixed Pt/Rh systems shows a synergism between the two metals. The OSC of Pt/Rh is 3.4 and 0.6 mol O<sub>2</sub> per 100 mol NM after ageing at 973 K and 1173 K (table 6, run 10) which is significantly higher than the values of 1.8 and 0.6 mol O<sub>2</sub> per 100 mol NM which we calculate by using the values reported for the single NM catalysts in table 6, runs 2 and 6. A similar synergism was also observed in HC/CO/NO conversions (Hu 1996).

Table 6  
Dynamic OSC measured over NM/CeO<sub>2</sub>/Al<sub>2</sub>O<sub>3</sub> catalysts (Su et al. 1985, Yao and Yu Yao 1984)

Run	NM and base-metal loading (wt%)			CeO <sub>2</sub> /NM	Dynamic-OSC <sup>a</sup> measured after ageing <sup>b</sup> at			
	Rh	Pt	CeO <sub>2</sub>		973 K		1173 K	
					ml/ml	mol/mol	ml/ml	mol/mol
1	0.022	—	—	—	0.33 <sup>c</sup>	10		
2	0.01	—	—	—	0.12	7.8	0.004	0.3
3	0.018	—	1.1	49			1.5	1.2
4	0.025	—	3.1	92	8	2.1	5.1	1.3
5	—	0.18	—	—	0.16 <sup>c</sup>	1.1		
6	—	0.15	—	—	0.15	1.2	0.03	0.2
7	—	—	1.2	—	0.23	0.17	0.13	0.10
8	—	0.14	1.2	12			2.6	1.7
9	—	0.033	3.1	130			6.1	1.7
10	0.013	0.14	—	—	0.48	3.4	0.08	0.6
11	0.014	0.12	1.3	11			2.6	1.9
12	—	—	20	—				0.4 <sup>d</sup>
13	—		20	—				0.006 <sup>e</sup>
14	0.021 <sup>f</sup>		12					1.8 <sup>d</sup>
15	1.0 <sup>e,f</sup>		20					0.7
16		0.05	23					1.9 <sup>d</sup>
17	0.03		20					0.7 <sup>d</sup>

<sup>a</sup> Measured at 773 K by alternatively pulsing 1% O<sub>2</sub> and 2% CO in He; ml/ml: ml O<sub>2</sub> per 100 ml honeycomb catalyst; second number: mol O<sub>2</sub> per 100 mol (NM+CeO<sub>2</sub>). Data from Su et al. (1985).

<sup>b</sup> Thermal ageing under 5% O<sub>2</sub>, 6% CO<sub>2</sub>, 12% H<sub>2</sub>O and balance N<sub>2</sub> for 8 hours.

<sup>c</sup> Ageing temperature 623–613 K.

<sup>d</sup> Ageing in air at 1073 K for 4 hours, pulses of 2% O<sub>2</sub> and 2% CO. Data from Yao and Yu Yao (1984).

<sup>e</sup> Data from Haneda et al. (1993).

<sup>f</sup> NM = Pd.

As expected on the basis of CO-TPR, the OSC of the CeO<sub>2</sub>/Al<sub>2</sub>O<sub>3</sub> system is beneficially affected by the presence of the supported metal. The improvement of the OSC is rather remarkable: after ageing at 1173 K, the OSC increases by one order of magnitude in Rh/CeO<sub>2</sub>/Al<sub>2</sub>O<sub>3</sub> compared to the metal-free sample (table 6, runs 7 and 3). Note that after such ageing, the OSC of both Rh/Al<sub>2</sub>O<sub>3</sub> and CeO<sub>2</sub>/Al<sub>2</sub>O<sub>3</sub> is small compared to that of the mixed system, indicating a synergistic effect of both the supported metal and CeO<sub>2</sub> on the dynamic-OSC. It is also worth noting that by increasing the ageing temperature from 973 K to 1173 K, an approximately 10-fold drop of OSC is observed in Rh/Al<sub>2</sub>O<sub>3</sub> (table 6, run 2). In contrast, such ageing decreases the OSC of Rh/CeO<sub>2</sub>/Al<sub>2</sub>O<sub>3</sub> by less than 40% (table 6, run 4).

The specific OSC, measured as mol O<sub>2</sub> per 100 mol (NM+CeO<sub>2</sub>), does not change as the CeO<sub>2</sub> loading is increased from 1.1% to 3.1% (table 6, runs 3, 4 and 8, 9) which could suggest that the higher the amount of CeO<sub>2</sub> added, the higher an OSC can be obtained.



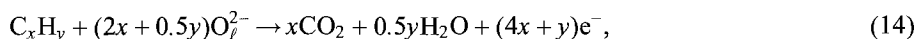
The  $\text{Al}_2\text{O}_3$  surface area is not given by Su et al. (1985), however, Yao and Yu Yao (1984) reported a surface area of  $80\text{ m}^2\text{ g}^{-1}$  for the same kind of  $\gamma\text{-Al}_2\text{O}_3$ . Assuming this surface area, the highest  $\text{CeO}_2$  loading of 3.1% wt employed by Su et al. (1985) is lower than the critical value of  $2.5\text{ }\mu\text{mol O}_2\text{ m}^{-2}$  (BET) found by Yao and Yu Yao (1984), at which point a change in  $\text{O}_2$  chemisorption ability is observed. This could account for the constant specific OSC efficiency. Apparently, such observation has induced in the past many catalyst manufacturers to increase the  $\text{CeO}_2$  content up to 30–50 wt% of the washcoat, leading to the 4th-generation TWCs. The comparison with data reported by Yao and Yu Yao (1984) and Haneda et al. (1993) (table 6, runs 12–17) nearly confirms the conclusion that high  $\text{CeO}_2$  loading favours OSC: except for  $\text{Rh/CeO}_2$  (20 wt%)/ $\text{Al}_2\text{O}_3$ , comparable specific OSC is found even for  $\text{CeO}_2$  loadings of about 20 wt% which are about 10-fold higher than those used by Su et al. (1985) (compare runs 8, 9, 14–17, table 6). However, ageing at 1173 K leads to low OSC in the NM-free  $\text{CeO}_2/\text{Al}_2\text{O}_3$  compared to the Pd-loaded sample, indicating that also for high  $\text{CeO}_2$  loading there is a metal-induced stabilisation of the OSC (table 6, runs 13 and 15). It should be noted that upon increasing the calcination temperatures from 773 K to 1173 K, the particle size of the supported  $\text{CeO}_2$  (20 wt%)/ $\text{Al}_2\text{O}_3$  increased from 7.6 nm to 12.6 nm, which suggests that  $\text{CeO}_2$  sintering is responsible for the low OSC.

In conclusion, the results of investigations of the dynamic OSC of  $\text{CeO}_2/\text{Al}_2\text{O}_3$  systems are in agreement with the essential features found when discussing total-OSC: (i) OSC is promoted by the supported noble metal; (ii)  $\text{Al}_2\text{O}_3$  favours a high dispersion of  $\text{CeO}_2$ , thereby increasing the effectiveness of the  $\text{Ce}^{4+}/\text{Ce}^{3+}$  redox couple; (iii) the presence of the noble metal stabilises the OSC against deactivation by thermal ageing.

The comparison of the dynamic and total OSC in  $\text{CeO}_2$ - and  $\text{CeO}_2/\text{Al}_2\text{O}_3$ -based systems indicates that the general conclusions drawn for total-OSC can be applied also to the dynamic conditions, even if the extent of the OSC is lower. This, of course, is only correct as long as the dynamic-OSC is measured in the range of temperatures 500–800 K, i.e. at temperatures where mainly surface reduction occurs. An important corollary of the similarity between the dynamic- and total-OSC is that the trends observed in the total-OSC measurements are generally reflected also under dynamic conditions in the  $\text{CeO}_2$ -based systems.

Besides the above-mentioned reducing agents, the exhausts also contain other reducing agents such as hydrocarbons. The contribution of these compounds to the OSC has been scarcely addressed by investigators even though evidence for hydrocarbon oxidation by lattice  $\text{CeO}_2$  oxygen has been reported in the literature (Su and Rothschild 1986, Choudhary and Rane 1992, Zhao and Baerns 1992, Mendelovici and Steinberg 1985).

Reduction by the hydrocarbon can be described by the following reaction (Trovarelli 1996):



where the lattice oxygen is identified as  $\text{O}_\ell$ ; this, however, does not take into account the observation that besides the oxidation products, carbon deposition on the catalyst under the rich excursion is generally observed.

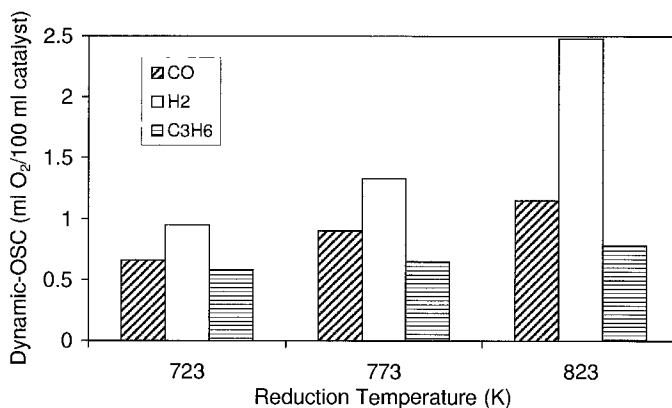


Fig. 25. Effect of reductant gas on dynamic-OSC. OSC was measured from the conversion of the reductant; washcoat composition (wt%): Pt 0.17, Rh 0.014, Ni 1.5, Ce 1.0, Pb 0.03, on  $\text{Al}_2\text{O}_3$ ; washcoat loading 10%; oxidant:  $\text{O}_2$  (1% in He); pulse volume: 3 ml. (Su and Rothschild 1986.)

A comparison of the relative reducing ability of  $\text{H}_2$ , CO and  $\text{C}_3\text{H}_6$  was investigated under dynamic conditions over a composite catalyst containing Pt, Rh, Ni,  $\text{CeO}_2$  and Pb (fig. 25; Su and Rothschild 1986). Notably, using both CO and  $\text{H}_2$  as reductant, the dynamic-OSC increases with temperature. In contrast, it remains almost constant when  $\text{C}_3\text{H}_6$  is employed as reductant, which could suggest a different mechanism in the latter case. In fact, the dynamic-OSC reported in fig. 25 was measured from the conversion of the reductant which, in the case of the HC, includes also its retention on the support. During the  $\text{C}_3\text{H}_6$  pulse,  $\text{H}_2$  and CO formation was detected, indicating that cracking of the HCs occurs over the catalyst, and about 50% of the  $\text{C}_3\text{H}_6$  was retained on the catalyst surface presumably as carbon particles (Su and Rothschild 1986, Mendelovici and Steinberg 1985). The amount of "carbon" deposits did not vary with temperature (Su and Rothschild 1986) which presumably also accounts for the constant dynamic-OSC shown in fig. 25. Clearly, if the majority of the  $\text{C}_3\text{H}_6$  conversion is attributed to its cracking, then the contribution of the HC to the OSC in terms of a  $\text{Ce}^{4+}/\text{Ce}^{3+}$  redox process should be rather small compared to the effects of both CO and  $\text{H}_2$ . Accordingly, we calculated from the data reported by Choudhary and Rane (1992) that by pulsing at 1073 K pure  $\text{CH}_4$ ,  $\text{C}_2\text{H}_6$  and  $\text{C}_2\text{H}_4$  over  $\text{CeO}_2$ , respectively  $3.0 \times 10^{-4}$ ,  $1.3 \times 10^{-3}$  and  $2.1 \times 10^{-3}$  mol  $\text{O}_2$  per mol  $\text{CeO}_2$  were released by the support. This is about one order of magnitude less than the values reported in table 6 which were measured at 773 K and using a diluted CO as reductant. This suggests that the interaction of HC with  $\text{CeO}_2$ -based catalysts should be properly considered as a reaction with the support rather than a conventional OSC in terms of a  $\text{Ce}^{4+}/\text{Ce}^{3+}$  redox process.

The possibility of using a simple thermal treatment as a mild reduction treatment was recently exploited by Bernal et al. (1997a). They used an experimental procedure that consists of evaluating in a quantitative manner the capacity of the oxide materials to attenuate (buffer) the oscillations in the oxygen partial pressure induced by fast pulsing

Table 7

Two-step reduction (step 1) and oxidation (step 2) of  $\text{CeO}_2$  (surface area  $18.8 \text{ m}^2 \text{ g}^{-1}$ ) and physical admixtures of  $\text{CeO}_2$  with NM (Otsuka et al. 1983)<sup>a</sup>

Additive (wt%)	Rate in step 1 at 823 K ( $10^{-8} \text{ mol s}^{-1} \text{ g}^{-1}$ )	Rate in step 2 at 298 K ( $10^{-8} \text{ mol s}^{-1} \text{ g}^{-1}$ )
None	1.75	0.26
Pd (1.7)	3.21	281
Pt (1.9)	2.30	323

<sup>a</sup> Reduction carried out at  $p_{\text{H}_2} = 1.36 \times 10^4 \text{ Pa}$ .

(0.1 Hz) of  $\text{O}_2$ (5%)/He in a helium stream continuously passing through the reactor (OBC, Oxygen Buffering Capacity). The advantage is that this procedure allows an easy and fast comparison of the ability of the  $\text{CeO}_2$ -based materials to release/store oxygen, even though the quantification of the stored/released oxygen may not be very simple. Of course, under such conditions, the degree of reduction is related to the intrinsic nature of the OSC material and its ability to release oxygen, since no “chemical reductant” is employed.

Up to this point, we have discussed the intrinsic factors which affect the OSC of  $\text{CeO}_2$ -containing materials, e.g. the nature of the catalyst and the reducing agent. It remains, however, to ascertain to what extent the OSC effectively operates under exhaust conditions. In fact, the importance of the OSC in improving the activity of the TWCs has been often questioned. An immediate observation is that under real exhaust conditions, the reduction of  $\text{CeO}_2$  – the slow step of the OSC – would have to occur in the presence of oxidants such as  $\text{H}_2\text{O}$  and  $\text{CO}_2$  which although weak, each represent about 10% of the exhaust.

The rates of oxidation and reduction of  $\text{CeO}_2$  with  $\text{H}_2\text{O}$  and  $\text{H}_2$  respectively, were measured by Otsuka et al. (1983). The data are reported in table 7. The oxidation of the reduced  $\text{CeO}_2$  moiety with water is fast and it occurs even at room temperature. Notably, at 823 K, the initial rate of  $\text{H}_2$  production from  $\text{H}_2\text{O}$ , i.e.  $\text{CeO}_2$  oxidation, was proportional to the concentration of oxygen vacancies created in step 1. The rate of reduction is increased upon mixing  $\text{CeO}_2$  with NM, which is in agreement with hydrogen being spilt over the support. The effect of the presence of NM on the oxidation rate is remarkable and it indicates that catalytic splitting of the HO–H bonds or spilling over some activated species onto the surface of the reduced  $\text{CeO}_2$  should be rate determining for NM-free  $\text{CeO}_2$ . There is however, one important point to be considered. The rate of oxidation and reduction did not vary as the surface area decreased from  $18.8$  to  $10.0 \text{ m}^2 \text{ g}^{-1}$  upon consecutive reduction/oxidation processes (Otsuka et al. 1983). Under the experimental conditions employed, the  $\gamma$  in  $\text{CeO}_\gamma$  was between 1.85 and 2.00. Since low surface areas were employed, it seems reasonable to assume that redox processes were occurring prevalently in the bulk of the  $\text{CeO}_2$  rather than on the surface. This, of course, must affect the measured reaction rates. It was indeed shown that the presence of oxygen vacancies located in the bulk of the reduced  $\text{CeO}_2$  moiety promotes a fast

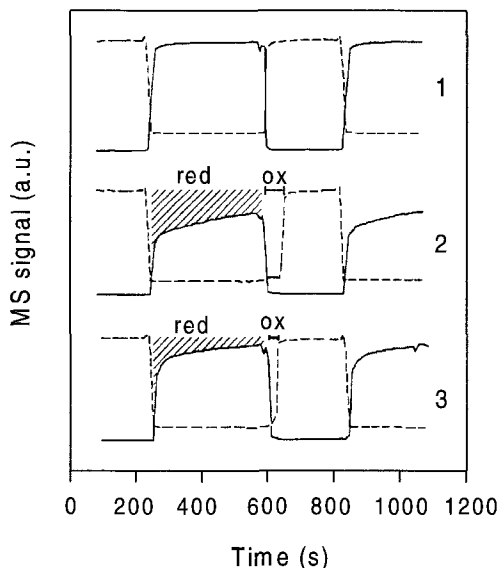


Fig. 26. Reduction/oxidation of  $\text{CeO}_2$  at 823 K (surface area  $30 \text{ m}^2 \text{ g}^{-1}$ ) in (1) empty reactor; (2) dry gas feed and (3) water-saturated feed by respectively cycling between  $\text{H}_2$  (solid curves) and  $\text{O}_2$  (dashed curves) in He. (Padeste et al. 1993.)

$\text{CO}_2$  and NO dissociation, in contrast to surface oxygen vacancies (Trovarelli et al. 1992, 1995, Ranga Rao et al. 1996). The gradient of oxygen vacancies from the bulk to the surface was suggested to provide the driving force for the fast activation of the X–O bond ( $\text{X}=\text{N}, \text{H}, \text{C}$ ) leading to the oxidation of the  $\text{CeO}_y$  (Trovarelli et al. 1992, 1995, Ranga Rao et al. 1996, Serre et al. 1993b).

Under dynamic conditions at 500–800 K, mostly surface redox processes are occurring. Also in these conditions, the kinetics of the  $\text{CeO}_2$  reduction are affected by the presence of  $\text{H}_2\text{O}$  (Padeste et al. 1993). This is exemplified in fig. 26 which shows that  $\text{H}_2$  consumption ( $\text{CeO}_2$  reduction) is depressed by addition of  $\text{H}_2\text{O}$  into the  $\text{H}_2$  stream. Notably, the oxidation step in fig. 26 occurs in a stepwise manner, suggesting that the modulation of the  $\text{H}_2$  curve is due to the slow reduction of  $\text{CeO}_2$ . The overall degree of reduction appears strongly affected by the presence of  $\text{H}_2\text{O}$  as expected on the basis of the phase diagram. Although, to the best of our knowledge, the effects of  $\text{CO}_2$  addition on  $\text{CeO}_2$  reduction under kinetic control have not been measured directly, it is reasonable to assume that the effects should be rather similar to  $\text{H}_2\text{O}$  addition. With respect to  $\text{H}_2\text{O}$ ,  $\text{CO}_2$  is less effective in re-oxidising the reduced  $\text{CeO}_2$ . A comparison of the effectiveness of  $\text{H}_2\text{O}$  and  $\text{CO}_2$  as oxidants showed that conversions of respectively 100% at 573 K and 50% at 673 K were achieved in re-oxidation of a reduced  $\text{CeO}_2$  (Otsuka et al. 1983).  $\text{CO}_2$  dissociation effectively occurred also over reduced NM/ $\text{CeO}_2$  moieties which resulted in a re-oxidation of the support (Trovarelli et al. 1992, 1995). In both cases, however, presence of oxygen vacancies in the bulk seems an essential pre-requisite to obtain highly efficient  $\text{CO}_2$  dissociation (Trovarelli et al. 1995).

In summary, the extent of the  $\text{Ce}^{4+}/\text{Ce}^{3+}$  redox processes, i.e. the OSC, should be heavily affected by the presence of both  $\text{H}_2\text{O}$  and  $\text{CO}_2$  under real exhaust conditions.

Nevertheless, as will be shown in subsequent sections, there is a clear evidence for a strong relationship between the total/dynamic-OSC and the catalyst efficiency of the TWCs.

## 2.2. Stabilisation of metal dispersion

Stabilisation of metal dispersion is an important topic for the development of active and thermally stable TWCs. In fact, given the high cost of the noble metals, there is a strong interest in maintaining high dispersion of the active metal phase even after severe ageing of the TWC. Several authors have reported the favourable effect of  $\text{CeO}_2$  in maintaining the high dispersion of noble metals (Diwell et al. 1991, Duplan and Praliaud 1991, Su et al. 1985, Su and Rothschild 1986, Summers and Aussen 1979). Figure 27 shows that addition of  $\text{CeO}_2$  to a  $\text{Pt}/\text{Al}_2\text{O}_3$  catalyst strongly increases the Pt dispersion up to 1100 K, as determined from pulse CO adsorption. Generally speaking, the stabilisation of the dispersion of the supported NM particles is observed for all noble metals of interest in the TWCs, i.e. Pt, Rh and Pd, even if it may happen to a different extent (Dictor and Roberts 1989, Duplan and Praliaud 1991, Murrell et al. 1991, Primet et al. 1990).

A key of this general behaviour seems to be related to some common characteristics of the NM particles on the  $\text{CeO}_2$  surface. As shown by HREM studies, the organisation of the metal-particle morphology over the  $\text{CeO}_2$  surface is such that there is a clear epitaxial relationship between the  $\text{CeO}_2$  (111) and NM (111) faces. After low-temperature reduction, the most common particle morphology is a truncated cubooctahedron in which the NM (111) planes grow epitaxially with the  $\text{CeO}_2$  planes (Bernal et al. 1993a, 1996, 1997b, Kepinski and Wolcyrz 1997). For example, for  $\text{Rh}/\text{CeO}_2$ , this epitaxy leads to a quite singular rhodium/ceria interface in which four Rh (111) planes ( $d(111)=0.220\text{ nm}$ ) fit three  $\text{CeO}_2$  (111) planes ( $d(111)=0.312\text{ nm}$ ). This implies the regular appearance of metal dislocations at the interface (Bernal et al. 1993a,c). Notice, however, that these dislocations cannot be unequivocally discerned from the HREM images, since electron-optical artefacts may present similar features (Bernal et al. 1995a). For reduction

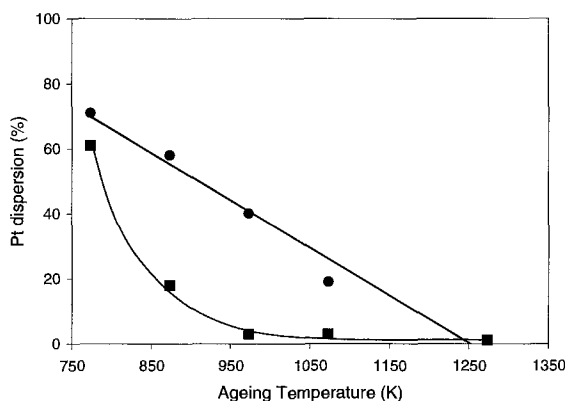
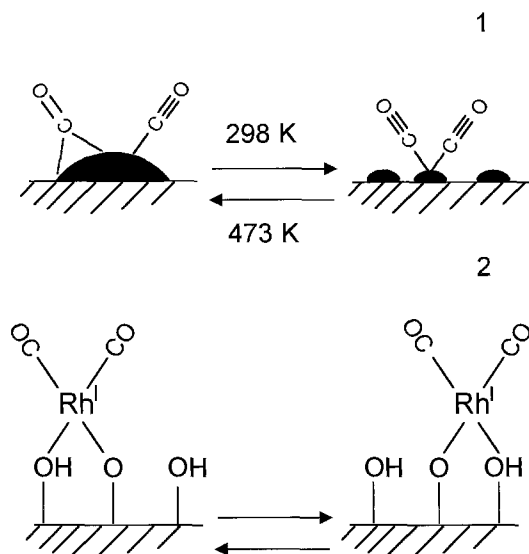


Fig. 27. Effect of  $\text{CeO}_2$  addition on stability of Pt dispersion in 0.9 wt%  $\text{Pt}/\text{Al}_2\text{O}_3$  (squares) and 0.9 wt%  $\text{Pt}/\text{CeO}_2(25\text{ wt}\%)/\text{Al}_2\text{O}_3$  (circles). (Diwell et al. 1991.)



Scheme 2. (1) CO-induced reductive agglomeration/oxidative disruption of Rh particles on oxide supports; (2) OH-promoted mobility of disrupted species on the support. (Dictor 1988, Dictor and Roberts 1989, Solymosi and Pasztor 1985, Solymosi et al. 1988.)

temperatures up to 773 K, metal sintering appears rather limited, even though the nature of the reductant may affect the particle stability. In fact, Dictor and Roberts observed that under a CO atmosphere, the metal particles in a 0.46 wt% Rh/CeO<sub>2</sub>(10 wt%)/Al<sub>2</sub>O<sub>3</sub> catalyst strongly agglomerated at 573 K, while little Rh agglomeration occurred upon reduction in H<sub>2</sub> (Dictor and Roberts 1989). This suggests that CO may act as a coalescing agent, in agreement with the occurrence of oxidative disruption/reductive agglomeration phenomena as detected by infrared spectroscopy (scheme 2). Notice that the agglomeration/disruption process is favoured by the high mobility of the rhodium dicarbonyl species which interacts with the surface hydroxyls (scheme 2).

The occurrence of the above reactions depends on the CO adsorption temperature and the nature of the support. Addition of CeO<sub>2</sub> was shown to inhibit the reductive agglomeration of rhodium at 573 K in comparison to Rh/SiO<sub>2</sub>, in agreement with the stabilisation effects of CeO<sub>2</sub> on Rh dispersion (Solymosi et al. 1988). This is consistent with the ability of CeO<sub>2</sub> to promote an intimate NM–O–Ce interaction, which helps maintaining a highly dispersed state of the NM under oxidising conditions (Brogan et al. 1994, Murrell et al. 1991) (compare sect. 2.4.1).

For reduction temperatures higher than 773 K, i.e. 873 K (Pd) and 973 K (Rh, Pt), decoration of metal particles by CeO<sub>2</sub> was observed, resulting in a decrease of the apparent dispersion on the NM (Bernal et al. 1995a, 1996, 1998a, Kepinski and Wolcyrz 1997). These effects can be reversed by an oxidation treatment, but it is observed that the higher the temperature of the reduction, the higher must be the oxidation temperature in order to completely reverse the effects of the high-temperature reduction (Bernal et al. 1994c, 1995a). Notably, this treatment may also lead to a redispersion of the metal phase (Bernal et al. 1995a, Dictor and Roberts 1989).

Some care, however, should be taken before the generalisation of the effects of CeO<sub>2</sub> on NM dispersion as detected by HREM. In fact, while decoration of Pd particles was observed at 873 K by HREM (Kepinski and Wolcyrz 1997), infrared studies showed that highly dispersed Pd on HSA CeO<sub>2</sub> (142 m<sup>2</sup> g<sup>-1</sup>) was irreversibly (upon oxidation at 673 K, *vide infra*) encapsulated into CeO<sub>2</sub> for reduction temperatures as low as 623 K (Badri et al. 1996). However, when Pd was supported on LSA CeO<sub>2</sub> (15 m<sup>2</sup> g<sup>-1</sup>), no encapsulation was observed and the decoration of the metal particles induced by the reduction could be partially reversed. This is a clear indication that texture of CeO<sub>2</sub> plays an important role in the stabilisation of the NM particles. In fact, due to the low textural stability of CeO<sub>2</sub> under reducing conditions (Perrichon et al. 1995), sintering of the CeO<sub>2</sub> support may possibly lead to loss of exposed metal surface area due to NM-particle encapsulation. A lack of observation of such phenomena by HREM does not exclude such phenomenon because in the HREM studies, due to the poor contrast between the CeO<sub>2</sub> and the NMs, low-surface-area, texturally stable CeO<sub>2</sub> was employed. In this respect, the presence of Al<sub>2</sub>O<sub>3</sub> may favourably affect the metal dispersion since CeO<sub>2</sub> sintering is prevented (sect. 2.1.2).

It is worth noting that the textural/particle stabilisations of the NM–CeO<sub>2</sub> couple is a mutual effect. An increase of CeO<sub>2</sub> surface area with Pt content was observed upon calcination at 1023 K (Murrell et al. 1991). Thus, the surface area of a HSA CeO<sub>2</sub> (130 m<sup>2</sup> g<sup>-1</sup>) decreased to 20 and 100 m<sup>2</sup> g<sup>-1</sup> for Pt loadings of 0.5 and 5 wt%, respectively, upon calcination at 1023 K. This is attributed to a strong NM-oxide–CeO<sub>2</sub> interaction as detected by Raman spectroscopy, which helps preventing the sintering process of the support.

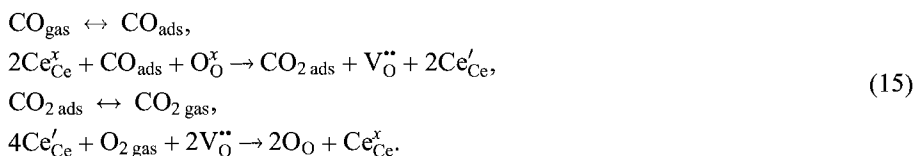
## 2.3. Catalytic activity

### 2.3.1. CO/NO/hydrocarbon reactions

2.3.1.1. *CO oxidation.* CO oxidation is a major reaction responsible for the removal of this pollutant from the exhausts. This apparently simple reaction has received considerable attention in the literature. Before discussing the effects of ceria addition upon the kinetics of CO oxidation it is worth to recall essential features of the CO oxidation over the NM. The kinetics of the reaction has been examined for Pt, Rh and Pd wires under stoichiometric to moderately oxidising conditions. First order in O<sub>2</sub> and inverse first order in CO was found with activation energies between 117 and 125 kJ mol<sup>-1</sup> (Yu Yao 1984). The favoured mechanism reported in the literature to explain these features is the interaction between adsorbed O<sub>2</sub> and CO (Langmuir–Hinshelwood mechanism) with the latter being strongly adsorbed on the surface, causing self-inhibition. The reaction is suggested to be structure-insensitive and, accordingly, under conditions where the surface is predominantly covered by CO, i.e., stoichiometric to reducing, an excellent agreement was found between the Rh(111) and Rh/Al<sub>2</sub>O<sub>3</sub> in both the specific activity (turnover frequencies) and activation energies (121 kJ mol<sup>-1</sup> for Rh(111) vs. 125 kJ mol<sup>-1</sup> for Rh/Al<sub>2</sub>O<sub>3</sub>) (Oh et al. 1986, Oh and Eickel 1990).

The kinetics of CO oxidation are affected by the presence of CeO<sub>2</sub> (Mannila et al. 1996, Shalabi et al. 1996, Hardacre et al. 1994, 1996, Bunluesin et al. 1995, 1996, Cordatos et al. 1996a, Oh and Eickel 1988, 1990, Zafiris and Gorte 1993a, Summers and Aussen 1979, Maunula et al. 1997) and CeO<sub>2</sub> itself catalyses this reaction (Tschope et al. 1995, Liu and Flytzani-Stephanopoulos 1995b, Breysse et al. 1972, 1973). Some of the kinetic parameters are gathered in table 8.

Over pure CeO<sub>2</sub> the reaction is zero-order in O<sub>2</sub> pressure and positive, nearly first-order, in CO pressure (Breysse et al. 1972, 1973). Adsorption of CO on hydroxylated CeO<sub>2</sub> surface above 473 K leads to the appearance of surface carbonate and inorganic carboxylate species, which indicates that CO is oxidised by surface oxygen species, i.e. CO reduces the CeO<sub>2</sub> surface (Li et al. 1989b). On de-hydroxylated surfaces, this reaction occurred even at room temperature. This observation is in agreement with the suggestion of Breysse et al. (1972, 1973) that lattice oxygens participate in the oxidation of CO by a mechanism involving cyclic reduction/oxidation of the surface, according to the following mechanism:



According to this mechanism, the reaction of CO with the lattice oxygen (O<sub>O</sub><sup>x</sup>) creates oxygen vacancies (V<sub>O</sub><sup>••</sup>) in the solid. Ce<sup>4+</sup> is reduced to Ce<sup>3+</sup> leading to n-type semiconductivity. In their elegant work, Breysse et al. (1972) showed that if the second step is rate determining, then, upon assumption of the steady-state hypothesis for the oxygen vacancies (V<sub>O</sub><sup>••</sup>), the electrical conductivity should be proportional to  $p_{\text{O}_2}^{-0.5}$ . They found experimentally that  $\sigma \propto p_{\text{O}_2}^{-0.50 \pm 0.03}$ .

Note that the assumption of the second step being rate determining is in agreement with the above observation that CeO<sub>2</sub> reduction is a difficult step. Further, the CO-TPR results discussed in sect. 2.1.1 showed that the sample morphology (crystallinity) strongly affects the TPR behaviour, which reasonably should be reflected also in the activity. Accordingly, nanocrystalline CeO<sub>2-x</sub> materials, generated by magnetron sputtering from metal targets, followed by controlled oxidation, showed a decrease of the light-off temperature (50% conversion) by 100–180 K, compared to ultrafine precipitated CeO<sub>2</sub> particles (Tschope et al. 1995). The remarkable difference in activity was discussed in terms of non-stoichiometry of the nanocrystalline CeO<sub>2-x</sub>, however, different crystalline habit in the conventional and nanocrystalline materials could be also indicated as responsible for the different activity. Indeed, computer simulation studies have indicated that the energetics for the creation of oxygen vacancies on the CeO<sub>2</sub> surface strongly depends on the face exposed, the more open (110) and (310) being favoured over the most dense (111) face (Conesa 1995, Sayle et al. 1992, 1994b). This suggests that appropriate synthesis leading to specific faces being exposed could generate highly active CeO<sub>2</sub> oxidation catalysts.



Table 8  
Kinetics of CO oxidation over NM, CeO<sub>2</sub>, NM/CeO<sub>2</sub> and NM/CeO<sub>2</sub>/Al<sub>2</sub>O<sub>3</sub> catalysts (rate =  $kP_{\text{O}_2}^m P_{\text{CO}}^n$ )

Run	Catalyst NM/CeO <sub>2</sub> (wt%) <sup>a</sup>	m	n	E <sub>a</sub> <sup>b</sup> (kJ mol <sup>-1</sup> )	Reaction rate/temperature <sup>c</sup>		CO pressure <sup>d</sup> (torr)	O <sub>2</sub> pressure <sup>d</sup> (torr)	Reference
					Rate (mol CO <sub>2</sub> g <sup>-1</sup> s <sup>-1</sup> )	T (K)			
1	Pt-wire	1	-1	125	100 <sup>e</sup>	573	3.8	3.8	Yu Yao (1984)
2	Pd-wire	1	-1	125	137 <sup>e</sup>	523	3.8	3.8	
3	Rh-wire	1	-1	117	300 <sup>e</sup>	523	3.8	3.8	
4	CeO <sub>2</sub> (100)	0	0.84	84 (588-635)	5.8 × 10 <sup>-4</sup>	595	253	253 (200-400)	Breysse et al. (1972)
5	Pt/CeO <sub>2</sub> (100)	0.46	0	54 (467-624)	-	573	24	0.3 (5-500)	Bunluesin et al. (1996)
6	Rh/CeO <sub>2</sub> (100)	0.40	0	50 (467-624)	-	573	170	0.3 (170-500)	
7		0.9	-1		-	573	8	0.3 (<170)	
8	Pd/CeO <sub>2</sub> (100)	0.44	0	54 (467-624)	-	573	46	0.3 (20-500)	
9		0.9	-1				6	(<20)	
10	Pd/CeO <sub>2</sub> (23)	0	1	38	1.4 × 10 <sup>-2</sup>	523	3.8	3.8	Yu Yao (1984)
11		0.5 <sup>f</sup>	0	84	3.3 × 10 <sup>-2</sup>	523	3.8	3.8	
12	Pt/CeO <sub>2</sub> (23)	0	1	50	1.4 × 10 <sup>-3</sup>	573	3.8	3.8	
13		0.3	0.3	79	7.6 × 10 <sup>-2</sup>	523	3.8	3.8	

<sup>a</sup> Balance Al<sub>2</sub>O<sub>3</sub>.

<sup>b</sup> Range of temperature where E<sub>a</sub> was measured is given in parentheses.

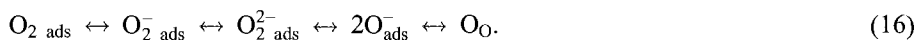
<sup>c</sup> Reaction rate (g catalysts, CeO<sub>2</sub> or NM) and temperature at which reaction rate and reaction order were measured.

<sup>d</sup> Pressure at which the reaction rate was measured. Range of validity of the kinetic law is given in parentheses.

<sup>e</sup> Mol CO<sub>2</sub> m<sup>-2</sup> of NM s<sup>-1</sup>.

<sup>f</sup> Reduced at ≥573 K with 1% CO for a few minutes.

Some authors favoured the CO oxidation mechanism over  $\text{CeO}_2$  *via* an adsorbed superoxide species (Sass et al. 1986, Tarasov et al. 1989). Superoxide and peroxide species can be considered as intermediates formed during  $\text{O}_2$  adsorption/dissociation according to the following scheme (Zhang and Klabunde 1992):



Formation of these species mainly depends on the electron-donating ability of the surface and the presence of suitable sites for stabilising the formed species (Li et al. 1989a). In fact,  $\text{O}_2^-$  radicals form only when anion vacancies are created on the  $\text{CeO}_2$  surface by a thermal evacuation at  $T \geq 473$  K (Li et al. 1989a, Soria et al. 1995) or reduction (Li et al. 1989a). These species show a relatively low thermal stability since all the EPR signal due to adsorbed paramagnetic oxygen adsorption-derived species, vanished after heating to 473 K (Soria et al. 1995). Generally speaking, the above equilibria shift to the right when the reaction temperature is raised, that is, at high temperatures the lattice oxygen will be a major component (Liu and Flytzani-Stephanopoulos 1995a). Mobile lattice oxygen species were detected by TPD of  $^{18}\text{O}_2$  (Liu and Flytzani-Stephanopoulos 1995a). Further, in the oxidation of  $\text{CH}_4$  by  $^{18}\text{O}_2$  at 773 K, presence of  $^{16}\text{O}$  was immediately detected in the  $\text{CO}_2$  produced, indicating that lattice oxygen effectively participates in the reaction (Haneda et al. 1995). Accordingly, depending on the reaction temperature, lattice oxygens may be involved either in the formation of the active catalyst or actively participate in the reaction itself. This has been confirmed by measurements of surface concentration of  $\text{O}_2^-$  radicals on a  $\text{Ce}_2\text{O}_3/\text{Al}_2\text{O}_3$  catalyst (Sass et al. 1986). Above 498 K, the calculated value of  $\text{O}_2^-$  radicals which should ensure the experimental CO oxidation rate was about 3 orders of magnitude greater than the experimental concentration of surface  $\text{O}_2^-$  radicals, indicating that lattice oxygen is the active oxygen form under these conditions (Sass et al. 1986).

A perusal of data reported in table 8 reveals that the pure  $\text{CeO}_2$  is at least two orders of magnitude less active than the NM-containing catalysts. This suggests that only the effects of the  $\text{CeO}_2$  on the activity of the noble metal are of real interest under TWC conditions, rather than the activity of  $\text{CeO}_2$  itself. One should also be aware that upon careful doping of  $\text{CeO}_2$  with other elements, Cu being the most effective, the CO oxidation activity can be effectively enhanced to achieve activities comparable with  $\text{Pt}/\text{Al}_2\text{O}_3$  (Liu and Flytzani-Stephanopoulos 1995a,b). Unfortunately, despite the extensive research on Cu-based catalysts for TWCs and especially for lean-DeNOx applications (Centi and Perathoner 1996), applicability of such systems in TWC catalysis is far away due to their low stability under hydrothermal conditions.

As shown in table 8, the presence of  $\text{CeO}_2$  significantly affects the kinetics of the CO oxidation over noble metals (Bunluesin et al. 1995, Hardacre et al. 1994, Zafiridis and Gorte 1993a, Oh and Eickel 1988). Typically, the apparent activation energy decreases from 110–130 to 50–85  $\text{kJ mol}^{-1}$  (Bunluesin et al. 1995, 1996, Yu Yao 1984, Engler et al. 1989). Over  $\text{Rh}/\text{CeO}_2\text{--Al}_2\text{O}_3$  catalysts, an almost linear relationships for the apparent activation energy with  $\text{CeO}_2$  loading was found (fig. 28), suggesting a direct correlation

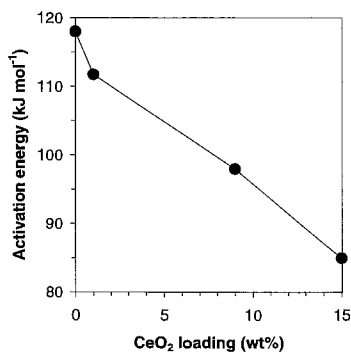


Fig. 28. Apparent activation energies for the CO oxidation over Rh/CeO<sub>2</sub>-Al<sub>2</sub>O<sub>3</sub> catalysts as a function of CeO<sub>2</sub> loading. Reactant stream CO (1 vol%) and O<sub>2</sub> (1 vol%) in N<sub>2</sub>. (Oh and Eickel 1988.)

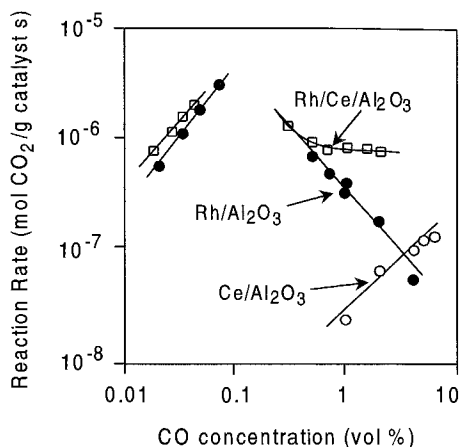


Fig. 29. CO oxidation rates over 0.014 wt% Rh/Al<sub>2</sub>O<sub>3</sub>, Rh/CeO<sub>2</sub>(9 wt%)-Al<sub>2</sub>O<sub>3</sub> and CeO<sub>2</sub>(9 wt%)-Al<sub>2</sub>O<sub>3</sub> vs. CO concentration. Reaction temperature 469 K, GHSV 32000 h<sup>-1</sup>. (Oh and Eickel 1988.)

between the CO oxidation activity and the presence of CeO<sub>2</sub>. Note that an equimolar repartition of Rh on CeO<sub>2</sub> and Al<sub>2</sub>O<sub>3</sub> would lead to a linear-type dependence of the activation energy upon CeO<sub>2</sub> loading.

Generally speaking, the effects of CeO<sub>2</sub> addition on the CO oxidation kinetics are revealed under stoichiometric to reducing conditions (Oh and Eickel 1988, Bunluesin et al. 1995, 1996, Zafiridis and Gorte 1993a). As shown in fig. 29, under strongly oxidising conditions, i.e. very low CO concentrations, both Rh/Al<sub>2</sub>O<sub>3</sub> and Rh/CeO<sub>2</sub>-Al<sub>2</sub>O<sub>3</sub> show a positive (+1) reaction rate dependency on the CO pressure. This is consistent with the studies carried out on model Rh (111) and Rh-wire catalysts (Oh et al. 1986). The implication is that under low CO pressure, the CO inhibition outlined above is ineffective since the surface is mainly covered by adsorbed oxygen (Oh et al. 1986). The transition from first-order to negative first-order dependence of the reaction rate on CO pressure, which is seen around 0.1 vol% for Rh/Al<sub>2</sub>O<sub>3</sub> (fig. 29), is a direct consequence of the increase of CO surface coverage. This inhibits dissociative O<sub>2</sub> adsorption, thus accounting for the negative dependence. At variance with Rh/Al<sub>2</sub>O<sub>3</sub>, the reaction rate is effectively enhanced over Rh/CeO<sub>2</sub>-Al<sub>2</sub>O<sub>3</sub> above 0.5 vol% CO. Moreover, a zero-order dependence on CO pressure is found.

According to Oh and Eickel (1988), the origin of this effect should not arise from modification of the CO adsorption characteristics since both TPD and infrared spectra were not significantly altered by the addition of CeO<sub>2</sub> to Rh/Al<sub>2</sub>O<sub>3</sub>. This finding was contradicted by subsequent studies which showed a strong modification of the CO-TPD spectra upon addition of CeO<sub>2</sub> to NM/Al<sub>2</sub>O<sub>3</sub> catalysts (Löf et al. 1991a) (for a discussion of this point see sect. 2.3.1.2). Also the CO-TPD profiles obtained on a Pt/CeO<sub>2</sub> catalyst showed different characteristics compared to conventional catalysts such as Pt/SiO<sub>2</sub> due

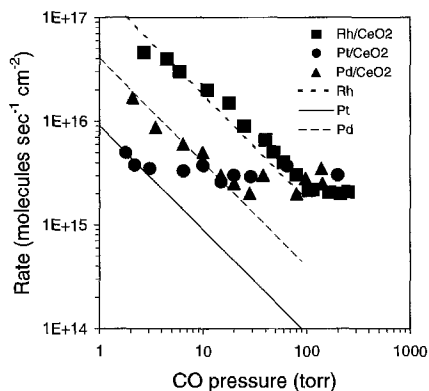


Fig. 30. CO oxidation reaction rates at 573 K on model Rh, Pd and Pt catalysts supported on CeO<sub>2</sub>. The lines correspond to the rates for pure Rh, Pd and Pt. (Bunluesin et al. 1996.)

to significant CO<sub>2</sub> formation (Jin et al. 1987). By pre-adsorbing either labelled <sup>18</sup>O or H<sub>2</sub>O before the CO-TPD, the authors were able to show that both water gas shift reaction with adsorbed H<sub>2</sub>O/-OH groups and reaction with oxygen from PtO were not responsible for this CO<sub>2</sub> formation. Accordingly, they suggested that the oxidation of adsorbed CO is promoted by the high mobility of CeO<sub>2</sub> lattice oxygen located at the periphery of the metal particles (Jin et al. 1987).

The influence of the NM and CeO<sub>2</sub> morphology on the ceria-promoted CO oxidation has been investigated in detail by Gorte and co-workers (Stubenrauch and Vohs 1996, 1997, Cordatos et al. 1996a,b, Bunluesin et al. 1995, 1996, Zafiridis and Gorte 1993a,b, Putna et al. 1996, 1997). They compared the CO oxidation activities of Pt, Pd and Rh supported on ceria films supported on an oxidised Al foil with those of NM/Al<sub>2</sub>O<sub>3</sub> (Bunluesin et al. 1996, Zafiridis and Gorte 1991). Under stoichiometric or slightly reducing conditions they obtained kinetic parameters which are typical of NM-catalysed CO oxidation (table 8, runs 7 and 9). In contrast, under strongly reducing conditions, a rate expression of the type

$$r = k p_{\text{CO}}^0 p_{\text{O}_2}^{0.4}$$

was observed (table 8, runs 5, 6 and 8). The CO pressure rate dependency is reported in fig. 30. Two features are worth noting: the almost constant rate for all NM/CeO<sub>2</sub> catalysts in the zero-order region, and the transition from the NM-mediated (first order in CO pressure) to the CeO<sub>2</sub>-promoted (zero order in CO pressure) rate expressions occurring at different CO pressures depending on the nature of the noble metal. The common reaction rate under the zero-order pressure [point (i)] is attributed to a common rate-determining step which could be either oxygen migration from CeO<sub>2</sub> to the metal particles or a reaction at the interface between the metal and oxide phases. Note that these two hypotheses are not in opposition, in the sense that oxygen migration to the metal certainly involves the metal-oxide interface. As will be shown below, the rate in the zeroth-order regime is very sensitive to ceria structure (Cordatos et al. 1996a) which may suggest that the former mechanism is more important. In agreement, the reaction

rates are similar even if there are some differences in the NM particle size (Rh, 2.3 nm; Pt, 2.7 nm; Pd, 4.2 nm; Bunluesin et al. 1996). The different CO pressures for transition to zero order [point (ii)] are due to different CO oxidation rates of the pure metals, which shifts the intersection of the rates due to the metal-mediated and CeO<sub>2</sub>-mediated reactions. Of course, the lower the specific activity of the noble metal, the higher is the promoting effect of CeO<sub>2</sub>. This is evident especially for Pt/CeO<sub>2</sub> where the transition occurs below 10 torr of CO (fig. 30).

The dependency of the reactivity of CO on the CeO<sub>2</sub> surface morphology was detected by TPD of CO pre-adsorbed on Rh/polycrystalline CeO<sub>2</sub>, Rh/CeO<sub>2</sub> (111) and Rh/CeO<sub>2</sub> (100) (Stubenrauch and Vohs 1996, Cordatos et al. 1996a). Up to 20% of CO desorbed as CO<sub>2</sub> from the polycrystalline sample, which decreased to about 2% over CeO<sub>2</sub> (111) and CeO<sub>2</sub> (100). Notably, at comparable Rh surface coverage (1–5 monolayers), the supported Rh featured particle sizes of 2.5–9.5 nm and 14–15 nm for the polycrystalline and single-crystal CeO<sub>2</sub>, respectively. The ratio of the number of Rh atoms at the Rh/CeO<sub>2</sub> interface to the total number of Rh atoms would be a nonlinear function of the Rh particle size, with small particles having a higher percentage of atoms at the interface. Consequently, the low CO<sub>2</sub> production rates observed on Rh/CeO<sub>2</sub> (111) and Rh/CeO<sub>2</sub> (100) do not represent conclusive evidence that low-index surface planes of ceria do not play an important role in terms of lattice-oxygen donation (Cordatos et al. 1996a). As already observed for CO-TPR (Padeste et al. 1993), defective/disordered structure clearly promotes the ability of CeO<sub>2</sub> to release lattice oxygen. The work reported by Cordatos et al. (1996a) is illustrative in this respect. They studied  $1.5 \times 10^{15}$  Rh/cm<sup>2</sup> films deposited on polycrystalline CeO<sub>2</sub> films annealed at 970 K and 1270 K to give CeO<sub>2</sub> particle sizes of 9–12 nm and 30–35 nm, respectively. The two CeO<sub>2</sub> samples showed dramatically different morphology: flat, slightly porous, regions separated by cracks at ~1 mm intervals were observed in the former case, while upon annealing at 1273 K, ceria formed particles with round surfaces which revealed facets of (111) and (100) surfaces.

Remarkably, significant CO<sub>2</sub> evolution is observed in CO-TPD (fig. 31) from the Rh on CeO<sub>2</sub> annealed at 973 K, which becomes negligible on the sample annealed at 1273 K. The latter sample shows only two CO desorption states at approximately 400 K and 500 K similar to what was observed for Rh on ZrO<sub>2</sub> or Al<sub>2</sub>O<sub>3</sub> (Zafiridis and Gorte 1991). The CO<sub>2</sub> evolution is attributed to reactive lattice oxygen species located on ceria, which migrate from ceria to the Rh particles providing oxygen supply for the oxidation of CO. As shown in fig. 32, the correlation between the reactive oxygen species detected in TPD of CO and the CeO<sub>2</sub>-promoted CO oxidation is straightforward. No zero-order CO pressure dependence is found for the Rh/CeO<sub>2</sub> catalysts annealed at 1273 K. Similar effects of the annealing temperature of the CeO<sub>2</sub> support on CO oxidation kinetics were reported for Pt/CeO<sub>2</sub> (Jin et al. 1987) and recently also for Pd/CeO<sub>2</sub> (Bunluesin et al. 1997), which confirms the strict correlation between the CeO<sub>2</sub> promotional effects and the CeO<sub>2</sub> particle morphology. Keeping in mind that thermal sintering of the NM/CeO<sub>2</sub> also leads to loss of the NM/CeO<sub>2</sub> interactions as detected by H<sub>2</sub>-TPR (sect. 2.1.3), the present data confirm the key role of these interactions in modifying the CO oxidation kinetics.

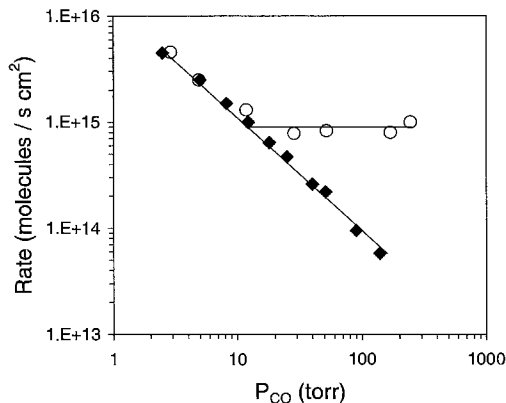
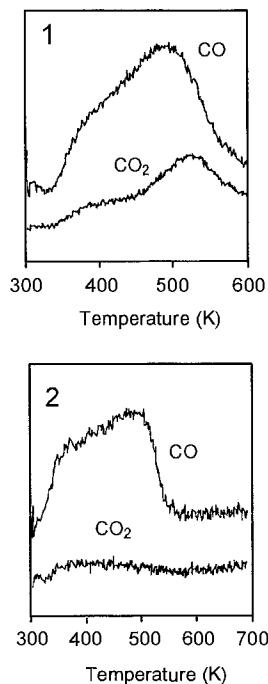


Fig. 32. Steady-state CO oxidation rates vs. CO partial pressure at 515 K on  $1.5 \times 10^{15}$  Rh/cm<sup>2</sup> films deposited on polycrystalline CeO<sub>2</sub> annealed at 970 K (circles) and 1270 K (squares). (Cordatos et al. 1996a.)

Fig. 31. CO TPD curves following adsorption of CO on  $1.5 \times 10^{15}$  Rh/cm<sup>2</sup> films deposited on polycrystalline CeO<sub>2</sub> annealed at (1) 970 K and (2) 1270 K. (Cordatos et al. 1996a.)

Also, under transient conditions, the kinetics of the CO oxidation are remarkably altered by the presence of CeO<sub>2</sub>. This is shown in fig. 33 where the effects of step-wise change of feed composition from CO to O<sub>2</sub> and *vice versa* are compared for Pt/Al<sub>2</sub>O<sub>3</sub> and Pt/CeO<sub>2</sub>-Al<sub>2</sub>O<sub>3</sub>. When the feed is switched from CO to O<sub>2</sub> on the Pt/Al<sub>2</sub>O<sub>3</sub>, adsorbed CO initially covers the Pt surface. This results in an immediate detection of O<sub>2</sub> at the outlet since no adsorption sites are available for O<sub>2</sub> adsorption and dissociation. Only when a significant fraction of CO has desorbed/reacted is the catalytic activity recovered, resulting in a minimum in the O<sub>2</sub> trace. When the feed is switched from O<sub>2</sub> to CO, CO<sub>2</sub> production is immediately started showing no inhibitory effects. Such a picture is fully compatible with a Langmuir-Hinshelwood mechanism, the Pt surface being preferentially covered by CO. Addition of CeO<sub>2</sub> to the catalyst considerably alters the reaction behaviour. The amount of CO<sub>2</sub> formed is higher compared to Pt/Al<sub>2</sub>O<sub>3</sub> and no inhibitory effect of CO pre-adsorption is observed.

Since equivalent CO chemisorption was found for the two catalysts (CO/Pt = 1.16 and 1.10 respectively for Pt/Al<sub>2</sub>O<sub>3</sub> and Pt/CeO<sub>2</sub>-Al<sub>2</sub>O<sub>3</sub>), a decrease of CO surface coverage for Pt/CeO<sub>2</sub>-Al<sub>2</sub>O<sub>3</sub> should be ruled out. The observed features can be explained by an additional supply of reactive oxygen species which is provided by the supported CeO<sub>2</sub> *via* a spillover-type mechanism. As discussed above, evidence for weakly bound oxygen species on CeO<sub>2</sub> which are responsible for CO oxidation were reported by Gorte

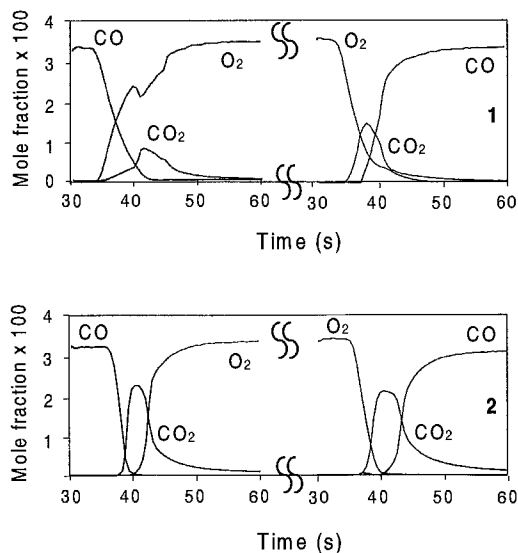


Fig. 33. Transient response to step-wise change of composition in the CO oxidation over (1) Pt/Al<sub>2</sub>O<sub>3</sub> and (2) Pt/CeO<sub>2</sub>-Al<sub>2</sub>O<sub>3</sub>. Left-hand side: CO/O<sub>2</sub> change; right-hand side: O<sub>2</sub>/CO change. Reaction conditions: 3.3% CO in He, 3.3% O<sub>2</sub> in He, reaction temperature 423 K. (Maunula et al. 1997.)

et al. for model NM-loaded and metal-free CeO<sub>2</sub> films (Putna et al. 1996, Zafiridis and Gorte 1993b).

CO conversion enhancements were neatly observed by Serre et al. (1993b) when a Pt/CeO<sub>2</sub>(14.5 wt%)-Al<sub>2</sub>O<sub>3</sub> catalyst was pre-reduced before the catalytic measurements, while pre-oxidation led to activity comparable to that of Pt/Al<sub>2</sub>O<sub>3</sub>. The authors claimed that the pre-oxidation was carried out under conditions where PtO<sub>2</sub> is unstable<sup>4</sup>, indicating that it is the Pt-CeO<sub>2</sub> interface which is affected by the oxidative/reductive pre-treatment (Serre et al. 1991, 1993a). CeO<sub>2</sub> is known to stabilise the oxidised state of platinum even at high temperatures due to a strong Pt-O-Ce interaction (Serre et al. 1991, 1993a, Summers and Ausen 1979, Brogan et al. 1994). This suggested that a highly reactive Pt-CeO<sub>2</sub> interface is generated by the reduction, which is responsible for the high CO oxidation activity, while pre-oxidation leads to an inactive PtO<sub>2</sub>-CeO<sub>2</sub> interface, leaving the bulk of the Pt in its metallic state as occurs in Pt/Al<sub>2</sub>O<sub>3</sub>. CO-TPD spectra support the evidence for the sensitivity of the NM/CeO<sub>2</sub> interaction to the pre-treatment conditions. In fact, as above quoted, Oh and Eickel (1988) did not find any appreciable effect of CeO<sub>2</sub> addition on CO-TPD from a non-pre-reduced Rh/Al<sub>2</sub>O<sub>3</sub> which showed a broad peak at 323 K and one or two other broad peaks at 500–515 K. In contrast, Lööf et al. (1991a) found on pre-reduced catalysts that after addition of CeO<sub>2</sub>, CO evolves in a minor peak at 350 K and a major one at 740 K, indicating that CO is strongly retained on the surface. Similar desorption features were observed on both Pt and Rh/CeO<sub>2</sub>, indicating that the nature of the NM-CeO<sub>2</sub> interface affects the CO bonding to the noble metal (Lööf et al. 1991a, Munuera et al. 1991).

<sup>4</sup> PtO<sub>2</sub> is stable in the range 673–823 K, approximately (Huizinga et al. 1984).

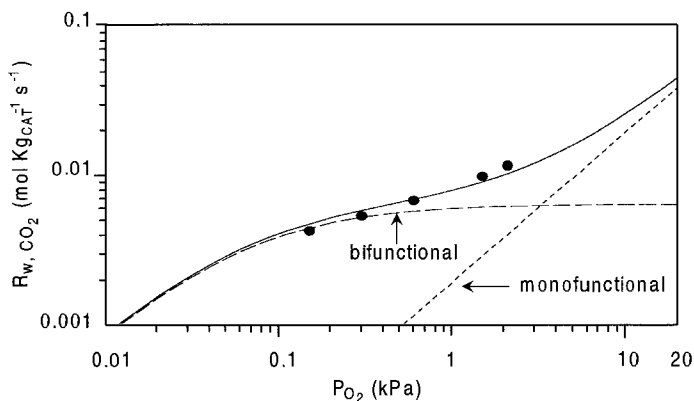


Fig. 34. Dependence of  $\text{CO}_2$  production rate on  $\text{O}_2$  pressure,  $p_{\text{CO}} = 0.30 \text{ kPa}$ ,  $p_{\text{H}_2\text{O}} = p_{\text{CO}_2} = 10 \text{ kPa}$ , reaction temperature 436 K. Circles indicate experimental rates, solid line is the sum of  $\text{CO}_2$  production rates calculated from mono-functional ( $\text{Pt}/\text{Al}_2\text{O}_3$ ) and bi-functional ( $\text{Pt}/\text{CeO}_2/\text{Al}_2\text{O}_3$ ) reaction paths. (Nibbelke et al. 1997.)

In summary, the effect of  $\text{CeO}_2$  addition upon the CO oxidation activity of the noble metals seems to be attributable essentially to the ability of  $\text{CeO}_2$  to provide reactive oxygen species to the noble metal, minimising the inhibition of  $\text{O}_2$  adsorption/dissociation by competitive CO adsorption. This effect is obviously observable under stoichiometric to net reducing conditions, while under net oxidising conditions the kinetics of the CO oxidation appear strictly related to those of the noble metal (Oh and Eickel 1988, 1990). In principle, it is difficult to evaluate to which extent these effects may be operative under real exhaust conditions. In fact, the above-described promoting effects of  $\text{CeO}_2$  addition to  $\text{NM}/\text{Al}_2\text{O}_3$  are strongly sensitive to the pre-treatment of the catalysts (Serre et al. 1993b, Summers and Aussen 1979, Yu Yao 1984).

However, recently a careful kinetic study of CO oxidation over a  $\text{Pt}/\text{CeO}_2/\text{Al}_2\text{O}_3$  catalyst carried out in the presence of  $\text{CO}_2$  and steam (10 kPa each) showed that for CO and  $\text{O}_2$  pressures ranging from 0.12 kPa to 4 kPa, the kinetics are conveniently described (fig. 34) by a kinetic model which includes mono- and bi-functional reaction paths (Nibbelke et al. 1997). The former reaction path could be described by the same rate expression as obtained for  $\text{Pt}/\text{Al}_2\text{O}_3$ , while the latter involves a reaction between adsorbed CO on the noble metal and oxygen from ceria.

**2.3.1.2. NO reduction.** Reduction of NO is an important topic within the framework of the reactions occurring in TWCs (table 2). This subject has been reviewed and the role of Rh discussed (Taylor 1984, 1993, Shelef and Graham 1994). Importantly, while the removal of the two other classes of pollutants, i.e. CO and HC occurs via an oxidation reaction, removal of NO requires that a simultaneous reduction occurs. Generally speaking, decomposition of NO to give  $\text{N}_2$  and  $\text{O}_2$  would certainly be the best option for the elimination of  $\text{NO}_x$  from the exhausts but unfortunately no catalyst has been reported so far which is sufficiently active and at the same time can withstand the



harsh conditions of the exhaust. Nor have the so called lean-DeNO<sub>x</sub> catalysts reached a sustainable activity to meet the legal requirements for the abatement of the NO<sub>x</sub> (Armor 1994, Shelef 1995). Accordingly, as discussed in sect. 1.3, the A/F ratio in the exhaust is kept close to the stoichiometric ratio to provide reductants necessary for NO<sub>x</sub> reduction. As outlined in table 2, it is generally considered that the reaction between CO and NO is responsible for the removal of the latter pollutant (Shelef and Graham 1994, Taylor 1984, 1993, Taylor and Schlatter 1980, Oh and Carpenter 1986), even if the contribution of the NO/H<sub>2</sub> reaction to NO removal should not be disregarded (Kobylinski and Taylor 1974). Under model conditions, using equal CO and H<sub>2</sub> concentrations (4.5 mol%), about 80% of the reacted NO was reduced by H<sub>2</sub> (Kobylinski and Taylor 1974). Despite this observation and the fact that the H<sub>2</sub> content in the exhausts is about one third of the CO content, excepting some early studies ((Taylor and Schlatter 1980) and references therein), this reaction has received scarce attention in the literature (Kobylinski and Taylor 1974, Hecker and Bell 1984, Sasahara et al. 1996, Dumpelmann et al. 1996, Maunula et al. 1997, deLange et al. 1995, Shinjoh et al. 1987, Otto and Yao 1980). To our knowledge, there is a limited number of reports in the open literature which specifically address the role of CeO<sub>2</sub> in the NO/H<sub>2</sub> reaction (Maunula et al. 1997, Dumpelmann et al. 1995). Surprisingly, there appear to be no conclusive studies of the NO/CO/H<sub>2</sub> reaction system despite the fact that all of these gases are present in the exhausts (Dumpelmann et al. 1995). Accordingly we will focus our attention mainly on the CO/NO reaction.

Rh has been generally added to TWCs due to its unique ability to efficiently promote NO dissociation which is believed to be rate determining (Taylor 1984, 1993, Oh and Eickel 1990, Hecker and Bell 1983), at least at low temperatures (Cho et al. 1989). An elementary step mechanism for NO reduction by using CO was suggested by Hecker and Bell (1983). Also, Cho (1992, 1994, 1996) performed a detailed kinetic investigation in order to elucidate the role of intermediates, including N<sub>2</sub>O, in the NO–CO reaction. Shelef and Graham (1994) noted that NO is adsorbed in a dinitrosyl mode on highly dispersed Rh and suggested that the unique efficiency of Rh to promote NO reduction is due to its ability to promote N pairing in adsorbed NO molecules prior to N–O bond rupture. In contrast, studies on model single Rh crystals suggested that recombination of adsorbed nitrogen atoms is the true reaction pathway, i.e. NO dissociation occurs first (Oh et al. 1986, Zhdanov and Kasemo 1996). Whatever are the details of the reaction mechanism on Rh, the overall reaction scheme for NO reduction by CO can be summarised as follows (Cho et al. 1989):



According to the reaction temperature the product selectivity shifts from N<sub>2</sub>O to N<sub>2</sub>, reaction (17) being favoured above approximately 573 K (Oh and Carpenter 1986, Hecker and Bell 1983, Kašpar et al. 1994, Cho et al. 1989). Note, however, that the reaction

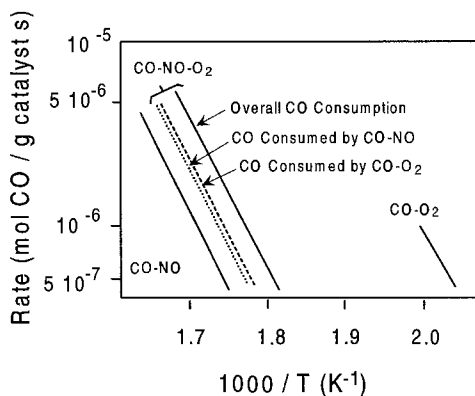


Fig. 35. Arrhenius plot for CO consumption rates in CO/O<sub>2</sub>, CO/NO and CO/O<sub>2</sub>/NO reactions over Rh(0.01 wt%)/Al<sub>2</sub>O<sub>3</sub>. Reactant concentration: 0.5 vol% each. (Oh and Carpenter 1986.)

temperature at which N<sub>2</sub>O formation is observed depends on the flow rate of the reactants, higher GHSV shifting the maximum of N<sub>2</sub>O formation to higher temperatures. This was explained in terms of N<sub>2</sub>O being an intermediate of the NO/CO reaction (Cho 1994).

The contribution of the above reaction network to the elimination of NO from the exhaust was confirmed by comparison of the CO/O<sub>2</sub>, CO/NO and CO/O<sub>2</sub>/NO kinetics (fig. 35).

The lines for the CO/O<sub>2</sub>/NO reaction lie close to those for the CO/NO reaction, indicating that the overall reaction kinetics are dominated by the kinetics of the CO/NO reaction rather than, as might be expected, those of the faster CO/O<sub>2</sub> reaction. Accordingly, apparent activation energies of 117, 197 and 175 kJ mol<sup>-1</sup> are found for the CO/O<sub>2</sub>, CO/NO and CO/O<sub>2</sub>/NO reactions, respectively (Oh et al. 1986). Further, the presence of even traces of NO prevents the occurrence of the CO/O<sub>2</sub> reaction until the extent of the NO/CO reaction becomes significant. This suggests that the onset of these reactions in the CO/O<sub>2</sub>/NO mixture is controlled by the same mechanistic step, i.e. blocking of the active sites by adsorbed molecular NO. Only when the reaction conditions become favourable to promote NO dissociation, are reactive sites made available for the oxidation of CO.

The effects of CeO<sub>2</sub> addition on the NO/CO kinetics over Rh/Al<sub>2</sub>O<sub>3</sub> were analysed by Oh (1990) and Cho et al. (1989) respectively under stationary and transient/feed-cycling conditions. Under stationary feed composition, addition of CeO<sub>2</sub> (9 wt%) to Rh/Al<sub>2</sub>O<sub>3</sub> suppressed the N<sub>2</sub>O formation in the range of temperatures 523–573 K in excess of CO (feed-stream: CO 1 vol% and NO 0.1 vol%) (Oh 1990). Conversely, under lean feed (CO 0.1 vol% and NO 0.5 vol%) no appreciable change of selectivity was induced by CeO<sub>2</sub> addition. Therefore, as already observed for CO oxidation (sect. 2.3.1.1), the kinetics of the CO/NO reactions are significantly affected by the CeO<sub>2</sub> addition.

Rh/CeO<sub>2</sub>Al<sub>2</sub>O<sub>3</sub> catalysts are characterised by a single apparent activation energy as long as sufficient CeO<sub>2</sub> is added (≥2 wt%) (Oh 1990). In contrast, Rh/Al<sub>2</sub>O<sub>3</sub> is characterised by two apparent activation energies above and below approximately 500 K (Pande and Bell 1986, Kašpar et al. 1994, Oh 1990, Oh and Eickel 1990, Hecker and

Table 9

Kinetic power-law parameters for NO reduction by CO over supported Rh catalysts (Oh 1990, Pande and Bell 1986)

Catalyst	$E_a$ (kJ mol <sup>-1</sup> )	NO consumption rate <sup>a</sup>			Reaction temperature (K)
		$m$	$n$	$k_{NO}$	
Rh/CeO <sub>2</sub> <sup>b</sup>	—	+0.54	-0.18	—	533
Rh/CeO <sub>2</sub> (9 wt%)/Al <sub>2</sub> O <sub>3</sub> <sup>b</sup>	75	+0.30	-0.19	—	533
Rh/Al <sub>2</sub> O <sub>3</sub> <sup>b</sup>	117	-0.14	+0.11	—	533
Rh/Al <sub>2</sub> O <sub>3</sub> <sup>c</sup>	101	-0.37	+0.03	$0.82 \times 10^{-3}$	483
Rh/SiO <sub>2</sub> <sup>c</sup>	140	-0.17	+0.08	$4.30 \times 10^{-3}$	483
Rh/MgO <sup>c</sup>	107	-0.15	+0.06	$2.92 \times 10^{-3}$	483
Rh/TiO <sub>2</sub> <sup>c</sup>	82	+0.09	-0.22	$7.75 \times 10^{-3}$	483
Rh/La <sub>2</sub> O <sub>3</sub> <sup>c</sup>	126	-0.16	+0.04	$4.75 \times 10^{-3}$	483

<sup>a</sup> Rate(TOF) =  $k_{NO} P_{NO}^m P_{CO}^n$ ;  $k_{NO} = \text{atm}^{-(m+n)} \text{s}^{-1}$ .<sup>b</sup> Data from Oh (1990); range of pressures:  $P_{CO} = 7.6\text{--}38$  torr,  $P_{NO} = 0.76\text{--}6.1$  torr.<sup>c</sup> Data from Pande and Bell (1986).

Bell 1983). This activation energy is significantly lower ( $75 \text{ kJ mol}^{-1}$ ) than the  $117$  and  $159 \text{ kJ mol}^{-1}$  observed on Rh/Al<sub>2</sub>O<sub>3</sub> below and above  $550 \text{ K}$ , respectively (Oh 1990). Except for a Rh/TiO<sub>2</sub> catalyst, apparent activation energies above  $100 \text{ kJ mol}^{-1}$  were observed also on other conventional supports (table 9). As shown in table 9, the presence of CeO<sub>2</sub> also alters the dependence of the reaction rate on the partial pressures of both CO and NO. With the exception of those containing CeO<sub>2</sub> and TiO<sub>2</sub> as supports, all the reported Rh catalysts show a zero- to weak positive-order dependence on the partial pressure of CO and a weak negative-order dependence on the NO pressure. This clearly indicates that both the reducible supports promote the NO/CO reaction. In fact, Rh/CeO<sub>2</sub>(9 wt%)/Al<sub>2</sub>O<sub>3</sub> showed reaction rates more than five times higher than those of Rh/Al<sub>2</sub>O<sub>3</sub> for  $T < 523 \text{ K}$  (Oh 1990).

Attempts to rationalise the above results have been made by comparing the TPD spectra of adsorbed CO and NO, respectively, on NM/Al<sub>2</sub>O<sub>3</sub> and NM/CeO<sub>2</sub> systems (Oh 1990, Löff et al. 1991a,b). Löff et al. showed that the desorption characteristics of CO are modified by the presence of ceria. The TPD spectra of Pt and Rh/Al<sub>2</sub>O<sub>3</sub> feature three overlapping peaks at approximately  $373 \text{ K}$ ,  $473 \text{ K}$  and  $623\text{--}673 \text{ K}$ , which is broadly in agreement with the TPD spectra previously reported by Oh (1990) and Pande and Bell (1986) for both Rh/Al<sub>2</sub>O<sub>3</sub> and Rh/CeO<sub>2</sub>(9 wt%)/Al<sub>2</sub>O<sub>3</sub>. However, while Oh did not find any significant modification of the TPD pattern in Rh/CeO<sub>2</sub>(2–9 wt%)/Al<sub>2</sub>O<sub>3</sub>, Löff et al. (1991a) found that either Pt, Rh or Pt–Rh supported on CeO<sub>2</sub>(20 wt%)/Al<sub>2</sub>O<sub>3</sub> featured a relatively small peak at  $353 \text{ K}$  and a large one at  $743 \text{ K}$ . The difference can be easily rationalised by the different experimental procedures employed. Reduction at  $900 \text{ K}$  was carried out before the CO adsorption by Löff et al. (1991a), with no pre-reduction in the other case. In fact, the pre-reduction strongly affects the adsorption properties of CeO<sub>2</sub>-based materials: On reduced (pure H<sub>2</sub>, 4 h,  $575 \text{ K}$ ) Rh/CeO<sub>2</sub>/SiO<sub>2</sub> and Rh/CeO<sub>2</sub>

a new infrared adsorption band due to strongly bound CO species, which exhibits a high thermal stability, was observed (Lavalley et al. 1990). This band was attributed to a NM-CO species with CO bound via oxygen to the reduced support (Lavalley et al. 1990). In fact, the amount of strongly adsorbed CO on CeO<sub>2</sub> increases with increasing degree of reduction (Li et al. 1993, Lavalley et al. 1990).

In contrast, in the absence of a strong pre-reduction, the CO adsorption appears unperturbed with respect to NM/Al<sub>2</sub>O<sub>3</sub> systems as found by Oh (1990). Since the re-oxidation of CeO<sub>2</sub> is easy, even in the presence of traces of NO (Padeste et al. 1994), it may be expected that under reaction conditions in the presence of NO and CO the catalyst would be in an oxidised state. Consequently, the modification of the kinetics of NO/CO reaction should be ascribed to the interaction of NO with the Rh/CeO<sub>2</sub>-based catalyst rather than that of CO. The interaction of NO with the NM/CeO<sub>2</sub> and CeO<sub>2</sub> moieties depends on the degree of pre-reduction of the system in a similar fashion as occurs for CO. One should also be aware that NO efficiently oxidises the reduced CeO<sub>2-x</sub> moieties according to reactions (2) and (3) (sect. 2.1) (Padeste et al. 1994, Kim 1982). After reduction up to 773 K, a Rh/CeO<sub>2-x</sub> catalyst decomposed NO at room temperature (rt) producing first N<sub>2</sub> as the main reaction product at the initial stage of reaction (Padeste et al. 1994). As the run progressed, N<sub>2</sub> and N<sub>2</sub>O were produced simultaneously. Most of the catalyst oxidation occurred at rt, however, some residual reaction occurred also at about 400–450 K. Interaction of NO with CeO<sub>2</sub> showed that reduction in H<sub>2</sub> at 723 K increased the NO dissociation and hence N<sub>2</sub> formation compared to a thermal evacuation (Niwa et al. 1982). The oxygen evolved is incorporated into the CeO<sub>2</sub>.

A further consideration is that a variety of nitrogen-derived species were detected on evacuated/reduced surfaces: nitrites, nitrates, and hyponitrites (Niwa et al. 1982, Martinez-Arias et al. 1995). The latter species has been proposed as an intermediate leading to N<sub>2</sub>O and N<sub>2</sub> formation (Niwa et al. 1982, Martinez-Arias et al. 1995).

The surface O<sup>2-</sup> species originated by breaking the N–O bond might constitute active oxygen species contributing to the formation of NO<sub>2</sub><sup>-</sup> and NO<sub>3</sub><sup>-</sup> species.

As far as the preferential formation of N<sub>2</sub> vs. N<sub>2</sub>O is concerned, it should be noted that N<sub>2</sub> formation has been detected on HSA CeO<sub>2</sub> after a deep reduction, while mild reduction treatments lead preferentially to N<sub>2</sub>O formation (Niwa et al. 1982). On the basis of kinetic studies it has been suggested that breaking of N–O bonds in the adsorbed N<sub>2</sub>O<sub>2</sub><sup>2-</sup> is the rate-limiting step for NO decomposition (Martinez-Arias et al. 1995). In the presence of a significant degree of reduction in the bulk, an oxygen vacancy gradient from the bulk to the surface would be established upon NO adsorption on the surface. This provides an extra driving force for an efficient NO decomposition, as has been proposed for CO<sub>2</sub> dissociation on reduced Rh/CeO<sub>2</sub> catalysts (Trovarelli et al. 1995, de Leitenburg et al. 1997). Refilling of the oxygen vacancies in the bulk annihilates this additional driving force for NO dissociation and reduction. At this point mainly formation of N<sub>2</sub>O is favoured. Further, the reaction of NO initially occurs with elimination of associated surface vacancies which are generated by high temperature outgassing (*vide infra*), while the isolated vacancies are affected only later (Martinez-Arias et al. 1995). Interestingly,

the ability to reductively activate NO at low temperatures depends on the ability of CeO<sub>2</sub> to form these associated vacancy sites. They exist on CeO<sub>2</sub> but their generation is more difficult on CeO<sub>2</sub>/Al<sub>2</sub>O<sub>3</sub> supports where CeO<sub>2</sub> is well dispersed on the alumina substrate (Padeste et al. 1993). In summary, the interaction of NO with CeO<sub>2</sub> (CeO<sub>2</sub>/Al<sub>2</sub>O<sub>3</sub>) leads respectively to its disproportionation and, at the same time, the formation of hyponitrite species. The decomposition of the latter species to give the reduction products is strongly dependent on the presence of oxygen vacancies; pre-oxidation by O<sub>2</sub> inhibiting the decomposition process.

Accordingly, the addition of CeO<sub>2</sub> to NM/Al<sub>2</sub>O<sub>3</sub> (or substitution of Al<sub>2</sub>O<sub>3</sub> with CeO<sub>2</sub>) strongly affects the interaction of these catalysts with NO. This has been successfully probed using the TPD technique (Cordatos and Gorte 1996, Valden et al. 1996, Löff et al. 1991a,b, Altman and Gorte 1988). Let us now examine the NO desorption from Rh catalysts. We will first discuss the TPD spectra of the Rh on Al<sub>2</sub>O<sub>3</sub> (Kašpar et al. 1994, Pande and Bell 1986, Altman and Gorte 1988, Löff et al. 1991a,b) and CeO<sub>2</sub> (Oh 1990, Löff et al. 1991a,b) due to the relevance of this metal to NO dissociation/reduction. Typically the TPD spectra of NO adsorbed on dispersed Rh/Al<sub>2</sub>O<sub>3</sub> catalysts feature desorption peaks due to NO, N<sub>2</sub>O and N<sub>2</sub>. Nitrogen evolution in the TPD of pre-adsorbed NO shows two peaks: the β<sub>1</sub> peak centred at about 450–480 K and the β<sub>2</sub> peak centred at about 550–650 K, attributed respectively to the following processes (Campbell and White 1978, Chin and Bell 1983, Root et al. 1983):



where \* denotes a Rh adsorption site.

The temperature of the β<sub>2</sub> peak depends on the surface coverage (Campbell and White 1978, Chin and Bell 1983, Root et al. 1983), which is consistent with a second-order desorption process. On increasing surface coverage, the β<sub>2</sub> peak fills up first and moves towards lower temperatures. At high coverage, most of the N<sub>2</sub> evolves as β<sub>1</sub>, β<sub>2</sub> being almost negligible (Chin and Bell 1983). In the presence of free re-adsorption, a single N<sub>2</sub> desorption peak was observed which was shifted to high temperatures (Kašpar et al. 1994).

Both the NO and N<sub>2</sub>O desorption features are affected to a minor extent by the Rh particle morphology. At variance, the N<sub>2</sub> desorption is strongly effected by the Rh particle size: larger particles favour N<sub>2</sub> formation and make the low-temperature N<sub>2</sub> desorption features prominent (Altman and Gorte 1988, Kašpar et al. 1994). This is in agreement with the suggestion that NO dissociation is sterically demanding and requires a certain number of adjacent Rh sites (Campbell and White 1978, Villarubia and Ho 1987, Oh et al. 1986). Similarly, a dependence on particle size of the NO desorption features was also observed for Pt and Pd model catalysts supported on α-Al<sub>2</sub>O<sub>3</sub> (0001) (Altman and Gorte 1988, 1989, Cordatos et al. 1995). On Pt/α-Al<sub>2</sub>O<sub>3</sub>(0001), the fraction of pre-adsorbed NO which reacted depended on particle size: about 85% of adsorbed NO dissociated on Pt-film which decreased to 45% for Pt particles of about 1.7 nm. This is

consistent with the above quoted structure sensitivity of the NO dissociation. In contrast, on Pd/ $\alpha$ -Al<sub>2</sub>O<sub>3</sub>(0001), as the metal particle size decreased, a larger fraction of adsorbed NO reacted (Cordatos et al. 1995). In both cases, however, in CO/NO co-desorption studies, formation of CO<sub>2</sub> was observed at the same temperature at which N<sub>2</sub> was formed in TPD measurements of NO (Cordatos et al. 1995, Xu and Goodman 1994). In contrast, CO<sub>2</sub> formation was observed on Rh/ $\alpha$ -Al<sub>2</sub>O<sub>3</sub>(0001) at temperatures lower than N<sub>2</sub> desorption, suggesting that rate of N<sub>2</sub> formation in the TPD is limited by NO dissociation on Pd and Pt, and by N<sub>2</sub> recombination on Rh (Cordatos et al. 1995, Altman and Gorte 1988, 1989).

The interaction of NO with model NM/CeO<sub>2</sub> systems shows different characteristics. Similarly to the TPD of CO discussed in sect. 2.3.1.1, the morphology of the ceria films plays a fundamental role in the NO desorption. Annealing at high temperatures which leads to ordered CeO<sub>2</sub> structures, brings to NO and CO desorption characteristics which are equal to those obtained on both oxidised Al foil and  $\alpha$ -Al<sub>2</sub>O<sub>3</sub> (0001) (Cordatos and Gorte 1996, Cordatos et al. 1996a, Zafirir and Gorte 1992). However, when highly disordered and presumably defective ceria films are investigated, the NO TPD appear strongly affected by CeO<sub>2</sub> (Cordatos and Gorte 1996). Under similar experimental conditions, desorption of NO from a Pd/CeO<sub>2</sub> model catalyst produced prevalently N<sub>2</sub>, while the TPD of NO from Pd/ $\alpha$ -Al<sub>2</sub>O<sub>3</sub>(0001) mostly showed evolution of NO and some dissociation as detected by production of N<sub>2</sub>O and N<sub>2</sub> (Cordatos et al. 1995, Cordatos and Gorte 1996). Further, a mild reduction of Pd/CeO<sub>2</sub> by CO (10 min, 650 K,  $p_{\text{CO}} = 1 \times 10^{-7}$  torr) strongly increased the intensity of the N<sub>2</sub> signal due to a strong increase of the overall amount of nitrogen-derived species on the catalyst. The sum of desorbed amounts of N<sub>2</sub>, N<sub>2</sub>O and NO were 0.8 and 3.5 respectively on the fresh and reduced catalysts (Cordatos and Gorte 1996) (fig. 36).

The increase of NO adsorption upon reduction of Pd/CeO<sub>2</sub> is clearly associated with the ability of reduced CeO<sub>2-x</sub> moieties to reductively activate the X–O bonds (X = C, N, H), except for CO which does not re-oxidise surface Ce<sup>3+</sup> sites (Otsuka et al. 1983, Ranga Rao et al. 1994, Trovarelli et al. 1992, Niwa et al. 1982, Arai et al. 1993). Accordingly, a reduced Rh/TiO<sub>2</sub> catalyst showed a significant increase of NO uptake compared to Rh/Al<sub>2</sub>O<sub>3</sub> or Rh/SiO<sub>2</sub> (Pande and Bell 1986). It is worth noting that the promotion of NO dissociation reported by Cordatos and Gorte (1996) was observed on both reduced and oxidised catalyst indicating that in both cases CeO<sub>2</sub> is prone to receive oxygen species, presumably via a spillover mechanism. The ability of the support to receive oxygen is higher as the degree of reduction of ceria is deeper. Accordingly, it has been shown on high surface area NN/CeO<sub>2</sub>/Al<sub>2</sub>O<sub>3</sub> (NM = Rh, Pt) catalysts that when oxygen is deposited on the noble metal and, consequently, on the reduced ceria by successive NO TPD runs, the NO dissociation is progressively inhibited (Löf et al. 1991a). Notably, the accumulation of oxygen *via* the reaction



leads to an initial inhibition of the low-temperature NO dissociation path ( $\beta_1$ ). The high-temperature  $\beta_2$  path is affected only in subsequent runs (fig. 37).

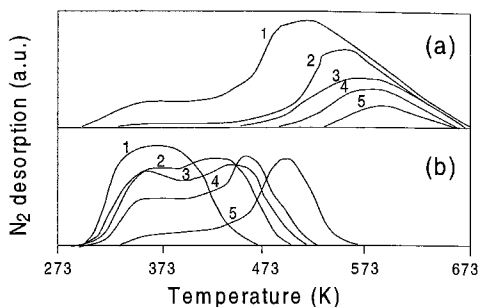
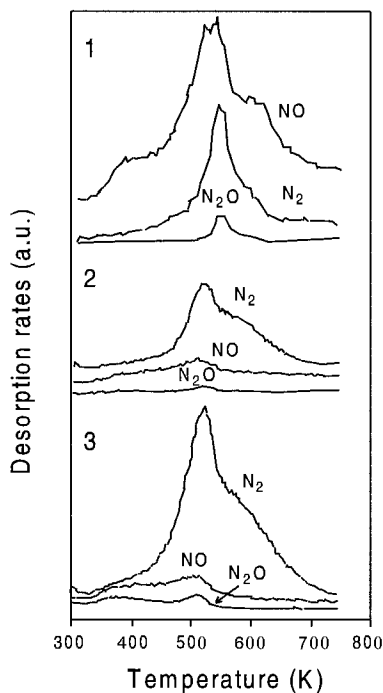


Fig. 37.  $\text{N}_2$  evolution in successive NO-TPD runs on initially reduced ( $\text{H}_2$  4% in Ar, 900 K, 5 min) (a)  $\text{Rh}/\text{Al}_2\text{O}_3$  and (b)  $\text{Rh}/\text{CeO}_2\text{-Al}_2\text{O}_3$ . (Löff et al. 1991a.)

Fig. 36. TPD spectra following NO adsorption at rt on (1)  $\text{Pd}/\alpha\text{-Al}_2\text{O}_3$  (0001), (2) fresh and (3) reduced Pd films on  $\text{CeO}_2$ . (Cordatos et al. 1995, Cordatos and Gorte 1996.)

The observation that  $\text{CeO}_2$  promotes NO dissociation at low temperatures (Oh 1990, Löff et al. 1991a,b) is consistent with the decrease of activation energy for the NO/CO reaction induced by  $\text{CeO}_2$ . Further, the oxygen-inhibiting effect on NO decomposition is much slower when ceria is added to the catalyst. In fact, more oxygen doses are necessary to block the NO dissociation (fig. 37). In summary,  $\text{CeO}_2$  appears to promote the NO/CO reaction by increasing the rate of NO dissociation. The promotional effect is affected by the pre-treatment/degree of reduction of ceria. On a pre-reduced catalyst,  $\text{CeO}_2$  may directly participate in the NO reduction via a redox-type mechanism. In fact, NO adsorption on the support is enhanced. Differently, on oxidised catalysts the ceria may enhance the activity by acting as an oxygen acceptor *via* oxygen spilling from the metal over the support.

The ability of  $\text{CeO}_2$  to affect the NO/CO reaction over Rh was clearly established under cycling conditions (Cho et al. 1989). When, under cycling conditions, the reactant flow is switched from CO to NO over the  $\text{Rh}/\text{Al}_2\text{O}_3$  catalyst, the NO decomposition activity starts to decay after 5–6 s into the NO half-cycle, yielding a time-averaged NO conversion of 76%. Using the  $\text{Rh}/\text{CeO}_2$  catalyst, despite comparable metal loading and dispersions ( $\text{CO}/\text{Rh} = 0.54$  and 0.47 respectively for  $\text{Rh}/\text{Al}_2\text{O}_3$  and  $\text{Rh}/\text{CeO}_2$ ), the decay of NO starts at 7 s, yielding a time-averaged NO conversion of 94% (fig. 38; Cho et al. 1989). This enhancement of conversion was attributed to the large oxygen storage capacity of  $\text{CeO}_2$  (Cho et al. 1989). Note that these experiments were carried out above the catalyst light-

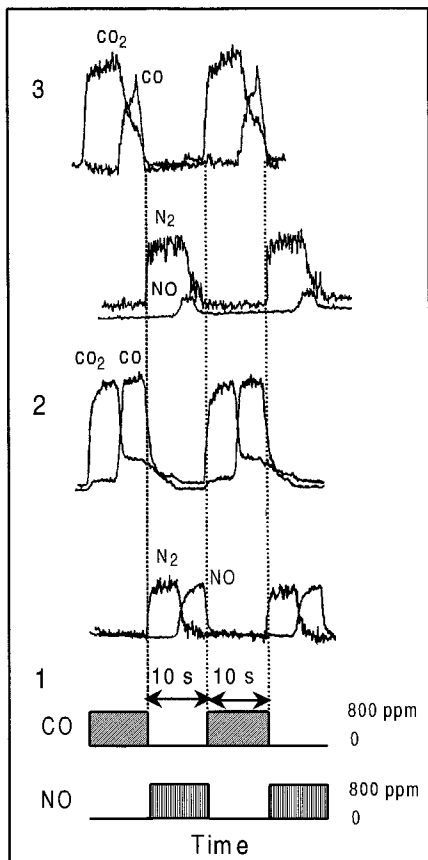


Fig. 38. Time variations of (1) reactor inlet and (2,3) reactor outlet concentrations at 773 K during symmetric cycling operations over (2) Rh(0.09 wt%)/Al<sub>2</sub>O<sub>3</sub> and (3) Rh(0.04 wt%)/CeO<sub>2</sub>. CO=NO=800 ppm in He, GHSV=82 000 h<sup>-1</sup>, *p*=1 atm). (Cho et al. 1989.)

off temperature where, according to Cho et al. (1989), the reaction rate is limited by the scavenging of surface oxygen accumulated on the metal by CO. This suggests that the increase of the NO conversion could be attributed rather to an increased efficiency in depleting the oxygen from Rh particles *via* the Rh–CeO<sub>2</sub> interface, as already proposed for CO oxidation, than to a direct participation of CeO<sub>2</sub> in NO decomposition.

The higher efficiency of pre-reduced CeO<sub>2</sub>-based catalysts in the reduction of NO compared to pre-oxidised ones was confirmed by step-wise H<sub>2</sub>/NO and NO/H<sub>2</sub> exchange experiments (Maunula et al. 1997). When the flow of reactants over a Rh/CeO<sub>2</sub>/Al<sub>2</sub>O<sub>3</sub> was switched from H<sub>2</sub> (1% in He) to NO (1% in He) and *vice versa*, in both cases an instantaneous N<sub>2</sub> production was detected. However, the amount of N<sub>2</sub> produced in the switch from H<sub>2</sub> to NO was at least twice that observed with the exchange order inverted.

Finally, whereas its relevance to three-way catalysis is to be ascertained, recently an interesting effect of CeO<sub>2</sub> addition to Pt/Al<sub>2</sub>O<sub>3</sub> was reported (Mergler and Nieuwenhuys 1996): under net reducing conditions (CO:NO=3:1 in He, concentrations <4% – not



specified), a Pt/Al<sub>2</sub>O<sub>3</sub> catalyst quickly deactivated on stream even at 673 K. On the contrary, Pt/CeO<sub>2</sub>/Al<sub>2</sub>O<sub>3</sub> showed oscillations in the reaction rates with a period of 18 min at this temperature. Apparently, the addition of ceria results in oscillatory behaviour and maintains the catalytic activity. The oscillatory behaviour is attributed to the build-up of a stable Pt<sup>n+</sup>-CO species responsible for the deactivation of the catalyst. This species is slowly removed by reaction with adsorbed O generated by the NO dissociation on CeO<sub>2-x</sub> or by the lattice oxygen of CeO<sub>2-x</sub>, thereby accounting for the lack of oscillatory phenomena on Pt/Al<sub>2</sub>O<sub>3</sub>.

### 2.3.2. Water-gas shift reaction

The water-gas shift (WGS) reaction is an important reaction in the framework of exhaust abatement since it can significantly promote the catalytic removal of CO by its reaction with H<sub>2</sub>O. Supported Group-VIII metals effectively catalyse this reaction, see for instance Taylor et al. (1974) and Grenoble et al. (1981). Schlatter and Mitchell (1980) clearly demonstrated that the WGS reaction induces a significant transient enhancement of the CO conversion during changes between rich and lean exhaust stoichiometry. During their transient experiments on a Pt-Rh/CeO<sub>2</sub>/Al<sub>2</sub>O<sub>3</sub> system, formation of equimolar amounts of CO<sub>2</sub> and H<sub>2</sub> has been observed (fig. 39), while no additional CO conversion was

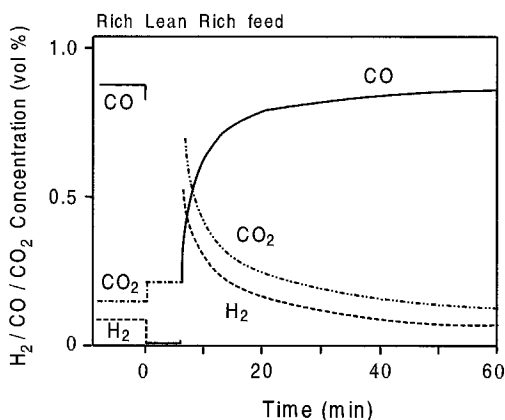


Fig. 39. CO<sub>2</sub> and H<sub>2</sub> production during a step change experiment at 823 K on 0.05 wt% Pt-0.005 wt% Rh/CeO<sub>2</sub>(0.7 wt%)/Al<sub>2</sub>O<sub>3</sub>, GHSV = 104 000 h<sup>-1</sup>; rich feed: 1% CO, 10% H<sub>2</sub>O, N<sub>2</sub> balance; lean feed: 0.2% CO, 1% O<sub>2</sub>, 10% H<sub>2</sub>O, N<sub>2</sub> balance. (Schlatter and Mitchell 1980.)

measured in the absence of water. Although their time scale (several minutes) during the step-change experiments was far from that of a real TWC, they clearly pointed out a potential additional pathway for CO conversion, which has induced a strong research interest towards additives/components for TWCs which improve the WGS reaction.

It has been reported that the support has a major effect on the activity for the WGS reaction. Grenoble et al. (1981) suggested that the metal activates carbon monoxide whereas support sites are the principal sites for water activation. They suggest that the interaction of water molecules with the support can occur both through a dissociative

adsorption (reaction 21) or a non-dissociative adsorption (reaction 22), depending on the reaction temperature, degree of dehydration and relative amount of Lewis acid centres:



They proposed formic acid as an intermediate since its decomposition involves both the product and the reactant of the WGS reaction. The formation of formic acid can be schematically represented as follows:



On the basis of this hypothesis, they suggested that the effects of support might be related to its acidity. The lower activity of the  $\text{SiO}_2$  support compared to that of  $\text{Al}_2\text{O}_3$  has therefore been interpreted in terms of a minor presence of Lewis sites.

It has been observed that by doping alumina with various alkali metals it is possible to promote the WGS reaction (Amenomiya and Pleizier 1982). Certainly,  $\text{CeO}_2$  is the most studied additive to TWCs, not only for its beneficial effects on the OSC, as already discussed, but also for its role in improving the WGS reaction. Partially reduced ceria decomposes water, producing hydrogen (Otsuka et al. 1983). In fact, the  $\Delta G$  for the reaction  $\text{Ce}_2\text{O}_3 + \text{H}_2\text{O} = 2\text{CeO}_2 + \text{H}_2$  is negative at the working temperature of such catalysts. Shido and Iwasawa (1992) studied the reaction mechanism of the WGS reaction over  $\text{CeO}_2$  by FTIR. They found that, on partially reduced ceria, CO interacts with terminal OH groups to form bridge formates, which convert to bidentate formates. The presence of water stabilises bidentate formates on  $\text{CeO}_2$  and therefore inhibits the backward decomposition of the formates to  $\text{OH} + \text{CO}$ . In the presence of water, the activation energy for the backward decomposition increases more than that for the forward decomposition, favouring the WGS reaction. The authors suggested that the bond scission of both C–H (formate) and O–H (hydroxyl) be involved in the transition of the rate-determining step of the WGS reaction. They proposed a mechanism in which the hydrogen of the C–H (formate) can interact with the hydrogen of the bridged OH groups to produce  $\text{H}_2$  and unidentate carbonate. Finally water molecules favour the decomposition of unidentate carbonate to  $\text{CO}_2$ , regenerating surface OH groups. In a following paper (Shido and Iwasawa 1993) they extended their investigation to the  $\text{Rh}/\text{CeO}_2$  system. By addition of a small amount of Rh (0.2%) to ceria, the WGS reaction rate increased dramatically, especially in the presence of water. They suggested that the mechanism proposed for the pure support is operative also for  $\text{Rh}/\text{CeO}_2$ . However, Rh promotes formation and decomposition of bidentate formates on  $\text{Rh}/\text{CeO}_2$  compared to  $\text{CeO}_2$ , as indicated by a lower activation energy and decomposition temperature. This effect has been correlated with the easier formation of oxygen defects in  $\text{Rh}/\text{CeO}_2$  with respect to  $\text{CeO}_2$ . In the presence of water the forward decomposition rate of formates on  $\text{Rh}/\text{CeO}_2$  increases and the relative activation energy decreases. From isotopic investigation, they suggested that the rate-determining step of the WGS reaction on  $\text{Rh}/\text{CeO}_2$  is the dissociation of the

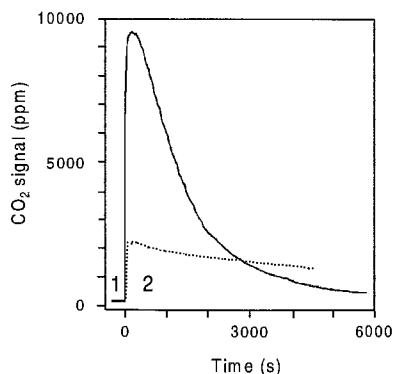


Fig. 40. (1) Steady-state and (2) transient water-gas shift activity at 723 K on 0.003 wt% Rh/ $\text{Al}_2\text{O}_3$  (dotted curve) and 0.003 wt% Rh/ $\text{CeO}_2$ (1.02 wt%)/ $\text{Al}_2\text{O}_3$  (solid curve) following an oxidation step in 1%  $\text{O}_2$  for 15 min. GHSV =  $100\,000\text{ h}^{-1}$ , 1% CO, 10%  $\text{H}_2\text{O}$ ,  $\text{N}_2$  balance; lean treatment: 1%  $\text{O}_2$ , 10%  $\text{H}_2\text{O}$ ,  $\text{N}_2$  balance. (Weibel et al. 1991.)

C–H bond of the bidentate formate. In contrast, a parallel experiment suggested that the activation of both the C–H bond of formate and the O–H bond of an adjacent bridge OH group in the transition state are necessary on pure  $\text{CeO}_2$ . This indicates that the presence of rhodium modifies the local electronic structure and the surface morphology around the active site (Martinez-Arias et al. 1997). It was suggested that the charge rearrangement and local reconstruction of the Ce–O sites due to the presence of Rh favours the activation of the C–H bond of the formate, leading to low activation energy.

Weibel et al. (1991) observed that, following a switch from a lean to a rich reaction mixture, Rh/ $\text{CeO}_2$ / $\text{Al}_2\text{O}_3$  shows a significantly higher transient WGS reaction activity compared to Rh/ $\text{Al}_2\text{O}_3$  (fig. 40). However, it should be noted that the activity decreases more rapidly when ceria is present. Remarkable is the fact that these significant changes are observed upon adding only 1.02 wt% of ceria. To account for the enhancement in the WGS reaction activity after  $\text{CeO}_2$  addition, they proposed a reaction mechanism based on the formation of an active Rh-oxide catalyst. It has been suggested that the interaction between Rh and Ce regulate the formation of the active sites, which are deactivated by adsorption of water and formation of hydroxyl groups strongly bonded to the active centre.

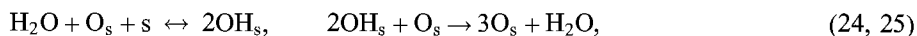
Herz and Sell (1985) mainly associated the increase of CO conversion for Pt/ $\text{CeO}_2$ / $\text{Al}_2\text{O}_3$  catalyst with the oxygen storage capacity of ceria, although their results do not completely exclude participation of the WGS reaction. They observed a different response for the Pt/Rh/ $\text{CeO}_2$ / $\text{Al}_2\text{O}_3$  catalyst, which suggests that the greater enhancement of CO conversion should be attributed to the WGS reaction.

Zafiridis and Gorte (1993a,b) suggested a different mechanism to account for the transient enhancement of the WGS reaction in the case of Rh/ $\text{CeO}_2$ . They have found evidence that oxygen can migrate from  $\text{CeO}_2$  onto supported Rh and there react with CO to form  $\text{CO}_2$  at relatively low temperature. The catalytic cycle can be completed by the re-oxidation of the partially reduced ceria by water. An interaction similar to that between ceria and Rh was not found for Pt/ $\text{CeO}_2$  catalysts, providing an explanation for the poor WGS reaction activity they observed on a Pt/ $\text{CeO}_2$  catalyst. However,  $\text{CO}_2$  formation was reported in a TPD study of CO on a high-surface-area Pt/ $\text{CeO}_2$  catalyst (Jin et al. 1987), suggesting

that oxygen migration can occur from ceria to Pt, but the rate might be lower than on Rh/CeO<sub>2</sub>.

There are some additional factors that must be considered in order to interpret the data concerning the WGS reaction on noble-metal-loaded ceria-containing materials: the redox properties of ceria strongly depend on its structure and surface; they are significantly effected by chemical/physical treatments; the loading and the dispersion of the supported metal have a great influence on type and intensity of the interactions between metal and support. On this basis it seems reasonable that the WGS reaction on noble metals supported on ceria or CeO<sub>2</sub>/Al<sub>2</sub>O<sub>3</sub> occurs through a bifunctional mechanism in which CO adsorbed on the noble metal is oxidised by ceria, which can then be re-oxidised by water. Differences in activity can be rationalised in terms of differences in the reducibility of ceria due to different crystallite size.

A detailed kinetic study of the CO oxidation over Pt/Al<sub>2</sub>O<sub>3</sub> and Pt/Rh/CeO<sub>2</sub>/Al<sub>2</sub>O<sub>3</sub> has been published recently by Nibbelke et al. (1997). They observed that the presence of steam significantly enhances the rate of CO oxidation, although in their reaction conditions the contribution of the WGS reaction to the conversion of CO seems to be negligible. They proposed the existence of two reaction paths to explain the kinetic data. The first one is catalysed by the metal only, while the second one involves a reaction between CO adsorbed on the metal and oxygen from ceria at the noble metal/ceria interface. In the case of Rh/Pt/CeO<sub>2</sub>/Al<sub>2</sub>O<sub>3</sub>, the accelerating effect of steam on the CO reaction rate was explained in terms of an increased rate of dissociation of molecular oxygen adsorbed on ceria, according to the following reaction steps:



where *s* is an adsorption site. The promoting effect of steam on the rate of CO oxidation over Pt/Al<sub>2</sub>O<sub>3</sub> has not been elucidated. The authors, however, suggested that water might affect the adsorption equilibrium of CO, resulting in a decreased CO inhibition, or it might increase oxygen adsorption on the Al<sub>2</sub>O<sub>3</sub> support in an bifunctional mechanism analogous to that proposed for the ceria-containing system.

A comparison between the experimental data for CO oxidation on Rh/Pt/CeO<sub>2</sub>/Al<sub>2</sub>O<sub>3</sub> and the modelling using both the proposed bifunctional mechanism and the metal-only mechanism is reported in fig. 34 (compare sect. 2.3.1.1). Although the authors did not distinguish between the specific activities of Pt and Rh, a satisfactory understanding of the kinetics of CO oxidation emerged.

Löff et al. (1991b) also pointed out the importance of considering the effective contribution of the WGS reaction in the real exhaust environment. They showed that the presence of traces of SO<sub>2</sub> has detrimental effects on the WGS reaction activity.

All these considerations suggest that the presence of CeO<sub>2</sub> in the NM/Al<sub>2</sub>O<sub>3</sub> catalysts favourably contributes to the removal of CO via the WGS reaction, CeO<sub>2</sub> being active itself. A comparison of the activities of Pt, Rh and mixed Pt–Rh catalysts in the presence of CeO<sub>2</sub> was reported by Barbier and Duprez (1993) (fig. 41). The presence of CeO<sub>2</sub> clearly promotes the effectiveness of the NM catalyst as the light-off temperatures always

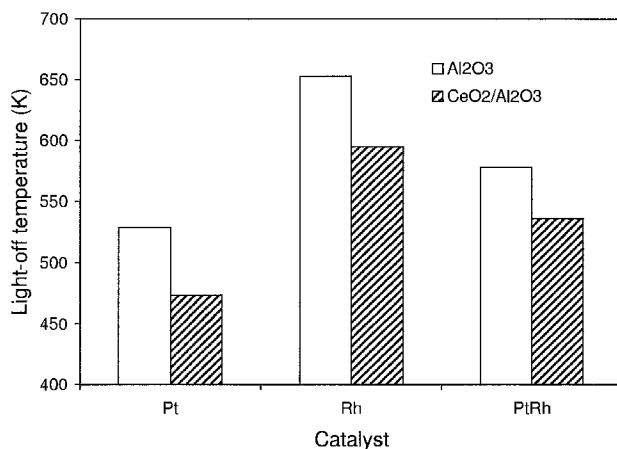


Fig. 41. Light-off temperatures for WGS reaction over  $\text{Al}_2\text{O}_3$ - and  $\text{CeO}_2/\text{Al}_2\text{O}_3$ -supported Pt, Rh, and PtRh catalysts. GHSV =  $250\,000\text{ h}^{-1}$ , feed 0.8% CO, 10%  $\text{H}_2\text{O}$  in  $\text{N}_2$ , catalysts: 1 wt% Pt/ $\text{Al}_2\text{O}_3$ , 0.2 wt% Rh/ $\text{Al}_2\text{O}_3$ , 1 wt% Pt–0.2 wt% Rh/ $\text{Al}_2\text{O}_3$ , 1 wt% Pt/ $\text{CeO}_2$ (12 wt%)/ $\text{Al}_2\text{O}_3$ , 0.2 wt% Rh/ $\text{CeO}_2$ (12 wt%)/ $\text{Al}_2\text{O}_3$ , 1 wt% Pt–0.2 wt% Rh/ $\text{CeO}_2$ (12 wt%)/ $\text{Al}_2\text{O}_3$ ,  $\text{CeO}_2$ (12 wt%)/ $\text{Al}_2\text{O}_3$ . (Barbier and Duprez 1993.)

decrease in the presence of  $\text{CeO}_2$  (fig. 41). Although the Pt catalysts appear more active than both the Rh and bimetallic ones, no direct comparison of the specific activities can be drawn from the light-off temperatures due to the fact that different metal loadings were employed. Cho (1991) clearly indicated that light-off temperatures can be taken as an indication of the specific activity of supported catalysts as long as equal areas of exposed metal are employed. This was confirmed in a study of the effects of metal dispersion in the NO/CO reaction (Kašpar et al. 1994). Nevertheless, the fact that addition of Rh to the Pt catalysts results in a decrease of activity suggests that Pt is more active compared to the Rh catalyst. The relative decrease of light-off temperatures upon  $\text{CeO}_2$  addition is 11%, 9% and 7% for Pt, Rh and PtRh catalysts, respectively. This also indicates that the Pt/ $\text{CeO}_2$  combination is more effective than the other ones in promoting the WGS reaction.

Comparisons of the specific activities of the Pt and Rh catalysts and the effects of  $\text{CeO}_2$  addition on the WGS reaction are reported in table 10. Under the reaction conditions employed, the activity of both Pt/ $\text{Al}_2\text{O}_3$  and Rh/ $\text{Al}_2\text{O}_3$  is approximately doubled upon addition of  $\text{CeO}_2$ .

Addition of  $\text{O}_2$  to the reaction feed-stream strongly inhibits the reaction rates. However, the effect of  $\text{CeO}_2$  is remarkable: there is a 2000–3000-fold drop of activity for the  $\text{Al}_2\text{O}_3$  supported catalysts, which decreases to less than 50-fold in the presence of  $\text{CeO}_2$ .

Bearing in mind that most of the above findings were obtained under stationary feeds, it seems reasonable to conclude that  $\text{CeO}_2$  effectively improves CO removal via the WGS reaction, however, under practical applications such effects are only significant above 600 K and under rich conditions, where  $\text{O}_2$  competition for CO is minimised.

Table 10  
Activation energies and turnover frequencies for Al<sub>2</sub>O<sub>3</sub>- and CeO<sub>2</sub>/Al<sub>2</sub>O<sub>3</sub>-supported Pt and Rh catalysts

Catalyst <sup>a</sup>	Inlet pressures (kPa)			$E_a$ (kJ mol <sup>-1</sup> )	$N_t$ <sup>b</sup>
	CO	H <sub>2</sub> O	O <sub>2</sub>		
Pt/Al <sub>2</sub> O <sub>3</sub>	0.8	10		54	680
Pt/CeO <sub>2</sub> /Al <sub>2</sub> O <sub>3</sub>	0.8	10			1450
Rh/Al <sub>2</sub> O <sub>3</sub>	0.8	10		80	16
Rh/CeO <sub>2</sub> /Al <sub>2</sub> O <sub>3</sub>	0.8	10		85	36
Pt/Al <sub>2</sub> O <sub>3</sub>	0.8	10	0.16	113	0.21
Pt/CeO <sub>2</sub> /Al <sub>2</sub> O <sub>3</sub>	0.8	10	0.16	96	125
Rh/Al <sub>2</sub> O <sub>3</sub>	0.8	10	0.16	110	0.009
Rh/CeO <sub>2</sub> /Al <sub>2</sub> O <sub>3</sub>	0.8	10	0.16	117	0.81

<sup>a</sup> GHSV = 250 000 h<sup>-1</sup>; catalysts: 1 wt% Pt/Al<sub>2</sub>O<sub>3</sub>, 0.2 wt% Rh/Al<sub>2</sub>O<sub>3</sub>, 1 wt% Pt/CeO<sub>2</sub>(12 wt%)/Al<sub>2</sub>O<sub>3</sub>, 0.2 wt% Rh/CeO<sub>2</sub>(12 wt%)/Al<sub>2</sub>O<sub>3</sub>.

<sup>b</sup> Turnover frequencies (h<sup>-1</sup>) per metal atom.

Accordingly, a significant increase of CO conversion upon addition of H<sub>2</sub>O was detected in the rich spike CO conversion (Diwell et al. 1991).

### 2.3.3. Steam reforming

In addition to its role as a reactant for CO removal by water–gas shift, steam can contribute to the removal of hydrocarbons via steam reforming. Steam reforming is indeed an industrial process, which is used for the production of hydrogen or syngas (Duprez 1992). Steam effects in three-way catalysis have been reviewed by Barbier and Duprez 1994, accordingly we will focus only on some relevant aspects related to the role of CeO<sub>2</sub>.

In steam reforming the hydrocarbons are converted into H<sub>2</sub> and CO<sub>2</sub>. Formally, the following equation describes the chemical process:



In principle, such a process can contribute to the removal of hydrocarbons, however it should be noted that other oxidants, particularly O<sub>2</sub> itself, are present in the exhaust and may compete with the steam. A comparison of the activities in the steam reforming, CO oxidation and WGS reactions on Pt, Pd and Rh catalysts was attempted by Whittington et al. (1995). The results reported in fig. 42 show that the light-off temperatures increase according to the following order: CO oxidation  $\ll$  C<sub>3</sub>H<sub>8</sub> oxidation (dry conditions)  $\leq$  C<sub>3</sub>H<sub>8</sub> oxidation (H<sub>2</sub>O present) < steam reforming  $\approx$  water–gas shift. Thus it appears that both steam reforming and water–gas shift reaction can occur in a TWC, but only at temperatures above those necessary to initiate oxidation. The comparison of the catalytic efficiency of the three noble metals investigated should be considered with caution. Similarly to the data discussed above for the WGS reaction, due to the fact that the authors did not report the metal dispersions, the trends of the light-off temperatures reported in

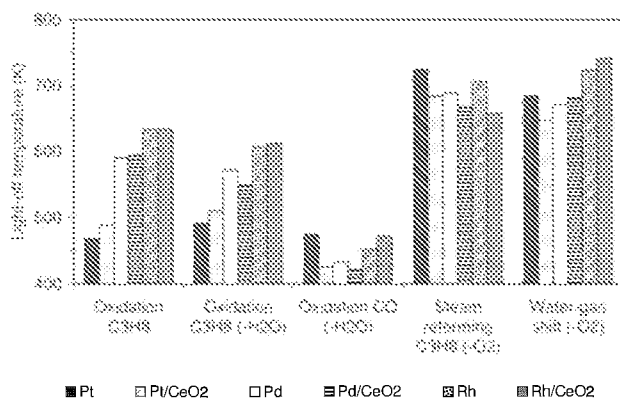


Fig. 42. Light-off temperatures for competing CO and propane oxidation, water–gas shift and steam reforming reactions. Full reaction mixture: GHSV = 19 000 h<sup>-1</sup>; 0.5% H<sub>2</sub>, 1.6% CO, 0.13% C<sub>3</sub>H<sub>8</sub>, 15.1% H<sub>2</sub>O, 13.4% CO<sub>2</sub>, N<sub>2</sub> balance. Other mixtures: H<sub>2</sub>O/O<sub>2</sub> are replaced with N<sub>2</sub>. Catalysts: 0.3 wt% of noble metal of CeO<sub>2</sub>–Al<sub>2</sub>O<sub>3</sub>. (Whittington et al. 1995.)

fig. 42 should be considered in a qualitative way. A perusal of fig. 42 reveals that while the oxidation and WGS activities roughly follow the order Pt < Pd < Rh, the opposite is being observed for steam reforming. The presence of CeO<sub>2</sub> seems to favour the steam reforming activity and CO oxidation, while no beneficial effect is observed in the other cases. Use of stationary feed and the non-specified loading of CeO<sub>2</sub> may explain this result.

Generally speaking, the contribution of steam reforming to HC removal was observed in model feeds as long as nearly stoichiometric or O<sub>2</sub>-deficient reaction conditions are investigated. Duprez and co-workers (Barbier and Duprez 1992–1994, 1995, Maillet et al. 1996) investigated the oxidation of propane in the presence of under-stoichiometric amounts of O<sub>2</sub> on Pt, Rh and Pd catalysts. Under such conditions the light-off curve of the propane oxidation presents two different regions (fig. 43). The first occurs at low temperatures where the oxidation with O<sub>2</sub> takes place; the second one, when O<sub>2</sub> is completely consumed, corresponds to the reaction of H<sub>2</sub>O produced by oxidation with residual propane (steam-reforming).

Remarkably, almost no H<sub>2</sub> was detected until all the added O<sub>2</sub> was consumed, indicating that the two reactions occur in a sequence. Once again, it appears that the contribution of steam reforming to the overall HC removal might be significant only at rich conditions when insufficient amounts of O<sub>2</sub> are present for the direct oxidation reaction. This was confirmed when the H<sub>2</sub> production was monitored in propane oxidation as a function of the stoichiometry of the feed (Barbier and Duprez 1992). In the presence of H<sub>2</sub>O and O<sub>2</sub>, propane can be oxidised according to the following reactions:



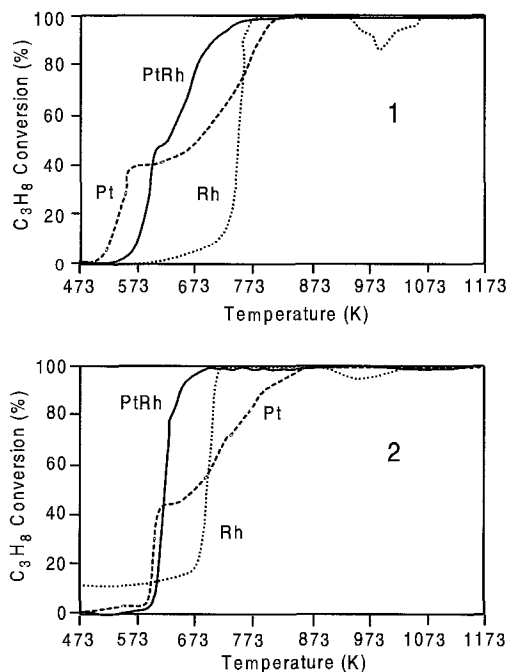


Fig. 43. Temperature-programmed oxidation/steam reforming of propane in an oxygen-deficient reaction medium. GHSV =  $250\,000\text{ h}^{-1}$ ; feed 0.8% CO, 0.16% O<sub>2</sub>, 10% H<sub>2</sub>O in N<sub>2</sub>; catalysts: (1) 1 wt% Pt/Al<sub>2</sub>O<sub>3</sub>, 0.2 wt% Rh/Al<sub>2</sub>O<sub>3</sub>, 1 wt% Pt–0.2 wt% Rh/Al<sub>2</sub>O<sub>3</sub>; (2) 1 wt% Pt/CeO<sub>2</sub>(12 wt%)/Al<sub>2</sub>O<sub>3</sub>, 0.2 wt% Rh/CeO<sub>2</sub>(12 wt%)/Al<sub>2</sub>O<sub>3</sub>, 1 wt% Pt–0.2 wt% Rh/CeO<sub>2</sub>(12 wt%)/Al<sub>2</sub>O<sub>3</sub>. (Barbier and Duprez 1993.)

where reaction (27) is the direct oxidation, while reactions (28) and (29) correspond to steam reforming. Data reported in fig. 44 show that as the ratio  $R$ , which is defined as the ratio of experimental O<sub>2</sub>/C<sub>3</sub>H<sub>8</sub> concentration to the stoichiometric ratio necessary for the oxidation of C<sub>3</sub>H<sub>8</sub>, increases to 1, i.e. stoichiometric oxidation (reaction 27), the amount of H<sub>2</sub> produced tends to zero. Noticeably, when the H<sub>2</sub> production starts, only small amounts of O<sub>2</sub> are present in the reaction mixture, which is a clear indication that the two sets of reaction occur consecutively.

It is worth noting that in the absence of O<sub>2</sub>, steam reforming is reversibly deactivated, presumably by coke deposition. This effect is particularly pronounced over Pt-containing catalysts, while Rh catalysts are less sensitive to the deactivation. This suggests that Rh is more effective as a steam-reforming catalyst compared to Pt. Under oxy-steam reforming conditions (0.4% C<sub>3</sub>H<sub>8</sub>, 0.8% O<sub>2</sub>, 10% H<sub>2</sub>O), the activity could be maintained for several hours and the presence of H<sub>2</sub>O clearly promoted the activity compared to the dry feed (Barbier and Duprez 1993). Note that steam reforming did not occur until all the O<sub>2</sub> was consumed in the oxidation reaction. Steam virtually does not react in excess of oxygen.

The relative activity of the Pt and Rh in the oxy-steam reforming is of interest. As shown in fig. 43, over Pt catalysts the two steps, i.e. oxidation and steam reforming, are clearly discernible, while for the Rh a typical light-off type of conversion curve is observed. This is attributed (Barbier and Duprez 1993, 1994) to both the low oxidation activity of the Rh catalyst and the high steam reforming activity which makes the two steps indistinguishable. The effects of CeO<sub>2</sub> are complex, especially



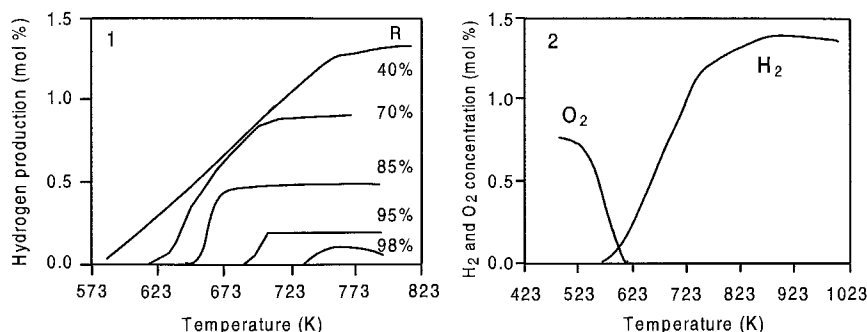


Fig. 44. Effect of  $R$  (% of  $O_2/C_3H_8$  ratio as defined in the text) on  $H_2$  production in temperature-programmed oxidation of propane on (1) 1 wt% Pt–0.2 wt% Rh/CeO<sub>2</sub>(12 wt%)/Al<sub>2</sub>O<sub>3</sub> and (2)  $O_2$  and  $H_2$  production at  $R = 70\%$ . (Barbier and Duprez 1993.)

in the mixed 1 wt% Pt–0.2 wt% Rh/CeO<sub>2</sub>(12 wt%)/Al<sub>2</sub>O<sub>3</sub> catalyst. CeO<sub>2</sub> promotes the Pt oxidation activity at 470–520 K, which depletes the  $O_2$  concentration, making the occurrence of steam reforming possible. Further it promotes the activity of Rh in steam reforming at low temperature, and finally it helps to eliminate, via the WGS reaction, the CO which is formed on Rh by steam reforming above 620 K.

In summary, there are some similarities between the WGS and steam reforming reactions over CeO<sub>2</sub>-promoted catalysts under TWC conditions. In fact, as long as  $O_2$  is present in the feed, it strongly competes with water as oxidant. This makes the occurrence of these reactions possible only under rich conditions, while under lean conditions significant promoting effects should not be expected. The inhibiting effect of  $O_2$  seems to be relaxed in the presence of CeO<sub>2</sub> compared to Al<sub>2</sub>O<sub>3</sub> as support, which could perhaps be related to the high ability of CeO<sub>2</sub> to activate/exchange  $O_2$ . However, the possibility that CeO<sub>2</sub> participates in the activation/reduction of H<sub>2</sub>O cannot be discounted, given its ability to promote splitting of the O–H bond in the water molecule (Otsuka et al. 1983).

#### 2.4. Supported-metal–CeO<sub>2</sub> interactions

The discovery by Tauster et al. (1978) that a high-temperature reduction, typically in H<sub>2</sub> at 773 K, strongly depresses the  $H_2$  and CO chemisorption of noble metals supported on reducible oxides, particularly TiO<sub>2</sub>, triggered a renewed interest in the study of mutual noble-metal–support interactions (supported-metal–support interaction or SMSI effect) and their effects on chemisorption and catalytic properties. Also ceria, being an easily reducible oxide, has been subject of such studies and typically the effects of high-temperature reduction have been investigated, see for example Bernal et al. (1994b, 1995a), Cunningham et al. (1992), Trovarelli et al. (1992, 1993), Fan and Fujimoto (1994), Datye et al. (1995), Meriaudeau et al. (1982), Da Silva et al. (1989), Cunningham et al. (1990), de Leitenburg and Trovarelli (1995), Trovarelli (1996), and references therein. A comprehensive discussion of metal–support interactions in the NM/CeO<sub>2</sub> systems is outside the scope of the present chapter and we refer the reader to the review

by Trovarelli (1996). Here we will focus our attention on some of the aspects, which specifically affect the activity and the activation/deactivation of the CeO<sub>2</sub>-based TWCs. Further, only the effects of oxidative and reductive pre-treatments will be addressed since the specific roles of CeO<sub>2</sub> in promoting the different reactions in three-way catalysts have been discussed in the previous sections.

#### 2.4.1. *Effects of high-temperature oxidising atmosphere*

The effects of high temperature calcination has been studied by different authors due to their inherent importance under the fuel-cut conditions, where the TWCs are subjected to extremely high temperatures under oxidising conditions (above 1273 K in the close-coupled catalyst).

Generally speaking, the effect of high-temperature calcination is to favour the interaction of the supported metal particles with oxygen species from CeO<sub>2</sub>. Evidence for Pt–O bonds not arising from the related oxide have been detected by comparison of Raman spectra supported on Al<sub>2</sub>O<sub>3</sub> and CeO<sub>2</sub>/Al<sub>2</sub>O<sub>3</sub> (Brogan et al. 1994). By varying the CeO<sub>2</sub> loading on Al<sub>2</sub>O<sub>3</sub>, two bands at 550 cm<sup>-1</sup> and 690 cm<sup>-1</sup> were detected which were absent on Pt/Al<sub>2</sub>O<sub>3</sub>. Note that the relative intensity of these two bands does not change with the CeO<sub>2</sub> loading although the intensity of the band at 465 cm<sup>-1</sup>, due to the triply degenerated T<sub>2g</sub> mode of CeO<sub>2</sub>, increases (fig. 45). This has been taken as an indication that these bands derive from Pt–CeO<sub>2</sub> species containing a Pt–O–Ce linkage. Accordingly, in another study (Murrell et al. 1991), an increase of Pt loading at a constant CeO<sub>2</sub> content led to an increase of the intensities of the two bands associated with the Pt–O bond. The two bands at 550 cm<sup>-1</sup> and 690 cm<sup>-1</sup> were attributed to respectively asymmetric and symmetric Pt–O–Ce stretching (Brogan et al. 1994). Formation of the M–O–Ce surface complex appears a common feature for the NM/CeO<sub>2</sub> systems as detected by bands at 630, 614 and 586 cm<sup>-1</sup> for Pd, Ir and Rh, respectively, on CeO<sub>2</sub> (Murrell et al. 1991). In summary, the interaction of surface oxygens of ceria with the noble metals appears established. The important point is to which extent this interaction affects the catalytic properties of the TWCs.

An immediate observation is that this kind of interaction could be responsible for the high mobility of the oxygen on the CeO<sub>2</sub> surface as detected in the CO TPDs reported by Gorte et al. (compare sect. 2.3.1.1). Unfortunately there is a lack of information on the correlation between the catalytic activity measurements and the presence of these M–O–Ce surface complexes. The presence of M–O–Ce interactions has been indirectly confirmed by XPS characterisation of Pd and Pt/Al<sub>2</sub>O<sub>3</sub> catalysts containing CeO<sub>2</sub> (Shyu et al. 1988a, Shyu and Otto 1989). As shown in table 11, CeO<sub>2</sub> stabilizes both the PdO and PtO on the surface compared to the Al<sub>2</sub>O<sub>3</sub> support. In fact, oxidation of Pt/Al<sub>2</sub>O<sub>3</sub> leads to PtO<sub>2</sub> formation on Al<sub>2</sub>O<sub>3</sub> while PtO is stabilised in the presence of ceria. Conversely, both the reduced Pt and Pd ceria-containing catalysts are easily oxidised back to the M<sup>II</sup> state upon exposure to air at rt. In contrast, in the case of alumina-supported catalysts only metallic Pt and Pd are detected, which may be taken as an indication that ceria surface oxygen directly interacts with the supported metal. In addition, Pt phase was detected by

Table 11

XPS binding energies of Pd and Pt supported on  $\text{Al}_2\text{O}_3$ ,  $\text{CeO}_2$  and  $\text{CeO}_2(7 \text{ wt}\%)/\text{Al}_2\text{O}_3$  after different treatments (Shyu et al. 1988a, Shyu and Otto 1989)

Sample	Pre-treatment	BE (eV) <sup>a</sup>	Assignment
<i>Pt catalysts</i>			
Pt(10 wt%)/ $\text{Al}_2\text{O}_3$	Calcined (1073 K)	317.0	$\text{PtO}_2$
	Reduced (773 K)	314.0	$\text{Pt}^0$
Pt(5 wt%)/ $\text{CeO}_2$	Calcined (1073 K)	315.3	PtO
	Reduced (773 K)	314.1	$\text{Pt}^0$
Pt(10 wt%)/ $\text{CeO}_2(20 \text{ wt}\%)/\text{Al}_2\text{O}_3$	Calcined (1073 K)	315.2	PtO
	Reduced (773 K)	313.9	$\text{Pt}^0$
<i>Pd catalysts</i>			
Pd(6.8 wt%)/ $\text{Al}_2\text{O}_3$	Calcined (1073 K)	337.1	PdO
	Reduced (773 K)	314.9	$\text{Pd}^0$
	Reduced (1193 K) and exposed to air (rt)	335.0	$\text{Pd}^0$
Pd(0.6 wt%)/ $\text{CeO}_2$	Calcined (1073 K)	336.9	$\text{Pd}^0$
	Reduced (773 K)	335.1	$\text{Pd}^0$
	Reduced (1193 K) and exposed to air (rt)	337.0	PdO
Pd(4.5 wt%)/ $\text{CeO}_2(18 \text{ wt}\%)/\text{Al}_2\text{O}_3$	Calcined (1073 K)	337.2	PdO
	Reduced (773 K)	335.0	$\text{Pd}^0$
	Reduced (1193 K) and exposed to air (rt)	335.8	

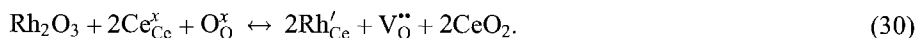
<sup>a</sup> Pd  $3d_{5/2}$ ; Pt  $4d_{5/2}$ .

XRD in the case of  $\text{Pt}/\text{Al}_2\text{O}_3$  and not in the case of  $\text{Pt}/\text{CeO}_2$ , suggesting that the noble metal is finely dispersed as a results of the Pt– $\text{CeO}_2$  interaction (Shyu and Otto 1989).

As far as the stabilisation of the metal dispersion is concerned, the presence of the metal–oxygen bonds certainly affects the rate of metal-particle sintering. Generally speaking, the rate of metal sintering at high temperatures is higher for metal particles than for the corresponding metal oxides. In this respect the presence of the M–O–Ce interaction definitely plays an important role in the stabilisation of the dispersed metal particles. This has been confirmed by thermogravimetric studies which showed that the thermal decomposition of PdO and the reformation of Pd to PdO is dependent on the support upon which they are dispersed (Farrauto et al. 1995). Pd/ $\text{CeO}_2$  showed small hysteresis between the PdO thermal decomposition/reformation under flowing air in the course of heating/cooling experiments in comparison to, for example, Pd/ $\text{ZrO}_2$  (Farrauto et al. 1995), because of a significant increase in the temperature for reformation of the PdO, as the sample cools. There exists a large region of temperature stability of PdO when dispersed on  $\text{CeO}_2$ , indicating a strong metal (oxide)–support interaction. In fact, Murrell et al. (1991) reported that the M–O–Ce surface complexes could be detected for calcination temperatures up to 1273 K, however, when the catalysts were redox aged at 1123 K, evidence for this complex could hardly be found. At the same time a strong sintering of the  $\text{Pt}/\text{CeO}_2$  catalysts was detected by CO chemisorption. In

general, it appears that as long as enough  $\text{CeO}_2$  surface area is available, the NM sintering is prevented by the presence of the M– $\text{CeO}_2$  interaction. This is a mutual effect since Pt itself stabilizes  $\text{CeO}_2$  against surface area loss (Murrell et al. 1991). However, under redox conditions, due to the high sintering rate of  $\text{CeO}_2$  under reducing conditions (Perrichon et al. 1995), the amount of surface oxygen sites available for the M–O–Ce interaction becomes low, and sintering of the supported metal readily occurs.

The interaction of Rh with  $\text{CeO}_2$  seems to be slightly different. On one hand, a number of authors detected or suggested the presence of Rh–O–Ce surface complexes and/or  $[\text{Rh–O}_2]^{2+}$  species after calcination (Munuera et al. 1991, Soria et al. 1992, Murrell et al. 1991). On the other hand, Cunningham et al. (1995) found that upon relatively mild calcination (573–1173 K) of a Rh(4 wt%)/ $\text{CeO}_2$  catalyst, all the Rh-oxide/Rh-metal-related XRD features disappeared. Only after further calcination at 1273 K do the rhodia-related peaks reappear, suggesting a metastable dissolution of rhodia into the ceria lattice according to the reaction



The latter process is supported by the prediction that metal ions preferentially segregate at the  $\text{CeO}_2$  surface (Sayle et al. 1994a). The actual nature of the interaction of Rh with the  $\text{CeO}_2$  under oxidizing conditions appears, however, strongly affected by the pre-treatment conditions. Thus, for example, after treatment in  $\text{O}_2$  (0.1 torr  $\text{O}_2$ , 30 min, 300–400 K) mainly  $\text{Rh}^+$  species were detected (Munuera et al. 1991), while above 473 K  $\text{Rh}^{3+}$  becomes the main species (Padeste et al. 1994, Munuera et al. 1991).

#### 2.4.2. *Effects of high-temperature reducing atmosphere*

As stated above, the observation of the SMSI effect has stimulated a strong interest in the effects of high-temperature reduction (HTR) upon the catalytic properties of the NM/metal oxide systems. There has been a strong discussion concerning the effectiveness of the  $\text{CeO}_2$ -based catalysts to deeply enter into a SMSI state after HTR, usually at 773 K. Generally speaking, HTR decreases the  $\text{H}_2$  and CO chemisorption capacities of the NM/ $\text{CeO}_2$  systems, but, with a few exceptions, no complete inhibition was observed after such a treatment (Badri et al. 1996, Rogemond et al. 1996, Bernal et al. 1993c, 1994b,c, 1995a, 1996, 1997b, Binet et al. 1992, Cunningham et al. 1990, 1992, Datye et al. 1995, de Leitenburg and Trovarelli 1995, de Leitenburg et al. 1997, Golunski et al. 1995, Kepinski and Wolcyrz 1997, Trovarelli et al. 1992). Apparently, the nature of the SMSI state in the  $\text{CeO}_2$ -based catalysts differs from the  $\text{TiO}_2$ -based systems mainly due to the following factors: (i) the ability of H species to quickly migrate over the  $\text{CeO}_2$  surface, making the  $\text{H}_2$  suppression less effective (spillover phenomenon); (ii) the need for reduction temperatures higher than 773 K to obtain significant decoration of NM particles by the support. In fact, metal decoration was observed by high-resolution electron microscopy (HREM) only at reduction temperatures at (or above) 873 K (Pd/ $\text{CeO}_2$ ) and 973 K (Pt/ $\text{CeO}_2$ , Rh/ $\text{CeO}_2$ ) (Bernal et al. 1995a, Kepinski and Wolcyrz 1997). Care should be taken, however, in considering such temperatures as the onset of metal decoration, since

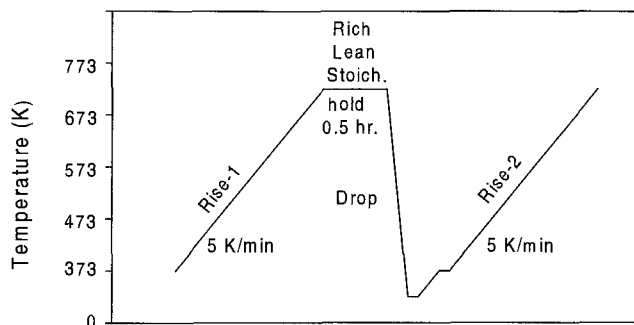


Fig. 46. Temperature profile used for catalyst testing. (Nunan et al. 1992.)

texturally stable, i.e. low-surface-area, materials and relatively high metal loading were employed in the HREM studies due to the low contrast between  $\text{CeO}_2$  and NM.

Researchers have therefore addressed the effects of a reduction treatment on the catalytic properties. It was observed that this treatment generates short-lived, but highly productive, interactions that can occur between the noble metal and the  $\text{CeO}_2$  (Golunski et al. 1995, Nunan et al. 1992). In fact, the comprehension of such transient improvements of activity at moderate temperatures may be an important break-through point for the development of efficient cold-start TWCs. Typically, it is observed that rich-fuel and/or  $\text{H}_2$  activation results in strong enhancement of the low-temperature activity resulting a decrease by about 100–150 K in the light-off temperatures. The results reported by Nunan et al. (1992) highlight these aspects. The activity of a series of  $\text{Pt,Rh/CeO}_2/\text{Al}_2\text{O}_3$  catalysts was investigated in a synthetic mixture containing  $\text{CO}$ ,  $\text{H}_2$ ,  $\text{C}_3\text{H}_8$ ,  $\text{C}_3\text{H}_6$ ,  $\text{NO}$ ,  $\text{O}_2$ ,  $\text{CO}_2$  and  $\text{H}_2\text{O}$  in  $\text{N}_2$ , with an equivalence ratio ( $\lambda$ ) alternatively varied between lean ( $\lambda = 2.0$ ), stoichiometric ( $\lambda = 1.0$ ) and rich ( $\lambda = 0.5$ ) feed. Typically, the catalysts were subjected to a thermal treatment such as depicted in fig. 46. The activity of fresh untreated catalysts was measured during the Rise-1 part of the thermal cycles. This activity was then compared to that obtained during the Rise-2 portion of the cycle, after subjecting the catalysts to a combination of lean, stoichiometric or rich treatments either in the hold or drop part of the cycle. It is observed that the conditions employed in the relatively short (10 min) drop part of the cycle are able to dramatically influence the activity in the subsequent Rise part of the cycle. In fact, this pre-conditioning is able to lower the light-off activity – measured as 50% conversion of  $\text{CO}$  – by about 120–180 K relative to the fresh (untreated) and lean-conditioned catalyst (fig. 47). A perusal of fig. 47 also reveals that the active state of the catalyst is reversibly deactivated by a lean treatment. Importantly, addition of 20 ppm  $\text{SO}_2$  did not adversely affected the nature of the active state since under such conditions, the difference of  $\text{CO}$  light-off activity between the lean and rich treated sample was nearly 250 K.

The comparison of different pre-treatments reveals that the presence of a reducing atmosphere is necessary to observe such an enhancement of activity. In order to identify the component responsible for the activation of the catalyst, a step-wise removal of the

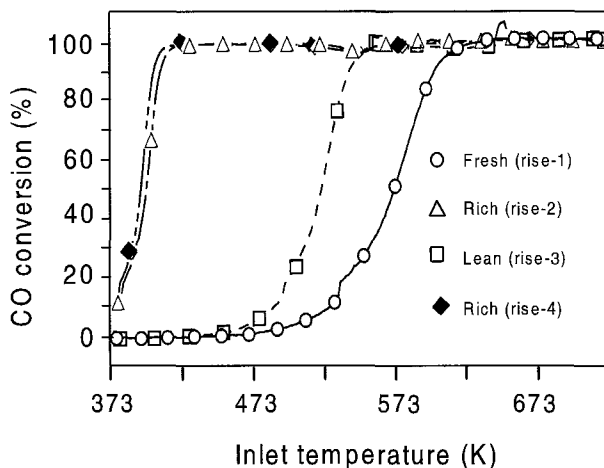


Fig. 47. Comparison of effects of pre-conditioning on the catalytic activity of Pt,Rh/CeO<sub>2</sub>(24 wt%)/Al<sub>2</sub>O<sub>3</sub> on the conversion of CO under a stoichiometric synthetic mixture containing CO (5775 ppm), H<sub>2</sub> (1925 ppm), C<sub>3</sub>H<sub>8</sub> (193 ppm), C<sub>3</sub>H<sub>6</sub> (167 ppm), NO (1835 ppm), O<sub>2</sub> (4645 ppm), CO<sub>2</sub> (118 800 ppm) and H<sub>2</sub>O (100 000 ppm) in N<sub>2</sub>. (Nunan et al. 1992.)

reactant was effected. It turned out that removal of CO, hydrocarbon (HC), and O<sub>2</sub> had no effect on catalyst activation. Only a subsequent removal of H<sub>2</sub> suppressed the activation of the catalyst under rich conditions, suggesting that H<sub>2</sub> is the agent which is responsible for the generation of the active state of the catalyst. Unfortunately, the effects of removal of H<sub>2</sub> alone were not reported. This would give insight in the importance of H<sub>2</sub> generated by occurrence of the WGS reaction upon generation of the active state of this Pt,Rh/CeO<sub>2</sub>/Al<sub>2</sub>O<sub>3</sub> catalyst.

Presence of a close contact between the Pt and CeO<sub>2</sub> appears a fundamental requirement for the occurrence of the "active" state. Consistently, a decrease of the particle size of the CeO<sub>2</sub> supported on Al<sub>2</sub>O<sub>3</sub> increases the efficiency in the improvement of the catalytic activity by the reduction treatment. These transient enhancements of the catalytic activity were attributed to the presence of a SMSI state induced by the reduction, which creates some highly active NM–CeO<sub>2</sub> interfacial sites (Golunski et al. 1995). In our view, the decrease of H<sub>2</sub> chemisorption alone is not sufficient to attribute this transient effect to a SMSI-type phenomenon. As discussed above, the onset of metal decoration requires reduction temperatures higher than 773 K.

Similar transient enhancement of catalytic activity in the NM/CeO<sub>2</sub> systems following a HTR were observed in several model reactions including CO<sub>2</sub> hydrogenation and NO/CO reaction (Fornasiero et al. 1998, Ranga Rao et al. 1994, 1996, Trovarelli et al. 1992, 1993, 1995). As will be discussed below (sect. 3.1.4), these transient promotional effects of reduced CeO<sub>2</sub> moieties seem to be related rather to the presence of oxygen vacancies in the bulk of the CeO<sub>2</sub>, which create an additional driving force for enhancing

the activity. In fact, a SMSI state would be easily destroyed in the presence of oxidants such as NO, O<sub>2</sub>, CO<sub>2</sub> and water (de Leitenburg et al. 1997, Fornasiero et al. 1998).

### 3. Advanced TWC technology

This section deals with the present and future technologies of TWCs. In this respect, TWCs containing CeO<sub>2</sub>–ZrO<sub>2</sub> mixed oxides represent the most advanced technology for the development of CCCs. Although this technology has been employed since the mid-1990s by some automobile companies (Heck and Farrauto 1995), it has not been openly presented by the washcoater companies until very recently. Thus, during the third CAPoC<sup>5</sup> meeting held in Brussels in 1994 only one independent academic group reported the effectiveness of ZrO<sub>2</sub> in promoting the OSC of CeO<sub>2</sub>, while catalyst manufacturers described non-specified promoters. Only at the CAPoC 4 meeting held in 1997 did the industrial researchers claim the effectiveness of ZrO<sub>2</sub> in stabilising CeO<sub>2</sub> against thermal deactivation. An entire mini-symposium dedicated to the role of ZrO<sub>2</sub> in catalysis was held at the SAE<sup>6</sup> conference in Detroit in February 1997. Accordingly, the data reported in the scientific literature are rather scarce, as most of the papers treating this issue appeared in commercial journals. These materials represent today's TWC technology, however there are a number of open issues to be addressed by researchers in order to fully understand the origin of their improved performance compared to the traditional CeO<sub>2</sub>-based technology. Further, due to future reduction of allowed exhaust emission limits all over the world (table 12, overleaf), it is imperative to further improve their performance and to develop year-2005 technology.

#### 3.1. CeO<sub>2</sub>–ZrO<sub>2</sub> mixed oxides

Before introducing the CeO<sub>2</sub>–ZrO<sub>2</sub> system, let us briefly recall some relevant findings concerning the CeO<sub>2</sub> system. The TPR profile of the high-surface-area CeO<sub>2</sub> reported in fig. 48 shows the well-known two-peak profile associated with reduction at the surface and in the bulk, respectively, of CeO<sub>2</sub> (Yao and Yu Yao 1984, Johnson and Mooi 1987). The presence of rhodium clearly promotes the reduction of the surface oxygen species as documented by the shift of the peak at 770 K below 500 K. As above discussed, the low-temperature reduction is strictly related to the extent of surface area. In fact, when a second TPR is performed after an oxidation of the reduced moieties, negligible peaks are observed below 700 K due to a collapse of surface area. This results in loss of metal–CeO<sub>2</sub> interactions as detected by the low-temperature TPR peak.

The correlation between the low-temperature reduction peaks in the TPR profile and the three-way activity appears well established now for the CeO<sub>2</sub>-based catalysts. The

---

<sup>5</sup> The symposium *Catalysis and automotive pollution control* (CAPoC) has been held in Brussels periodically since 1986.

<sup>6</sup> SAE, Society of Automotive Engineers.

Table 12

US federal, Californian and European emission standards in  $\text{g km}^{-1}$  for gasoline fuelled automobiles ( $\text{CH}_4$  is excluded in the US and Californian standards)

Enactment	CO	HC	$\text{NO}_x$	Comments
<i>US federal</i>				
1987	2.11	0.25	0.62	MT 91, tier 0
1994	2.11	0.16	0.25	MT 94, tier 1
2003	1.06	0.08	0.124	proposed
<i>California</i>				
TLEV	2.11	0.08	0.25	
LEV	2.11	0.05	0.12	
ULEV	1.06	0.02	0.12	
<i>European Union</i>				
1996/97	2.7	0.341	0.252	directive 94/12
2000/2001	2.3	0.20	0.15	proposed
2005/2006	1.0	0.10	0.08	indicated

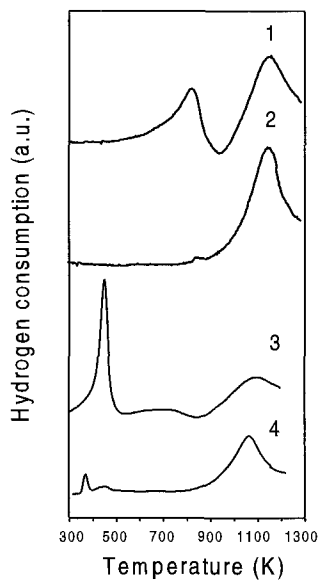


Fig. 48. Temperature-programmed reduction of  $\text{CeO}_2$  and  $\text{Rh/CeO}_2$  and the effects of redox ageing: (1)  $\text{CeO}_2$  ( $194 \text{ m}^2 \text{ g}^{-1}$ ); (2) sample from run (1), oxidised at 700 K ( $<10 \text{ m}^2 \text{ g}^{-1}$ ); (3)  $\text{Rh/CeO}_2$  ( $194 \text{ m}^2 \text{ g}^{-1}$ ); (4) sample from run (3), oxidised at 700 K ( $<10 \text{ m}^2 \text{ g}^{-1}$ ). (Fornasiero et al. 1997.)

thermal ageing leads to loss of noble metal– $\text{CeO}_2$  interactions as detected by TPR, and simultaneously a significant deactivation of the catalysts is observed (fig. 49). It is worth noting that the deactivation seems to be related to two different phenomena: (i) sintering on the noble metal particles leading to a loss of metal surface area; (ii) loss of



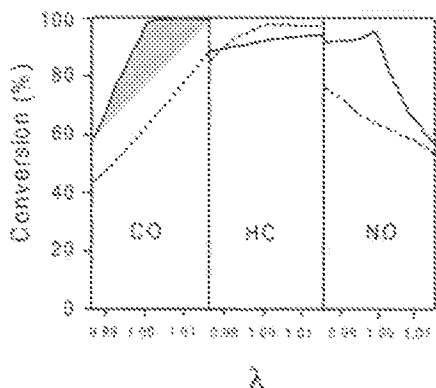


Fig. 49. Effects of thermal ageing at 1173 K on CO, HC and NO<sub>x</sub> conversion on a Rh/CeO<sub>2</sub>/Al<sub>2</sub>O<sub>3</sub> catalysts during cyclic sweep test: solid curves, fresh; dashed curves, aged; GHSV = 65 000 h<sup>-1</sup>, reaction temperature 823 K. For the shaded area, see the text. (Permana et al. 1997.)

CeO<sub>2</sub> surface area leading to a loss of OSC. It is conceivable that the loss of metal surface area leads to a monotonic decrease of activity which indicates that the shaded area in fig. 49 is attributable to a high OSC in the fresh catalyst.

In summary, it appears that whatever is the true nature of the CeO<sub>2</sub> promotion effects in the TWCs, these effects are noticeable as long as high surface area, and consequently low-temperature reduction features, are present in the CeO<sub>2</sub>-based catalysts. Accordingly, the research activity in the 1990s has been focussed mainly on the improvement of the surface-area stability in the CeO<sub>2</sub> promoter. Among different systems tested, ZrO<sub>2</sub> appeared to be the most effective thermal stabiliser of CeO<sub>2</sub>, particularly when it forms a mixed oxide with ceria (Heck and Farrauto 1995). This system will be discussed in the following sections.

### 3.1.1. *Synthesis and phase diagram*

Before entering into the details of the advanced properties of the CeO<sub>2</sub>-ZrO<sub>2</sub> mixed oxides compared to the CeO<sub>2</sub>-based TWC technology it is worthwhile to briefly discuss the appearance of the CeO<sub>2</sub>-ZrO<sub>2</sub> phase diagram. The CeO<sub>2</sub>-ZrO<sub>2</sub> system has long been investigated due to its importance in the fields of ceramics and as solid state electrolytes (Duwez and Odell 1950, Leonov et al. 1966a,b). The exact appearance of this diagram is still a matter of debate despite extensive work by several research groups (Yashima et al. 1993a,b, 1994a,c, 1995a,b, Du et al. 1994, McHale 1991, Meriani 1985, 1986, Tani et al. 1983b). The main reason for this uncertainty is that besides the thermodynamically stable phases, a number of metastable phases have been reported in the literature. As shown in fig. 50, below 1273 K the phase diagram shows a monophasic region of monoclinic (*m*) symmetry for CeO<sub>2</sub> molar content less than ~10%, while for CeO<sub>2</sub> content higher than 80% a cubic (*c*) phase was reported (Duran et al. 1990, Tani et al. 1983b). In the intermediate region, the true nature of the CeO<sub>2</sub>-ZrO<sub>2</sub> phase diagram is still unclear. In this region indeed a number of stable and metastable phases of tetragonal symmetry are observed (Meriani 1985, 1986, 1989). According to Yashima et al. (1993a,b, 1994a) three different phases designated *t*, *t'* and *t''* can be distinguished on the basis of XRD and Raman characterisation. These phases can be prepared at

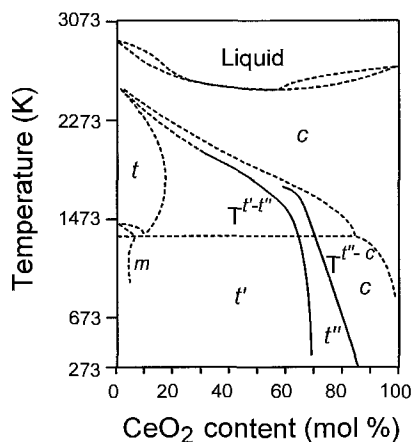


Fig. 50. Phase diagram of the CeO<sub>2</sub>-ZrO<sub>2</sub> system. (Yashima et al. 1993a,b, 1994a.)

Table 13  
Classification of the phases in the CeO<sub>2</sub>-ZrO<sub>2</sub> binary system<sup>a</sup>

Phase	Composition range (% mol Ce)	Tetragonality <sup>b</sup>	Space group
Monoclinic ( <i>m</i> )	0–10	–	P2 <sub>1</sub> /c
Tetragonal ( <i>t</i> )	10–30	>1	P4 <sub>2</sub> /nmc
Tetragonal ( <i>t'</i> )	30–65	>1	P4 <sub>2</sub> /nmc
Tetragonal ( <i>t''</i> ) <sup>c</sup>	65–80	1	P4 <sub>2</sub> /nmc
Cubic ( <i>c</i> )	80–100	1	Fm3m

<sup>a</sup> The classification here reported follows that proposed by Yashima et al. (1994a). The *t*- and *t'*-phases correspond to the TZ<sup>o</sup> and TZ' phases previously reported by Meriani (1985, 1989).

<sup>b</sup> Defined as axial ratio *c/a*.

<sup>c</sup> As described in the text, on the basis of the XRD pattern this phase is commonly indexed in the Fm3m space group (Meriani 1985, 1989).

high temperatures by solid-state synthesis, and upon cooling the *t*-form, which is stable, can be formed through a diffusional phase decomposition, while the *t'*-form is obtained through a diffusionless transition and is metastable. The *t''*-form is metastable as well, and it is intermediate between *t'* and *c*. The *t''*-phase shows no tetragonality and it exhibits an oxygen displacement from ideal fluorite sites. It is often referred to as a *cubic* phase because its XRD pattern is indexed in the cubic Fm3m space group (Fornasiero et al. 1996a). This is due to the fact that the cation sublattice prevalently generates the XRD pattern. For the sake of clarity the characteristics of all the phases are summarised in table 13.

The phase boundaries as indicated in fig. 50 should be considered very approximate due to the fact that in the case of the metastable tetragonal phases, the kind of distortion from the fluorite type structure is highly sensitive to the particle size.

Thus Yashima et al. (1994a) observed that the  $t''$ -phase is formed for  $\text{CeO}_2$  contents above 65 mol%, while we reported the formation of the same phase for a  $\text{Ce}_{0.5}\text{Zr}_{0.5}\text{O}_2$  sample (Fornasiero et al. 1996a). The reasons for such apparent discrepancies can be rationalised by analogy with pure  $\text{ZrO}_2$ . In fact, at room temperature the  $m$ - $\text{ZrO}_2$  is the thermodynamically stable phase, however, either tetragonal and cubic  $\text{ZrO}_2$  have been stabilised at rt provided that fine particles are formed in the synthesis. Different explanations have been advanced to account for the stabilisation of  $t$ - $\text{ZrO}_2$ : surface and strain energy effects (Garvie and Goss 1986, Garvie 1965, 1978); strain energy effects generated at domain boundaries (Mitsuhashi et al. 1974); structural similarity between the amorphous  $\text{ZrO}_2$  and  $t$ - $\text{ZrO}_2$  (Livage et al. 1968) and/or topotactic crystallisation from the amorphous precursor (Tani et al. 1983a) of  $t$ - $\text{ZrO}_2$  from the amorphous phase. The latter two explanations are kinetic rather than thermodynamic, and they rely on the fact that in the amorphous  $\text{ZrO}_2$  bands attributed to the  $t$ -phase were detected by Raman spectroscopy, indicating that a partial ordering of the structure is present already in the precursor (Keramidas and White 1974). Nevertheless, all these investigations point out that below a critical crystallite size, the tetragonal phase is favoured over the monoclinic one. Consistently, by using extremely fine particles, even  $c$ - $\text{ZrO}_2$  was stabilised at rt (Chatterjee et al. 1994, Yoldas 1982, Stefanic et al. 1997).

In addition to the above considerations, one should note that specific compounds have also been proposed to exist in the  $\text{CeO}_2$ - $\text{ZrO}_2$  system: tetragonal  $\text{Ce}_2\text{Zr}_3\text{O}_{10}$  (Longo and Minichelli 1973) and cubic  $\text{Ce}_3\text{ZrO}_8$  (Kawabata et al. 1996). The existence of the former compound, however, has not been confirmed (Tani et al. 1983a). Finally, in the discussion of the features of the  $\text{CeO}_2$ - $\text{ZrO}_2$  phase diagrams, it must be considered that upon reduction of the  $\text{CeO}_2$ - $\text{ZrO}_2$  mixed oxides a still different situation is observed (Leonov et al. 1966a) and the presence of different phases was inferred (Pijolat et al. 1995). For example, Otsuka-Yao-Matsuo and colleagues suggested that under reducing conditions at high temperatures ( $>1273$  K), the pyrochlore  $\text{Ce}_2\text{Zr}_2\text{O}_7$  may originate (Izu et al. 1998, Otsuka-Yao-Matsuo et al. 1998b). By a re-oxidation around 873 K, the pyrochlore compound produces a so-called  $\kappa$ -phase, which seems to be structurally related to the cubic phase with a double pseudofluorite cell (Otsuka-Yao-Matsuo et al. 1996, 1998a). This phase in itself may originate another  $t^*$  tetragonal phase upon high-temperature oxidation (1323–1423 K). The appearance of the different phases is clearly related to the metastable nature of the  $\text{CeO}_2$ - $\text{Ce}_2\text{O}_3$ - $\text{ZrO}_2$  system.

The presence of metastable phases in the phase diagram immediately points out the critical importance of the method of synthesis of the mixed oxides and the relevance of the kinetic lability/inertness towards phase separation. Accordingly, a number of different synthetic methods have been applied to prepare  $\text{CeO}_2$ - $\text{ZrO}_2$  and related mixed oxides: solid state synthesis (Ranga Rao et al. 1994, Fornasiero et al. 1995); co-precipitation (de Leitenburg et al. 1996b, Sinev et al. 1996, Murota et al. 1993, Ozawa et al. 1993), high energy ball-milling (de Leitenburg et al. 1995, Chen et al. 1994, Michel et al. 1993), use of different additives/gelification agents such as hydrazine (Kawabata et al. 1996), oxalic acid (Zhang et al. 1995, Settu and Gobinathan 1994, 1996), citric acid (Yashima et al. 1994b, Vidmar et al. 1997), sol-gel methods using alkoxide precursors (Balducci et al. 1995,

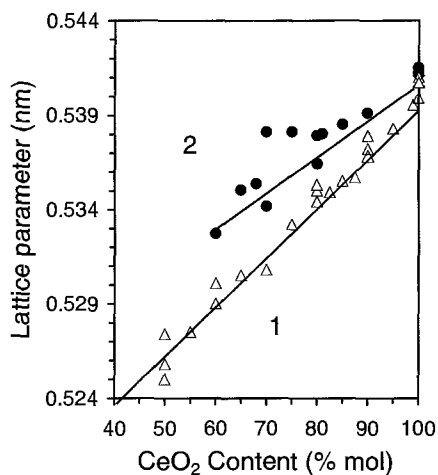


Fig. 51. Experimental lattice parameters reported for the  $\text{CeO}_2\text{-ZrO}_2$  mixed oxides: circles, LSA ceramic materials; triangles, HSA materials. (de Leitenburg et al. 1995, 1996b, Zhang et al. 1995, Ozawa et al. 1993, Pal'ghev et al. 1959.)

Meriani and Soraru 1983, Nagarajan and Rao 1992), formation of aerogels by supercritical drying of hydrogels (Sun and Sermon 1996), microemulsion method (Masui et al. 1998).

As will be shown in the following sections, the homogeneity of a  $\text{CeO}_2\text{-ZrO}_2$  solid solution critically affects both the redox and textural properties, which explains the need for an appropriate method of synthesis. Generally speaking, Vegard's law is widely employed by the researchers to assess the presence of a solid solution. Due to the different ionic radii of  $\text{Ce}^{4+}$  (0.097 nm) and  $\text{Zr}^{4+}$  (0.084 nm) (Shannon 1976, Shannon and Prewitt 1969, 1970), a linear relationship between the cell parameter and the  $\text{ZrO}_2$  content is expected for the cubic samples. Due to the variable  $c/a$  ratio, in the tetragonal region this relationship is related to the cell volume rather than to a single cell parameter. A number of empirical or semi-empirical models have been reported to quantitatively evaluate this variation of the cell parameter (Hong and Virkar 1995, Yashima et al. 1992a,b, Kim 1989). In fact, several authors experimentally found rather good linear relationships (fig. 51), however, comparison between the results of different researchers, and even results within the same laboratory when different synthesis methods are employed (de Leitenburg et al. 1995, 1996b), leads to a significant disagreement in the data. Also, the presence of a solid solution is often found only in a limited range of compositions as denoted by a constant lattice parameter in the data taken from (Ozawa et al. 1993) (fig. 51).

The model reported in fig. 51 (Yashima et al. 1992a,b) fits fairly well the cell parameters reported for a ceramic type of  $\text{CeO}_2\text{-ZrO}_2$  solid solutions, i.e. dense materials with low surface areas. This model has been derived from data reported by Tani et al. (1983a), Okikawa et al. (1970) and Duwez and Odell (1950), which have not been reported in fig. 51 but obviously fit the model (Yashima et al. 1992a,b). In contrast, the lattice parameters of the high-surface-area samples, which were prepared by co-precipitation (de Leitenburg et al. 1996b, Ozawa et al. 1993) or co-impregnation on  $\text{Al}_2\text{O}_3$  (Yao et al. 1997), are significantly higher. This suggests that the intrinsic nature/structural properties of the HSA and LSA  $\text{CeO}_2\text{-ZrO}_2$  mixed oxides could be different.

### 3.1.2. Thermal stability

The thermal stability of  $\text{CeO}_2$  critically affects the efficiency of the  $\text{CeO}_2$  promoter. As soon as significant sintering of  $\text{CeO}_2$  particles occurs, both OSC and metal-support interactions appear inhibited. Industry spent significant efforts on finding a solution for improving the thermal stability both by modification of the  $\text{CeO}_2$  synthesis and by looking for different types of promoters and stabilisers. Use of  $\text{ZrO}_2$  resulted in effectively improving the thermal stability of  $\text{CeO}_2$ , as reported in patent literature (Dettling and Lui 1992, Fujitani et al. 1982, Matsumoto et al. 1988). In the early attempts the addition of  $\text{ZrO}_2$  was made in an uncontrolled way, mostly by impregnation, and no characterisation of the obtained phases was reported. Further work suggested that the appropriate way of adding  $\text{ZrO}_2$  is by the formation of a solid solution between the  $\text{CeO}_2$  and  $\text{ZrO}_2$ . Since the early 1990s, evidence has been reported in the open literature showing the effectiveness of structural doping of  $\text{CeO}_2$  with  $\text{ZrO}_2$  in improving the redox and catalytic properties of  $\text{CeO}_2$  (Ozawa et al. 1993, Matsumoto et al. 1991, Murota et al. 1993, Ranga Rao et al. 1994).

These reports were concerned mainly with the OSC and catalytic activity. The effects of foreign cation doping (0.5–10 mol%) on the thermal stability of  $\text{CeO}_2$  has been investigated extensively by Pijolat and colleagues (Pijolat et al. 1993, 1994a,b, 1995, Gruy and Pijolat 1994). They tried to rationalise the ability of foreign cations to stabilise  $\text{CeO}_2$  against sintering by developing a complete set of equations based on the diffusion of cerium vacancies as the rate-limiting step in the sintering process. Among the different cations investigated ( $\text{Th}^{4+}$ ,  $\text{Zr}^{4+}$ ,  $\text{Si}^{4+}$ ,  $\text{La}^{3+}$ ,  $\text{Y}^{3+}$ ,  $\text{Sc}^{3+}$ ,  $\text{Al}^{3+}$ ,  $\text{Ca}^{2+}$ , and  $\text{Mg}^{2+}$ ), those with ionic radii smaller than that of  $\text{Ce}^{4+}$  effectively stabilised the  $\text{CeO}_2$  against sintering (Pijolat et al. 1995). As a general trend an increase of the amount of added cation decreased the rate of sintering. For the tetravalent cations the following order of rates of sintering is found:  $\text{Th}^{4+} < \text{Zr}^{4+} \ll \text{Si}^{4+}$ . The presence of associated defects of the type  $(\text{M}_{\text{Ce}}, \text{Ce}_{\text{Ce}})'$ , where electrons in the reduced cerium cation are associated with the neighbouring foreign cation, was invoked to explain these observation. The higher the electronegativity of the foreign atom, the higher tendency to form such associated defects. Qualitatively such defects should be less mobile than  $\text{Ce}'_{\text{Ce}}$ , accounting for the low rate of sintering. Unfortunately, neither experimental nor calculated evidence has been reported so far for such type of defects. Also, it seems reasonable that the ability of the foreign cation to share electrons with  $\text{Ce}'_{\text{Ce}}$  should preferably be related to the fourth ionisation energy, which, however, does not follow the observed order ( $\text{Th}$  28.8 eV,  $\text{Zr}$  34.34 eV,  $\text{Si}$  45.41 eV). Significantly, both magnetic susceptibility and XANES measurements indicated that reduction of  $\text{CeO}_2$ – $\text{ZrO}_2$  leads to formation of reduced  $\text{Ce}^{3+}$  sites ( $\text{Ce}'_{\text{Ce}}$ ) and no evidence for  $\text{Zr}^{4+}$  accepting electrons was found (Fornasiero et al. 1995, Ranga Rao et al. 1994). This is in agreement with the higher fourth ionisation energy for cerium (36.72 eV) compared to zirconium. In our view, further work is needed before the general validity of the Pijolat et al. model (Pijolat et al. 1995) can be assessed. In fact, although the authors claimed structural homogeneity of their solid solutions (Prin 1991), it is worth noting that all the samples were prepared by an incipient

Table 14

Effect of trivalent dopants on stabilization of CeO<sub>2</sub> surface after high-temperature calcination (Kubsch et al. 1991)

Dopant (mol%)	BET surface area (m <sup>2</sup> g <sup>-1</sup> ) after 1 h calcination at	
	813 K	1253 K
None	80	5
La <sub>2</sub> O <sub>3</sub> (5%)	84	33
Nd <sub>2</sub> O <sub>3</sub> (5%)	80	26
Y <sub>2</sub> O <sub>3</sub> (5%)	92	26
Al <sub>2</sub> O <sub>3</sub> (5%)	88	11

wetness method, followed by a calcination at 723 K for 4 hours. Keeping in mind the relatively large average particle diameter (13.7 nm) and the mild calcination conditions, it cannot be excluded that the observed phenomena could be related simply to the higher ability of small cations, compared to large ones, of migrating into the CeO<sub>2</sub> lattice and forming a solid solution.

Thermal stabilisation of CeO<sub>2</sub> surface area was observed also in mixed oxides prepared by co-precipitation (Kubsch et al. 1991). Remarkably, all dopants whose radii are larger than that of Ce<sup>4+</sup>, e.g. La, Nd, and Y, significantly stabilise CeO<sub>2</sub> with respect to high-temperature calcination (table 14). No evidence for separation of the added oxide was found by XRD, suggesting that solid solutions were formed. Notably, XPS measurements carried out on La/CeO<sub>2</sub> calcined at 813 K and 1253 K showed La/Ce ratios of 0.19 and 0.25, respectively, indicating that the calcination induced a surface enrichment in the La/CeO<sub>2</sub> mixed oxide with respect to the bulk value (0.11). Remarkably, in an impregnated sample the La/Ce ratio (La/Ce = 0.25 in fresh sample) was as high as 0.75 after calcination at 1275 K. A similar surface enrichment was observed for Nd/CeO<sub>2</sub>. It appears that the common mechanism of the stabilisation of surface area with these trivalent dopants is a surface M<sup>3+</sup> enrichment that impedes ceria crystallite growth under oxidising conditions (Harrison et al. 1996, Kubsch et al. 1991). Segregation at the surface of low-valent cations together with oxygen vacancies is energetically favoured and may represent the driving force for this surface area stabilisation (Sayle et al. 1994a).

The effectiveness of high ZrO<sub>2</sub> content (>10 mol%) on the surface area stability of CeO<sub>2</sub> was also reported (Trovarelli et al. 1997, Cuif et al. 1997). Generally speaking, it has been reported for commercial products that an increase of ZrO<sub>2</sub> increases the surface area stability up to approximately 60 mol%. At higher ZrO<sub>2</sub> contents, the surface area is constant (fig. 52). The OSC appears maximum for intermediate ZrO<sub>2</sub> contents (25–50 mol%). A rationale for this behaviour cannot be given at present, due to a number of reasons. In fact, as above discussed, formation of a homogeneous solid solution over the whole range of composition by using a single optimised process appears unreliable. Accordingly, the authors claimed that homogeneous solid solutions were detected for ZrO<sub>2</sub> molar contents up to 50 mol% (Cuif et al. 1997).

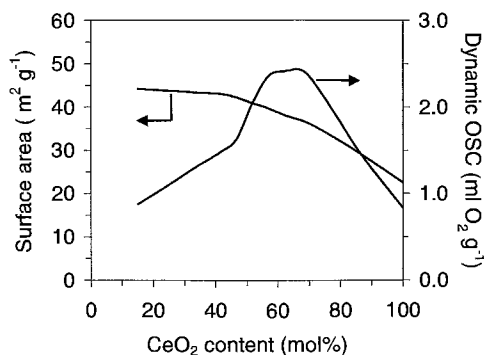


Fig. 52. Thermal stability and OSC at 673 K of “state of the art” CeO<sub>2</sub>–ZrO<sub>2</sub> mixed oxides after ageing at 1173 K for 6 hours under air atmosphere; OSC was measured at 673 K by alternatively pulsing 2.5% O<sub>2</sub> in He and 5% CO in He over the catalyst. (Cuif et al. 1997.).

Another important point is that the intrinsic effect of ZrO<sub>2</sub> on the stability of the CeO<sub>2</sub> surface area, i.e. effects which can be related simply to a compositional change, cannot be detected unless the samples are prepared by a single synthesis method, giving common textural and morphological properties. It is well known that surface areas, particle morphology and even the phase nature of ZrO<sub>2</sub> are strongly affected by the synthesis conditions (Chuah and Jaenicke 1997, Stefanic et al. 1997, Chatterjee et al. 1994). In fact, by using a high-energy ball milling method for the synthesis of Ce<sub>x</sub>Zr<sub>1-x</sub>O<sub>2</sub> mixed oxides ( $x = 1, 0.8, 0.5, 0.2, 0$ ) (Zamar et al. 1996), it was observed that the surface area increased with CeO<sub>2</sub> content, reaching a maximum for  $x = 0.8$ . This is exactly the opposite of the trend reported in fig. 52. Very recently a series of high-surface-area CeO<sub>2</sub>–ZrO<sub>2</sub> mixed oxides have been characterised both fresh and after ageing at 1173 K for 140 h in the presence of water vapour (Colon et al. 1998). Both fresh and aged samples showed comparable surface areas irrespectively of the ZrO<sub>2</sub> content, suggesting absence of significant effects of ZrO<sub>2</sub> addition on the surface area stability. Further studies are necessary to elucidate this point.

An important factor for the stabilisation of the surface area is the homogeneity of the CeO<sub>2</sub>–ZrO<sub>2</sub> mixed oxide. In a comparative study of co-precipitated and impregnated–precipitated CeO<sub>2</sub>(26 mol%)–ZrO<sub>2</sub> aerogels were prepared and characterised (Sun and Sermon 1996). XRD patterns showed traces of *m*-ZrO<sub>2</sub> in the latter sample while a homogeneous solid solution was formed in the former case. The sintering behaviour was investigated. Surface areas of 39 and 12 m<sup>2</sup> g<sup>-1</sup>, respectively, were measured after calcination at 1223 K. Both samples sintered to a similar particle size (12–14 nm), however, as evidenced by SEM and TEM, the particles remained disperse and relatively separated in the homogeneous solid solution. In contrast, the particles were severely agglomerated in the precipitated–impregnated sample, indicating a different type of sintering behaviour. Surface enrichment in ceria was detected by XPS in the non-homogeneous sample, suggesting that its presence is responsible for the easy particle agglomeration.

The effect of synthesis conditions of the surface area stability of CeO<sub>2</sub>–ZrO<sub>2</sub> mixed oxides was recently addressed by Terribile et al. (1998b). They compared the surface areas of samples prepared by the conventional co-precipitation route with those prepared by

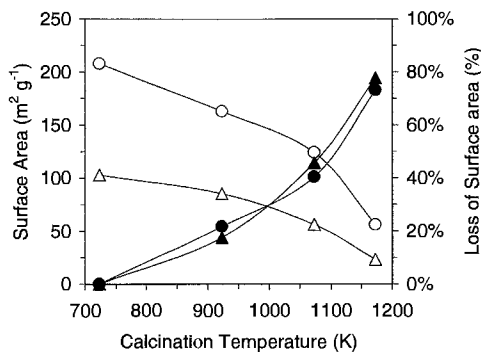


Fig. 53. Surface areas (open symbols) and percentage loss of surface area (solid symbols) upon calcination at 773–1173 K of surfactant route (circles) and co-precipitated (triangles)  $\text{CeO}_2$ – $\text{ZrO}_2$  mixed oxides. (Terribile et al. 1998b.)

carrying out the synthesis in the presence of surfactants. As shown in fig. 53, remarkably high surface areas were obtained by the surfactant route, which persisted after calcination. This effect seems to be ascribed to the presence of an initial surface area, rather than to a modification of the sintering mechanism. Both the co-precipitated and surfactant-route samples show indeed comparable percentages of loss of surface area upon calcination (fig. 53).

In summary, the efficiency of  $\text{ZrO}_2$  in improving the thermal stability of  $\text{CeO}_2$  is now well established, but the intrinsic role of  $\text{ZrO}_2$  in determining these improved properties is far from being understood. Systematic studies on well-defined materials are necessary to elucidate this important point.

The thermal stability of  $\text{CeO}_2$ – $\text{ZrO}_2$  mixed oxides supported on  $\text{Al}_2\text{O}_3$  has been investigated by researchers from Ford (Yao et al. 1997). Samples of the type  $\text{Ce}_x\text{Zr}_{1-x}\text{O}_2/\text{Al}_2\text{O}_3$  ( $x=0.92, 0.81, 0.65, 0.49, 0$ ) with nominal loading of the mixed oxide ranging from 18 to 44 wt% have been prepared by wet impregnation of  $\text{Al}_2\text{O}_3$  with ceria- and zirconia-containing nitrate solution to the incipient wetness. After calcination at 673 K for 4 hours, formation of  $\text{CeO}_2$ – $\text{ZrO}_2$  solid solutions supported on  $\text{Al}_2\text{O}_3$  was detected by XRD. However, all the observed lattice parameters were systematically higher than the reference JPCDS<sup>7</sup> files. This suggested that by this methodology, the insertion of  $\text{ZrO}_2$  into the  $\text{CeO}_2$  lattice was only partially accomplished, the rest of  $\text{ZrO}_2$  being anchored to the  $\text{Al}_2\text{O}_3$  support in a highly dispersed form. Accordingly, no evidence for crystalline  $\text{ZrO}_2$  is found in the XRD pattern of the fresh  $\text{ZrO}_2$ -only/ $\text{Al}_2\text{O}_3$  sample (fig. 54).

The favourable effects of  $\text{ZrO}_2$  addition to  $\text{CeO}_2$  were observed after ageing under both hydrothermal and reducing conditions: after hydrothermal ageing a particle size of  $\sim 27$  nm was found for  $\text{CeO}_2/\text{Al}_2\text{O}_3$ , which decreased below 20 nm for the  $\text{ZrO}_2$ -containing samples. As detected by TEM and XRD in the aged samples, the  $\text{CeO}_2$ – $\text{ZrO}_2$  particle size decreased as the  $\text{ZrO}_2$  content increased from 0 to 50 mol%. This is an interesting result since the  $\text{CeO}_2$ – $\text{ZrO}_2$  loading was increased from 26 to 44 wt% in these samples. The favourable effect of  $\text{Al}_2\text{O}_3$  on  $\text{CeO}_2$  dispersion should be less effective increasing the content of the supported phase. However, a possible drawback of using

<sup>7</sup> Joint Committees on Powder Diffraction Standards.



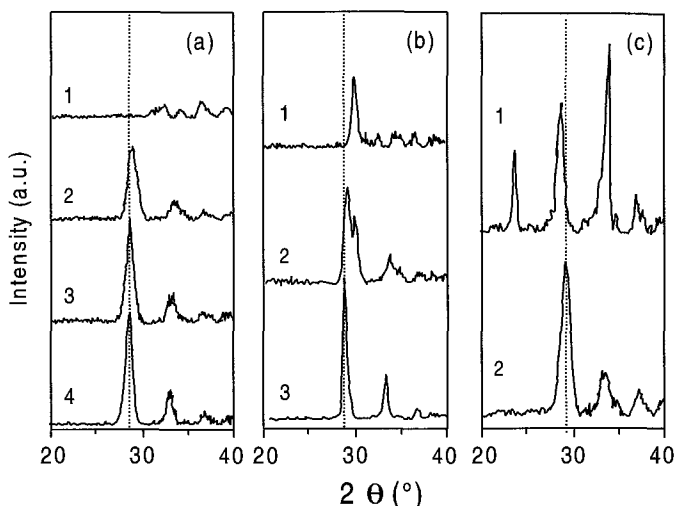


Fig. 54. XRD patterns of (a) fresh, (b) steamed (24 h, 10%  $\text{H}_2\text{O}$ , 1273 K) and (c) reduced ( $\text{H}_2/\text{Ar}$  8.85%, 1173 K)  $\text{Ce}_x\text{Zr}_{1-x}\text{O}_2$  mixed oxides supported on  $\text{Al}_2\text{O}_3$ : (1)  $\text{ZrO}_2$ (18 wt%)/ $\text{Al}_2\text{O}_3$ ; (2)  $\text{Ce}_{0.49}\text{Zr}_{0.51}\text{O}_2$ (44 wt%)/ $\text{Al}_2\text{O}_3$ ; (3)  $\text{Ce}_{0.81}\text{Zr}_{0.19}\text{O}_2$ (28 wt%)/ $\text{Al}_2\text{O}_3$ ; (4)  $\text{CeO}_2$ (26 wt%)/ $\text{Al}_2\text{O}_3$ . (Yao et al. 1997.)

such high  $\text{ZrO}_2$  contents is apparent from fig. 54. The splitting of the (111) peak indicates that a partial separation of a tetragonal  $\text{Ce}_x\text{Zr}_{1-x}\text{O}_2$  phase occurred in the  $\text{Ce}_{0.49}\text{Zr}_{0.51}\text{O}_2$ (44 wt%)/ $\text{Al}_2\text{O}_3$ . This phase separation is consistent with the limited mutual solubility of the  $\text{CeO}_2$ – $\text{ZrO}_2$  system (Tani et al. 1983a) and represents a drawback for the development of thermally stable  $\text{CeO}_2$ – $\text{ZrO}_2$ -based TWCs. Modification of the catalysts upon ageing is undesirable. At present, however, it cannot be excluded that the phase separation may be attributed to intrinsic sample non-homogeneity due to the synthesis method, i.e. co-precipitation. In fact, the particle sizes as determined by XRD were systematically lower than those measured by HREM, suggesting the presence of compositional fluctuation, which leads to apparent XRD peak broadening. Statistically, the higher the Zr loading, the greater the opportunity for compositional fluctuation. This interpretation seems to be substantiated by the XRD patterns reported in fig. 55.

Both the as-prepared samples (fig. 55) do not show evidence for the presence of a  $\text{CeO}_2$ – $\text{ZrO}_2$  mixed oxide due to the high dispersion of the supported phase. On progressively raising the calcination temperature, a single-phase product is observed for the optimised synthesis, producing a solid solution. A tetragonal and a cubic phase are observed in the case of the co-impregnated product. No significant evidence for change of relative intensities of the (111) reflection is observed in the latter case. This suggests that the observed modifications of the XRD patterns can be associated with a parallel growth of particle size of the two phases rather than to a phase separation induced by the calcination. This result highlights the necessity of extremely careful characterisation of the as-synthesised products before the effects of the thermal treatments of the phase stability can be accurately assessed.

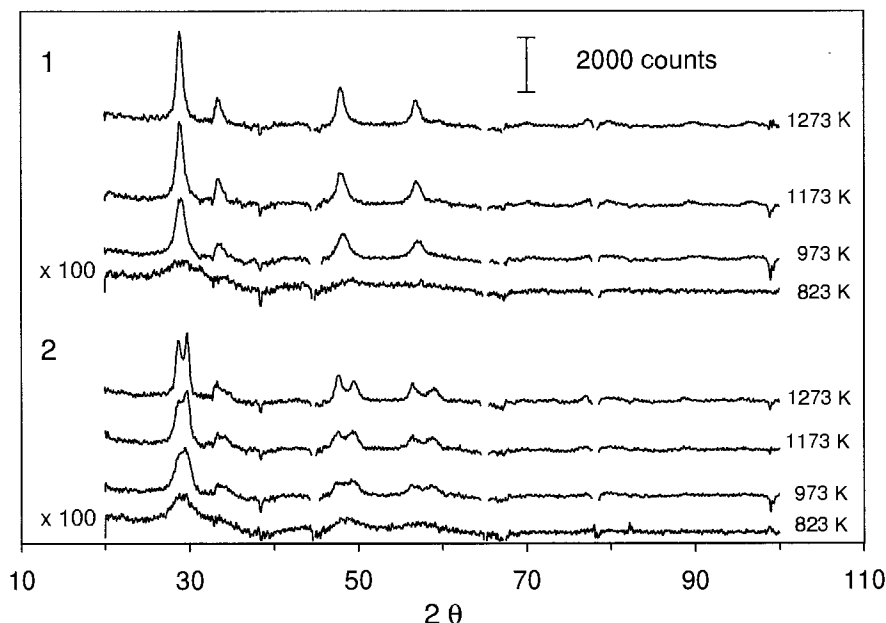


Fig. 55. Effect of calcination (5 h at the indicated temperature) on powder XRD patterns of  $\text{Ce}_{0.6}\text{Zr}_{0.4}\text{O}_2/\text{Al}_2\text{O}_3$  samples prepared by different synthetic methods. XRD patterns are subtracted from the  $\text{Al}_2\text{O}_3$  contribution. (1) proprietary sample; (2) co-impregnated sample. (Di Monte et al. 1998a.)

Figure 54c shows another interesting observation. The presence of  $\text{ZrO}_2$  inhibits the undesirable interaction of  $\text{CeO}_2$  with  $\text{Al}_2\text{O}_3$ , preventing the deactivation of the  $\text{Ce}^{4+}/\text{Ce}^{3+}$  redox couple due to formation of  $\text{CeAlO}_3$  (Shyu et al. 1988b). The latter species is clearly detected in  $\text{CeO}_2/\text{Al}_2\text{O}_3$  after reduction at 1173 K.

### 3.1.3. Redox properties: textural and structural dependence

Evidence for the importance of  $\text{ZrO}_2$  in modifying the redox behaviour of  $\text{CeO}_2$  was first reported in the open literature by Japanese authors (Matsumoto et al. 1991, Ozawa et al. 1993, Murota et al. 1993). Formation of  $\text{CeO}_2$ – $\text{ZrO}_2$  mixed oxides by a co-precipitation method decreased the temperature of the reduction in the bulk from 1100 K to about 900 K (Murota et al. 1993). This was attributed to the high oxygen mobility in the bulk of the oxide induced by the insertion of  $\text{ZrO}_2$  into the  $\text{CeO}_2$  lattice. Shortly afterwards we reported the unusual observation (Ranga Rao et al. 1994) that reduction in the bulk of Rh-loaded  $\text{CeO}_2$ – $\text{ZrO}_2$  solid solutions occurred at very mild temperatures (600–700 K), despite the fact that these systems were prepared by solid-state synthesis. This synthesis, which consists of firing a mixture of oxides at 1873 K, produces dense ceramic materials, which feature very low surface area (LSA,  $\sim 1 \text{ m}^2 \text{ g}^{-1}$ ). The ability of the sintered Rh/ $\text{CeO}_2$ – $\text{ZrO}_2$  solid solutions to undergo reduction at mild temperatures is exemplified in fig. 56, which reports the TPR profiles for Rh-loaded and metal-free

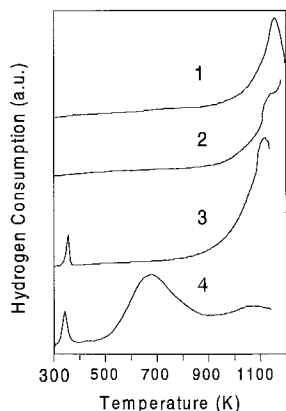


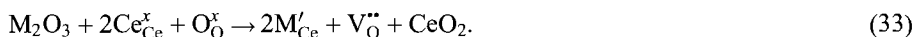
Fig. 56.  $H_2$ -TPR profiles of LSA samples: (1)  $CeO_2$ ; (2)  $Ce_{0.6}Zr_{0.4}O_2$ ; (3) 0.5 wt% Rh/ $CeO_2$ ; (4) 0.5 wt% Rh/ $Ce_{0.6}Zr_{0.4}O_2$ . (Ranga Rao et al. 1994.)

$Ce_{0.6}Zr_{0.4}O_2$ . Comparison of the TPR traces of the Rh-loaded  $CeO_2$  and  $Ce_{0.6}Zr_{0.4}O_2$  immediately reveals that there is a strong reduction peak at  $\sim 700$  K in the  $ZrO_2$ -containing catalyst, which is missing in the other systems. This feature is attributed to the promotion of the reduction in the bulk of the mixed oxide, since surface effects can be excluded in these samples.

These initial studies have stimulated interest in investigating the effects of doping  $CeO_2$  with  $ZrO_2$  and other related materials to promote the  $CeO_2$  redox properties (de Leitenburg et al. 1995, Zamar et al. 1995, Sinev et al. 1996, Fornasiero et al. 1995, Usmen et al. 1995, Bernal et al. 1997c, Logan and Shelef 1994, Kubsch et al. 1991). As early recognised by Miki et al. (1990) and Cho (1991), structural doping of  $CeO_2$  may provide an efficient route to enhance its oxygen storage capacity and hence its catalytic activity under transient conditions. In these early studies, the idea was that insertion of a low-valent ion, such as the trivalent La or Gd, should enhance the oxygen anion mobility in the  $CeO_2$ , increasing the OSC of these materials. According to Cho (1991), two types of oxygen vacancies are created in the doped ceria: intrinsic and extrinsic. The former is due to the reduction of  $Ce^{4+}$  according to the reaction



while the latter is created by the insertion of the bi- or trivalent cation according to the reaction



Both of these vacancies were believed to provide a practical way to increase the OSC of  $CeO_2$ . This is true if the oxygen anion mobility is considered. Solid  $CeO_2$ -based electrolytes show indeed an increased ionic mobility when doped with low-valent cations (Tuller and Nowick 1975). However, the doping may lead to a decrease of the total-OSC.

In fact, the overall degree of reduction of  $\text{CeO}_2$  is generally limited by some kind of a non-stoichiometric compound. This means that starting from an oxygen-deficient system of the type  $\text{M}_x\text{Ce}_{1-x}\text{O}_{2-x/2}$  less oxygen vacancies are needed to achieve a certain degree of non-stoichiometry compared to a fully oxidised  $\text{CeO}_2$ .

The interpretation of the reduction features reported in fig. 56 seems straightforward (Fornasiero et al. 1995, Ranga Rao et al. 1994).  $\text{ZrO}_2$  promotes the reduction in the bulk of the mixed oxide; to observe this effect the presence of the noble metal is necessary. In agreement with the NM/ $\text{CeO}_2$  system, the NM activates and spills  $\text{H}_2$  over the support, favouring its reduction.

A detailed structural characterisation of these solid solutions by XRD, Raman and EXAFS techniques (Fornasiero et al. 1995, Vlaic et al. 1997) suggested some fundamental relationships between the redox properties and the structure in these ceramic-type  $\text{CeO}_2$ - $\text{ZrO}_2$  solid solutions. Insertion of progressively increasing amounts of  $\text{ZrO}_2$  into the  $\text{CeO}_2$  fluorite lattice up to 50 mol% is responsible for (i) a decrease of lattice parameter, due to the smaller  $\text{Zr}^{4+}$  (0.084 nm) compared to  $\text{Ce}^{4+}$  (0.097 nm) (Fornasiero et al. 1995); (ii) an increase of the channel diameter for the oxygen migration in the lattice; (iii) a progressive increase of structural defects; (iv) a decrease of the number of nearest-neighbour oxygens around the  $\text{Zr}^{4+}$  from 8 to 6 in  $\text{Ce}_{0.5}\text{Zr}_{0.5}\text{O}_2$ ; and (v) no variation of the Ce-O coordination sphere except for some shortening of the Ce-O bond length consistent with the contraction of the cell parameter (Vlaic et al. 1997). Given the stoichiometry of the  $\text{CeO}_2$ - $\text{ZrO}_2$  solid solutions, the apparent decrease of the coordination number was attributed to a high structural disorder of the “missed” oxygens induced by the insertion of  $\text{ZrO}_2$  (Vlaic et al. 1997). These two “invisible” oxygens are located at a Zr-O bond distance higher than 2.7 Å, suggesting large oxygen lability.

A different situation is found in the tetragonal region, i.e. for  $\text{ZrO}_2 \geq 50$  mol%. Here  $\text{ZrO}_2$  becomes the dominant factor determining the phase. The Zr-O bonds now assume the typical geometry of tetragonal zirconias, i.e. 4 short and 4 long Zr-O bonds, indicating that the structural disorder found in the cubic phase is no longer present. Consistently, the amount of lattice defects, as detected by density measurements, remains constant in the tetragonal region (Fornasiero et al. 1995). The progressive tetragonalisation with increasing amounts of  $\text{ZrO}_2$  now provides an effective route for the release of the lattice stress induced by the  $\text{ZrO}_2$  insertion, resulting in low oxygen mobility. All these results indicate that the oxygen mobility in the lattice is a key factor in determining the facility of  $\text{Ce}^{4+}$  reduction in the bulk of these highly sintered  $\text{CeO}_2$ - $\text{ZrO}_2$  solid solutions.

Whether these results can be extended to the redox properties of the high-surface-area systems remains, however, to be ascertained. In fact, the dependence of the reduction behaviour of the  $\text{CeO}_2$ - $\text{ZrO}_2$  mixed oxides upon textural properties is rather intriguing. For example, for the  $\text{Ce}_{0.5}\text{Zr}_{0.5}\text{O}_2$  composition the following TPR behaviour was observed: a single peak at 950 K (de Leitenburg et al. 1995) and two peaks at 880 K and 1000 K (Fornasiero et al. 1996a) for surface areas of  $22 \text{ m}^2 \text{ g}^{-1}$  and  $64 \text{ m}^2 \text{ g}^{-1}$ , respectively. In another investigation two peaks at 800 K and 1000 K were found (Murota et al. 1993). In contrast, the ultimate degree of reduction is approximately constant, i.e. a composition of  $\text{Ce}_{0.5}\text{Zr}_{0.5}\text{O}_{1.85}$  is obtained after reduction at 1273 K

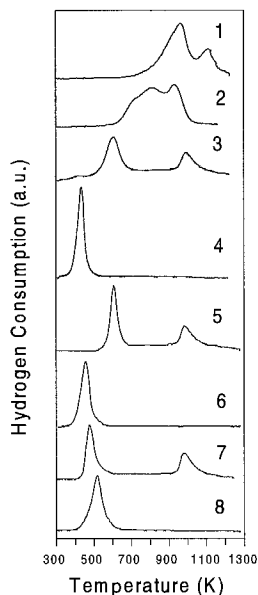


Fig. 57.  $H_2$ -TPR profiles of fresh samples and samples recycled/oxidised at 700 K: (1) fresh and (2) recycled  $Ce_{0.5}Zr_{0.5}O_2$ ; (3) fresh and (4) recycled  $Rh/Ce_{0.5}Zr_{0.5}O_2$ ; (5) fresh and (6) recycled  $Pt/Ce_{0.5}Zr_{0.5}O_2$ ; (7) fresh and (8) recycled  $Pd/Ce_{0.5}Zr_{0.5}O_2$ . (Balducci et al. 1995, Di Monte et al. 1998b, Fornasiero et al. 1996a.)

(de Leitenburg et al. 1995, Fornasiero et al. 1996a). Further, treatment under  $H_2$  in the TPR leads to a strong sintering of the mixed oxides and the surface area drops to or below  $10\text{ m}^2\text{ g}^{-1}$ . This leads to a decrease of the reduction temperature compared to the fresh, high-surface-area sample (HSA) (fig. 57) (Fornasiero et al. 1996a, Balducci et al. 1995). This effect is even more remarkable in the presence of the supported noble metal where the reduction of the aged samples occurs at a temperature as low as 440 K for Rh. Clearly, both textural and structural factors govern the redox behaviour of these mixed oxides. Also worth noting is that conventional characterisation methods may fail in determining the presence of microdomains in the mixed oxide, which may affect the redox behaviour (Vidmar et al. 1997, Egami et al. 1997).

A possible interpretation of the unusual redox behaviour reported in fig. 57 was highlighted by comparison of the Raman spectra of the fresh and aged HSA  $Ce_{0.5}Zr_{0.5}O_2$ . Both the fresh metal-free and Rh-loaded HSA  $Ce_{0.5}Zr_{0.5}O_2$  featured a strong  $T_{2g}$  band at  $465\text{ cm}^{-1}$  – attributed to a totally symmetric M–O (M=Zr, Ce) stretching mode – whose intensity strongly decreased upon ageing in TPR/oxidation processes. This was taken as an indication of a progressive breaking of the symmetry of the M–O bond leading to an oxygen sublattice as observed in LSA  $Ce_{0.5}Zr_{0.5}O_2$ . This interpretation is consistent with the TPR profiles of the noble-metal-loaded HSA  $Ce_{0.5}Zr_{0.5}O_2$ . In the presence of the noble metal, hydrogen activation is unlikely rate limiting for the reduction process. Thus, spilling of  $H_2$  to the support surface is responsible for the shift of the surface reduction from 770 K to 400–450 K in the HSA  $CeO_2$  in the presence of the noble metal (Harrison et al. 1988) (fig. 48). Accordingly, the reduction peak observed at 880 K in the fresh HSA  $Ce_{0.5}Zr_{0.5}O_2$  shifts to 500–700 K in the presence of Rh, Pt or Pd, leaving

the peak at 1100 K unaffected. Notice that due to sample inhomogeneity some  $\text{CeO}_2$  was present in the initial sample, which was incorporated into a solid solution upon reduction (*vide infra*). The sintering occurring in the TPR modifies the oxygen sublattice, which increases the oxygen mobility in the bulk and shifts the whole reduction process to low temperatures. At variance, the NM/ $\text{CeO}_2$  system is deactivated by this treatment.

The importance of the oxygen migration in controlling the rate of  $\text{CeO}_2$ – $\text{ZrO}_2$  reduction was recently questioned by Hori et al. (1998). In fact, by measuring the rate of CO oxidation carried out by pulsing CO over Pt/ $\text{CeO}_2$ – $\text{ZrO}_2$  at 873 K, the calculated flux of oxygen from the bulk of the oxide to the surface was reported to be several orders of magnitude higher than that experimentally measured. This suggested that surface processes rather than migration of oxygen in the bulk were rate-limiting the reduction process. Unfortunately, there are wide variations in the values of oxygen diffusion coefficients reported in the literature. It turns out that, for example, upon applying those reported by Martin and Duprez (1996) and Taha et al. (1996) surface reaction is found to be faster than oxygen migration in the bulk at the reaction temperature employed by the authors. Reduction of  $\text{Ce}_x\text{Zr}_{1-x}\text{O}_2$  and the Rh-loaded mixed oxides was recently studied by X-ray near edge spectroscopy (Overbury et al. 1998). They suggested that water desorption could be a possible rate-determining step, the enhancing effect of Rh being that of catalysing its removal from the support. This would account for the decrease of the reduction temperature in  $\text{Ce}_{0.5}\text{Zr}_{0.5}\text{O}_2$  upon addition of Rh, previously observed (Fornasiero et al. 1997). However, water desorption was completed by about 500 K on HSA  $\text{Ce}_{0.5}\text{Zr}_{0.5}\text{O}_2$ , suggesting that it should not limit the rate of the reduction process (Fornasiero et al. 1999).

Figure 58 reports the TPR profiles of  $\text{Ce}_{0.5}\text{Zr}_{0.5}\text{O}_2$  prepared as a single phase, as detected by Rietveld analysis of the XRD pattern (Fornasiero et al., 1999). The TPR profiles were obtained using either  $^1\text{H}_2/\text{Ar}$  or  $^2\text{H}_2/\text{Ar}$  mixtures as reducing agents. As discussed in sect. 2.1.1, the reduction of  $\text{CeO}_2$  can be separated into fast surface-related steps which involve the activation of the reducing agent ( $^1\text{H}_2/\text{Ar}$  or  $^2\text{H}_2/\text{Ar}$ ) or activated reductants, and a slow migration of oxygen in the bulk. The absence of the isotope effect was observed for the low-temperature reduction feature, as documented by the invariable TPR profiles. Consistently, by varying the heating rate apparent activation energies of  $41.5 \pm 2.3$  and  $38.8 \pm 6.6$   $\text{kJ mol}^{-1}$  were calculated from the shifts of the peak around 660 K using  $^2\text{H}_2$  and  $^1\text{H}_2$ , respectively. This is a very strong indication that the surface steps should not be rate limiting for reduction of the mixed oxide at low temperatures.

Also worth noting is that the fresh single-phase  $\text{Ce}_{0.5}\text{Zr}_{0.5}\text{O}_2$  shows a single reduction peak (fig. 58). We believe that observation of a single reduction feature in HSA samples is a good indication of sample homogeneity, since non-homogeneous HSA systems invariably showed two reduction features (Vidmar et al. 1997). This is in agreement with a recent model calculation which suggested that the energy for creation of a surface oxygen vacancy is very close to that calculated for the bulk of the  $\text{CeO}_2$ – $\text{ZrO}_2$  solid solution (Balducci et al. 1997, 1998).

The redox behaviour of ternary  $\text{CeO}_2$ – $\text{ZrO}_2$  systems using trivalent oxides as dopants was also investigated (Vidmar et al. 1997, Yamada et al. 1997).  $\text{Ga}^{3+}$ ,  $\text{Y}^{3+}$  and  $\text{La}^{3+}$

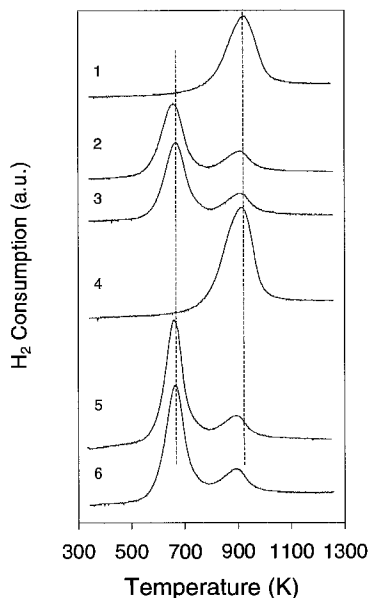


Fig. 58. TPR profiles obtained for  $\text{Ce}_{0.5}\text{Zr}_{0.5}\text{O}_2$ . Consecutive runs using (1–3)  $^2\text{H}_2$  and (4–6)  $^1\text{H}_2$ . Sample pre-treatment: runs 1, 4,  $\text{O}_2/\text{Ar}$  at 1273 K; runs 2, 3, 5, 6,  $\text{O}_2/\text{Ar}$  at 700 K. (Fornasiero et al. 1999.)

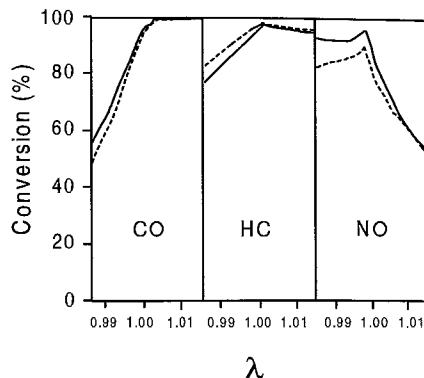


Fig. 59. Effects of thermal ageing at 1173 K on  $\text{CO}$ ,  $\text{HC}$  and  $\text{NO}_x$  conversion efficiency (%) for  $\text{NM}/\text{Ce}_{0.75}\text{Zr}_{0.25}\text{O}_2/\text{Al}_2\text{O}_3$  during cycled sweep test; solid curves, fresh; dashed curves, aged for 8 hours in cycled  $\text{H}_2/\text{N}_2$  5% and  $\text{O}_2/\text{N}_2$  5% feed-stream,  $\text{GHSV} = 65\,000\text{ h}^{-1}$ , reaction temperature 823 K. (Permana et al. 1997.)

were inserted into the  $\text{Ce}_{0.6}\text{Zr}_{0.4}\text{O}_2$  lattice (Vidmar et al. 1997). Of these cations, the ionic radius of  $\text{Y}^{3+}$  (1.1015 Å) is very close to the critical one, while  $\text{Ga}^{3+}$  (0.62 Å) and  $\text{La}^{3+}$  (1.18 Å) are undersized and oversized, respectively. Conventionally, the critical radius is defined as that radius which causes no expansion of the lattice upon substitution. Remarkable modifications of the TPR profiles were found, which can be summarised as follows: (i) an appropriate amount (2.5–5.0 mol%) of the trivalent dopants is necessary to achieve a significant improvement of the reduction; (ii) among the cations investigated, the one whose ionic radius is closest to the critical radius of  $\text{Ce}_{0.6}\text{Zr}_{0.4}\text{O}_2$  is the most effective in promoting the reducibility at low temperature; (iii) the OSC measured after a low-temperature reduction is improved by about 30% compared to the undoped sample. In contrast, the total-OSC measured after a reduction at 1273 K is less affected (see above).

A remarkable point in all these investigations is that redox ageing often leads to improved TPR behaviour at moderate temperatures (compare fig. 57), suggesting a high thermal stability of the OSC in the  $\text{CeO}_2\text{--ZrO}_2$  mixed oxides. Accordingly, Permana et al. (1997) found that a  $\text{NM}/\text{CeO}_2\text{--ZrO}_2/\text{Al}_2\text{O}_3$  catalyst is far less deactivated by thermal ageing with respect to  $\text{NM}/\text{CeO}_2/\text{Al}_2\text{O}_3$  (fig. 59). The comparison with data reported in fig. 49 clearly shows the superior thermal stability of the  $\text{ZrO}_2$ -containing catalysts. The lack of OSC deactivation appears in agreement with the results of the investigation of the redox behaviour.

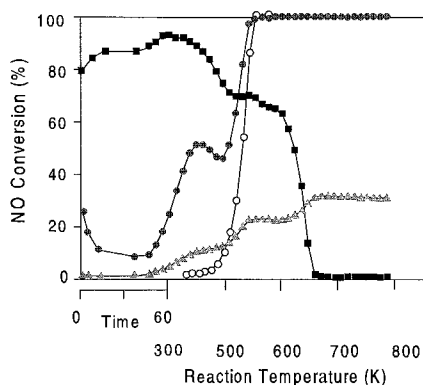


Fig. 60. Reduction of NO with CO over  $\text{Rh/Ce}_{0.6}\text{Zr}_{0.4}\text{O}_2$ : reaction profile vs. temperature obtained after an initial period of 60 min at 300 K (reaction conditions:  $\text{NO}(1\%)$  and  $\text{CO}(3\%)$  in He, heating/cooling rate  $1\text{ K min}^{-1}$ ,  $W/F = 1 \times 10^{-3} \text{ g}_{\text{catalyst}} \text{ ml}^{-1} \text{ min}$ ). Selectivity in  $\text{N}_2\text{O}$  formation (squares) and CO conversion (triangles) measured on a freshly reduced catalyst; NO conversion measured in run-up experiment on a freshly reduced catalyst (solid circles) and run-down experiment on an aged catalyst (open circles). (Fornasiero et al. 1998.)

### 3.1.4. Catalytic reactions

The catalytic activity of the  $\text{CeO}_2\text{--ZrO}_2$ -based catalysts has been investigated in some model TWC reactions, e.g. CO and  $\text{CH}_4$  oxidation (Trovarelli et al. 1997, Bekyarova et al. 1998, Zamar et al. 1995), CO/NO reaction (Di Monte et al. 1998a,b, Fornasiero et al. 1998, Ranga Rao et al. 1994, 1996), CO/ $\text{O}_2$ /NO (Fajardie et al. 1998) and full synthetic mixture (Murota et al. 1993, Permana et al. 1997). A number of SAE technical papers have recently appeared describing different roles of  $\text{ZrO}_2$  in promoting the OSC, thermal stability and TWC activity (Anonymous 1997). Also some model studies on NM/ $\text{CeO}_2\text{--ZrO}_2$  films have recently been reported (Bunluesin et al. 1997, Putna et al. 1997, 1998).

The effects of the  $\text{CeO}_2\text{--ZrO}_2$  mixed oxides on the Rh activity in the reduction of NO with CO has been investigated by Kašpar and colleagues on both LSA and HSA NM/ $\text{CeO}_2\text{--ZrO}_2$  catalysts (Di Monte et al. 1998a,b, Fornasiero et al. 1996b, 1998, Ranga Rao et al. 1994, 1996). The influence of pre-reduction and of the textural/structural properties of the  $\text{CeO}_2\text{--ZrO}_2$  upon the catalytic activity were analysed. Figure 60 shows a conversion vs. temperature reaction profile obtained for a freshly reduced ( $\text{H}_2$ , 473 K, 2 h) HSA  $\text{Rh/Ce}_{0.6}\text{Zr}_{0.4}\text{O}_2$  (Fornasiero et al. 1998). Noticeably, there is an initial NO conversion at rt, which re-oxidizes the support, and no concomitant CO oxidation is observed. Conversion of both NO and CO starts at about 350 K and it progressively increases with temperature up to approximately 470 K where a sudden decrease of activity in the NO reduction is observed. This behaviour is less pronounced for the CO conversion where an additional plateau of activity is observed around 550 K, due to a change of the stoichiometry of the reaction as the product selectivity changes from  $\text{N}_2\text{O}$  to  $\text{N}_2$ . The peak of activity at 470 K is attributed to the presence of an active state of the freshly reduced catalysts. This state is deactivated by treating the catalyst in the presence of NO and CO above 500 K. Consistently, in the run-down part of the thermal cycle no such peak is observed for the NO conversion (fig. 60). The active state could be regenerated by a  $\text{H}_2$  treatment at 473 K carried out immediately after the run-down cycle, indicating that the activation/deactivation process is reversible. The NO conversion initially exceeds that



Table 15

Reaction rates for the NO/CO reaction and apparent activation energies observed over 0.5 wt% Rh/Al<sub>2</sub>O<sub>3</sub>, Rh/CeO<sub>2</sub>-ZrO<sub>2</sub> and Rh/CeO<sub>2</sub>-ZrO<sub>2</sub>-Y<sub>2</sub>O<sub>3</sub> catalysts (Di Monte et al. 1998b)

Run	Support	Pre-treatment	Reaction rate <sup>a</sup> ( $\times 10^3$ )	Activation energy <sup>b</sup> (kJ mol <sup>-1</sup> )	
				Run up	Run down
1	Al <sub>2</sub> O <sub>3</sub>	H <sub>2</sub> , 473 K, 2 h	70	115	121
2		NO + CO, 473–773 K	32	134	131
3	Ce <sub>0.4</sub> Zr <sub>0.6</sub> O <sub>2</sub>	H <sub>2</sub> , 473 K, 2 h	331	67	93
4		NO + CO, 473–773 K	90	85	87
5	Ce <sub>0.6</sub> Zr <sub>0.4</sub> O <sub>2</sub>	H <sub>2</sub> , 473 K, 2 h	336	67	86
6		NO + CO, 473–773 K	46		
7	Ce <sub>0.5</sub> Zr <sub>0.5</sub> O <sub>2</sub>	H <sub>2</sub> , 473 K, 2 h	224	66	87
8		NO + CO, 473–773 K	117	118	138
9		NO + CO, 473–773 K <sup>c</sup>	25	129	139
10		O <sub>2</sub> , 700 K, 0.5 h, H <sub>2</sub> , 1073 K, 2 h	179	86	106
11	Ce <sub>0.6</sub> Zr <sub>0.4</sub> O <sub>2</sub> <sup>d</sup>	H <sub>2</sub> , 473 K, 2 h <sup>d</sup>	1630	71	76
12		NO + CO, 433–773 K <sup>d</sup>	1590		
13	Ce <sub>0.6</sub> Zr <sub>0.35</sub> Y <sub>0.05</sub> O <sub>1.975</sub>	H <sub>2</sub> , 473 K, 2 h <sup>d</sup>	4500	60	80
14		NO + CO, 473–773 K <sup>d</sup>	2000		

<sup>a</sup> Mol NO converted (g catalysts)<sup>-1</sup> s<sup>-1</sup>, measured in steady-state conditions at 473 K.

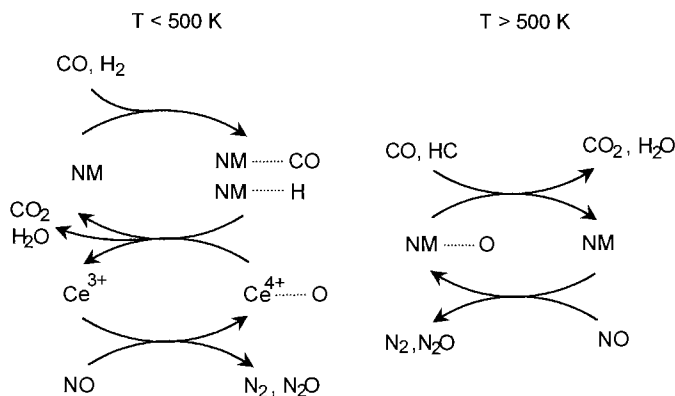
<sup>b</sup> Measured during the run-up/run-down cycles in the range of temperatures 473–530 K. Conversions <20%, standard deviation  $\pm 8$  kJ mol<sup>-1</sup>.

<sup>c</sup> Aged catalyst.

<sup>d</sup> Rh(NO<sub>3</sub>)<sub>3</sub> precursor, reaction rate measured at 433 K.

of CO due to an initial NO conversion occurring partly at the expense of a Ce<sup>3+</sup> oxidation. Oxidation of the Ce<sup>3+</sup> to give Ce<sup>4+</sup> was confirmed by *in situ* XANES spectra taken at the Ce L<sub>III</sub> edge; further, no oxygen was detected in the outlet of the reactor.

The activity data of these catalysts prepared from the RhCl<sub>3</sub> precursor are summarised in table 15. Use of a CeO<sub>2</sub>-ZrO<sub>2</sub> support clearly improves the activity of the supported rhodium as denoted by the 3–5 times increase of activity compared to Rh/Al<sub>2</sub>O<sub>3</sub> (table 15, runs 1, 3, 5, 7). This increase of activity was found for a range of CeO<sub>2</sub>-ZrO<sub>2</sub> compositions, indicating that this phenomenon is related to the mixed oxide rather than to its particular composition. An apparent activation energy of 66–67 kJ mol<sup>-1</sup> is observed with all the fresh CeO<sub>2</sub>-ZrO<sub>2</sub>-based catalysts (table 15, runs 1, 3, 5, 7), suggesting that a support-promoted reaction mechanism is operative under these conditions below 500 K. Ageing under reaction conditions gradually deactivated the catalyst to obtain an activity level comparable to that of Rh/Al<sub>2</sub>O<sub>3</sub> (table 15, run 9). However, oxidation followed by a reduction at 1073 K re-activates the catalyst and a “durable low-temperature active” state of Rh/Ce<sub>0.5</sub>Zr<sub>0.5</sub>O<sub>2</sub> is again obtained. Such a treatment strongly improves the reducibility of the catalyst at low temperatures (compare sect. 3.1.3) (Fornasiero et al. 1997),



Scheme 3. Catalytic reduction of NO by CO over NM promoted by  $\text{CeO}_2\text{--ZrO}_2$  solid solutions.

suggesting that the redox properties of  $\text{Ce}_{0.5}\text{Zr}_{0.5}\text{O}_2$  play a key role in the generation of the active state.

Use of chloride-free precursors dramatically enhances the effectiveness of the “active” state of the  $\text{Rh/CeO}_2\text{--ZrO}_2$  catalysts (compare runs 5 and 11 in table 15), suggesting that spillover phenomena also play a key role in the  $\text{CeO}_2\text{--ZrO}_2$ -mediated reaction mechanism. Chloride is indeed removed with difficulty from  $\text{CeO}_2$ -based catalysts (Bernal et al. 1993a) and it acts as a highly efficient killer of the spillover phenomena (Taha et al. 1996). However, at this stage inherent lower concentration of oxygen vacancies, due to residual chlorine, cannot be excluded to be responsible for the low activity. Notice that the redox properties of the support again affect the catalytic efficiency, since by insertion of 5 mol%  $\text{Y}^{3+}$  into the  $\text{CeO}_2\text{--ZrO}_2$  mixed oxide, both the catalytic activity and the OSC of the system are further improved (compare sect. 3.1.3).

Summarising, the data show a strong increase of the activity over the freshly reduced catalyst, which is associated with the ability of the  $\text{Rh/CeO}_2\text{--ZrO}_2$  to undergo reduction of the support at low temperatures. The reduction of the catalyst affects the activity mainly in three ways:

- (1) A strong, transient increase of NO conversion which is already observed at room temperature;
- (2) An “active” state of the catalyst, which exists below 500 K in the reaction conditions and which is reversibly deactivated above this temperature.

The above findings concerning the active state of the  $\text{Rh/CeO}_2\text{--ZrO}_2$  catalysts can be rationalised in terms of NO reduction promoted by a  $\text{Ce}^{4+}/\text{Ce}^{3+}$  redox couple according to scheme 3. In this scheme, the key role of the  $\text{CeO}_2\text{--ZrO}_2$  is suggested to be the ability to promote the oxygen migration from the oxidant to the reductant via the  $\text{Ce}^{4+}/\text{Ce}^{3+}$  redox couple. The interaction of NO with the reduced  $\text{CeO}_2\text{--ZrO}_2$  moieties is direct below 500 K (Ranga Rao et al. 1996), while above 500 K the oxygen transfer is mediated by the noble metal. Accordingly, two activation energies are found under stationary conditions. The initial transient high activity is associated with the annihilation

of bulk oxygen vacancies created by the initial reduction of the support. This provides the driving force for an efficient NO reduction to give mainly  $N_2O$ , in agreement with the ability of reduced ceria-containing moieties to be easily oxidised by weak oxidants (sect. 2.3.1.2). Under steady-state conditions below 500 K, the  $Ce^{4+}/Ce^{3+}$  redox process seems to be related mainly to surface and near-subsurface regions. Accordingly, the reduction at 1073 K of  $Rh/Ce_{0.5}Zr_{0.5}O_2$  does not deactivate the catalyst despite a strong collapse of surface area. Since  $Ce^{3+}$  oxidation at the expense of NO reduction is easy, it seems reasonable that the reduction of  $Ce^{4+}$  is the rate-limiting step in the scheme. The supported metal promotes this process: no catalytic reaction is observed in its absence. The model is further substantiated by the power-type dependence of reaction rates measured on  $Rh/Ce_{0.5}Zr_{0.5}O_2$  at 473 K by varying the NO and CO pressure in the range 7–25 torr. The data can be conveniently fitted to a power-type law:

$$\text{Rate(NO conversion)} = k_{NO} p_{NO}^m p_{CO}^n,$$

with  $k_{NO} = 3.2 \pm 0.5 \times 10^{-8} \text{ ml g}_{\text{catalyst}}^{-1} \text{ s}^{-1}$ ,  $m = -2.0 \pm 0.7 \times 10^{-1}$ ,  $n = 2.4 \pm 0.2 \times 10^{-1}$ . A comparison with the kinetic data reported in table 9 (sect. 2.3.1.2) shows that these values are in line with the reaction orders found for  $Rh/CeO_2$  and  $Rh/CeO_2/Al_2O_3$ . According to scheme 3, reduction of the  $CeO_2-ZrO_2$  support favours the NO conversion. In agreement, the reaction order with respect to  $p_{CO}$  is positive. In the presence of  $H_2$ , the reduction of the support is promoted via  $H_2$  activation by the supported metal, which provides active hydrogen to be spilled over the support, favouring its reduction. In CO atmosphere, formation of carbonates on the  $CeO_2$  surface was observed (Badri et al. 1991) whose desorption, leading to the reduction of the support, is not an easy process (Laachir et al. 1991). However, a rapid CO oxidation occurs at the periphery of the metal particles in NM/ $CeO_2$  systems, accounting for the promotional effect of NM in close contact with  $CeO_2-ZrO_2$ . Under these conditions, a long-range effect may become important and the oxygen migration towards the metal particles would be rate limiting as proposed by Gorte and colleagues in the CO oxidation over  $Rh/CeO_2$  (Bunluesin et al. 1995, Cordatos et al. 1996a). Consistently, the very high activity of the chloride-free catalysts may be accounted for by assuming a high efficiency of the reverse spillover of oxygen species. As far as the deactivation of the support mediated cycle above 500 K is concerned, it should be noted that this process may be operative as long as the reduced  $CeO_2-ZrO_2$  moiety shows a strong tendency to be oxidised by NO. Nitric oxide adsorption was used as a valuable tool to determine the presence of reactive oxygen species on the  $CeO_2$  surface (Martinez-Arias et al. 1995). As shown in fig. 61, NO adsorption at 473 K on pre-reduced  $Rh/Ce_{0.5}Zr_{0.5}O_2$  leads to formation of a broad infrared band centred at  $1396 \text{ cm}^{-1}$ , attributable to nitrite/nitrate species on zirconium sites. In contrast, an equivalent experiment carried out at 523 K does not lead to formation of nitrite/nitrate species, suggesting the absence of reactive oxygen species in the latter case (Di Monte et al. 1998b). Since the catalyst was pre-reduced, the presence of reactive oxygen species is associated with a concomitant NO reduction (Martinez-Arias et al. 1995). The lack of their observation after treatment at 523 K suggests that NO reduction,

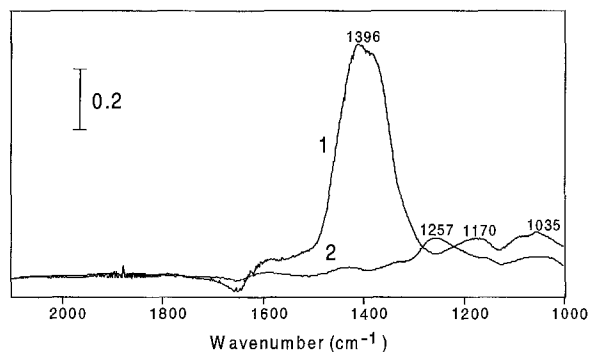


Fig. 61. Adsorption of NO ( $p_{\text{NO}} = 7$  torr) on Rh/Ce<sub>0.6</sub>Zr<sub>0.4</sub>O<sub>2</sub> at (1) 473 K and (2) 523 K. (Di Monte et al. 1998b.)

leading to reactive surface oxygen species, does not occur at this temperature. Due to the high lability of the surface oxygen species at 523 K, surface oxidation by interaction with NO is no longer favoured. According to this model the driving force for NO reduction is related to the stability of the surface oxygen vacancies according to the equilibrium



where  $\text{V}_{\text{O}}^{\bullet\bullet}$  and  $\text{O}_{\text{s}}$  represent surface oxygen vacancy and surface oxygen, respectively. Below 500 K, the equilibrium would be shifted to the right, which provides the driving force for NO reduction. Above 500 K, the equilibrium is shifted to the left and the catalytic cycle mediated by CeO<sub>2</sub>–ZrO<sub>2</sub> is deactivated.

The validity of the above hypothesis on a CeO<sub>2</sub>–ZrO<sub>2</sub>-promoted reaction mechanism was recently confirmed by the observation that such effects are also found in a Pd/Ce<sub>0.6</sub>Zr<sub>0.4</sub>O<sub>2</sub>/Al<sub>2</sub>O<sub>3</sub> catalyst (Di Monte et al. 1998a).

The effectiveness of the CeO<sub>2</sub>–ZrO<sub>2</sub> mixed oxides to effectively promote the catalytic removal of NO by CO was observed also in the presence of oxygen (Fajardie et al. 1998). The interesting point is that the authors provided evidence that Rh<sup>x+</sup> species, rather than Rh metal, are the active species under the reaction conditions. This is due to the ability of the CeO<sub>2</sub>–ZrO<sub>2</sub> mixed oxide to donate oxygen to the Rh particles, in a similar fashion as CeO<sub>2</sub> does (Martinez-Arias et al. 1997). Accordingly, infrared spectroscopy showed that Rh supported on CeO<sub>2</sub>–ZrO<sub>2</sub> is oxidatively disrupted under CO atmosphere at temperatures up to 523 K to give >Rh<sup>I</sup>(CO)<sub>2</sub> species (Fornasiero et al. 1998). In contrast, on alumina this species is agglomerated to Rh metal above 500 K (scheme 2, sect. 2.2; Kašpar et al. 1994), indicating the ability of the CeO<sub>2</sub>–ZrO<sub>2</sub> mixed oxide to maintain the Rh species in a highly dispersed form. On dispersed Rh, NO conversion then proceeds via a dinitrosyl or mixed NO/CO–rhodium species as suggested by Shelef and Graham (1994).

The overall impression is that the effects of CeO<sub>2</sub>–ZrO<sub>2</sub> mixed oxides in promoting the catalytic activity of the noble metals show features common to the NM/CeO<sub>2</sub> systems. There is, however, a strong difference in that the improved redox properties/migration of oxygen species at the surface and in the bulk make these systems thermally stable in comparison to CeO<sub>2</sub>-based catalysts (fig. 59).

### 3.2. Other systems

A great number of systems, e.g.  $\text{CeO}_2\text{--Al}_2\text{O}_3$  and  $\text{CeO}_2\text{--La}_2\text{O}_3\text{--Al}_2\text{O}_3$  (Miki et al. 1990, Graham et al. 1993, Usmen et al. 1995),  $\text{CeO}_2\text{--Gd}_2\text{O}_3$  (Cho 1991),  $\text{CeO}_2\text{--SiO}_2$  (Bensalem et al. 1995, Pijolat et al. 1994a),  $\text{CeO}_2\text{--ZrO}_2\text{--M}_2\text{O}_3$  ( $M = \text{Y, La, Ga}$ ) (Vidmar et al. 1997),  $\text{CeO}_2\text{--ZrO}_2\text{--MnO}_x$  and  $\text{CeO}_2\text{--ZrO}_2\text{--CuO}_x$  (de Leitenburg et al. 1996a),  $\text{CeO}_2\text{--HfO}_2$  (Zamar et al. 1995),  $\text{CeO}_2\text{--La}_2\text{O}_3$  (Bernal et al. 1997c, Usmen et al. 1995, Pijolat et al. 1993, Kubsch et al. 1991),  $\text{CeO}_2\text{--Nd}_2\text{O}_3$  (Kubsch et al. 1991),  $\text{CeO}_2\text{--TbO}_x$  (Bernal et al. 1997a, 1998c),  $\text{CeO}_2\text{--La}_2\text{O}_3\text{--TbO}_x$  (Bernal et al. 1994a),  $\text{CeO}_2\text{--PrO}_x$  (Logan and Shelef 1994),  $\text{CeO}_2\text{--PrO}_x$  and  $\text{PrO}_x\text{--ZrO}_2$  (Sinev et al. 1996),  $\text{CeO}_2\text{--TiO}_2$  (Dauscher et al. 1992, Guglielminotti and Boccuzzi 1996),  $\text{CeO}_2\text{--Y}_2\text{O}_3$  (Kubsch et al. 1991),  $\text{BaO--CeO}_2$  (Funabiki et al. 1991), have been examined with the aim to increase the thermal stability of  $\text{CeO}_2$  and to increase OSC or prevent OSC decline. Effects of doping of  $\text{CeO}_2$  with a variety of di-, tri-, and tetravalent dopants on thermal stability and OSC has also been reported (Pijolat et al. 1995, Zhang et al. 1995). Doping of  $\text{CeO}_2$  has also been shown to significantly enhance the rate of CO oxidation, Cu being the most effective promoter (Liu and Flytzani-Stephanopoulos 1995a,b).

As already observed for the  $\text{CeO}_2\text{--ZrO}_2$  systems, a general comparison of the properties of these systems cannot be made at present, due to different synthesis procedures, dopant loadings, reaction conditions, etc. Nevertheless, it seems that incorporation of the dopant into a mixed oxide/solid solution appears to be the most investigated route to promote the  $\text{CeO}_2$ . Secondly, the use of a low-valent dopant (less than IV) appears promising for most of the authors. As suggested in the pioneering works of Cho (1991) and Miki et al. (1990), the presence of a trivalent dopant should increase the oxygen mobility in the bulk of  $\text{CeO}_2$ , since extrinsic oxygen vacancies are created in the lattice (compare sect. 3.1.3). This has indeed been observed in some of the investigated systems, however, very often the introduction of a trivalent dopant can lead to a decrease of TWC activity, as was observed for La, Nd and Y (Kubsch et al. 1991). There are a number of factors which, in our view, should be fully considered before the effects of dopants can be assessed. The addition of the low-valent dopant may enhance the oxygen-ion mobility by a mechanism which is similar to the increase of the ionic conductivity of stabilised zirconias observed upon addition of bi- or trivalent dopants. Some correlation between the conductivity and the catalytic activity has been reported in the literature, but such concepts cannot be indiscriminately extended to other catalytic systems (Bernal et al. 1994b, Breyse et al. 1972, Herrmann et al. 1996, Ioannides and Verykios 1996, Papadakis et al. 1997, Pliangos et al. 1997). In addition it should be considered that at the usual TWC temperatures  $\text{CeO}_2$  behaves as a mixed conductor or an electronic conductor rather than ionic one (Tuller and Nowick 1975). The choice of the low-valent dopant must also be considered very carefully. Generally speaking, the use of a cation with a radius close to the critical one may be preferred, because it is known that for such systems the ionic conductivity is maximised (Butler et al. 1983, Etsell and Flengas 1970). Also the choice of the amount of dopant might be critical. Typically the ionic conductivity increases up to approximately 8 mol% of the trivalent dopant, then decreases

due to association of oxygen vacancies. This association is also present when bivalent dopants are employed, making the oxygen mobility low. In summary, it seems that at present there is not enough evidence that an increase of ionic conductivity is directly correlated to the efficiency of the OSC property. Accordingly, the  $\text{CeO}_2\text{--ZrO}_2$  mixed oxides, which do not contain a low-valent dopant, show improved properties and higher OSC compared to the binary  $\text{M}_2\text{O}_3$  (MO)– $\text{CeO}_2$  systems. As discussed in sect. 3.1.3, the mechanism by which the oxygen migration is promoted seems to be related to the structural disorder of the  $\text{CeO}_2$  lattice induced by the insertion of the  $\text{ZrO}_2$ .

A different situation is observed when variable valence dopants are employed.  $\text{TbO}_x$ - or  $\text{PrO}_x$ -containing  $\text{CeO}_2$  mixed oxides show high ability to release oxygen, even under mild reduction conditions (Logan and Shelef 1994, Bernal et al. 1997a, Sinev et al. 1996). It appears that there is some kind of mutual improvement of the redox properties of both reducible components (Bernal et al. 1998c, Sinev et al. 1996). This could tentatively be explained by suggesting that both tetravalent Pr and Tb can promote the oxygen mobility by a mechanism which is similar to that of  $\text{ZrO}_2$  in the  $\text{CeO}_2\text{--ZrO}_2$ . In addition, both the dopants can easily change their own oxidation state, thus contributing to the overall OSC.

In summary, there is a strong interest in the investigation of doped  $\text{CeO}_2$  systems, and encouraging improvements of the OSC have been observed. To which extent these improvements are of practical interest still remains still unclear. Among other consideration, the addition of expensive dopants is not favourably considered by industry.

## 4. Conclusions

### 4.1. *Summary of state of art and future perspectives*

For twenty years, the three-way catalysts have represented the most important technology for automotive pollution control. As discussed in this chapter, the efficiency and the durability of these systems is very high, ceria-based compounds playing a key role in obtaining such advanced properties. In fact the advent of  $\text{CeO}_2$  into TWC technology represented an important breakthrough in the catalytic abatement of the automotive exhaust. Among the different promoting roles of  $\text{CeO}_2$  discussed here, apart from the stabilisation of NM dispersion, most of the  $\text{CeO}_2$  functionality in three-way catalysis seems to be correlated to its ability to promote a highly efficient oxygen migration/exchange. By making available/accepting the oxygen at the catalytic centre,  $\text{CeO}_2$  allows the catalyst to cope with both the oxidation and reduction processes, which are needed to simultaneously eliminate the three classes of the pollutants.

As shown in sect. 3,  $\text{CeO}_2\text{--ZrO}_2$  mixed oxides represent a fundamental advance of TWC technology from the advent of the  $\text{CeO}_2$  in exhaust control in the early 1980s. As discussed above, particularly thermal stability of both surface area and OSC are positively affected by the insertion of  $\text{ZrO}_2$  in the catalyst formulation. Consequently, the development of the close-coupled catalyst has become a reality. This technology

now appears quite mature and ready to anticipate requirements that will apply in the new century. However, despite increasing evidence, a fundamental knowledge of the role of  $\text{ZrO}_2$  is still lacking. The variability of the redox properties seems to be related to the synthesis conditions and hence to sample homogeneity (Vidmar et al. 1997). An understanding of how the homogeneity/inhomogeneity of the mixed oxide influences the catalytic activity would represent an important breakthrough point for the development of new-generation TWCs.

In summary, new challenges are still open for the researcher in the field of automotive exhaust abatement. The recent world environmental conference in Tokyo indicated the need for a significant reduction of  $\text{CO}_2$  evolution and hence fuel consumption in the developed countries. This target cannot be accomplished by employing present TWC technology due to its inherent limitations, e.g. the necessity of using a stoichiometric air-to-fuel ratio. Development of a successful lean-burn technology, which allows significant fuel saving, has therefore become a priority target. In this framework, the advanced TWC still plays an important role since the so-called partial burn, i.e.  $\text{NO}_x$  accumulation under lean-burn and their reduction on a TWC under stoichiometric burn ( $\text{NO}_x$  storage/reduction), appears to be the most reliable and ready-to-use technology.

We have observed that notwithstanding the strong advance obtained by employing  $\text{CeO}_2$ - $\text{ZrO}_2$ -based TWCs, there is a wide area of open problems which need to be addressed by the researcher to further advance our knowledge in this area. For example: "Are true solid-solution or mixed-phase systems the most effective catalysts? How do synthesis conditions affect OSC? How are these factors correlated? How do pre-treatment and ageing conditions affect OSC?" These are just a few open questions, the understanding of which is necessary for the development of future generations of automotive exhaust catalysts.

## Acknowledgements

Dr Neal Hickey (University of Trieste) is gratefully acknowledged for helpful discussions. University of Trieste, the Ministero dell'Ambiente (Roma), contract n. DG 164/SCOC/97, CNR (Roma) Programmi Finalizzati "Materiali Speciali per Tecnologie Avanzate II", Contract n. 97.00896.34 are gratefully acknowledged for financial support.

## References

- Altman, E.I., and R.J. Gorte, 1988, *J. Catal.* **113**, 185.
- Altman, E.I., and R.J. Gorte, 1989, *J. Phys. Chem.* **93**, 1993.
- Amenomiya, Y., and G. Pleizier, 1982, *J. Catal.* **76**, 345.
- Amiridis, M.D., T.J. Zhang and R.J. Farrauto, 1996, *Appl. Catal. B* **10**, 203.
- Anonymous, 1997, *Zirconium in Emission Control* (Society of Automotive Engineers, Inc., Warrendale, PA).
- Arai, T., K. Maruya, K. Domen and T. Onishi, 1993, *J. Catal.* **141**, 533.
- Armor, J.N., 1994, *Mobile engine emission control: An overview*, in: *Environmental Catalysis*, ed. J.N.

- Armor (American Chemical Society, Washington, DC) pp. 90–93.
- Badri, A., J. Lamotte, J.C. Lavalley, A. Laachir, V. Perrichon, O. Touret, N.S. Sauvion and E. Quemere, 1991, *Eur. J. Solid State Inorg. Chem.* **28**, 445.
- Badri, A., C. Binet and J.C. Lavalley, 1996, *J. Chem. Soc. Faraday Trans.* **92**, 1603.
- Balducci, G., P. Fornasiero, R. Di Monte, J. Kašpar, S. Meriani and M. Graziani, 1995, *Catal. Lett.* **33**, 193.
- Balducci, G., J. Kašpar, P. Fornasiero, M. Graziani, M.S. Islam and J.D. Gale, 1997, *J. Phys. Chem. B* **101**, 1750.
- Balducci, G., J. Kašpar, P. Fornasiero, M. Graziani and M.S. Islam, 1998, *J. Phys. Chem. B* **102**, 557.
- Barbier, J., and D. Duprez, 1994, *Appl. Catal. B* **4**, 105.
- Barbier Jr, J., and D. Duprez, 1992, *Appl. Catal. A* **85**, 89.
- Barbier Jr, J., and D. Duprez, 1993, *Appl. Catal. B* **3**, 61.
- Barbier Jr, J., and D. Duprez, 1995, Reactivity of steam in exhaust catalysis. Part II. Sintering and regeneration of Rh and PtRh catalysts in propane oxidation, in: *Catalysis and Automotive Pollution Control III*, eds A. Frennet and J.-M. Bastin (Elsevier, Amsterdam) pp. 73–84.
- Barbier Jr, J., F. Marsollier and D. Duprez, 1992, *Appl. Catal. A* **90**, 11.
- Bekyarova, E., P. Fornasiero, J. Kašpar and M. Graziani, 1998, *Catal. Today* **45**, 179.
- Bensalem, A., F. Bozon-Verduraz, M. Delamar and G. Bugli, 1995, *Appl. Catal. A* **121**, 81.
- Bernal, S., F.J. Botana, R. Garcia, Z.C. Kang, M.L. Lopez, M. Pan, F. Ramirez and J.M. Rodriguez-Izquierdo, 1988, *Catal. Today* **2**, 653.
- Bernal, S., J.J. Calvino, G.A. Cifredo, J.M. Rodriguez-Izquierdo, V. Perrichon and A. Laachir, 1992a, *J. Chem. Soc. Chem. Commun.*, p. 460.
- Bernal, S., J.J. Calvino, G.A. Cifredo, J.M. Rodriguez-Izquierdo, V. Perrichon and A. Laachir, 1992b, *J. Catal.* **137**, 1.
- Bernal, S., F.J. Botana, J.J. Calvino, M.A. Cauqui, G.A. Cifredo, A. Jobacho, J.M. Pintado and J.M. Rodriguez-Izquierdo, 1993a, *J. Phys. Chem.* **97**, 4118.
- Bernal, S., J.J. Calvino, G.A. Cifredo, J.M. Gatica, J.A. Perez-Omil and J.M. Pintado, 1993b, *J. Chem. Soc. Faraday Trans.* **89**, 3499.
- Bernal, S., J.J. Calvino, M.A. Cauqui, G.A. Cifredo, A. Jobacho and J.M. Rodriguez-Izquierdo, 1993c, *Appl. Catal.* **99**, 1.
- Bernal, S., G. Blanco, F.J. Botana, J.M. Gatica, J.A. Perez-Omil, J.M. Pintado, J.M. Rodriguez-Izquierdo, P. Maestro and J.J. Braconnier, 1994a, *J. Alloys & Compounds* **207**, 196.
- Bernal, S., J.J. Calvino, G.A. Cifredo, A. Laachir, V. Perrichon and J.M. Herrmann, 1994b, *Langmuir* **10**, 717.
- Bernal, S., G. Blanco, J.J. Calvino, G.A. Cifredo, J.A. Perez-Omil, J.M. Pintado and A. Varo, 1994c, HREM and TPO Study of the Behaviour under Oxidizing Conditions of some Rh/CeO<sub>2</sub> Catalysts, in: *New Developments in Selective Oxidation II*, eds C. Cortés and B. Vic (Elsevier, Amsterdam) pp. 507–510.
- Bernal, S., F.J. Botana, J.J. Calvino, G.A. Cifredo and J.A. Perez-Omil, 1995a, *Catal. Today* **23**, 219.
- Bernal, S., J.J. Calvino, G.A. Cifredo and J.M. Rodriguez-Izquierdo, 1995b, *J. Phys. Chem.* **99**, 11794.
- Bernal, S., M.A. Cauqui, G.A. Cifredo, J.M. Gatica, C. Larese and J.A. Perez-Omil, 1996, *Catal. Today* **29**, 77.
- Bernal, S., G. Blanco, M.A. Cauqui, P. Corchado, J.M. Pintado and J.M. Rodriguez-Izquierdo, 1997a, *Chem. Commun.*, p. 1545.
- Bernal, S., J.J. Calvino, J.M. Gatica, C. Larese, C. Lopez-Cartes and J.A. Perez-Omil, 1997b, *J. Catal.* **169**, 510.
- Bernal, S., G. Blanco, G.A. Cifredo, J.A. Perez-Omil, J.M. Pintado and J.M. Rodriguez-Izquierdo, 1997c, *J. Alloys & Compounds* **250**, 449.
- Bernal, S., J.J. Calvino, M.A. Cauqui, J.A. Perez-Omil, J.M. Pintado and J.M. Rodriguez-Izquierdo, 1998a, *Appl. Catal. B* **16**, 127.
- Bernal, S., G. Blanco, M.A. Cauqui, G.A. Cifredo, J.M. Pintado and J.M. Rodriguez-Izquierdo, 1998b, *Catal. Lett.* **53**, 51.
- Bernal, S., G. Blanco, M.A. Cauqui, P. Corchado, J.M. Pintado, J.M. Rodriguez-Izquierdo and H. Vidal, 1998c, Fundamental properties of a new cerium-based mixed oxide alternative as TWC component, in: *Catalysis and automotive pollution control IV*, eds N. Kruse, A. Frennet and J.M. Bastin (Elsevier, Amsterdam) pp. 611–618.
- Bevan, D.J.M., 1955, *J. Inorg. Nucl. Chem.* **1**, 49.
- Binet, C., A. Jadi, J.C. Lavalley and M. Boutonnet-Kizling, 1992, *J. Chem. Soc. Faraday Trans.* **88**, 2079.



- Bozon-Verduraz, F., and A. Bensalem, 1994, *J. Chem. Soc. Faraday Trans.* **90**, 653.
- Breyse, M., M. Guenin, B. Claudel, H. Latreille and J. Veron, 1972, *J. Catal.* **27**, 275.
- Breyse, M., M. Guenin, B. Claudel, H. Latreille and J. Veron, 1973, *J. Catal.* **28**, 54.
- Brogan, M.S., T.J. Dines and J.A. Cairns, 1994, *J. Chem. Soc. Faraday Trans.* **90**, 1461.
- Bruce, L.A., M. Hoang, A.E. Hughes and T.W. Turner, 1996, *Appl. Catal. A* **134**, 351.
- Bunluesin, T., H. Cordatos and R.J. Gorte, 1995, *J. Catal.* **157**, 222.
- Bunluesin, T., E.S. Putna and R.J. Gorte, 1996, *Catal. Lett.* **41**, 1.
- Bunluesin, T., R.J. Gorte and G.W. Graham, 1997, *Appl. Catal. B* **14**, 105.
- Butler, V., C.R.A. Catlow, B.E.F. Fender and J.H. Harding, 1983, *Solid State Ionics* **8**, 109.
- Campbell, C.T., and J.M. White, 1978, *Appl. Surf. Sci.* **1**, 347.
- Centi, G., and S. Perathoner, 1996, *Catal. Today* **29**, 117.
- Chatterjee, A., S.K. Pradhan, A. Datta, M. De and D. Chakravorty, 1994, *J. Mater. Res.* **9**, 263.
- Chen, Y.L., M. Qi, D.Z. Yang and K.H. Wu, 1994, *Mater. Sci. Eng. A* **183**, L9.
- Chiang, H.W., R.N. Blumenthal and R.A. Fournelle, 1993, *Solid State Ionics* **66**, 85.
- Chin, A.A., and A.T. Bell, 1983, *J. Phys. Chem.* **87**, 3700.
- Cho, B.K., 1991, *J. Catal.* **131**, 74.
- Cho, B.K., 1992, *J. Catal.* **138**, 255.
- Cho, B.K., 1994, *J. Catal.* **148**, 697.
- Cho, B.K., 1996, *J. Catal.* **162**, 149.
- Cho, B.K., B.H. Shanks and J.A. Bailey, 1989, *J. Catal.* **115**, 489.
- Choudhary, V.R., and V.H. Rane, 1992, *J. Catal.* **135**, 310.
- Chuah, G.K., and S. Jaenicke, 1997, *Appl. Catal. A* **163**, 261.
- Church, M.L., B.J. Cooper and P.J. Willson, 1989, SAE publication 890815.
- Colon, G., M. Pijolat, F. Valdivieso, H. Vidal, J. Kašpar, E. Finocchio, M. Daturi, C. Binet, J.C. Lavalley, R.T. Baker and S. Bernal, 1998, *J. Chem. Soc. Faraday Trans.* **94**, 3717.
- Conesa, J.C., 1995, *Surf. Sci.* **339**, 337.
- Cordatos, H., and R.J. Gorte, 1996, *J. Catal.* **159**, 112.
- Cordatos, H., T. Bunluesin and R.J. Gorte, 1995, *Surf. Sci.* **323**, 219.
- Cordatos, H., T. Bunluesin, J. Stubenrauch, J.M. Vohs and R.J. Gorte, 1996a, *J. Phys. Chem.* **100**, 785.
- Cordatos, H., D. Ford and R.J. Gorte, 1996b, *J. Phys. Chem.* **100**, 18128.
- Cuif, J.P., G. Blanchard, O. Touret, A. Seigneurin, M. Marzi and E. Quémeré, 1997, SAE publication 970463.
- Cunningham, J., S. O'Brien, J. Sanz, J.M. Rojo, J. Soria and J.L.G. Fierro, 1990, *J. Mol. Catal.* **57**, 379.
- Cunningham, J., D. Cullinane, J. Sanz, J.M. Rojo, J. Soria and J.L.G. Fierro, 1992, *J. Chem. Soc. Faraday Trans.* **88**, 3233.
- Cunningham, J., D. Cullinane, F. Farrell, J.P. Odriscoll and M.A. Morris, 1995, *J. Mater. Chem.* **5**, 1027.
- Da Silva, P.N., M. Guenin, C. Leclercq and R. Frety, 1989, *Appl. Catal.*, 203.
- Daturi, M., C. Binet, J.C. Lavalley, H. Vidal, J. Kašpar, M. Graziani and G. Blanchard, 1998, *J. Chim. Phys.* **95**, 2048.
- Datye, A.K., D.S. Kalakkad, M.H. Yao and D.J. Smith, 1995, *J. Catal.* **155**, 148.
- Dauscher, A., P. Wehrer and L. Hilaire, 1992, *Catal. Lett.* **14**, 171.
- de Leitenburg, C., and A. Trovarelli, 1995, *J. Catal.* **156**, 171.
- de Leitenburg, C., A. Trovarelli, F. Zamar, S. Maschio, G. Dolcetti and J. Llorca, 1995, *J. Chem. Soc. Chem. Commun.*, p. 2181.
- de Leitenburg, C., D. Goi, A. Primavera, A. Trovarelli and G. Dolcetti, 1996a, *Appl. Catal. B* **11**, L29.
- de Leitenburg, C., A. Trovarelli, J. Llorca, F. Cavani and G. Bini, 1996b, *Appl. Catal. A* **139**, 161.
- de Leitenburg, C., A. Trovarelli and J. Kašpar, 1997, *J. Catal.* **166**, 98.
- Degobert, P., 1995, *Automobiles and Pollution* (Society of Automotive Engineers, Inc., Warrendale, PA).
- deLange, M., Y. Mergler and B. Nieuwenhuys, 1995, *Catal. Lett.* **35**, 383.
- Detting, J.C., and Y.K. Lui, 1992, *Inventors, Engelhard Corp., USA. US Patent 5,128,306*, issued July 7, 1992 (patent applied for June 21, 1990).
- Di Monte, R., J. Kašpar, P. Fornasiero, A. Ferrero, G. Gubitosa and M. Graziani, 1998a, *Stud. Surf. Sci. Catal.* **116**, 559.
- Di Monte, R., P. Fornasiero, M. Graziani and J. Kašpar, 1998b, *J. Alloys & Compounds* **277**, 877.
- Dietor, R., 1988, *J. Catal.* **109**, 89.
- Dietor, R., and S. Roberts, 1989, *J. Phys. Chem.* **93**, 5846.

- Diwell, A.F., R.R. Rajaram, H.A. Shaw and T.J. Truex, 1991, The role of ceria in three-way catalysts, in: *Catalysis and Automotive Pollution Control II*, ed. A. Crueg (Elsevier, Amsterdam) pp. 139–152.
- Du, Y., M. Yashima, T. Koura, M. Kakihana and M. Yoshimura, 1994, *Scripta Metall. Mater.* **31**, 327.
- Dumpelmann, R., N.W. Cant and D.L. Trimm, 1995, Enhancement of the reaction of nitric oxide and carbon monoxide by hydrogen and water over platinum and rhodium-containing catalysts, in: *Catalysis and Automotive Pollution Control III*, eds A. Frennet and J.-M. Bastin (Elsevier, Amsterdam) pp. 123–135.
- Dumpelmann, R., N.W. Cant and D.L. Trimm, 1996, *J. Catal.* **162**, 96.
- Duplan, J.L., and H. Praliaud, 1991, *Appl. Catal.* **67**, 325.
- Duprez, D., 1992, *Appl. Catal. A* **82**, 111.
- Duran, P., M. Gonzales, C. Moure, J.R. Jurdo and C. Pascal, 1990, *J. Mater. Sci.* **25**, 5001.
- Duwez, P., and F. Odell, 1950, *J. Am. Ceram. Soc.* **33**, 274.
- Egami, T., W. Dmowski and R. Brezny, 1997, SAE publication 970461.
- El Fallah, J., S. Boujana, H. Dexpert, A. Kiennemann, J. Majerus, O. Touret, F. Villain and F. Le Normand, 1994, *J. Phys. Chem.* **98**, 5522.
- Engler, B., R. Koberstein and P. Schubert, 1989, *Appl. Catal.* **48**, 71.
- Etsell, T.H., and S.N. Flengas, 1970, *Chem. Rev.* **70**, 339.
- Eyzat, P., 1995, Internal combustion engines – probable evolutions and trends, in: *Catalysis and Automotive Pollution Control III*, eds A. Frennet and J.-M. Bastin (Elsevier, Amsterdam) pp. 33–52.
- Fajardie, F., J.F. Tempere, J.M. Manoli, O. Touret, F. Blanchard and G. Djega-Mariadassou, 1998, *J. Catal.* **179**, 469.
- Fan, L., and K. Fujimoto, 1994, *J. Catal.* **150**, 217.
- Farrauto, R.J., J.K. Lampert, M.C. Hobson and E.M. Waterman, 1995, *Appl. Catal. B* **6**, 263.
- Fierro, J.L.G., J. Soria, J. Sanz and J.M. Rojo, 1987, *J. Solid State Chem.* **66**, 154.
- Fornasiero, P., R. Di Monte, G. Ranga Rao, J. Kašpar, S. Meriani, A. Trovarelli and M. Graziani, 1995, *J. Catal.* **151**, 168.
- Fornasiero, P., G. Balducci, R. Di Monte, J. Kašpar, V. Sergo, G. Gubitosa, A. Ferrero and M. Graziani, 1996a, *J. Catal.* **164**, 173.
- Fornasiero, P., G. Balducci, J. Kašpar, S. Meriani, R. Di Monte and M. Graziani, 1996b, *Catal. Today* **29**, 47.
- Fornasiero, P., J. Kašpar and M. Graziani, 1997, *J. Catal.* **167**, 576.
- Fornasiero, P., G. Ranga Rao, J. Kašpar, F. L'Erario and M. Graziani, 1998, *J. Catal.* **175**, 269.
- Fornasiero, P., J. Kašpar and M. Graziani, 1999, *Appl. Catal. B* **000**, in press.
- Fujitani, Y., H. Muraki, S. Kondoh, M. Tomita, K. Yokota, H. Sobukawa and T. Nakamura, 1982, Inventors, Kabushiki Kaisha Toyota Chuo Kenkyusho, Aichi, Japan. US Patent 4,316,822, issued February 23, 1982 (patent applied for December 8, 1980).
- Funabiki, T., K. Yamada and K. Kayano, 1991, *Catal. Today* **10**, 33.
- Gandhi, H.S., A.G. Piken, M. Shelef and R.G. Delosh, 1976, SAE, 760201, 55.
- Garvie, R.C., 1965, *J. Phys. Chem.* **69**, 1238.
- Garvie, R.C., 1978, *J. Phys. Chem.* **82**, 218.
- Garvie, R.C., and M.F. Goss, 1986, *J. Mater. Sci.* **21**.
- Golunski, S.E., H.A. Hatcher, R.R. Rajaram and T.J. Truex, 1995, *Appl. Catal. B* **5**, 367.
- Graham, G.W., P.J. Schmitz, R.K. Usmen and R.W. McCabe, 1993, *Catal. Lett.* **17**, 175.
- Grenoble, D.C., M.M. Estadt and D.F. Ollis, 1981, *J. Catal.* **67**, 90.
- Gruy, F., and M. Pijolat, 1994, *J. Am. Ceram. Soc.* **77**, 1537.
- Guglielminotti, E., and F. Boccuzzi, 1996, *J. Mol. Catal. A* **104**, 273.
- Haneda, M., T. Mizushima, N. Kakuta, A. Ueno, Y. Sato, S. Matsuura, K. Kasahara and M. Sato, 1993, *Bull. Chem. Soc. Jpn.* **66**, 1279.
- Haneda, M., T. Mizushima and N. Kakuta, 1995, *J. Chem. Soc. Faraday Trans.* **91**, 4459.
- Hardacre, C., R.M. Ormerod and R.M. Lambert, 1994, *J. Phys. Chem.* **98**, 10901.
- Hardacre, C., T. Rayment and R.M. Lambert, 1996, *J. Catal.* **158**, 102.
- Harrison, B., A.F. Diwell and C. Hallett, 1988, *Plat. Met. Rev.* **32**, 73.
- Harrison, P.G., D.A. Creaser, B.A. Wolfendale, K.C. Waugh, M.A. Morris and W.C. Mackrodt, 1996, The surface chemistry of ceria doped with lanthanide oxides, in: *Catalysis and Surface Characterisation*, eds T.J. Dines, C.H. Rochester and J. Thomson (The Royal Society of Chemistry, Cambridge) pp. 76–86.

- Heck, R.M., and R.J. Farrauto, 1995, Catalytic Air Pollution Control. Commercial Technology (Van Nostrand Reinhold, New York) 206 pp.
- Heck, R.M., and R.J. Farrauto, 1997, CATTECH **2**, 117.
- Hecker, W.C., and A.T. Bell, 1983, J. Catal. **84**, 200.
- Hecker, W.C., and A.T. Bell, 1984, J. Catal. **88**, 289.
- Herrmann, J.M., C. Hoang-Van, L. Dibansa and R. Harivololona, 1996, J. Catal. **159**, 361.
- Hertz, R.K., and E.J. Shinouskis, 1985, Ind. Eng. Chem. Prod. Res. Dev. **24**, 385.
- Herz, R.K., 1981, Ind. Eng. Chem. Prod. Res. Dev. **20**, 451.
- Herz, R.K., and A.T. Sell, 1985, J. Catal. **94**, 125.
- Holgado, J.P., and G. Munuera, 1995, XPR/TPR study of the reducibility on M/CeO<sub>2</sub> catalysts (M = Pt, Rh): Does the junction effect theory apply?, in: Catalysis and Automotive Pollution Control III, eds A. Frennet and J.-M. Bastin (Elsevier, Amsterdam) pp. 109–122.
- Hong, S.J., and A.V. Virkar, 1995, J. Am. Ceram. Soc. **78**, 433.
- Hori, C.E., H. Permana, K.Y.S. Ng, A. Brenner, K. More, K.M. Rahmoeller and D.N. Belton, 1998, Appl. Catal. B **16**, 105.
- Hoskins, B.F., and R.L. Martin, 1995, Aust. J. Chem. **48**, 709.
- Hu, Z., 1996, Chem. Commun., p. 879.
- Huizinga, T., J. van Grondelle and R. Prins, 1984, Appl. Catal. **10**, 199.
- Ioannides, T., and X.E. Verykios, 1996, J. Catal. **161**, 560.
- Izu, N., T. Omata and S. Otsuka-Yao-Matsuo, 1998, J. Alloys & Compounds **270**, 107.
- Jin, T., T. Okuara, G.J. Mains and J.M. White, 1987, J. Phys. Chem. **91**, 3310.
- Johnson, M.F.L., and J. Mooi, 1987, J. Catal. **103**, 502; errata corrige: 1993, J. Catal. **140**, 612.
- Kang, Z.C., and L. Eyring, 1992, J. Alloys & Compounds **181**, 483.
- Kang, Z.C., and L. Eyring, 1997a, J. Alloys & Compounds **249**, 206.
- Kang, Z.C., and L. Eyring, 1997b, Aust. J. Chem. **49**, 981.
- Kang, Z.C., J. Zhang and L. Eyring, 1996, Z. Anorg. Allg. Chem. **622**, 465.
- Kašpar, J., C. de Leitenburg, P. Fornasiero, A. Trovarelli and M. Graziani, 1994, J. Catal. **146**, 136.
- Kawabata, A., S. Hirano, M. Yoshimaka, K. Hirota and O. Yamaguchi, 1996, J. Mater. Sci. **31**, 4945.
- Kepinski, L., and M. Wolcyrz, 1997, Appl. Catal. A **150**, 197.
- Keramidas, V.G., and W.B. White, 1974, J. Am. Ceram. Soc. **57**, 22.
- Kim, D.J., 1989, J. Am. Ceram. Soc. **72**, 1415.
- Kim, G., 1982, Ind. Eng. Chem. Prod. Res. Dev. **21**, 267.
- Kobylinski, T.P., and B.W. Taylor, 1974, J. Catal. **33**, 376.
- Kubsch, J.E., J.S. Rieck and N.D. Spencer, 1991, Cerium oxide stabilization: physical property and three-way activity considerations, in: Catalysis and Automotive Pollution Control II, ed. A. Cruick (Elsevier, Amsterdam) pp. 125–138.
- Kummer, J.T., 1986, J. Phys. Chem. **90**, 4747.
- Laachir, A., V. Perrichon, A. Badri, J. Lamotte, E. Catherine, J.C. Lavalley, J. El Fallah, L. Hilaire, F. Le Normand, E. Quémeré, N.S. Sauvion and O. Touret, 1991, J. Chem. Soc. Faraday Trans. **87**, 1601.
- Laachir, A., V. Perrichon, S. Bernal, J.J. Calvino and G.A. Cifredo, 1994, J. Mol. Catal. A **89**, 391.
- Lamonier, C., G. Wrobel and J.P. Bonnelle, 1994, J. Mater. Chem. **4**, 1927.
- Lavalley, J.C., J. Saussey, J. Lamotte, R. Breault, J.P. Hindermann and A. Kiennemann, 1990, J. Phys. Chem. **94**, 5941.
- Le Normand, F., L. Hilaire, K. Kili, G. Krill and G. Maire, 1988, J. Phys. Chem. **92**, 2561.
- Leonov, A.I., A.B. Andreeva and E.K. Keler, 1966a, Izv. Akad. Nauk SSSR, Neorg. Mater. **2**, 137.
- Leonov, A.I., E.K. Keler and A.B. Andreeva, 1966b, Ogneupory **3**, 42.
- Li, C., K. Domen, K. Maruya and T. Onishi, 1989a, J. Am. Chem. Soc. **111**, 7683.
- Li, C., Y. Sakata, T. Arai, K. Domen, K. Maruya and T. Onishi, 1989b, J. Chem. Soc. Faraday Trans. I **85**, 929.
- Li, C., K. Domen, K. Maruya and T. Onishi, 1993, J. Catal. **141**, 540.
- Li, P., I.W. Chen and J.E. Penner-Hahn, 1994, J. Am. Ceram. Soc. **77**, 118.
- Liu, W., and M. Flytzani-Stephanopoulos, 1995a, J. Catal. **153**, 317.
- Liu, W., and M. Flytzani-Stephanopoulos, 1995b, J. Catal. **153**, 304.
- Livage, J., K. Doi and C. Mazieres, 1968, J. Am. Ceram. Soc. **51**, 349.
- Logan, A.D., and M. Shelef, 1994, J. Mater. Res. **9**, 468.

- Longo, V., and D. Minichelli, 1973, *J. Am. Ceram. Soc.* **56**, 1186.
- Löf, P., B. Kasemo, S. Andersson and A. Frestad, 1991a, *J. Catal.* **130**, 181.
- Löf, P., B. Kasemo, L. Bjornkvist, S. Andersson and A. Frestad, 1991b, TPD and XPS studies on CO and NO on highly dispersed Pt + Rh automotive exhaust catalysts: Evidence for noble metal–ceria interaction, in: *Catalysis and Automotive Pollution Control II*, ed. A. Crucg (Elsevier, Amsterdam) pp. 253–274.
- Maillet, T., J. Barbier and D. Duprez, 1996, *Appl. Catal. B* **9**, 251.
- Mannila, P., T. Salmi, H. Haario, M. Luoma, M. Harkonen and J. Sohlö, 1996, *Appl. Catal. B* **7**, 179.
- Martin, D., and D. Duprez, 1996, *J. Phys. Chem.* **100**, 9429.
- Martin, D., and D. Duprez, 1997, *J. Phys. Chem. B* **101**, 4428.
- Martin, R.L., 1974, *J. Chem. Soc. Dalton Trans.*, 1335.
- Martínez-Arias, A., J. Soria, J.C. Conesa, X.L. Seoane, A. Arcoya and R. Cataluna, 1995, *J. Chem. Soc. Faraday Trans.* **91**, 1679.
- Martínez-Arias, A., J. Soria and J.C. Conesa, 1997, *J. Catal.* **168**, 364.
- Masui, T., K. Fujiwara, K. Machida, G. Adachi, T. Sakata and H. Mori, 1997, *Chem. Mater.* **9**, 2197.
- Masui, T., K. Fujiwara, Y.M. Peng, T. Sakata, K. Machida, H. Mori and G. Adachi, 1998, *J. Alloys & Compounds* **269**, 116.
- Matsumoto, S., N. Miyoshi, M. Kimura, M. Ozawa and A. Isogai, 1988, Inventors, Toyota Motor Corp. & Toyota Central Research and Development Laboratories, Japan. German Patent DE 3737419, issued May 19, 1988 (patent applied for November 4, 1987).
- Matsumoto, S., N. Miyoshi, T. Kanazawa, M. Kimura and M. Ozawa, 1991, The effect of complex oxides in Ce–La and Ce–Zr systems on thermal resistant three way catalyst, in: *Catalytic Science and Technology*, ed. S. Yoshida (VCH/Kodansha, Weinheim/Tokyo) pp. 335–338.
- Maunula, T., J. Ahola, T. Salmi, H. Haario, M. Harkonen, M. Luoma and V.J. Pohjola, 1997, *Appl. Catal. B* **12**, 287.
- McCabe, R.W., and J.M. Kisenyi, 1995, *Chem. Ind. London*, p. 605.
- McHale, A.E., 1991, Phase diagrams for ceramists. Annual 1991 (American Ceramic Society, Columbus, OH) p. 20.
- Mendelovici, L., and M. Steinberg, 1985, *J. Catal.*, 353.
- Mergler, Y.J., and B.E. Nieuwenhuys, 1996, *J. Catal.* **161**, 292.
- Meriani, S., 1985, *Mater. Sci. Eng. A* **71**, 365.
- Meriani, S., 1986, *J. Phys. Paris* **47**, C1–485.
- Meriani, S., 1989, *Mater. Sci. Eng. A* **109**, 121.
- Meriani, S., and G. Soraru, 1983, Ultra fine ceria zirconia powders obtained via metallorganic precursors, in: *Ceramic Powders*, ed. P. Vicenzini (Elsevier, Amsterdam) pp. 547–554.
- Meriaudeau, P., J.F. Dutel, M. Dufuax and C. Nacache, 1982, *Stud. Surf. Sci. Catal.* **11**, 95.
- Michel, D., L. Mazerolles, P. Berthet and E. Gaffet, 1993, *J. Am. Ceram. Soc.* **76**, 2884.
- Miki, T., T. Ogawa, A. Ueno, S. Matsuura and M. Sato, 1988, *Chem. Lett.*, p. 565.
- Miki, T., T. Ogawa, M. Haneda, N. Kakuta, A. Ueno, S. Tateishi, S. Matsuura and M. Sato, 1990, *J. Phys. Chem.* **94**, 6464.
- Mitsuhashi, T., M. Ichihara and U. Tatsuke, 1974, *J. Am. Ceram. Soc.* **57**, 97.
- Moeller, T., 1982, The lanthanides, in: *Comprehensive Inorganic Chemistry*, eds J.C. Bailar, H.J. Emeleus, R. Nyholm and A.F. Trotman-Dickenson (Pergamon Press, Oxford) p. 1.
- Munuera, G., A. Fernandez and A.R. Gonzales-Elipse, 1991, The role of the oxygen vacancies at the support in the CO oxidation on Rh/CeO<sub>2</sub> and Rh/TiO<sub>2</sub> autocatalysts, in: *Catalysis and Automotive Pollution Control II*, ed. A. Crucg (Elsevier, Amsterdam) pp. 207–219.
- Murota, T., T. Hasegawa, S. Aozasa, H. Matsui and M. Motoyama, 1993, *J. Alloys & Compounds* **193**, 298.
- Murrell, L.L., S.J. Tauster and D.R. Anderson, 1991, Laser Raman characterization of surface phase precious metal oxides formed on CeO<sub>2</sub>, in: *Catalysis and Automotive Pollution Control II*, ed. A. Crucg (Elsevier, Amsterdam) pp. 275–289.
- Nagarajan, V.S., and K.J. Rao, 1992, *Philos. Mag. A* **65**, 771.
- Nibbelke, R.H., M.A.J. Campman, J.H.B.J. Hoebink and G.B. Marin, 1997, *J. Catal.* **171**, 358.
- Niwa, M., Y. Furukawa and Y. Murakami, 1982, *J. Coll. Interface Sci.* **86**, 260.
- Nunan, J.G., H.J. Robota, M.J. Cohn and S.A. Bradley, 1992, *J. Catal.* **133**, 309.

- Oh, S.H., 1990, *J. Catal.* **124**, 477.
- Oh, S.H., and J.E. Carpenter, 1986, *J. Catal.* **101**, 114.
- Oh, S.H., and C.C. Eickel, 1988, *J. Catal.* **112**, 543.
- Oh, S.H., and C.C. Eickel, 1990, *J. Catal.* **128**, 526.
- Oh, S.H., G.B. Fisher, J.E. Carpenter and D.W. Goodman, 1986, *J. Catal.* **100**, 360.
- Okikawa, S., S. Takano, S. Saito and S. Somiya, 1970, *Bull. Tokyo Inst. Technol.* **98**, 53.
- Otsuka, K., M. Hatano and A. Morikawa, 1983, *J. Catal.* **79**, 493.
- Otsuka-Yao-Matsuo, S., H. Morikawa, N. Izu and K. Okuda, 1996, *J. Jpn Inst. Met.* **59**, 1237.
- Otsuka-Yao-Matsuo, S., T. Omata, N. Izu and H. Kishimoto, 1998a, *J. Solid State Chem.* **138**, 47.
- Otsuka-Yao-Matsuo, S., N. Izu, T. Omata and K. Ikeda, 1998b, *J. Electrochem. Soc.* **145**, 1406.
- Otto, K., and H.C. Yao, 1980, *J. Catal.* **66**, 229.
- Overbury, S.H., D.R. Huntley, D.R. Mullins and G.N. Glavee, 1998, *Catal. Lett.* **51**, 133.
- Ozawa, M., M. Kimura and A. Isogai, 1993, *J. Alloys & Compounds* **193**, 73.
- Padeste, C., N.W. Cant and D.L. Trimm, 1993, *Catal. Lett.* **18**, 305.
- Padeste, C., N.W. Cant and D.L. Trimm, 1994, *Catal. Lett.* **28**, 301.
- Pal'guyev, S.F., S.I. Alyamosvkii and Z.S. Volchenkova, 1959, *Russ. J. Inorg. Chem.* **4**, 1185.
- Pande, N.K., and A.T. Bell, 1986, *J. Catal.* **98**, 7.
- Papadakis, V.G., C.A. Pliangos, I.V. Yentekakis, X.E. Verykios and C.G. Vayenas, 1997, *Nonlinear Anal. Theor. Methods Appl.* **30**, 2353.
- Permana, H., D.N. Belton, M. Rahmoeller, S.J. Schmieg, C.E. Hori, A. Brenner and K.Y.S. Ng, 1997, *SAE*, 970462.
- Perrichon, V., A. Laachir, G. Bergeret, R. Frety, L. Tournayan and O. Touret, 1994, *J. Chem. Soc. Faraday Trans.* **90**, 773.
- Perrichon, V., A. Laachir, S. Abouarnadasse, O. Touret and G. Blanchard, 1995, *Appl. Catal. A* **129**, 69.
- Pijolat, M., M. Prin, M. Soustelle, O. Touret and P. Nortier, 1993, *Solid State Ionics* **63-65**, 781.
- Pijolat, M., M. Prin, M. Soustelle and P. Nortier, 1994a, *J. Chim. Phys. Phys.-Chim. Biol.* **91**, 51.
- Pijolat, M., M. Prin, M. Soustelle and O. Touret, 1994b, *J. Chim. Phys. Phys.-Chim. Biol.* **91**, 37.
- Pijolat, M., M. Prin, M. Soustelle, O. Touret and P. Nortier, 1995, *J. Chem. Soc. Faraday Trans.* **91**, 3941.
- Pliangos, C., I.V. Yentekakis, V.G. Papadakis, C.G. Vayenas and X.E. Verykios, 1997, *Appl. Catal. B* **14**, 161.
- Primet, M., M. El Azhar, R. Frety and M. Guenin, 1990, *Appl. Catal.* **59**, 153.
- Prin, M., 1991, PhD Thesis (Ecole Nationale Supérieure des Mines, Saint Etienne, France).
- Putna, E.S., J.M. Vohs and R.J. Gorte, 1996, *J. Phys. Chem.* **100**, 17862.
- Putna, E.S., J.M. Vohs and R.J. Gorte, 1997, *Catal. Lett.* **45**, 143.
- Putna, E.S., R.J. Gorte, J.M. Vohs and G.W. Graham, 1998, *J. Catal.* **178**, 598.
- Ranga Rao, G., J. Kašpar, R. Di Monte, S. Meriani and M. Graziani, 1994, *Catal. Lett.* **24**, 107.
- Ranga Rao, G., P. Fornasiero, R. Di Monte, J. Kašpar, G. Vlaic, G. Balducci, S. Meriani, G. Gubitosa, A. Cremona and M. Graziani, 1996, *J. Catal.* **162**, 1.
- Ricken, M., J. Nolting and I. Riess, 1984, *J. Solid State Chem.* **54**, 89.
- Rogemond, E., N. Essayem, R. Frety, V. Perrichon, M. Primet, M. Chevrier, C. Gauthier and F. Mathis, 1996, *Catal. Today* **29**, 83.
- Root, T.W., L.W. Schmidt and G.B. Fisher, 1983, *Surf. Sci.* **134**, 30.
- Sasahara, A., H. Tamura and K. Tanaka, 1996, *J. Phys. Chem.* **100**, 15229.
- Sass, A.S., V.A. Shvets, G.A. Savel'eva, N.M. Popova and V.B. Kazansky, 1986, *Kinet. Catal. USSR* **26**, 799.
- Sayle, T.X.T., S.C. Parker and C.R.A. Catlow, 1992, *J. Chem. Soc. Chem. Commun.*, p. 977.
- Sayle, T.X.T., S.C. Parker and C.R.A. Catlow, 1994a, *J. Phys. Chem.* **98**, 13625.
- Sayle, T.X.T., S.C. Parker and C.R.A. Catlow, 1994b, *Surf. Sci.* **316**, 329.
- Schlatter, J.C., and P.J. Mitchell, 1980, *Ind. Eng. Chem. Prod. Res. Dev.* **19**, 288.
- Schmieg, S.J., and D.N. Belton, 1995, *Appl. Catal. B* **6**, 127.
- Sergo, V., and D.R. Clarke, 1995, *J. Am. Ceram. Soc.* **78**, 641.
- Serre, C., F. Garin, G. Belot, G. Maire and R. Roche, 1991, Characterization of oxidation catalysts by CO-TPR and selective carbon-carbon bond rupture, in: *Catalysis and Automotive Pollution Control II*, ed. A. Crueg (Elsevier, Amsterdam) pp. 153-165.
- Serre, C., F. Garin, G. Belot and G. Maire, 1993a, *J. Catal.* **141**, 1.

- Serre, C., F. Garin, G. Belot and G. Maire, 1993b, *J. Catal.* **141**, 9.
- Settu, T., and R. Gobinathan, 1994, *Bull. Chem. Soc. Jpn.* **67**, 1999.
- Settu, T., and R. Gobinathan, 1996, *J. Eur. Ceram. Soc.* **16**, 1309.
- Shalabi, M.A., B.H. Harji and C.N. Kenney, 1996, *J. Chem. Technol. Biotechnol.* **65**, 317.
- Shannon, R.D., 1976, *Acta Crystallogr. A* **32**, 751.
- Shannon, R.D., and C.T. Prewitt, 1969, *Acta Crystallogr. B* **25**, 925.
- Shannon, R.D., and C.T. Prewitt, 1970, *Acta Crystallogr. B* **26**, 1046.
- Shelef, M., 1995, *Chem. Rev.* **95**, 209.
- Shelef, M., and G.W. Graham, 1994, *Catal. Rev. Sci. Eng.* **36**, 433.
- Shido, T., and Y. Iwasawa, 1992, *J. Catal.* **136**, 493.
- Shido, T., and Y. Iwasawa, 1993, *J. Catal.* **141**, 71.
- Shinjo, H., H. Muraki and Y. Fujitani, 1987, Periodic operation effects on automotive noble metal catalysts: Reaction analysis of binary gas systems, in: *Catalysis and Automotive Pollution Control*, eds A. Cruce and A. Frennet (Elsevier, Amsterdam) pp. 187–197.
- Shyu, J.Z., and K. Otto, 1989, *J. Catal.* **115**, 16.
- Shyu, J.Z., K. Otto, W.L.H. Watkins, G.W. Graham, R.K. Belitz and H.S. Gandhi, 1988a, *J. Catal.* **114**, 23.
- Shyu, J.Z., W.H. Weber and H.S. Gandhi, 1988b, *J. Phys. Chem.* **92**, 4964.
- Sinev, M.Y., G.W. Graham, L.P. Haack and M. Shelef, 1996, *J. Mater. Res.* **11**, 1960.
- Solymosi, F., and M. Pasztor, 1985, *J. Phys. Chem.* **89**, 4789.
- Solymosi, F., M. Pasztor and G. Rakhely, 1988, *J. Catal.* **110**, 413.
- Sorensen, O.T., 1981, Thermodynamics and defect structure of nonstoichiometric oxides, in: *Nonstoichiometric Oxides*, ed. O.T. Sorensen (Academic Press, New York) pp. 1–59.
- Soria, J., A. Martinez-Arias and J.C. Conesa, 1992, *Vacuum* **43**, 437.
- Soria, J., A. Martinez-Arias and J.C. Conesa, 1995, *J. Chem. Soc. Faraday Trans.* **91**, 1669.
- Stefanic, G., S. Popovic and S. Music, 1997, *Thermochim. Acta* **303**, 31.
- Stubenrauch, J., and J.M. Vohs, 1996, *J. Catal.* **159**, 50.
- Stubenrauch, J., and J.M. Vohs, 1997, *Catal. Lett.* **47**, 21.
- Su, E.C., and W.G. Rothschild, 1986, *J. Catal.* **99**, 506.
- Su, E.C., C.N. Montreuil and W.G. Rothschild, 1985, *Appl. Catal.* **17**, 75.
- Summers, J.C., and S.A. Ausen, 1979, *J. Catal.* **58**, 131.
- Summers, J.C., and D.R. Monroe, 1981, *Ind. Eng. Chem. Prod. Res. Dev.* **20**,.
- Sun, Y., and P.A. Sermon, 1996, *J. Mater. Chem.* **6**, 1025.
- Taha, R., D. Martin, S. Kacimi and D. Duprez, 1996, *Catal. Today* **29**, 89.
- Taha, R., D. Duprez, N. Mouaddib-Moral and C. Gauthier, 1998, Oxygen storage capacity of three-way catalysts: a global test for catalyst deactivation, in: *Catalysis and Automotive Pollution Control IV*, eds N. Kruse, A. Frennet and J.-M. Bastin (Elsevier, Amsterdam) pp. 549–558.
- Tani, E., M. Yoshimura and S. Somiya, 1983a, *J. Am. Ceram. Soc.* **66**, 506.
- Tani, E., M. Yoshimura and S. Somiya, 1983b, *J. Am. Ceram. Soc.* **66**, 11.
- Tarasov, A.L., L.K. Przhval'skaya, V.A. Shvets and V.B. Kazanskii, 1989, *Kinet. Catal. USSR* **29**, 1020.
- Tauster, S.J., S.C. Fung and R.L. Garten, 1978, *J. Am. Chem. Soc.* **100**, 170.
- Taylor, K.C., 1984, Automobile catalytic converters, in: *Catalysis – Science and Technology*, eds J.R. Anderson and M. Boudart (Springer, Berlin) pp. 119–170.
- Taylor, K.C., 1993, *Catal. Rev.-Sci. Eng.* **35**, 457.
- Taylor, K.C., and J.C. Schlatter, 1980, *J. Catal.* **63**, 53.
- Taylor, K.C., R.M. Sinkewitch and R.L. Klimisch, 1974, *J. Catal.* **35**, 34.
- Terribile, D., A. Trovarelli, C. de Leitenburg, G. Dolcetti and J. Llorca, 1997, *Chem. Mater.* **9**, 2676.
- Terribile, D., A. Trovarelli, J. Llorca, C. de Leitenburg and G. Dolcetti, 1998a, *J. Catal.* **178**, 299.
- Terribile, D., A. Trovarelli, J. Llorca, C. de Leitenburg and G. Dolcetti, 1998b, *Catal. Today* **43**, 79.
- Terribile, D., J. Llorca, M. Boaro, C. de Leitenburg, G. Dolcetti and A. Trovarelli, 1998c, *Chem. Commun.*, p. 1897.
- Tournayan, L., N.R. Marcilio and R. Frety, 1991, *Appl. Catal.* **78**, 31.
- Trovarelli, A., 1996, *Catal. Rev. Sci. Eng.* **38**, 439.

- Trovarelli, A., G. Dolcetti, C. de Leitenburg, J. Kašpar, P. Finetti and A. Santoni, 1992, *J. Chem. Soc. Faraday Trans.* **88**, 1311.
- Trovarelli, A., G. Dolcetti, C. de Leitenburg and J. Kašpar, 1993, CO<sub>2</sub> hydrogenation over platinum group metals supported on CeO<sub>2</sub>: evidence for a transient metal-support interaction, in: *New Frontiers in Catalysis*, eds L. Guczi, F. Solymosi and P. Tétényi (Elsevier, Amsterdam) pp. 2781–2785.
- Trovarelli, A., C. de Leitenburg, G. Dolcetti and J.L. Lorca, 1995, *J. Catal.* **151**, 111.
- Trovarelli, A., C. de Leitenburg and G. Dolcetti, 1997, *Chemtech* **27**, 32.
- Tschope, A., W. Liu, M. Flytzani-Stephanopoulos and J.Y. Ying, 1995, *J. Catal.* **157**, 42.
- Tuller, H.L., and A.S. Nowick, 1975, *J. Electrochem. Soc.* **122**, 255.
- Usmen, R.K., G.W. Graham, W.L.H. Watkins and R.W. McCabe, 1995, *Catal. Lett.* **30**, 53.
- Valden, M., R.L. Keiski, N. Xiang, J. Pere, J. Aaltonen, M. Pessa, T. Maunula, A. Savimäki, A. Lahti and M. Harkonen, 1996, *J. Catal.* **161**, 614.
- Vidmar, P., P. Fornasiero, J. Kašpar and M. Graziani, 1997, *J. Catal.* **171**, 160.
- Villarubia, J.S., and H. Ho, 1987, *J. Chem. Phys.* **87**, 750.
- Vlaic, G., P. Fornasiero, S. Geremia, J. Kašpar and M. Graziani, 1997, *J. Catal.* **168**, 386.
- Weibel, M., F. Garin, P. Bernhardt, G. Maire and M. Prigent, 1991, Influence of water in the activity of catalytic converters, in: *Catalysis and Automotive Pollution Control II*, ed. A. Cruick (Elsevier, Amsterdam) pp. 195–205.
- Whittington, B.J., J.C. Jiang and D.L. Trimm, 1995, *Catal. Today* **26**, 41.
- Xu, X., and D.W. Goodman, 1994, *Catal. Lett.* **24**, 31.
- Yamada, K., H. Tanaka and M. Yamamoto, 1997, *SAE*, 970464.
- Yao, H.C., and Y.F. Yu Yao, 1984, *J. Catal.* **86**, 254.
- Yao, M.H., R.J. Baird, F.W. Kunz and T.E. Hoost, 1997, *J. Catal.* **166**, 67.
- Yashima, M., N. Ishizawa and M. Yoshimura, 1992a, *J. Am. Ceram. Soc.* **75**, 1550.
- Yashima, M., N. Ishizawa and M. Yoshimura, 1992b, *J. Am. Ceram. Soc.* **75**, 1541.
- Yashima, M., K. Morimoto, N. Ishizawa and M. Yoshimura, 1993a, *J. Am. Ceram. Soc.* **76**, 2865.
- Yashima, M., K. Morimoto, N. Ishizawa and M. Yoshimura, 1993b, *J. Am. Ceram. Soc.* **76**, 1745.
- Yashima, M., H. Arashi, M. Kakihana and M. Yoshimura, 1994a, *J. Am. Ceram. Soc.* **77**, 1067.
- Yashima, M., K. Ohtake, M. Kakihana and M. Yoshimura, 1994b, *J. Am. Ceram. Soc.* **77**, 2773.
- Yashima, M., H. Takashina, M. Kakihana and M. Yoshimura, 1994c, *J. Am. Ceram. Soc.* **77**, 1869.
- Yashima, M., T. Hirose, S. Katano, Y. Suzuki, M. Kakihana and M. Yoshimura, 1995a, *Phys. Rev. B* **51**, 8018.
- Yashima, M., T. Mitsunashi, H. Takashina, M. Kakihana, T. Ikegami and M. Yoshimura, 1995b, *J. Am. Ceram. Soc.* **78**, 2225.
- Yoldas, B.E., 1982, *J. Am. Ceram. Soc.* **65**, 387.
- Yu Yao, Y.F., 1984, *J. Catal.* **87**, 152.
- Zafiris, G.S., and J. Gorte, 1993a, *J. Catal.* **143**, 86.
- Zafiris, G.S., and J. Gorte, 1993b, *J. Catal.* **139**, 561.
- Zafiris, G.S., and R.J. Gorte, 1991, *J. Catal.* **132**, 275.
- Zafiris, G.S., and R.J. Gorte, 1992, *Surf. Sci.* **276**, 86.
- Zamar, F., A. Trovarelli, C. de Leitenburg and G. Dolcetti, 1995, *J. Chem. Soc. Chem. Commun.*, p. 965.
- Zamar, F., A. Trovarelli, C. de Leitenburg and G. Dolcetti, 1996, *Stud. Surf. Sci. Catal.* **101**, 1283.
- Zhang, X., and K.J. Klabunde, 1992, *Inorg. Chem.* **31**, 1706.
- Zhang, Y., S. Andersson and M. Muhammed, 1995, *Appl. Catal. B* **6**, 325.
- Zhao, Z.L., and M. Baerns, 1992, *J. Catal.* **135**, 317.
- Zhdanov, V.P., and B. Kasemo, 1996, *Catal. Lett.* **40**, 197.
- Zotin, F.M.Z., L. Tournayan, J. Varlout, V. Perrichon and R. Frety, 1993, *Appl. Catal. A* **98**, 99.

## Chapter 185

# THE USE OF RARE-EARTH-CONTAINING ZEOLITE CATALYSTS

A. CORMA and J.M. LÓPEZ NIETO

*Instituto de Tecnología Química, UPV-CSIC, Avda. Los Naranjos s/n,  
 46022 Valencia, Spain*

### Contents

Symbols and abbreviations	269	3.1.2. Alkylation of isobutane/butene	290
1. Zeolite characteristics and main commercial uses	270	3.2. Petrochemistry	295
2. Zeolite modification with rare earths	273	3.2.1. Alkylation of aromatics	295
2.1. Preparation of R-containing zeolites	273	3.2.2. Isomerization of C <sub>8</sub> alkylaromatics	298
2.2. Physico-chemical characterization of R-containing zeolites	278	3.2.3. Methanol conversion	298
2.2.1. Effect of R exchange on zeolite stability and acidity	280	3.3. Production of chemicals and fine chemicals	299
3. Zeolite catalysts containing rare earths	284	3.3.1. Acylations	299
3.1. Oil refining for gasoline production	284	3.3.2. Condensation of carbonyl compounds	301
3.1.1. Rare earths in FCC catalysts	284	3.4. Other reactions and uses	302
3.1.1.1. Rare earths in SO <sub>x</sub> and NO <sub>x</sub> abatement additives for FCC	288	3.4.1. NO <sub>x</sub> elimination	303
		4. Conclusions	305
		References	305

### Symbols and abbreviations

A	Linde type A zeolite, an 8-membered ring zeolite, see table 2. Me-A or R-A correspond to metal- or rare-earth-exchanged materials	LPG	Liquefied petroleum gas
D <sub>i</sub>	Intracrystalline diffusion coefficient	MCM-22	Zeolitic material with characteristics of both 10- and 12-membered ring zeolites and supercages of 7.1×7.1×18.2 Å <sup>3</sup>
DMB	Dimethylbutane	MH	Methylhexane
DMH	Dimethylhexane	MON	Motor octane number
DMP	Dimethylpentane	MOR	Mordenite, a 12-membered ring zeolite, see table 2.
EDTA	Ethylenediaminetetracetic acid	MRI	Magnetic resonance imaging
EMT	Hexagonal faujasite zeolite, a 12-membered ring zeolite	R	Rare earth
FCC	Fluid catalytic cracking	RON	Research octane number
		SCR	Selective catalytic reduction



TMP	Trimethylpentanes	Y	Zeolite with faujasite structure, a 12-membered ring zeolite, see table 2.
USY	Ultrastable Y zeolite. Me-USY and R-USY correspond to metal- and rare-earth-exchanged material		Me-Y and R-Y correspond to metal- and rare-earth-exchanged materials
X	Zeolite with faujasite structure, a 12-membered ring zeolite, see table 2. Me-X or R-X correspond to metal- and rare-earth-exchanged materials	ZSM- <i>n</i>	Zeolites with different structures ( $n=3, 4, 5, 8, 12, 18, 20$ or $23$ ); see table 2

## 1. Zeolite characteristics and main commercial uses

During the last sixteen years the crystalline aluminosilicates, named zeolites, have attracted the attention of industrialists and scientists, because of their possible uses as catalysts, adsorbents and molecular sieves. Zeolite minerals were first identified in 1756 by Baron Crostedt, a Swedish mineralogist (Occelli and Robson 1989). They are natural adsorbents, and for this use they are efficient and more cost-effective than synthetic zeolites. However, since naturally occurring zeolites very frequently contain metal impurities, which can strongly modify their catalytic behaviour, their use as catalysts is limited and synthetic zeolites are preferred for catalytic applications.

In 1948, researchers at Union Carbide synthesized zeolites A and X. After these first experiences, the number of new synthetic materials has now increased to well over 150 structures (Breck 1974, Dyer 1988, Roland 1989, Occelli and Robson 1989, van Bekkum et al. 1990, Venuto 1994, 1997, Corma 1995, Meier et al. 1996, Treacy et al. 1996).

Since then, zeolites have been developed into key materials in the chemical industry. While the production of synthetic zeolites in 1986 exceeded some 1100 million lbs worldwide (Chen and Degnan 1988), a similar production is expected in the USA within the next few years. Table 1 gives the US demand for zeolites in 1995 and the demand expected in 2000 (Hairston 1996). Although ion-exchange applications in detergents (using zeolite A) are the largest zeolite uses, one of the most potentially lucrative markets

Table 1  
Demand for zeolites in the USA (million LB)

Product	1995	2000
<i>Detergents</i>		
Powdered household detergents	690	760
Other detergents and cleaners	2	10
<i>Catalysts</i>		
Petroleum refining	153	170
Other applications	10	25
<i>Other markets</i>	127	155
<b>Total</b>	<b>982</b>	<b>1120</b>

for zeolites is their use as catalysts. In this way, while oil refining is the most important field of application, the replacement of liquid acid catalysts (hydrofluoric and sulphuric acids) and aluminium chloride by zeolites in an important number of petrochemical and fine chemical processes are increasing in the last decade.

Zeolites are tridimensional crystalline aluminosilicates with the following formula in the as-synthesized form:  $mM_{2/n}O[xAl_2O_3-ySiO_2]wH_2O$ , where M is a cation which can belong to group IA or IIA or can be an organic cation, while  $n$  is the cation valence, and  $w$  represents water contained in the zeolite voids. The main characteristic of the zeolites is that the tetrahedral primary building blocks are linked in such a way that a three-dimensional network containing channels and cavities of molecular dimensions is produced.

Considering the size of the channels, they are conventionally defined as ultralarge (>12-), large (12-), medium (10-), or small (8-membered ring) pore materials depending on the smallest number of O or T (T=Si, Al) atoms that limit the pore aperture of the largest channel, and whose diameter varies between 5 and 20 Å. A summary of the different types of zeolites is shown in table 2.

In the case of rare-earth-exchanged zeolite, structures A, X and Y have been the most studied. The synthesis and structures of these zeolites are well known (Stiles and Koch 1995), and the structures are all based on the sodalite (β-cage) unit (fig. 1) (Smith 1976). The A zeolite (fig. 2, top) is obtained by replacing each 4-ring of the sodalite cage at the corner of the unit cell by a cube. Each sodalite cage at the body center of the unit cell transforms into a truncated cuboctahedron with twelve 4-rings, eight 6-rings, and six 8-rings. The truncated octahedra form a system of pores linked in three directions by windows of 8-rings. The sodalite units are separated from each other, and access to them is via 6-rings.

The topology of faujasite (and of the related X and Y zeolites) is obtained by linking sodalite units with hexagonal prisms (fig. 2, bottom). Each sodalite unit is linked to four sodalite units in a tetrahedral configuration by hexagonal prisms which are attached to four of the eight hexagonal faces; the other four hexagonal faces are unshared, as are the 4-rings. The framework of faujasite is very open and encloses a system of large cages linked by four windows of 12-rings to adjacent pores (fig. 3). Each of the faujasite cages is bounded by eighteen 4-rings, four 6-rings and four 12-rings.

Zeolites, especially the silica-rich materials, often exhibit a high thermal and hydrothermal stability. They show very high surface area and pore volume, and so are capable of adsorbing great amounts of hydrocarbons. In addition, acidity in zeolites can be very high, being about 1000 times higher than that of amorphous silica-alumina. Acidity is related to the framework aluminium content and is easily tuneable by controlling some physicochemical properties, such as the framework Al content, by ion exchange, or by replacing Al by other elements (Ga, Fe, B). The framework Al content can be controlled either by direct synthesis or by post-synthesis dealumination treatments. The dealumination is generally performed by hydrothermal treatment followed by hydrochloric acid leaching as well as by complexing and abstracting the framework Al using EDTA,  $SiCl_4$  or  $(NH_4)_2F_6Si$  as reactants. In these cases, dealumination occurs, with a mechanism

Table 2  
Structural characteristics of different zeolites

Zeolite	Structure type Code <sup>a</sup>	Diameter of largest channel (Å)	Dimensionality	Ring size of channels
Rho	RHO	3.6	3	8–8–8
Chabattite	CHA	3.8×3.8	3	8–8–8
Linde Type A	LTA	4.1	3	8–8–8
Erionite	ERI	3.6×5.1	3	8–8–8
Ferrierite	FER	4.2×5.4 3.5×4.8	2	10–8
ZSM-22/Theta-1	TON	4.4×5.5	1	10
ZSM-23	MTT	4.5×5.2	1	10
Heulandite	HEU	3.0×7.6 2.6×4.7	2	10–8–8
NV-87	NES	4.7×6.0	2	10–10
ZSM-5	MFI	5.3×5.6 5.1×5.5	3	10–10–10
ZSM-11	MEL	5.3×5.4	3	10–10–10
ZSM-12	MTW	5.5×5.9	1	12
Linde type L	LTL	7.1	1	12
ZSM-4/Omega	MAZ	7.4 3.4×5.6	1	12–8
Mordenite	MOR	6.5×7.0 2.6×5.7	2	12–8
ZSM-18	MEI	6.9 3.2×3.5	3	12–7
Offretite	OFF	6.7 3.6×4.9	3	12–8
Beta	BEA	7.6×6.4 5.5×5.5	3	12–12
Faujasite (Y, X)	FAU	7.4	3	12–12–12
VPI-5	VFI	12.1	1	18

<sup>a</sup> Meier et al. 1996; Treacy et al. 1996.

that is now well known (Fleisch et al. 1986, Scherzer 1986, Corma et al. 1990b, 1992, Occelli and Robson 1992).

**Isomorphous substitution** of aluminium or silicon by other trivalent (B, Cr, Ga, Fe) or tetravalent (V, Ti, Ge) elements, can be carried out either by direct synthesis (by adding the appropriate salt in the medium) or by post-synthesis modification employing metal halides. **Grafting** of a given compound at sites located on the surface or inside the channels or cavities of crystallites, contributes to introduce new catalytic sites or to modify the accessibility and diffusivity of reactants and products. Thus, the possibility of tuning the adsorption properties together with the possibility of generating active sites

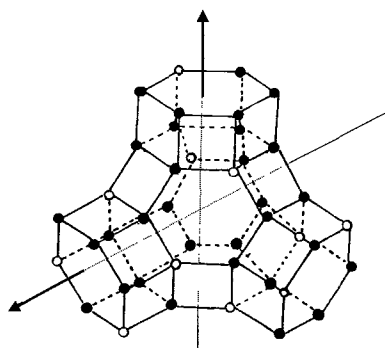


Fig. 1. Idealized projection and section through a sodalite  $\beta$ -cage unit. (After Smith 1976.)

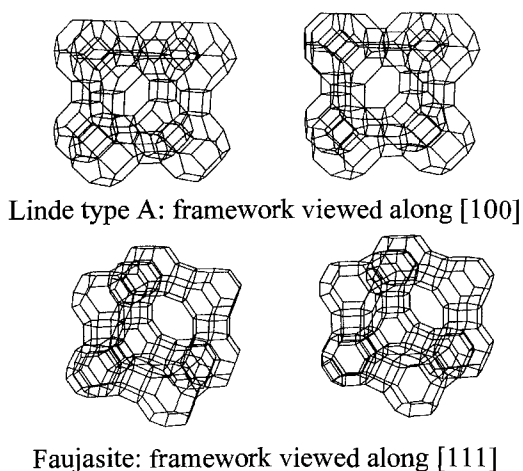


Fig. 2. Stereodiagram of framework topology of (a) A zeolites and (b) faujasite zeolites. (After Meier et al. 1996.)

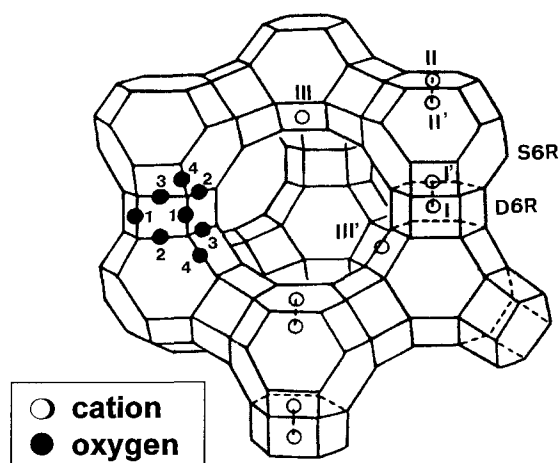


Fig. 3. Faujasite structure. Roman numerals indicate cation positions. The different types of framework oxygen atoms are indicated by the numbers 1–4. (After Yeom et al. 1997.)

inside the channels and cavities of zeolites results in a very important type of catalyst, which by itself can be considered as a catalytic microreactor (Corma 1995).

## 2. Zeolite modification with rare earths

### 2.1. Preparation of R-containing zeolites

The modification of zeolites by ion exchange provides a useful means of tailoring their properties for particular applications. Several authors have reviewed a large body of

Table 3  
Preparation of rare-earth zeolites by ion exchange

Zeolite	Precursor	Si/Al	Cation	Me-ion exchange <sup>a</sup>	Temp. (°C)	Ref.
Y	Na-form	n.d. <sup>b</sup>	La-nitrate	71.1 <sup>c</sup>		Zinner et al. 1993
		3.5			70	Mostad et al. 1997
		2.5		15–69	70	Gaare and Akporiaye 1996; Flego et al. 1995
		2.4		26–70	70	Akporiaye et al. 1993
		2.4		63–92		Weiß et al. 1997
	Na- or NH <sub>4</sub> -form	2.68			70	Spiridonov et al. 1992
	H-form		La-chloride	70	25	Gauthier et al. 1989
	Na-form		Ce-nitrate	65.8 <sup>c</sup>		Zinner et al. 1993
		3		33–98		Choudhary et al. 1989
				70	80	Chiche et al. 1986
	Na-form		Ce-chloride	70	25	Gauthier et al. 1989
	Na-form		Pr-nitrate	70	25	Gauthier et al. 1989
	Na-form		Yb-nitrate	70	25	Gauthier et al. 1989
	Na- or NH <sub>4</sub> -form	2.68				Spiridonov et al. 1992
	Na-form		Gd-nitrate	56.8 <sup>c</sup>		Zinner et al. 1993
				70	25	Gauthier et al. 1989
	Na-form		Tb-nitrate			Hong et al. 1995
	K-form		Eu-nitrate			Baba et al. 1995
	Na-form <sup>c</sup>	5.9	Nd-nitrate			Azbel et al. 1989
	Na-form			60.5 <sup>c</sup>		Zinner et al. 1993
	Na- or NH <sub>4</sub> -form	2.68			70	Spiridonov et al. 1992
X	Na-form	1.3	La-chloride			Gaare and Akporiaye 1997
			La-nitrate		25–82	Sherry 1968, 1997
	Na-form	23.3	Ce-acetate	18.5	25	Yasuda et al. 1995
		1.25	Ce-nitrate	90		Choudhary et al. 1989
	Na-form	1.16	Eu-chloride	11–59	25	Liu et al. 1994
Beta	H-form	11	La-nitrate	30	70	Mostad et al. 1997
MCM-22	Na-form	14.7	La-nitrate	40	70	Mostad et al. 1997
H-ZSM-5	Na-form	23.3	La-nitrate			Mori et al. 1993
	Cu-form	n.d.			85	Rokosz et al. 1997
	Na-form	42	Ce-nitrate	67		Pillai 1996
	Cu-form	20		11–60	25	Zhang and Flytzami-Stephanopoulos 1996
	Na-form	23.3	Nd-nitrate			Mori et al. 1993
	Na-form	23.3	Yb-nitrate			Mori et al. 1993

*continued on next page*

Table 3, *continued*

Zeolite	Precursor	Si/Al	Cation	Me-ion exchange <sup>a</sup>	Temp. (°C)	Ref.
Mordenite	Na-form	13.1	La-chloride	57	70–100	Ito et al. 1994
	Na-form	23–128	Ce-nitrate	0.27 <sup>d</sup>	90	Sugi et al. 1994b
		13.1	Ce-acetate	58	70–100	Ito et al. 1994
EMT	Na-form	n.d.	La-nitrate		70	Rørbik et al. 1997
	NH <sub>4</sub> -form	3.5		40–80	70	Mostad et al. 1997
A	Na-form		Gd-chloride	0.8–5.0 <sup>f</sup>	25	Hazenkamp et al. 1992a
	Na-form		Eu-chloride	5.0 <sup>f</sup>	25	Hazenkamp et al. 1992b

<sup>a</sup> From the theoretical ion-exchange capacity.<sup>d</sup> Ce/Al ratio.<sup>b</sup> n.d., not determined.<sup>e</sup> Dealuminated Na-Y.<sup>c</sup> Me,Ca:Na-Y.<sup>f</sup> In wt%.

pertinent literature on ion exchange in zeolites (Magee and Blazek 1976, Cremers 1977, Townsend 1986, 1991, Ben Taarit 1992). Also, the relative affinities of different cations in A, X and Y zeolites have been established, and the exchange kinetics have been investigated especially in relation to detergency (Sherry 1966).

Usually, the introduction of rare-earth cations in zeolites can be achieved by ion exchange of the sodium or ammonium forms of zeolites, using a suspension of these starting materials in a solution of the cation to be introduced (table 3). In the case of the faujasite structure, although conventional ion exchange can be used in order to introduce rare-earth cations, it becomes difficult to surpass a degree of exchange higher than about 75% which corresponds to the exchangeable positions in the supercage. Indeed, the exchange of the remaining 25% positions which are located within the sodalite cages is strongly hampered by the small dimensions of the sodalite windows, which limit the diffusion of the H<sub>2</sub>O-solvated rare-earth cations (Karge et al. 1988a).

A high degree of exchange can only be obtained when the exchange procedure is repeated several times and intermediate calcinations are carried out in order to push the desolvated M<sup>3+</sup> cations into the sodalite cages (Keir et al. 1988). Then, during the calcination, water molecules could be removed from the rare-earth ions which then could move into the network of sodalite cages and hexagonal prisms, while the sodium ions migrate from those into the supercage (Sherry 1976). Recently, it has been observed that the amount of rare-earth fixation is independent of time and temperature of calcination but depends on the water content of the calcined sample (Sherry 1997).

During the preparation of R-exchanged zeolites (R=rare-earth atoms) it was found that reversible ion-exchange isotherms could be obtained in the La,Na-X and La,Na-Y systems, and these depend on the temperature and the zeolite type. Thus, rare earths cannot diffuse into the small cages of synthetic faujasites at 25°C within a reasonable time,

but this is accelerated at higher temperatures (Sherry 1968). At room temperature, a lanthanum exchange of 69% and 85% for Na-Y and Na-X, respectively, has been reported. This is so because the sodium ions in the small cages are difficult to remove. However, when the exchange is carried out at 100°C,  $\text{La}^{3+}$  ions can replace the  $\text{Na}^+$  ions located in the small cages, and higher levels of exchange are achieved.

On the other hand, if zeolites are treated at high temperatures, a complete ion exchange can be achieved. The radius of the hydrated  $\text{La}^{3+}$  ion is 3.96 Å whereas the free diameter of the entrances to the network of the small cavities is 2.4 Å (Herreros et al. 1992). However, when the zeolite is heated to about 320°C, the hydration sphere is lost (the Pauling radius of  $\text{La}^{3+}$  is 1.13 Å) and some of the lanthanum cations migrate into the sodalite cages.

We must indicate that, generally, the degree of exchange is markedly influenced by the type and concentration of the rare earth as well as by the nature of the compensation cation pre-existing in the zeolite. Thus, Rees and Zuyi (1986) reported kinetic and thermodynamic values for the exchange of the rare-earth cations La, Ce, Y and Lu, at 25 and 65°C, with Na-Y. They observed that up to a 50% level of exchange the selectivity for R exchange was in the order  $\text{La} = \text{Ce} > \text{Lu} = \text{Y}$ . In agreement with this, Das and Upreti (1995) observed that, at room temperature, the exchange obtained on zeolite X with  $\text{La}^{3+}$  was higher than that with  $\text{Pr}^{3+}$ .

The level of ion exchange also depends on the cation present in the zeolite. Thus, Keane (1996) reports ion exchange isotherms at 25°C of  $\text{Ce}^{3+}$  with alkaline-exchanged  $\text{Me}^+$ -Y zeolite,  $\text{Me}^+$  being Li, Na, K, Rb-Na, Cs-Na. According to these results it can be concluded that the progress of exchange and the overall preference of the zeolite phase for the  $\text{Ce}^{3+}$  ions decreases in the order  $\text{Li-Y} > \text{Na-Y} > \text{K-Y} > \text{Rb,Na-Y} > \text{Cs,Na-Y}$ , while the maximum level of cerium exchanged is achieved in the Ce,K-Y system. In this respect, a clear example of the influence of the method of cation incorporation on the catalytic behaviour of exchanged zeolites is the variation of the catalytic activity of Ce,Cu-ZSM-5 zeolite (Zhang and Flytzani-Stephanopoulos 1994), an active catalyst for the reduction of  $\text{NO}_x$ , where the best catalyst is that prepared by exchanging Cu ions into the ZSM-5, followed by Ce ion exchange.

Although it can be of interest from a fundamental point of view to study zeolites exchanged with a single rare-earth cation, from an industrial point of view it is most interesting to use the natural mixture of rare earths. Accordingly, some authors have described the preparation of rare-earth-exchanged zeolite X (Venuto et al. 1966a,b), zeolite Y (Venuto et al. 1966a,b, Hickson and Csicsery 1968, Ward 1969, Magee and Blazek 1976, Fleisch et al. 1986, Reddy and Varma 1997a) and Mordenite (Sakamoto et al. 1994) using commercial rare-earth chloride ( $\text{RECl}_3 \cdot 6\text{H}_2\text{O}$ ).

In the last decade, zeolite ion exchange has also been carried out in the **solid state**. Zeolites can be exchanged by solid-state exchange using different salts of the desired cation, and the zeolite in the ammonium, hydrogen or sodium form (Beyer et al. 1988, Karge 1992, 1994, 1997, Karge et al. 1988a,b, 1990, 1991, 1994, Karge and Beyer 1991, Karge and Jozefowicz 1994). As an example, fig. 4 shows the catalytic behaviour of La-exchanged H-Y and Na-Y zeolites prepared by both solid-state reaction and conventional ion exchange (Karge and Beyer 1991, Karge 1992) during the selective

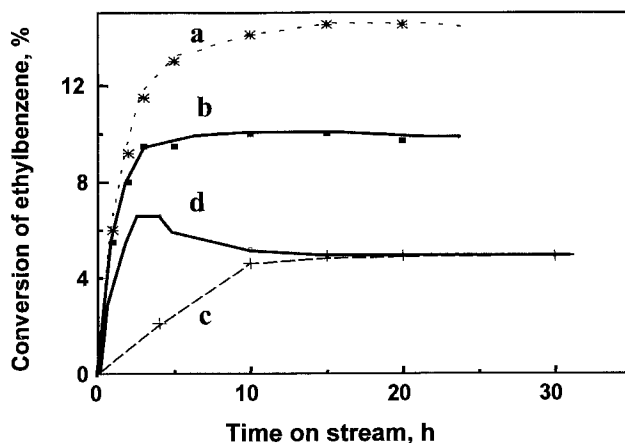


Fig. 4. Selective disproportionation of ethylbenzene over La,H-Y zeolites. The catalysts were prepared (a) by a solid-state reaction between  $\text{LaCl}_3$  and the corresponding zeolite and (b) by conventional ion exchange. Experimental conditions:  $T = 182^\circ\text{C}$ ; 1.3 vol% ethylbenzene in He, total flow  $5 \text{ ml min}^{-1}$ ,  $m(\text{cat}) = 0.25 \text{ g}$ . (After Karge et al. 1988a.)

disproportionation of ethylbenzene. It can be seen that both preparation methods give active catalysts, and the differences observed between both methods can be related to the optimal amount of La incorporated into the framework of the zeolite obtained by solid-state exchange.

Solid-state ion exchange of deammoniated  $\text{NH}_4\text{Na-Y}$  with lanthanum chloride results in a complete replacement of the OH groups of the deammoniated  $\text{NH}_4\text{Na-Y}$  material with the evolution of HCl. However, a complete replacement does not occur, and partially exchanged zeolites are obtained by solid-state ion exchange in H-ZSM-5/ $\text{LaCl}_3$  or H-MOR/ $\text{LaCl}_3$  (Karge et al. 1988b). Indeed, in the case of H-ZSM-5/ $\text{LaCl}_3$ , only about 60% of the protons are replaced by  $\text{La}^{3+}$  under the same conditions. This is probably due to the difficulty in counter-balancing the negative charges widely dispersed in samples with a Si/Al ratio  $>23$  (Karge 1994, Karge et al. 1994). Recently, Sulikowski et al. (1997) have reported the solid-state reaction of  $\text{LaCl}_3$  with different zeolites, i.e. ferrierite, mordenite, zeolite L and stabilised faujasite, under anhydrous conditions.

We must indicate that in addition to the type of zeolite, the conditions used in the solid-state ion exchange determine the catalytic behaviour of the metal-containing zeolites. Thus, stoichiometric mixtures of  $\text{NH}_4\text{Na-Y/LaCl}_3$  after a heat treatment at  $402^\circ\text{C}$ , yield a material inactive for catalyzing hydrocarbon reactions such as disproportionation of ethylbenzene and cracking of *n*-decane. However, if the same heat-treatment is followed by admission of small amounts of water, an active  $\text{La}_3\text{Na-Y}$  catalyst with a catalytic behaviour similar to a material obtained by conventional ion exchange is obtained (Karge et al. 1988a, 1991). The interaction of the cations introduced with water molecules generates OH groups (Bönsted acid sites) as evidenced by in-situ IR spectroscopy before and after the hydration steps (Karge et al. 1991).



Solid-state ion exchange does not occur only with the hydrogen form of zeolites but also with the sodium form. Thus, a solid-state reaction between  $\text{LaCl}_3$  and Na-Y has also been observed (Karge 1994, Karge et al. 1994).

Although R-containing zeolites are generally prepared by solution or solid-state ion exchange of alkaline zeolites, they can also be prepared using other methods. One of these consists in the incorporation of the metal precursor salts into the zeolite by impregnation with an aqueous solution (Zhang and Flytzani-Stephanopoulos 1996, Al-jarallah et al. 1997) or an ethanolic solution (Sugi et al. 1994a), or with the R metal dissolved in liquid ammonia (Baba et al. 1991, 1993).  $\text{La}_2\text{H-ZSM-5}$  (Li et al. 1993) and R-ZSM-5 (Yiguang et al. 1992) zeolites have also been obtained by an hydrothermal exchange from  $\text{NH}_4\text{-ZSM-5}$  zeolite, although R incorporation was not very effective using this procedure. On the other hand, Gd-containing silicalite has also been obtained by hydrothermal synthesis (Bresinska et al. 1993).

## 2.2. *Physico-chemical characterization of R-containing zeolites*

The distribution of the cations between different positions and the structural characteristics of fresh and hydrothermally treated rare-earth-exchanged zeolites has been investigated by X-ray (Olson et al. 1968, Bennett and Smith 1969, Hunter and Scherzer 1971, Smith 1976, Costenoble et al. 1978, Dyer et al. 1978, Herreros et al. 1992, Nery et al. 1997) and neutron diffraction (Cheetham et al. 1984). Other physico-chemical techniques have also been reported to be useful for the characterization of the R-zeolites. These include the determination of ionic conductivities (Slade et al. 1992), IR spectroscopy (Rabo et al. 1968, Ward 1968, 1971, Jacobs and Uytterhoeven 1973, Scherzer and Bass 1975, Scherzer et al. 1975, Jia et al. 1992, Nasukhanov et al. 1993, Sousa-Aguiar et al. 1998), XPS (Grünert et al. 1993, Haack et al. 1995), EPR (Ulla et al. 1990, Nicula and Trif 1991), EXAFS-XANES (Suib et al. 1984, Berry et al. 1993, Baba et al. 1993, Tanaka et al. 1995, Antonio et al. 1997) and luminescence spectroscopy (Arakawa et al. 1982, Suib et al. 1984, Yiguang et al. 1992, Tian et al. 1992, Hazenkamp et al. 1992a,b, Hazenkamp and Blasse 1993, Serra et al. 1993, Hong et al. 1995, Rosa et al. 1997). However, solid-state NMR spectroscopy appears to be the most sensitive technique in the study of the location of rare-earth trivalent cations: results of  $^{129}\text{Xe}$ -NMR (Chen et al. 1991, Liu et al. 1994, Kim et al. 1994, Hunger et al. 1995, Timonen and Pakkanen 1997),  $^{23}\text{Na}$ -NMR (Lin and Chao 1991, Beyer et al. 1993, Liu et al. 1994, Hunger et al. 1995, Karge 1997),  $^{27}\text{Al}$ -NMR (Iyer et al. 1988, Hunger et al. 1995),  $^{29}\text{Si}$ -NMR (Roelofsen et al. 1986, Iyer et al. 1988, Chao and Lin 1992, Li et al. 1994, Hunger et al. 1995, Gaare and Akporiaye 1997) and  $^{139}\text{La}$ -NMR (Herreros et al. 1992, Hunger et al. 1995) in R-exchanged zeolites have been reported.

In the case of the most widely used R-Y zeolite, there are six different sites for the rare earth (see fig. 3) (Smith et al. 1967, Smith 1976): site I is located at the centre of a hexagonal prism (D6R), site I' is located in the sodalite ( $\beta$ ) cage approximately 1 Å from the D6R that comprise the hexagonal prism, site II' is located inside the sodalite cavity near a single six-ring (S6R, shared by a  $\beta$  and a supercage), site II is located in the

supercage adjacent to a S6R, site III is located in the supercage opposite a four-ring between two 12-rings, and site VI is somewhat off site III (off the 2-fold axis).

The position occupied by the R cation in the zeolite depends both on the particular cation and on the zeolite type. Olson et al. (1968) reported the structures of cerium-exchanged natural faujasite and lanthanum-exchanged X zeolite. Cerium ions were found to occupy sites III and to be randomly distributed in the supercages in hydrated cerium-exchanged natural faujasite. Meanwhile lanthanum ions occupy sites I' and II, being in positions II' in the case of hydrated La-exchanged X. A different distribution is observed on dehydrated samples. Thus, cerium ions partially occupy site III in the large cavity and site I' in the sodalite cage in the case of cerium-exchanged X zeolite (Hunter and Scherzer 1971), while in La-Y the lanthanum ions also occupy sites I' (Smith et al. 1967).

However, the positions of these cations change after calcination as a consequence of the dehydration/dehydroxylation of the cation, which allows it to migrate through the six-ring opening of the sodalite cage, and then occupy sites I, I' and III (Smith et al. 1967, Hunter and Scherzer 1971, Lee and Rees 1987a,b, Nery et al. 1997). In general, variations in R location were also observed depending on the calcination temperature, the exchanged cation and zeolite type. Accordingly, it has been proposed that when coordinated with H<sub>2</sub>O or OH<sup>-</sup> the R ions prefer to occupy sites I', while in the absence of H<sub>2</sub>O or OH<sup>-</sup> the preferred locations for the La<sup>3+</sup> ions are sites I and, to a lesser degree, sites I' (Smith 1976).

Computer modelling of the position of La<sup>3+</sup> has been carried out by Brenan et al. (1994a,b). These authors found that their predictions in anhydrous (Brenan et al. 1994a) and hydrated La-Y (Brenan et al. 1994b) zeolites were consistent with the diffraction structure reported by Cheetham et al. (1984). In addition, they found that the relaxation of O<sup>2-</sup> ions is an important factor in determining the stability of the La<sup>3+</sup> sites in faujasite. However, the composition of the zeolites also influences the positions in which the cations are incorporated. Thus, when in the R,Ca,Na-Y zeolite Ca<sup>2+</sup> ions are introduced before the R<sup>3+</sup> ions, they direct the latter to sites in the supercages, while no such directing effect is observed when the R<sup>3+</sup> ions are introduced first. In the case of an R<sub>2</sub>Na-Y zeolite, R<sup>3+</sup> ions preferentially occupy sites other than those in the supercages (Winkler et al. 1984). Winkler and Steimberg (1989) proposed that the number of R<sup>3+</sup> ions in the supercages of R<sub>2</sub>Na-Y zeolites after calcination can be derived from the longitudinal proton NMR relaxation time  $T_1$  of water adsorbed in R<sub>2</sub>Na-Y zeolite. They proposed that about 70% of these R ions are paramagnetic and dominate the proton  $T_1$ .

Shiralkar and Kulkarni (1982) studied the thermal and structural properties of rare-earth-exchanged Na-X and Na-Y zeolites by thermal analysis (TG/DTA), X-ray diffraction (XRD) and infrared (IR) spectroscopy. The cation exchange was carried out by contacting the zeolite powder with 5% mixed rare-earth chloride RCl<sub>3</sub>, composed of lighter rare earths such as La, Pr and Sm with traces of heavy rare earths. A better thermal stability was observed upon the replacement of sodium with a rare earth, although a partial replacement of rare earth with ammonium/hydrogen enhances the thermal stability. This trend has been observed on both R<sub>2</sub>Na-X and R<sub>2</sub>Na-Y zeolites, although Y is more stable than X zeolite.

Lee and Rees (1987a,b) described in detail the influence of calcination on the location and the valency of lanthanum (Lee and Rees 1987a) and cerium (Lee and Rees 1987b) cations in zeolite Y. They conclude that the number of rare-earth ions locked in the small cages (and thus the number of R ions in the supercage) is a function of the calcination temperature, and the migration of  $\text{La}^{3+}$  and  $\text{Ce}^{3+}$  cations outside the supercages occurs during the calcination step. The results show that, regardless of the calcination mode, both La and Ce migrate to sites I', located inside the sodalite cage, whereas Na cations migrate to sites II'. In addition, they observed that the total number of cations located in the small cages of the calcined Ce,Na-Y reached a maximum of 18 ions per unit cell (i/u.c.) which is slightly higher than the 17 i/u.c. found with the calcined La,Na-Y (Lee and Rees 1987b). On the other hand, the aluminium generated by the dealumination process due to the incorporation of  $\text{R}^{3+}$  cations and the calcination step is located inside the sodalite cage. In this way, dealumination is likely to occur due to the presence of protons produced during the formation of hydroxyl groups associated with the rare-earth cations. The migration of lanthanum ions from the supercages to the small cages causes the redistribution of sodium ions after dehydration of La,Na-Y zeolite at 350°C (Lin and Chao 1991). It has to be taken into account that although the migration of R ions is produced after calcination, La and Ce ions appear to resist migration out of the framework (Haack et al. 1995).

#### 2.2.1. *Effect of R exchange on zeolite stability and acidity*

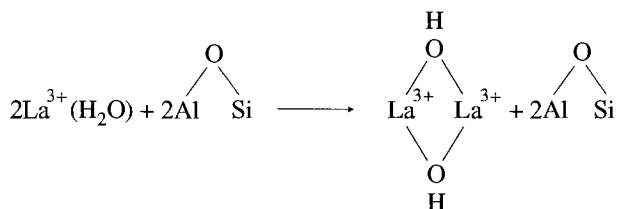
The success of zeolites as catalysts is based on their thermal and hydrothermal stability, together with the strong acidities achieved on their surface. The presence of rare-earth ions plays an important role in both properties, and therefore the impact of R on the stability and acidity of zeolites is presented below.

Concerning the stability of R-exchanged Y zeolite, it appears that the dealumination of the zeolite framework is strongly inhibited by the presence of a rare earth (Roelofsen et al. 1986, Nasukhanov et al. 1993). In this way, the introduction of an additional level of acidity during the thermal activation, due to the presence of the highly polarising  $\text{Ce}^{3+}$  ions, could serve to suppress crystallite growth, as has been observed in Ce,Ni-Y materials (Coughlan and Keane 1991). On the other hand, since  $\text{La}^{3+}$  ions can stabilise the Si (3Al) and Si (2Al) units of the framework they could affect the coordination distribution of the next-nearest-neighbour Al atom (Li et al. 1994). Consequently, they can affect the concentration and strength of the Brønsted acid sites in the resultant  $\text{R}_x\text{H-Y}$  zeolites.

It has been observed that the stability of both  $\text{R}_x\text{Na-Y}$  (Chen et al. 1991) and  $\text{R}_x\text{Na-X}$  (Kim et al. 1994) zeolites also depends on the dehydration-rehydration of zeolites.  $\text{La}^{3+}$  and  $\text{Ce}^{3+}$  cations are found in the supercages after exchange with  $\text{Na}^+$  at 25°C. They all migrate from these to the sodalite cages and hexagonal prisms when  $[\text{La}(\text{OH})]^{2+}$  and  $[\text{Ce}(\text{OH})]^{2+}$  decompose. However,  $\text{La}^{3+}$  cations will retromigrate from the sodalite cages and prisms towards the supercages at 25°C if the sample stays in contact with water vapour for a long time. In the case of  $\text{R}_x\text{Na-X}$  zeolites (Kim et al. 1994), it has been observed that both  $\text{La}^{3+}$  and  $\text{Ce}^{3+}$  are located outside the supercages. In this way, when the  $\text{R}_x\text{H-Y}$  zeolites are treated with steam, there is a migration of cations from the sodalite cells into the

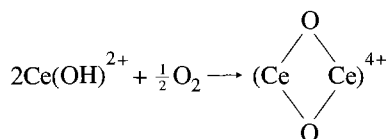
large cavities (Spiridonov et al. 1992). Similar conclusions were achieved by using other characterization techniques (Sherry 1966, Lai and Rees 1976, Marynen et al. 1984).

The exchange of rare-earth cations into faujasite-type zeolites is known to produce acidic zeolite catalysts of high thermal stability. This high stability has been ascribed to the presence of extra-framework oxygen linkages between two  $\text{La}^{3+}$  cations in sodalite cages at elevated temperatures (Smith et al. 1967, Rabo et al. 1968, Cheetham et al. 1984, Marynen et al. 1984, Maugé et al. 1986, Lee and Rees 1987a, Carvajal et al. 1990, Akporiaye et al. 1993):



Support for the existence and stability of the bridged La-O structure was provided by X-ray diffraction (Smith et al. 1967, Maugé et al. 1986, Lee and Rees 1987a) and XPS (Grünert et al. 1993) studies. In the last case, it has been excluded that lanthanum is present in the zeolite in a physical mixture or as a supported bulk phase.

In the same way, Hunter and Scherzer (1971) proposed the formation of  $\text{Ce}(\text{OH})^{3+}$  and  $\text{Ce}(\text{OH})^{2+}$  ions during the calcination in air of hydrated Ce-X zeolite. However, Lee and Rees (1987b) observed in Ce-Y zeolite the formation of an oxycerium complex during the oxidation:



The formation of hydroxycerium ions up to 250°C, and oxycerium ions at 300°C and above, was found to be irreversible, and these species remain unchanged in the small cages on rehydration (Lee and Rees 1987b).

In the case of Eu-exchanged zeolites, a tetrahedral  $[\text{Eu}_4\text{O}]^{10+}$  complex has been proposed to be formed on dehydration (Simon et al. 1992). This indicates that  $\text{Eu}^{3+}$  ions migrate into sodalite cages (Suib et al. 1984, Simon et al. 1992).

Lin and Chao (1991) studied the variation of the cation distribution with the lanthanum exchange level in hydrated La,Na-Y zeolites by two-dimensional  $^{23}\text{Na}$  nutation NMR spectra in which the chemical shift and the quadrupole interaction could be separated. They proposed that the mobility of both water molecules and sodium ions can be reduced by lowering the temperature of the sample, and the migration of lanthanum ions from supercages to small cages causes the redistribution of sodium after dehydration

at 350°C. Similar observations were made with the system  $\text{LaCl}_3/\text{Na-Y}$  during solid-state reactions in which contact-induced solid-state exchange was revealed by  $^{23}\text{Na}$  MAS NMR with a replacement of  $\text{Na}^+$  with  $\text{La}^{3+}$ ,  $\text{La}(\text{OH})^{3+}$  or  $\text{La}(\text{OH})_2^+$ , and the corresponding formation of  $\text{NaCl}$  (Karge 1997).

Not only do rare earths contribute strongly to the thermal stability of zeolites, but they also have the function of enhancing or creating acidity. As occurs in hydrogen and alkaline-earth Y zeolites, rare-earth-exchanged Y zeolites (RY) present Brönsted acid sites after calcination at 480°C (Ward 1969, Ward and Hansford 1969, Scherzer and Bass 1975, Scherzer et al. 1975, Zinner and Araujo 1992, Sousa-Aguiar et al. 1998), and Lewis sites if the calcination is carried out at 700°C (Ward 1969, Ward and Hansford 1969, Scherzer and Bass 1975, Scherzer et al. 1975, Spiridonov et al. 1992, Nasukhanov et al. 1993) as determined by IR studies of chemisorbed pyridine. IR spectroscopy also shows that the lanthanum content of the zeolite and the type and treatment have a significant effect on the spectrum in the hydroxyl-stretching region (Scherzer and Bass 1975, Scherzer et al. 1975).

Typical IR spectra for a mixed rare-earth-exchanged Y zeolite show hydroxyl bands at 3740, 3640 and 3530  $\text{cm}^{-1}$  after evacuation at about 450°C, while they are observed at 3550 and 3618  $\text{cm}^{-1}$  at lower temperatures (Ward 1976, Sousa-Aguiar et al. 1998). However, the frequency of the absorption band near 3500  $\text{cm}^{-1}$  decreases with cation radius from 3522  $\text{cm}^{-1}$  for La-Y to 3470  $\text{cm}^{-1}$  for Yb-Y.

Ikemoto et al. (1972) studied the influence of the pre-treatment temperature, silica-to-alumina ratio, cation species and degree of cation exchange on the number and strength of acid sites of zeolite catalysts by means of amine titration using Hammett indicators. They observed that only the La form of Y-zeolite has strong acid sites ( $H_0 < -10.8$ ), while the acid strength of Y and MOR zeolites in acid form is distributed in the  $H_0$  range from  $-8.2$  to  $-10.8$ . However, the acid strength of La-Y is dependent on the degree of La exchange. Thus, if the degree of La exchange exceeds 85 mol%, the catalysts shows an acid coloration even with dinitrotoluene with a  $\text{pK}_a < -12.8$ .

Bolton (1971) suggested that some of the O-H present in rare-earth-exchanged Y zeolites result from direct exchange of  $\text{Na}^+$  ions by  $\text{H}_3\text{O}^+$  during the exchange with  $\text{R}^{3+}$  since this operation must be carried out under acidic conditions (pH 4.5) to avoid precipitation of hydrolysed R salts.

Keir et al. (1988) studied a sample of Y zeolite in which all of the sodium ions in the original sample were replaced with lanthanum (from 16 to 29 lanthanum ions per unit cell). They observed a higher number and strength of Brönsted acid sites on La-containing materials. More recently, Karge and Jozefowicz (1994) studied the acidity of various zeolites using the differential heats of ammonia adsorption as measured by high-vacuum microcalorimetry. They observed that the strength of Brönsted acidity follows the sequence  $\text{H-ZSM-5} > \text{H-Y} > \text{La,Na-Y} > \text{La,Na-X}$ . Choudhary et al. (1989) employed temperature-programmed desorption of benzene to study Ce-exchanged Na-Y and Na-X zeolites, but this appears to be not very specific to determine acid sites. In fact the heat of sorption of benzene was:  $\text{Na-Y} < \text{Ce,Na-Y}(33) > \text{Ce,Na-Y}(73) < \text{Ce,Na-X}(90) < \text{Ce,Na-Y}(98)$  (the values in parentheses indicate the percentage of  $\text{Ce}^{3+}$  exchange in Ce,Na-Y zeolite). These

results could indicate that benzene interacts more strongly with  $\text{Na}^+$  than with the acidic sites (i.e., the hydroxyl groups responsible for the protonic acidity). However, the fact that different desorption peaks appear in Ce,Na zeolites, whereas the benzene sorption sites do not differ significantly in Na-Y, could indicate that Ce-exchanged materials show different sites with different sorption energies.

Recently, Weiß et al. (1997) have studied the factors influencing the length of the induction period in ethylbenzene disproportionation over La,Na-Y zeolites with different degrees of lanthanum exchange. They propose that the catalytic behaviour is related to the number and strength of Brönsted acid sites in the catalyst. Figure 4 (above) shows the variation of the ethylbenzene conversion during the disproportionation of ethylbenzene on lanthanum-exchanged faujasites (at different degrees of lanthanum exchange, i.e. 63, 72 and 92 equiv.-%) at 180°C. From the comparison between catalytic results and  $^1\text{H}$  MAS NMR spectra of catalysts it can be concluded that both the catalytic activity and the acid strength increases with the degree of La exchange. A correlation between structural characteristics and catalytic properties of rare-earth Y zeolites have been discussed by several authors (Corma et al. 1986, Lemos et al. 1987, Keir et al. 1988, Carvajal et al. 1990, Algarra et al. 1993, Ivanova et al. 1994).

On the basis of ion exchange of zeolites, it is also possible to modify the characteristics of the cavities of the sieves leading to potential applications in purification and separation processes as well as in catalytic reactions. However, the sorption capacities of R-exchanged zeolites depend on the nature and content of R.

During the study of a series of rare-earth-exchanged X and Y zeolites, it was observed that the sorption capacity for nitrogen (Shiralkar and Kulkarni 1978) or hydrocarbons (Lee and Ma 1977) decreases when the rare-earth content of the zeolites or the size of adsorbed molecules is increased.

Thus, a reduction in the void volume from  $0.36 \text{ cm}^3 \text{ g}^{-1}$  in Na-X to  $0.29 \text{ cm}^3 \text{ g}^{-1}$  in R-X in which 97%  $\text{Na}^+$  ions were replaced with  $\text{R}^{3+}$  ions has been observed (Shiralkar and Kulkarni 1978).

Lee and Ma (1977) observed that the intracrystalline diffusion coefficients ( $D_i$ ) of *n*-butane, isobutane and 1-butene in the Na-, Ca- and La-forms of synthetic faujasite, determined in a constant volume, decrease in the following order for all three hydrocarbons (table 4):  $D_i(\text{La-X}) > D_i(\text{Ca-X}) > D_i(\text{Na-X})$ . This is caused by the

Table 4  
Diffusion coefficients of  $\text{C}_4$ -hydrocarbons in Me-X zeolites (Me=Na, Ca, La)<sup>a</sup>

Hydrocarbon	$D_i \times 10^{13} \text{ (cm}^2 \text{ s}^{-1} \text{, at } 35^\circ\text{C)}$		
	Na-X	Ca-X	La-X
<i>n</i> -butane	0.432	2.226	121.1
Isobutane	10.38	18.03	29.96
1-butene	0.049	0.0970	5.463

<sup>a</sup> After Lee and Ma (1977).

replacement of  $\text{Na}^+$  cations by one third their number of  $\text{La}^{3+}$  or one-half their number of  $\text{Ca}^{2+}$  cations, which have different sites in the zeolite framework and offer different resistance to sorbate diffusion. However, we must indicate that the order of the magnitudes of the crystalline diffusion coefficients for isobutane and *n*-butane is reversed for La-X with respect to Na-X or Ca-X. This effect has been explained by the stronger interaction between the  $\text{La}^{3+}$  cation and the diffusing molecules.

It is known that the number and size of cations in the channels and cavities as well as the polarizability of the sorbate molecules influence the sorption properties of zeolites. This effect must also be considered in the case of R-exchanged zeolites.

### 3. Zeolite catalysts containing rare earths

Molecular-sieve-enclosed paramagnetic ions have been proposed as image-brightening or imaging-contrast agents. Thus, zeolite-enclosed trivalent gadolinium (as ion or ligated with a chelator) is useful as contrast medium in magnetic resonance imaging (MRI) studies of the entire gastrointestinal tract (Young et al. 1995, Balkus and Shi 1997). However, owing to the high stability and acidity of rare-earth-exchanged zeolites, it is not surprising that a large number of papers on acid catalysis using R-exchanged zeolites had already appeared in the 1960s (Plank et al. 1964, Rabo et al. 1961, 1968, Landis and Venuto 1966, Venuto et al. 1966a–c). These have found wide use in a large number of reactions in the fields of oil refining, petrochemistry and the production of fine chemical processes.

#### 3.1. *Oil refining for gasoline production*

##### 3.1.1. *Rare earths in FCC catalysts*

The catalysts which consume the largest amount of rare earths are very probably those used in fluid catalytic cracking (FCC). Everything started when zeolites X and Y were introduced as cracking catalysts, showing their superior activity and selectivity towards amorphous silica-aluminas (Hatch 1969, Plank 1984, Corma 1992). However, cracking catalysts need to be continuously regenerated by burning off the coke which is produced during the process and which causes catalyst deactivation. This regeneration process produces high temperatures on the surface of the zeolite catalyst, and this together with the presence of steam is responsible for the destruction of the zeolite structure. It was then necessary to improve the thermal and hydrothermal stability of X and Y zeolites in order to achieve their practical use as catalytic cracking catalysts. The commercial impact of zeolites came when Davinson's XZ-25, a rare-earth-exchanged X zeolite, was introduced. It was demonstrated that the introduction of a rare earth increased the stability of X and Y zeolites, increasing their activity and selectivity towards the production of gasoline (Goodall 1962, Magee 1972). Today most of the FCC catalysts contain zeolite Y with different levels of R exchange (Kitto et al. 1992, Rhodes 1997, Brait et al. 1998).

Table 5  
Comparison of rare-earth oxide content of two source materials

Rare earth	Content (wt%)		Rare earth	Content (wt%)	
	Monazite	Bastnaesite		Monazite	Bastnaesite
Cerium	46	50	Samarium	3	1
Lanthanum	24	24	Gadolinium	2	0.5
Neodymium	17	10	Others	2	0.5
Praseodymium	6	4			

The R sources used for preparing FCC catalysts are monazite and bastnaesite sands which predominantly contain cerium, lanthanum and neodymium; their detailed composition is given in table 5 (Magee and Blazek 1976).

When the R are introduced by exchange in zeolite Y, there is no selectivity towards the different components in the mixture, provided that the pH of the exchange is kept between 3.5 and 5.5 in order to avoid precipitation of  $\text{Ce}_2\text{O}_3$ . Concerning the R composition, it has no influence on cracking activity and selectivity. However, the stability of the resultant R-Y zeolite is directly proportional to La content, and inversely proportional to Ce content (Scherzer et al. 1971, Lemos et al. 1987). Therefore, commercially, La-rich exchange solutions are preferred and up to 17 wt%  $\text{R}_2\text{O}_3$  is introduced in zeolite Y carrying out the exchange at 70–90°C.

The first FCC catalysts contained zeolite Y with a high level of R (CRY and RHY). They were prepared following two different pathways. The most direct one consisted in an exchange of the parent Na-Y with an aqueous solution of R and ammonium salts. The ionic exchange occurs primarily with supercage sodium ions, due to the inability of the hydrated R cations to surpass the 6-member ring of the sodalite cage as was described above. However, in a following process the R-exchanged Y zeolite is calcined, and then the cations without the water coordination sphere can penetrate into the sodalite cages. Meanwhile, most of the  $\text{Na}^+$  present in the sodalite cages, which was not exchanged, migrates into the supercage and can be exchanged in a second step.

In the second method of preparation the parent Na-Y zeolite is first exchanged with  $\text{NH}_4^+$ , and in this process up to 80% of the sodium ions are removed, while reducing the alkalinity of the zeolite. Then, the  $\text{NH}_4\text{-Na-Y}$  resulting zeolite is exchanged with R. Zeolites containing low levels of Na (~0.35 wt%) can be obtained in a single exchange without intermediate calcination, when the exchange is carried out in an autoclave at 168°C for 3 h.

Solid-state ion exchange between  $\text{LaCl}_3$  and  $\text{NH}_4\text{-Y}$  zeolites can also occur, yielding catalysts active for hydrocarbon cracking (Karge et al. 1991). Their catalytic behaviour is similar to those obtained by conventional exchange in suspensions of the starting zeolite Na-Y with La salt solutions. It has been found that residual water is not necessary to conduct solid-state ion exchange successfully. However, brief contact with small amounts of water vapour is required to render the resultant materials active cracking catalysts.



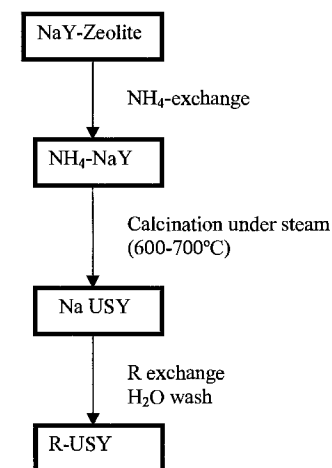
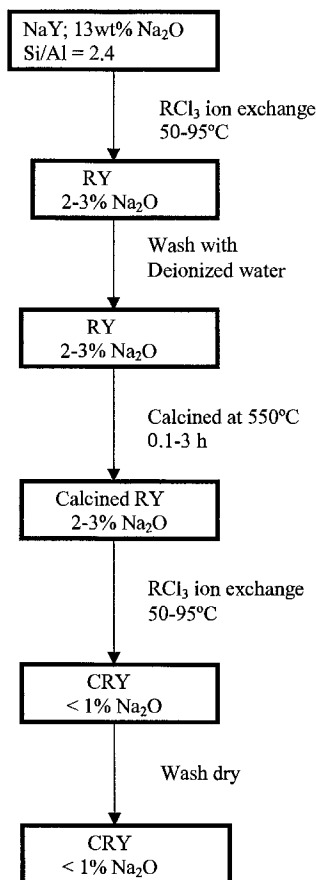
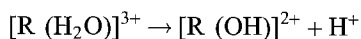


Fig. 6. Preparation of R-USY zeolite for FCC catalysts.

Fig. 5. Production process for calcined rare earth Y (CRY).

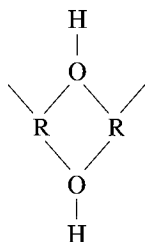
A scheme of the process for producing CRY zeolites for FCC is given in fig. 5 (Maher and McDaniel 1986).

During calcination of R-Y zeolites, acid sites are formed by hydrolysis of the water associated to the exchanged cations via the following mechanism:



The protons formed in this way are associated with the T-O-T' framework units generating bridging hydroxyl groups, which give the corresponding infrared bands at 3640 and 3520 cm<sup>-1</sup> and which are acidic towards accessible basic molecules. They are responsible for the hydrocarbon cracking activity of the resultant materials.

The thermal and hydrothermal stability of the R-exchanged Y zeolites has been related to the formation of hydroxycomplexes in the sodalite units:



which stabilizes the framework towards dealumination (Iyer et al. 1988).

Based on this, it has been found that it is possible to control the level of dealumination, and therefore the unit cell size of the zeolite, by introducing different levels of R into the zeolite. In this way, the higher the R content of the zeolite is, the lower will be the dealumination, and consequently the larger the unit cell size of the zeolite, upon steaming. This in turn indicates that the higher the R content of the zeolite Y containing catalyst is, the higher will be the conversion of the FCC catalyst, but at the same time the lower will be the octane of the gasoline produced, the higher the amount of coke, and the lower the amount of olefins in gases (Scherzer 1989). Consequently, a series of ultrastable Y zeolites (USY) with different levels of R content (R-USY) can be produced to adjust the gasoline octane number, coke, and olefins to the requirements of the different refiners. The scheme of preparation of R-USY zeolites is given in fig. 6.

As said before, the R content controls the level of dealumination, i.e. the decrease in size of the unit cell, produced during the regeneration of the catalyst. Thus, fig. 7 shows that from the point of view of the gasoil cracking activity there is a maximum for framework Al contents of  $\sim 20$  Al per unit cell size, which corresponds to a Y zeolite with  $\sim 24.40$  Å unit cell size. The stabilisation in the regenerator of a zeolite with this unit cell size is achieved by introducing about 14 wt%  $R_2O_3$  in the Y zeolite which conforms the FCC catalyst (Corma et al. 1988). Furthermore, it has been shown that by decreasing the level of rare-earth content of the zeolite, and therefore decreasing the unit cell size of the equilibrated catalyst, the selectivity to dry gas first decreases for cell size reductions down to  $24.32$  Å ( $\sim 10\%$   $R_2O_3$  in zeolite) and then increases. Inversely, gasoline selectivity first increases for cell size reductions down to  $\sim 24.32$  Å and then decreases upon further unit cell reduction. Coke decreases upon dealumination down to a unit cell size of  $\sim 24.28$  Å ( $\sim 8\%$   $R_2O_3$  in zeolite) and then remains practically constant. Furthermore, LPG olefinicity increases slowly until the unit cell size is reduced to  $\sim 24.35$  Å, and then increases strongly. The changes in selectivity due to R content (and concomitant unit cell size of the zeolite) have a strong influence on gasoline octane, increasing this when decreasing the R content of the ultrastable Y zeolite (Pine et al. 1984, Corma et al. 1990a). The effect of R on zeolite stability is generally accepted for Y zeolites, but it is less notable for other zeolites.

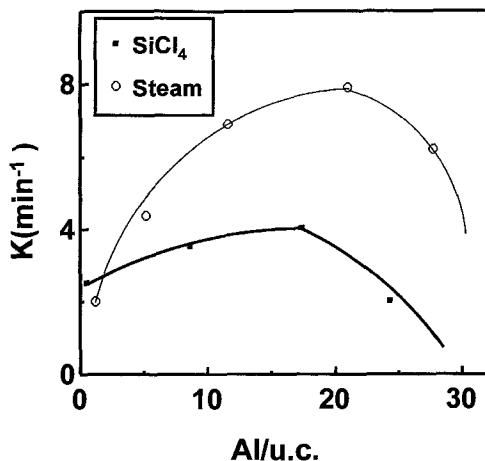


Fig. 7. Activity for gas-oil cracking as a function of FAL per unit cell, for samples dealuminated by  $\text{SiCl}_4$  (solid circles) or steam (open circles).

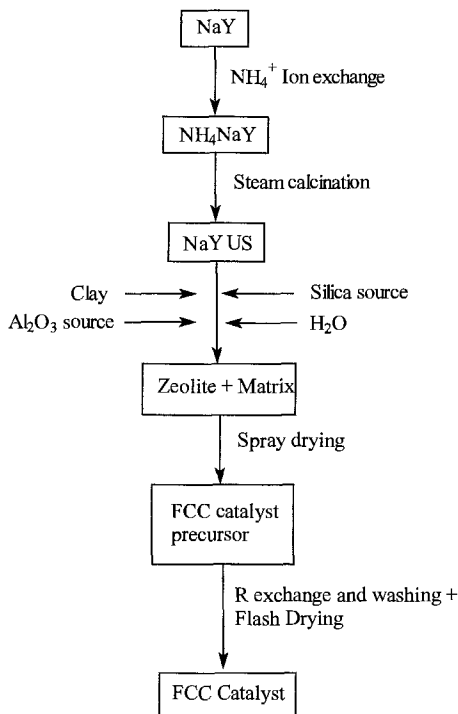


Fig. 8. Preparation procedure of the global catalyst FCC.

It is clear that the zeolite is only one of the several components (although the most important) of the global FCC catalysts. Indeed, the matrix also plays an important role, giving to the final FCC catalyst the density, attrition resistance, macroporosity, etc. for accomplishing the required fluidodynamic and resistance properties of a successful FCC catalyst. The preparation procedure for the global catalyst is given in fig. 8.

**3.1.1.1. Rare earths in  $\text{SO}_x$  and  $\text{NO}_x$  abatement additives for FCC.** Sulfur oxides can be formed in the regenerator due to the oxidation of the sulfur compounds contained in the coke. There are four options to abate  $\text{SO}_x$  emissions in FCC units: Processing low-sulfur feeds ( $\text{S} < 0.3\%$ ), hydrosulfurization of the feed, flue gas scrubbing, and the use of  $\text{SO}_x$  additives.

The first option, while being direct, presents major drawbacks associated with the high price of sweet crudes, and the restrictions in refiners' crude options. Hydrosulfurization of FCC unit feeds not only can reduce the sulfur content but also makes the feed less refractory to cracking, improving therefore the total conversion and gasoline and coke selectivities. Unfortunately, the dehydrosulfurization of the feed requires a large capital investment and has a high operating cost. Stack scrubbing of the flue gas is the best solution when very low levels of  $\text{SO}_x$  emission occur, but it demands a large capital investment and has high operating costs.

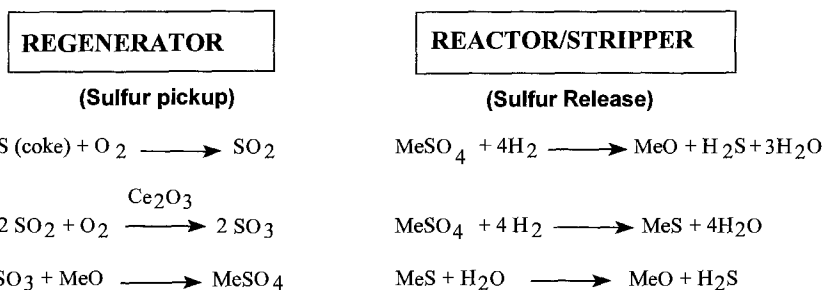


Fig. 9. Reactions involved in both reactor/stripper and regenerator during the abatement of  $\text{SO}_x$  emissions in FCC units by the use of  $\text{SO}_x$  additives.

$\text{SO}_x$  abatement additives have a low capital cost and the operating cost per pound of  $\text{SO}_x$  removed is similar to that for flue gas scrubbing. The use of additives is advantageous when the  $\text{SO}_x$  emissions need to be lowered only moderately below base operation.

The  $\text{SO}_x$  additives are formed by an oxide function, usually  $\text{Ce}_2\text{O}_3$ , which can rapidly oxidize  $\text{SO}_2$  to  $\text{SO}_3$ . This then reacts with a more basic oxide, such as  $\text{MgO}$  or  $\text{MgO}-\text{Al}_2\text{O}_3$ , also present in the additive, and forms the corresponding metal sulfate. All these processes occur in the regenerator unit. Then, when the additive is passed to the reactor, it reacts with  $\text{H}_2$  to either be regenerated, forming  $\text{H}_2\text{S}$  and  $\text{H}_2\text{O}$ , or to form a sulfide and  $\text{H}_2\text{O}$ . The sulfide can then be hydrolyzed in the stripper to form  $\text{H}_2\text{S}$ . The different reactions occurring are schematized in fig. 9.

Besides removal of  $\text{SO}_x$ , refiners are also interested in removing  $\text{NO}_x$  which is also formed during the combustion of the basic compounds containing nitrogen, present in the coke. It has been claimed that, among other catalysts, a Group III B base additive, such as lanthanum or yttrium oxides, reduces  $\text{NO}_x$  emissions even in the presence of Pt, CO combustion promoter, and excess of oxygen (Nunan et al. 1995). Zeolite ZSM-5 exchanged with copper or rare-earth cations are also effective for reducing  $\text{NO}_x$  emissions in FCC. Finally, it has been recently reported that a  $\text{Ce}_2\text{O}_3$ -containing Cu-Mg hydrotalcite is able to reduce both  $\text{SO}_x$  and  $\text{NO}_x$  emissions (Corma et al. 1993, 1997).

The amount of  $\text{SO}_x$  and  $\text{NO}_x$  emissions in FCC strongly increases when processing residues which contain a larger amount of sulfur and nitrogen compounds. Moreover, in these feeds larger amounts of vanadium-containing compounds are present in the form of V-porphyrins. These react on the surface of the catalyst under the reducing atmosphere of the reactor, leaving  $\text{V}^{3+}$  and  $\text{V}^{4+}$  species on the coke formed. Then, in the regenerator  $\text{V}_2\text{O}_5$  species on the surface of the catalyst are formed, which react with the steam present to form highly mobile vanadic acid ( $\text{VO}(\text{OH})_3$ ). The mobile vanadic acid migrates to the zeolite and reacts with the rare earths present there, forming R-vanadates and destabilising the zeolite, leading to its destruction.

There are several options to prevent metal contamination: addition of fresh catalyst, feed hydrotreatment, and the use of metal-tolerant catalysts; it is obvious that the first two can become expensive and efforts have been made in improving the last two solutions.

Metal-tolerant catalysts are formed by active matrices with macropores which can entrap large molecules such as the vanadium-containing compounds and, ideally, can produce metal agglomeration and a strong interaction with the matrix. However, most of these catalysts have to balance between metal tolerance and other desired catalyst characteristics such as yield and cost. Due to this, separate metal-trap additives have been used, and in the case of vanadium besides MgO-containing materials (von Ballmoos 1993) and a liquid vanadium passivator (Stonecipher 1997), a new rare-earth-based dual particle system has been introduced (Dogan 1994).

In conclusion, we have shown here that rare earths play an important role in improving the stability of Y zeolite in FCC catalysts. Moreover, by an adequate control of the zeolite rare-earth content, it is possible to control the activity and selectivity of the catalyst by controlling the unit cell size or framework aluminium content of the equilibrated zeolite.

Rare earths either in zeolite (ZSM-5) or on  $\text{Al}_2\text{O}_3$ ,  $\text{MgO-Al}_2\text{O}_3$  supports play an important role in  $\text{SO}_x$  removal additives by catalyzing the oxidation of  $\text{SO}_2$  into  $\text{SO}_3$ . They also intervene in the processes directed to  $\text{NO}_x$  removal. However, the R contained in the zeolite Y of FCC catalysts, reacts with vanadic acid, forming vanadates and leading to the destruction of the zeolite with the corresponding loss of the FCC catalyst activity (Occelli 1991, Yang et al. 1994, Occelli 1996). Vanadium traps based on rare earths can help to reduce zeolite destruction by vanadium (Feron et al. 1992).

### 3.1.2. Alkylation of isobutane/butene

Gasoline obtained by alkylation of isobutane with  $\text{C}_3\text{-C}_5$  olefins is an ideal blending component for reformulated gasoline, since alkylate has a high octane number with a low octane sensitivity (difference between RON and MON), and is mainly formed by multibranched paraffins. If replacement of the environmentally hazardous sulfuric and hydrofluoric acids used as commercial alkylation catalysts by more friendly solid-acid catalysts becomes technically and economically feasible, this would greatly enhance alkylation capacity (Corma and Martinez 1993).

Table 6 shows a comparison of the product distributions observed during the alkylation of isobutane with 2-butene on both a silicoaluminate and an industrial  $\text{H}_2\text{SO}_4$  catalyst (Kirsch et al. 1972). Despite the differences observed in the distribution of trimethylpentanes (TMP), the close similarity observed on both catalysts led to the conclusion that the same chain mechanism is operative in both cases. In fact, a similar product distribution during the alkylation of isobutane with 1- or 2-butene on an R-Y catalyst and on an  $\text{H}_2\text{SO}_4$  catalyst can be observed (Kirsch et al. 1972).

Some specific factors should be considered when using zeolites as catalysts in isobutane/olefin alkylation. The first is the strong hydrocarbon adsorption of zeolites, especially at low temperatures, which makes the actual concentration of the reactants in the zeolite quite high. In addition, and due to the high concentration of acid sites in the zeolite cavities, zeolite would behave as a liquid-acid catalyst but with a high solubility of reactants. Taking this into account it can be easily assumed that the Si/Al ratio can determine the nature of reaction products. In this way, it has been proposed that zeolites

Table 6  
Product compositions in isobutane/2-butene alkylation.

Compound	Zeolite <sup>a</sup>		H <sub>2</sub> SO <sub>4</sub> (vol%)
	(wt%)	(wt%)	
i-pentane	3.40	5.78	4.16
2,3-DMB + MP	3.59	3.46	4.58
2,4-DMP	4.14	3.58	2.37
2,2,3-TMB	0.21	0.10	—
All MH	0.35	0.32	—
2,3-DMP	1.67	1.26	1.38
2,2,4-TMP	16.22	17.70	30.64
All DMH	8.59	8.89	9.02
2,2,3-TMP	3.54	3.97	—
2,3,4-TMP	—	—	—
2,3,3-TMP	47.34	48.16	41.55
2,2,5-TMP	0.78	0.71	1.88
Other C <sub>9</sub>	9.21	6.06	4.41

<sup>a</sup> For different catalysts and conditions (Corma and Martinez 1993).

with low Si/Al ratio strongly enhance olefin polymerization but decrease the alkylation reactions (Corma et al. 1990a). In order to make a successful zeolite catalyst, the pore diameter of the channels should not only allow the reactants to go in, but also the products to migrate out of the pore system quickly. This means that in some cases the diffusion limitations in the zeolite pores can determine the life of the catalyst and the product distribution obtained. Thus, and from a structural point of view, large-pore zeolites (12-member-ring zeolites or even zeolites with larger pore openings) which can allow the diffusion of the multibranched products formed should be better than medium-pore-size zeolites. In fact, ZSM-5 is inactive for alkylation of isobutane and butene due to its constrained pores, and it mainly catalyzes the oligomerization of butene (Chu and Chester 1986). Zeolites capable of allowing the diffusion of 2,2,4-trimethylpentane, i.e. Faujasite, Beta, ZSM-20, ZSM-3, ZSM-4, ZSM-18, etc. (Huang 1983, Corma and Martinez 1993, Corma et al. 1994a,b, 1996a,b), have been used in the patent literature, although X and Y zeolites, with different mono-, di- and trivalent cations (especially rare-earth-metal exchanged faujasite-type zeolites) have been the most widely studied.

On the other hand, ethylene cannot be used in isobutane/olefin alkylation on sulphuric acid, because of the formation of stable ethylsulfates. However, when using a R,Ca-Y catalysts in combination with transition-metal cations (especially Ni) (Minachev et al. 1977) an alkylate containing octane isomers as the major product (about 80%), without the formation of hexanes has been obtained. They observed a strong influence of the chemical composition on the catalytic behaviour of R,Ca-Y zeolites, showing a maximum on a R,Ca-Y (16.6% Ca and 64.2% R) zeolite.

Table 7  
Isobutane/butenes alkylation on Ce-exchanged zeolites<sup>a,b</sup>

Product	Catalyst/time on stream				
	Ce-Y (46) <sup>c</sup>	Ce-Y (98) <sup>c</sup>		Ce-X (96) <sup>c</sup>	
	9	1	30	1	40
<b>Carbon number distribution (wt%)</b>					
C <sub>5</sub>	5.7	22.6	6.1	26.0	8.9
C <sub>6</sub>	5.9	11.9	5.0	14.4	7.6
C <sub>7</sub>	5.9	9.0	5.3	10.4	7.9
C <sub>8</sub>	65.9	47.0	53.8	45.8	49.8
C <sub>9</sub>	6.1	6.4	8.1	2.3	7.0
C <sub>10</sub> -C <sub>12</sub>	10.5	3.1	21.7	1.1	18.8
<b>C<sub>8</sub> isomers distribution (wt%)</b>					
TMP	37.1	76.9	53.9	80.4	59.0
DMH	60.9	21.5	45	19.3	39.3
Otros	2.0	1.6	1.1	0.3	1.7

<sup>a</sup> After Weitkamp (1980a).

<sup>b</sup> Experimental conditions: 80°C; pressure 3.1 MPa, liquid feed rate 7.5 cm<sup>3</sup> h<sup>-1</sup>. Isobutane/1-butene molar ratio 11.1/1 in Ce-X(96) and Ce-Y(46); isobutane/2-*cis*-butene molar ratio 11/1 in Ce-Y(98).

<sup>c</sup> Numbers in parentheses after catalysts denote formal degree of cerium exchange as calculated from the cerium and sodium contents; times on stream are listed under the catalysts.

Gárdos et al. (1980a,b) studied the catalytic behaviour of a R-Y (17.1 wt% R<sub>2</sub>O<sub>3</sub>; SiO<sub>2</sub>/Al<sub>2</sub>O<sub>3</sub> molar ratio of 5.08) during the alkylation of isobutane with 1-butene at a pressure of 2.0 MPa, and they observed that the maximum yield can be achieved (C<sub>8</sub>: 91%; TMP=50%, especially 2,3,3-TMP; DMHx=27%) at 343 K and with an isobutane/1-butene molar ratio of 8/1. The activity and yield to TMP during the alkylation of isobutane on NH<sub>4</sub>La-Y zeolite depends on the La content: the higher the La incorporated the higher the yield to alkylation products (Gárdos et al. 1982).

Weitkamp (1980a,b) studied Faujasite X and Y zeolites with different degrees of cerium exchange (table 7) and from their results it can be concluded that a high degree of cerium exchange is desirable for isobutane/butene alkylation. In addition, Ce-Y(98) ages more slowly than Ce-Y(46), and the Brönsted acid sites formed by direct exchange as well as those formed by hydrolysis of the water associated to the R cations are responsible for the formation of the precursors for alkylation.

A similar trend in the influence of the R content in Y zeolites on their catalytic behavior has also been reported by other authors (Kirsch et al. 1972, Gárdos et al. 1983). Thus, it appears that an increase in the R content produces an increase in the yield of hydrocarbons with more than 5 carbon atoms (C<sub>5+</sub>) and a better product distribution (a higher yield of C<sub>8</sub> and TMP/DMP ratio).

A comparative study between the catalytic properties in the alkylation of isobutane and the changes of Brönsted acid sites by IR spectroscopy on Ce,L<sub>a</sub>-Y zeolites (with Ce/L<sub>a</sub> ratios from 0.75/0.25 to 0.25/0.75) has been carried out (Gárdos et al. 1984). It was observed that the Ce/L<sub>a</sub> distribution does not modify the catalytic behaviour of Ce,L<sub>a</sub>-Y zeolites. In addition they observed that the IR absorption band at 3630 cm<sup>-1</sup> can be related to the acidic OH groups responsible for the catalytic activity in the alkylation of isobutane with 1-butene.

Since it is well known that increasing the R content results in an increased number of framework Al remaining after thermal and hydrothermal treatments, and the hydrogen transfer ability of the zeolite is also higher, it can be concluded that no very strong acid sites are necessary to carry out the alkylation of isobutane with butenes on zeolites. However, the most important factor is to achieve a high Al and cation content, and therefore a high density of framework Al which favours both a high activity and high hydrogen transfer.

The catalytic behaviour in the alkylation reaction of Ce-Y zeolite has been compared with those obtained on superacid catalysts such as Nafion-H (Rørbik et al. 1995). They observed that both catalysts show a high initial activity for the alkylation reaction with a rapid decrease in the alkylation selectivity. Nevertheless, the Ce-Y catalyst showed the highest molar ratio of trimethylpentanes (TMP) to dimethylhexanes and can be considered a better catalyst for the alkylation reaction. However, the different distribution of TMP and especially the highest formation of the isomer 2,2,4-trimethylpentane (2,2,4-TMP) on Nafion-H has been explained by the acidity distribution. It is likely that the strongest acid sites in a zeolite deactivate first. Since 2,2,4-TMP is formed mainly in the first minutes on zeolitic materials, its formation is probably more dependent on the presence of strong acidic sites than any of the other isomers.

Recently, the group of Rørbik (1996) has compared the catalytic behaviour of acidic faujasites, i.e., H-Y and Ce-Y(98) (98 representing 98% of exchange), with a hexagonal faujasite (EMT) in a semibatch slurry reactor. H-EMT exhibited better results during the reaction with respect to an improved deactivation profile and moderate loss of alkylate selectivity than the acidic cubic Y zeolite. In this way, this group has compared the catalytic behaviour of different La-exchanged zeolites, i.e. La-Y, La-MCM-22, La-Beta and La-EMT, for the isobutane/2-butene alkylation (Mostad et al. 1997). The catalytic results at 80°C are shown in table 8. La-EMT zeolite (La-EMT-40 sample with 40% La exchanged) shows the highest activity and selectivity to C<sub>8</sub> paraffins, especially to trimethylpentanes (TMP). A recent paper compares the catalytic behaviour of hydrogen and 51% La-exchanged EMT zeolites (Rørbik et al. 1997). The La-exchanged sample presents a very slightly enhanced alkylate activity and yield, in particular towards the 2,2,4-TMP among the isocyanates, compared to the H-EMT zeolite. On the other hand, this zeolite was regenerated by burning off coke in air and reused in alkylation showing a slight loss in its alkylation activity.

IR and UV-VIS spectroscopies have been employed in order to understand the mechanism in the isobutane/2-butene alkylation on La-Beta (Kiricsi et al. 1995) and on La,H-Y zeolites (Flego et al. 1995). It has been observed that the formation of alkenyl



Table 8  
Isobutane/2-butene alkylation on La-exchanged zeolites<sup>a,b</sup>

Catalyst	2-Butene conversion (wt%)	Product distribution (wt%)			C <sub>8</sub> distribution (wt%)		
		C <sub>5</sub> -C <sub>7</sub> paraffins	C <sub>8</sub> paraffins	C <sub>8</sub> olefins	C <sub>9+</sub> paraffins + olefins	TMP (2,2,4-; 2,3,3-; 2,3,4-)	DMH (2,3-; 2,4-; 3,4-)
H-EMT	88	8.4	78.9	2.9	9.7	80.8	11
La-EMT-40	100	10.2	84.5	0.8	4.5	78.9	9.4
La-EMT-80	81	10.1	77.3	0.9	11.7	82.4	12.5
La-EMT-30	76	10.1	77.3	0.9	11.7	80.9	12.2
La-Beta-30	70	16.5	55.2	8.7	19.6	72.9	20.8
La-FAU-40	78	15.7	58.3	7.3	18.7	76.7	17.6

<sup>a</sup> After 3 hours reaction time in a semibatch slurry reactor (Mostad et al. 1997).

<sup>b</sup> Reaction conditions: 80°C; isobutane/2-butene ratio 10/1; WHSV = 1.2 g 2-butene per hour per g dry catalyst.

ions is strongly suppressed in the presence of isobutane, and the role of isobutane can be explained by its enhanced hydride ion donor character. On the other hand, UV–VIS spectroscopic studies of La,H-Y catalyst deactivation in the alkylation of isobutane with 1-butene (Flego et al. 1995) indicate the presence of unsaturated carbenium ions immediately after the adsorption of 1-butene and/or 1-butene/isobutane mixtures. These ions are probably part of high-molecular-weight oligomers which remain attached to the active site, producing catalyst deactivation by poisoning.

Recently, Diaz-Mendoza et al. (1998) have studied the catalytic behaviour and the catalyst decay of Beta, RY and USY zeolites. They propose that Lewis acid sites promote the formation of unsaturated compounds (favoring coke formation). However, Brønsted acid sites with intermediate acid strength appear to be appropriate sites for maintaining good alkylation catalytic performance. They observe that the best catalytic performance and the slowest deactivation were achieved with Beta zeolite, followed by RY and USY with low sodium content. However, only butene isomerization was observed over USY zeolite with high sodium content.

### 3.2. Petrochemistry

#### 3.2.1. Alkylation of aromatics

Electrophilic alkylation of aromatics (especially benzene, toluene and biphenils) are generally carried out on a variety of reactants such as olefins, alcohols, and halogenated hydrocarbons (Venuto 1994, Corma 1995). Commercial catalytic processes leading to the formation of ethylbenzene, *p*-xylene, propylbenzenes, ethyltoluene and 4,4'-isopropylbiphenyl have been developed. In addition, alkylation of aromatics is a good example of reactions where the diffusion and transition-state shape selectivity play a predominant role in controlling the selectivity of zeolite catalysts. Thus, depending on the size of the reactant and product molecules, shape selectivity applies to either medium- or larger-pore zeolites, and selective alkylation processes have been developed using both types of zeolites. In this way, the Mobil–Badger ethylbenzene process is based on the use of ZSM-5 zeolite catalyst to produce ethylbenzene, for the production of styrene, by alkylation of benzene with ethylene (Dwyer 1981). By an adequate choice of the benzene-to-ethylene ratio it is possible to limit the formation of diethylbenzene, and an overall yield of 99% of ethylbenzene is obtained.

Venuto et al. (1966a) studied the alkylation of benzene with ethylene on R-Y, R-X and H-Y zeolites, and they observed that the conversion of ethylene to ethylbenzene increases as  $H-Y < R-X < R-Y$  (fig. 10). Optimum conditions were also investigated in the alkylation of benzene or phenol using other olefins, alcohols and alkyl halides as alkylating agents and R-X as catalyst (Venuto et al. 1966a). In general, *ortho/para* orientation of substituents was usually observed in the alkylation of substituted benzenes, while in alkylations with alkylating agents with three or more carbon atoms, the monoalkylate consisted of a mixture of isomers. In the case of the alkylation with ethylene, a mono-/poly-ethylbenzene molar ratio of 4.65 was observed.

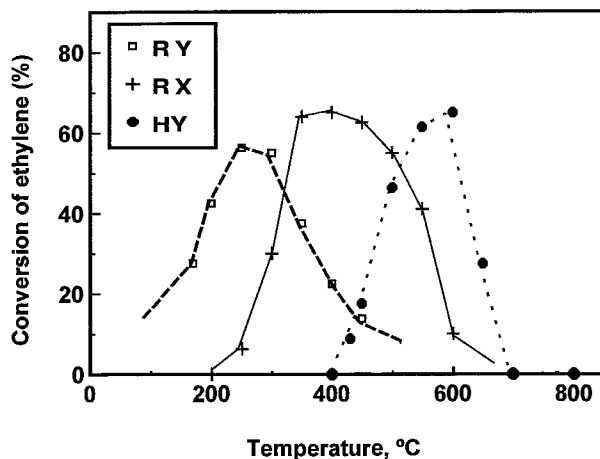


Fig. 10. Conversion of ethylene to ethylbenzenes during the alkylation of benzene with ethylene on H-Y, R-Y and R-X zeolites. Experimental conditions: 177°C; 1 atm;  $C_6H_6/C_2H_4 = 12$  molar ratio; contact time, LHSV, 5.4. (After Venuto et al. 1966a.)

On the other hand, and in order to study the competitive effect between the alkylation of both benzene and phenol with ethylene at 205°C, a clear selectivity to the more reactive aromatic was observed ( $k_{C_6H_5OH}/k_{C_6H_6} = 6.95$ ), indicating that the reaction proceeds through an electrophilic attack of the aromatic ring by the protonated ethylene (Venuto et al. 1966b).

Pradhan and Rao (1991) observed that La,H-Y and H-MOR catalysts have good initial activity for the isopropylation of benzene (80% selectivity to cumene at 99% propylene conversion), although they deactivate within a span of 8–10 h. However, while the deactivation of La,H-Y is due to poisoning (blocking) of active sites, the deactivation of zeolite MOR (a unidirectional pore system) is due to blocking of the channels by bulkier molecules like di-isopropylbenzene, which is the major by-product in this reaction. It has also been observed that La,H-Y, as occurs with large-pore zeolites, e.g. H-Beta, is also selective in the transalkylation of di-isopropylbenzenes with toluene or benzene (Pradhan and Rao 1991). Thus the high yield to monoalkylated product observed on this catalyst could be explained by the fact that, although di-isopropylbenzene is formed, it is transalkylated, favouring also the formation of monoalkylated by consecutive reactions.

Zinner et al. (1993) observed that the alkylation of benzene with 1-dodecene over rare-earth-doped Y zeolite, R,Ca:Na-Y (R = La, Ce, Nd or Gd) can be carried out at relatively low temperatures (80°C) forming selectively linear alkylbenzenes. This has been explained by the appearance of R hydroxyl cations in the zeolite cages after exchange and thermal treatment, resulting in the generation of Brønsted and Lewis acid sites. They observed that the catalytic activity decreases with the lanthanide contraction in the order La- > Ce > Nd- > Gd-. Although 2-phenyl dodecane is the most important reaction product, dodecane isomers (6-, 5-, 4- and 3-phenyl dodecane) are also observed.

R-Si-ZSM-5 catalysts have been reported as active and selective in the ethylation of ethylbenzene to *para*-diethylbenzene (PDB), with a yield of 95–98% (Xiangsheng et al. 1997). The high *para*-selectivity is due, according to the authors, to the reduction in acid strength within the pores and the reduction in acid sites on the crystal's external surface.

In the case of the alkylation of phenol or aniline, the attack on the functional group, in addition to the attack on the aromatic nucleus, can be observed. In this way, aniline can be alkylated with *n*-propyl alcohol (Pillai and Pillai 1993) or (Ione and Kikhtyanin 1989) methanol using zeolitic materials. N- and C-alkylation took place in both cases, although the selectivity to C-alkylated products depends on the reaction temperature. Thus, the selectivity to N-alkylated products decreases from 100 to 0.3 as the temperature increases from 270 to 450°C (Ione and Kikhtyanin 1989). Then, Ce-exchanged Y and ZSM-5 zeolites are active and selective in N-alkylation reaction although Ce-Y shows the higher yield to N-*n*-propylaniline, the reaction probably occurring through a  $SN_2$  mechanism (Pillai 1996).

More recently, Reddy and Varma (1997a) showed that Ce,Na-Y zeolite (72% of Ce exchanged) is an effective catalyst in the synthesis of organic sulfides from cyclohexanethiols and thiophenol with alkyl halides. Yields to alkylated products from 72 to 92%, depending on the reactants, have been reported.

Goux et al. (1994) have proposed the alkylthiolation of phenol with dimethyldisulfide over zeolites. They observe that on faujasite-type zeolites the reaction leads to the formation of 2- and/or 4-(methyl-thio)phenol (*o*- and *p*-isomers), although the ratio of *o*-/*p*- isomers depends on the composition of zeolite. In this way, it has been observed that Ce,Na-Y catalyst favours the highest *p*-/*o*- ratio (76/24).

Polynuclear aromatics have also been employed in order to study shape-selectivity effects for the alkylation reactions (Song and Kirby 1993). This is the case for the alkylation of naphthalene with propylene on Ce-modified H-Mordenite zeolite (Sugi et al. 1994a, Mravec et al. 1997). Although Ce-doped H-MOR zeolites can be prepared by either impregnation or ion exchange, H-MOR catalysts impregnated with cerium (30 wt%) exhibited the highest selectivity for 2,6-di-isopropyl-naphthalene (Sugi et al. 1994a). This catalytic behavior has been explained by a selective deactivation of acid sites on the external surface during cerium impregnation.

Moreau et al. (1992) studied the isopropylation of naphthalene over H-Y and H-mordenite zeolites using isopropylbromide. In both cases, a high  $\beta$ -selectivity was observed in the monoalkylation and dialkylation reactions. However, the better  $\beta$ -selectivity (94%) was obtained on the Y zeolite exchanged with  $Ce^{3+}$  cations (Ce,Na-Y): 2-isopropyl-naphthalene (selectivity 66%) and 2,6- and 2,7-di-isopropyl-isomers (28%) at a conversion of 73%. Cerium-impregnated H-MOR appears also to be an active and selective catalyst for the isopropylation of naphthalene (Kim et al. 1995). In this case, the selectivity to 2,6-di-isopropyl-naphthalene was enhanced by the impregnation of cerium (the highest selectivity was achieved up to 70% over a highly dealuminated H-MOR with 30 wt% cerium) without significant decrease of catalytic activity. The enhancement of the selectivity is ascribed to the deactivation of external acid sites judging from the activity of the cracking reaction of 1,3,5-tri-isopropyl-naphthalene. On the other hand, the presence

of lanthanum and neodymium inhibited catalytic activity, probably because the pores are narrowed by their impregnation. The different behaviour of Ce with respect to La or Nd has been explained by its amphoteric properties.

Long-chain alkyl-substituted naphthalenes can be produced by alkylating naphthalene with olefins on USY zeolite having rare-earth cations, and both ammonium and protonic species, associated with the exchangeable sites of the zeolite (Ardito et al. 1997). In this case, the presence of rare earths and both ammonium and protonic species appears to be very important in order to achieve a high selectivity to long-chain mono-alkyl-substituted naphthalenes.

Isopropylation of biphenyl with propylene on cerium-exchanged sodium mordenite (Ce,Na-MOR) gives 4,4'-di-isopropylbiphenyl (4,4'-DIPB) with high selectivity under any propylene pressure (Sugi et al. 1994b). However, 4,4'-DIPB is only selectively formed on H-MOR under high propylene pressure. It has been suggested that cerium-exchanged sodium mordenite acts as a shape-selective catalyst, in which Brönsted acid sites produced by cerium cation exchange are the active sites. In addition, it has been proposed that the better selectivity to 4,4'-DIPB on Ce,Na-MOR in comparison with H-MOR can be explained by the fact that external acid sites, responsible for isomerization reactions and coke deposition, are not present on Ce-containing catalyst while they are observed on H-MOR.

### 3.2.2. *Isomerization of C<sub>8</sub> alkylaromatics*

Venuto et al. (1966a) studied the isomerization of *o*-xylene and diethylbenzene to *m*- and *p*-xylene and diethylbenzene, respectively.

The isomerization of diethylbenzenes and *t*-butylphenols have also been studied on R-exchanged Y zeolite (Bolton et al. 1968a,b). In both cases, the catalyst employed was a 45% rare-earth cation-exchanged 45% decationized type Y zeolite (SiO<sub>2</sub>/Al<sub>2</sub>O<sub>3</sub> molar ratio of 5). They proposed that the isomerization proceeds via a transalkylation mechanism rather than through intramolecular rearrangements. However, more recent studies using deuterated alkyl chains in C<sub>8</sub> alkylaromatics show that isomerization occurs by both a unimolecular 1,2 methyl shift and a bimolecular transalkylation process (Corma and Sastre 1991).

Ring-shift isomerization of 1,2,3,4,5,6,7,8-octahydro-phenanthrene (syn-OHP) to 1,2,3,4,5,6,7,8-octahydro-anthracene (syn-OHAn) was studied on several hydrogen- and Me-exchanged Y zeolites (Song and Moffatt 1993). La,H-Y zeolite (8.4 wt% La<sub>2</sub>O<sub>3</sub>) appears to be an active and selective catalysts. Thus, a selectivity to syn-OHAn of 44.9% at a conversion of 74.93% at 250°C (yield of 30.43) have been reported. However, the catalytic behaviour was strongly influenced by the solvent, and the best catalytic behaviour was obtained using decaline as solvent.

### 3.2.3. *Methanol conversion*

In 1976 Mobil announced the conversion of methanol to hydrocarbons and water using zeolites as catalysts (Meisel et al. 1976, Chang and Silvestri 1977, Chang 1983,

Harandi 1993). The hydrocarbons produced in this process are aliphatic and aromatic, and are predominantly in the gasoline range ( $C_4$  to  $C_{10}$ ). The gasoline thus produced is chemically conventional, with unleaded research octane numbers of 90 to 95. Activity, selectivity and catalyst decay strongly depend on the structure of the zeolite.

Schulz et al. (1986) compared the catalytic behaviour in methanol conversion of H-ZSM-5, H-MOR, R-Y zeolites and a commercial cracking catalyst. They observed that H-ZSM-5 is a better catalyst because it produces a lower amount of methane and coke.

Some times it is desired to produce olefins instead of gasoline. Then, a ZSM-5 zeolite catalyst modified with phosphorus, rare-earth elements and pore structure regulators (Wang et al. 1996), as well as silicalite impregnated with  $LaNO_3$  (Al-jarallah et al. 1997) have been claimed to be effective catalysts to convert methanol/dimethyl ether to light olefins. A selectivity to  $C_2$ – $C_4$  of 85% at 100% methanol conversion can be obtained and the possibility for producing short-chain olefins is opened, provided that the price of methanol is low enough.

### 3.3. *Production of chemicals and fine chemicals*

The use of molecular sieves as catalysts for the production of chemicals and fine chemicals has increased over the last two decades (Hölderich and van Bekkum 1991, Venuto 1994, 1997, Feast and Lercher 1996, Corma and Garcia 1997). In this way, rare-earth-containing microporous materials appear to be interesting catalysts in fine chemical reactions. This is the case for the synthesis of ketone acetals. Thus, Ce-Y, La-Y and R-Y zeolites are very effective catalysts in the synthesis of cyclohexanone diethyl acetal (Wortel et al. 1977). However, the results obtained in acylation and carbonyl condensation reactions are particularly relevant.

#### 3.3.1. *Acylation*

The application of zeolitic catalysts to the acylation of aromatics has been described in the literature (Chiche et al. 1986, Floor et al. 1989, Corma et al. 1989, Richard et al. 1993, Armengol et al. 1995, Spagnol et al. 1996), and the electronic effects have been shown to be analogous to those reported in the case of classical electrophilic aromatic substitution. Chiche et al. (1986) studied the direct acylation of toluene and *p*-xylene by  $C_2$  to  $C_{22}$  straight-chain carboxylic acids, at 150°C, using a Ce,Na-Y catalyst (the level of Ce exchange was 70% of the theoretically possible). They observed that the activity and yield of acylated products depends on both the acid used as acylating agent and the Ce content of the zeolite. The yield to acylated products initially increases with the length of the acylating agent, showing a maximum (96%) with dodecanoic acid, and decreases when the number of C-atoms is increased above 12. On the other hand, it has been observed that  $Ce^{3+}$ -Y zeolites are more active than the corresponding clay,  $Ce^{3+}$ -montmorillonite (Chiche et al. 1987), their selectivities being different. Exchanged montmorillonite and  $AlCl_3$  do not show shape selectivity, and the *meta* isomer was observed, while the *para* isomer (selectivities of 94%) was the main product obtained on exchanged zeolites.

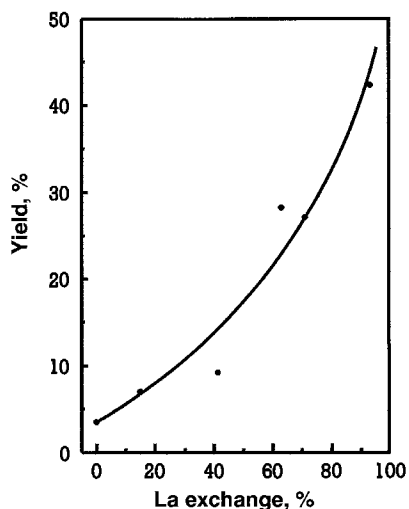


Fig. 11. Variation of the yield of para-product with La content of La,H-Y zeolite during the reaction of acetyl chloride and anisole at 70°C and 6 h time on stream. (After Gaare and Akporiaye 1996.)

Gauthier et al. (1989) studied the activity of various cation-exchanged Y-type zeolites in the acylation of toluene with octanoic acid, obtaining selectivities to the *para* isomer of 94% at 75% yield of acylated product. The most efficient catalysts were rare-earth-exchanged zeolites (70% exchange), the following order of activity being observed:  $\text{Cr}^{3+}$ ,  $\text{Zr}^{4+} < \text{M}^{2+}$ ,  $\text{Cu}^{2+}$ ,  $\text{Co}^{2+} \ll \text{H}^+ \ll \text{Pr}^{3+}$ ,  $\text{La}^{3+}$ ,  $\text{Gd}^{3+}$ ,  $\text{Yb}^{3+}$ ,  $\text{Ce}^{3+}$ .

During acylation of phenol with acetic anhydride on modified ZSM-5 catalysts (Subba Rao et al. 1995), it has been observed that Co, Cu, La and, especially, Ce show an important promoting effect in the formation of *o*-hydroxyacetophenone by C-acylation. Meanwhile the presence of others elements, such as Zr, V, Pd, Cr, Rh, favours the formation of phenylacetate by promoting the O-acylation of phenol. In addition, it has been observed that the reaction conditions, especially the phenol/acetic anhydride molar ratio and the reaction temperature, determine the distribution of O- and C-acylation.

More recently, Gaare and Akporiaye (1996) studied the acylation of anisole by acetyl chloride and acetic anhydride. They observed that the activity of La-exchanged H-Y zeolite depends on the lanthanum content. In fact, as can be seen in fig. 11, the highest yield to acylated compounds was obtained on catalysts with a 93% exchange. However, the activity to acylation reactions depends not only on the catalyst compositions but also on the acylating agents. Thus, it has been shown that activities for the acylation of anisole increases in the order benzoyl < acetyl < propionyl chloride, but, in all cases, a high selectivity to the *para* isomer was observed (Akporiaye et al. 1993).

Acylation of heterocyclics on R-exchanged zeolites has been also reported. This is the case for the acylation of furan with acetic anhydride to form 2-acetylfuran Ce,B- and La,B-ZSM-5 catalysts (Lermer et al. 1987) or the acylation of substituted benzofuran (Amouzegh et al. 1995).

On the other hand, Ce,Na- and Zn,Na-Y zeolites have also been studied in the formation of antraquinone from benzene and phthalic anhydride (ref. 149 in Hölderich and van Bekkum 1991).

### 3.3.2. Condensation of carbonyl compounds

Venuto and Landis (1966) studied the condensation of phenol and formaldehyde on different zeolitic materials. The activity at 182°C decreases as follows: H-Y > R-Y > H-Mordenite > R-X > Ca-X. However, although the highest selectivity to 2,4'-bis(hydroxyphenyl)methane was obtained on H-Y, the greatest selectivity to the isomer 2,2'-bis(hydroxyphenyl)methane was observed on R-X and Ca-X at low formaldehyde conversions. Only traces of dypione were observed during the aldol condensation of acetophenone on R-X zeolite.

Mori et al. (1993) studied the liquid reaction of acetaldehyde over various ZSM-5 zeolites. Although *cis*-paraldehyde and *trans*-paraldehyde were the main reaction products, rare-earth (La, Ce, Nd, Y) exchanged H-ZSM-5 or Na-ZSM-5 zeolites exhibited high activities for the formation of *trans*-paraldehyde while neither *cis*-paraldehyde nor *trans*-paraldehyde were formed over alkaline-exchanged zeolite. As for other reactions it is not surprising that the catalytic behaviour depends on the zeolite used. Thus, catalysts prepared from H-ZSM-5 exhibited a higher activity than those prepared from Na-ZSM-5. This particular effect has been explained on the basis of the presence of Brønsted acid sites in the neighbourhood of a  $M^{n+}$  site in the ZSM-5 zeolite pore.

Condensation reactions using rare-earth-exchanged zeolites have been studied by Reddy et al. (1993) and Reddy and Varma (1997b). In this way, nitroketene S,N-acetals, useful intermediates for the construction of several nitroheterocycles, have been obtained from the condensation of dimethyl carbonimidithioates with nitromethane in the presence of R,Na-Y zeolite with yields of 50% (Reddy et al. 1993). The dimethyl carbonimidithioates derived from various primary amines and amino-acid esters, i.e. glycine, (S)-alanine or (L)-phenylalanine were used in order to obtain a large number of condensation products. However, a crystalline product was also obtained in addition to the condensation products, probably by the reaction of two molecules of the starting material.

Knoevenagel condensation on R,Na-Y zeolite has also been recently reported: Reddy and Varma 1997b studied the condensation of arylaldehydes (benzaldehyde, *p*-bromobenzaldehyde, *p*-nitrobenzaldehyde or vanillin) with methylene compounds (malonitrile, ethylcyanoacetate or 2-cyanoacetamide) on zeolites in order to achieve the corresponding olefinic products. The yield of condensation products decreases as R(72%)Y > Ce(70%)Y > La(70%)Y > Zn(70%)Y > NaY > CaY > H-ZSM-5 (numbers in parentheses represent maximum percentage exchange obtained), and yields between 70 and 85% depending on the reactants were obtained. According to the authors, the overall condensation is probably facilitated by the electrostatic interactions between the exchanged cations and the included organic guests.

Michael reaction of cyclopent-2-enone with dimethyl malonate has been studied on europium-containing Y zeolite at 30°C (Baba et al. 1995). In this case, europium was introduced into K<sup>+</sup>-exchanged zeolite by impregnation from a solution of the metal on



NH<sub>3</sub>, and the catalytic activity depends on the evacuation temperature of the impregnated catalyst. Thus, the yield to 3-(1,1-bismethoxycarbonyl)cyclopent-1-one increased by increasing the evacuation temperature, reaching a maximum of 81%, with a selectivity of 100% at around 147°C.

### 3.4. Other reactions and uses

R-exchanged zeolites are acid materials, and therefore they have been used for carrying out hydration and dehydration of hydrocarbons. This is the case for the hydration of bicyclo[2.2.1]hepta-2,5-diene (Azbel et al. 1989), the cyclodehydration of *N*-ethanolamine (Pillai 1995) and the dehydration of 2,3-dimethyl-2,3-butanediol, pinacol (Bezouhanova and Jabur 1994).

On the other hand, R-exchanged zeolites have also been used in combination with a metal function, for carrying out the isomerization and hydrocracking of paraffins and cycloalkanes. This is the case for isomerization of *n*-hexane to isohexane and 2,2-dimethyl-butane (Rabo et al. 1961); the isomerization of *n*-undecane to mixed C<sub>11</sub> isomers at 275°C on Pt/Ce-Y zeolite (Weitkamp et al. 1985); the isomerization of *endo-exo*-tricyclo[5.2.1.0<sup>2,6</sup>]-decane or *exo*-tricyclo[6.2.1.0<sup>2,7</sup>]-undecane into adamantane or 1-methyladamantane, respectively, on R-Y at 150–270°C (Lau and Maier 1987); the isomerization of tetrahydrodicyclopentadiene into adamantane on Re-Y in a H<sub>2</sub>/HCl atmosphere at 250°C (Honna et al. 1986); or the double bond relocation of 2-alkyl acrolein into *trans*-2-methyl-2-alkenals over Ce,B-ZSM-5 (Fisher et al. 1986). Recently, it has been reported that Ce-promoted Pd/ZSM-5 is an active and selective catalyst in the dehydroisomerization of  $\alpha$ -limonene to *p*-cymene (Weyrich et al. 1997).

In addition, Diels–Alder reactions have also been studied on R-containing microporous materials. Murthy and Pillai (1991) reported the reaction of cyclopentadiene, cyclohexadiene or furan with less reactive dienophiles (acrolein, acrylamide or methyl acrylate). They observed that microporous materials give high yields in Diels–Alder reactions although exclusive endoselectivity was only obtained on a combined catalyst (Ce-Y zeolite with anhydrous ZnBr<sub>2</sub>).

On the other hand, zeolites may serve as cocatalysts or as a carrier for oxidising cations. This is the case of R,Fe-Y zeolite an active catalyst in the oxidation of CO or NO (Aparicio et al. 1988) or Fe–Gd–K–O/mordenite and Fe–Tb–K–O/clinoptilolite catalysts which give a yield of 45–75% styrene from the oxidative dehydrogenation of ethylbenzene (Alimardanov and Addullayev 1996).

Although La-ZSM-5 has been reported as a selective catalyst in the oxidation of phenol with N<sub>2</sub>O to give *p*-hydroquinone with a selectivity of 82.1% (Deng et al. 1997), Ce-containing microporous materials have been the most studied catalysts in redox processes. Thus, Ce-Y zeolite has been used in the complete oxidation of methylene chloride in air (Chatterjee and Greene 1991). However, Ce-modified zeolites can also be used in selective oxidation reactions. This is the case for the selective oxidation of *p*-xylene at 130°C on Ce-containing Mordenite (Hasimoto et al. 1997) or the selective oxidation of cyclohexane on Ce-exchange Y (Pires et al. 1997). Recently, it has been

reported that cerium oxide supported on zeolite X showed a higher activity than those supported on zeolite Y and Kisselguhr, or cobalt-based catalysts for the liquid-phase oxidation of cyclohexanone to dibasic acids (adipic acid and glutaric acid) and caprolactone with glacial acetic acid as solvent and molecular oxygen as oxidant (Yao and Weng 1992).

#### 3.4.1. $\text{NO}_x$ elimination

There is an important number of commercial approaches to  $\text{NO}_x$  removal, including adsorptive, thermal and catalytic techniques (Armor 1994, Centi and Forzatti 1995, Fritz and Pitchon 1997). In the case of catalytic processes, the elimination of  $\text{NO}_x$  can be carried out by direct catalytic decomposition, or by selective catalytic reduction (SCR) using hydrocarbons or ammonia as reductant. Although several catalytic system have been studied, zeolites have been proposed as interesting catalysts for both reactions.

The direct catalytic decomposition of nitric oxide is one of the most attractive alternatives for removing  $\text{NO}_x$  from flue gas streams. The most promising catalyst for NO decomposition is presently the copper ion-exchanged ZSM-5 zeolite (Iwamoto et al. 1986, Lei et al. 1995, Lee et al. 1995). Recently, it has been reported that  $\text{Ce}^{3+}$  (Li and Armor 1992, Zhang and Flytzani-Stephanopoulos 1994) or  $\text{Sm}^{3+}$  (Parvulescu et al. 1998) ions promote the low-temperature NO decomposition. However, a different performance has been proposed depending on the ion incorporated. It has been proposed that the presence of  $\text{Sm}^{3+}$  ions promotes both the low-temperature NO decomposition (Li and Armor 1992, Zhang and Flytzani-Stephanopoulos 1994) and the hydrothermal stability of Cu-ZSM-5 catalysts in the presence of water (Zhang and Flytzani-Stephanopoulos 1996), although the method used in the incorporation of both Cu and Ce ions strongly influence the catalytic activity (Zhang and Flytzani-Stephanopoulos 1994). On the other hand, the incorporation of Sm ions could modify the exchange of copper with the zeolite and, consequently, the dispersion and aggregation of copper (Parvulescu et al. 1998).

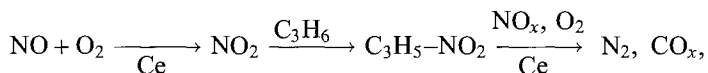
Besides transition metals (Cu, Co and Zn) (Amiridis et al. 1996, Sato et al. 1991, Ito et al. 1994), rare-earth-ion exchanged Y zeolites have also been tested for the reduction of nitrogen oxides with hydrocarbons (Misono and Kondo 1991, Yokoyama and Misono 1992, 1994a,b, Sakamoto et al. 1994, Orlik et al. 1994, Yasuda et al. 1995, Swaroop and Wurisika 1996) and ammonia (Ito et al. 1994, 1995a,b, 1996). In general, it can be concluded that the catalytic activity of these materials is governed by the nature of the cation exchanged, the degree of sodium exchanging for the corresponding cation, by the  $\text{SiO}_2/\text{Al}_2\text{O}_3$  ratio of the zeolite, and by the acidity of the catalyst surface (Orlik et al. 1994).

Misono and Kondo (1991) studied Ce-containing catalysts, i.e., Ce-ZSM-5, Ce-Y and  $\text{CeO}_2/\text{Al}_2\text{O}_3$ . They observed that Ce-containing microporous materials, especially Ce-ZSM-5 (Yokoyama and Misono 1994b), were more active than the  $\text{CeO}_2/\text{Al}_2\text{O}_3$  catalyst, suggesting a promoting effect of the zeolite structure on the activity of Ce. The high activity of Ce-ZSM-5 was attributed to its high selectivity and the high efficiency of the use of propene for the reduction.

Ce-Y and Pr-Y zeolites were found to exhibit significant activity using propene as reductant and they show temperatures of maximum NO conversion within the range reported for the transition-metal-exchanged ZSM-5 and Y zeolites. In this way, Nishizaka and Misono (1993) have reported that, when methane was used as the reductant, the activity of two palladium loaded catalysts (i.e., Pd-H- and Pd-Ce-H-ZSM-5) was found to be comparable to the activity of transition-metal-exchanged ZSM-5. However, these catalysts were ineffective for the reduction of NO by propylene. On the other hand, the addition of alkaline-earth-metal ions (Mg, Ca, Sr, and Ba) enhanced the activity of the Ce-ZSM-5 catalysts, particularly at temperatures above 350°C (Yokoyama and Misono 1992, 1994a,b).

Sakamoto et al. (1994) studied the catalytic properties of Ln-Pt ion-exchanged mordenite for the system NO-O<sub>2</sub>-C<sub>3</sub>H<sub>8</sub>. They observed that the amounts of N<sub>2</sub>O, which is a by-product in the catalytic reduction of NO, differ largely with the type of rare-earth ions. However, the activity of Ln-Pt ion-exchanged mordenite was decreased in the presence of gaseous oxygen.

According to the reaction network proposed by Yokoyama and Misono (1994a),



where Ce ions participate in both step 1 (the oxidation of NO to NO<sub>2</sub> is accelerated by the Ce ion) and step 3 (in which the Ce ion also acts as a catalytic center).

Recently, it has been proposed that the bi-cation Ce-Ag-ZSM-5 zeolite is a selective catalyst for the reduction of nitric oxide by methane in the presence of excess oxygen (Li and Flytzani-Stephanopoulos 1997). The coexistence of both Ce and Ag is, according to these authors, crucial for achieving high NO conversion to N<sub>2</sub>.

In the case of the selective catalytic reduction using ammonia as reductant but in excess O<sub>2</sub>, Ce-exchanged sodium-type mordenite (CeNa-MOR) has been reported as an active catalyst in the 250–560°C temperature range with respect to non-redox La,Na- and H-mordenite catalysts (Ito et al. 1994). In this case, the reduction of nitric oxide is thought to proceed with crucial involvement of a Ce<sup>3+</sup>/Ce<sup>4+</sup> redox couple, although the intermediate reaction pathway depends on the reaction temperature.

More recently, infrared studies on the adsorption of NO and the coadsorption of NO and O<sub>2</sub> onto Ce,Na-mordenite zeolite indicate that the redox properties of cerium (Ce<sup>3+</sup>/Ce<sup>4+</sup>) may contribute to the easier desorption of oxidized NO species (Ito et al. 1995a,b, 1996). In this way, the formation of NO<sup>+</sup> is associated with zeolite acid sites, and NO<sub>3</sub><sup>-</sup> species associated to La cations, both NO<sup>+</sup> and NO<sub>3</sub><sup>-</sup> were found to desorb more easily from Ce,Na-mordenite than from La,Na-mordenite (Ito et al. 1995a).

However, although Cu-containing zeolite-based catalysts present a high productivity they have not yet been implemented in practice. This is a consequence of the rapid deactivation under lean NO<sub>x</sub> reduction conditions, i.e. in an atmosphere containing a high concentration of steam at a temperature of 400–800°C. A comparative study of Ce,Cu-mordenite and a commercially available V<sub>2</sub>O<sub>5</sub>/TiO<sub>2</sub>/WO<sub>3</sub>-type catalyst for the

selective catalytic reduction of  $\text{NO}_x$  in diesel-exhaust gases with  $\text{NH}_3$  was presented by Hultermans et al. (1995).

On the other hand, it has been observed that both by increasing the Cu loading to above 68% of the exchange capacity and by La addition it is possible to improve the stability of Cu-zeolite-based catalysts, presumably because these decrease the concentration of protons which are important in the dealumination of the ZSM-5 framework (Yan et al. 1997). However, this positive effect was not observed with the addition of Ce ions, because  $\text{CeO}_2$  was formed.

Rokosz et al. (1997) have studied several ions as stabilizers, i.e., Co, Ni, Pd, Cu, Ga, Al, Fe, La and Ce. They observe that  $\text{La}^{3+}$  and  $\text{Ce}^{3+}$  suppress the dealumination of Cu-ZSM-5 catalysts, although samples containing the active  $\text{Cu}^{2+}$  and the  $\text{La}^{3+}$  are not stable as singly modifier materials and they are not more active than non-modified ones. However, by incorporating ~5% of La or Ce, a part of the copper (20–30%) preserves the active square-planar  $\text{Cu}^{2+}$  co-ordination even at high temperature.

This apparent discrepancy between the results obtained by Rokosz et al. (1997) and Yan et al. (1997) can be explained by taking account of the method used in the incorporation of the R ion. An ion-exchange method was used by Rokosz et al. (1997), while impregnation with an aqueous solution was employed by Yan et al. (1997). Thus, as was discussed in sect. 2.2, the incorporation of R ions and their stability under steaming conditions will determine their distribution in the zeolite. However, the possible stabilization of  $\text{Cu}^{2+}$  topography in ZSM-5 and of the Si–O–Al linkages by rare-earth modifiers is not fully understood at present.

#### 4. Conclusions

In conclusion, it has been shown that zeolites are largely stabilised by the presence of rare earths in extra-framework positions. The acidity generated during the exchange yields catalysts that are active and selective, either by themselves or in combination with metals, for acid catalysed processes involving carbonium and carbenium ions. They are of practical importance in processes related with oil refining petrochemistry and also in the production of chemicals.

Finally, new types of  $\text{NO}_x$  and  $\text{SO}_x$  abatement catalysts use rare earths in their formulations, helping to increase the activity and stability of transition-metal-containing zeolites.

#### References

- |   |   |
|---|---|
| Akporiaye, D.E., K. Daasvatn, J. Solberg and M. Stöcker, 1993, Modified zeolites as active catalysts in Friedel–Crafts acylation, in: <i>Heterogeneous Catalysis and Fine Chemicals III</i> , eds | M. Guisnet, J. Barbier, J. Barrault, C. Bouchoule, D. Duprez, G. Perot and C. Montassier, Vol. 78 of <i>Studies in Surface Science and Catalysis</i> (Elsevier, Amsterdam) pp. 521–526. |
|---|---|

- Al-jarallah, A.M., U.A. El-nafaty and M.M. Abdillahi, 1997, *Appl. Catal.* **154**, 117.
- Algarra, F., A. Corma, V. Fornés, H. Garcia, A. Martinez and J. Primo, 1993, Rearrangement of acetals of 2-bromopropiophenone as a test reaction to characterize the Lewis sites in large pore zeolites, in: *Heterogeneous Catalysis and Fine Chemicals III*, eds M. Guisnet, J. Barbier, J. Barrault, C. Bouchoule, D. Duprez, G. Perot and C. Montassier, Vol. 78 of *Studies in Surface Science and Catalysis* (Elsevier, Amsterdam) pp. 653–660.
- Alimardanov, K.M., and A.F. Addullayev, 1996, *Petr. Chem.* **35**, 508.
- Amiridis, M.D., T. Zhang and R.J. Farrauto, 1996, *Appl. Catal.* **10**, 203.
- Amouzegh, P., A. Finniels, P. Geneste, E. Ginestar and P. Moreau, 1995, *Catal. Lett.* **34**, 389.
- Antonio, M.R., L. Soderholm and I. Song, 1997, *J. Appl. Electrochem.* **27**, 784.
- Aparicio, L.M., M.A. Ulla, W.S. Millman and J.A. Dumesic, 1988, *J. Catal.* **110**, 330.
- Arakawa, T., T. Toshihawa, M. Takakuwa, G. Adachi and J. Shiokawa, 1982, *Mater. Res. Bull.* **17**, 171.
- Ardito, S.C., H. Ashjian, T.F. Degnan, T.E. Helton, Q.N. Le and A.R. Quinones, 1997, US Patent 5,629,463.
- Armengol, E., A. Corma, H. Garcia and J. Primo, 1995, *Appl. Catal. A* **126**, 391.
- Armor, J.M., 1994, NO<sub>x</sub> removal: an overview, in: *Environmental Catalysis*, ed. J.M. Armor, Vol. 552 of ACS Symposium Series (American Chemical Society, Washington, DC) pp. 2–6.
- Azbel, B.I., N.F. Goldshleger, E.T. Epelbaum, Yu.Yu. Yamplo-Skii, M.L. Khidekel, Ya.I. Isakov and Kh.M. Minachev, 1989, Catalytic properties of a zeolite system in bicyclo[2,2,1]hepta-2,5-diene reaction, in: *Zeolites: Facts, Figures and Future*, eds P.A. Jacobs and R.A. van Santen, Vol. 49 of *Studies in Surface Science and Catalysis* (Elsevier, Amsterdam) pp. 1407–1412.
- Baba, T., R. Koide and Y. Ono, 1991, *J. Chem. Soc. Chem. Commun.*, p. 691.
- Baba, T., S. Hikita, R. Koide, Y. Ono, T. Hanada, T. Tanaka and S. Yoshida, 1993, *J. Chem. Soc. Faraday Trans.* **89**, 3177.
- Baba, T., S. Hikita, Y. Ono, T. Yoshida, T. Tanaka and S. Yoshida, 1995, *J. Mol. Catal. A* **98**, 49.
- Balkus, K.J., and J. Shi, 1997, *Microporous Mater.* **11**, 325.
- Ben Taarit, Y., 1992, Catalysis by exchanged cation and zeolite framework sites, in: *Zeolite Microporous Solids: Synthesis, Structure, and Reactivity*, eds E.G. Derouane, F. Lemos, G. Naccache and F.T. Ribeiro, Vol. C-352 of NATO ASI Series (Kluwer Academic Publishers, Dordrecht) pp. 347–371.
- Bennett, J.M., and J.V. Smith, 1969, *Mater. Res. Bull.* **4**, 343.
- Berry, F.J., J.F. Marco and A.T. Steel, 1993, *J. Alloys & Compounds* **194**, 167.
- Beyer, H.K., H.G. Karge and G. Pal-Borbely, 1988, *Zeolites* **8**, 79.
- Beyer, H.K., G. Pal-Borbely and H.G. Karge, 1993, *Microporous Mater.* **1**, 67.
- Bezouhanova, C.P., and F.A. Jabur, 1994, *J. Mol. Catal.* **87**, 39.
- Bolton, A.P., 1971, *J. Catal.* **22**, 9.
- Bolton, A.P., M.A. Lanewala and P.E. Pickert, 1968a, *J. Org. Chem.* **33**, 1513.
- Bolton, A.P., M.A. Lanewala and P.E. Pickert, 1968b, *J. Org. Chem.* **33**, 3415.
- Brait, A., K. Seshan and J.A. Lercher, 1998, *Appl. Catal. A* **169**, 299.
- Breck, D.W., 1974, *Zeolite Molecular Sieves* (Wiley, New York) pp. 725–755.
- Brenan, D., R.G. Bell, C.R.A. Catlow and R.A. Jackson, 1994a, *Zeolites* **14**, 650.
- Brenan, D., C.R.A. Catlow and R.A. Jackson, 1994b, *Zeolites* **14**, 660.
- Bresinska, I., K.J. Balkus and S. Kowalak, 1993, Synthesis of Silicalite-1 containing Gadolinium, Vol. 38 of *Preprints, Division of Petroleum Chemistry* (American Chemical Society, Washington, DC) pp. 494–497.
- Carvajal, R., P.-J. Chu and J.H. Lunsford, 1990, *J. Catal.* **125**, 123.
- Centi, G., and P. Forzatti, eds, 1995, 1st World Conference on Environmental Catalysis for a Better World and Life, *Catal. Today* **27**, Special Issue.
- Chang, C.D., 1983, *Catal. Rev. Sci. Eng.* **25**, 1.
- Chang, C.D., and A.J. Silvestri, 1977, *J. Catal.* **47**, 249.
- Chao, K.-J., and Ch.-F. Lin, 1992, *Collect. Czech. Chem. Commun.* **57**, 710.
- Chatterjee, S., and H.L. Greene, 1991, *J. Catal.* **130**, 76.
- Cheetham, A.K., M.M. Eddy and J.M. Thomas, 1984, *J. Chem. Soc. Chem. Commun.*, p. 1337.
- Chen, N.Y., and T.F. Degnan, 1988, *Chem. Eng. Prog.* **84**, 32.
- Chen, Q.J., T. Ito and J. Fraissard, 1991, *Zeolites* **11**, 239.

- Chiche, B., A. Finiels, C. Gauthier and P. Geneste, 1986, *J. Org. Chem.* **51**, 2128.
- Chiche, B., A. Finiels, C. Gauthier and P. Geneste, 1987, *J. Mol. Catal.* **42**, 229.
- Choudhary, V.R., K.R. Srinivasan and D.B. Akolekar, 1989, *Zeolites* **9**, 115.
- Chu, Y.F., and A.W. Chester, 1986, *Zeolites* **6**, 195.
- Corma, A., 1992, Zeolites in oil refining and petrochemistry, in: *Zeolite Microporous Solids: Synthesis, Structure, and Reactivity*, eds E.G. Derouane, F. Lemos, G. Naccache and F.T. Ribeiro, Vol. C-352 of NATO ASI Series (Kluwer Academic Publishers, Dordrecht) pp. 347–371.
- Corma, A., 1995, *Chem. Rev.* **95**, 559.
- Corma, A., and H. Garcia, 1997, *Catal. Today* **38**, 257.
- Corma, A., and A. Martinez, 1993, *Catal. Rev. Sci. Eng.* **35**, 483.
- Corma, A., and E. Sastre, 1991, *J. Chem. Soc. Chem. Commun.*, p. 594.
- Corma, A., V. Fornés, J.B. Montón and V. Orchillés, 1986, *Ind. Eng. Chem. Prod. Res. Dev.* **25**, 231.
- Corma, A., V. Fornés, A. Martínez and A.V. Orchillés, 1988, Parameters in addition to the unit cell that determine the cracking activity and selectivity of dealuminated HY zeolite, in: *ACS Symposium Series*, Vol. 368, eds W.H. Flank and T.E. Whyte (ACS, Washington, DC) pp. 542–554.
- Corma, A., M.J. Climent, H. Garcia and J. Primo, 1989, *Appl. Catal.* **49**, 109.
- Corma, A., M. Faraldos, A. Martinez and A. Mifsud, 1990a, *J. Catal.* **122**, 230.
- Corma, A., F.V. Melo and D.J. Rawlance, 1990b, *Zeolites* **10**, 690.
- Corma, A., F.V. Melo and D.J. Rawlance, 1992, *Zeolites* **12**, 261.
- Corma, A., A.E. Palomares and F. Rey, 1993, *European Patent* 9301712.
- Corma, A., M.I. Juan-Rajadell, J.M. López Nieto, A. Martínez and C. Martínez, 1994a, *Appl. Catal. A* **111**, 175.
- Corma, A., V. Gómez and A. Martínez, 1994b, *Appl. Catal. A* **119**, 83.
- Corma, A., A. Martínez and C. Martínez, 1996a, *Appl. Catal. A* **134**, 169.
- Corma, A., A. Martínez, P.A. Arroyo, J.L.F. Monteiro and E.F. Sousa-Aguiar, 1996b, *Appl. Catal. A* **142**, 139.
- Corma, A., A.E. Palomares, F. Rey and F. Marquez, 1997, *J. Catal.* **170**, 140.
- Costenoble, M.L., W.J. Mortier and J.B. Uytterhoeven, 1978, *J. Chem. Soc. Faraday Trans. I*, **74**, 466.
- Coughlan, B., and M.A. Keane, 1991, *Zeolites* **11**, 2.
- Cremers, A., 1977, Ion exchange in zeolites, in: *Molecular Sieve II*, ed. J.R. Katzer, Vol. 40 of ACS Symposium Series (American Chemical Society, Washington, DC) pp. 179–193.
- Das, D., and M.C. Upreti, 1995, *Indian J. Chem. A* **34**(5), 383.
- Deng, G., Z. Liu and R. Mu, 1997, *CN Patent* 1145280A.
- Diaz-Mendoza, F.A., L. Pernett-Bolano and N. Cardona-Martinez, 1998, *Termochim. Acta* **312**(1–2), 47.
- Dougan, T.J., 1994, *Advances in FCC Vanadium Tolerance*, NPRA AM 94–96.
- Dwyer, F.G., 1981, in: *Catalysis Organic Reactions*, ed. W.R. Moser (Marcel Dekker, New York) p. 39.
- Dyer, A., 1988, *Zeolite Molecular Sieves* (Wiley, Chichester).
- Dyer, A., M. Shesheniah and J.G. Brown, 1978, *J. Inorg. Nucl. Chem.* **40**, 99.
- Feast, S., and J.A. Lercher, 1996, Synthesis of intermediates and fine chemicals using molecular sieve, in: *Recent Advances and New Horizons in Zeolite Science and Technology*, eds H. Chon, S.I. Wo and S.E. Park, Vol. 102 of *Studies in Surface Science and Catalysis* (Elsevier, Amsterdam) pp. 363–412.
- Feron, B., P. Gallezot and M. Bourgogne, 1992, *J. Catal.* **134**, 469.
- Fisher, R., W.F. Hölderich, W.D. Moss and H.H. Weits, 1986, *European Patent Application* 0 167 021.
- Flego, C., I. Kiricsi, W.O. Parker Jr and M.G. Clerici, 1995, *Appl. Catal. A* **124**, 107.
- Fleisch, T.H., B.L. Meyers, G.J. Ray, J.B. Hall and C.L. Marshall, 1986, *J. Catal.* **99**, 117.
- Floor, M., A.P.G. Kieboom and H. Van Bekkum, 1989, *Recl. Trav. Chim. Pays-Bas*, **108**, 128.
- Fritz, A., and V. Pitchon, 1997, *Appl. Catal. B* **13**, 1.
- Gaare, K., and D. Akporiaye, 1996, *J. Mol. Catal. A* **109**, 177.
- Gaare, K., and D. Akporiaye, 1997, *J. Phys. Chem. B* **101**, 48.
- Gárdos, G., L. Pechy, A. Redey and Ch. Okonji, 1980a, *Hung. J. Ind. Chem. Veszprém.* **8**, 363.
- Gárdos, G., L. Pechy, A. Redey and Y. Sokobai, 1980b, *Hung. J. Ind. Chem. Veszprém.* **8**, 371.
- Gárdos, G., J. Kristóf, L. Pechy and A. Redey, 1982, *Hung. J. Ind. Chem. Veszprém.* **10**, 251.

- Gárdos, G., A. Redey and J. Kristóf, 1983, *Geterog. Katal.* **5**, 447.
- Gárdos, G., A. de Jonge, F. Halmos, J. Kristóf and A. Redey, 1984, *Hung. J. Ind. Chem. Veszprém.* **12**, 251.
- Gauthier, C., B. Chiche, A. Finiels and P. Geneste, 1989, *J. Mol. Catal.* **50**, 219.
- Goodall, R.D., 1962, *Davison Catalagram* **13**, 2.
- Goux, A., P. Geneste and P. Moreau, 1994, *J. Mol. Catal.* **89**, 383.
- Grünert, W., U. Sauerlandt, R. Schlögl and H.G. Karge, 1993, *J. Phys. Chem.* **97**, 1413.
- Haack, L.P., C.P. Hubbard and M. Shelef, 1995, X-ray photoelectron-spectroscopy of metal exchanged Na-ZSM-5 zeolites, Vol. 587 of ACS Symposium Series (American Chemical Society, Washington, DC) pp. 166–182.
- Hairston, D.W., 1996, *Chem. Eng.*, July, p. 57.
- Harandi, M.N., 1993, US Patent 5,177,279.
- Hasimoto, K., K. Matzuo, H. Kominami and Y. Kera, 1997, *J. Chem. Soc. Faraday Trans.* **93**, 3729.
- Hatch, L.F., 1969, *Hydrocarbon Process.* **48**, 77.
- Hazenkamp, M.F., and G. Blasse, 1993, *Res. Chem. Intermed.* **19**, 343.
- Hazenkamp, M.F., A.M.H. van der Veen and G. Blasse, 1992a, *J. Chem. Soc. Faraday Trans.* **88**, 133.
- Hazenkamp, M.F., A.M.H. van der Veen, N. Feiken and G. Blasse, 1992b, *J. Chem. Soc. Faraday Trans.* **88**, 141.
- Herreros, B., P.P. Man, J.-M. Manoli and J. Fraissard, 1992, *J. Chem. Soc. Chem. Commun.*, p. 464.
- Hickson, D.A., and S.M. Csicsery, 1968, *J. Catal.* **10**, 27.
- Hölderich, W.F., and H. van Bekkum, 1991, Zeolites in organic synthesis, in: *Introduction to Zeolite Science and Practice*, eds H. van Bekkum, E.M. Flanigen and J.C. Jansen, Vol. 58 of *Studies in Surface Science and Catalysis* (Elsevier, Amsterdam) pp. 631–726.
- Hong, S.B., J.S. Seo, Ah.-H. Pyun, Ch.-H. Kim and Y.S. Uh, 1995, *Catal. Lett.* **30**, 87.
- Honna, K., M. Sugimoto, N. Shimizu and K. Kurisaki, 1986, *Chem. Lett.*, p. 315.
- Huang, T.J., 1983, US Patent 4,384,161.
- Hultermans, R.J., E. Ito, A. Jozsef, P.M. Lugt and C.M. van den Bleek, 1995, Selective catalytic reduction of NO<sub>x</sub> in diesel exhaust-gases with NH<sub>3</sub> over Ce and Cu mordenite and V<sub>2</sub>O<sub>5</sub>/TiO<sub>2</sub>/WO<sub>3</sub> type catalysts – Can Ce solve the NH<sub>3</sub> slip problem?, in: *Catalysis and Automotive Pollution Control III*, eds A. Frennet and J.-M. Bastin, Vol. 96 of *Studies in Surface Science and Catalysis* (Elsevier, Amsterdam) pp. 645–653.
- Hunger, M., G. Engelhardt and J. Weitkamp, 1995, *Microporous Mater.* **3**, 497.
- Hunter, F.D., and J. Scherzer, 1971, *J. Catal.* **20**, 246.
- Ikemoto, M., K. Tsutsumi and H. Takahashi, 1972, *Bull. Chem. Soc. Japan* **45**, 1330.
- Ione, K.G., and O.V. Kikhtyanin, 1989, Reactions of electrophilic substitution on zeolite catalysts. Aniline alkylation by methanol, in: *Zeolites: Facts, Figures and Future*, eds P.A. Jacobs and R.A. van Santen, Vol. 49 of *Studies in Surface Science and Catalysis* (Elsevier, Amsterdam) pp. 1073–1083.
- Ito, E., R.J. Hultermans, P.M. Lugt, M.H.W. Burgers, M.S. Rigutto, H. van Bekkum and C.M. van den Bleek, 1994, *Appl. Catal. B* **4**, 95.
- Ito, E., Y.J. Mergler, B.E. Nieuwenhuys, H. van Bekkum and C.M. van den Bleek, 1995a, *Microporous Mater.* **4**, 455.
- Ito, E., R.J. Hultermans, P.M. Lugt, M.H.W. Burgers, H. van Bekkum and C.M. van den Bleek, 1995b, Selective reduction of NO<sub>x</sub> with ammonia over cerium exchanged zeolite catalysts – Towards a solution for an ammonia slip problem, in: *Catalysis and Automotive Pollution Control III*, eds A. Frennet and J.-M. Bastin, Vol. 96 of *Studies in Surface Science and Catalysis* (Elsevier, Amsterdam) pp. 661–673.
- Ito, E., Y.J. Mergler, B.E. Nieuwenhuys, H.P.A. Calis, H. van Bekkum and C.M. van den Bleek, 1996, *J. Chem. Soc. Faraday Trans.* **92**, 1799.
- Ivanova, I.I., A.D. Kazenina, B.V. Romanovsky and I.M. Gerzeliev, 1994, Application of iodometry for zeolite active sites characterization and modification, in: *Zeolites and Related Microporous Materials: State of the Art 1994*, eds J. Weitkamp, H.G. Karge, H. Pfeifer and W. Hölderich, Vol. 84 of *Studies in Surface Science and Catalysis* (Elsevier, Amsterdam) p. 717–724.
- Iwamoto, M., H. Furukawa, Y. Mine, F. Uemura, S. Mikuriya and S. Kagawa, 1986, *J. Chem. Soc. Chem. Commun.* **15**, 1272.
- Iyer, P.S., J. Scherzer and Z.C. Mester, 1988, <sup>29</sup>Si and <sup>27</sup>Al Magic angle spinning-NMR spectroscopy study of rare-earth-exchanged zeolites, in: *Perspectives in Molecular Sieve Science*, eds W.H. Flank and T.E. White, Vol. 368 of ACS Symposium Series (American Chemical Society, Washington, DC) pp. 48–65.

- Jacobs, P.A., and J.B. Uytterhoeven, 1973, *J. Chem. Soc. Faraday Trans. 1*, **69**, 373.
- Jia, M., H. Lechert and H. Föster, 1992, *Zeolites* **12**, 32.
- Karge, H.G., 1992, Modification of zeolites and new routes to ion exchange, in: *Zeolite Microporous Solids: Synthesis, Structure, and Reactivity*, eds E.G. Derouane, F. Lemos, G. Naccache and F.T. Ribeiro, Vol. C-352 of NATO ASI Series (Kluwer Academic Publishers, Dordrecht) pp. 273–290.
- Karge, H.G., 1994, Solid-state reactions in zeolites, in: *Zeolites and Microporous Materials*, eds Y. Hattori and T. Yashima, Vol. 83 of *Studies in Surface Science and Catalysis* (Elsevier, Amsterdam) pp. 135–146.
- Karge, H.G., 1997, Post-synthesis modifications of microporous materials by solid-state reactions, in: *Progress in Zeolite and Microporous Materials*, eds H. Chon, S.-K. Ihm and Y.S. Uh, Vol. 105 of *Studies in Surface Science and Catalysis* (Elsevier, Amsterdam) pp. 1901–1948.
- Karge, H.G., and H.K. Beyer, 1991, Introduction of cations into zeolites by solid-state reaction, in: *Zeolite Chemistry and Catalysis*, eds P.A. Jacobs, N.I. Jaeger, L. Kubelkova and B. Wichterlova, Vol. 69 of *Studies in Surface Science and Catalysis* (Elsevier, Amsterdam) pp. 43–64.
- Karge, H.G., and L.C. Jozefowicz, 1994, A comparative study of the acidity of various zeolites using the differential heats of ammonia adsorption as measured by high-vacuum microcalorimetry, in: *Zeolites and Related Microporous Materials: State of the Art 1994*, eds J. Weitkamp, H.G. Karge, H. Pfeifer and W. Hölderich, Vol. 84 of *Studies in Surface Science and Catalysis* (Elsevier, Amsterdam) pp. 685–692.
- Karge, H.G., G. Borbely, H.K. Beyer and G. Onyestyak, 1988a, Solid-state ion exchange in zeolites. Part III. Preparation and test of lanthanum zeolite catalysts, in: *Proc. 9th Int. Congress on Catalysis*, Ottawa, 1988, eds M.J. Phillips and M. Ternan (The Chemical Institute of Canada, Ontario) pp. 396–403.
- Karge, H.G., H.K. Beyer and G. Borbely, 1988b, *Catal. Today* **3**, 41.
- Karge, H.G., V. Mavrodinova, Z. Zheng and H.K. Beyer, 1990, Solid-state ion exchange – phenomenon and mechanism, in: *Guidelines for Mastering the Properties of Molecular Sieves*, eds D. Bartomeuf, E.G. Derouane and W. Hölderich, Vol. B 221 of NATO ASI Series (Plenum Press, New York) pp. 157–168.
- Karge, H.G., V. Mavrodinova, Z. Zheng and H.K. Beyer, 1991, *Appl. Catal.* **75**, 343.
- Karge, H.G., G. Pal-Borbely and H.K. Beyer, 1994, *Zeolites* **14**, 512.
- Keane, M.A., 1996, *Microporous Mater.* **7**, 51.
- Keir, D., E.F.T. Lee and L.V.C. Rees, 1988, *Zeolites* **8**, 228.
- Kim, J.-G., T. Kompany, R. Ryoo, T. Ito and J. Fraissard, 1994, *Zeolites* **14**, 427.
- Kim, J.H., Y. Sugi, T. Matsuzaki, T. Hanaoka, Y. Kubota, X. Tu, M. Matsumoto, S. Naakata, A. Kato, G. Seo and C. Park, 1995, *Appl. Catal. A* **131**, 15.
- Kiricsi, Y., C. Flego and G. Bellussi, 1995, *Appl. Catal. A* **126**, 401.
- Kirsch, F.W., J.D. Potts and D.S. Barmby, 1972, *J. Catal.* **27**, 142.
- Kitto, M.E., D.L. Anderson, G.E. Gordon and I. Olmez, 1992, *Environ. Sci. Technol.* **26**, 1368.
- Lai, P.P., and L.V.C. Rees, 1976, *J. Chem. Soc. Faraday Trans. 1*, **72**, 1809.
- Landis, P.S., and P.B. Venuto, 1966, *J. Catal.* **6**, 245.
- Lau, G.C., and W.F. Maier, 1987, *Langmuir* **3**, 164.
- Lee, C.-Y., K.-Y. Choi and B.-H. Ha, 1995, *Appl. Catal. B* **5**, 7.
- Lee, E.F.T., and L.V.C. Rees, 1987a, *Zeolites* **7**, 143.
- Lee, E.F.T., and L.V.C. Rees, 1987b, *Zeolites* **7**, 446.
- Lee, T.Y., and Y.H. Ma, 1977, Ion exchange in zeolites, in: *Molecular Sieve II*, ed. J.R. Katzer, Vol. 40 of ACS Symposium Series (American Chemical Society, Washington, DC) pp. 428–438.
- Lei, G.D., B.J. Adelman, J. Sarkany and W.M.H. Sachtler, 1995, *Appl. Catal. B* **5**, 245.
- Lemos, F., F. Ramoa Ribeiro, M. Kern, G. Gianetto and M. Guisnet, 1987, *Appl. Catal.* **29**, 43.
- Lerner, H., W. Holderich and M. Schwarzmann, 1987, *German Patent DE 3618964 A1*.
- Li, Q., L. Dai, J. Xiong, L. Zhu and Z. Xue, 1994, *Zeolites* **14**, 367.
- Li, R.-S., R.-W. Wen, W.-Y. Zhang and Q. Wei, 1993, *Zeolites* **13**, 229.
- Li, Y., and J.N. Armor, 1992, *US Patent* 5,149,512.
- Li, Z., and M. Flytzani-Stephanopoulos, 1997, *Appl. Catal. A* **165**, 15.
- Lin, C.F., and K.J. Chao, 1991, *J. Phys. Chem.* **23**, 9411.
- Liu, S.-B., Y.-J. Shu and Ch.-T. Chang, 1994, *J. Chin. Chem. Soc.* **41**, 53.
- Magee, J.S., 1972, *Davison Catalagram* **41**, 3.



- Magee, J.S., and J.J. Blazek, 1976, Preparation and performance of zeolite cracking catalysts, in: *Zeolite Chemistry and Catalysis*, ed. J.E. Rabo, ACS Monograph 171 (American Chemical Society, Washington, DC) pp. 615–679.
- Maher, P.K., and C.V. McDaniel, 1986, US Patent 3,402,996.
- Marynen, P., A. Maes and A. Cremers, 1984, *Zeolites* **4**, 287.
- Maugé, F., P. Gallezot, J.-C. Courcelle, P. Engelhard and J. Grosmangin, 1986, *Zeolites* **6**, 261.
- Meier, W.M., D.H. Olson and Ch. Baerlocher, 1996, *Zeolites*, **17**, 1.
- Meisel, S.L., J.P. McCullough, C.H. Lechtaler and P.B. Weisz, 1976, *Chemtech* **6**, 86.
- Minachev, K.M., E.S. Mortinov, S.M. Zen'kovski, N.V. Mostovoy and N.F. Kononov, 1977, Isoparaffin-olefin alkylation over zeolite catalysts, in: *Industrial and Laboratory Alkylations*, Vol. 55 of ACS Symposium Series (American Chemical Society, Washington, DC) pp. 89–95.
- Misono, M., and K. Kondo, 1991, *Chem. Lett.*, No. 6, 1001.
- Moreau, P., A. Finiels, P. Geneste and J. Solofo, 1992, *J. Catal.* **136**, 487.
- Mori, H., T. Yamazaki, S. Ozawa and Y. Ogino, 1993, *Bull. Chem. Soc. Jpn.* **66**, 2504.
- Mostad, H., M. Stöcker, A. Karlsson, H. Junggreen and B. Hustad, 1997, La-EMT, a promising catalyst for isobutane/2-butene alkylation, in: *Progress in Zeolite and Microporous Materials*, eds H. Chon, S.-K. Ihm and Y.S. Uh, Vol. 105 of *Studies in Surface Science and Catalysis* (Elsevier, Amsterdam) pp. 1413–1422.
- Mravec, D., M. Michouk and M. Honec, 1997, *Petr. Coal.* **39**, 27.
- Murthy, Y.V.S.N., and C.N. Pillai, 1991, *Synth. Commun.* **21**, 783.
- Nasukhanov, Kh.S.U., S.E. Spiridonov, O.V. Kyukov and S.N. Khadzhiev, 1993, *Kinet. Catal.*, **34**, 158.
- Nery, J.G., Y.P. Mascarenhas, T.J. Bonagamba, N.C. Mello and E.F. Souza-Aguiar, 1997, *Zeolites* **18**, 44.
- Nicula, A., and E. Trif, 1991, *Rev. Roum. Phys.* **36**, 861.
- Nishizaka, Y., and M. Misono, 1993, *Chem. Lett.* 1295.
- Nunan, J.G., K.C.C. Kharas and H.J. Robota, 1995, WO Patent 9509687 A1.
- Occelli, M.L., 1991, *Catal. Rev. Sci Eng.* **33**, 241.
- Occelli, M.L., 1996, Vanadium resistant fluid cracking catalysts, in: *Catalyst in Petroleum Refining and Petrochemical Industries 1995*, eds M. Absi-Halabi, J. Beshara, H. Qabazard and A. Stanislaus, Vol. 100 of *Studies in Surface Science and Catalysis* (Elsevier, Amsterdam) pp. 25–47.
- Occelli, M.L., and H.E. Robson, 1989, *Zeolite Synthesis* (American Chemical Society, Washington, DC) 662 pp.
- Occelli, M.L., and H.E. Robson, 1992, *Molecular Sieves* (van Nostrand Reinhold, New York) 563 pp.
- Olson, D.H., G.T. Kokotailo and J.F. Charnell, 1968, *J. Colloid Interface Sci.* **28**, 305.
- Orlik, S.N., V.L. Struzhko, V.P. Stasevich and M.G. Martsenyukukharuk, 1994, *Teor. Eksp. Khim.* **30**(6), 350.
- Parvulescu, V.I., P. Oelker, P. Grange and B. Delmon, 1998, *Appl. Catal. B* **16**, 1.
- Pillai, R.B.C., 1995, *Current Sci.* **68**, 732.
- Pillai, R.B.C., 1996, *React. Kinet. Catal. Lett.* **58**, 145.
- Pillai, R.B.C., and C.N. Pillai, 1993, *Indian J. Chem.* **32B**, 592.
- Pine, L.A., P.J. Maher and W.A. Watcher, 1984, *J. Catal.* **85**, 466.
- Pires, E.L., M. Wallau and U. Schuchardt, 1997, Selective oxidation of cyclohexane over rare earth exchanged zeolite Y, in: *3rd World Congr. on Oxidation Catalysis*, eds R.K. Grasselli, S.T. Oyama, A.M. Gaffney and J.E. Lyons, Vol. 110 of *Studies in Surface Science and Catalysis* (Elsevier, Amsterdam) pp. 1025–1027.
- Plank, C.J., 1984, *CHEMTECH*, April, 243.
- Plank, C.J., E.J. Rosinski and W.P. Hawthorne, 1964, *Ind. Eng. Chem. Prod. Res. Dev.* **3**, 165.
- Pradhan, A.R., and B.S. Rao, 1991, *J. Catal.* **132**, 79.
- Rabo, J.A., P.E. Pickert, D.N. Stamires and J.E. Boyle, 1961, Molecular sieve catalysts in hydrocarbon reactions, in: *Actes 2me Congr. Int. on Catalyse*, Vol. 2 (Editions Technip, Paris) pp. 2055–2073.
- Rabo, J.A., C.A. Angell and V. Schomaker, 1968, Catalytic and structural properties of rare-earth exchanged forms of type Y zeolite, in: *Proc. 4th Int. Congr. on Catalysis*, Moscow (Nauka, Moscow) preprint 54, pp. 96–113.
- Reddy, T.I., and R.S. Varma, 1997a, *Chem. Commun.*, p. 621.
- Reddy, T.I., and R.S. Varma, 1997b, *Tetrahedron Lett.* **38**, 1721.
- Reddy, T.I., B.M. Bhawal and S. Rajappa, 1993, *Tetrahedron* **49**, 2101.

- Rees, L.V.C., and T. Zuyi, 1986, *Zeolites* **6**, 201.
- Rhodes, A.K., 1997, *Oil Gas J.*, October 6, p. 41. OGI Special on Worldwide Catalyst Report.
- Richard, F., J. Drouillard, H. Carreyre, J.L. Lember-ton and G. Perot, 1993, Zeolite catalyzed acylation of heterocyclic aromatic compounds. 1. Acylation of benzofuran, in: *Heterogeneous Catalysis and Fine Chemicals III*, eds M. Guisnet, J. Barbier, J. Barrault, C. Bouchoule, D. Duprez, G. Perot and C. Montassier, Vol. 78 of *Studies in Surface Science and Catalysis* (Elsevier, Amsterdam) pp. 601–606.
- Roelofsen, J.W., H. Mathies, R.L. de Groot, P.C.M. van Woerkom and H.A. Gaur, 1986, Effect of rare earth loading in Y-zeolite on its dealumination during thermal treatment, in: *New Developments in Zeolite Science and Technology*, eds Y. Murakami, A. Iijima and J.W. Ward, Vol. 28 of *Studies in Surface Science and Catalysis* (Elsevier, Amsterdam) pp. 337–344.
- Rokosz, M.J., A.V. Kucherov, H.-W. Jen and M. Shelef, 1997, *Catal. Today* **35**, 65.
- Roland, E., 1989, Industrial zeolite production, in: *Zeolites as Catalysts, Sorbents and Detergent Builders*, eds H.G. Karge and J. Weitkamp, Vol. 46 of *Studies in Surface Science and Catalysis* (Elsevier, Amsterdam) pp. 645–659.
- Rørbik, T., I.M. Dahl, H.B. Mostad and O.H. Ellestad, 1995, *Catal. Lett.* **33**, 127.
- Rørbik, T., H.B. Mostad, O.H. Ellestad and M. Stöcker, 1996, *Appl. Catal. A* **137**, 235.
- Rørbik, T., H.B. Mostad, A. Karlsson and O.H. Ellestad, 1997, *Appl. Catal. A* **156**, 267.
- Rosa, I.L.V., O.A. Serra and E.J. Nassar, 1997, *J. Lumin.* **72**, 532.
- Sakamoto, E., T. Ohnishi and T. Arakawa, 1994, Catalytic reduction of nitric oxide with propane over Ln–Pt ion exchanged zeolites (Ln = rare earth), in: *Zeolites and Related Microporous Materials: State of the Art 1994*, eds J. Weitkamp, H.G. Karge, H. Pfeifer and W. Holderich, Vol. 84 of *Studies in Surface Science and Catalysis* (Elsevier, Amsterdam) pp. 1537–1540.
- Sato, S., Y. Yu-u, H. Yahiro, N. Mizuno and M. Iwamoto, 1991, *Appl. Catal.* **70**, L1.
- Scherzer, J., 1986, *ACS Symposium Series*, Vol. **248**, p. 157.
- Scherzer, J., 1989, *Catal. Rev. Sci. Eng.* **31**, 215.
- Scherzer, J., and J.L. Bass, 1975, *J. Phys. Chem.* **79**, 1200.
- Scherzer, J., G.C. Edwards, R.W. Baker, E.A. Albers and P.K. Maher, 1971, *German Patent* 2,125,980.
- Scherzer, J., J.L. Bass and F.D. Hunter, 1975, *J. Phys. Chem.* **79**, 1194.
- Schulz, H., W. Böhringer, W. Baumgartner and Z. Siwei, 1986, Comparative investigation of time on stream selectivity changes during methanol conversion on different zeolites, in: *New Developments in Zeolite Science and Technology*, eds Y. Murakami, A. Iijima and J.W. Ward, Vol. 28 of *Studies in Surface Science and Catalysis* (Elsevier, Amsterdam) pp. 915–922.
- Serra, O.A., I.L. Rosa and E.F. Sousa-Aguiar, 1993, *J. Braz. Chem. Soc.* **4**, 154.
- Sherry, H.S., 1966, *J. Phys. Chem.* **70**, 1158.
- Sherry, H.S., 1968, *J. Colloid Interface Sci.* **28**, 288.
- Sherry, H.S., 1976, *J. Colloid Interface Sci.* **35**, 321.
- Sherry, H.S., 1997, The contribution of ion exchange to the understanding and modification of the properties of zeolites, in: *Blending Research and Innovative Technology at Las Vegas*, eds M.L. Occelli, V.S. Ozkan and J. Sinfelt, Vol. 42(4) of *Preprints, Division of Petroleum Chemistry* (American Chemical Society, Washington, DC) pp. 870–872.
- Shiralkar, V.P., and S.B. Kulkarni, 1978, *Indian J. Chem.* **16a**, 665.
- Shiralkar, V.P., and S.B. Kulkarni, 1982, *J. Thermal Anal.* **25**, 399.
- Simon, M.W., A.M. Efstathiou, C.O. Bennett and S.L. Suib, 1992, *J. Catal.* **138**, 1.
- Slade, R.C.T., H. Jinku and G.B. Hix, 1992, *Solid State Ionics* **57**, 177.
- Smith, J.V., 1976, Origin and structure of zeolites, in: *Zeolite Chemistry and Catalysis*, ed. J.E. Rabo, ACS Monograph 171 (American Chemical Society, Washington, DC) pp. 1–79.
- Smith, J.V., J.M. Bennett and E.M. Flanigan, 1967, *Nature* **215**, 241.
- Song, Ch., and S. Kirby, 1993, Shape-selective alkylation of naphthalene over molecular sieves, in: *Preprints, Division of Petroleum Chemistry*, Vol. 38 (American Chemical Society, Washington, DC) pp. 784–787.
- Song, Ch., and K. Moffatt, 1993, Zeolite-catalyzed ring shift and conformational isomerization reactions of polycyclic hydrocarbons, in: *Preprints, Division of Petroleum Chemistry*, Vol. 38 (American Chemical Society, Washington, DC) pp. 779–783.
- Sousa-Aguiar, E.F., V.L.D. Camorim, F.M.Z. Zotin and R.L.C. dos Santos, 1998, *Microporous Mater.* **25**, 25.

- Spagnol, M., L. Gilbert and D. Alby, 1996, Friedel–Crafts acylation of aromatics using zeolites, in: *The Roost of Organic Development*, eds J.R. Desmurs and S. Ratton (Elsevier, Amsterdam) pp. 29–38.
- Spiridonov, S.E., Kh.S.-U. Nasukhanov, O.V. Kryukov, E.B. Pod'yacheva and S.N. Khadzhiev, 1992, *Kinet. Catal.* **33**, 317.
- Stiles, A.B., and T.A. Koch, 1995, *Catalyst Manufacture* (Marcel Dekker, New York) pp. 122–135.
- Stonecipher, D.L., 1997, *Advances in FCC Vanadium Tolerance*, NPRA AM 97–29.
- Subba Rao, Y.V., S.J. Kulkarni, M. Subrahmanyam and A.V. Rama Rao, 1995, *Appl. Catal. A* **122**, L1.
- Sugi, Y., J.-H. Kim, T. Matsuzaki, T. Hanaoka, Y. Kubota, X. Tu and M. Matsumoto, 1994a, The isopropylation of naphthalene over cerium modified H-mordenite, in: *Zeolites and Related Microporous Materials: State of the Art 1994*, eds J. Weitkamp, H.G. Karge, H. Pfeifer and W. Hölderich, Vol. 84 of *Studies in Surface Science and Catalysis* (Elsevier, Amsterdam) pp. 1837–1844.
- Sugi, Y., T. Matsuzaki, T. Hanaoka, Y. Kubota, J.-H. Kim, X. Tu and M. Matsumoto, 1994b, *Catal. Lett.* **27**, 315.
- Suib, S.L., R.P. Zerger, G.D. Stucky, T.I. Morrison and G.K. Shenoy, 1984, *J. Chem. Phys.* **80**, 2203.
- Sulikowski, B., J. Find, H.G. Karge and D. Herein, 1997, *Zeolites* **19**, 395.
- Swaroop, S.H., and R.R. Wurisika, 1996, US Patent 5,587,137.
- Tanaka, T., T. Yoshida, S. Yoshida, T. Baba and Y. Ono, 1995, *Physica B* **209**, 687.
- Tian, Y.G., S.L. Qiu, F.Q. Zhou, W.Q. Pang and S.G. Hou, 1992, *J. Alloys & Compounds* **186**, 267.
- Timonen, J.T., and T.T. Pakkanen, 1997, *Microporous Mater.* **8**, 57.
- Townsend, R.P., 1986, Ion exchange in zeolites: Some recent developments in theory and practice, in: *New Developments in Zeolite Science and Technology*, eds A. Iijima and J.W. Ward, Vol. 28 of *Studies in Surface Science and Catalysis* (Elsevier, Amsterdam) pp. 273–282.
- Townsend, R.P., 1991, Ion exchange in zeolites, in: *Introduction to Zeolite Science and Practice*, eds H. van Bekkum, E.M. Flanigen and J.C. Jansen, Vol. 58 of *Studies in Surface Science and Catalysis* (Elsevier, Amsterdam) pp. 359–390.
- Treacy, M.M., J.B. Higgins and R. Von Ballmoos, 1996, *Zeolite* **16**, 327.
- Ulla, M.A., L.A. Aparicio, V.R. Balse, J.A. Dumesic and W.S. Millman, 1990, *J. Catal.* **123**, 195.
- van Bekkum, H., E.M. Flanigen and J.C. Jansen, eds, 1990, *Introduction to Zeolite Science and Practice*, Vol. 58 of *Studies in Surface Science and Catalysis* (Elsevier, Amsterdam) 754 pp.
- Venuto, P.B., 1994, *Microporous Mater.* **2**, 297.
- Venuto, P.B., 1997, Structure–reactivity–selectivity relationships in reaction of organics over zeolite catalysts, in: *Progress in Zeolite and Microporous Materials*, eds H. Chon, S.-K. Ihm and Y.S. Uh, Vol. 105 of *Studies in Surface Science and Catalysis* (Elsevier, Amsterdam) pp. 811–852.
- Venuto, P.B., and P.S. Landis, 1966, *J. Catal.* **6**, 237.
- Venuto, P.B., L.A. Hamilton, P.S. Landis and J.J. Wise, 1966a, *J. Catal.* **4**, 81.
- Venuto, P.B., L.A. Hamilton and P.S. Landis, 1966b, *J. Catal.* **5**, 484.
- Venuto, P.B., E.N. Givens, L.A. Hamilton and P.S. Landis, 1966c, *J. Catal.* **6**, 253.
- von Ballmoos, R.A., 1993, *Advances in FCC Vanadium Tolerance*, NPRA AM 93–30.
- Wang, G., M. Ying, X. Wang and G. Chen, 1996, US Patent 5,573,990.
- Ward, J.W., 1968, *J. Phys. Chem.* **72**, 4211.
- Ward, J.W., 1969, *J. Catal.* **13**, 321.
- Ward, J.W., 1971, *Adv. Chem.* **101**, 380.
- Ward, J.W., 1976, Infrared studies of zeolite surface and surface reactions, in: *Zeolite Chemistry and Catalysis*, ed. J.E. Rabo, ACS Monograph 171 (American Chemical Society, Washington, DC) pp. 118–284.
- Ward, J.W., and R.C. Hansford, 1969, *J. Catal.* **13**, 364.
- Weiß, U., M. Weihe, M. Hunger, H.G. Karge and J. Weitkamp, 1997, The induction period in ethylbenzene disproportionation over large pore zeolites, in: *Progress in Zeolite and Microporous Materials*, eds H. Chon, S.-K. Ihm and Y.S. Uh, Vol. 105 of *Studies in Surface Science and Catalysis* (Elsevier, Amsterdam) pp. 973–980.
- Weitkamp, J., 1980a, Isobutane/butene alkylation on cerium exchanged X and Y Zeolites, in: *Catalysis by Zeolites*, eds B. Imelik, C. Naccache, Y. Ben Taarit, J.C. Vedrine, G. Coudurier and H. Praliaud, Vol. 5 of *Studies in Surface Science and Catalysis* (Elsevier, Amsterdam) pp. 65–75.
- Weitkamp, J., 1980b, Isoalkane/alkene alkylation and alkene oligomerization on zeolites. 1. Time on stream effects with isobutane/cis-2-butene on CeY, in: *Catalysis by Zeolites*, eds B. Imelik, C. Naccache, Y. Ben Taarit, J.C. Vedrine, G. Coudurier and H. Praliaud, Vol. 5 of

- Studies in Surface Science and Catalysis (Elsevier, Amsterdam) pp. 858–865.
- Weitkamp, J., W. Gerhard and P.A. Jacobs, 1985, *Acta Phys. Chem. (Szeged)* **31**, 261.
- Weyrich, P.A., H. Treviño, W.F. Hölderich and W.M.H. Sachtler, 1997, *Appl. Catal. A*, **163**, 31.
- Winkler, H., and K.-H. Steinberg, 1989, *Zeolites* **9**, 445.
- Winkler, H., K.-H. Steinberg and G. Kapphahn, 1984, *J. Colloid Interface Sci.* **98**, 144.
- Wortel, Th.M., W.H. Esser, G. Van Minnen-Pathuis, R. Taal, D.P. Roelofsen and H. van Bekkum, 1977, *J.R. Neth. Chem. Soc.* **96**, 44.
- Xiangsheng, W., W. Guiru and G. Hongchen, 1997, Ethylation of ethylbenzene to produce para-diethylbenzene, in: *Progress in Zeolite and Microporous Materials*, eds H. Chon, S.-K. Ihm and Y.S. Uh, Vol. 105 of *Studies in Surface Science and Catalysis* (Elsevier, Amsterdam) pp. 1357–1364.
- Yan, J.Y., W.M.H. Sachtler and H.H. Kung, 1997, *Catal. Today* **33**, 279.
- Yang, S.-J., Y.-W. Chen and Ch. Li, 1994, *Appl. Catal. A* **117**, 109.
- Yao, C.S., and H.S. Weng, 1992, *Chem. Eng. Sci.* **47**, 2745.
- Yasuda, H., T. Miyamoto and M. Misono, 1995, IR study of catalytic reduction of NO<sub>x</sub> by propene in the presence of O<sub>2</sub> over CeZSM-5, in: *ACS Symposium Series*, Vol. 587, eds U.S. Ozkan, S.K. Agarwal and G. Marcelin (American Chemical Society, Washington, DC) pp. 110–122.
- Yeom, Y.H., Y. Kim, S.H. Song and K. Seff, 1997, *J. Phys. Chem. B* **101**, 2138.
- Yiguang, T., Q. Shilun, Z. Fengqi, P. Wenqin and H. Shangong, 1992, *J. Alloys & Compounds*, **186**, 267.
- Yokoyama, Ch., and M. Misono, 1992, *Chem. Lett.*, 1669.
- Yokoyama, Ch., and M. Misono, 1994a, *J. Catal.* **150**, 9.
- Yokoyama, Ch., and M. Misono, 1994b, *Bull. Chem. Soc. Jpn.* **67**, 557.
- Young, S.W., K.J. Balkus and A.D. Sherry, 1995, US Patent 5,429,814.
- Zhang, Y., and M. Flytzani-Stephanopoulos, 1994, Catalytic decomposition of nitric oxide over promoted copper-ion-exchanged ZSM-5 zeolites, in: *Environmental Catalysis*, ed. J.M. Armor, Vol. 552 of *ACS Symposium Series* (American Chemical Society, Washington, DC) pp. 7–21.
- Zhang, Y., and M. Flytzani-Stephanopoulos, 1996, *J. Catal.* **164**, 131.
- Zinner, L.B., and A.S. Araujo, 1992, *J. Alloys & Compounds* **180**, 289.
- Zinner, L.B., K. Zinner, M. Ishige and A.S. Araujo, 1993, *J. Alloys & Compounds* **193**, 65.

## Chapter 186

### TRIFLATES

Shū KOBAYASHI

*Graduate School of Pharmaceutical Sciences, The University of Tokyo,  
 Hongo, Bunkyo-ku, Tokyo, 113-0033, Japan*

#### Contents

List of symbols, abbreviations, and acronyms	315	4.2. Allylation of imines	340
1. Introduction	316	5. Strecker-type reactions	340
2. Aldol reactions	317	6. Diels–Alder reactions	345
2.1. Aldol reactions in aqueous media	317	7. Aza Diels–Alder reactions	347
2.2. Recovery and reuse of the catalyst	323	7.1. Reactions of imines with dienes or alkenes	347
2.3. Aldol reactions in organic solvents	324	7.2. Three-component coupling reactions of aldehydes, amines, and dienes or alkenes	348
2.4. Aldol reactions in micellar systems	326	7.3. Reaction mechanism	351
3. Mannich-type reactions	327	8. Asymmetric Diels–Alder reactions	354
3.1. Reactions of imines with silyl enolates	327	9. Asymmetric aza Diels–Alder reactions	362
3.2. One-pot synthesis of $\beta$ -amino esters from aldehydes	330	10. Asymmetric 1,3-dipolar cycloadditions	365
3.3. Use of acylhydrazones as electrophiles in Mannich-type reactions	333	11. Conclusions	370
3.4. Aqueous Mannich-type reaction	336	Acknowledgments	370
4. Allylation reactions	337	References and Notes	371
4.1. Allylation of aldehydes and ketones	337		

#### List of symbols, abbreviations, and acronyms

Ac	acetyl	DTMP	2,6-di- <i>t</i> -butyl-4-methylpyridine
<i>p</i> -Ans	<i>p</i> -methoxyphenyl	Et	ethyl
BINOL	1,1'-bi-2-naphthol	hfc	3-(heptafluoropropylhydroxymethylene)-(-)-camphorate
Bn	benzyl	HOMO	highest occupied molecular orbital
Boc	<i>t</i> -butoxycarbonyl	imid.	imidazole
Bu	butyl	LDA	lithium diisopropylamide
CTAB	cetyltrimethylammonium bromide	Ln	lanthanide
DBU	diazabicyclo-[5,4,0]-undec-7-ene	LUMO	lowest unoccupied molecular orbital
DMF	<i>N,N</i> -dimethylformamide	Me	methyl
DPP	2,6-diphenylpyridine	MID	<i>N</i> -methylimidazole
DTBMP	2,6-di- <i>t</i> -butyl-4-methylpyridine	MNEA	<i>N</i> -methyl-bis(1-naphthylethyl)amine
DTBP	2,6-di- <i>t</i> -butylpyridine		

MPEA	<i>N</i> -methyl-bis(1-phenylethyl)amine	TBS	<i>t</i> -butyldimethylsilyl
MS 4A	molecular sieves 4A	Tf	trifluoromethanesulfonyl
$\alpha$ -Nap	1-naphthyl	THF	tetrahydrofuran
PAA	3-phenylacetylacetone	TMP	<i>cis</i> -1,2,6-trimethylpiperidine
Ph	phenyl	TMS	trimethylsilyl
Pr	propyl	Ts	<i>p</i> -toluenesulfonyl
SDS	sodium dodecyl sulfate		

---

## 1. Introduction

Rare-earth triflates mean group-3 metal triflates. While actinides are not commonly used, the term lanthanide triflates ( $\text{Ln}(\text{OTf})_3$ ) has often been used to include Sc, Y, La–Lu triflates.  $\text{Ln}(\text{OTf})_3$  are classified into hard Lewis acids. The trifluoromethanesulfonyl group (OTf) is one of the strongest electron-withdrawing groups and thus, the  $\text{Ln}(\text{OTf})_3$  compounds are expected to be stronger Lewis acids compared to  $\text{LnCl}_3$  or  $\text{LnBr}_3$ . Their preparation method was briefly reported in a US patent in 1973; however, for 15 years after, no reports concerning  $\text{Ln}(\text{OTf})_3$  appeared in the literature. In 1989, the  $\text{Ln}(\text{OTf})_3$  were focused in the field of synthetic organic chemistry, and used as one of the alkylating reagents. In 1991, the  $\text{Ln}(\text{OTf})_3$  were first used as stable Lewis acid catalysts in water. This was remarkable because most Lewis acids were believed to be unstable in the presence of even a small amount of water.

Due to the great interest in Lewis-acid-catalyzed reactions which attain unique reactivities and selectivities under mild conditions (Schinzer 1989), the  $\text{Ln}(\text{OTf})_3$  have been focused as among the most unique Lewis acid catalysts. While various kinds of Lewis-acid-promoted reactions have been developed, and many have been applied in industry, these reactions must be carried out under strict anhydrous conditions. The presence of even a small amount of water stops the reaction, because most Lewis acids immediately react with water rather than with the substrates and decompose or deactivate, and this has restricted the use of Lewis acids in organic synthesis. On the other hand, rare-earth compounds were expected to act as strong Lewis acids because of their hard character and to have strong affinity toward carbonyl oxygens (Molander 1992). Of these,  $\text{Ln}(\text{OTf})_3$  were expected to be among the strongest Lewis acids as mentioned above. Their hydrolysis was postulated to be slow, based on their hydration energies and hydrolysis constants (Baes and Mesmer 1976). In fact, while most metal triflates are prepared under strict anhydrous conditions, the  $\text{Ln}(\text{OTf})_3$  have been reported to be prepared in aqueous solution (Thom 1971, Forsberg et al. 1987, Collins and Hong 1987, Almasio et al. 1983, Harrowfield et al. 1983). The large radius and the specific coordination number of lanthanide(III) are also unique, and many investigations using the  $\text{Ln}(\text{OTf})_3$  as Lewis acids have been performed.

In this chapter, an overview is presented of the use of the  $\text{Ln}(\text{OTf})_3$  as Lewis acid catalysts in carbon–carbon bond-forming reactions in both aqueous and organic solvents.

## 2. Aldol reactions

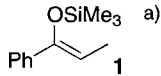
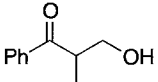
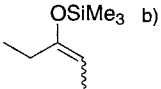
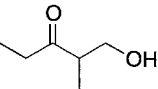
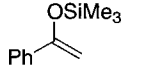
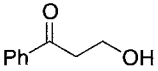
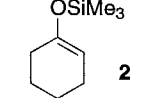
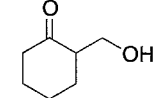
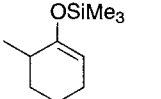
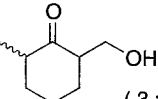
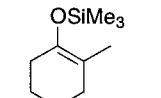
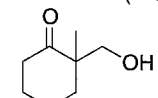
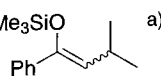
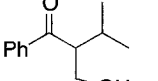
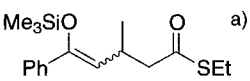
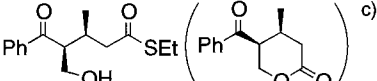
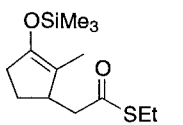
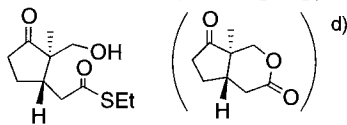
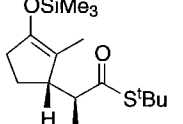
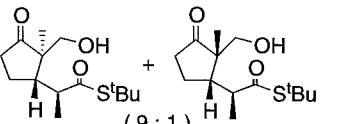
### 2.1. Aldol reactions in aqueous media

The titanium tetrachloride-mediated aldol reaction of silyl enol ethers with aldehydes was first reported in 1973 (Mukaiyama et al. 1973, 1974). The reaction is notably distinguished from the conventional aldol reactions carried out under basic conditions; it proceeds in a highly regioselective manner to afford cross aldols in high yields (Mukaiyama 1982). Since this pioneering effort, several efficient activators such as trityl salts (Kobayashi et al. 1985), Clay montmorillonite (Kawai et al. 1986, 1988), fluoride anions (Noyori et al. 1977, Nakamura et al. 1983), and others (Takai and Heathcock 1985, Vougioukas and Kagan 1987, Gong and Streitwieser 1990, Mikami et al. 1993), have been developed to realize high yields and selectivities, and now the reaction is considered to be one of the most important carbon-carbon bond-forming reactions in organic synthesis. These reactions are usually carried out under strictly anhydrous conditions. The presence of even a small amount of water causes lower yields, probably due to the rapid decomposition or deactivation of the promoters and hydrolysis of the silyl enol ethers. Furthermore, the promoters can not be recovered and reused because they decompose under usual quenching conditions (adding water).

On the other hand, the water-promoted aldol reaction of silyl enol ethers with aldehydes was reported in 1986 (Lubineau 1986, Lubineau and Meyer 1988). While the report that the aldol reactions proceeded without a catalyst in water was unique, the yields and the substrate scope were not satisfactory. In 1991, the first example of Lewis acid catalysis in aqueous media was reported; that is the hydroxymethylation reaction of silyl enol ethers with commercial formaldehyde solution using the  $\text{Ln}(\text{OTf})_3$  as catalysts (Kobayashi 1991). Formaldehyde is a versatile reagent, being one of the most highly reactive C1 electrophiles in organic synthesis (Hajos and Parrish 1973, Stork and Isobe 1975, Lucast and Wemple 1976, Ono et al. 1983, Tsuji et al. 1986, Larsen et al. 1986). Dry gaseous formaldehyde required for many reactions has some disadvantages because it must be generated before use from solid polymer paraformaldehyde by way of thermal depolymerization and it self-polymerizes easily (Snider et al. 1982, Snider 1989, Maruoka et al. 1990, 1993a). On the other hand, the commercial formaldehyde solution, an aqueous solution containing 37% formaldehyde and 8–10% methanol, is cheap, easy to handle, and stable even at room temperature. However, the use of this reagent is strongly restricted due to the existence of a large amount of water. For example, the titanium tetrachloride ( $\text{TiCl}_4$ )-promoted hydroxymethylation reaction of silyl enol ethers was carried out by using trioxane as a  $\text{HCHO}$  source under strict anhydrous conditions (Mukaiyama et al. 1974, Murata et al. 1980). A formaldehyde water solution could not be used because  $\text{TiCl}_4$  and the silyl enol ether reacted with water rather than  $\text{HCHO}$  in that water solution.

The effects of the  $\text{Ln}(\text{OTf})_3$  in the reaction of 1-phenyl-1-trimethylsiloxypropene (**1**) with commercial formaldehyde solution were examined (Kobayashi 1991). In most cases, the reactions proceeded smoothly to give the corresponding adducts in high yields.

Table 1  
Reaction of silyl enol ethers with commercial formaldehyde solution catalyzed by  $\text{Yb}(\text{OTf})_3$

Entry	Silyl enol ether	Product	Yield/%
1	 a)		94
2	 b)		85
3			77
4	 2		82
5		 (3 : 2)	86
6			92
7	 a)		92
8	 a)	 c)	88
9		 d)	83
10		 (9 : 1)	90

<sup>a</sup>  $Z/E \geq 98/2$ .

<sup>b</sup>  $Z/E = 1/4$ .

<sup>c</sup> A mixture of hydroxy thioester and lactone (2:1) was obtained. Other diastereomers were not observed.

<sup>d</sup> A mixture of hydroxy thioester and lactone (3:1) was obtained. Less than 3% yield of other diastereomers was observed.



Table 2  
Effect of lanthanide triflates

$\text{PhCHO} + \text{2} \xrightarrow[\text{rt, 20 h}]{\text{Ln(OTf)}_3 \text{ (10 mol\%)}, \text{H}_2\text{O-THF (1:4)}} \text{Ph-CH(OH)-C(=O)-cyclohexyl}$			
Ln(OTf) <sub>3</sub>	Yield (%)	Ln(OTf) <sub>3</sub>	Yield (%)
La(OTf) <sub>3</sub>	8	Dy(OTf) <sub>3</sub>	73
Pr(OTf) <sub>3</sub>	28	Ho(OTf) <sub>3</sub>	47
Nd(OTf) <sub>3</sub>	83	Er(OTf) <sub>3</sub>	52
Sm(OTf) <sub>3</sub>	46	Tm(OTf) <sub>3</sub>	20
Eu(OTf) <sub>3</sub>	34	Yb(OTf) <sub>3</sub>	91
Gd(OTf) <sub>3</sub>	89	Lu(OTf) <sub>3</sub>	88

The reactions were most effectively carried out in commercial formaldehyde solution–THF media under the influence of a catalytic amount of Yb(OTf)<sub>3</sub>.

Several examples of the hydroxymethylation reaction of silyl enol ethers with commercial formaldehyde solution are summarized in table 1. The following characteristic features of this reaction are noted: (1) In every case, the reactions proceeded smoothly under extremely mild conditions (almost neutral) to give the corresponding hydroxymethylated adducts in high yields. Sterically hindered silyl enol ethers also worked well and the diastereoselectivities were high. (2) Di- and poly-hydroxymethylated products were not observed (Gaut and Skoda 1946). (3) The absence of equilibrium (double-bond migration) in silyl enol ethers allowed for a regiospecific hydroxymethylation reaction. (4) Only a catalytic amount of Yb(OTf)<sub>3</sub> was required to complete the reaction. The amount of catalyst was examined by taking the reaction of **1** with commercial formaldehyde solution as a model, and the reaction was found to be catalyzed by even 1 mol% of Yb(OTf)<sub>3</sub>: 1 mol% (90% yield); 5 mol% (90% yield); 10 mol% (94% yield); 20 mol% (94% yield); 100 mol% (94% yield).

The use of the Ln(OTf)<sub>3</sub> in the activation of aldehydes other than formaldehyde was also investigated (Kobayashi and Hachiya 1992). The model reaction of 1-trimethylsiloxy-cyclohexene (**2**) with benzaldehyde under the influence of a catalytic amount of Yb(OTf)<sub>3</sub> (10 mol%) was examined. The reaction proceeded smoothly in H<sub>2</sub>O–THF (1:4), but the yields were low when water or THF was used alone. Among several Ln(OTf)<sub>3</sub> screened, neodymium triflate (Nd(OTf)<sub>3</sub>), gadolinium triflate (Gd(OTf)<sub>3</sub>), Yb(OTf)<sub>3</sub>, and lutetium triflate (Lu(OTf)<sub>3</sub>) were quite effective, while the yield of the desired aldol adduct was lower in the presence of lanthanum triflate (La(OTf)<sub>3</sub>), praseodymium triflate (Pr(OTf)<sub>3</sub>) or thulium triflate (Tm(OTf)<sub>3</sub>) (table 2).

Table 3  
 Effect of Yb salts

$  \text{PhCHO} + \text{2} \xrightarrow[\text{rt, 19 h}]{\text{Yb salt (10 mol\%)}, \text{H}_2\text{O-THF (1:4)}} \text{Product}  $			
Yb salt	Yield (%)	Yb salt	Yield (%)
Yb(OTf) <sub>3</sub>	91 <sup>a</sup>	Yb(OAc) <sub>3</sub> ·8H <sub>2</sub> O	14
Yb(ClO <sub>4</sub> ) <sub>4</sub>	88 <sup>b</sup>	Yb(NO <sub>3</sub> ) <sub>3</sub> ·5H <sub>2</sub> O	7
YbCl <sub>3</sub>	3	Yb(SO <sub>4</sub> ) <sub>3</sub> ·5H <sub>2</sub> O	trace

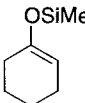
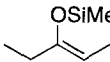
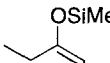
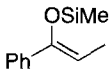
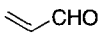
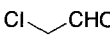
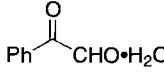
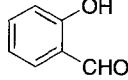
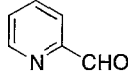
<sup>a</sup> *syn/anti* = 73/27.<sup>b</sup> *syn/anti* = 76/24.

The Ln(OTf)<sub>3</sub> were found to be effective for the activation of formaldehyde water solution. The effect of ytterbium salts was also investigated (table 3) (Kobayashi and Hachiya 1994). While Yb salts with less nucleophilic counter anions such as OTf<sup>-</sup> or ClO<sub>4</sub><sup>-</sup> effectively catalyzed the reaction, only low yields of the product were obtained when Yb salts with more nucleophilic counter anions such as Cl<sup>-</sup>, OAc<sup>-</sup>, NO<sub>3</sub><sup>-</sup>, and SO<sub>4</sub><sup>2-</sup> were employed. The Yb salts with less nucleophilic counter anions are more cationic and the high Lewis acidity promotes the desired reaction.

Several examples of the present aldol reaction of silyl enol ethers with aldehydes are listed in table 4. In every case, the aldol adducts were obtained in high yields in the presence of a catalytic amount of Yb(OTf)<sub>3</sub>, Gd(OTf)<sub>3</sub>, or Lu(OTf)<sub>3</sub> in aqueous media. Diastereoselectivities were generally good to moderate. One feature in the present reaction is that water-soluble aldehydes – for instance acetaldehyde, acrolein, and chloroacetaldehyde – can be reacted with silyl enol ethers to afford the corresponding cross aldol adducts in high yields (entries 5–7 in table 4). Some of these aldehydes are commercially supplied as water solutions and are appropriate for direct use. Phenylglyoxal monohydrate also worked well (entry 8). It is known that water often interferes with the aldol reactions of metal enolates with aldehydes and that in cases where such water soluble aldehydes are employed, some troublesome purifications including dehydration are necessary. Moreover, salicylaldehyde (entry 9) and 2-pyridinecarboxaldehyde (entry 10) could be successfully employed. The former has a free hydroxy group which is incompatible with metal enolates or Lewis acids, and the latter is generally difficult to use under the influence of Lewis acids because the coordination of the nitrogen atom to the Lewis acids results in the deactivation of the acids.

The aldol reactions of silyl enol ethers with aldehydes were also found to proceed smoothly in water-ethanol-toluene (Kobayashi et al. 1994a). Some reactions proceeded much faster in this solvent system than in THF-water. Furthermore, the new solvent system realized continuous use of the catalyst by a very simple procedure.

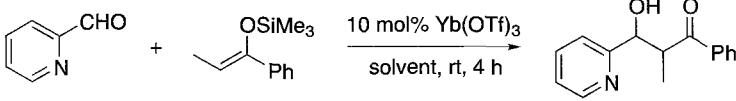
Table 4  
Lanthanide triflate-catalyzed aldol reactions in aqueous media

$\text{R}^1\text{CHO} + \text{R}^2\text{C}(\text{OSiMe}_3)\text{=CH-R}^3 \xrightarrow[\text{H}_2\text{O-THF, rt}]{\text{Yb(OTf)}_3 \text{ (10 mol\%)}} \text{R}^1\text{CH(OH)CH(R}^3\text{)C(=O)R}^2$			
Entry	Aldehyde	Silyl Enol Ether	Yield/%
1	PhCHO	 <b>2</b>	91 <sup>a)</sup>
2	PhCHO		89 <sup>b)</sup>
3	PhCHO		93 <sup>c)</sup>
4	PhCHO	 <b>1</b>	81 <sup>d)</sup>
5	CH <sub>3</sub> CHO	<b>1</b>	93 <sup>e, f)</sup>
6		<b>1</b>	82 <sup>e, g)</sup>
7		<b>1</b>	95 <sup>h)</sup>
8		<b>1</b>	67 <sup>i)</sup>
9		<b>1</b>	81 <sup>j, k)</sup>
10		<b>1</b>	87 <sup>j, l)</sup>

<sup>a</sup> *syn/anti* = 73/27.<sup>b</sup> *syn/anti* = 63/37.<sup>c</sup> *syn/anti* = 71/29.<sup>d</sup> *syn/anti* = 53/47.<sup>e</sup> Gd(OTf)<sub>3</sub> was used instead of Yb(OTf)<sub>3</sub>.<sup>f</sup> *syn/anti* = 46/54.<sup>g</sup> *syn/anti* = 60/40.<sup>h</sup> *syn/anti* = 45/55.<sup>i</sup> *syn/anti* = 27/73.<sup>j</sup> Lu(OTf)<sub>3</sub> was used instead of Yb(OTf)<sub>3</sub>.<sup>k</sup> *syn/anti* = 55/45.<sup>l</sup> *syn/anti* = 42/58.

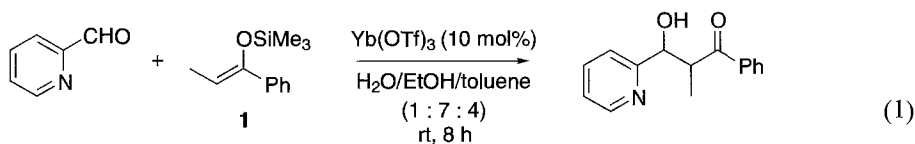
Several water-organic solvent systems were examined in the model reaction of 1-phenyl-1-trimethylsiloxypropene (**1**) with 2-pyridinecarboxaldehyde under the influence of 10 mol% Yb(OTf)<sub>3</sub> (table 5). While the reaction proceeded sluggishly in a water-toluene system, the adduct was obtained in good yield when ethanol was added to this

Table 5  
 Effect of solvents

			
Solvent		Yield (%)	<i>syn/anti</i>
H <sub>2</sub> O/toluene	(1:4)	0	—
H <sub>2</sub> O/EtOH/toluene	(1:3:4)	30	37/63
	(1:5:4)	41	39/61
	(1:7:4)	70	41/59
	(1:10:4)	96	40/60
H <sub>2</sub> O/THF	(1:4)	12	43/57

system. The yield increased with the amount of ethanol, and it was noted that the reaction proceeded much faster in the water–ethanol–toluene system than in the original water–THF system.

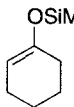
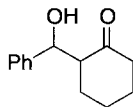
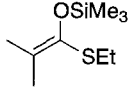
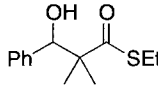
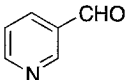
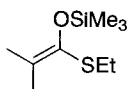
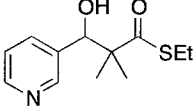
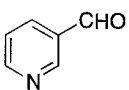
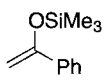
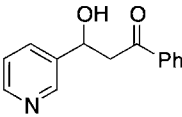
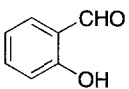
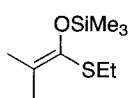
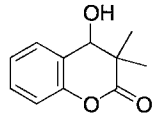
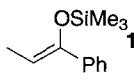
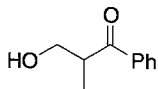
Although the water–ethanol–toluene (1:7:4) system was one phase, it easily became two phases by adding toluene after the reaction was completed. The product was isolated from the organic layer by a usual work-up. On the other hand, the catalyst remained in the aqueous layer, which was used directly in the next reaction without removing water. It is noteworthy that the yields of the 2nd, 3rd and 4th runs were comparable to that of the 1st run:



1st run: 86% (*syn/anti* = 38/62)    3rd run: 90% (*syn/anti* = 38/62)  
 2nd run: 82% (*syn/anti* = 38/62)    4th run: 82% (*syn/anti* = 39/61)

Several examples of the present aldol reactions of silyl enol ethers with aldehydes in water–ethanol–toluene are summarized in table 6. 3-Pyridinecarboxaldehyde as well as 2-pyridinecarboxaldehyde, salicylaldehyde, and formaldehyde–water solution worked well. As for silyl enol ethers, not only ketone enol ethers but also silyl enolates derived from thioesters were used. In every case, the adducts were obtained in high yields in the presence of 10 mol% Yb(OTf)<sub>3</sub>.

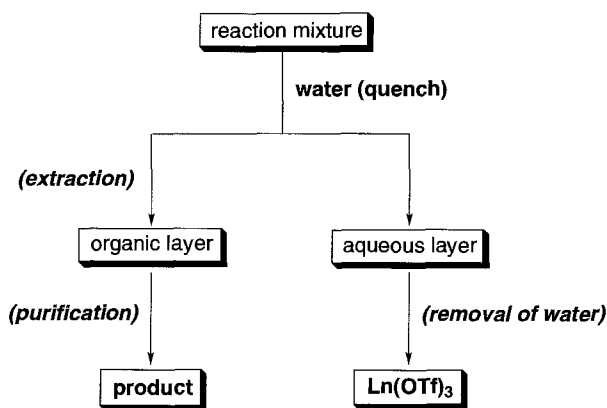
Table 6  
Yb(OTf)<sub>3</sub>-catalyzed aldol reactions of silyl enol ethers with aldehydes in water-ethanol-toluene

$\text{R}^1\text{CHO} + \text{R}^2\text{C}(\text{OSiMe}_3)=\text{R}^3\text{R}^4 \xrightarrow[\text{H}_2\text{O/EtOH/Toluene, rt (1:7:4)}]{\text{Yb(OTf)}_3 (10 \text{ mol}\%)} \text{R}^1\text{CH}(\text{OH})\text{C}(\text{R}^2)(\text{R}^3)\text{C(=O)R}^4$			
Aldehyde	Silyl Enol Ether	Product	Yield / %
PhCHO	 <b>2</b>		89 <sup>a)</sup>
PhCHO			95
			87
			82
			96
HCHO aq.	 <b>1</b>		90

<sup>a</sup> *syn/anti* = 74/26.

## 2.2. Recovery and reuse of the catalyst

While continuous use of Ln(OTf)<sub>3</sub> is possible, it is also easy to recover the Ln(OTf)<sub>3</sub> themselves. The Ln(OTf)<sub>3</sub> are more soluble in water than in organic solvents such as dichloromethane. Almost 100% of the Ln(OTf)<sub>3</sub> was quite easily recovered from the aqueous layer after the reaction was completed, and it could be reused. For example: 1st use (20 mol% Yb(OTf)<sub>3</sub>) in the reaction of **1** with formaldehyde–water solution gave 94% yield; 2nd use, 91% yield; 3rd use, 93% yield. The reactions are usually quenched with water and the products are extracted with an organic solvent (for example, dichloromethane). The Ln(OTf)<sub>3</sub> are in the aqueous layer, and only removal of water gives the catalysts which can be used in the next reaction (scheme 1). It is noteworthy that the



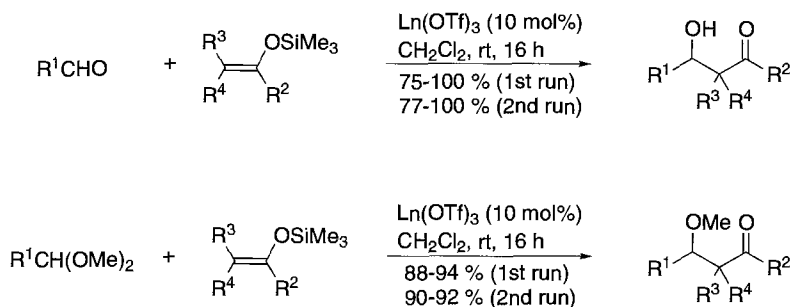
Scheme 1. Recovery of the catalyst.

Ln(OTf)<sub>3</sub> are expected to solve some severe environmental problems induced by Lewis-acid-promoted reactions in industrial chemistry (Haggin 1994).

### 2.3. Aldol reactions in organic solvents

Lanthanide triflates were found to be excellent Lewis acid catalysts not only in aqueous media but also in organic solvents. The reaction of ketene silyl acetal **3** with benzaldehyde proceeded smoothly in the presence of 10 mol% Yb(OTf)<sub>3</sub> in dichloromethane at  $-78^{\circ}\text{C}$ , to afford the corresponding aldol-type adduct in 94% yield. The same reaction at room temperature also went quite cleanly without side reactions and the desired adduct was obtained in 95% yield. No adduct was obtained in THF–water or toluene–ethanol–water, because hydrolysis of the ketene silyl acetal preceded the desired aldol reaction in such solvents. In other organic solvents such as toluene, THF, acetonitrile, and DMF, Yb(OTf)<sub>3</sub> worked well, and it was found that other Ln(OTf)<sub>3</sub> also catalyzed the above aldol reaction effectively (85–95% yields).

Silyl enolates derived from not only esters but also thioesters and ketones reacted with aldehydes to give the corresponding adducts in high yields (scheme 2) (Kobayashi et al. 1993a). Furthermore, acetals reacted smoothly with silyl enolates to afford the



Scheme 2. Aldol reactions in organic solvent.

Table 7  
Effect of catalysts

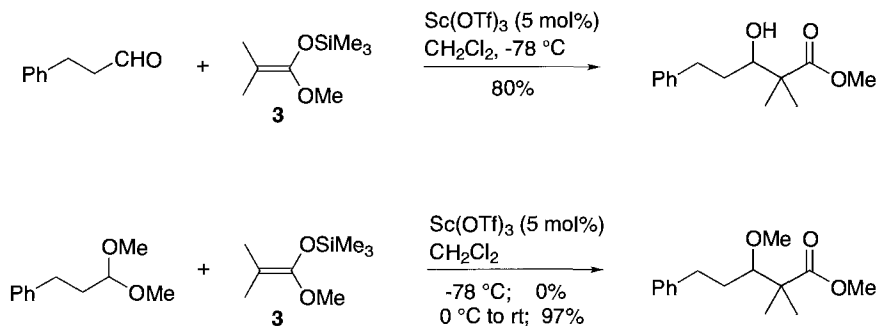
$\text{PhCHO} + \text{2} \xrightarrow[\text{CH}_2\text{Cl}_2, -78^\circ\text{C}, 15\text{ h}]{\text{Catalyst (5 mol\%)}} \text{Product}$		
Entry	Catalyst	Yield/%
1	Sc(OTf) <sub>3</sub>	81
2	Y(OTf) <sub>3</sub>	trace
3	Yb(OTf) <sub>3</sub>	trace

corresponding aldol-type adducts in high yields. It should be noted that the catalysts could be easily recovered from the aqueous layer after the reactions were quenched with water and could be reused, and that the yields of the 2nd run were almost comparable to those of the 1st run in every case.

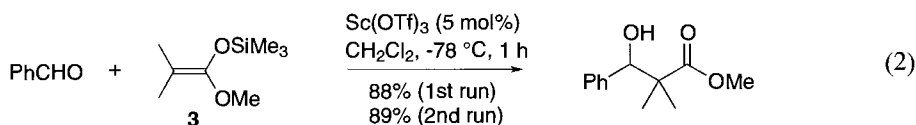
Scandium triflate (Sc(OTf)<sub>3</sub>) was found to be an effective catalyst in the aldol reactions (Kobayashi et al. 1993b). The activities of various triflate catalysts were evaluated in the aldol reaction of 1-trimethylsilyloxycyclohexene (**2**) with benzaldehyde in dichloromethane (table 7). While the reaction scarcely proceeded at  $-78^\circ\text{C}$  in the presence of Yb(OTf)<sub>3</sub> or Y(OTf)<sub>3</sub>, the aldol adduct was obtained in an 81% yield in the presence of Sc(OTf)<sub>3</sub>. Obviously, Sc(OTf)<sub>3</sub> is more active than Y(OTf)<sub>3</sub> or Yb(OTf)<sub>3</sub> in this case.

Several examples of the Sc(OTf)<sub>3</sub>-catalyzed aldol reactions of silyl enolates with aldehydes were examined, and it was found that silyl enolates derived from ketones, thioesters, and esters reacted smoothly with aldehydes in the presence of 5 mol% Sc(OTf)<sub>3</sub> to afford the aldol adducts in high yields. Sc(OTf)<sub>3</sub> was also found to be an effective catalyst in the aldol-type reaction of silyl enolates with acetals. The reactions proceeded smoothly at  $-78^\circ\text{C}$  or room temperature to give the corresponding aldol-type adducts in high yields without side reaction products. It should be noted that aldehydes were more reactive than acetals (Noyori et al. 1981, Mukai et al. 1990, Mukaiyama et al. 1991). For example, while 3-phenylpropionaldehyde reacted with the ketene silyl acetal of methyl 2-methylpropionate (**3**) at  $-78^\circ\text{C}$  to give the aldol adduct in 80% yield, no reaction occurred at  $-78^\circ\text{C}$  in the reaction of the same ketene silyl acetal with 3-phenylpropionaldehyde dimethylacetal. The acetal reacted with the ketene silyl acetal at  $0^\circ\text{C}$  to room temperature to give the aldol-type adduct in 97% yield (scheme 3).

Sc(OTf)<sub>3</sub> can behave as a Lewis acid catalyst even in aqueous media. Sc(OTf)<sub>3</sub> was stable in water and was effective in the aldol reactions of silyl enolates with aldehydes in aqueous media. The reactions of usual aromatic and aliphatic aldehydes such as benzaldehyde and 3-phenylpropionaldehyde with silyl enolates were carried out in both aqueous and organic solvents, and water-soluble formaldehyde and chloroacetaldehyde were directly treated as water solutions with silyl enolates to afford the aldol adducts

Scheme 3.  $\text{Sc}(\text{OTf})_3$ -catalyzed aldol reactions.

in good yields. Moreover, the catalyst could be recovered almost quantitatively from the aqueous layer after the reaction was completed. The recovered catalyst was also effective in the 2nd reaction, and the yield of the 2nd run was comparable to that of the 1st run:



#### 2.4. Aldol reactions in micellar systems

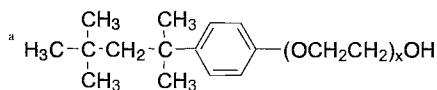
$\text{Sc}(\text{OTf})_3$ -catalyzed aldol reactions of silyl enol ethers with aldehydes were successfully carried out in micellar systems. While the reactions proceeded sluggishly in pure water, a remarkable enhancement of the reactivity was observed in the presence of a small amount of a surfactant. In these systems, versatile carbon–carbon bond-forming reactions proceeded in water without using any organic solvents.

Lewis acid catalysis in micellar systems was first found in the model reaction of **1** with benzaldehyde (table 8) (Kobayashi et al. 1997a). While the reaction proceeded sluggishly in the presence of 0.2 eq.  $\text{Yb}(\text{OTf})_3$  in water, remarkable enhancement of the reactivity was observed when the reaction was carried out in the presence of 0.2 eq.  $\text{Yb}(\text{OTf})_3$  in an aqueous solution of sodium dodecyl sulfate (SDS, 0.2 eq., 35 mM), and the corresponding aldol adduct was obtained in 50% yield. In the absence of the Lewis acid and the surfactant (water-promoted conditions), only 20% yield of the aldol adduct was isolated after 48 h, while 33% yield of the aldol adduct was obtained after 48 h in the absence of the Lewis acid in an aqueous solution of SDS. The amounts of surfactant also influenced the reactivity, and the yield was improved when  $\text{Sc}(\text{OTf})_3$  was used as a Lewis acid catalyst. Judging from the critical micelle concentration, micelles would be formed in these reactions, and it is noteworthy that the Lewis-acid-catalyzed reactions proceeded smoothly in micellar systems (Fendler and Fendler 1975, Holland and Rubingh 1992, Cramer and Truhlar 1994, Sabatini et al. 1995). It was also found that the surfactants



Table 8  
Effect of  $\text{Ln}(\text{OTf})_3$  and surfactants

$\text{PhCHO} + \text{Ph}-\text{CH}=\text{CH}-\text{OSiMe}_3 \xrightarrow[\text{H}_2\text{O}]{\text{cat. Ln(OTf)}_3, \text{surfactant}} \text{Ph}-\text{CH}(\text{OH})-\text{CH}(\text{Ph})-\text{C}(=\text{O})\text{Ph}$			
$\text{Ln}(\text{OTf})_3/\text{eq.}$	Surfactant/eq.	Time (h)	Yield (%)
$\text{Yb}(\text{OTf})_3/0.2$	—	48	17
$\text{Yb}(\text{OTf})_3/0.2$	SDS/0.04	48	12
$\text{Yb}(\text{OTf})_3/0.2$	SDS/0.1	48	19
$\text{Yb}(\text{OTf})_3/0.2$	SDS/0.2	48	50
$\text{Yb}(\text{OTf})_3/0.2$	SDS/1.0	48	22
$\text{Sc}(\text{OTf})_3/0.2$	SDS/0.2	17	73
$\text{Sc}(\text{OTf})_3/0.1$	SDS/0.2	4	88
$\text{Sc}(\text{OTf})_3/0.1$	TritonX-100 <sup>a</sup> /0.2	60	89
$\text{Sc}(\text{OTf})_3/0.1$	CTAB/0.2	4	trace



influenced the yield, and that TritonX-100 was effective in the aldol reaction (but required long reaction time), while only a trace amount of the adduct was detected when using cetyltrimethylammonium bromide (CTAB) as a surfactant.

Several examples of  $\text{Sc}(\text{OTf})_3$ -catalyzed aldol reactions in micellar systems are shown in table 9 (overleaf). Not only aromatic, but also aliphatic and  $\alpha,\beta$ -unsaturated aldehydes reacted with silyl enol ethers to afford the corresponding aldol adducts in high yields. Formaldehyde–water solution also worked well. Ketene silyl acetal **3**, which is known to hydrolyze very easily even in the presence of a small amount of water, reacted with an aldehyde in the present micellar system to afford the corresponding aldol adduct in high yield.

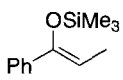
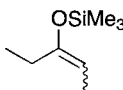
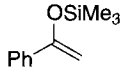
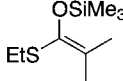
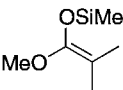
It should be noted that the reactions were successfully carried out in water without using any organic solvents. Use of the reusable scandium catalyst and water as a solvent would result in clean and environmentally friendly systems.

### 3. Mannich-type reactions

#### 3.1. Reactions of imines with silyl enolates

The Mannich and related reactions provide one of the most fundamental and useful methods for the synthesis of  $\beta$ -amino ketones or esters. Although the classical protocols

Table 9  
Sc(OTf)<sub>3</sub>-catalyzed aldol reactions in micellar systems

$\text{R}^1\text{CHO} + \text{R}^2\text{C}(\text{OSiMe}_3)=\text{CH}\text{R}^3 \xrightarrow[\text{H}_2\text{O, rt}]{\text{Sc(OTf)}_3 (0.1 \text{ eq.}), \text{SDS} (0.2 \text{ eq.})} \text{R}^2\text{C}(\text{O})\text{CH}(\text{OH})\text{R}^1$		
Aldehyde	Silyl Enol Ether	Yield/%
PhCHO	 <b>1</b>	88 <sup>a)</sup>
PhCH <sub>2</sub> CH <sub>2</sub> CHO	<b>1</b>	86 <sup>b)</sup>
PhCH=CHCHO	<b>1</b>	88 <sup>c)</sup>
HCHO	<b>1</b>	82 <sup>d)</sup>
PhCHO		88 <sup>e)</sup>
PhCHO		75 <sup>f,g)</sup>
PhCHO		94
PhCHO	 <b>3</b>	84 <sup>g)</sup>

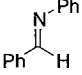
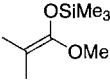
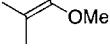
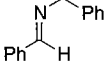
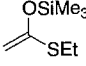
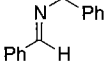
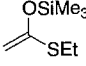
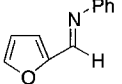
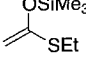
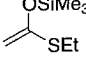
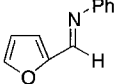
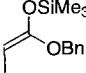
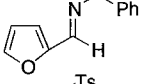
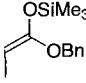
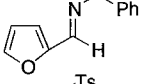
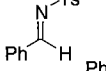
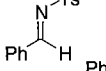
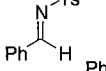
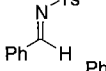
<sup>a</sup> *syn/anti* = 50/50.<sup>b</sup> *syn/anti* = 45/55.<sup>c</sup> *syn/anti* = 41/59.<sup>d</sup> Commercially available HCHO aq. (3 ml), **1** (0.5 mmol), Sc(OTf)<sub>3</sub> (0.1 mmol), and SDS (0.1 mmol) were combined.<sup>e</sup> *syn/anti* = 57/43.<sup>f</sup> Sc(OTf)<sub>3</sub> (0.2 eq.) was used.<sup>g</sup> Additional silyl enolate (1.5 eq.) was charged after 6 h.

include some severe side reactions, new modifications using preformed iminium salts and imines have been developed (Kleinman 1991). Among them, reactions of imines with enolate components, especially silyl enolates, provide useful and promising methods leading to β-amino ketones or esters. The first report using a stoichiometric amount of TiCl<sub>4</sub> as a promoter appeared in 1977 (Ojima et al. 1977), and since then, some efficient catalysts have been developed (Ikeda et al. 1983, Mukaiyama et al. 1989, 1990, Onaka et al. 1993, Dubois and Axiotis 1984, Colvin and McGarry 1985, Shimada et al. 1992, Hattori and Yamamoto 1994).

In aqueous media, water coordinates the  $\text{Ln}(\text{OTf})_3$  under equilibrium conditions, and thus activation of carbonyl compounds using a catalytic amount of the Lewis acid has been performed. Based on the same consideration, it was expected that the catalytic activation of imines would be possible by using the  $\text{Ln}(\text{OTf})_3$ .

The reactions of imines with silyl enolates were tested in the presence of 5 mol%  $\text{Ln}(\text{OTf})_3$ , and selected examples are shown in table 10 (Kobayashi et al. 1995a). In

Table 10  
Reactions of imines with silyl enolates

$\text{R}^1\text{C}(\text{H})=\text{N}-\text{R}^2 + \text{R}^3\text{C}(\text{OSiMe}_3)=\text{CH}-\text{R}^5 \xrightarrow[\text{CH}_2\text{Cl}_2, 0^\circ\text{C}]{\text{Ln}(\text{OTf})_3 (5 \text{ mol}\%)} \text{R}^1\text{CH}(\text{NHR}^2)\text{C}(\text{R}^3)(\text{R}^4)\text{C}(=\text{O})\text{R}^5$			
Imine	Silyl enolate	Ln	Yield/%
	 <b>3</b>	Yb	97 <sup>a</sup> )
		Y	81
		Yb	95
	<b>3</b>	Y	86
		Yb	86
	<b>3</b>	Y	78
		Yb	65
		Sc	80
		Yb	80 <sup>b</sup> )
	<b>3</b>	Yb	95
		Yb	67 <sup>c</sup> )
	<b>3</b>	Yb	88
	<b>3</b>	Yb	88
	<b>3</b>	Yb	88
	<b>3</b>	Yb	88
	<b>3</b>	Yb	60
	<b>3</b>	Yb	47

<sup>a</sup> 2nd use = 96% yield; 3rd use = 98% yield.

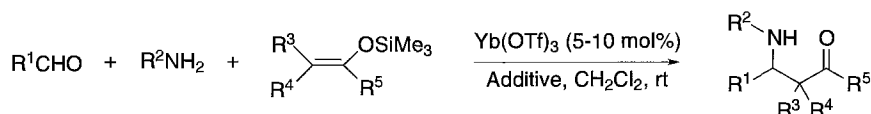
<sup>b</sup> *syn/anti* = 18/82.

<sup>c</sup> *syn/anti* = 21/79.

most cases, the reactions proceeded smoothly in the presence of 5 mol%  $\text{Yb}(\text{OTf})_3$  (a representative  $\text{Ln}(\text{OTf})_3$ ) to afford the corresponding  $\beta$ -amino ester derivatives in good to high yields. Yttrium triflate ( $\text{Y}(\text{OTf})_3$ ) was also effective, and the yield was improved when  $\text{Sc}(\text{OTf})_3$  was used instead of  $\text{Yb}(\text{OTf})_3$  as the catalyst. Not only silyl enolates derived from esters, but also that derived from a thioester worked well to give the desired  $\beta$ -amino esters and thioester in high yields. In the reactions of the silyl enolate derived from benzyl propionate, *anti* adducts were obtained in good selectivities. In addition, the catalyst could be recovered after the reaction was completed and could be reused.

### 3.2. One-pot synthesis of $\beta$ -amino esters from aldehydes

While the Lewis-acid-catalyzed reactions of imines with silyl enolates constitute one of the most efficient methods for the preparation of  $\beta$ -amino esters, many imines are hygroscopic, unstable at high temperatures, and difficult to purify by distillation or column chromatography. It is desirable from a synthetic point of view that imines, generated *in situ* from aldehydes and amines, immediately react with silyl enolates and provide  $\beta$ -amino esters in a one-pot reaction. However, most Lewis acids can not be used in this reaction because they decompose or deactivate in the presence of the amines and water that exist during imine formation. Judging from the unique properties of the  $\text{Ln}(\text{OTf})_3$ , their efficient use as catalysts for the above one-pot preparation of  $\beta$ -amino esters from aldehydes was expected.

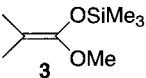
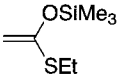
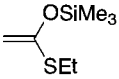
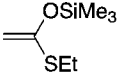
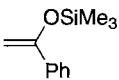


Scheme 4. One-pot synthesis of  $\beta$ -amino esters.

A general scheme for one-pot synthesis of  $\beta$ -amino esters from aldehydes is shown in scheme 4 (Kobayashi et al. 1995b). In the presence of a catalytic amount of  $\text{Yb}(\text{OTf})_3$  and an additive (a dehydrating reagent such as MS 4A or  $\text{MgSO}_4$ ), an aldehyde was treated with an amine and then with a silyl enolate in the same vessel. Several examples are shown in tables 11 and 12, and the following characteristic features of this reaction are noted:

- (1) In every case,  $\beta$ -amino esters were obtained in high yields. Silyl enolates derived from esters as well as thioesters reacted smoothly to give the adducts. No adducts between aldehydes and the silyl enolates were observed in any reactions.
- (2) A silyl enol ether derived from a ketone also worked well to afford the  $\beta$ -amino ketone in high yield (table 11, entry 10).
- (3) Aliphatic aldehydes reacted with amines and silyl enolates to give the corresponding  $\beta$ -amino esters in high yields. In some reactions of imines, it is known that aliphatic enolizable imines prepared from aliphatic aldehydes gave poor results.

Table 11  
One-pot synthesis of  $\beta$ -amino esters from aldehydes

Entry	R <sup>1</sup>	R <sup>2</sup>	Silyl enolate	Additive <sup>a)</sup>	Yield/%
1	Ph	Ph		MS4A MgSO <sub>4</sub>	90 89
2	Ph	Bn	<b>3</b>	MS4A	85
3	Ph	p-MeOPh	<b>3</b>	MgSO <sub>4</sub>	91 <sup>b)</sup>
4	Ph	o-MeOPh	<b>3</b>	MS4A	96
5	Ph	Ph		MS4A	90
6	Ph	Bn		MS4A	62 <sup>b)</sup>
7	Ph	p-MeOPh		MS4A	79 84, <sup>b)</sup> 87 <sup>b,c)</sup>
8	Ph	C <sub>4</sub> H <sub>9</sub>	<b>3</b>	MS4A	89
9	PhCO <sup>d)</sup>	Ph	<b>3</b>	MgSO <sub>4</sub>	82
10	PhCO <sup>d)</sup>	Ph		MgSO <sub>4</sub>	87
11	PhCH=CH	p-MeOPh	<b>3</b>	MgSO <sub>4</sub>	92 <sup>e)</sup>
12	Ph(CH <sub>2</sub> ) <sub>2</sub>	Bn	<b>3</b>	MgSO <sub>4</sub>	83 <sup>f)</sup>
13	C <sub>4</sub> H <sub>9</sub>	Bn	<b>3</b>	MgSO <sub>4</sub>	77 <sup>f)</sup>
14	C <sub>8</sub> H <sub>17</sub>	Bn	<b>3</b>	MgSO <sub>4</sub>	81 <sup>f)</sup>
15	C <sub>8</sub> H <sub>17</sub>	Ph <sub>2</sub> CH	<b>3</b>	MgSO <sub>4</sub>	89 <sup>g)</sup>

<sup>a</sup> MS4A or MgSO<sub>4</sub> was used. Almost comparable yields were obtained in each case.

<sup>b</sup> CH<sub>3</sub>CN was used as a solvent.

<sup>c</sup> Sc(OTf)<sub>3</sub> was used instead of Yb(OTf)<sub>3</sub>.

<sup>d</sup> Monohydrate.

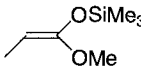
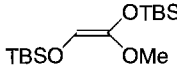
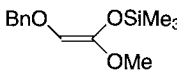
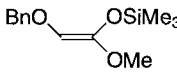
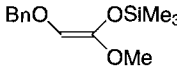
<sup>e</sup> C<sub>2</sub>H<sub>5</sub>CN, -78°C.

<sup>f</sup> -78°C to 0°C.

<sup>g</sup> 0°C.

(4) Phenylglyoxal monohydrate also worked well in this reaction. The imine derived from phenylglyoxal is unstable, and a troublesome treatment is known to be required for its use (Lucchini et al. 1988).

Table 12  
Diastereoselective one-pot synthesis of  $\beta$ -amino esters from aldehydes

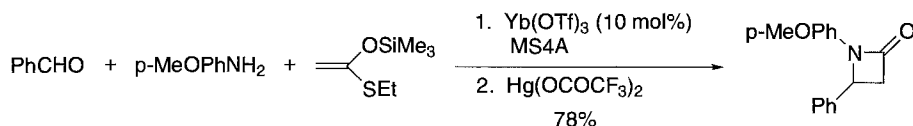
$\text{R}^1\text{CHO} + \text{R}^2\text{NH}_2 + \begin{array}{c} \text{R}^3 \\ \diagup \\ \text{C}=\text{C} \\ \diagdown \\ \text{R}^4 \end{array} \begin{array}{c} \text{OSiMe}_3 \\ \\ \text{OMe} \end{array} \xrightarrow[\text{MS4A, C}_2\text{H}_5\text{CN, -78 }^\circ\text{C}]{\text{Yb(OTf)}_3 \text{ (5-10 mol\%)}} \begin{array}{c} \text{R}^2 \\   \\ \text{NH} \\   \\ \text{R}^1-\text{CH}-\text{CH}-\text{C}(=\text{O})-\text{R}^4 \\   \\ \text{R}^3 \end{array}$					
Entry	R <sup>1</sup>	R <sup>2</sup>	Silyl enolate	Yield/%	<i>syn</i> / <i>anti</i> <sup>a)</sup>
1	Ph	Bn		90	1 / 13.3
2	Ph	Bn		78	1 / 9.0
3	Ph(CH <sub>2</sub> ) <sub>2</sub>	Ph <sub>2</sub> CH		88	8.1 / 1
4	C <sub>4</sub> H <sub>9</sub>	Ph <sub>2</sub> CH		90	8.1 / 1
5	(CH <sub>3</sub> ) <sub>2</sub> CHCH <sub>2</sub>	Ph <sub>2</sub> CH		86	7.3 / 1

<sup>a)</sup> Determined by <sup>1</sup>H NMR analysis.

- (5) The catalyst could be recovered after the reaction was completed and could be reused [1st run, 91%; 2nd run, 92%, in the reaction of benzaldehyde, *p*-anisidine, and silyl enolate 3 (table 12, entry 3)].
- (6) As for the diastereoselectivity of this reaction, good results were obtained after examination of the reaction conditions. While *anti* adducts were produced preferentially in the reactions of benzaldehyde, *syn* adducts were obtained with high selectivities in the reactions of aliphatic aldehydes (table 12).
- (7) The high yields of the present one-pot reactions depend on the unique properties of the Ln(OTf)<sub>3</sub> as the Lewis acid catalysts. Although TiCl<sub>4</sub> and TMSOTf are known to be effective for the activation of imines (Ojima et al. 1977, Guanti et al. 1987), the use of even stoichiometric amounts of TiCl<sub>4</sub> and TMSOTf instead of the Ln(OTf)<sub>3</sub> in the present one-pot reactions gave only trace amounts of the product in both cases (table 13).
- (8) One-pot preparation of a  $\beta$ -lactam from an aldehyde, an amine, and a silyl enolate has been achieved based on the present reaction (scheme 5). The reaction of the aldehyde, the amine, and 2 was carried out under the standard conditions, and Hg(OCOCF<sub>3</sub>)<sub>2</sub> was then added to the same pot. The desired  $\beta$ -lactam was isolated in 78% yield.

Table 13  
Effect of catalysts

$\text{C}_8\text{H}_{17}\text{CHO} + \text{Ph}_2\text{CHNH}_2 + \text{3} \xrightarrow[\text{MgSO}_4, \text{CH}_2\text{Cl}_2, 0^\circ\text{C}]{\text{Activator}} \text{Product}$			
Entry	Activator		Yield (%)
1	Yb(OTf) <sub>3</sub>	10 mol%	89
2	TiCl <sub>4</sub>	100 mol%	trace
3	TMSOTf	100 mol%	trace



Scheme 5. One-pot synthesis of a  $\beta$ -lactam from an aldehyde.

### 3.3. Use of acylhydrazones as electrophiles in Mannich-type reactions

Hydrazones are aldehyde and ketone equivalents as well as imines. Their stability is much higher than imines, and actually hydrazones derived from aliphatic aldehydes are often crystalline and can be isolated and stored at room temperature. However, their reactivity as electrophiles is known to be low, and there have been many fewer reports on the reactions of hydrazones with nucleophiles than on those of imines (Kodata et al. 1996, Enders et al. 1986, 1996, Denmark et al. 1987, Claremon et al. 1986, Takahashi et al. 1979, Burk and Feaster 1992).

While 3-phenylpropionaldehyde phenylhydrazone did not react with ketene silyl acetal (**3b**) ( $\text{R}^2 = \text{'Bu}$ ) derived from methyl isobutyrate at all, 3-phenylpropionaldehyde acylhydrazones reacted with **3b** in the presence of a catalytic amount of  $\text{Sc(OTf)}_3$ . Among the acylhydrazones tested, 4-trifluoromethylbenzoylhydrazone (**4a**,  $\text{R}^1 = \text{CF}_3$ ) gave the best yield (table 14). It is noteworthy that the electronic effect of the benzoyl moieties influenced the yields dramatically. While hydrazones with electron-donating groups gave lower yields, higher yields were obtained using hydrazones with electron-withdrawing groups. As for Lewis acids,  $\text{Sc(OTf)}_3$  gave an excellent yield (Oyamada and Kobayashi 1998, Kobayashi and Nagayama 1997a, Kobayashi et al. 1997b,c, 1998a,b), and much lower yields were obtained by using typical Lewis acids such as  $\text{TiCl}_4$ ,  $\text{SnCl}_4$ , and  $\text{BF}_3 \cdot \text{OEt}_2$  [ $\text{Yb(OTf)}_3$  was effective for the activation of the acylhydrazone, although the yield was ca. 10% lower than that using  $\text{Sc(OTf)}_3$  in a preliminary experiment].

Several examples of the reactions of 4-trifluoromethylbenzoylhydrazones with silyl enolates are shown in table 15. Hydrazones derived from aromatic, aliphatic, and

Table 14  
Effect of R<sup>1</sup> and Lewis acids

Entry	Lewis acid	R <sup>1</sup>	R <sup>2</sup>	Temperature (°C)	Yield (%)
1	Sc(OTf) <sub>3</sub>	H	<sup>t</sup> Bu	-20	37
2	Sc(OTf) <sub>3</sub>	MeO	<sup>t</sup> Bu	-20	7
3	Sc(OTf) <sub>3</sub>	NO <sub>2</sub>	<sup>t</sup> Bu	-20	77
4	Sc(OTf) <sub>3</sub>	CF <sub>3</sub>	<sup>t</sup> Bu	-20	88
5	Sc(OTf) <sub>3</sub>	CF <sub>3</sub>	Me	-20	97
					75 <sup>a,b</sup>
6	BF <sub>3</sub> ·OEt <sub>2</sub>	CF <sub>3</sub>	Me	0	4 <sup>a</sup>
7	TiCl <sub>4</sub>	CF <sub>3</sub>	Me	0	13 <sup>a</sup>
8	SnCl <sub>4</sub>	CF <sub>3</sub>	Me	0	46 <sup>a</sup>

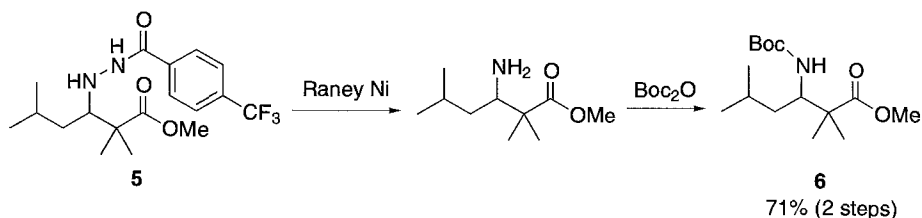
<sup>a</sup> Dichloromethane was used as a solvent.<sup>b</sup> 0°C.

Table 15  
Reactions of acylhydrazones with silyl enolates

Entry	R <sup>1</sup>	R <sup>2</sup>	R <sup>3</sup>	R <sup>4</sup>	Temperature (°C)	Yield (%)
1	Ph(CH <sub>2</sub> ) <sub>2</sub>	Me	Me	OMe	-20	97
2	(CH <sub>3</sub> ) <sub>2</sub> CHCH <sub>2</sub>	Me	Me	OMe	rt	88
3	CH <sub>3</sub> (CH <sub>2</sub> ) <sub>5</sub>	Me	Me	OMe	0	95
4	Ph	Me	Me	OMe	rt	73
5	CH <sub>2</sub> CH=CH	Me	Me	OMe	0-rt	80
6	PhCH=CH	Me	Me	OMe	rt	75
7	Ph(CH <sub>2</sub> ) <sub>2</sub>	H	H	SEt	0	79
8	CH <sub>3</sub> (CH <sub>2</sub> ) <sub>5</sub>	H	H	SEt	0	80
9	(CH <sub>3</sub> ) <sub>2</sub> CHCH <sub>2</sub>	H	H	SEt	0-rt	68
10	<i>c</i> -C <sub>6</sub> H <sub>11</sub>	H	H	SEt	0	68
11	(CH <sub>3</sub> ) <sub>2</sub> CHCH <sub>2</sub>	Me	Me	SEt	0-rt	83
12	Ph(CH <sub>2</sub> ) <sub>2</sub>	OBn	H	O <sup>i</sup> Pr	-78	90 <sup>a,b</sup>
13	Ph(CH <sub>2</sub> ) <sub>2</sub>	H	Me	OPh	-45-0	95 <sup>a,c</sup>
14	Ph(CH <sub>2</sub> ) <sub>2</sub>	H	H	Ph	rt	66

<sup>a</sup> Propionitrile was used as a solvent.<sup>b</sup> *syn/anti* = 75/25.<sup>c</sup> *syn/anti* = 64/36.



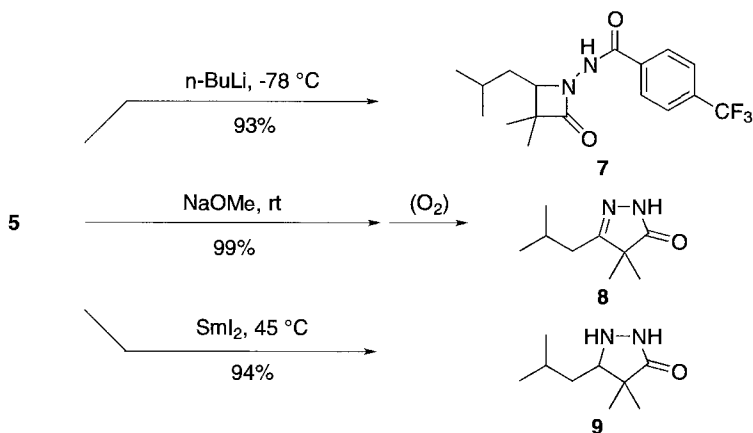


Scheme 6. Conversion to aminoester derivative.

$\alpha,\beta$ -unsaturated aldehydes reacted with silyl enolates smoothly to afford the corresponding  $\beta$ - $N'$ -acylhydrazinocarbonyl compounds in high yields. It is noted that several aliphatic hydrazones, readily prepared from aliphatic aldehydes, reacted with silyl enolates smoothly to afford the corresponding adducts in high yields. All aliphatic acylhydrazones tested were crystalline and could be stored at room temperature. As for silyl enolates, the enolates derived from both esters and thioesters worked well. 1-Phenyl-1-trimethylsiloxyethene (a ketone-derived silyl enolate) also reacted with an aliphatic acylhydrazone to afford the corresponding adduct in a good yield.

Quite recently, benzoylhydrazones derived from  $\alpha$ -functionalized aldehydes and formaldehyde have been prepared as stable equivalent of unstable imines, and successfully used in Mannich-type reactions (Manabe et al. 2000).

Reductive cleavage of the nitrogen–nitrogen bond of the hydrazino compound (**6a**) was successfully carried out using Raney Ni under  $\text{H}_2$  atmosphere (scheme 6) (Alexakis et al. 1991, Seebach and Wykypiel 1979, Kodata et al. 1996, Enders et al. 1986, 1996, Denmark et al. 1987, Claremon et al. 1986, Takahashi et al. 1979). Thus, adduct **5** was treated with a catalytic amount of Raney Ni (W-3) under  $\text{H}_2$  (1 atm) at ambient temperature. After cleavage of the nitrogen–nitrogen bond, the resulting amine was protected as its *t*-butoxycarbonyl (Boc) group (**6**). It was found (scheme 7) that  $\beta$ -lactam (**7**) was obtained

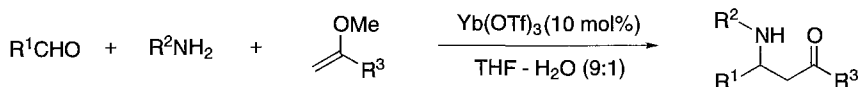
Scheme 7. Conversion to  $\beta$ -lactam, pyrazolone, and pyrazolidinone.

by treatment of **5** with *n*-BuLi at  $-78^{\circ}\text{C}$ , while pyrazolone **8** was produced in the presence of NaOMe at room temperature. Since isomerization from **7** to **8** was observed under these conditions (NaOMe), **7** and **8** were expected to be kinetic and thermodynamic products, respectively. Moreover, pyrazolidinone (**9**) was obtained in the presence of samarium diiodide ( $\text{SmI}_2$ ) (Burk and Feaster 1992, Overman et al. 1997) in THF-MeOH at room temperature.

### 3.4. Aqueous Mannich-type reaction

As mentioned in the previous sections, silyl enolates are excellent enolate components in the Mannich-type reactions with imines. Alternatively, it was found that vinyl ethers also reacted with imines smoothly in the presence of a catalytic amount of  $\text{Ln}(\text{OTf})_3$ , to afford the corresponding  $\beta$ -amino ketones. In addition, the reactions proceeded smoothly by the combination of aldehydes, amines, and vinyl ethers in aqueous media (Kobayashi and Ishitani 1995).

A general scheme for the new Mannich-type reaction is shown in scheme 8. In the presence of 10 mol%  $\text{Yb}(\text{OTf})_3$ , an aldehyde, an amine, and a vinyl ether are combined in a solution of THF–water (9:1) at room temperature to afford a  $\beta$ -amino ketone.



Scheme 8. Novel Mannich-type reaction.

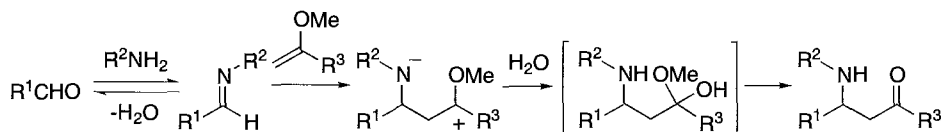
Selected examples of the reaction are shown in table 16. In all cases,  $\beta$ -amino ketones were obtained in good yields. Several characteristic features are noteworthy in this reaction. The procedure is very simple, consisting of simply mixing an aldehyde, an amine, a vinyl ether, and a small amount of  $\text{Ln}(\text{OTf})_3$  in aqueous solution. The catalyst could be recovered after the reaction was completed and could be reused (1st run, 93%; 2nd run, 83%; 3rd run, 87%, in the reaction of phenylglyoxal-monohydrate, *p*-chloroaniline, and 2-methoxypropene). Commercially available formaldehyde and chloroacetaldehyde water solutions were used directly and the corresponding  $\beta$ -amino ketones were obtained in good yields. Phenylglyoxal monohydrate, methyl glyoxylate, an aliphatic aldehyde, and an  $\alpha,\beta$ -unsaturated ketone also worked well to give the corresponding  $\beta$ -amino esters in high yields. In some Mannich reactions with preformed iminium salts and imines, it is known that yields are often low because of the instability of the imines derived from these aldehydes, or troublesome treatments are known to be required for their use (Lucchini et al. 1988).

A possible mechanism for the present reaction is shown in scheme 9. It should be noted that dehydration accompanied by imine formation and successive addition of a vinyl ether proceed smoothly in aqueous solution and that the first aqueous Mannich-type reaction catalyzed by  $\text{Ln}(\text{OTf})_3$  has been developed. Use of the  $\text{Ln}(\text{OTf})_3$ , a water-tolerant Lewis acid, is key and essential in this reaction.

Table 16  
Synthesis of  $\beta$ -amino ketones in aqueous media

R <sup>1</sup>	R <sup>2</sup>	R <sup>3</sup>	Yield (%)
H	<i>p</i> -ClPh	Me	92
H	<i>p</i> -Ans <sup>a</sup>	Me	76
H	<i>p</i> -Ans	Ph	quant.
Ph	<i>p</i> -ClPh	Me	90
Ph	<i>p</i> -Ans	Me	74
Ph(CH <sub>2</sub> ) <sub>2</sub>	<i>p</i> -ClPh	Me	55
ClCH <sub>2</sub>	<i>p</i> -ClPh	Me	59
PhCH=CH	<i>p</i> -ClPh	Me	73
PhCO	<i>p</i> -ClPh	Me	93
PhCO	Ph	Me	90
PhCO	<i>p</i> -Ans	Me	75
PhCO	<i>p</i> -Ans	Ph	85
MeO <sub>2</sub> C	<i>p</i> -Ans	Me	67
MeO <sub>2</sub> C	<i>p</i> -Ans	Ph	58

<sup>a</sup> *p*-Ans = *p*-Anisidine.



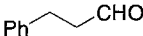
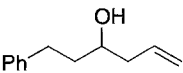
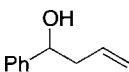
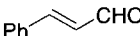
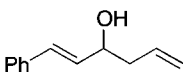
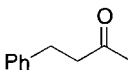
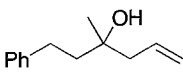
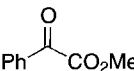
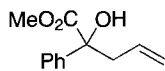
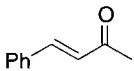
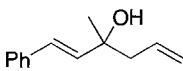
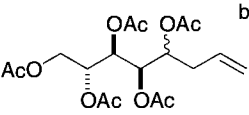
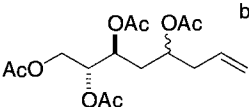
Scheme 9. Possible reaction mechanism.

## 4. Allylation reactions

### 4.1. Allylation of aldehydes and ketones

Synthesis of homoallylic alcohols by the reaction of allyl organometallics with carbonyl compounds is one of the most important processes in organic synthesis (Yamamoto and Asao 1993). The allylation reactions of carbonyl compounds were found to proceed smoothly under the influence of 5 mol% Sc(OTf)<sub>3</sub> (Hachiya and Kobayashi 1993) by using tetraallyltin as an allylating reagent (Peet and Tam 1983, Daude and Pereyre 1980, Harpp and Gingras 1988, Fukuzawa et al. 1983, Yamamoto et al. 1980, Pereyre et al. 1987, Yanagisawa et al. 1993). Several examples of the allylation reactions are shown in table 17. The reactions proceeded smoothly in the presence of only a catalytic amount of Sc(OTf)<sub>3</sub> under extremely mild conditions (Kobayashi et al. 1985), and the adducts, homoallylic alcohols, were obtained in high yields. Ketones could also be used in the reaction (entries 4 and 5). In most cases, the reactions were successfully carried out in aqueous media. It is noteworthy that unprotected sugars reacted directly to give the adducts in high yields (entries 7–9). The allylated adducts are intermediates for the

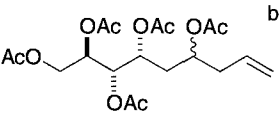
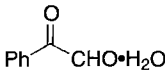
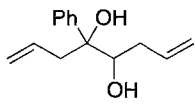
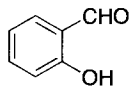
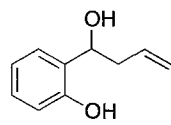
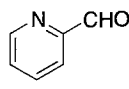
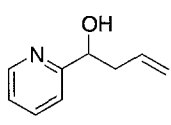
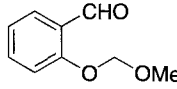
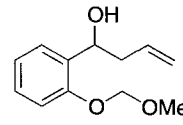
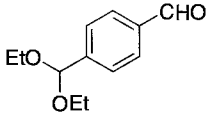
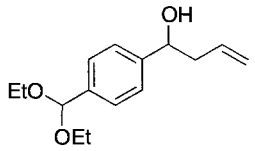
Table 17  
 $\text{Sc}(\text{OTf})_3$ -catalyzed allylation reactions of carbonyl compounds with tetraallyltin

Entry	Carbonyl compound	Product	Solvent	Yield (%)
1			$\text{H}_2\text{O} : \text{THF}$ (1 : 9)	92
			$\text{H}_2\text{O} : \text{EtOH}$ (1 : 9)	96
			$\text{H}_2\text{O} : \text{CH}_3\text{CN}$ (1 : 9)	96
			$\text{EtOH}$	86
			$\text{CH}_3\text{CN}$	94
2	$\text{PhCHO}$		$\text{H}_2\text{O} : \text{THF}$ (1 : 9)	94
			$\text{CH}_3\text{CN}$	82
3			$\text{H}_2\text{O} : \text{THF}$ (1 : 9)	98
			$\text{CH}_3\text{CN}$	94
4			$\text{CH}_2\text{Cl}_2$	78
5			$\text{H}_2\text{O} : \text{THF}$ (1 : 9)	87
6			$\text{CH}_2\text{Cl}_2$	82
7	D-arabinose		$\text{H}_2\text{O} : \text{THF}$ (1 : 4)	81 <sup>c)</sup>
			$\text{H}_2\text{O} : \text{EtOH}$ (1 : 4)	89 <sup>d)</sup>
			$\text{H}_2\text{O} : \text{CH}_3\text{CN}$ (1 : 9)	93 <sup>e)</sup>
8	2-deoxy-D-ribose		$\text{H}_2\text{O} : \text{THF}$ (1 : 9)	89 <sup>f)</sup>

continued on next page

synthesis of higher sugars (Schmid and Whitesides 1991, Kim et al. 1993). Moreover, an aldehyde containing water of crystallization such as phenylglyoxal monohydrate reacted with tetraallyltin to give the di-allylated adduct in high yield (entry 10). Under the present reaction conditions, salicylaldehyde and 2-pyridinecarboxaldehyde reacted with

Table 17, *continued*

Entry	Carbonyl compound	Product	Solvent	Yield (%)
9	2-deoxy-D-glucose		H <sub>2</sub> O : THF (1 : 9)	88 <sup>f)</sup>
10			CH <sub>3</sub> CN	78 <sup>g)</sup>
11			H <sub>2</sub> O : THF (1 : 9) CH <sub>3</sub> CN	quant. 90
12			H <sub>2</sub> O : THF (1 : 9) CH <sub>3</sub> CN	quant. 84
13			CH <sub>3</sub> CN	87
14			CH <sub>3</sub> CN	90

<sup>a</sup> Carried out at 25°C except for entries 8 and 9 (60°C).

<sup>b</sup> The products were isolated after acetylation.

<sup>c</sup> *syn/anti* = 28/72.

<sup>d</sup> *syn/anti* = 27/73.

<sup>e</sup> *syn/anti* = 26/74.

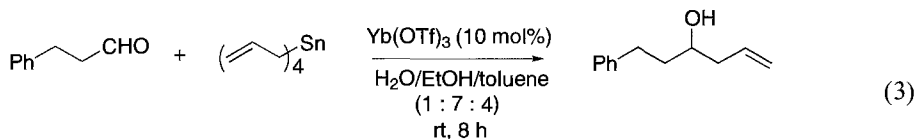
<sup>f</sup> *syn/anti* = 50/50.

<sup>g</sup> Diastereomer ratio = 88/12. Relative configuration assignment was not made.

tetraallyltin to afford the homoallylic alcohols in good yields (entries 11 and 12). Under general Lewis-acidic conditions, these compounds react with the Lewis acids rather than the nucleophile. Furthermore, several kinds of solvents could be used. The reactions also proceeded under non-aqueous conditions. Water-sensitive substrates under Lewis-acidic conditions could be reacted in an appropriate organic solvent (entries 13 and 14).

Not only Sc(OTf)<sub>3</sub> but also Yb(OTf)<sub>3</sub> is effective in the present allylation reactions. For example, 3-phenylpropionaldehyde reacted with tetraallyltin in the presence of 5 mol% Yb(OTf)<sub>3</sub> to afford the adduct in 90% yield.

The water–ethanol–toluene system could be successfully applied to the present allylation reactions. An example of the allylation reaction of tetraallyltin with aldehyde is shown in eq. (3), and in this case also continuous use of the catalyst was realized:



1st run: 90%;      2nd run: 95%;      3rd run: 96%;      4th run: 89%

Furthermore, the  $\text{Sc(OTf)}_3$ -catalyzed allylation reactions of aldehydes with tetraallyltin proceeded smoothly in micellar systems to afford the corresponding homoallylic alcohols in high yields. The reactions were successfully carried out in the presence of a small amount of surfactant in water without using any organic solvents.

#### 4.2. Allylation of imines

Three-component reactions of aldehydes, amines, and allyltributylstannane proceeded smoothly in water without using any organic solvents, in the presence of a small amount of scandium triflate ( $\text{Sc(OTf)}_3$ ) and sodium dodecyl sulfate (SDS), to afford the corresponding homoallylic amines in high yields (Kobayashi et al. 1998b). Several examples of the three-component reactions of aldehydes, amines, and allyltributylstannane are shown in table 18. Not only aromatic aldehydes but also aliphatic, unsaturated, and heterocyclic aldehydes worked well. It is known that severe side reactions occur to decrease yields in the reactions of imines having  $\alpha$ -protons with allyltributylstannane (Yamamoto and Asao 1993). It should be noted that aliphatic aldehydes, especially non-branched aliphatic aldehydes, reacted smoothly under these conditions to afford the homoallylic amines in high yields. In all cases, no aldehyde adducts (homoallylic alcohols) were obtained. It was suggested that the imine formation from aldehydes and amines was very fast in the coexistence of  $\text{Sc(OTf)}_3$  and SDS (Kobayashi and Ishitani 1995), and that the selective activation of imines rather than aldehydes was achieved using  $\text{Sc(OTf)}_3$  as a catalyst (Kobayashi and Nagayama 1997b). It is also noteworthy that using a small amount of surfactant created efficient hydrophobic reaction fields and achieved the dehydration and addition reactions in water.

### 5. Strecker-type reactions

$\alpha$ -Amino nitriles are useful intermediates for the synthesis of amino acids (Shafran et al. 1989) and nitrogen-containing heterocycles such as thiadiazoles, imidazole derivatives, etc. (Weinstock et al. 1967, Matier et al. 1973). Use of cyanotrimethylsilane (TMSCN) instead of HCN as a cyano anion source provides promising and safer routes to these compounds. The synthetic routes to  $\alpha$ -amino nitriles using TMSCN are divided into

Table 18  
Three-component reactions of aldehydes, amines, and allyltributylstannane

$\text{R}^1\text{CHO} + \text{R}^2\text{NH}_2 + \text{CH}_2=\text{CH}-\text{CH}_2\text{SnBu}_3 \xrightarrow[\text{H}_2\text{O, rt., 20 h}]{\text{Sc(OTf)}_3 (0.2 \text{ eq.)}, \text{SDS} (0.2 \text{ eq.)}}$ $\text{R}^1-\text{CH}(\text{NHR}^2)-\text{CH}_2-\text{CH}=\text{CH}_2$		
R <sup>1</sup>	R <sup>2</sup>	Yield (%)
Ph	Ph	83
Ph	<i>p</i> -ClPh	90
Ph	<i>p</i> -MeOPh	81
<i>p</i> -ClPh	<i>p</i> -ClPh	70
2-furyl	<i>p</i> -ClPh	67
		71 <sup>a</sup>
		82 <sup>c</sup>
2-thiophene	<i>p</i> -ClPh	67 <sup>a</sup>
		78 <sup>c</sup>
Ph(CH <sub>2</sub> ) <sub>2</sub>	<i>p</i> -ClPh	78
CH <sub>3</sub> (CH <sub>2</sub> ) <sub>8</sub>	<i>p</i> -ClPh	66
<i>c</i> -C <sub>6</sub> H <sub>11</sub>	Ph	80
		83 <sup>b</sup>
<i>c</i> -C <sub>6</sub> H <sub>11</sub>	<i>p</i> -MeOPh	74
PhCO	<i>p</i> -ClPh	71
		83 <sup>c</sup>
( <i>E</i> )-PhCH=CH	<i>p</i> -ClPh	80
		82 <sup>a</sup>

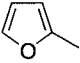
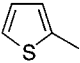
<sup>a</sup> SDS, 0.4 eq.<sup>b</sup> 0.6 eq.<sup>c</sup> 1.0 eq.

two categories: the reactions of O-silylated cyanohydrins (prepared from aldehydes and TMSCN) with amines (Mai and Patil 1984), and the reactions of imines with TMSCN (Ojima et al. 1975). While these methods have both merits and demerits, use of a Lewis acid is one of the keys to performing the reactions efficiently in both cases.

It was reported that imines reacted with TMSCN in the presence of 10 mol% Yb(OTf)<sub>3</sub> in dichloromethane at 0°C, to afford the corresponding α-amino nitriles in high yields (Kobayashi et al. 1997c) (table 19).

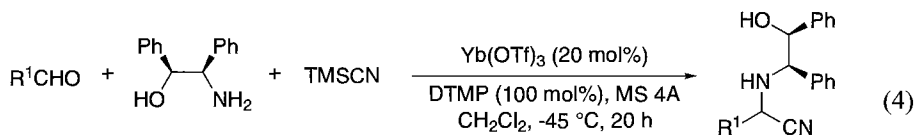
In the reactions of imines, one drawback is their instability. It is desirable from a synthetic point of view that imines, generated *in situ* from aldehydes and amines, immediately react with TMSCN and provide α-amino nitriles in a one-pot reaction. However, most Lewis acids cannot be used in this reaction because they decompose or deactivate in the presence of the amines and water that exist during imine formation. On the other hand, it was reported that α-amino nitriles were prepared by simply mixing aldehydes, amines, and TMSCN without any catalysts (Leblanc and Gibson 1992, Chakraborty et al. 1991). The reports insisted that water which was produced in the imine formation catalyzed the reactions. It was assumed that water would react with TMSCN

Table 19  
Yb(OTf)<sub>3</sub>-catalyzed reactions of imines with TMSCN

$\text{R}^1\text{-CH=N-R}^2 + \text{TMSCN} \xrightarrow[\text{CH}_2\text{Cl}_2, 0^\circ\text{C}]{\text{Yb(OTf)}_3 (10 \text{ mol}\%)} \text{R}^1\text{-CH(NH-R}^2\text{)-CN}$			
Entry	R <sup>1</sup>	R <sup>2</sup>	Yield/%
1	Ph	Ph <sub>2</sub> CH	99
2	Ph	<i>p</i> -ClPh	quant.
3		Ph	94
4		Ph	97
5	<i>o</i> -C <sub>6</sub> H <sub>11</sub>	Ph <sub>2</sub> CH	quant.

immediately to form HCN and that HCN would react with the imines to give  $\alpha$ -amino nitriles in these reactions. Because the existence of water during the reactions caused the HCN problem, it is desirable to perform the reactions in the presence of a dehydration reagent such as MS 4A. It was found that the reaction of an aldehyde, an amine, and TMSCN proceeded sluggishly in the presence of MS 4A without any catalysts. On the other hand, the reaction proceeded smoothly in the presence of 10 mol% Yb(OTf)<sub>3</sub> under the same reaction conditions. The reactions of several aldehydes, amines, and TMSCN were carried out in the presence of Yb(OTf)<sub>3</sub> and MS 4A, and the results are summarized in table 20. In all cases, the three-component reactions proceeded smoothly to afford the corresponding  $\alpha$ -amino nitriles in high yields. In these reactions, other Ln(OTf)<sub>3</sub> such as Sc(OTf)<sub>3</sub>, Y(OTf)<sub>3</sub>, Er(OTf)<sub>3</sub>, Tm(OTf)<sub>3</sub>, etc., were also effective.

The present Strecker-type reactions were successfully applied to asymmetric reactions. In the presence of 10 mol% Yb(OTf)<sub>3</sub> and 100 mol% 2,6-di-*t*-butyl-4-methylpyridine (DTMP), the three-component reaction of benzaldehyde, (1*S*,2*R*)-(+)-2-amino-1,2-diphenylethanol, and TMSCN proceeded smoothly at  $-45^\circ\text{C}$ , to afford the corresponding  $\alpha$ -amino nitrile in an excellent diastereoselectivity. In the reaction using cyclohexanecarboxaldehyde, the selectivity decreased slightly:



R<sup>1</sup> = Ph, 78% yield, ds = 16:1

R<sup>1</sup> = *o*-C<sub>6</sub>H<sub>11</sub>, 87% yield, ds = 7.5:1



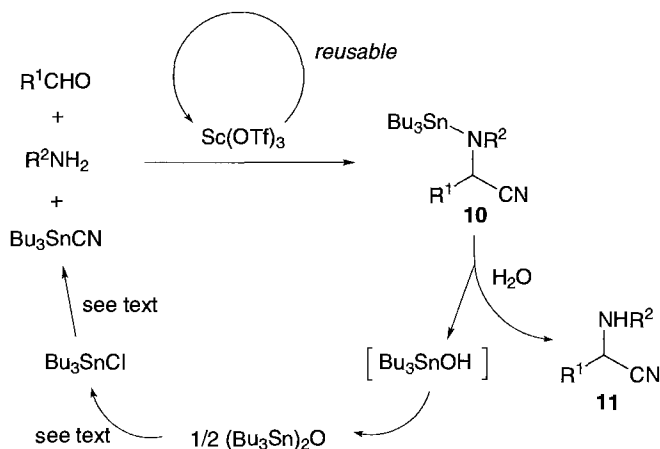
Table 20  
Yb(OTf)<sub>3</sub>-catalyzed three-component reactions of aldehydes, amines, and TMSCN

$\text{R}^1\text{CHO} + \text{R}^2\text{NH}_2 + \text{TMSCN} \xrightarrow[\text{MS 4A}]{\text{Yb(OTf)}_3 \text{ (5-10 mol\%)}} \text{R}^1\text{CH}(\text{CN})\text{NHR}^2$				
Entry	R <sup>1</sup>	R <sup>2</sup>	Conditions <sup>a</sup>	Yield (%)
1	Ph	MeOPh	A	92
2	Ph	Ph <sub>2</sub> CH	A	88
3	α-Nap	MeOPh	A	91
4	α-Nap	Ph <sub>2</sub> CH	A	85
5	<i>c</i> -C <sub>6</sub> H <sub>11</sub>	MeOPh	A	86
6	<i>c</i> -C <sub>6</sub> H <sub>11</sub>	Ph <sub>2</sub> CH	A	85
7	C <sub>3</sub> H <sub>7</sub>	Ph <sub>2</sub> CH	B	91
8	(CH <sub>3</sub> ) <sub>2</sub> CHCH <sub>2</sub>	Ph <sub>2</sub> CH	B	84
9	(CH <sub>3</sub> ) <sub>2</sub> CH	Ph <sub>2</sub> CH	B	91

<sup>a</sup> Conditions A: Yb(OTf)<sub>3</sub> 5 mol%, CH<sub>3</sub>CN, rt; B: Yb(OTf)<sub>3</sub> 10 mol%, C<sub>2</sub>H<sub>5</sub>CN, -78°C to 0°C.

While use of trimethylsilyl cyanide (TMSCN) as a cyano anion source provides promising and safer routes to these compounds, TMSCN is easily hydrolyzed in the presence of water, and it is necessary to perform the reactions under strict anhydrous conditions. On the other hand, tributyltin cyanide (Bu<sub>3</sub>SnCN) (Luijten and van der Kerk 1955, Tanaka 1980, Harusawa et al. 1987) is stable in water and is a potential cyano anion source, although there have been no reports of Strecker-type reactions using Bu<sub>3</sub>SnCN. In this section, we report scandium triflate-catalyzed Strecker-type reactions of aldehydes, amines, and Bu<sub>3</sub>SnCN in both organic and aqueous solutions. Complete recovery of the toxic tin compounds is also described.

The Strecker-type reaction of valeraldehyde, diphenylmethylamine, and Bu<sub>3</sub>SnCN was first performed in the presence of 10 mol% Sc(OTf)<sub>3</sub> in organic solvents. The reactions proceeded smoothly at room temperature in acetonitrile, benzene, dichloromethane, and toluene to afford the corresponding α-amino nitrile in high yields. Among these solvents tested, acetonitrile–toluene (1:1) gave the best yield (84%). It was interesting to find that no dehydration reagents such as molecular sieves, MgSO<sub>4</sub>, drierite, etc. were needed in these reactions. In addition, the reaction was also carried out successfully in water. It was found that the above Strecker-type reaction proceeded smoothly in the presence of a catalytic amount of Sc(OTf)<sub>3</sub> in water to give the corresponding α-amino nitrile in 94% yield (Kobayashi et al. 1998c). No surfactant was needed in this reaction. The reaction is assumed to proceed via imine formation and successive cyanation; it was confirmed that imine formation was much faster than cyanohydrin ether formation under these reaction conditions, and it is noted that the dehydration process (imine formation) proceeded smoothly in water. Moreover, it was found that the reaction rate in water was almost the same as those in organic solvents.



Scheme 10. Recycling system of novel Strecker-type reactions.

While the desired reaction proceeded smoothly, it was thought that use of the toxic tin reagent might restrict the application of the reaction (Davies 1997). An attempt was made to recover the tin materials after the reaction (scheme 10). A Strecker-type reaction was performed using an equimolar amount of an aldehyde and an amine, and a slight excess of  $\text{Bu}_3\text{SnCN}$ . After the reaction was completed, excess  $\text{Bu}_3\text{SnCN}$  was treated with a weak acid to form bis(tributyltin) oxide (Brown et al. 1972). On the other hand, the adduct,  $\alpha$ -(*N*-tributyltin)amino nitrile (**10**), was hydrolyzed by adding water to produce  $\alpha$ -amino nitrile (**11**) and tributyltin hydroxide, that was readily converted to bis(tributyltin) oxide (Brown et al. 1972). Thus, all tin sources were converted to bis(tributyltin) oxide, which could be recovered quantitatively. It has already been reported that bis(tributyltin) oxide can be converted to tributyltin chloride (Davies et al. 1971) and then to  $\text{Bu}_3\text{SnCN}$  (Luijten and van der Kerk 1955, Tanaka 1980, Harusawa et al. 1987). Since the catalyst,  $\text{Sc(OTf)}_3$ , is also recoverable and reusable (Kobayashi 1994, Kobayashi et al. 1993c), the present Strecker-type reactions have achieved a completely recyclable system.

Several examples of the Strecker-type reaction are shown in table 21. In all cases, including aromatic, aliphatic, heterocyclic, as well as  $\alpha,\beta$ -unsaturated aldehydes, the reactions proceeded smoothly to afford the corresponding  $\alpha$ -amino nitriles in high yields. While the adducts,  $\alpha$ -(*N*-benzhydryl)amino nitriles, were readily converted to  $\alpha$ -amino acids (Iyer et al. 1996), the present Strecker-type reactions using other amines such as aniline and benzylamine also proceeded smoothly to afford the corresponding adducts in high yields.

Thus, Strecker-type reactions of aldehydes, amines, and  $\text{Bu}_3\text{SnCN}$  were successfully performed using  $\text{Sc(OTf)}_3$  as a catalyst. The reactions proceeded smoothly in both organic and aqueous solutions to afford  $\alpha$ -amino nitriles in high yields. It is noted that the experimental procedure is very simple; just mixing the three components and  $\text{Sc(OTf)}_3$  in an appropriate solvent at room temperature. Moreover, complete recovery of the tin materials in these reactions has been achieved. While many useful tin reagents have been

Table 21  
Sc(OTf)<sub>3</sub>-catalyzed Strecker-type reactions

$\text{RCHO} + \text{Ph}_2\text{CHNH}_2 + \text{Bu}_3\text{SnCN} \xrightarrow[\text{solvent, rt}]{\text{Sc(OTf)}_3 \text{ (10 mol\%)}} \text{R}-\text{CH}(\text{CN})-\text{NH}-\text{CHPh}_2$		
R	Yield (%)	
	In CH <sub>3</sub> CN–toluene (1 : 1)	In H <sub>2</sub> O
Ph	88	88
PhCH=CH	83	84
2-furyl	88	89
Ph(CH <sub>2</sub> ) <sub>2</sub>	94	79
C <sub>4</sub> H <sub>9</sub>	84	94
<i>n</i> -C <sub>6</sub> H <sub>11</sub>	86	94

developed, their toxicity has sometimes limited their use in organic synthesis. The present method provides a solution to this problem toward environmentally-friendly chemical processes.

## 6. Diels–Alder reactions

Although many Diels–Alder reactions have been carried out at higher reaction temperatures without catalysts, such reactions can not be applied to heat-sensitive compounds in complex and multistep syntheses. While Lewis acid catalysts allow the reactions to proceed at room temperature with satisfactory yields, they are often accompanied by diene polymerization, and excess amounts of the catalyst are often needed to catalyze carbonyl-containing dienophiles (Yates and Eaton 1960, Hollis et al. 1992, Carruthers 1990).

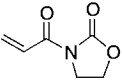

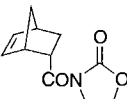
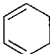
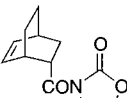
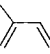
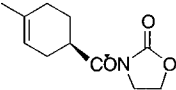
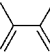
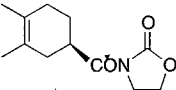
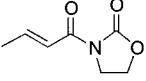

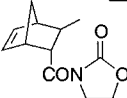
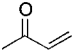

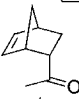
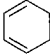
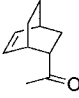
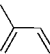
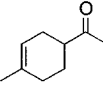
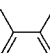
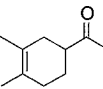
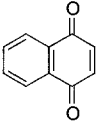

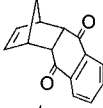
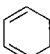
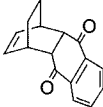
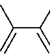
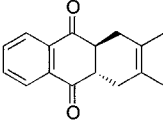
The Ln(OTf)<sub>3</sub> were also found to be efficient catalysts in Diels–Alder reactions of carbonyl-containing dienophiles with cyclopentadiene (Kobayashi et al. 1992). A catalytic amount of Yb(OTf)<sub>3</sub> was enough to promote the reactions to give the corresponding adducts in high yields, and the catalyst could be easily recovered and reused.

In the Diels–Alder reactions, Sc(OTf)<sub>3</sub> was clearly the most effective of the Ln(OTf)<sub>3</sub> as a catalyst (Kobayashi et al. 1992). While in the presence of 10 mol% Y(OTf)<sub>3</sub> or Yb(OTf)<sub>3</sub>, only a trace amount of the adduct was obtained in the Diels–Alder reaction of methyl vinyl ketone with isoprene, the reaction proceeded quite smoothly to give the adduct in 91% yield in the presence of 10 mol% Sc(OTf)<sub>3</sub>.

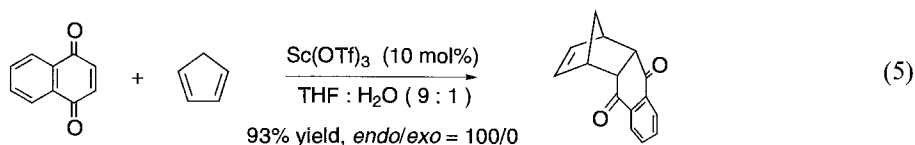
Several examples of Sc(OTf)<sub>3</sub>-catalyzed Diels–Alder reactions are shown in table 22. In all cases, the Diels–Alder adducts were obtained in high yields with *endo* selectivities.

The present Diels–Alder reactions proceeded even in aqueous media (eq. 5) (Kobayashi et al. 1993c; cf. Rideout and Breslow 1980, Grieco et al. 1983). Thus, naphthoquinone

Table 22  
 $\text{Sc}(\text{OTf})_3$ -catalyzed Diels–Alder reactions

Dienophile	Diene	Product	Yield /%	endo / exo
			95	87 / 13
			89	100 / 0
			90	—
			86	—
			97	84 / 16
			96	89 / 11
			83	>95 / 5
			91	—
			73	—
			83	100 / 0
			89	94 / 3
			92	—

reacted with cyclopentadiene in THF–H<sub>2</sub>O (9:1) at room temperature to give the corresponding adduct in 93% yield (*endo/exo* = 100/0):



Recovery and reuse of the catalyst were also possible in this reaction. After the reaction was completed, the aqueous layer was concentrated to give the catalyst. The recovered catalyst was effective in subsequent Diels–Alder reactions, and it should be noted that the yields of the 2nd and even the 3rd runs were comparable to that of the 1st run.

## 7. Aza Diels–Alder reactions

### 7.1. Reactions of imines with dienes or alkenes

The aza Diels–Alder reaction is among the most powerful synthetic tools for constructing *N*-containing six-membered heterocycles, such as pyridines and quinolines (Weinreb 1991, Boger and Weinreb 1987). Although Lewis acids often promote these reactions, more than stoichiometric amounts of the acids are required due to the strong coordination of the acids to nitrogen atoms (Weinreb 1991, Boger and Weinreb 1987). Use of the Ln(OTf)<sub>3</sub> as a catalyst was investigated in this reaction.

In the presence of 10 mol% Yb(OTf)<sub>3</sub> (a representative lanthanide triflate), *N*-benzylideneaniline (**12a**) was treated with 2-trimethylsiloxy-4-methoxy-1,3-butadiene (Danishefsky's diene, **13**) (Danishefsky and Kitahara 1974) in acetonitrile at room temperature. The aza Diels–Alder reaction proceeded smoothly to afford the corresponding tetrahydropyridine derivative in 93% yield (table 23). The adduct was obtained quantitatively when Sc(OTf)<sub>3</sub> was used as a catalyst. Imines **12b** and **12c** also reacted smoothly with **13** to give the corresponding adducts in high yields. The reaction of **12a** with cyclopentadiene was next performed under the same reaction conditions. It was found that the reaction course changed in this case and that a tetrahydroquinoline derivative was obtained in 69% yield. In this reaction, the imine worked as an azadiene toward one of the double bonds of cyclopentadiene as a dienophile (Lucchini et al. 1988, Boger 1983, Grieco and Bahsas 1988). In the reactions of 2,3-dimethylbutadiene, mixtures of tetrahydropyridine and tetrahydroquinoline derivatives were obtained.

Other examples and effects of the Ln(OTf)<sub>3</sub> are shown in tables 24 and 25, respectively (Kobayashi et al. 1995c,d). A vinyl sulfide, a vinyl ether, and a silyl enol ether worked well as dienophiles to afford tetrahydroquinoline derivatives in high yields (Joh and Hagihara 1967, Povarov 1967, Worth et al. 1970, Kametani et al. 1986, Cheng et al. 1985, Narasaka and Shibata 1993, Makioka et al. 1995). Among the Ln(OTf)<sub>3</sub>, heavy lanthanides such as Er, Tm, and Yb gave better results.

Table 23  
Syntheses of pyridine derivatives catalyzed by  $\text{Ln}(\text{OTf})_3$

$\text{R}^1$	Diene	$\text{Ln}(\text{OTf})_3$ (mol%)	Product	Yield/%
H ( <b>12a</b> ) OMe ( <b>12b</b> ) Cl ( <b>12c</b> )		$\text{Yb}(\text{OTf})_3$ (10)	<b>14a</b> <b>14b</b> <b>14c</b>	93 (99) <sup>a</sup> 82 92
H ( <b>12a</b> ) OMe ( <b>12b</b> ) Cl ( <b>12c</b> )		$\text{Sc}(\text{OTf})_3$ (20)	<b>15a+16a</b> <b>15b+16b</b> <b>15c+16c</b>	54 <sup>b</sup> 71 <sup>c</sup> 50 <sup>d</sup>
H ( <b>12a</b> ) OMe ( <b>12b</b> ) Cl ( <b>12c</b> )		$\text{Yb}(\text{OTf})_3$ (10)	<b>17a</b> <b>17b</b> <b>17c</b>	69 (91) <sup>e,f</sup> 38 <sup>f</sup> 85 <sup>f</sup>

<sup>a</sup> 10 mol%  $\text{Sc}(\text{OTf})_3$  was used. The reaction was carried out at  $0^\circ\text{C}$ .

<sup>b</sup> **15a** 37%, **16a** 17%.

<sup>c</sup> **15b** 8%, **16b** 63%.

<sup>d</sup> **15c** 37%, **16c** 13%.

<sup>e</sup> 20 mol%  $\text{Sc}(\text{OTf})_3$  was used.

<sup>f</sup> *cis/trans* = 94/6.

## 7.2. Three-component coupling reactions of aldehydes, amines, and dienes or alkenes

One synthetic problem in the aza Diels–Alder reactions is the stability of the imines under the influence of Lewis acids. It is desirable that the imines activated by Lewis acids are immediately trapped by dienes or dienophiles (Larsen et al. 1986, Grieco and Bahsas 1988). In 1989, Weinreb and coworkers reported (Sisko and Weinreb 1989) a convenient procedure for the imino Diels–Alder reaction of an aldehyde and a 1,3-diene with *N*-sulfinyl *p*-toluenesulfonamide via *N*-sulfonyl imine produced *in situ*, by using a stoichiometric amount of  $\text{BF}_3 \cdot \text{OEt}_2$  as a promoter.

Bearing in mind the usefulness and efficiency of one-pot procedures, three-component coupling reactions between aldehydes, amines, and alkenes via imine formation and aza Diels–Alder reactions were examined using the  $\text{Ln}(\text{OTf})_3$  as a catalyst.

Table 24  
Syntheses of quinoline derivatives catalyzed by  $\text{Ln}(\text{OTf})_3$

R <sup>1</sup>	R <sup>2</sup>	Alkene	Product	Yield/%	<i>cis/trans</i>	
H	H (12a)		<b>18a</b>	75	57/43	
OMe	H (12b)		<b>18b</b>	0	—	
Cl	H (12c)		<b>18c</b>	quant.	nd <sup>a)</sup>	
H	OMe (12d)		<b>18d</b>	70	nd <sup>a)</sup>	
H	H (12a)		<b>19a</b>	96	nd <sup>a)</sup>	
OMe	H (12b)		<b>19b</b>	77	67/33	
Cl	H (12c)		<b>19c</b>	95	nd <sup>a)</sup>	
OMe	H (12b)		<b>20</b>	quant.	83/17 <sup>b)</sup>	


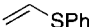
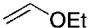
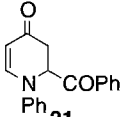

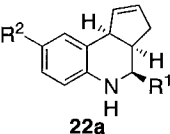
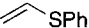
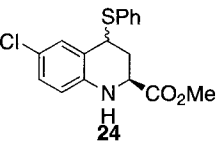

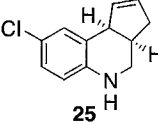
<sup>a</sup> Not determined.<sup>b</sup> Relative configuration assignment was not made.

Table 25  
Effects of  $\text{Ln}(\text{OTf})_3$  (**1**)

Ln	Yield (%)	Ln	Yield (%)
Sc	94	Gd	76
V	60	Dy	63
La	45	Ho	64
Pr	57	Er	97
Nd	60	Tm	92
Sm	63	Yb	85
Eu	63	Lu	72

In the presence of 10 mol%  $\text{Yb}(\text{OTf})_3$  and magnesium sulfate, benzaldehyde was treated with aniline and **13** successively in acetonitrile at room temperature. The

Table 26  
One-pot syntheses of pyridine and quinoline derivatives

$\text{R}^1\text{CHO} + \text{H}_2\text{N}-\text{C}_6\text{H}_4-\text{R}^2 + \text{diene or alkene} \xrightarrow[\text{CH}_3\text{CN, rt}]{\text{Yb(OTf)}_3 (5-20 \text{ mol}\%)} \text{pyridine or quinoline derivatives}$					
R <sup>1</sup>	R <sup>2</sup>	Diene or Alkene	Product	Yield/%	cis/trans
Ph	H	<b>13</b>	<b>14a</b>	80 (83) <sup>a</sup>	—
			<b>17a</b>	56	94/ 6
			<b>18a</b>	70	nd <sup>b</sup>
	Cl		<b>18c</b>	quant.	nd <sup>b</sup>
	H		<b>19a</b>	60	79/21
PhCO	H	<b>13</b>		76	—
	H			94 (97) <sup>c</sup>	96/ 4 (96/ 4)
			<b>22a</b>		
	OMe		<b>22b</b>	94	94/ 6
	Cl		<b>22c</b>	quant.	96/ 4
MeO <sub>2</sub> C	H		<b>23a</b>	82	99/ 1
	Cl		<b>23c</b>	84	99/ 1
	Cl			65	nd <sup>b</sup>
H <sup>d</sup>	Cl			90 <sup>c</sup>	—
			<b>25</b>		

<sup>a</sup> Sc(OTf)<sub>3</sub> (10 mol%) was used.

<sup>b</sup> Not determined.

<sup>c</sup> The reactions were carried out in aqueous solution (H<sub>2</sub>O:EtOH:toluene = 1:9:4).

<sup>d</sup> Commercial formaldehyde water solution was used.



Table 27  
Effects of  $\text{Ln}(\text{OTf})_3$  (2)

$\text{PhCOCHO} + \text{4-methoxyaniline} + \text{cyclopentadiene} \xrightarrow[\text{CH}_3\text{CN, rt, 20h}]{\text{Ln}(\text{OTf})_3 (10 \text{ mol}\%)}$			
Ln	Yield (%)	Ln	Yield (%)
Sc	63	Gd	91
Y	77	Dy	87
La	88	Ho	76
Pr	75	Er	84
Nd	97	Tm	84
Sm	91	Yb	94
Eu	87	Lu	80

three-component coupling reaction proceeded smoothly to afford the corresponding tetrahydropyridine derivative in 80% yield. It is noteworthy that  $\text{Yb}(\text{OTf})_3$  kept its activity and effectively catalyzed the reaction even in the presence of water and the amine. When typical Lewis acids such as  $\text{BF}_3 \cdot \text{OEt}_2$  and  $\text{ZnCl}_2$  (100 mol%) were used instead of the  $\text{Ln}(\text{OTf})_3$  under the same reaction conditions, lower yields were observed (23% and 12%, respectively). Use of  $\text{Sc}(\text{OTf})_3$  slightly improved the yield. Other examples of the three-component coupling reaction are shown in table 26. In the reaction between benzaldehyde, anisidine, and cyclopentadiene under the same reaction conditions, the reaction course changed and the tetrahydroquinoline derivative was obtained in 56% yield. A vinyl sulfide and a vinyl ether, and a silyl enol ether worked well as dienophiles to afford tetrahydroquinoline derivatives in high yields. Phenylglyoxal monohydrate reacted with amines and **13** or cyclopentadiene to give the corresponding tetrahydropyridine or quinoline derivatives in high yields. As mentioned in the previous section, the imine derived from phenylglyoxal is known to be highly hygroscopic and its purification by distillation or chromatography is very difficult due to its instability (Lucchini et al. 1988). Moreover, the three-component coupling reactions proceeded smoothly in aqueous solution, and commercial formaldehyde–water solution could be used directly. Most lanthanide triflates tested were effective in the three-component coupling reactions (table 27). These reactions provide very useful routes for the synthesis of pyridine and quinoline derivatives.

### 7.3. Reaction mechanism

In the reactions of **12a–12c** with cyclopentadiene, a vinyl sulfide, or a vinyl ether (**12a–c** work as azadienes), **12c** gave the best yields, while the yields using **12b** were

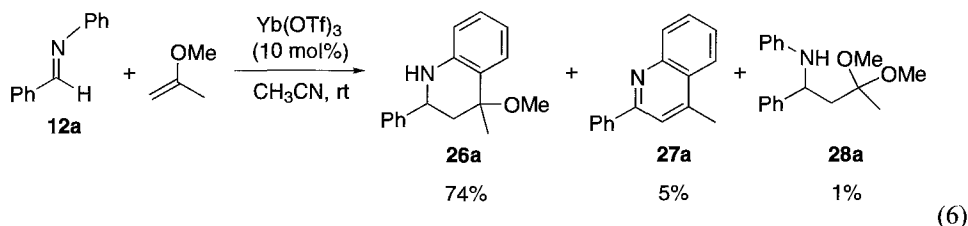
Table 28  
HOMO and LUMO energies and coefficients of **12a–c**<sup>a</sup>

	HOMO (eV)	Coefficient				LUMO (eV)	Coefficient			
		C1	N2	C3	C4		C1	N2	C3	C4
<b>12a</b>	-8.97	0.32	0.35	-0.34	-0.24	-0.69	0.43	-0.38	-0.30	0.27
<b>12b</b>	-8.68	0.32	0.29	-0.40	-0.24	-0.64	0.43	-0.38	-0.28	0.28
<b>12c</b>	-8.93	0.30	0.31	-0.35	-0.22	-0.85	0.43	-0.35	-0.33	0.27
<b>12a–H<sup>+</sup></b>	-13.19	0.15	0.31	-0.39	-0.19	-5.75	0.63	-0.48	-0.09	0.21
<b>12b–H<sup>+</sup></b>	-12.53	0.20	0.18	-0.46	-0.08	-5.58	0.62	-0.49	-0.07	0.21
<b>12c–H<sup>+</sup></b>	-12.58	0.16	0.15	-0.37	-0.10	-5.77	0.63	-0.47	-0.19	0.21

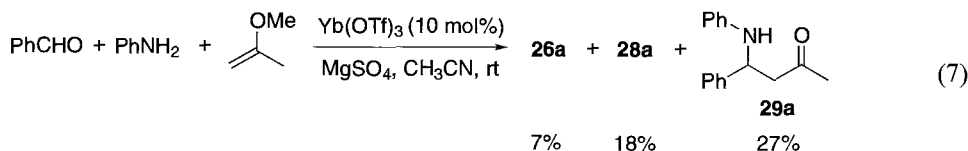
<sup>a</sup> Calculated with MOPAC Ver 6.01 using the PM3 Hamiltonian. MOPAC Ver. 6, Stewart, J.J.P. QCPE Bull. 1989, **10**, 9. Revised as Ver. 6.01 by Tsuneo Hirano, University of Tokyo, for HITAC and UNIX machines, JCPE Newsletter, 1989, **10**, 1.

lowest. The HOMO and LUMO energies and coefficients of **12a–c** and protonated **12a–c** are summarized in table 28. These data do not correspond to the differences in reactivity between **12a–c**, if the reactions are postulated to proceed via concerted [4+2] cycloaddition. On the other hand, the high reactivity of **12c** toward electrophiles compared to **12a** and **12b** may be accepted by assuming a stepwise mechanism.

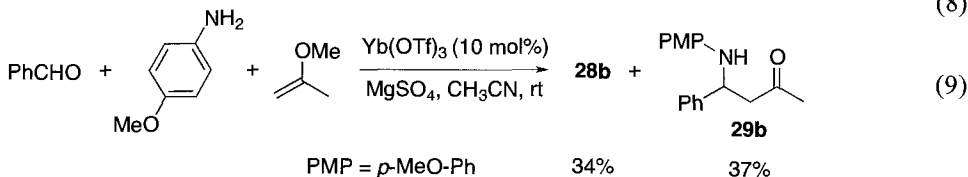
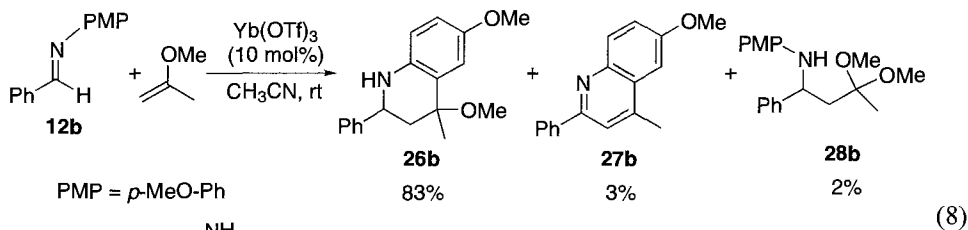
The reaction of **12a** with 2-methoxypropene was tested in the presence of Yb(OTf)<sub>3</sub> (10 mol%). The main product was tetrahydroquinoline derivative **26a**; small amounts of quinoline **27a** and β-amino ketone dimethylacetal **28a** were also obtained:



On the other hand, the three-component coupling reaction between benzaldehyde, aniline, and 2-methoxypropene gave only a small amount of tetrahydroquinoline derivative **26a**, and the main products in this case were β-amino ketone **29a** and its dimethylacetal **28a**:

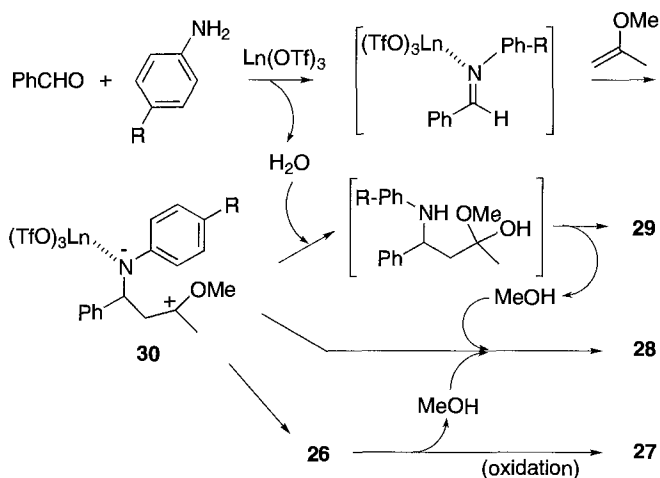


Similar results were obtained in the reaction of **12b** with 2-methoxypropene and the three-component coupling reaction between benzaldehyde, anisidine, and 2-methoxypropene:



A possible mechanism for these reactions is shown in scheme 11. Intermediate **30** is quenched by water and methanol generated *in situ* to afford **28** and **29**, respectively. While **26** is predominantly formed from **30** under anhydrous conditions, formation of **28** and **29** predominates in the presence of even a small amount of water. It is noted that these results suggest a stepwise mechanism in these types of aza Diels–Alder reactions (Nomura et al. 1978).

Thus, this new type of Lewis acid, the  $\text{Ln}(\text{OTf})_3$ , is quite effective for the catalytic activation of imines, and has achieved aza Diels–Alder reactions of imines with dienes or alkenes. The unique reactivities of imines which work as both dienophiles and azadienes under certain conditions were also revealed. Three-component coupling reactions between



Scheme 11. Possible mechanism for three-component coupling reaction.

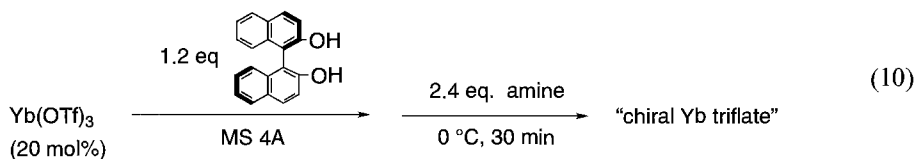
aldehydes, amines, and dienes or alkenes were successfully carried out by using the  $\text{Ln}(\text{OTf})_3$  as catalysts to afford pyridine and quinoline derivatives in high yields. The triflates were stable and kept their activity even in the presence of water and amines. According to these reactions, many substituted pyridines and quinolines can be prepared directly from aldehydes, amines, and dienes or alkenes.

## 8. Asymmetric Diels–Alder reactions

Some efficient asymmetric Diels–Alder reactions catalyzed by chiral Lewis acids have been reported (Hashimoto et al. 1979, Narasaka et al. 1989, Chapuis and Jurczak 1987, Maruoka et al. 1988, 1993b, Corey et al. 1989, 1991, Kaufmann and Boese 1990, Sartor et al. 1991, Mikami et al. 1991, Evans et al. 1993, Ishihara et al. 1993, Seerden and Scheeren 1993; reviews by Narasaka 1991 and Kagan and Riant 1992). The chiral Lewis acids employed in these reactions are generally based on traditional acids such as titanium, boron, or aluminum reagents, and they are well modified to realize high enantioselectivities. Although lanthanide compounds were expected to be Lewis-acid reagents, only a few asymmetric reactions catalyzed by chiral lanthanide Lewis acids were reported. Danishefsky's pioneer work demonstrated that  $\text{Eu}(\text{hfc})_3$  (a NMR shift reagent) catalyzed hetero-Diels–Alder reactions of aldehydes with siloxydienes, but enantiomeric excesses were moderate (Bednarski et al. 1983; see also Quimpere and Jankowski 1987, Sasai et al. 1993).

As shown in the previous section, the  $\text{Ln}(\text{OTf})_3$  were found to be good catalysts in Diels–Alder reactions of various dienophiles with cyclic and acyclic dienes. The reactions proceeded smoothly in the presence of a catalytic amount of the triflate to give the corresponding adducts in high yields. Moreover, the catalyst was stable in water and was easily recovered from the aqueous layer after the reaction was completed, and could be reused. These unique properties were considered to be dependent on the specific characters of the lanthanides(III) (Cotton and Wilkinson 1988), and design of chiral  $\text{Ln}(\text{OTf})_3$  which could work as an efficient catalyst in the asymmetric Diels–Alder reaction was performed.

First,  $\text{Yb}(\text{OTf})_3$  was chosen as a representative of the lanthanide triflates. The chiral Yb triflate was prepared *in situ* from  $\text{Yb}(\text{OTf})_3$ , (*R*)-binaphthol, and a tertiary amine:



while  $\text{Yb}(\text{OTf})_3$  or (*R*)-binaphthol dissolved only sluggishly in dichloromethane, the mixture of  $\text{Yb}(\text{OTf})_3$ , (*R*)-binaphthol, and an amine became an almost clear solution; a model reaction of 3-(2-butenoyl)-1,3-oxazolidin-2-one (**31**) with cyclopentadiene was examined (Narasaka et al. 1989).

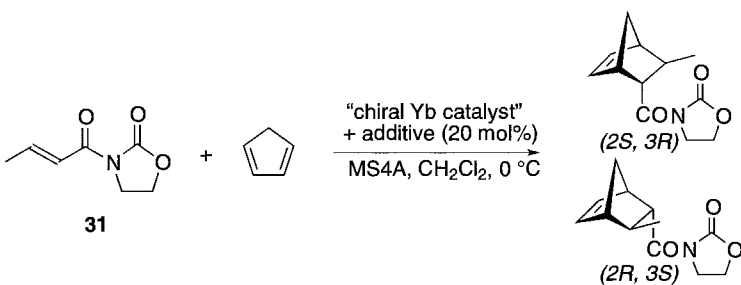
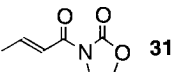
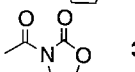
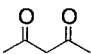
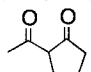
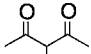
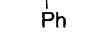
Thus, in the presence of a chiral Yb triflate prepared from  $\text{Yb}(\text{OTf})_3$ , (*R*)-binaphthol, and triethylamine at 0°C for 0.5 h in dichloromethane, **31** reacted with cyclopentadiene at room temperature to afford the Diels–Alder adduct in 87% yield (*endo/exo* = 76/24) and the enantiomeric excess of the *endo* adduct was shown to be 33%. After screening several reaction conditions, it was found that the amine employed at the stage of the preparation of the chiral ytterbium triflate strongly influenced the diastereo- and enantioselectivities. In general, bulky amines gave better results, and 70%, 75%, and 71% ee were observed when diisopropylethylamine, *cis*-2,6-dimethylpiperidine, and *cis*-1,2,6-trimethylpiperidine were used, respectively. In addition, a better result was obtained when the amine was combined with molecular sieves 4A (*cis*-1,2,6-trimethylpiperidine, 91% yield, *endo/exo* = 86/14, *endo* = 90% ee), and the enantiomeric excess was further improved to 95% when the reaction was carried out at 0°C (Kobayashi et al. 1993d).

At this stage, although the reaction conditions were optimized, aging of the catalyst was found to take place. High selectivities (77% yield, *endo/exo* = 89/11, *endo* = 95% ee) were obtained when the diene and the dienophile were added just after  $\text{Yb}(\text{OTf})_3$ , (*R*)-binaphthol and a tertiary amine were stirred at 0°C for 0.5 h in dichloromethane (the original catalyst system). On the other hand, the selectivities decreased with the stirring time of the catalyst solution and the temperature. These results seemed to be ascribed to the aging of the catalyst, but the best result (77% yield, *endo/exo* = 89/11, *endo* = 95% ee) was obtained when the mixture (the substrates and 20 mol% of the catalyst) was stirred at 0°C for 20 h. It was suggested from this result that the substrates or the product stabilized the catalyst. The effect of the substrates or the product on the stabilization of the catalyst was then examined, and the dienophile (**31**) was found to be effective in preventing the catalyst from aging. When 20 mol% of the original catalyst system and **31** (additive) were stirred at 0°C for 5.5 h in dichloromethane, the product was obtained in 66% yield, *endo/exo* = 87/13, and the enantiomeric excess of the *endo* adduct was 88%.

Moreover, after screening several additives other than **31**, it was found that some additives were effective not only in stabilizing the catalyst but also in controlling the enantiofacial selectivities in the Diels–Alder reaction. Selected examples are shown in table 29. When 3-acetyl-1,3-oxazolidin-2-one (**32**) was combined with the original catalyst system (to form catalyst A), the *endo* adduct was obtained in 93% ee and the absolute configuration of the product was 2*S*, 3*R*. On the other hand, when acetyl acetone derivatives were mixed with the catalyst, reverse enantiofacial selectivities were observed. The *endo* adduct with an absolute configuration of 2*R*, 3*S* was obtained in 81% ee when 3-phenylacetylacetone (PAA) was used as an additive (catalyst B). In these cases, the chiral source was the same (*R*)-binaphthol. Therefore, the enantioselectivities were controlled by the achiral ligands, 3-acetyl-1,3-oxazolidin-2-one and PAA (Kobayashi and Ishitani 1994).

As shown in table 30, the same selectivities were observed in the reactions of other 3-acyl-1,3-oxazolidin-2-ones. Thus, by using the same chiral source (*R*)-binaphthol, both enantiomers of the Diels–Alder adducts between 3-acyl-1,3-oxazolidin-2-ones and cyclopentadiene were prepared. Traditional methods have required both enantiomers of chiral sources in order to prepare both enantiomers stereoselectively (Stinson 1993), but

Table 29  
 Effect of additives

			
Additive	Yield/%	<i>endo/exo</i>	<i>2S,3R/2R,3S</i> (ee (%)) <sup>a)</sup>
 <b>31</b>	66	87/13	<b>94.0</b> / 6.0 (88)
 <b>32</b>	77	89/11	<b>96.5</b> / 3.5 (93)
<hr/>			
	80	88/12	22.5/ <b>77.5</b> (55)
	36	81/19	19.0/ <b>81.0</b> (62)
	69	88/12	15.5/ <b>84.5</b> (69)
 Ph	83	93/ 7	9.5/ <b>90.5</b> (81) <sup>c)</sup>

<sup>a</sup> Enantiomer ratios of *endo* adducts.

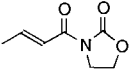
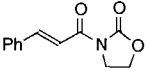
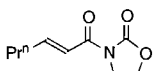
<sup>b</sup> 1,2,2,6,6-Pentamethylpiperidine was used instead of *cis*-1,2,6-trimethylpiperidine. Yb(OTf)<sub>3</sub>, MS4A, and the additive were stirred in dichloromethane at 40°C for 3 h.

the counterparts of some chiral sources are of poor quality or are hard to obtain (for example, sugars, amino acids, alkaloids, etc.). *It is noted that the chiral catalysts with reverse enantiofacial selectivities could be prepared by using the same chiral source and a choice of achiral ligands.*

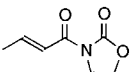
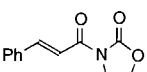
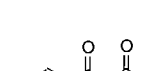
These exciting selectivities are believed to be strongly dependent on the specific coordination number of Yb(III) (Cotton and Wilkinson 1988) (scheme 12). Two binding sites for the ligands are now postulated in the Yb catalysts. **31** or **32** coordinates in site A under equilibrium conditions to stabilize the original catalyst system. When **31** coordinates Yb(III), cyclopentadiene attacks from the *si* face of **31** (site A favors *si* face attack). On the other hand, in catalyst B (the original catalyst system and PAA), site A is occupied by PAA. [3-acyl-1,3-oxazolidin-2-ones are weakly coordinating ligands, whereas PAA is stronger coordinating. From the experiments, site A seems to be more easily available for coordination than site B]. Since another coordination site still remains

Table 30

Synthesis of both enantiomers of the Diels–Alder adducts between cyclopentadiene and dienophiles by use of catalysts A<sup>a</sup> and B<sup>b</sup>

Dienophile	Yield/%	Catalyst A	
		<i>endo/exo</i>	<i>2S,3R/2R,3S</i> (ee (%)) <sup>c</sup>
 31	77	89/11	<b>96.5</b> / 3.5 (93)
	77	89/11	<b>97.5</b> / 2.5 (95) <sup>d</sup>
	40	81/19	<b>91.5</b> / 8.5 <sup>d</sup> (83)
	34	80/20	<b>93.0</b> / 7.0 (86)
	81	80/20	<b>91.5</b> / 8.5 (83) <sup>d</sup>

Dienophile	Yield/%	Catalyst B <sup>b</sup>	
		<i>endo/exo</i>	<i>2S,3R/2R,3S</i> (ee (%)) <sup>c</sup>
 31	83	93/ 7	9.5/ <b>90.5</b> (81)
	60	89/11	10.5/ <b>89.5</b> <sup>f</sup> (79)
	51	89/11	8.5/ <b>91.5</b> <sup>f</sup> (83)
	51	89/11	5.5/ <b>94.5</b> <sup>f</sup> (89) <sup>g</sup>
	81	91/ 9	10.0/ <b>90.0</b> (80)
	85	91/ 9	9.0/ <b>91.0</b> (82) <sup>g</sup>
	60	91/ 9	7.5/ <b>92.5</b> (85) <sup>h</sup>

<sup>a</sup> Catalyst A: Yb(OTf)<sub>3</sub> + (*R*)-(+)-binaphthol + *cis*-1,2,6-trimethylpiperidine + MS4A + 3-acetyl-1,3-oxazolidin-2-one (**32**).

<sup>b</sup> Catalyst B: Yb(OTf)<sub>3</sub> + (*R*)-(+)-binaphthol + *cis*-1,2,6-trimethylpiperidine + MS4A + 3-phenylacetylacetonate (PAA).

<sup>c</sup> 1,2,2,6,6-Pentamethylpiperidine was used instead of 1,2,6-trimethylpiperidine.

<sup>d</sup> Enantiomer ratios of *endo* adducts.

<sup>g</sup> Tm(OTf)<sub>3</sub>.

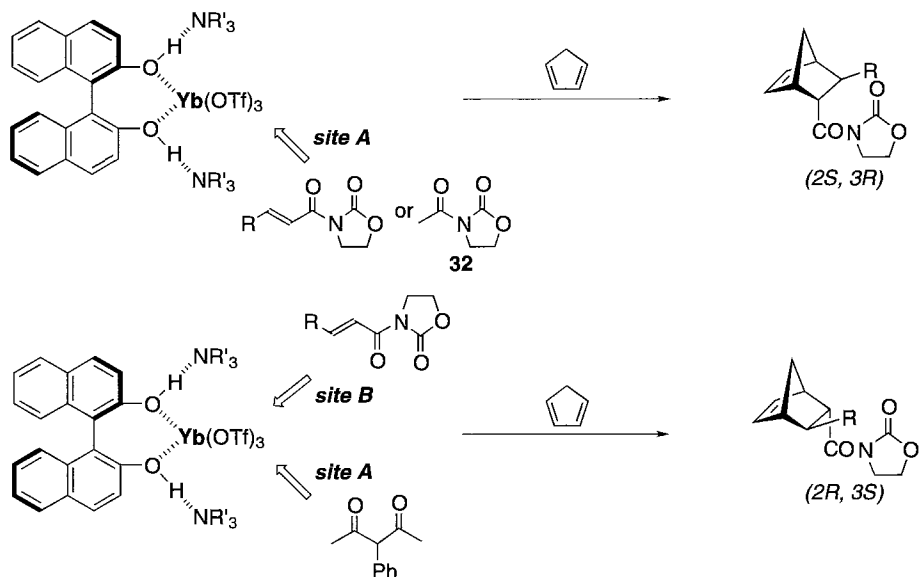
<sup>e</sup> Without additive.

<sup>h</sup> Er(OTf)<sub>3</sub> was used instead of Yb(OTf)<sub>3</sub>.

<sup>f</sup> 2*R*,3*R*/2*S*,3*S*.

in the Yb(III) catalyst owing to the specific coordination numbers, **31** coordinates at site B and cyclopentadiene attacks from the *re* face (site B favors *re* face attack).

The effect of other Ln(OTf)<sub>3</sub> was also examined. As shown in table 31, the choice of lanthanide element strongly influenced the yields and selectivities. A slight difference between the two catalyst systems (catalysts A and B) on the effect of the lanthanide elements was also observed. In catalyst A, lutetium triflate (Lu(OTf)<sub>3</sub>) was also effective in generating the *endo* Diels–Alder adduct in 93% ee. The yields and selectivities diminished rapidly in accordance with the enlargement of the ionic radii. In catalyst B, on the other hand, the best results were obtained when thulium triflate (Tm(OTf)<sub>3</sub>) or erbium triflate (Er(OTf)<sub>3</sub>) was employed. Deviations to either larger or smaller ionic



Scheme 12. Synthesis of both enantiomers using the same chiral source.

radii resulted in decreased selectivities, however, the Diels–Alder adduct was obtained in 85% yield with good selectivities (*endo/exo* = 92/8, *endo* isomer = 61% ee) even when holmium triflate ( $\text{Ho}(\text{OTf})_3$ ) was used.

Although  $\text{Sc}(\text{OTf})_3$  has slightly different properties compared with other lanthanide triflates, the chiral Sc catalyst could be prepared from  $\text{Sc}(\text{OTf})_3$ , (*R*)-binaphthol and a tertiary amine in dichloromethane (Kobayashi et al. 1994b). The catalyst was also found to be effective in the Diels–Alder reactions of acyl-1,3-oxazolidin-2-ones with dienes. The amines employed in the preparation of the catalyst influenced the enantioselectivities strongly. For example, in the Diels–Alder reaction of 3-(2-butenoyl)-1,3-oxazolidin-2-one with cyclopentadiene ( $\text{CH}_2\text{Cl}_2$ ,  $0^\circ\text{C}$ ), the enantiomeric excesses of the *endo* adduct depended crucially on the amines employed; aniline, 14% ee; lutidine, 46% ee; triethylamine, 51% ee; 2,2,6,6-tetramethylpiperidine, 51% ee; diisopropylethylamine, 69% ee; 2,6-dimethylpiperidine, 69% ee; 1,2,2,6,6-pentamethylpiperidine, 72% ee; and *cis*-1,2,6-trimethylpiperidine, 84% ee.

Several examples of the chiral Sc(III)-catalyzed Diels–Alder reactions are shown in table 32. The highest enantioselectivities were observed when *cis*-1,2,6-trimethylpiperidine was employed as an amine. 3-(2-butenoyl)-, 3-cinnamoyl-, and 3-(2-hexenoyl)-1,3-oxazolidin-2-ones reacted with cyclopentadiene smoothly in the presence of the chiral Sc catalyst to afford the corresponding Diels–Alder adducts in high yields and high selectivities. It should be noted that even 3 mol% of the catalyst was enough to complete the reaction, and the *endo* adduct was obtained in 92% ee.

The catalyst was also found to be effective for the Diels–Alder reactions of an acrylic acid derivative (Narasaka et al. 1991). 3-Acryloyl-1,3-oxazolidin-2-one reacted with



Table 31  
Effect of Ln(OTf)<sub>3</sub>

Ln	Yield (%)	<i>endo/exo</i>	2 <i>S</i> ,3 <i>R</i> /2 <i>R</i> ,3 <i>S</i>	(ee) (%) <sup>a</sup>
<b>Catalyst A</b>				
Lu	60	89/11	96.5/3.5	(93)
Yb	77	89/11	96.5/3.5	(93)
Tm	46	86/14	87.5/12.5	(75)
Er	24	83/17	84.5/15.5	(69)
Ho	12	73/27	62.5/37.5	(25)
Y	6	70/30	60.0/40.0	(20)
Gd	0	—	—	—
<b>Catalyst B</b>				
Lu	30	89/11	24.5/75.5	(51)
Yb	88	92/8	15.0/85.0	(70)
Tm	72	91/9	13.0/87.0	(74)
Er	59	90/10	13.0/87.0	(74)
Ho	70	84/16	21.0/79.0	(58)
Y	85	91/9	19.5/80.5	(61)
Gd	61	85/15	28.5/71.5	(43)

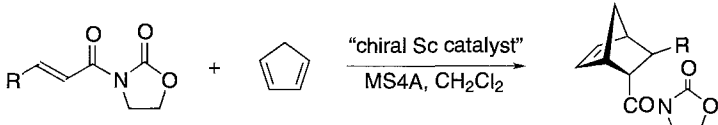
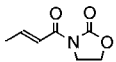
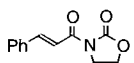
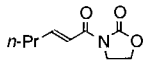
<sup>a</sup> Enantiomer ratios of *endo* adducts.

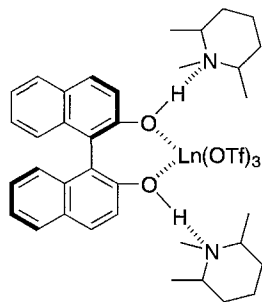
2,3-dimethylbutadiene to afford the corresponding Diels–Alder adduct in 78% yield and 73% ee, whereas the reaction of 3-acryloyl-1,3-oxazolidin-2-one with cyclohexadiene gave 72% ee for the *endo* adduct (88% yield, *endo/exo* = 100/0).

Similar to the chiral Yb catalyst, aging was observed in the chiral Sc catalyst. It was also found that **32** or 3-benzoyl-1,3-oxazolidin-2-one was a good additive for stabilization of the catalyst, but that reverse enantioselectivities by additives were not observed. This can be explained by the coordination numbers of Yb(III) and Sc(III); while Sc(III) has up to seven ligands, specific coordination numbers allow Yb(III) to have up to twelve ligands (Cotton and Wilkinson 1988; for a review see Hart 1987).

As for the chiral ytterbium and scandium catalysts, the following structures were postulated. The unique structure shown in scheme 13 was indicated by <sup>13</sup>C NMR and IR spectra. The most characteristic point of the catalysts was the existence of hydrogen bonds between the phenolic hydrogens of (*R*)-binaphthol and the nitrogens of the tertiary amines. The <sup>13</sup>C NMR spectra indicated these interactions, and the existence of the hydrogen bonds was confirmed by the IR spectra (Fritsch and Zundel 1981). The coordination form of these catalysts may be similar to that of the lanthanide(III)–water or –alcohol complex (for a review see Hart 1987). It is noted that the structure is quite different from those of conventional chiral Lewis acids based on aluminum (Maruoka and Yamamoto 1989, Bao et al. 1993), boron (Hattori and Yamamoto 1992), or titanium

Table 32  
Enantioselective Diels–Alder reactions using a chiral scandium catalyst

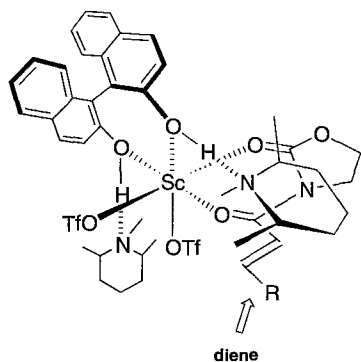
				
Dienophile	Catalyst/mol%	Yield/%	<i>endo/exo</i>	ee/% ( <i>endo</i> )
 31	20	94	89/11	92 (2 <i>S</i> ,3 <i>R</i> )
	10	84	86/14	96 (2 <i>S</i> ,3 <i>R</i> )
	5	84	87/13	93 (2 <i>S</i> ,3 <i>R</i> )
	3	83	87/13	92 (2 <i>S</i> ,3 <i>R</i> )
	20	99	89/11	93 (2 <i>R</i> ,3 <i>R</i> )
	10	96	90/10	97 (2 <i>R</i> ,3 <i>R</i> )
	20	95	78/22	74 (2 <i>S</i> ,3 <i>R</i> )
	10	86	78/22	75 (2 <i>S</i> ,3 <i>R</i> )



Scheme 13. Chiral rare-earth metal triflates.

(Reetz et al. 1986, Mikami et al. 1990). In the present chiral catalysts, the axial chirality of (*R*)-binaphthol is transferred via the hydrogen bonds to the amine parts, which shield one side of the dienophile effectively (Bao et al. 1993; see also Bednarski et al. 1983). This is consistent with the experimental results showing that amines employed in the preparation of the chiral catalysts strongly influenced the selectivities and that bulky amines gave better selectivities.

Although the transition states of the chiral lanthanide(III)-catalyzed reactions are rather complicated due to the specific coordination number and stereochemistry of the lanthanide(III), the sense of asymmetric induction in the chiral scandium-catalyzed reactions can be rationalized by assuming an intermediate octahedral Sc(III)–dienophile complex (scheme 14). The axial chirality of (*R*)-binaphthol is transferred to the amine,



Scheme 14. Assumed transition state.

the *re* face of the acyl-1,3-oxazolidin-2-one is effectively shielded by the amine part, and a diene approaches the dienophile from the *si* face to afford the adduct in a high enantioselectivity.

It was also suggested that aggregation of the catalysts influenced the selectivities in the Diels–Alder reactions; the reaction of 3-(2-butenoyl)-1,3-oxazolidin-2-one with cyclopentadiene using (*R*)-binaphthol in lower enantiomeric excesses was examined (Oguni et al. 1988, Kitamura et al. 1989, Puchot et al. 1986). The results are shown in fig. 1. Very interestingly, a positive nonlinear effect was observed in the chiral Sc catalyst.

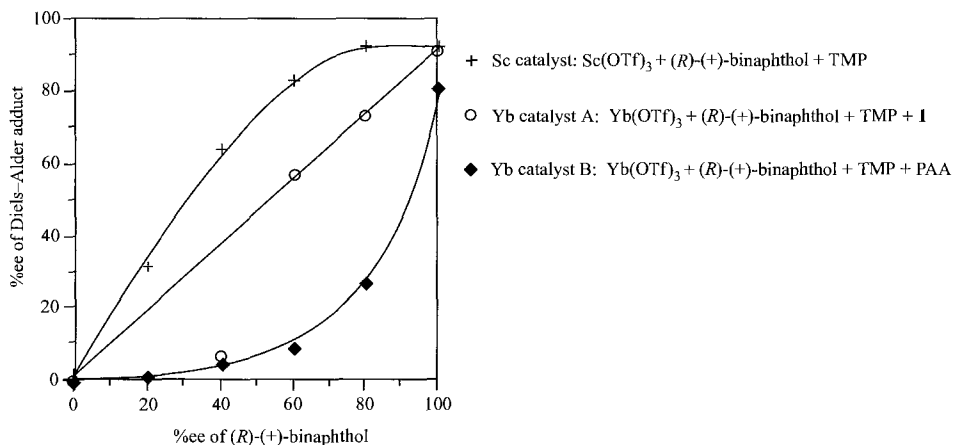


Fig. 1. Correlation between the ee of the Diels–Alder adduct and the ee of (*R*)-(+)-binaphthol.

In the chiral Yb catalysts, on the other hand, the effect was dependent on the additives. The extent of asymmetric induction in catalyst A did not deviate from the enantiomeric excesses of (*R*)-binaphthol in the range 60–100% ee<sup>1</sup> while a negative nonlinear effect

<sup>1</sup> Lower enantiomeric excesses of the product were observed when (*R*)-binaphthol in less than 60% ee was used. This may be ascribed to turnover of the catalyst.

was observed in catalyst B. These results can be ascribed to a difference in aggregation between the Sc catalyst, Yb catalyst A, and Yb catalyst B.

## 9. Asymmetric aza Diels–Alder reactions

While asymmetric reactions using chiral Lewis acids have been demonstrated to achieve several highly enantioselective carbon–carbon bond-forming processes using catalytic amounts of chiral sources (Maruoka and Yamamoto 1993, Narasaka 1991), chiral Lewis-acid-catalyzed asymmetric reactions of nitrogen-containing substrates are rare, probably because most chiral Lewis acids would be trapped by the basic nitrogen atoms to block the catalytic cycle. For example, aza Diels–Alder reactions are among the most basic and versatile reactions for the synthesis of nitrogen-containing heterocyclic compounds (Weinreb 1991, Boger and Weinreb 1987, Kametani and Kasai 1989, Grigos et al. 1965, 1966). Although asymmetric versions using chiral auxiliaries or a stoichiometric amount of a chiral Lewis acid have been reported (Waldmann 1994, Borriore et al. 1989, Ishihara et al. 1994), examples using a catalytic amount of a chiral source are unprecedented.

In the previous section, the  $\text{Ln}(\text{OTf})_3$  were shown to be excellent catalysts for achiral aza Diels–Alder reactions. While stoichiometric amounts of Lewis acids are required in many cases, a small amount of triflate effectively catalyzes the reactions. On the other hand, chiral lanthanide Lewis acids have been developed to realize highly enantioselective Diels–Alder reactions of 2-oxazolidin-1-one with dienes (Kobayashi et al. 1994c). The reaction of *N*-benzylideneaniline with cyclopentadiene was first performed under the influence of 20 mol% of a chiral ytterbium Lewis acid prepared from  $\text{Yb}(\text{OTf})_3$ , (*R*)-BINOL, and trimethylpiperidine (TMP). The reaction proceeded smoothly at room temperature to afford the desired tetrahydroquinoline derivative in 53% yield; however, no chiral induction was observed. At this stage, it was indicated that bidentate coordination between a substrate and a chiral Lewis acid would be necessary for reasonable chiral induction. *N*-Benzylidene-2-hydroxyaniline (**33a**) was then prepared, and the reaction with cyclopentadiene (**34a**) was examined. It was found that the reaction proceeded smoothly to afford the corresponding 8-hydroxyquinoline derivative (**35a**) (Rauckman et al. 1989, Johnson et al. 1989, Ife et al. 1992, Sarges et al. 1993, Mongin et al. 1995) in a high yield. The enantiomeric excess of the *cis* adduct in the first trial was only 6%, however, the selectivity increased when diazabicyclo-[5,4,0]-undec-7-ene (DBU) was used instead of TMP (table 33). It was also indicated that the phenolic hydrogen of **33a** would interact with DBU, which should interact with the hydrogen of (*R*)-BINOL (Kobayashi et al. 1994d), to decrease the selectivity. Additives which interact with the phenolic hydrogen of **33a** were then examined. When 20 mol% *N*-methylimidazole (MID) was used, 91% ee of the *cis* adduct was obtained, however, the chemical yield was low. Other additives were screened and it was found that the desired tetrahydroquinoline derivative was obtained in 92% yield with high selectivities (*cis/trans* = > 99/1, 71% ee), when 2,6-di-*t*-butylpyridine (DTBP) was used.

Table 33  
 Effect of additive

Additive (mol%)	Temperature (°C)	Yield (%)	<i>cis/trans</i>	ee ( <i>cis</i> ) (%)
—	0	71	98/2	62
—	−15 to 0	48	99/1	68
MID <sup>b</sup> (20)	−15 to 0	21	98/2	91
DTBP <sup>c</sup> (20)	0	49	95/5	31
DTBP <sup>c</sup> (100)	0	67	99/1	61
DMP <sup>d</sup> (100)	0	14	98/2	56
DTBMP <sup>e</sup> (100)	−15	82	>99/1	70
DTBP <sup>c</sup> (100)	−15	92	>99/1	71

<sup>a</sup> Prepared from Yb(OTf)<sub>3</sub>, (*R*)-(+)-BINOL, and DBU.

<sup>b</sup> MID, 1-Methylimidazole.

<sup>c</sup> DTBP, 2,6-Di-*t*-butylpyridine.

<sup>d</sup> DMP, 2,6-Dimethylpyridine.

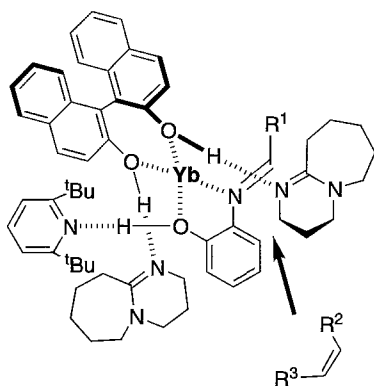
<sup>e</sup> DTBMP, 2,6-Di-*t*-butyl-4-methylpyridine.

Other substrates were tested, and the results are summarized in table 34 (Ishitani and Kobayashi 1996). Vinyl ethers (**34b–d**) also worked well to afford the corresponding tetrahydroquinoline derivatives (**35b–e**) in good to high yields with good to excellent diastereo- and enantioselectivities (entries 1–9). Use of 10 mol% of the chiral catalyst also gave the adduct in high yields and selectivities (entries 2 and 6). As for additives, 2,6-di-*t*-butylpyridine (DTBP) gave the best result in the reaction of imine **33a** with ethyl vinyl ether (**34b**), while higher selectivities were obtained when DTBMP or 2,6-diphenylpyridine (DPP) was used in the reaction of imine **33b** with **33b**. This could be explained by the slight difference in the asymmetric environment created by Yb(OTf)<sub>3</sub>, (*R*)-BINOL, DBU, and the additive (see below). While use of butyl vinyl ether (**34c**) decreased the selectivities (entry 7), dihydrofuran (**34d**) reacted smoothly to achieve high levels of selectivity (entries 8, 9). It was found that the imine (**33c**) prepared from cyclohexanecarboxaldehyde and 2-hydroxyaniline was unstable and difficult to purify. The asymmetric aza Diels–Alder reaction was successfully carried out using the three-component coupling procedure (successively adding the aldehyde, the amine, and cyclopentadiene) in the presence of Sc(OTf)<sub>3</sub> (instead of Yb(OTf)<sub>3</sub>), (*R*)-BINOL, DBU, and DTBMP.

The assumed transition state of this reaction is shown in scheme 15. Yb(OTf)<sub>3</sub>, (*R*)-BINOL and DBU form a complex with two hydrogen bonds, and the axial chirality of (*R*)-BINOL is transferred via the hydrogen bonds to the amine parts. The additive would interact with the phenolic hydrogen of the imine, which is fixed by bidentate coordination

Table 34  
Asymmetric synthesis of tetrahydroquinoline derivatives

Entry	R <sup>1</sup>	Alkene	Additive <sup>a</sup>	Amount of Catalyst /mol%	Temp /°C	Product	Yield /%	<i>cis/trans</i>	Ee/% ( <i>cis</i> )	
1	Ph ( <b>33a</b> )	(34b)	DTBP	20	-45	<b>35b</b>	58	94 / 6	61	
2	Ph ( <b>33a</b> )	<b>34b</b>	DTBP	10	-45	<b>35b</b>	52	94 / 6	77	
3	$\alpha$ -Naph ( <b>33b</b> )	<b>34b</b>	DTBP	20	-15	<b>35c</b>	69	>99/ 1	86	
4	$\alpha$ -Naph ( <b>33b</b> )	<b>34b</b>	DPP <sup>b</sup>	20	-15	<b>35c</b>	65	99/ 1	91	
5	$\alpha$ -Naph ( <b>33b</b> )	<b>34b</b>	DTBMP	20	-15	<b>35c</b>	74	>99/ 1	91	
6	$\alpha$ -Naph ( <b>33b</b> )	<b>34b</b>	DTBMP	10	-15	<b>35c</b>	62	98/ 2	82	
7	$\alpha$ -Naph ( <b>33b</b> )	(34c)	DTBMP	20	-15	<b>35d</b>	80	66/34	70	
8	$\alpha$ -Naph ( <b>33b</b> )	(34d)	DTBMP	20	-15	<b>35e</b>	90	91 / 9	78	
9	$\alpha$ -Naph ( <b>33b</b> )	<b>34d</b>	DPP <sup>b</sup>	20	-15	<b>35e</b>	67	93 / 7	86	
10	$\alpha$ -Naph ( <b>33b</b> )	(34a)	DTBMP	20	-15	<b>35f</b>	69	>99/ 1	68	
11 <sup>c</sup>	<i>o</i> -C <sub>6</sub> H <sub>11</sub> ( <b>33c</b> )	<b>34a</b>	DTBMP	20	-15	<b>35g</b>	58	>99/ 1	73	

<sup>a</sup> See table 29.<sup>b</sup> 2,6-Diphenylpyridine.<sup>c</sup> Sc(OTf)<sub>3</sub> was used.

Scheme 15. Assumed transition state; triflate anions are omitted for clarity.

to Yb(III). Since the top face of the imine is shielded by the amine, the dienophiles approach from the bottom face to achieve high levels of selectivity.

Thus, catalytic asymmetric aza Diels–Alder reactions of imines with alkenes have been developed using a chiral lanthanide Lewis acid, to afford 8-hydroxyquinoline derivatives in high yields with high diastereo- and enantioselectivities. Characteristic points of this reaction are as follows:

- (i) Asymmetric aza Diels–Alder reactions between achiral azadienes and dienophiles have been achieved using a catalytic amount of a chiral source.
- (ii) The unique reaction pathway in which the chiral Lewis acid activates not dienophiles but dienes, is revealed. In most asymmetric Diels–Alder reactions reported using chiral Lewis acids, the Lewis acids activate dienophiles (Maruoka and Yamamoto 1993, Narasaka 1991, Posner et al. 1994, Markó and Evans 1994).
- (iii) A unique lanthanide complex including an azadiene and an additive, which is quite different from the conventional chiral Lewis acids, has been developed.

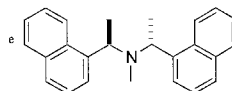
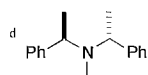
## 10. Asymmetric 1,3-dipolar cycloadditions

1,3-Dipolar cycloadditions between nitrones and alkenes are most useful and convenient for the preparation of isoxazolidine derivatives, which are readily converted to 1,3-amino alcohol equivalents under mild reducing conditions (Tufariello 1984, Torssell 1988). In spite of the importance of chiral amino alcohol units for the synthesis of biologically important alkaloids, amino acids,  $\beta$ -lactams, and amino sugars, etc. (for a review see Frederickson 1997), catalytic enantioselective 1,3-dipolar cycloadditions remain relatively unexplored (Seerden et al. 1994, 1995, Gothelf and Jørgensen 1994, Gothelf et al. 1996, Hori et al. 1996, Seebach et al. 1996, Jensen et al. 1997). Catalytic enantioselective 1,3-dipolar cycloadditions of nitrones with alkenes using a chiral lanthanide catalyst were investigated. It was recently found that the  $\text{Ln}(\text{OTf})_3$  are excellent catalysts in achiral 1,3-dipolar cycloadditions between nitrones and alkenes and also in three-component coupling reactions of aldehydes, hydroxylamines, and alkenes (Kobayashi et al. 1997b, Minakata et al. 1997, see also Sanchez-Blanco et al. 1997). First, the 1,3-dipolar cycloaddition reaction of *N*-benzylidenebenzylamine *N*-oxide (**36**) with 3-(2-butenoyl)-1,3-oxazolidin-2-one (**31**) was performed in the presence of a chiral Yb(III) catalyst (20 mol%) prepared from  $\text{Yb}(\text{OTf})_3$ , (*S*)-BINOL, and triethylamine ( $\text{Et}_3\text{N}$ ). The reaction proceeded smoothly at room temperature to afford the corresponding isoxazolidine derivative in a 65% yield with high *endo/exo* selectivity (99/1), and a moderate ee of the *endo* adduct was observed (table 35). The enantiomeric excess was improved to 78% when *cis*-1,2,6-trimethylpiperidine (TMP) was used instead of  $\text{Et}_3\text{N}$ . Furthermore, it was found that *use of chiral amines influenced the selectivity dramatically, and that combination of the chirality of BINOL and the amine was crucial for the selectivity*. Namely, 71% ee of the *endo* adduct was obtained in the model reaction using a catalyst prepared by the combination of (*S*)-BINOL and *N*-methyl-bis[(*R*)-1-phenylethyl]amine [(*R*)-MPEA], while only 35% ee was observed by the combination of

Table 35  
 Effect of amines

Amine	Yield (%)	<i>endo/exo</i>	ee <sup>b</sup> (%)
Et <sub>3</sub> N	65	99/1	63
<sup>t</sup> Pr <sub>2</sub> NEt	73	>99/1	62
<i>cis</i> -1,2,6-TMp <sup>c</sup>	73	99/1	78
( <i>R</i> )-MPEA <sup>d</sup>	92	>99/1	71
( <i>S</i> )-MPEA	80	97/3	35
( <i>R</i> )-MNEA <sup>e</sup>	92	99/1	96
( <i>S</i> )-MNEA	87	99/1	62

<sup>a</sup> Chiral Yb(III) = Yb(OTf)<sub>3</sub> + (*S*)-BINOL + amine. <sup>b</sup> ee of the *endo* adducts. <sup>c</sup> *cis*-1,2,6-Trimethylpiperidine.



(*S*)-BINOL and (*S*)-MPEA. Moreover, it was found that 96% ee of the *endo* adduct was obtained with an excellent yield (92%) and diastereoselectivity (*endo/exo* = 99/1) by the combination of (*S*)-BINOL and a newly prepared chiral amine, *N*-methyl-bis[(*R*)-1-(1-naphthyl)ethyl]amine [(*R*)-MNEA]; the latter was prepared from (*R*)-1-(1-naphthyl)ethylamine. The chiral Yb(III) catalyst thus prepared has two independent chiralities (*hetero-chiral Yb(III) catalyst, vide infra*) and it was found that the sense of the chiral induction in these reactions was mainly determined by BINOL and that the chiral amine increased or decreased the induction relatively.

Several examples of the 1,3-dipolar cycloadditions between nitrones and 3-(2-alkenoyl)-1,3-oxazolidin-2-ones using the novel hetero-chiral Yb(III) catalyst are shown in table 36. In most cases, the desired isoxazolidine derivatives were obtained in excellent yields with excellent diastereo- and enantioselectivities. It is noted that high levels of selectivities were attained at room temperature. Nitrones derived from aromatic and heterocyclic aldehydes gave satisfactory results, and even in the reaction using the nitrone derived from an aliphatic aldehyde, the cycloaddition proceeded smoothly to give the *endo* adduct in an excellent enantiomeric excess, albeit low *endo/exo* selectivity was observed. Moreover, it was found that alkenes which could be employed in the present 1,3-dipolar cycloaddition were not limited to 3-(2-alkenoyl)-1,3-oxazolidin-2-one derivatives. When *N*-phenylmaleimide was used as a dipolarophile, the desired isoxazolidine derivative was obtained in a 70% yield with *endo/exo* = >99/1, and the enantiomeric excess of the *endo* adduct was 70% ee under the standard reaction conditions. It is believed that bidentate coordination [e.g. Yb(III)-3-(2-alkenoyl)-1,3-oxazolidin-2-one] is necessary to obtain



Table 36  
Catalytic enantioselective 1,3-dipolar cycloadditions

R <sup>1</sup>	R <sup>2</sup>	Yield (%)	<i>endo</i> / <i>exo</i>	ee <sup>b</sup> (%)
Ph	CH <sub>3</sub>	92	99/1	96
<i>p</i> -Cl-Ph	CH <sub>3</sub>	93	99/1	92
<i>p</i> -MeO-Ph	CH <sub>3</sub>	82	95/5	90
2-furyl	CH <sub>3</sub>	89	95/5	89
1-naphthyl	CH <sub>3</sub>	88	98/2	85
Ph	H	91	>99/1	79
Ph	C <sub>3</sub> H <sub>7</sub>	89	98/2	93
C <sub>2</sub> H <sub>5</sub>	CH <sub>3</sub>	88	53/47	96

<sup>a</sup> Chiral Yb(III) = Yb(OTf)<sub>3</sub> + (*S*)-BINOL + (*R*)-MNEA.

<sup>b</sup> ee of the *endo* adducts.

high selectivities in many chiral lanthanide-catalyzed reactions. These results are very interesting and promising because it has been shown that even monodentate coordination can achieve good selectivities by using the hetero-chiral Yb(III) catalyst (Markó and Evans 1994, Burgess et al. 1996).

On the other hand, molecular sieves 4A (MS 4A) were essential to provide high enantioselectivity in this reaction. While MS 4A was first used as a dehydration agent to remove a small amount of water existing in a solvent, etc., it was found that reverse enantiofacial selectivity was obtained in the absence of MS 4A (quite recently, a similar effect of MS 4A was reported by Gothelf et al. 1998). That is, in the presence of MS 4A the absolute configuration of the major product of the cycloaddition of nitron **36** to *N*-crotonoyl-1,3-oxazolidin-2-one (**31**) was 3*R*, 4*S*, 5*R*, while an adduct with the absolute configuration of 3*S*, 4*R*, 5*S* was obtained in moderate selectivity in the absence of MS 4A. We already reported that a similar ytterbium catalyst was effective for asymmetric Diels–Alder reactions. However, in the Diels–Alder reaction of cyclopentadiene with **31**, the same enantiofacial selectivities were obtained using the same chiral Yb(III) catalyst in the presence and absence of MS 4A. These results suggested that the nitron would affect the enantiofacial selectivity in the 1,3-dipolar cycloaddition. On the other hand, it was found that the 3*S*, 4*R*, 5*S* selectivity was increased when one equivalent of the nitron was added to the chiral Yb(III) catalyst as an additive before adding the substrates, **36** and **31**. Namely, when an equimolar amount of Yb(OTf)<sub>3</sub>, (*S*)-BINOL, (*R*)-MNEA, and **1** were combined and then **36** and **31** were added, the desired *endo* adduct was obtained in 90% yield with 83% ee (*endo*/*exo*=99/1). Several additives other than **36** were then examined, and the results are summarized in table 37. It is noted that amine *N*-oxides such

Table 37  
 Effect of additives

Additive	(mol%)	Yield (%)	<i>endo/exo</i>	ee (%)	Config.
MS 4A		92	99/1	96	<i>3R, 4S, 5R</i>
none		83	98/2	50	<i>3S, 4R, 5S</i>
H <sub>2</sub> O	(20)	81	95/5	8	<i>3S, 4R, 5S</i>
NMO	(20)	68	98/2	81	<i>3S, 4R, 5S</i>
Me <sub>3</sub> N <sup>+</sup> -O <sup>-</sup>	(20)	79	>99/1	74	<i>3S, 4R, 5S</i>
	(20)	72	>99/1	72	<i>3S, 4R, 5S</i>
	(20)	78	99/1	65	<i>3S, 4R, 5S</i>
<b>36</b>	(20)	90	99/1	83	<i>3S, 4R, 5S</i>
<b>36</b>	(40)	83	>99/1	65	<i>3S, 4R, 5S</i>
	(20)	69	>99/1	41	<i>3S, 4R, 5S</i>

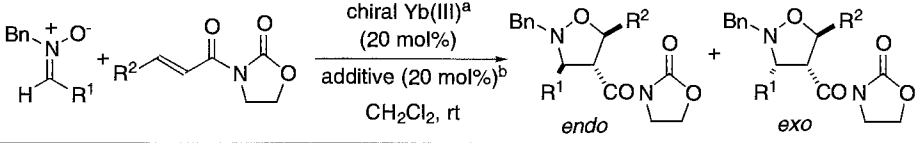
<sup>a</sup> Chiral Yb(III) = Yb(OTf)<sub>3</sub> + (*S*)-BINOL + (*R*)-MNEA.

<sup>b</sup> ee of the *endo* adducts.

as *N*-methylmorpholine oxide (NMO) were also effective for obtaining the cycloaddition adduct with *3R, 4S, 5R* configuration in high selectivity. The best selectivity was obtained by using one equivalent of (**36**) as an additive, while the selectivity decreased when two equivalents of (**36**) were used.

Several examples of the 1,3-dipolar cycloaddition of nitrones using the heterochiral Yb(III) catalyst in the absence of MS 4A are shown in table 38. The reactions were performed by adding one equivalent of the corresponding nitron to the Yb(III) catalyst and then, successively, the same nitron and a dipolarophile. In all cases, reverse enantiofacial selectivities compared with those obtained in the presence of MS 4A were observed. When *N*-acryloyl-1,3-oxazolidin-2-one was used as a dipolarophile, the desired isoxazolidine derivative was obtained in 88% ee. Other substrates also gave high diastereo- and enantioselectivities in most cases. In the reaction of an aliphatic nitron, low diastereoselectivity was observed, albeit the *endo* adduct was obtained in good yield and ee.

Table 38  
Catalytic enantioselective 1,3-dipolar cycloadditions

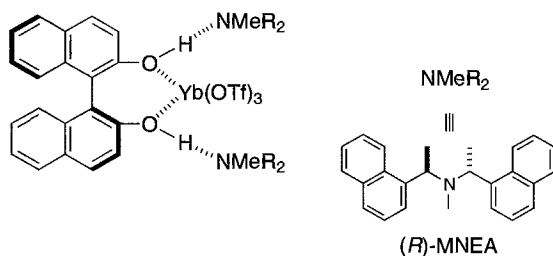
							
R <sup>1</sup>	R <sup>2</sup>	Without MS 4A			With MS 4A <sup>d</sup>		
		Yield (%)	endo/exo	ee <sup>c</sup> (%)	Yield (%)	endo/exo	ee (%)
Ph	CH <sub>3</sub>	90	99/1	83	92	99/1	−96
Ph	H	72	>99/1	88	91	>99/1	−79
Ph	C <sub>3</sub> H <sub>7</sub>	82	>99/1	83	89	98/2	−93
2-furyl	CH <sub>3</sub>	75	99/1	76	89	95/5	−89
1-naphthyl	CH <sub>3</sub>	83	97/3	81	88	98/2	−85
C <sub>2</sub> H <sub>5</sub>	CH <sub>3</sub>	79	53/47	79	88	53/47	−96

<sup>a</sup> Chiral Yb(III) = Yb(OTf)<sub>3</sub> + (*S*)-BINOL + (*R*)-MNEA.

<sup>b</sup> The corresponding nitron was added as an additive (see text).

<sup>c</sup> ee of the *endo* adducts.

<sup>d</sup> Reverse enantioselectivities were observed. See table 37.

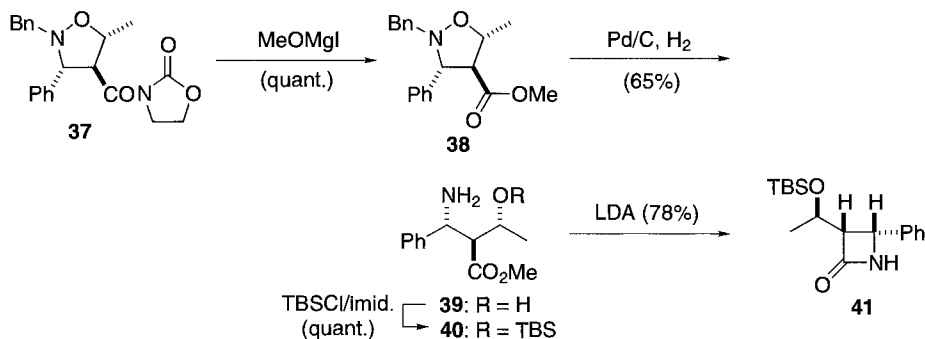


Scheme 16. Novel chiral hetero-chiral Yb(III) catalyst.

As for the structure of the hetero-chiral Yb(III) catalyst, the structure shown in scheme 16 was supported. Actually, the existence of hydrogen bonds between the phenolic hydrogens of (*S*)-BINOL and the nitrogens of (*R*)-MNEA was confirmed by the IR spectra of the catalyst<sup>2</sup>. Direct coordination of the amine to Yb(III) is doubtful in light of the fact that the 1,3-dipolar cycloaddition proceeded very slowly when Yb(OTf)<sub>3</sub> and (*R*)-MNEA were first combined and then (*S*)-BINOL was added (Fritsch and Zundel 1981).

6-Hydroxyethyl  $\beta$ -lactam derivative was synthesized using the present reactions (scheme 17). Isoxazolidine derivative **37**, prepared via the catalytic enantioselective 1,3-dipolar cycloaddition, was treated with methoxymagnesium iodide (Evans et al. 1985) to give methyl ester **38**. Reductive N–O bond cleavage and deprotection of

<sup>2</sup> A bond pair (953 and 987 cm<sup>−1</sup>), which indicated hydrogen bonds (the OH...N and O<sup>−</sup>...H<sup>+</sup>N equilibrium), was observed in the area from 930 to 1000 cm<sup>−1</sup> in the IR spectra of the hetero-chiral Yb(III) catalyst (Evans et al. 1985).

Scheme 17. Conversion to  $\beta$ -lactam.

the *N*-benzyl part of **38** was performed in the same pot using Pd/C under hydrogen atmosphere (10 kg/cm<sup>2</sup>) (Kametani et al. 1982) to afford amino ester **39**. After the resulting alcohol moiety was protected as its *t*-butyldimethylsilyl (TBS) ether, cyclization of **40** proceeded smoothly using lithiumdiisopropylamide (LDA) (Sekiya et al. 1981) to afford the corresponding  $\beta$ -lactam (**41**) (as for carbapenems and penems, Palomo 1990, Perrone and Franceschi 1990) in good yield.

## 11. Conclusions

The Ln(OTf)<sub>3</sub> are new types of Lewis acids different from typical Lewis acids such as AlCl<sub>3</sub>, BF<sub>3</sub>, SnCl<sub>4</sub>, etc. While most Lewis acids are decomposed or deactivated in the presence of water, the Ln(OTf)<sub>3</sub> are stable and work as Lewis acids in water solutions. Many nitrogen-containing compounds such as imines and hydrazones are also successfully activated by using a small amount of the Ln(OTf)<sub>3</sub>. The Ln(OTf)<sub>3</sub> are also excellent Lewis acid catalysts in organic solvents. A catalytic amount of Ln(OTf)<sub>3</sub> is enough to complete reactions in most cases, and the Ln(OTf)<sub>3</sub> can be recovered after the reactions, and can be reused. Moreover, asymmetric catalyses using chiral rare-earth catalysts are successfully carried out.

Recently, polymer-supported rare-earth catalysts have become an area of great interest. Use of rare-earth catalysts in the solid-phase organic synthesis is now well-recognized (Kobayashi 1999). There have also been many other transformations than carbon-carbon bond-forming reactions in organic synthesis using the Ln(OTf)<sub>3</sub> as catalysts, and all these will be reviewed in the near future.

## Acknowledgments

Our work in this area was partially supported by CREST, Japan Science and Technology Corporation (JST), and a Grant-in-Aid for Scientific Research from the Ministry of Education, Science, Sports, and Culture, Japan. The author thanks and expresses his deep gratitude to his coworkers whose names appear in the references. Mrs. Yuri Nakasugi is also acknowledged for her help in preparing the manuscript.

## References and Notes

- Alexakis, A., N. Lensen and P. Mangeney, 1991, *Synlett*, p. 625. Cf. Seebach and Wykypiel (1979).
- Almasio, M.-C., F. Arnaud-Neu and M.-J. Schwing-Weill, 1983, *Helv. Chim. Acta* **66**, 1296.
- Baer Jr, C.F., and R.E. Mesmer, 1976, *The Hydrolysis of Cations* (Wiley, New York) p. 129.
- Bao, J., W.D. Wulff and A.L. Rheingold, 1993, *J. Am. Chem. Soc.* **115**, 3814.
- Bednarski, M., C. Maring and S. Danishefsky, 1983, *Tetrahedron Lett.* **24**, 3451.
- Boger, D.L., 1983, *Tetrahedron* **39**, 2869.
- Boger, D.L., and S.M. Weinreb, 1987, *Hetero Diels-Alder Methodology in Organic Synthesis* (Academic Press, San Diego, CA) chs. 2, 9.
- Borrione, E., M. Prato, G. Scorrano and M. Stiranello, 1989, *J. Chem. Soc. Perkin Trans. 1*, 2245.
- Brown, J.M., A.C. Chapman, R. Harper, D.J. Mowthorpe, A.G. Davies and P.J. Smith, 1972, *J. Chem. Soc. Dalton Trans.*, p. 338.
- Burgess, K., H.-J. Lim, A.M. Porte and G.A. Sullikowski, 1996, *Angew. Chem. Int. Ed. Engl.* **35**, 220.
- Burk, M.J., and J.E. Feaster, 1992, *J. Am. Chem. Soc.* **114**, 6266.
- Carruthers, W., 1990, *Cycloaddition Reactions in Organic Synthesis* (Pergamon Press, Oxford).
- Chakraborty, T.K., G.V. Reddy and K.A. Hussain, 1991, *Tetrahedron Lett.* **32**, 7597.
- Chapuis, C., and J. Jurczak, 1987, *Helv. Chim. Acta* **70**, 436.
- Cheng, Y.S., E. Ho, P.S. Mariano and H.L. Ammon, 1985, *J. Org. Chem.* **56**, 5678, and references cited therein. As for the reactions of vinyl sulfides, see Narasaka and Shibata (1993).
- Claremon, D.A., P.K. Lumma and B.T. Phillips, 1986, *J. Am. Chem. Soc.* **108**, 8265.
- Collins, S., and Y. Hong, 1987, *Tetrahedron Lett.* **28**, 4391.
- Colvin, E.W., and D.G. McGarry, 1985, *J. Chem. Soc. Chem. Commun.*, p. 539.
- Corey, E.J., R. Imwinkelried, S. Pikul and Y.B. Xiang, 1989, *J. Am. Chem. Soc.* **111**, 5493.
- Corey, E.J., N. Imai and H.Y. Zhang, 1991, *J. Am. Chem. Soc.* **113**, 728.
- Cotton, F.A., and G. Wilkinson, 1988, *Advanced Inorganic Chemistry*, 5th Ed. (Wiley, New York) p. 973.
- Cramer, C.J., and D.G. Truhlar, eds, 1994, *Structure and Reactivity in Aqueous Solution* (American Chemical Society, Washington, DC).
- Danishefsky, S., and T. Kitahara, 1974, *J. Am. Chem. Soc.* **96**, 7807.
- Daude, G., and M. Pereyre, 1980, *J. Organometal. Chem.* **190**, 43.
- Davies, A.G., 1997, *Organotin Chemistry* (VCH, Weinheim).
- Davies, A.G., D.C. Kleinschmidt, P.R. Palan and S.C. Vasishtha, 1971, *J. Chem. Soc. C*, p. 3972.
- Denmark, S.E., T. Weber and D.W. Piotrowski, 1987, *J. Am. Chem. Soc.* **109**, 2224.
- Dubois, J.-E., and G. Axiotis, 1984, *Tetrahedron Lett.* **25**, 2143.
- Enders, D., H. Schubert and C. Nubling, 1986, *Angew. Chem. Int. Ed. Engl.* **25**, 1109.
- Enders, D., D. Ward, J. Adam and G. Raabe, 1996, *Angew. Chem. Int. Ed. Engl.* **35**, 981.
- Evans, D.A., M.M. Morrissey and R.L. Dorow, 1985, *J. Am. Chem. Soc.* **107**, 4346.
- Evans, D.A., S.J. Miller and T. Lectka, 1993, *J. Am. Chem. Soc.* **115**, 6460.
- Fendler, J.H., and E.J. Fendler, 1975, *Catalysis in Micellar and Macromolecular Systems* (Academic Press, London).
- Forsberg, J.H., V.T. Spaziano, T.M. Balasubramanian, G.K. Liu, S.A. Kinsley, C.A. Duckworth, J.J. Poteruca, P.S. Brown and J.L. Miller, 1987, *J. Org. Chem.* **52**, 1017.
- Frederickson, M., 1997, *Tetrahedron* **53**, 403.
- Fritsch, J., and G. Zundel, 1981, *J. Phys. Chem.* **85**, 556.
- Fukuzawa, S., K. Sato, T. Fujinami and S. Sakai, 1983, *J. Chem. Soc. Chem. Commun.*, p. 853.
- Gaut, H., and J. Skoda, 1946, *Bull. Soc. Chim. Fr.* **13**, 308.
- Gong, L., and A. Streitwieser, 1990, *J. Org. Chem.* **55**, 6235.
- Gothelf, K.V., and K.A. Jørgensen, 1994, *J. Org. Chem.* **59**, 5687.
- Gothelf, K.V., I. Thomsen and K.A. Jørgensen, 1996, *J. Am. Chem. Soc.* **118**, 59.
- Gothelf, K.V., R.G. Hazell and K.A. Jørgensen, 1998, *J. Org. Chem.* **63**, 5483.
- Grieco, P.A., and A. Bahsas, 1988, *Tetrahedron Lett.* **29**, 5855.
- Grieco, P.A., P. Garner and Z. He, 1983, *Tetrahedron Lett.* **24**, 1897.

- Grigos, V.I., L.S. Povarov and B.M. Mikhailov, 1965, *Izv. Akad. Nauk SSSR, Ser. Khim.*, p. 2163.
- Grigos, V.I., L.S. Povarov and B.M. Mikhailov, 1966, *Chem. Abstr.* **64**, 9680.
- Guanti, G., E. Narisano and L. Banfi, 1987, *Tetrahedron Lett.* **28**, 4331.
- Hachiya, I., and S. Kobayashi, 1993, *J. Org. Chem.* **58**, 6958.
- Haggin, J., 1994, *Chem. Eng. News*, April 18, p. 22.
- Hajos, Z.G., and D.R. Parrish, 1973, *J. Org. Chem.* **38**, 3244.
- Harpp, D.N., and M. Gingras, 1988, *J. Am. Chem. Soc.* **110**, 7737.
- Harrowfield, J.M., D.L. Kepert, J.M. Patrick and A.H. White, 1983, *Aust. J. Chem.* **36**, 483.
- Hart, F.A., 1987, in: *Comprehensive Coordination Chemistry*, Vol. 3, ed. G. Wilkinson (Pergamon Press, New York) p. 1059.
- Harusawa, S., R. Yoneda, Y. Omori and T. Kurihara, 1987, *Tetrahedron Lett.* **28**, 4189.
- Hashimoto, S., N. Komeshita and K. Koga, 1979, *J. Chem. Soc. Chem. Commun.*, p. 437.
- Hattori, K., and H. Yamamoto, 1992, *J. Org. Chem.* **57**, 3264.
- Hattori, K., and H. Yamamoto, 1994, *Tetrahedron* **50**, 2785.
- Holland, P.M., and D.N. Rubingh, eds, 1992, *Mixed Surfactant Systems* (American Chemical Society, Washington, DC).
- Hollis, T.K., N.P. Robinson and B. Bosnich, 1992, *J. Am. Chem. Soc.* **114**, 5464.
- Hori, K., H. Kodama, T. Ohta and I. Furukawa, 1996, *Tetrahedron Lett.* **37**, 5947.
- Ife, R.J., T.H. Brown, D.J. Keeling, C.A. Leach, M.L. Meeson, M.E. Parsons, D.R. Reavill, C.J. Theobald and K.J. Wiggall, 1992, *J. Med. Chem.* **35**, 3413.
- Ikeda, K., K. Achiwa and M. Sekiya, 1983, *Tetrahedron Lett.* **24**, 4707.
- Ishihara, K., Q. Gao and H. Yamamoto, 1993, *J. Am. Chem. Soc.* **115**, 10412.
- Ishihara, K., M. Miyata, K. Hattori, T. Tada and H. Yamamoto, 1994, *J. Am. Chem. Soc.* **116**, 10520.
- Ishitani, H., and S. Kobayashi, 1996, *Tetrahedron Lett.* **37**, 7357.
- Iyer, M.S., K.M. Gigstad, N.D. Namdev and M. Lipton, 1996, *J. Am. Chem. Soc.* **118**, 4910.
- Jensen, K.B., K.V. Gothelf, R.G. Hazell and K.A. Jørgensen, 1997, *J. Org. Chem.* **62**, 2471.
- Joh, T., and N. Hagihara, 1967, *Tetrahedron Lett.* 4199.
- Johnson, J.V., B.S. Rauckman, D.P. Baccanari and B. Roth, 1989, *J. Med. Chem.* **32**, 1942.
- Kagan, H.B., and O. Riant, 1992, *Chem. Rev.* **92**, 1007.
- Kametani, T., and H. Kasai, 1989, *Stud. Nat. Prod. Chem.* **3**, 385.
- Kametani, T., S.P. Huang, A. Nakayama and T. Honda, 1982, *J. Org. Chem.* **47**, 2328.
- Kametani, T., H. Takeda, Y. Suzuki, H. Kasai and T. Honda, 1986, *Heterocycles* **24**, 3385.
- Kaufmann, D., and R. Boese, 1990, *Angew. Chem. Int. Ed. Engl.* **29**, 545.
- Kawai, M., M. Onaka and Y. Izumi, 1986, *Chem. Lett.*, p. 1581.
- Kawai, M., M. Onaka and Y. Izumi, 1988, *Bull. Chem. Soc. Jpn.* **61**, 1237.
- Kim, E., D.M. Gordon, W. Schmid and G.M. Whitesides, 1993, *J. Org. Chem.* **58**, 5500.
- Kitamura, M., S. Okada, S. Suga and R. Noyori, 1989, *J. Am. Chem. Soc.* **111**, 4028.
- Kleinman, E.F., 1991, in: *Comprehensive Organic Synthesis*, Vol. 2, ed. B.M. Trost (Pergamon Press, Oxford) p. 893.
- Kobayashi, S., 1991, *Chem. Lett.*, p. 2187.
- Kobayashi, S., 1994, *Synlett*, p. 689.
- Kobayashi, S., 1999, *Chem. Soc. Rev.* **28**, 1.
- Kobayashi, S., and I. Hachiya, 1992, *Tetrahedron Lett.* **33**, 1625.
- Kobayashi, S., and I. Hachiya, 1994, *J. Org. Chem.* **59**, 3590.
- Kobayashi, S., and H. Ishitani, 1994, *J. Am. Chem. Soc.* **116**, 4083.
- Kobayashi, S., and H. Ishitani, 1995, *J. Chem. Soc. Chem. Commun.*, p. 1379.
- Kobayashi, S., and S. Nagayama, 1997a, *J. Am. Chem. Soc.* **119**, 10049.
- Kobayashi, S., and S. Nagayama, 1997b, *J. Org. Chem.* **62**, 232.
- Kobayashi, S., M. Murakami and T. Mukaiyama, 1985, *Chem. Lett.*, p. 1535.
- Kobayashi, S., I. Hachiya, T. Takahori, M. Araki and H. Ishitani, 1992, *Tetrahedron Lett.* **33**, 6815.
- Kobayashi, S., I. Hachiya and T. Takahori, 1993a, *Synthesis*, p. 371.
- Kobayashi, S., I. Hachiya, H. Ishitani and M. Araki, 1993b, *Synlett*, p. 472.
- Kobayashi, S., I. Hachiya, M. Araki and H. Ishitani, 1993c, *Tetrahedron Lett.* **34**, 3755.
- Kobayashi, S., I. Hachiya, H. Ishitani and M. Araki, 1993d, *Tetrahedron Lett.* **34**, 4535.

- Kobayashi, S., I. Hachiya and Y. Yamanoi, 1994a, *Bull. Chem. Soc. Jpn.* **67**, 2342.
- Kobayashi, S., M. Araki and I. Hachiya, 1994b, *J. Org. Chem.* **59**, 3758.
- Kobayashi, S., H. Ishitani, I. Hachiya and M. Araki, 1994c, *Tetrahedron* **50**, 11623.
- Kobayashi, S., H. Ishitani, M. Araki and I. Hachiya, 1994d, *Tetrahedron Lett.* **35**, 6325.
- Kobayashi, S., M. Araki, H. Ishitani, S. Nagayama and I. Hachiya, 1995a, *Synlett*, p. 233.
- Kobayashi, S., M. Araki and M. Yasuda, 1995b, *Tetrahedron Lett.* **36**, 5773.
- Kobayashi, S., H. Ishitani and S. Nagayama, 1995c, *Chem. Lett.*, p. 423.
- Kobayashi, S., H. Ishitani and S. Nagayama, 1995d, *Synthesis*, p. 1195.
- Kobayashi, S., T. Wakabayashi, S. Nagayama and H. Oyamada, 1997a, *Tetrahedron Lett.* **38**, 4559.
- Kobayashi, S., R. Akiyama, M. Kawamura and H. Ishitani, 1997b, *Chem. Lett.*, p. 1039.
- Kobayashi, S., H. Ishitani and M. Ueno, 1997c, *Synlett*, p. 115.
- Kobayashi, S., T. Furuta, K. Sugita and H. Oyamada, 1998a, *Synlett*, p. 1019.
- Kobayashi, S., T. Busujima and S. Nagayama, 1998b, *J. Chem. Soc. Chem. Commun.*, p. 19.
- Kobayashi, S., T. Busujima and S. Nagayama, 1998c, *J. Chem. Soc. Chem. Commun.*, p. 981.
- Kodata, I., J.-Y. Park and Y. Yamamoto, 1996, *J. Chem. Soc. Chem. Commun.*, p. 841.
- Larsen, S.D., P.A. Grieco and W.F. Fobare, 1986, *J. Am. Chem. Soc.* **108**, 3512.
- Leblanc, J., and H.W. Gibson, 1992, *Tetrahedron Lett.* **33**, 6295.
- Lubineau, A., 1986, *J. Org. Chem.* **51**, 2142.
- Lubineau, A., and E. Meyer, 1988, *Tetrahedron* **44**, 6065.
- Lucast, D.H., and J. Wemple, 1976, *Synthesis*, p. 724.
- Lucchini, V., M. Prato, G. Scorrano and P. Tecilla, 1988, *J. Org. Chem.* **53**, 2251.
- Luijten, J.G.A., and G.J.M. van der Kerk, 1955, *Investigations in the Field of Organotin Chemistry* (Tin Research Institute, Greenford) p. 106.
- Mai, K., and G. Patil, 1984, *Tetrahedron Lett.* **25**, 4583.
- Makioka, Y., T. Shindo, Y. Taniguchi, K. Takaki and Y. Fujiwara, 1995, *Synthesis*, p. 801.
- Manabe, K., H. Oyamada, K. Sugita and S. Kobayashi, 2000, *J. Org. Chem.*, in press.
- Markó, I.E., and G.R. Evans, 1994, *Tetrahedron Lett.* **35**, 2771.
- Maruoka, K., and H. Yamamoto, 1989, *J. Am. Chem. Soc.* **111**, 789.
- Maruoka, K., and H. Yamamoto, 1993, in: *Catalytic Asymmetric Synthesis*, ed. I. Ojima (VCH, Weinheim) p. 413.
- Maruoka, K., T. Itoh, T. Shirasaki and H. Yamamoto, 1988, *J. Am. Chem. Soc.* **110**, 310.
- Maruoka, K., A.B. Conception, N. Hirayama and H. Yamamoto, 1990, *J. Am. Chem. Soc.* **112**, 7422.
- Maruoka, K., A.B. Conception, N. Murase, M. Oishi and H. Yamamoto, 1993a, *J. Am. Chem. Soc.* **115**, 3943.
- Maruoka, K., N. Murase and H. Yamamoto, 1993b, *J. Org. Chem.* **5**, 2938.
- Matier, W.L., D.A. Owens, W.T. Comer, D. Deitchman, H.C. Ferguson, R.J. Seidehamel and J.R. Young, 1973, *J. Med. Chem.* **16**, 901.
- Mikami, K., M. Terada and T. Nakai, 1990, *J. Am. Chem. Soc.* **112**, 3949.
- Mikami, K., M. Terada, Y. Motoyama and T. Nakai, 1991, *Tetrahedron: Asymmetry* **2**, 643.
- Mikami, K., M. Terada and T. Nakai, 1993, *J. Chem. Soc. Chem. Commun.*, p. 343.
- Minakata, S., T. Ezoe, R. Ilhyong, M. Komatsu and Y. Ohshiro, 1997, presented at 72nd Annual Meeting of the Chemical Society of Japan, Tokyo, paper 2F3 37.
- Molander, G.A., 1992, *Chem. Rev.* **92**, 29.
- Mongin, F., J.-M. Fourquez, S. Rault, V. Levacher, A. Godard, F. Trecoart and G. Queguiner, 1995, *Tetrahedron Lett.* **36**, 8415.
- Mukai, C., S. Hashizume, K. Nagami and M. Hanaoka, 1990, *Chem. Pharm. Bull.* **38**, 1509.
- Mukaiyama, T., 1982, *Org. React.* **28**, 203.
- Mukaiyama, T., K. Narasaka and T. Banno, 1973, *Chem. Lett.*, p. 1011.
- Mukaiyama, T., K. Banno and K. Narasaka, 1974, *J. Am. Chem. Soc.* **96**, 7503.
- Mukaiyama, T., K. Kashiwagi and S. Matsui, 1989, *Chem. Lett.*, p. 1397.
- Mukaiyama, T., H. Akamatsu and J.S. Han, 1990, *Chem. Lett.*, p. 889.
- Mukaiyama, T., T. Ohno, J.S. Han and S. Kobayashi, 1991, *Chem. Lett.*, p. 949.
- Murata, S., M. Suzuki and R. Noyori, 1980, *Tetrahedron Lett.* **21**, 2527.
- Nakamura, E., M. Shimizu, I. Kuwajima, J. Sakata, K. Yokoyama and R. Noyori, 1983, *J. Org. Chem.* **48**, 932.
- Narasaka, K., 1991, *Synthesis*, p. 1.

- Narasaka, K., and T. Shibata, 1993, *Heterocycles* **35**, 1039.
- Narasaka, K., N. Iwasawa, M. Inoue, T. Yamada, M. Nakashima and J. Sugimori, 1989, *J. Am. Chem. Soc.* **111**, 5340.
- Narasaka, K., H. Tanaka and F. Kanai, 1991, *Bull. Chem. Soc. Jpn.* **64**, 387.
- Nomura, Y., M. Kimura, Y. Takeuchi and S. Tomoda, 1978, *Chem. Lett.*, p. 267.
- Noyori, R., K. Yokoyama, J. Sakata, I. Kuwajima, E. Nakamura and M. Shimizu, 1977, *J. Am. Chem. Soc.* **99**, 1265.
- Noyori, R., S. Murata and M. Suzuki, 1981, *Tetrahedron* **37**, 3899.
- Oguni, N., Y. Matsuda and T. Kaneko, 1988, *J. Am. Chem. Soc.* **110**, 7877.
- Ojima, I., S. Inaba and K. Nakatsugawa, 1975, *Chem. Lett.*, p. 331.
- Ojima, I., S.-I. Inaba and K. Yoshida, 1977, *Tetrahedron Lett.* 3643.
- Onaka, M., R. Ohno, N. Yanagiya and Y. Izumi, 1993, *Synlett*, p. 141.
- Ono, N., H. Miyake, M. Fujii and A. Kaji, 1983, *Tetrahedron Lett.* **24**, 3477.
- Overman, L.E., B.N. Rogers, J.E. Tellew and W.C. Trenkle, 1997, *J. Am. Chem. Soc.* **119**, 7159.
- Oyamada, H., and S. Kobayashi, 1998, *Synlett*, p. 249.
- Palomo, C., 1990, in: *Recent Progress in the Chemical Synthesis of Antibiotics*, eds G. Lukacs and M. Ohno (Springer, Heidelberg) p. 565.
- Peet, W.G., and W. Tam, 1983, *J. Chem. Soc. Chem. Commun.*, p. 853.
- Pereyre, M., J.-P. Quintard and A. Rahm, 1987, *Tin in Organic Synthesis* (Butterworths, London) p. 216.
- Perrone, E., and G. Franceschi, 1990, in: *Recent Progress in the Chemical Synthesis of Antibiotics*, eds G. Lukacs, M. Ohno (Springer, Heidelberg) p. 613.
- Posner, G.H., J.-C. Carry, J.K. Lee, D.S. Bull and H. Dai, 1994, *Tetrahedron Lett.* **35**, 1321.
- Povarov, L.S., 1967, *Russ. Chem. Rev.* **36**, 656.
- Puchot, C., O. Samuel, E. Dunach, S. Zhao, C. Agami and H. Kagan, 1986, *J. Am. Chem. Soc.* **108**, 2353.
- Quimpere, M., and K. Jankowski, 1987, *J. Chem. Soc. Chem. Commun.*, p. 676.
- Rauckman, B.S., M.Y. Tidwell, J.V. Johnson and B. Roth, 1989, *J. Med. Chem.* **32**, 1927.
- Reetz, M.T., S.-H. Kyung, C. Bolm and T. Zierke, 1986, *Chem. Ind.*, p. 824.
- Rideout, D.C., and R. Breslow, 1980, *J. Am. Chem. Soc.* **102**, 7816.
- Sabatini, D.A., R.C. Knox and J.H. Harwell, eds, 1995, *Surfactant-Enhanced Subsurface Remediation* (American Chemical Society, Washington, DC).
- Sanchez-Blanco, A.I., K.V. Gothelf and K.A. Jørgensen, 1997, *Tetrahedron Lett.* **38**, 7923.
- Sarges, R., A. Gallagher, T.J. Chambers and L.-A. Yeh, 1993, *J. Med. Chem.* **36**, 2828.
- Sartor, D., J. Saffrich, G. Helmchen, C.J. Richard and H. Lambert, 1991, *Tetrahedron Asym.* **2**, 639.
- Sasai, H., T. Suzuki, N. Itoh, K. Tanaka, T. Date, K. Okumura and M. Shibasaki, 1993, *J. Am. Chem. Soc.* **115**, 10372.
- Schinzer, D., ed., 1989, *Selectivities in Lewis Acid Promoted Reactions* (Kluwer Academic Publishers, Dordrecht).
- Schmid, W., and G.M. Whitesides, 1991, *J. Am. Chem. Soc.* **113**, 6674.
- Seebach, D., and W. Wykypiel, 1979, *Synthesis*, p. 423.
- Seebach, D., R.E. Marti and T. Hintermann, 1996, *Helv. Chim. Acta* **79**, 1710.
- Seerden, J.-P.G., A.W.A. Scholte op Reimer and H.W. Scheeren, 1994, *Tetrahedron Lett.* **35**, 4419.
- Seerden, J.-P.G., M.M.M. Kuypers and H.W. Scheeren, 1995, *Tetrahedron Asym.* **6**, 1441.
- Seerden, J.G., and H.W. Scheeren, 1993, *Tetrahedron Lett.* **34**, 2669.
- Sekiya, M., K. Ikeda and Y. Terao, 1981, *Chem. Pharm. Bull.* **29**, 1747.
- Shafran, Y.M., V.A. Bakulev and V.S. Mokrushin, 1989, *Russ. Chem. Rev.* **58**, 148.
- Shimada, S., K. Saigo, M. Abe, A. Sudo and M. Hasegawa, 1992, *Chem. Lett.*, p. 1445.
- Sisko, J., and S.M. Weinreb, 1989, *Tetrahedron Lett.* **30**, 3037.
- Snider, B.B., 1989, in: *Selectivities in Lewis Acid Promoted Reactions*, ed. D. Schinzer (Kluwer Academic Publishers, Dordrecht) pp. 147-167.
- Snider, B.B., D.J. Rodini, T.C. Kirk and R. Cordova, 1982, *J. Am. Chem. Soc.* **104**, 555.
- Stinson, S.C., 1993, *Chem. Eng. News*, September 27, p. 38.
- Stork, G., and M. Isobe, 1975, *J. Am. Chem. Soc.* **97**, 4745.
- Takahashi, H., K. Tomita and H. Otomasu, 1979, *J. Chem. Soc. Chem. Commun.*, p. 668.
- Takai, K., and C.H. Heathcock, 1985, *J. Org. Chem.* **50**, 3247.



- Tanaka, M., 1980, *Tetrahedron Lett.* **21**, 2959.
- Thom, K.F., 1971, US Patent 3615169; *Chem. Abstr.* **76**, 5436a.
- Torsell, K.B.G., 1988, *Nitrile Oxides, Nitrones and Nitronates in Organic Synthesis* (VCH, Weinheim).
- Tsuji, J., M. Nisar and I. Minami, 1986, *Tetrahedron Lett.* **27**, 2483.
- Tufariello, J.J., 1984, in: *1,3-Dipolar Cycloaddition Chemistry*, ed. A. Padwa (Wiley, Chichester) Vol. 2, p. 83.
- Vougioukas, A.E., and H.B. Kagan, 1987, *Tetrahedron Lett.* **28**, 5513.
- Waldmann, H., 1994, *Synthesis*, p. 535.
- Weinreb, S.M., 1991, in: *Comprehensive Organic Synthesis*, ed. B.M. Trost (Pergamon Press, Oxford) Vol. 5, p. 401.
- Weinstock, L.M., P. Davis, B. Handelsman and R. Tull, 1967, *J. Org. Chem.* **32**, 2823.
- Worth, D.F., S.C. Perricini and E.F. Elslager, 1970, *J. Heterocyclic Chem.* **7**, 1353.
- Yamamoto, Y., and N. Asao, 1993, *Chem. Rev.* **93**, 2207.
- Yamamoto, Y., H. Yatagai, Y. Naruta and K. Maruyama, 1980, *J. Am. Chem. Soc.* **102**, 7107.
- Yanagisawa, A., H. Inoue, M. Morodome and H. Yamamoto, 1993, *J. Am. Chem. Soc.* **115**, 10356.
- Yates, D., and P.E. Eaton, 1960, *J. Am. Chem. Soc.* **82**, 4436.

## AUTHOR INDEX

- Aaltonen, J., see Valden, M. 217  
 Abdillahi, M.M., see Al-jarallah, A.M. 278, 299  
 Abe, K., see Imamura, H. 58, 62, 63  
 Abe, M., see Shimada, S. 328  
 Abouarnadasse, S., see Perrichon, V. 181, 203, 232  
 Abul Milh, M., see Lindstedt, A. 142  
 Achard, J.C., see Barrault, J. 14, 15, 23, 24, 36, 40, 41  
 Achard, J.C., see Paul-Boncour, V. 22, 24, 41  
 Achard, J.C., see Wang, Z.L. 24, 25, 41  
 Achiwa, K., see Ikeda, K. 328  
 Adachi, G., see Arakawa, T. 278  
 Adachi, G., see Corré, S. 17  
 Adachi, G., see Masui, T. 185, 240  
 Adam, J., see Enders, D. 333, 335  
 Addullayev, A.F., see Alimardanov, K.M. 302  
 Adelman, B.J., see Lei, G.D. 303  
 Agami, C., see Puchot, C. 361  
 Agarwal, D.D. 90, 91  
 Ahola, J., see Maunula, T. 204, 211, 213, 220  
 Aiko, K.I. 34  
 Akamatsu, H., see Mukaiyama, T. 328  
 Akiyama, R., see Kobayashi, S. 333, 365  
 Akolekar, D.B., see Choudhary, V.R. 274, 282  
 Akporiaye, D., see Gaare, K. 274, 278, 300  
 Akporiaye, D.E. 274, 281, 300  
 Al-jarallah, A.M. 278, 299  
 Albers, E.A., see Scherzer, J. 285  
 Alby, D., see Spagnol, M. 299  
 Alcock, C.B. 99, 100  
 Alcock, C.B., see Gunasekaran, N. 123, 124  
 Alexakis, A. 335  
 Algarra, F. 283  
 Alimardanov, K.M. 302  
 Almasio, M.-C. 316  
 Altman, E.I. 217, 218  
 Alyamosvkii, S.I., see Pal'guev, S.F. 240  
 Amenomiya, Y. 222  
 Amesz, D.J., see Schaper, H. 83  
 Amiridis, M.D. 160, 303  
 Ammon, H.L., see Cheng, Y.S. 347  
 Amouzegh, P. 300  
 Andersen, A.G., see Yi, G. 90, 91  
 Andersen, J.E.T., see Warren, J.P. 9, 39  
 Andersen, J.N. 63–65  
 Anderson, D.L., see Kitto, M.E. 284  
 Anderson, D.R., see Murrell, L.L. 201–203, 230–232  
 Andersson, A., see Hansen, S. 90, 91  
 Andersson, S., see Löf, P. 207, 211, 215, 217–219, 224  
 Andersson, S., see Zhang, Y. 239, 240, 257  
 Andersson, S.L.T., see Otamiri, J.C. 131  
 Ando, H. 22  
 Andreeva, A.B., see Leonov, A.I. 237, 239  
 Andresen, A.F. 63  
 Andriamasinoro, D., see Rehmspringer, J.L. 100  
 Andrianova, M.P., see Isupova, L.A. 128  
 Andryushkova, O.V., see Isupova, L.A. 128  
 Angell, C.A., see Rabo, J.A. 278, 281, 284  
 Anonymous 252  
 Antonio, M.R. 278  
 Aozasa, S., see Murota, T. 239, 241, 246, 248, 252  
 Apai, G., see Gysling, H.J. 84, 85, 107–109  
 Aparicio, L.A., see Ulla, M.A. 278  
 Aparicio, L.M. 302  
 Arai, H. 116, 117, 121, 122, 126–128  
 Arai, H., see Machida, M. 127  
 Arai, T. 218  
 Arai, T., see Li, C. 187, 204  
 Arakawa, T. 115, 278  
 Arakawa, T., see Sakamoto, E. 276, 303, 304  
 Araki, M., see Kobayashi, S. 325, 329, 330, 344, 345, 355, 358, 362  
 Arashi, H., see Yashima, M. 237–239  
 Araujo, A.S., see Zinner, L.B. 274, 282, 296  
 Arcoya, A., see Martinez-Arias, A. 216, 255  
 Ardito, S.C. 298  
 Armengol, E. 299  
 Armor, J.M. 303  
 Armor, J.N. 213

- Armor, J.N., see Li, Y. 303  
 Arnaud-Neu, F., see Almasio, M.-C. 316  
 Arroyo, P.A., see Corma, A. 291  
 Asao, N., see Yamamoto, Y. 337, 340  
 Ashjian, H., see Ardito, S.C. 298  
 Atkinson, G.B. 22  
 Atkinson, G.B., see Baglin, E.G. 26, 27  
 Ausen, S.A., see Summers, J.C. 201, 204, 211, 212  
 Avudaitalai, M., see Kutty, T.R.N. 151  
 Avvakumov, E.G., see Isupova, L.A. 128  
 Axiotis, G., see Dubois, J.-E. 328  
 Azbel, B.I. 274, 302
- Baba, T. 54, 56, 274, 278, 301  
 Baba, T., see Tanaka, T. 55, 56, 278  
 Baccanari, D.P., see Johnson, J.V. 362  
 Badri, A. 187, 203, 232, 255  
 Badri, A., see Laachir, A. 172, 174, 179, 181, 183, 192, 255  
 Baerlocher, Ch., see Meier, W.M. 270, 272, 273  
 Baerns, M., see Zhang, Z. 100  
 Baerns, M., see Zhao, Z.L. 197  
 Baes Jr, C.F. 316  
 Baglin, E.G. 26, 27  
 Bahsas, A., see Grieco, P.A. 347, 348  
 Baiker, A. 115, 117  
 Baiker, A., see Kritzenberger, J. 49  
 Baiker, A., see Marti, P.E. 82, 115, 117  
 Bailey, J.A., see Cho, B.K. 213, 214, 219, 220  
 Baird, R.J., see Yao, M.H. 240, 244, 245  
 Baker, R.T., see Colon, G. 243  
 Baker, R.W., see Scherzer, J. 285  
 Bakshi, N., see Gunasekaran, N. 123, 124  
 Bakulev, V.A., see Shafraun, Y.M. 340  
 Balachandran, U. 96, 97  
 Balandin, A.A. 66  
 Balasubramanian, T.M., see Forsberg, J.H. 316  
 Baldi, G., see Saracco, G. 80, 125, 126  
 Balducci, G. 239, 249, 250  
 Balducci, G., see Fornasiero, P. 174, 181, 195, 238, 239, 248, 249, 252  
 Balducci, G., see Ranga Rao, G. 172, 200, 234, 252, 254  
 Balkus, K.J. 284  
 Balkus, K.J., see Bresinska, I. 278  
 Balkus, K.J., see Young, S.W. 284  
 Ballivet-Tkatchenko, D. 38  
 Balse, V.R., see Ulla, M.A. 278
- Banfi, L., see Guanti, G. 332  
 Bankirov, A.N., see Kagan, Y.B. 27  
 Banno, K., see Mukaiyama, T. 317  
 Banno, T., see Mukaiyama, T. 317  
 Bao, J. 359, 360  
 Baran, J.E. 77  
 Barbier, J. 162, 226–228  
 Barbier, J., see Maillet, T. 162, 227  
 Barbier Jr, J. 181, 191, 192, 224, 225, 227–229  
 Barmby, D.S., see Kirsch, F.W. 290, 292  
 Barrault, J. 14, 15, 23, 24, 36, 40, 41, 77  
 Barrault, J., see Paul-Boncour, V. 22, 24, 41  
 Barrault, J., see Wang, Z.L. 24, 25, 41  
 Bartley, G.J.J. 30  
 Bass, J.L., see Scherzer, J. 278, 282  
 Batwara, J.M., see Mehrotra, R.C. 48  
 Baumgartner, W., see Schulz, H. 299  
 Bechman, C.A., see Wallace, W.E. 32  
 Bednarski, M. 354, 360  
 Beguin, B. 83  
 Beguin, F., see Moreau, S. 78, 82, 83  
 Bekyarova, E. 252  
 Belhekar, A.A., see Choudhary, V.R. 92–96  
 Belitz, R.K., see Shyu, J.Z. 230, 231  
 Bell, A.T., see Brown Bourzutschky, J.A. 109–111  
 Bell, A.T., see Chin, A.A. 217  
 Bell, A.T., see Hecker, W.C. 213, 214  
 Bell, A.T., see Pande, N.K. 214, 215, 217, 218  
 Bell, A.T., see Rojas, M.L. 109, 110  
 Bell, A.T., see Tascón, J.M.D. 85  
 Bell, R.G., see Brennan, D. 279  
 Bellussi, G., see Kiricsi, Y. 293  
 Belot, G., see Serre, C. 185, 190, 193, 200, 211, 212  
 Belton, D.N., see Hori, C.E. 250  
 Belton, D.N., see Permana, H. 237, 251, 252  
 Belton, D.N., see Schmieg, S.J. 172  
 Belzner, A., see Gur, T.M. 95  
 Ben Taarit, Y. 275  
 Bennett, C.O., see Simon, M.W. 281  
 Bennett, J.M. 278  
 Bennett, J.M., see Smith, J.V. 278, 279, 281  
 Bensalem, A. 257  
 Bensalem, A., see Bozon-Verduraz, F. 187  
 Bergeret, G., see Perrichon, V. 172, 175, 177, 179–181, 184  
 Berlo, R.C., see Furst, A. 70  
 Bernal, S. 175, 177, 179, 181–183, 192, 193, 198, 201, 202, 229, 232, 247, 254, 257, 258  
 Bernal, S., see Colon, G. 243

- Bernal, S., see Laachir, A. 185  
 Bernhardt, P., see Weibel, M. 223  
 Berry, F.J. 278  
 Bertel, E., see Netzer, F. 6, 13, 22, 31  
 Bertel, E., see Netzer, F.P. 63  
 Berthet, P., see Michel, D. 239  
 Bevan, D.J.M. 175  
 Beyer, H.K. 276, 278  
 Beyer, H.K., see Karge, H.G. 275–278, 285  
 Bezouhanova, C.P. 302  
 Bhasin, M.M., see Keller, G.E. 97  
 Bhawal, B.M., see Reddy, T.I. 301  
 Binet, C. 232  
 Binet, C., see Badri, A. 203, 232  
 Binet, C., see Colon, G. 243  
 Binet, C., see Daturi, M. 181  
 Bini, G., see de Leitenburg, C. 90, 91, 174, 179, 239, 240  
 Bini, G., see Lago, R. 94  
 Bjornkvist, L., see Löf, P. 215, 217, 219, 224  
 Blanchard, F., see Fajardie, F. 252, 256  
 Blanchard, G., see Cuif, J.P. 2, 242, 243  
 Blanchard, G., see Daturi, M. 181  
 Blanchard, G., see Perrichon, V. 181, 203, 232  
 Blanco, G., see Bernal, S. 175, 198, 202, 232, 247, 257, 258  
 Blasse, G., see Hazenkamp, M.F. 275, 278  
 Blazek, J.J., see Magee, J.S. 275, 276, 285  
 Blouri, B. 47  
 Blumenthal, R.N., see Chiang, H.W. 178  
 Boaro, M., see Terribile, D. 185  
 Boccuzzi, F., see Guglielminotti, E. 257  
 Boersma, J., see Hogerheide, M.P. 46  
 Boese, R., see Kaufmann, D. 354  
 Boger, D.L. 347, 362  
 Böhlinger, W., see Schulz, H. 299  
 Bolm, C., see Reetz, M.T. 360  
 Bolton, A.P. 282, 298  
 Bonagamba, T.J., see Nery, J.G. 278, 279  
 Bond, G.C. 69  
 Bonelle, J.P., see Sohier, M.P. 9, 19  
 Bonnelle, J.P., see Lamonier, C. 177  
 Bonvin, J.O., see Hansen, S. 90, 91  
 Borbely, G., see Karge, H.G. 275–277  
 Borovinskaya, I.P., see Merzhanov, A.G. 78  
 Borrione, E. 362  
 Bose, A.C., see Balachandran, U. 96, 97  
 Bosnich, B., see Hollis, T.K. 345  
 Bossi, A. 33  
 Botana, F.J., see Bernal, S. 192, 193, 201, 202, 229, 232, 254, 257  
 Boujana, S., see El Fallah, J. 179, 181–184, 191, 195  
 Bourgogne, M., see Feron, B. 290  
 Boutonnet-Kizling, M., see Binet, C. 232  
 Boyle, J.E., see Rabo, J.A. 284, 302  
 Bozon-Verduraz, F. 187  
 Bozon-Verduraz, F., see Bensalem, A. 257  
 Braaten, N.A. 9  
 Braconnier, J.J., see Bernal, S. 257  
 Bradley, S.A., see Nunan, J.G. 233, 234  
 Brait, A. 284  
 Branco, J., see Ballivet-Tkatchenko, D. 38  
 Breault, R., see Lavalley, J.C. 216  
 Breck, D.W. 270  
 Brenan, D. 279  
 Brenner, A., see Halasz, I. 132  
 Brenner, A., see Hori, C.E. 250  
 Brenner, A., see Permana, H. 237, 251, 252  
 Bresinska, I. 278  
 Breslow, R., see Rideout, D.C. 345  
 Breyse, M. 204, 205, 257  
 Brezny, R., see Egami, T. 249  
 Brieger, G. 70  
 Brinen, J.S. 108  
 Brogan, M.S. 202, 211, 230  
 Brousard, J.A. 109  
 Brown, J.G., see Dyer, A. 278  
 Brown, J.M. 344  
 Brown, L.M. 48  
 Brown, P.S., see Forsberg, J.H. 316  
 Brown, T.H., see Ife, R.J. 362  
 Brown Bourzutschky, J.A. 109–111  
 Bruce, L.A. 174, 179–181, 183  
 Brundle, C.R., see Siegmann, H.C. 8, 40  
 Bruning, H.C.A.M., see van Vucht, J.H.N. 63  
 Bryan, S.J. 7, 28  
 Bugli, G., see Bensalem, A. 257  
 Buitrago, R.H., see Marcos, J. 86, 87, 112, 113  
 Bull, D.S., see Posner, G.H. 365  
 Bunluesin, T. 204–209, 252, 255  
 Bunluesin, T., see Cordatos, H. 194, 204, 208–210, 217–219, 255  
 Burch, R. 30  
 Burch, R., see Bartley, G.J.J. 30  
 Burewicz, A., see Wachowski, L. 84  
 Burgers, M.H.W., see Ito, E. 275, 303, 304  
 Burgess, K. 367  
 Burk, M.J. 333, 336  
 Burwell Jr, R.L. 67  
 Burwell Jr, R.L., see Rowlinson, H.C. 67  
 Buschow, K.H.J. 63

- Busujima, T., see Kobayashi, S. 333, 340, 343  
 Butler, V. 257  
  
 Cable, T.L., see Mazanec, T.J. 95  
 Cabrera, A.L., see Luengo, C.A. 22  
 Cairns, J.A., see Brogan, M.S. 202, 211, 230  
 Calis, H.P.A., see Ito, E. 303, 304  
 Calleja, G., see van Grieken, R. 109–111  
 Calvino, J.J., see Bernal, S. 175, 177, 179, 181–183, 193, 201, 202, 229, 232, 254, 257  
 Calvino, J.J., see Laachir, A. 185  
 Camorim, V.L.D., see Sousa-Aguiar, E.F. 278, 282  
 Campbell, C.T. 217  
 Campbell, K.D. 102, 103  
 Campman, M.A.J., see Nibbelke, R.H. 212, 224  
 Cant, N.W., see Dumpelmann, R. 213  
 Cant, N.W., see Padeste, C. 177, 187, 200, 209, 216, 217, 232  
 Carberry, J.J., see Alcock, C.B. 99, 100  
 Carberry, J.J., see Gunasekaran, N. 122–124, 139  
 Cardona-Martinez, N., see Diaz-Mendoza, F.A. 295  
 Carpenter, J.E., see Oh, S.H. 203, 207, 213, 214, 217  
 Carreiro, L. 84  
 Carreyre, H., see Richard, F. 299  
 Carruthers, W. 345  
 Carry, J.-C., see Posner, G.H. 365  
 Carvajal, R. 281, 283  
 Cataluna, R., see Martinez-Arias, A. 216, 255  
 Catherine, E., see Laachir, A. 172, 174, 179, 181, 183, 192, 255  
 Catlow, C.R.A., see Brenan, D. 279  
 Catlow, C.R.A., see Butler, V. 257  
 Catlow, C.R.A., see Sayle, T.X.T. 176, 179, 204, 232, 242  
 Cauqui, M.A., see Bernal, S. 175, 193, 198, 201, 202, 232, 254, 257, 258  
 Cavani, F., see de Leitenburg, C. 90, 91, 174, 179, 239, 240  
 Centi, G. 206, 303  
 Cha, C., see Yang, M. 3  
 Chakraborty, T.K. 341  
 Chakravorty, D., see Chatterjee, A. 239, 243  
 Chambers, T.J., see Sarges, R. 362  
 Chan, K.S. 88, 89  
 Chandler, C.D. 78  
 Chang, C.D. 298  
 Chang, Ch.-T., see Liu, S.-B. 274, 278  
 Chao, K.J., see Foley, H.C. 108  
 Chao, K.J., see Lin, C.F. 278, 280, 281  
 Chao, K.-J. 278  
 Chaouki, J., see Kirchnerova, J. 123  
 Chapman, A.C., see Brown, J.M. 344  
 Chappell, R.J., see Burch, R. 30  
 Chapuis, C. 354  
 Charnell, J.F., see Olson, D.H. 278, 279  
 Chatikavanij, V., see Klier, K. 110  
 Chatterjee, A. 239, 243  
 Chatterjee, S. 302  
 Cheetham, A.K. 278, 279, 281  
 Chen, G., see Wang, G. 299  
 Chen, I.W., see Li, P. 177  
 Chen, N.Y. 270  
 Chen, Q.J. 278, 280  
 Chen, Y.L. 239  
 Chen, Y.-W., see Yang, S.-J. 290  
 Chen, Z., see Yang, M. 3  
 Cheng, Y.S. 347  
 Chester, A.W., see Chu, Y.F. 291  
 Chetina, O.V. 37, 40  
 Chevrier, M., see Rogemond, E. 184, 232  
 Chiang, H.W. 178  
 Chiang, P.H. 152, 153  
 Chiche, B. 274, 299  
 Chiche, B., see Gauthier, C. 274, 300  
 Chien, M.W. 80  
 Chin, A.A. 217  
 Chinchin, G.C. 27, 30  
 Cho, B.K. 213, 214, 219, 220, 225, 247, 257  
 Choi, J.G., see Jung, H.J. 130  
 Choi, K.-Y., see Lee, C.-Y. 303  
 Choisset, J., see Moreau, S. 78, 82, 83  
 Chojnacki, T. 10, 11, 40  
 Chorkendorff, I., see Andersen, J.N. 65  
 Choudhary, V.R. 92–96, 119, 197, 198, 274, 282  
 Christiansen, N., see Gordes, P. 78  
 Christmann, K. 59  
 Christopher, J., see Swamy, C.S. 137  
 Chu, P.-J., see Carvajal, R. 281, 283  
 Chu, Y.F. 291  
 Chuah, G.K. 243  
 Chuah, G.K., see Chan, K.S. 88, 89  
 Church, M.L. 162, 163  
 Chyou, P., see Johnson, J.R. 14, 16, 40  
 Cifredo, G.A., see Bernal, S. 175, 177, 179, 181–183, 193, 201, 202, 229, 232, 247, 254, 257

- Cifredo, G.A., see Laachir, A. 185  
 Claremon, D.A. 333, 335  
 Clarke, D.R., see Sergo, V. 175  
 Claudel, B., see Breysse, M. 204, 205, 257  
 Clerici, M.G., see Flego, C. 274, 293, 295  
 Climent, M.J., see Corma, A. 299  
 Cohn, M.J., see Nunan, J.G. 233, 234  
 Colliex, C., see Wang, Z.L. 24, 25, 41  
 Collin, J., see Kagan, H.B. 3  
 Collins, S. 316  
 Colon, G. 243  
 Colvin, E.W. 328  
 Comer, W.T., see Matier, W.L. 340  
 Concepcion, A.B., see Maruoka, K. 317  
 Conception, A.B., see Maruoka, K. 317  
 Conesa, J.C. 176, 179, 180, 204  
 Conesa, J.C., see Martinez-Arias, A. 216, 223, 255, 256  
 Conesa, J.C., see Soria, J. 206, 232  
 Conner Jr, W.C. 69  
 Coon, V.T. 22  
 Coon, V.T., see Wallace, W.E. 32  
 Cooper, A.S., see Voorhoeve, R.J.H. 140  
 Cooper, B.J., see Church, M.L. 162, 163  
 Corchado, P., see Bernal, S. 198, 257, 258  
 Cordatos, H. 171, 194, 204, 208–210, 217–219, 255  
 Cordatos, H., see Bunluesin, T. 204, 206–208, 255  
 Cordova, R., see Snider, B.B. 317  
 Corey, E.J. 354  
 Corma, A. 270, 272, 273, 283, 284, 287, 289–291, 295, 298, 299  
 Corma, A., see Algarra, F. 283  
 Corma, A., see Armengol, E. 299  
 Corré, S. 17  
 Costenoble, M.L. 278  
 Cotton, F.A. 354, 356, 359  
 Coughlan, B. 280  
 Coulon, M., see Barrault, J. 23, 24, 41  
 Courcelle, J.-C., see Maugé, F. 281  
 Courtine, P., see Sri Rahayu, W. 122, 123  
 Craig, R.S., see Coon, V.T. 22  
 Craig, R.S., see Elattar, A. 22  
 Craig, R.S., see Takeshita, T. 31  
 Craig, R.S., see Wallace, W.E. 32, 63  
 Cramer, C.J. 326  
 Creaser, D.A., see Harrison, P.G. 242  
 Cremers, A. 275  
 Cremers, A., see Marynen, P. 281  
 Cremona, A., see Ranga Rao, G. 172, 200, 234, 252, 254  
 Crespin, M. 84, 85, 107  
 Crespin, M., see Levitz, P. 85  
 Crow, J.E., see Otamiri, J.C. 131  
 Csicsery, S.M., see Hickson, D.A. 276  
 Cuif, J.P. 2, 242, 243  
 Cullinane, D., see Cunningham, J. 193, 229, 232  
 Cunningham, J. 181, 182, 193, 229, 232  
 Da Silva, P.N. 229  
 Daasvatn, K., see Akporiaye, D.E. 274, 281, 300  
 Dahl, I.M., see Rørbik, T. 293  
 Dahl, L., see Skoglundh, M. 142, 143  
 Dai, H., see Posner, G.H. 365  
 Dai, L., see Li, Q. 278, 280  
 D'Angremond, M., see Struijk, J. 51  
 Danishefsky, S. 347  
 Danishefsky, S., see Bednarski, M. 354, 360  
 Das, D. 276  
 Date, T., see Sasai, H. 354  
 Datta, A., see Chatterjee, A. 239, 243  
 Daturi, M. 181  
 Daturi, M., see Colon, G. 243  
 Datye, A.K. 2, 229, 232  
 Daude, G. 337  
 Dauscher, A. 257  
 Davies, A.G. 344  
 Davies, A.G., see Brown, J.M. 344  
 Davis, P., see Weinstock, L.M. 340  
 De, M., see Chatterjee, A. 239, 243  
 de Collongue, B. 80, 126  
 de Groot, R.L., see Roelofsen, J.W. 278, 280  
 de Jonge, A., see Gárdos, G. 293  
 de Leitenburg, C. 90, 91, 174, 179, 216, 229, 232, 235, 239, 240, 247–249, 257  
 de Leitenburg, C., see Kašpar, J. 213, 214, 217, 225, 256  
 de Leitenburg, C., see Terribile, D. 185, 243, 244  
 de Leitenburg, C., see Trovarelli, A. 177, 181, 189–191, 200, 216, 218, 229, 232, 234, 242, 252  
 de Leitenburg, C., see Zamar, F. 174, 243, 247, 252, 257  
 DeCanio, S.J., see Foley, H.C. 108  
 Degnan, T.F., see Ardito, S.C. 298  
 Degnan, T.F., see Chen, N.Y. 270  
 Degobert, P. 161, 167, 168

- Deitchman, D., see Matier, W.L. 340  
 Delamar, M., see Bensalem, A. 257  
 deLange, M. 213  
 Delmon, B., see Parvulescu, V.I. 303  
 Delosh, R.G., see Gandhi, H.S. 169  
 Deng, G. 302  
 Deng, J.F., see Jiang, A.R. 132  
 Denmark, S.E. 333, 335  
 Denny, P.J., see Chinchin, G.C. 30  
 Dent, A., see Shaw, E.A. 27  
 Dettling, J.C. 241  
 Dexpert, H., see El Fallah, J. 179, 181–184, 191, 195  
 Dexpert, H., see Paul-Boncour, V. 22  
 Di Monte, R. 246, 249, 252, 253, 255, 256  
 Di Monte, R., see Balducci, G. 239, 249  
 Di Monte, R., see Fornasiero, P. 174, 181, 195, 238, 239, 241, 247–249, 252  
 Di Monte, R., see Ranga Rao, G. 172, 200, 218, 234, 239, 241, 246–248, 252, 254  
 Diaz-Mendoza, F.A. 295  
 Dibansa, L., see Herrmann, J.M. 257  
 Dictor, R. 201, 202  
 Dines, T.J., see Brogan, M.S. 202, 211, 230  
 Dion, M., see Barrault, J. 77  
 Disalvo, F.J., see Voorhoeve, R.J.H. 140  
 Diwell, A.F. 201, 226  
 Diwell, A.F., see Harrison, B. 186, 187, 191, 249  
 Dixon, A.G., see Tsai, C.Y. 97  
 Djega-Mariadassou, G., see Fajardie, F. 252, 256  
 Dmowski, W., see Egami, T. 249  
 Dobson, N.A. 53  
 Doesburg, E.B.M., see Schaper, H. 83  
 Doi, K., see Livage, J. 239  
 Dolcetti, G., see de Leitenburg, C. 239, 240, 247–249, 257  
 Dolcetti, G., see Terribile, D. 185, 243, 244  
 Dolcetti, G., see Trovarelli, A. 177, 181, 189–191, 200, 216, 218, 229, 232, 234, 242, 252  
 Dolcetti, G., see Zamar, F. 174, 243, 247, 252, 257  
 Domen, K. 151, 152  
 Domen, K., see Arai, T. 218  
 Domen, K., see Li, C. 187, 204, 206, 216  
 Donato, A., see Galvagno, S. 51  
 Dorow, R.L., see Evans, D.A. 369  
 dos Santos, R.L.C., see Sousa-Aguiar, E.F. 278, 282  
 Doshi, R., see Alcock, C.B. 99, 100  
 Dougan, T.J. 290  
 Drouillard, J., see Richard, F. 299  
 Du, Y. 237  
 Dubois, J.-E. 328  
 Duckworth, C.A., see Forsberg, J.H. 316  
 Dufuax, M., see Meriaudeau, P. 229  
 Dumesic, J.A., see Aparicio, L.M. 302  
 Dumesic, J.A., see Ulla, M.A. 278  
 Dumpelmann, R. 213  
 Dunach, E., see Puchot, C. 361  
 Duplan, J.L. 201  
 Duprez, D. 226  
 Duprez, D., see Barbier, J. 162, 226–228  
 Duprez, D., see Barbier Jr, J. 181, 191, 192, 224, 225, 227–229  
 Duprez, D., see Barrault, J. 23, 36  
 Duprez, D., see Maillat, T. 162, 227  
 Duprez, D., see Martin, D. 184, 193, 194, 250  
 Duprez, D., see Taha, R. 179, 193, 250, 254  
 Duran, P. 237  
 Dusek, J.T., see Balachandran, U. 96, 97  
 Dutel, J.F., see Meriaudeau, P. 229  
 Duwez, P. 237, 240  
 Dwight, K., see Carreiro, L. 84  
 Dwyer, F.G. 295  
 Dybowski, C., see Foley, H.C. 108  
 Dyer, A. 270, 278  
 Eaton, P.E., see Yates, D. 345  
 Ebina, Y., see Domen, K. 151, 152  
 Eddy, M.M., see Cheetham, A.K. 278, 279, 281  
 Edelmann, F.T. 46  
 Edwards, G.C., see Scherzer, J. 285  
 Efsthathiou, A.M., see Simon, M.W. 281  
 Egami, T. 249  
 Eglinton, G., see Dobson, N.A. 53  
 Eguchi, K., see Arai, H. 116, 117, 121, 122, 126–128  
 Eguchi, K., see Machida, M. 127  
 Eguchi, K., see Seiyama, T. 88  
 Eickel, C.C., see Oh, S.H. 203, 204, 206, 207, 211–214  
 El Azhar, M., see Primet, M. 201  
 El Fallah, J. 179, 181–184, 191, 195  
 El Fallah, J., see Laachir, A. 172, 174, 179, 181, 183, 192, 255  
 El-nafaty, U.A., see Al-jarallah, A.M. 278, 299  
 Elattar, A. 22  
 Elattar, A., see Wallace, W.E. 32, 63  
 Ellestad, O.H., see Rørbik, T. 275, 293

- Elslager, E.F., see Worth, D.F. 347  
 Enders, D. 333, 335  
 Eng, D. 152  
 Eng, D., see Chiang, P.H. 152, 153  
 Engelhard, P., see Maugé, F. 281  
 Engelhardt, G., see Hunger, M. 278  
 Engler, B. 206  
 Epelbaum, E.T., see Azbel, B.I. 274, 302  
 Eriksson, B., see Andersen, J.N. 63–65  
 Ertl, G., see Christmann, K. 59  
 Essayem, N., see Rogemond, E. 184, 232  
 Esser, W.H., see Wortel, Th.M. 299  
 Estadt, M.M., see Grenoble, D.C. 221  
 Etsell, T.H. 257  
 Evans, D.A. 354, 369  
 Evans, G.R., see Markó, I.E. 365, 367  
 Eyring, L., see Kang, Z.C. 175–177, 180  
 Eyzat, P. 171  
 Ezerets, A.M., see Forni, L. 142  
 Ezoe, T., see Minakata, S. 365
- Fajardie, F. 252, 256  
 Fan, L. 229  
 Faraldos, M., see Corma, A. 287, 291  
 Farrauto, R.J. 231  
 Farrauto, R.J., see Amiridis, M.D. 160, 303  
 Farrauto, R.J., see Heck, R.M. 162–165, 167, 235, 237  
 Farrell, F., see Cunningham, J. 232  
 Feast, S. 299  
 Feaster, J.E., see Burk, M.J. 333, 336  
 Feiken, N., see Hazenkamp, M.F. 275, 278  
 Fender, B.E.F., see Butler, V. 257  
 Fendler, E.J., see Fendler, J.H. 326  
 Fendler, J.H. 326  
 Fengqi, Z., see Yiguang, T. 278  
 Fengyi, Li, see Jianhui, Li 9, 13, 36  
 Fengyi, Li, see Weiqi, Lu 9, 13, 36, 40  
 Ferguson, H.C., see Matier, W.L. 340  
 Fernandez, A., see Munuera, G. 211, 232  
 Feron, B. 290  
 Ferrero, A., see Di Monte, R. 246, 252, 256  
 Ferrero, A., see Fornasiero, P. 174, 181, 195, 238, 239, 248, 249  
 Fierro, J.L.G. 84, 85, 110, 129, 130, 172, 181, 182  
 Fierro, J.L.G., see Cunningham, J. 181, 182, 193, 229, 232  
 Fierro, J.L.G., see Lago, R. 94  
 Fierro, J.L.G., see Milt, V.G. 123, 124, 141
- Fierro, J.L.G., see Rodríguez-Ramos, I. 145–148  
 Fierro, J.L.G., see Rojas, M.L. 109, 110  
 Fierro, J.L.G., see Tascón, J.M.D. 84  
 Fierro, J.L.G., see Tejuca, L.G. 76, 85, 106, 140  
 Fierro, J.L.G., see van Grieken, R. 109–111  
 Find, J., see Sulikowski, B. 277  
 Finetti, P., see Trovarelli, A. 177, 181, 191, 200, 218, 229, 232, 234  
 Finiels, A., see Chiche, B. 274, 299  
 Finiels, A., see Gauthier, C. 274, 300  
 Finiels, A., see Moreau, P. 297  
 Finniels, A., see Amouzegh, P. 300  
 Finocchio, E., see Colon, G. 243  
 Fisher, G.B., see Oh, S.H. 203, 207, 213, 214, 217  
 Fisher, G.B., see Root, T.W. 217  
 Fisher, R. 302  
 Flanigan, E.M., see Smith, J.V. 278, 279, 281  
 Flanigen, E.M., see van Bekkum, H. 270  
 Flego, C. 274, 293, 295  
 Flego, C., see Kiricsi, Y. 293  
 Fleisch, T.H. 272, 276  
 Flengas, S.N., see Etsell, T.H. 257  
 Floor, M. 299  
 Flytzani-Stephanopoulos, M., see Li, Z. 304  
 Flytzani-Stephanopoulos, M., see Liu, W. 204, 206, 257  
 Flytzani-Stephanopoulos, M., see Tschope, A. 204  
 Flytzani-Stephanopoulos, M., see Zhang, Y. 274, 276, 278, 303  
 Fobare, W.F., see Larsen, S.D. 317, 348  
 Foley, H.C. 108  
 Ford, D., see Cordatos, H. 171, 208  
 Fornasiero, P. 174, 181, 191–193, 195, 234–236, 238, 239, 241, 247–253, 256  
 Fornasiero, P., see Balducci, G. 239, 249, 250  
 Fornasiero, P., see Bekyarova, E. 252  
 Fornasiero, P., see Di Monte, R. 246, 249, 252, 253, 255, 256  
 Fornasiero, P., see Kašpar, J. 213, 214, 217, 225, 256  
 Fornasiero, P., see Ranga Rao, G. 172, 200, 234, 252, 254  
 Fornasiero, P., see Vidmar, P. 239, 249–251, 257, 259  
 Fornasiero, P., see Vlaic, G. 248  
 Fornés, V., see Algarra, F. 283  
 Fornés, V., see Corma, A. 283, 287



- Forni, L. 142  
 Forost, M.P., see Petrov, A.A. 53  
 Forsberg, J.H. 316  
 Forzatti, P., see Centi, G. 303  
 Föster, H., see Jia, M. 278  
 Fournelle, R.A., see Chiang, H.W. 178  
 Fourquez, J.-M., see Mongin, F. 362  
 Fraissard, J., see Chen, Q.J. 278, 280  
 Fraissard, J., see Herreros, B. 276, 278  
 Fraissard, J., see Kim, J.-G. 278, 280  
 France, J., see Wallace, W.E. 26  
 France, J.E. 13, 24, 26, 41  
 Franceschi, G., see Perrone, E. 370  
 Frederickson, M. 365  
 Freeland, P.E., see Voorhoeve, R.J.H. 115  
 Freifelder, M. 53  
 Frestad, A., see Löf, P. 207, 211, 215, 217–219, 224  
 Frety, R., see Da Silva, P.N. 229  
 Frety, R., see Perrichon, V. 172, 175, 177, 179–181, 184  
 Frety, R., see Primet, M. 201  
 Frety, R., see Rogemond, E. 184, 232  
 Frety, R., see Tournayan, L. 174  
 Frety, R., see Zotin, F.M.Z. 173, 177, 181, 192  
 Fripiat, J., see Crespin, M. 85  
 Fritsch, E., see Baiker, A. 115, 117  
 Fritsch, J. 359, 369  
 Fritz, A. 303  
 Frost, J.C. 30  
 Frye Jr, J.G., see Mazanec, T.J. 95  
 Fu, X., see Zhong, Z. 124, 125  
 Fujii, H. 82  
 Fujii, H., see Mizuno, N. 80, 81  
 Fujii, M., see Ono, N. 317  
 Fujii, T. 66  
 Fujimoto, K., see Fan, L. 229  
 Fujimoto, K., see Nozaki, T. 105  
 Fujinami, T., see Fukuzawa, S. 337  
 Fujita, K., see Imamura, H. 70–72  
 Fujita, T., see Matsuda, T. 149  
 Fujitani, Y. 241  
 Fujitani, Y., see Shinjoh, H. 213  
 Fujiwara, K., see Masui, T. 185, 240  
 Fujiwara, M., see Ando, H. 22  
 Fujiwara, Y., see Makioka, Y. 347  
 Fukuda, H., see Teraoka, Y. 132  
 Fukuoka, Y. 51  
 Fukuzawa, S. 337  
 Funabiki, T. 257  
 Fung, S.C., see Tauster, S.J. 229  
 Furst, A. 70  
 Furukawa, H., see Iwamoto, M. 303  
 Furukawa, H., see Teraoka, Y. 132, 133  
 Furukawa, I., see Hori, K. 365  
 Furukawa, S., see Teraoka, Y. 95  
 Furukawa, Y., see Niwa, M. 216, 218  
 Furuta, T., see Kobayashi, S. 333  
 Gaare, K. 274, 278, 300  
 Gaffet, E., see Michel, D. 239  
 Galasso, F.S. 77  
 Gale, J.D., see Balducci, G. 250  
 Gallagher, A., see Sarges, R. 362  
 Gallagher, P.K. 80  
 Gallagher, P.K., see Johnson Jr, D.W. 80, 122  
 Gallagher, P.K., see Vogel, E.M. 84  
 Gallagher, P.K., see Voorhoeve, R.J.H. 140  
 Gallezot, P., see Feron, B. 290  
 Gallezot, P., see Maugé, F. 281  
 Galvagno, S. 51  
 Gandhi, H.S. 169  
 Gandhi, H.S., see Shyu, J.Z. 188, 190, 230, 231, 246  
 Ganne, M., see Barrault, J. 77  
 Gao, L., see Yu, Z. 148  
 Gao, P.Y., see Jiang, A.R. 132  
 Gao, Q., see Ishihara, K. 354  
 Garbassi, F., see Bossi, A. 33  
 Garbowski, E., see Beguin, B. 83  
 Garbowski, E., see de Collongue, B. 80, 126  
 Garcia, H., see Algarra, F. 283  
 Garcia, H., see Armengol, E. 299  
 Garcia, H., see Corma, A. 299  
 Garcia, R., see Bernal, S. 192  
 Gárdos, G. 292, 293  
 Garin, F., see Serre, C. 185, 190, 193, 200, 211, 212  
 Garin, F., see Weibel, M. 223  
 Garner, P., see Grieco, P.A. 345  
 Garten, R.L., see Tauster, S.J. 229  
 Garvie, R.C. 239  
 Gates, B.C., see Foley, H.C. 108  
 Gatica, J.M., see Bernal, S. 175, 177, 181–183, 193, 201, 202, 232, 257  
 Gatineau, L., see Crespin, M. 85, 107  
 Gatineau, L., see Levitz, P. 85  
 Gauckler, L.J., see Nakamura, T. 84  
 Gaur, H.A., see Roelofsen, J.W. 278, 280  
 Gaut, H. 319  
 Gauthier, C. 274, 300  
 Gauthier, C., see Chiche, B. 274, 299

- Gauthier, C., see Rogemond, E. 184, 232  
 Gauthier, C., see Taha, R. 179  
 Gavra, Z., see Johnson, J.R. 14–16, 40  
 Gellman, A.J., see Jaffey, D.M. 65  
 Geneste, P., see Amouzegh, P. 300  
 Geneste, P., see Chiche, B. 274, 299  
 Geneste, P., see Gauthier, C. 274, 300  
 Geneste, P., see Goux, A. 297  
 Geneste, P., see Moreau, P. 297  
 Gerard, V.K., see Hogerheide, M.P. 46  
 Geremia, S., see Vlaic, G. 248  
 Gerhard, W., see Weitkamp, J. 302  
 German, R.G., see Klier, K. 110  
 Gerzeliev, I.M., see Ivanova, I.I. 283  
 Ghatikar, M.N., see Hatwar, T.K. 55  
 Ghijsen, J., see Andersen, J.N. 65  
 Gianetto, G., see Lemos, F. 283, 285  
 Gibson, H.W., see Leblanc, J. 341  
 Gigstad, K.M., see Iyer, M.S. 344  
 Gilbert, L., see Spagnol, M. 299  
 Gillis-D'Hamers, I., see Voort, P.V.D. 48  
 Ginestar, E., see Amouzegh, P. 300  
 Gingras, M., see Harpp, D.N. 337  
 Girard, P., see Le Normand, F. 35, 41  
 Givens, E.N., see Venuto, P.B. 284  
 Glavee, G.N., see Overbury, S.H. 250  
 Gobinathan, R., see Settu, T. 239  
 Godard, A., see Mongin, F. 362  
 Goi, D., see de Leitenburg, C. 257  
 Goldschmidt, V.M. 76  
 Goldshleger, N.F., see Azbel, B.I. 274, 302  
 Golunski, S.E. 232–234  
 Golunski, S.E., see Burch, R. 30  
 Gómez, V., see Corma, A. 291  
 Gong, J., see Zhong, Z. 124, 125  
 Gong, L. 317  
 Gonzales, M., see Duran, P. 237  
 Gonzales-Elipse, A.R., see Munuera, G. 211, 232  
 Goodall, R.D. 284  
 Goodenough, J.B. 77  
 Goodman, D.W., see Oh, S.H. 203, 207, 213, 214, 217  
 Goodman, D.W., see Xu, X. 218  
 Gopalakrishnan, J., see Rao, C.N.R. 77  
 Gordes, P. 78  
 Gordon, D.M., see Kim, E. 338  
 Gordon, G.E., see Kitto, M.E. 284  
 Gorte, J., see Zafiris, G.S. 194, 204, 206–208, 211, 223  
 Gorte, R.J., see Altman, E.I. 217, 218  
 Gorte, R.J., see Bunluesin, T. 204–209, 252, 255  
 Gorte, R.J., see Cordatos, H. 171, 194, 204, 208–210, 217–219, 255  
 Gorte, R.J., see Putna, E.S. 208, 211, 252  
 Gorte, R.J., see Zafiris, G.S. 208, 209, 218  
 Goss, M.F., see Garvie, R.C. 239  
 Goswami, H.S., see Agarwal, D.D. 90, 91  
 Gothelf, K.V. 365, 367  
 Gothelf, K.V., see Jensen, K.B. 365  
 Gothelf, K.V., see Sanchez-Blanco, A.I. 365  
 Gotoh, Y., see Corré, S. 17  
 Gounlett, R.M., see Shaw, E.A. 27  
 Goux, A. 297  
 Graham, G.W. 257  
 Graham, G.W., see Bunluesin, T. 209, 252  
 Graham, G.W., see Putna, E.S. 252  
 Graham, G.W., see Shelef, M. 160, 163, 212, 213, 256  
 Graham, G.W., see Shyu, J.Z. 230, 231  
 Graham, G.W., see Sinev, M.Y. 239, 247, 257, 258  
 Graham, G.W., see Usmen, R.K. 247, 257  
 Grange, P., see Parvulescu, V.I. 303  
 Graziani, M., see Balducci, G. 239, 249, 250  
 Graziani, M., see Bekyarova, E. 252  
 Graziani, M., see Daturi, M. 181  
 Graziani, M., see Di Monte, R. 246, 249, 252, 253, 255, 256  
 Graziani, M., see Fornasiero, P. 174, 181, 191–193, 195, 234–236, 238, 239, 241, 247–253, 256  
 Graziani, M., see Kašpar, J. 213, 214, 217, 225, 256  
 Graziani, M., see Ranga Rao, G. 172, 200, 218, 234, 239, 241, 246–248, 252, 254  
 Graziani, M., see Vidmar, P. 239, 249–251, 257, 259  
 Graziani, M., see Vlaic, G. 248  
 Greene, H.L., see Chatterjee, S. 302  
 Grenoble, D.C. 221  
 Grepstad, J.K., see Braaten, N.A. 9  
 Grey, F., see Andersen, J.N. 65  
 Grieco, P.A. 345, 347, 348  
 Grieco, P.A., see Larsen, S.D. 317, 348  
 Griffin, T.A., see Zwinkels, M.F.M. 115, 125, 129  
 Griffith, W.P., see Hewkin, D.J. 48  
 Grigos, V.I. 362  
 Grosmanin, J., see Maugé, F. 281  
 Grosset, C., see Barrault, J. 77

- Grünert, W. 278, 281  
 Gruy, F. 241  
 Guanti, G. 332  
 Gubitosa, G., see Di Monte, R. 246, 252, 256  
 Gubitosa, G., see Fornasiero, P. 174, 181, 195, 238, 239, 248, 249  
 Gubitosa, G., see Ranga Rao, G. 172, 200, 234, 252, 254  
 Guenin, M., see Breyse, M. 204, 205, 257  
 Guenin, M., see Da Silva, P.N. 229  
 Guenin, M., see Primet, M. 201  
 Guerrero-Ruiz, A., see Rodríguez-Ramos, I. 145–148  
 Guglielminotti, E. 257  
 Guilleminot, A., see Barrault, J. 14, 15, 23, 24, 36, 40, 41  
 Guiru, W., see Xiangsheng, W. 297  
 Guisnet, M., see Lemos, F. 283, 285  
 Gunasekaran, N. 122–124, 139  
 Gunasekaran, N., see Alcock, C.B. 99, 100  
 Gupta, L.C., see Hatwar, T.K. 55  
 Gupta, L.C., see Rao, C.N.R. 55  
 Gur, T.M. 95  
 Gutmann, V., see Warf, J.C. 48  
 Gysling, H.J. 84, 85, 107–109
- Ha, B.-H., see Lee, C.-Y. 303  
 Ha, Y.H., see Tsai, C.Y. 97  
 Haack, L.P. 278, 280  
 Haack, L.P., see Sinev, M.Y. 239, 247, 257, 258  
 Haario, H., see Mannila, P. 204  
 Haario, H., see Maunula, T. 204, 211, 213, 220  
 Haas, O., see Müller, S. 152  
 Hachiya, I. 337  
 Hachiya, I., see Kobayashi, S. 319, 320, 324, 325, 329, 344, 345, 355, 358, 362  
 Hadenfeldt, C. 48, 54  
 Hadenfeldt, C., see Juza, R. 46, 53, 54  
 Haggin, J. 324  
 Hagihara, N., see Joh, T. 347  
 Hairston, D.W. 270  
 Hajos, Z.G. 317  
 Haku, E., see Imamura, H. 51  
 Halasz, I. 132  
 Hall, J.B., see Fleisch, T.H. 272, 276  
 Hall, W.K., see Crespin, M. 84, 85  
 Hall, W.K., see van Damme, H. 151  
 Haller, G.L., see Oyama, S.T. 63  
 Hallett, C., see Harrison, B. 186, 187, 191, 249  
 Halmos, F., see Gárdos, G. 293  
 Hamakawa, S., see Yi, G. 90, 91  
 Hamilton, L.A., see Venuto, P.B. 276, 284, 295, 296, 298  
 Hampden-Smith, M.J., see Chandler, C.D. 78  
 Han, J.S., see Mukaiyama, T. 325, 328  
 Hanada, T., see Baba, T. 54, 56, 278  
 Hanada, T., see Tanaka, T. 55  
 Hanaoka, M., see Mukai, C. 325  
 Hanaoka, T., see Kim, J.H. 297  
 Hanaoka, T., see Sugi, Y. 275, 278, 297, 298  
 Handelsman, B., see Weinstock, L.M. 340  
 Haneda, M. 196, 197, 206  
 Haneda, M., see Miki, T. 190, 247, 257  
 Hansen, S. 90, 91  
 Hansford, R.C., see Ward, J.W. 282  
 Harada, T., see Teraoka, Y. 132, 133  
 Harandi, M.N. 299  
 Hardacre, C. 39, 204, 206  
 Harding, J.H., see Butler, V. 257  
 Harivololona, R., see Herrmann, J.M. 257  
 Harji, B.H., see Shalabi, M.A. 204  
 Harkonen, M., see Mannila, P. 204  
 Harkonen, M., see Maunula, T. 204, 211, 213, 220  
 Harkonen, M., see Valden, M. 217  
 Harper, R., see Brown, J.M. 344  
 Harpp, D.N. 337  
 Harrison, B. 186, 187, 191, 249  
 Harrison, P.G. 242  
 Harrowfield, J.M. 316  
 Hart, F.A. 359  
 Hartner, H. 70  
 Harusawa, S. 343, 344  
 Harwell, J.H., see Sabatini, D.A. 326  
 Hasegawa, M., see Shimada, S. 328  
 Hasegawa, T., see Murota, T. 239, 241, 246, 248, 252  
 Hashimoto, S. 354  
 Hashizume, S., see Mukai, C. 325  
 Hasimoto, K. 302  
 Hatano, M., see Otsuka, K. 172, 199, 200, 218, 222, 229  
 Hatch, L.F. 284  
 Hatcher, H.A., see Golunski, S.E. 232–234  
 Hattori, K. 328, 359  
 Hattori, K., see Ishihara, K. 362  
 Hatwar, T.K. 55  
 Hawkes, C.M., see Owen, G. 26–30  
 Hawthorne, W.P., see Plank, C.J. 284  
 Hay, C.M. 29  
 Hayakawa, T., see Yi, G. 90, 91  
 Hazell, R.G., see Gothelf, K.V. 367

- Hazell, R.G., see Jensen, K.B. 365  
 Hazen, E.E., see Thompson, D.S. 46, 53  
 Hazenkamp, M.F. 275, 278  
 He, Z., see Grieco, P.A. 345  
 Heathcock, C.H., see Takai, K. 317  
 Heck, R.M. 162–165, 167, 235, 237  
 Hecker, W.C. 213, 214  
 Hegarty, B.F. 67  
 Hegde, M., see Ramesh, S. 131, 132  
 Helmchen, G., see Sartor, D. 354  
 Helton, T.E., see Ardito, S.C. 298  
 Herein, D., see Sulikowski, B. 277  
 Herpin, A. 13  
 Herreros, B. 276, 278  
 Herrmann, J.M. 257  
 Herrmann, J.M., see Bernal, S. 229, 232, 257  
 Hertz, R.K. 170, 171  
 Herz, R.K. 172, 173, 223  
 Hewkin, D.J. 48  
 Hickson, D.A. 276  
 Higgins, J.B., see Treacy, M.M. 270, 272  
 Hikita, S., see Baba, T. 54, 56, 274, 278, 301  
 Hilaire, L., see Barrault, J. 23, 24, 41  
 Hilaire, L., see Dauscher, A. 257  
 Hilaire, L., see Laachir, A. 172, 174, 179, 181, 183, 192, 255  
 Hilaire, L., see Le Normand, F. 35, 41, 181, 183  
 Hilaire, L., see Sim, K.S. 17, 18  
 Hindermann, J.P., see Lavalley, J.C. 216  
 Hintermann, T., see Seebach, D. 365  
 Hiranaka, S., see Imamura, H. 57, 59, 61, 62, 64, 65, 71  
 Hirano, S., see Kawabata, A. 239  
 Hirayama, N., see Maruoka, K. 317  
 Hirose, T., see Yashima, M. 237  
 Hirota, K., see Kawabata, A. 239  
 Hishida, T. 66  
 Hix, G.B., see Slade, R.C.T. 278  
 Ho, E., see Cheng, Y.S. 347  
 Ho, H., see Villarubia, J.S. 217  
 Hoang, M., see Bruce, L.A. 174, 179–181, 183  
 Hoang-Van, C., see Herrmann, J.M. 257  
 Hobson, M.C., see Farrauto, R.J. 231  
 Hoebink, J.H.B.J., see Nibbelke, R.H. 212, 224  
 Hogerheide, M.P. 46  
 Holderich, W., see Lerner, H. 300  
 Hölderich, W.F. 299, 301  
 Hölderich, W.F., see Fisher, R. 302  
 Hölderich, W.F., see Weyrich, P.A. 302  
 Holgado, J.P. 191, 193  
 Holland, P.M. 326  
 Hollis, T.K. 345  
 Homs, N., see Brown Bourzutschky, J.A. 109–111  
 Honda, T., see Kametani, T. 347, 370  
 Honec, M., see Mravec, D. 297  
 Hong, S.B. 274, 278  
 Hong, S.J. 240  
 Hong, Y., see Collins, S. 316  
 Hongchen, G., see Xiangsheng, W. 297  
 Honna, K. 302  
 Hoost, T.E., see Yao, M.H. 240, 244, 245  
 Hooton, S., see Furst, A. 70  
 Hori, C.E. 250  
 Hori, C.E., see Permana, H. 237, 251, 252  
 Hori, H., see Aiko, K.I. 34  
 Hori, K. 365  
 Hoskins, B.F. 176, 177  
 Hou, S.G., see Tian, Y.G. 278  
 Howell, K. 54  
 Hu, Z. 195  
 Huang, S.P., see Kametani, T. 370  
 Huang, T.J. 291  
 Hubbard, C.P., see Haack, L.P. 278, 280  
 Huggins, R.A., see Gur, T.M. 95  
 Hughes, A.E., see Bruce, L.A. 174, 179–181, 183  
 Huizinga, T. 211  
 Hultermans, R.J. 305  
 Hultermans, R.J., see Ito, E. 275, 303, 304  
 Hunger, M. 278  
 Hunger, M., see Weiß, U. 274, 283  
 Hunter, F.D. 278, 279, 281  
 Hunter, F.D., see Scherzer, J. 278, 282  
 Huntley, D.R., see Overbury, S.H. 250  
 Hussain, K.A., see Chakraborty, T.K. 341  
 Hustad, B., see Mostad, H. 274, 275, 293, 294  
 Iannibello, A., see Saracco, G. 80, 125, 126  
 Ichihara, M., see Mitsuhashi, T. 239  
 Ichikawa, M., see Imamura, H. 72  
 Ichiki, T., see Nitadori, T. 115–117, 138  
 Ichimura, K. 106, 107  
 Ife, R.J. 362  
 Igarashi, H., see Mizuno, N. 80, 81  
 Igawa, K., see Imamura, H. 68  
 Ihm, S.-K., see Moon, Y.H. 38, 39  
 Ikeda, K. 328  
 Ikeda, K., see Otsuka-Yao-Matsuo, S. 239  
 Ikeda, K., see Sekiya, M. 370  
 Ikeda, S., see Domen, K. 151, 152

- Ikeda, S., see Soga, K. 13, 63  
 Ikegami, T., see Yashima, M. 237  
 Ikemoto, M. 282  
 Iler, R.K. 47, 48  
 Ilhyong, R., see Minakata, S. 365  
 Imai, H. 37  
 Imai, H., see Tagawa, T. 98  
 Imai, N., see Corey, E.J. 354  
 Imamoto, T. 19, 20, 46  
 Imamura, H. 8, 9, 13, 34, 35, 37, 38, 46–54,  
 56–66, 68, 70–72  
 Imamura, H., see Konishi, T. 49, 53  
 Imamura, H., see Soga, K. 13, 63  
 Imamura, H., see Wallace, W.E. 16, 63  
 Imwinkelried, R., see Corey, E.J. 354  
 Inaba, S., see Ojima, I. 341  
 Inaba, S.-I., see Ojima, I. 328, 332  
 Inoue, H., see Yanagisawa, A. 337  
 Inoue, M., see Narasaka, K. 354  
 Inoue, Y., see Ichimura, K. 106, 107  
 Inui, T. 1  
 Inumaru, K. 46  
 Inumaru, K., see Wang, Y. 137, 138  
 Ioannides, T. 257  
 Ione, K.G. 297  
 Isakov, Ya.I., see Azbel, B.I. 274, 302  
 Ishige, M., see Zinner, L.B. 274, 296  
 Ishihara, K. 354, 362  
 Ishii, Y., see Shiraishi, H. 3  
 Ishitani, H. 363  
 Ishitani, H., see Kobayashi, S. 325, 329, 333,  
 336, 340, 341, 344, 345, 347, 355, 362, 365  
 Ishizawa, N., see Yashima, M. 237, 238, 240  
 Islam, M.S., see Balducci, G. 250  
 Isobe, M., see Stork, G. 317  
 Isogai, A., see Matsumoto, S. 241  
 Isogai, A., see Ozawa, M. 2, 239–241, 246  
 Isupova, L.A. 128  
 Ito, E. 275, 303, 304  
 Ito, E., see Hultermans, R.J. 305  
 Ito, T., see Chen, Q.J. 278, 280  
 Ito, T., see Kim, J.-G. 278, 280  
 Itoh, N., see Sasai, H. 354  
 Itoh, T., see Maruoka, K. 354  
 Ivanov, V.P., see Isupova, L.A. 128  
 Ivanova, I.I. 283  
 Iwamoto, M. 303  
 Iwamoto, M., see Sato, S. 303  
 Iwasawa, N., see Narasaka, K. 354  
 Iwasawa, Y. 12  
 Iwasawa, Y., see Shido, T. 222  
 Iyer, M.S. 344  
 Iyer, P.S. 278, 287  
 Izu, N. 239  
 Izu, N., see Otsuka-Yao-Matsuo, S. 239  
 Izumi, Y., see Kawai, M. 317  
 Izumi, Y., see Onaka, M. 328  
 Jabur, F.A., see Bezouhanova, C.P. 302  
 Jackson, R.A., see Brenan, D. 279  
 Jacobs, H., see Hadenfeldt, C. 48, 54  
 Jacobs, P.A. 278  
 Jacobs, P.A., see Weitkamp, J. 302  
 Jadi, A., see Binet, C. 232  
 Jaenicke, S., see Chan, K.S. 88, 89  
 Jaenicke, S., see Chuah, G.K. 243  
 Jaffey, D.M. 65  
 Janaceck, I., see Pollert, E. 131  
 Jankowski, K., see Quimper, M. 354  
 Jansen, J.C., see van Bekkum, H. 270  
 Jansson, K., see Skoglundh, M. 142, 143  
 Jansson, K., see Teraoka, Y. 144  
 Järås, S.G., see Zwinkels, M.F.M. 115, 125,  
 129  
 Jehanno, G., see Paul-Boncour, V. 24, 41  
 Jen, H.-W., see Rokosz, M.J. 274, 305  
 Jennings, J.R. 31  
 Jennings, J.R., see Bryan, S.J. 7, 28  
 Jennings, J.R., see Hay, C.M. 29  
 Jennings, J.R., see Nix, R.M. 11, 28, 29, 33, 41  
 Jennings, J.R., see Owen, G. 26–30  
 Jennings, J.R., see Shaw, E.A. 27  
 Jennings, J.R., see Walker, A.P. 31  
 Jensen, E.J., see Gordes, P. 78  
 Jensen, K.B. 365  
 Jia, M. 278  
 Jiang, A.R. 132  
 Jiang, J.C., see Whittington, B.J. 226, 227  
 Jianhui, Li 9, 13, 36  
 Jianhui, Li, see Weiqi, Lu 9, 13, 36, 40  
 Jin, T. 208, 209, 223  
 Jinku, H., see Slade, R.C.T. 278  
 Jirak, Z., see Pollert, E. 131  
 Jobacho, A., see Bernal, S. 193, 201, 232, 254  
 Jobson, E., see Kritzenberger, J. 49  
 Joh, T. 347  
 Johnson, D.W., see Vogel, E.M. 85  
 Johnson Jr, D.W. 80, 122  
 Johnson Jr, D.W., see Gallagher, P.K. 80  
 Johnson Jr, D.W., see Vogel, E.M. 84  
 Johnson, J.R. 14–16, 40  
 Johnson, J.V. 362

- Johnson, J.V., see Rauckman, B.S. 362  
 Johnson, M.F.L. 177–181, 235  
 Johnson, R.L., see Andersen, J.N. 65  
 Johnstone, R.A.W. 70  
 Jørgensen, K.A., see Gothelf, K.V. 365, 367  
 Jørgensen, K.A., see Jensen, K.B. 365  
 Jørgensen, K.A., see Sanchez-Blanco, A.I. 365  
 Jozefowicz, L.C., see Karge, H.G. 276, 282  
 Jozsef, A., see Hultermans, R.J. 305  
 Juan-Rajadell, M.I., see Corma, A. 291  
 Judd, R.W., see Nix, R.M. 29, 41, 63–65  
 Jung, H.J. 130  
 Junggreen, H., see Mostad, H. 274, 275, 293, 294  
 Jurczak, J., see Chapuis, C. 354  
 Jurdo, J.R., see Duran, P. 237  
 Juza, R. 46, 53, 54  
 Juza, R., see Hadenfeldt, C. 48, 54  
 Juza, R., see Linde, V.G. 48
- Kacimi, S., see Taha, R. 193, 250, 254  
 Kaddouri, A., see Reh Springer, J.L. 100  
 Kagan, H., see Puchot, C. 361  
 Kagan, H.B. 3, 354  
 Kagan, H.B., see Vougioukas, A.E. 317  
 Kagan, Y.B. 27  
 Kagawa, S., see Iwamoto, M. 303  
 Kagawa, S., see Teraoka, Y. 132, 133, 144  
 Kaji, A., see Ono, N. 317  
 Kakihana, M., see Du, Y. 237  
 Kakihana, M., see Yashima, M. 237–239  
 Kakuta, N., see Haneda, M. 196, 197, 206  
 Kakuta, N., see Miki, T. 190, 247, 257  
 Kalakkad, D.S., see Datye, A.K. 2, 229, 232  
 Kalenik, Z., see Miró, E.E. 98  
 Kamegashira, N. 86  
 Kametani, T. 347, 362, 370  
 Kanai, F., see Narasaka, K. 358  
 Kanazawa, T., see Matsumoto, S. 241, 246  
 Kandala, M.A., see Forni, L. 142  
 Kaneko, T., see Oguni, N. 361  
 Kang, Z.C. 175–177, 180  
 Kang, Z.C., see Bernal, S. 192  
 Kapphahn, G., see Winkler, H. 279  
 Karge, H.G. 275–278, 282, 285  
 Karge, H.G., see Beyer, H.K. 276, 278  
 Karge, H.G., see Grünert, W. 278, 281  
 Karge, H.G., see Sulikowski, B. 277  
 Karge, H.G., see Weiß, U. 274, 283  
 Karlicek, R.F., see Wallace, W.E. 16  
 Karlicek Jr, R.F., see Wallace, W.E. 63
- Karlsson, A., see Mostad, H. 274, 275, 293, 294  
 Karlsson, A., see Rørbik, T. 275, 293  
 Karnatak, R.C., see Paul-Boncour, V. 22  
 Kasahara, K., see Haneda, M. 196, 197  
 Kasahara, S., see Imamura, H. 9, 37, 38, 66  
 Kasai, H., see Kametani, T. 347, 362  
 Kasemo, B., see Löf, P. 207, 211, 215, 217–219, 224  
 Kasemo, B., see Zhdanov, V.P. 213  
 Kashiwagi, K., see Mukaiyama, T. 328  
 Kašpar, J. 213, 214, 217, 225, 256  
 Kašpar, J., see Balducci, G. 239, 249, 250  
 Kašpar, J., see Bekyarova, E. 252  
 Kašpar, J., see Colon, G. 243  
 Kašpar, J., see Daturi, M. 181  
 Kašpar, J., see de Leitenburg, C. 216, 232, 235  
 Kašpar, J., see Di Monte, R. 246, 249, 252, 253, 255, 256  
 Kašpar, J., see Fornasiero, P. 174, 181, 191–193, 195, 234–236, 238, 239, 241, 247–253, 256  
 Kašpar, J., see Ranga Rao, G. 172, 200, 218, 234, 239, 241, 246–248, 252, 254  
 Kašpar, J., see Trovarelli, A. 177, 181, 191, 200, 218, 229, 232, 234  
 Kašpar, J., see Vidmar, P. 239, 249–251, 257, 259  
 Kašpar, J., see Vlaic, G. 248  
 Kasuga, Y., see Imamura, H. 58, 60, 62–64, 68  
 Katano, S., see Yashima, M. 237  
 Kato, A. 83  
 Kato, A., see Kim, J.H. 297  
 Kato, A., see Matsuda, S. 83  
 Kato, Y., see Imamura, H. 8, 13  
 Kaufmann, D. 354  
 Kawabata, A. 239  
 Kawai, M. 317  
 Kawamura, M., see Kobayashi, S. 333, 365  
 Kawasaki, Y., see Shiraishi, H. 3  
 Kayano, K., see Funabiki, T. 257  
 Kazanskii, V.B., see Tarasov, A.L. 206  
 Kazansky, V.B., see Sass, A.S. 206  
 Kazenina, A.D., see Ivanova, I.I. 283  
 Keane, M.A. 276  
 Keane, M.A., see Coughlan, B. 280  
 Keeling, D.J., see Ife, R.J. 362  
 Keir, D. 275, 282, 283  
 Keiski, R.L., see Valden, M. 217  
 Keler, E.K., see Leonov, A.I. 237, 239  
 Keller, G.E. 97  
 Kennedy, L.A., see Prasad, R. 114

- Kenney, C.N., see Shalabi, M.A. 204  
 Kepert, D.L., see Harrowfield, J.M. 316  
 Kepinski, L. 201–203, 232  
 Kera, Y., see Hasimoto, K. 302  
 Keramidas, V.G. 239  
 Kern, M., see Lemos, F. 283, 285  
 Kershaw, R., see Carreiro, L. 84  
 Keusch, P., see Baiker, A. 115, 117  
 Khadzhiiev, S.N., see Nasukhanov, Kh.S.U. 278, 280, 282  
 Khadzhiiev, S.N., see Spiridonov, S.E. 274, 281, 282  
 Kharas, K.C.C., see Nunan, J.G. 289  
 Khidekel, M.L., see Azbel, B.I. 274, 302  
 Kieboom, A.P.G., see Floor, M. 299  
 Kiennemann, A., see El Fallah, J. 179, 181–184, 191, 195  
 Kiennemann, A., see Lavalley, J.C. 216  
 Kiennemann, A., see Rehspringer, J.L. 100  
 Kikhyanin, O.V., see Ione, K.G. 297  
 Kili, K., see Le Normand, F. 181, 183  
 Kim, Ch.-H., see Hong, S.B. 274, 278  
 Kim, D.J. 240  
 Kim, E. 338  
 Kim, G. 172, 216  
 Kim, G.J., see Baba, T. 54  
 Kim, J.-G. 278, 280  
 Kim, J.H. 297  
 Kim, J.-H., see Sugi, Y. 275, 278, 297, 298  
 Kim, Y., see Yeom, Y.H. 273  
 Kim, Y.R., see Jung, H.J. 130  
 Kimura, M., see Matsumoto, S. 241, 246  
 Kimura, M., see Nomura, Y. 353  
 Kimura, M., see Ozawa, M. 2, 239–241, 246  
 Kimura, T., see Sakai, M. 51  
 Kinsley, S.A., see Forsberg, J.H. 316  
 Kipling, S.J., see Bryan, S.J. 7, 28  
 Kirby, S., see Song, Ch. 297  
 Kirchmayr, H.R. 13  
 Kirchnerova, J. 123  
 Kiricsi, I., see Flego, C. 274, 293, 295  
 Kiricsi, Y. 293  
 Kirk, T.C., see Snider, B.B. 317  
 Kirsch, F.W. 290, 292  
 Kisenyi, J.M., see McCabe, R.W. 160, 166, 171  
 Kishimoto, H., see Otsuka-Yao-Matsuo, S. 239  
 Kitahara, T., see Danishefsky, S. 347  
 Kitajima, K., see Imamura, H. 50, 52, 53, 58  
 Kitamura, M. 361  
 Kitto, M.E. 284  
 Klabunde, K.J., see Zhang, X. 206  
 Kleefisch, M.S., see Balachandran, U. 96, 97  
 Kleinman, E.F. 328  
 Kleinschmidt, D.C., see Davies, A.G. 344  
 Klier, K. 110  
 Klimisch, R.L., see Taylor, K.C. 221  
 Klvana, D., see Kirchnerova, J. 123  
 Knizek, K., see Pollert, E. 131  
 Knox, R.C., see Sabatini, D.A. 326  
 Kobayashi, S. 317, 319, 320, 324–326, 329, 330, 333, 336, 337, 340, 341, 343–345, 347, 355, 358, 362, 365, 370  
 Kobayashi, S., see Hachiya, I. 337  
 Kobayashi, S., see Ishitani, H. 363  
 Kobayashi, S., see Manabe, K. 335  
 Kobayashi, S., see Mukaiyama, T. 325  
 Kobayashi, S., see Oyamada, H. 333  
 Koberstein, R., see Engler, B. 206  
 Kobylinski, T.P. 213  
 Kobylinski, T.P., see Balachandran, U. 96, 97  
 Koch, T.A., see Stiles, A.B. 271  
 Kodama, H., see Hori, K. 365  
 Kodata, I. 333, 335  
 Koga, K., see Hashimoto, S. 354  
 Koide, R., see Baba, T. 54, 56, 278  
 Kojima, I., see Ichimura, K. 107  
 Kokotailo, G.T., see Olson, D.H. 278, 279  
 Kolomiichuk, V.N., see Isupova, L.A. 128  
 Komatsu, M., see Minakata, S. 365  
 Komeshita, N., see Hashimoto, S. 354  
 Kominami, H., see Hasimoto, K. 302  
 Kompany, T., see Kim, J.-G. 278, 280  
 Kondo, J.N., see Domen, K. 151, 152  
 Kondo, K., see Misono, M. 303  
 Kondoh, S., see Fujitani, Y. 241  
 Konishi, T. 49, 53  
 Konishi, T., see Imamura, H. 47–49, 51, 53, 54, 56  
 Kononov, N.F., see Minachev, K.M. 291  
 Koura, T., see Du, Y. 237  
 Kowalak, S., see Bresinska, I. 278  
 Krause, K., see Chojnacki, T. 10, 11, 40  
 Krause, K.R. 11  
 Kremenić, G. 90, 116  
 Krill, G., see Le Normand, F. 35, 41, 181, 183  
 Krishnamurti, M., see Dobson, N.A. 53  
 Kristóf, J., see Gardos, G. 292, 293  
 Kritzenberger, J. 49  
 Kryukov, O.V., see Spiridonov, S.E. 274, 281, 282  
 Kryukova, G.N., see Isupova, L.A. 128  
 Kubota, Y., see Kim, J.H. 297

- Kubota, Y., see Sugi, Y. 275, 278, 297, 298  
 Kubsch, J.E. 242, 247, 257  
 Kuchеров, A.V., see Rokosz, M.J. 274, 305  
 Kudo, T. 154  
 Kuijpers, F.A. 63, 64  
 Kuijpers, F.A., see van Vucht, J.H.N. 63  
 Kulkarni, G.U. 131  
 Kulkarni, S.B., see Shiralkar, V.P. 279, 283  
 Kulkarni, S.J., see Subba Rao, Y.V. 300  
 Kummer, J.T. 160  
 Kung, H.H., see Yan, J.Y. 305  
 Kunz, F.W., see Yao, M.H. 240, 244, 245  
 Kuraishi, M., see Imai, H. 37  
 Kurihara, T., see Harusawa, S. 343, 344  
 Kurisaki, K., see Honna, K. 302  
 Kutty, T.R.N. 151  
 Kuwajima, I., see Nakamura, E. 317  
 Kuwajima, I., see Noyori, R. 317  
 Kuypers, M.M.M., see Seerden, J.-P.G. 365  
 Kyukov, O.V., see Nasukhanov, Kh.S.U. 278, 280, 282  
 Kyung, S.-H., see Reetz, M.T. 360  
  
 Laachir, A. 172, 174, 179, 181, 183, 185, 192, 255  
 Laachir, A., see Badri, A. 187, 255  
 Laachir, A., see Bernal, S. 179, 182, 193, 229, 232, 257  
 Laachir, A., see Perrichon, V. 172, 175, 177, 179–181, 184, 203, 232  
 Ladavos, A.K. 142  
 Lago, R. 94  
 Lahti, A., see Valden, M. 217  
 Lai, P.P. 281  
 Lambert, H., see Sartor, D. 354  
 Lambert, R.M., see Bryan, S.J. 7, 28  
 Lambert, R.M., see Hardacre, C. 39, 204, 206  
 Lambert, R.M., see Hay, C.M. 29  
 Lambert, R.M., see Jaffey, D.M. 65  
 Lambert, R.M., see Jennings, J.R. 31  
 Lambert, R.M., see Nix, R.M. 11, 28, 29, 33, 41, 63–65  
 Lambert, R.M., see Owen, G. 26–30  
 Lambert, R.M., see Shaw, E.A. 27, 29–31  
 Lambert, R.M., see Walker, A.P. 9, 31–34  
 Lambert, R.M., see Warren, J.P. 9, 39  
 Lamonier, C. 177  
 Lamotte, J., see Badri, A. 187, 255  
 Lamotte, J., see Laachir, A. 172, 174, 179, 181, 183, 192, 255  
 Lamotte, J., see Lavalley, J.C. 216  
 Lampert, J.K., see Farrauto, R.J. 231  
 Landis, P.S. 284  
 Landis, P.S., see Venuto, P.B. 276, 284, 295, 296, 298, 301  
 Lanewala, M.A., see Bolton, A.P. 298  
 Larese, C., see Bernal, S. 201, 202, 232  
 Larsen, S.D. 317, 348  
 Latreille, H., see Breyse, M. 204, 205, 257  
 Lau, G.C. 302  
 Lauder, A. 140  
 Lavalley, J.C. 216  
 Lavalley, J.C., see Badri, A. 187, 203, 232, 255  
 Lavalley, J.C., see Binet, C. 232  
 Lavalley, J.C., see Colon, G. 243  
 Lavalley, J.C., see Daturi, M. 181  
 Lavalley, J.C., see Laachir, A. 172, 174, 179, 181, 183, 192, 255  
 Le, Q.N., see Ardito, S.C. 298  
 Le Normand, F. 35, 41, 181, 183  
 Le Normand, F., see El Fallah, J. 179, 181–184, 191, 195  
 Le Normand, F., see Laachir, A. 172, 174, 179, 181, 183, 192, 255  
 Le Normand, F., see Sim, K.S. 17, 18  
 Leach, C.A., see Ife, R.J. 362  
 Leblanc, J. 341  
 Lechert, H., see Jia, M. 278  
 Lechtaler, C.H., see Meisel, S.L. 298  
 Leclercq, C., see Da Silva, P.N. 229  
 Lectka, T., see Evans, D.A. 354  
 Lee, C.-Y. 303  
 Lee, E.F.T. 279–281  
 Lee, E.F.T., see Keir, D. 275, 282, 283  
 Lee, J.K., see Posner, G.H. 365  
 Lee, J.Y., see Chan, K.S. 88, 89  
 Lee, S.H., see Jung, H.J. 130  
 Lee, T.Y. 283  
 Lei, G.D. 303  
 Lei, G.-D., see Zhang, Z.C. 12  
 Lei, Y., see Zhu, G. 17  
 Lemberston, J.L., see Richard, F. 299  
 Lemos, F. 283, 285  
 Lensen, N., see Alexakis, A. 335  
 Leonov, A.I. 237, 239  
 L'Erario, F., see Fornasiero, P. 234, 235, 252, 256  
 Lercher, J.A., see Brait, A. 284  
 Lercher, J.A., see Feast, S. 299  
 Lermer, H. 300  
 Levacher, V., see Mongin, F. 362  
 Levitz, P. 85



- Levitz, P., see Crespin, M. 107  
 Lewis, F.A. 68  
 Li, C. 187, 204, 206, 216  
 Li, Ch., see Yang, S.-J. 290  
 Li, P. 177  
 Li, Q. 278, 280  
 Li, R.-S. 278  
 Li, Y. 303  
 Li, Z. 304  
 Liang, J.J. 146, 149  
 Libby, W.F. 106  
 Liberov, L.G., see Kagan, Y.B. 27  
 Libowitz, G.G. 68  
 Lim, H.-J., see Burgess, K. 367  
 Lim, J.T., see Jung, H.J. 130  
 Lin, C.F. 278, 280, 281  
 Lin, Ch.-F., see Chao, K.-J. 278  
 Lin, E.V., see Kagan, Y.B. 27  
 Lin, Y. 137  
 Lin, Y.S., see Wang, W. 104  
 Linde, V.G. 48  
 Lindstedt, A. 142  
 Lintz, H.G. 118  
 Lipton, M., see Iyer, M.S. 344  
 Liu, Ch. 146, 150  
 Liu, G.K., see Forsberg, J.H. 316  
 Liu, S.-B. 274, 278  
 Liu, W. 204, 206, 257  
 Liu, W., see Tschope, A. 204  
 Liu, Z., see Deng, G. 302  
 Livage, J. 239  
 Llorca, J., see de Leitenburg, C. 90, 91, 174, 179, 239, 240, 247–249  
 Llorca, J., see Terribile, D. 185, 243, 244  
 Lloyd, D., see Owen, G. 26–30  
 Logan, A.D. 174, 247, 257, 258  
 Loktev, S.M., see Kagan, Y.B. 27  
 Lombardo, E.A. 86, 106  
 Lombardo, E.A., see Crespin, M. 85  
 Lombardo, E.A., see Marcos, J. 86, 87, 112, 113  
 Lombardo, E.A., see Milt, V.G. 78, 123, 124, 141  
 Lombardo, E.A., see Nudel, J.N. 80, 106  
 Lombardo, E.A., see Petunchi, J.O. 85, 106, 107, 113  
 Lombardo, E.A., see Ulla, M.A. 106, 112, 113  
 Longo, J.M., see Goodenough, J.B. 77  
 Longo, V. 239  
 Löf, P. 207, 211, 215, 217–219, 224  
 Loopstra, B.A., see Kuijpers, F.A. 63  
 Lopez, M.L., see Bernal, S. 192  
 Lopez-Cartes, C., see Bernal, S. 201, 232  
 López Nieto, J.M., see Corma, A. 291  
 Lorca, J.L., see Trovarelli, A. 189, 190, 200, 216, 234  
 Löwendahl, L., see Skoglundh, M. 142, 143  
 Lubineau, A. 317  
 Lucas, A., see van Grieken, R. 109–111  
 Lucas-De Regt, W.J.M., see Struijk, J. 51  
 Lucast, D.H. 317  
 Lucchini, V. 331, 336, 347, 351  
 Luengo, C.A. 22  
 Lugt, P.M., see Hultermans, R.J. 305  
 Lugt, P.M., see Ito, E. 275, 303, 304  
 Lui, Y.K., see Dettling, J.C. 241  
 Luijten, J.G.A. 343, 344  
 Lumma, P.K., see Claremon, D.A. 333, 335  
 Lunin, V.V., see Chetina, O.V. 37, 40  
 Lunsford, J.H., see Carvajal, R. 281, 283  
 Luoma, M., see Mannila, P. 204  
 Luoma, M., see Maunula, T. 204, 211, 213, 220  
 Ma, J., see Chan, K.S. 88, 89  
 Ma, Y.H., see Lee, T.Y. 283  
 Machida, K., see Masui, T. 185, 240  
 Machida, M. 127  
 Machida, M., see Arai, H. 126–128  
 Maciejewski, M., see Marti, P.E. 82  
 Mackrodt, W.C., see Harrison, P.G. 242  
 Madhok, K.L. 90  
 Maeland, A.J., see Libowitz, G.G. 68  
 Maes, A., see Marynen, P. 281  
 Maestro, P., see Bernal, S. 257  
 Magee, J.S. 275, 276, 284, 285  
 Maher, P.J., see Pine, L.A. 287  
 Maher, P.K. 286  
 Maher, P.K., see Scherzer, J. 285  
 Mai, K. 341  
 Maier, W.F., see Lau, G.C. 302  
 Maillet, T. 162, 227  
 Mains, G.J., see Jin, T. 208, 209, 223  
 Maire, G., see Le Normand, F. 35, 41, 181, 183  
 Maire, G., see Serre, C. 185, 190, 193, 200, 211, 212  
 Maire, G., see Weibel, M. 223  
 Majerus, J., see El Fallah, J. 179, 181–184, 191, 195  
 Makioka, Y. 347  
 Malera, A., see Brinen, J.S. 108  
 Man, P.P., see Herreros, B. 276, 278

- Manabe, K. 335  
 Mangeney, P., see Alexakis, A. 335  
 Mannila, P. 204  
 Manoli, J.M., see Fajardie, F. 252, 256  
 Manoli, J.-M., see Herreros, B. 276, 278  
 Maple, M.B., see Luengo, C.A. 22  
 Marcelin, G., see Öcal, M. 141  
 Marcilio, N.R., see Tournayan, L. 174  
 Marco, J.F., see Berry, F.J. 278  
 Marcos, J. 86, 87, 112, 113  
 Marcos, J., see Crespín, M. 85  
 Marcos, J.A., see Petunchi, J.O. 106, 107, 113  
 Marcq, J.P., see Sohler, M.P. 9, 19  
 Marczi, M., see Cuif, J.P. 242, 243  
 Mariano, P.S., see Cheng, Y.S. 347  
 Marin, G.B., see Nibbelke, R.H. 212, 224  
 Maring, C., see Bednarski, M. 354, 360  
 Markó, I.E. 365, 367  
 Marquez, F., see Corma, A. 289  
 Marshall, C.L., see Fleisch, T.H. 272, 276  
 Marsollier, F., see Barbier Jr, J. 181, 191, 192  
 Martensson, N., see Andersen, J.N. 63–65  
 Martí, P.E. 82, 115, 117  
 Martí, P.E., see Baiker, A. 115, 117  
 Martí, R.E., see Seebach, D. 365  
 Martin, D. 184, 193, 194, 250  
 Martin, D., see Taha, R. 193, 250, 254  
 Martin, R.L. 176  
 Martin, R.L., see Hoskins, B.F. 176, 177  
 Martinez, A., see Algarra, F. 283  
 Martinez, A., see Corma, A. 287, 290, 291  
 Martínez, A., see Corma, A. 287  
 Martinez, C., see Corma, A. 291  
 Martinez-Arias, A. 216, 223, 255, 256  
 Martinez-Arias, A., see Soria, J. 206, 232  
 Martsenyukukharuk, M.G., see Orlik, S.N. 303  
 Maruoka, K. 317, 354, 359, 362, 365  
 Maruya, K., see Arai, T. 218  
 Maruya, K., see Domen, K. 151, 152  
 Maruya, K., see Li, C. 187, 204, 206, 216  
 Maruyama, K., see Yamamoto, Y. 337  
 Marynen, P. 281  
 Mascarenhas, Y.P., see Nery, J.G. 278, 279  
 Maschio, S., see de Leitenburg, C. 239, 240, 247–249  
 Masui, T. 185, 240  
 Mathias, B.T., see Voorhoeve, R.J.H. 115  
 Mathies, H., see Roelofsen, J.W. 278, 280  
 Mathis, F., see Rogemond, E. 184, 232  
 Matier, W.L. 340  
 Matsuda, H., see Shimizu, Y. 152  
 Matsuda, S. 83  
 Matsuda, S., see Kato, A. 83  
 Matsuda, T. 149  
 Matsuda, Y., see Oguni, N. 361  
 Matsui, H., see Murota, T. 239, 241, 246, 248, 252  
 Matsui, S., see Mukaiyama, T. 328  
 Matsumoto, M., see Kim, J.H. 297  
 Matsumoto, M., see Sugi, Y. 275, 278, 297, 298  
 Matsumoto, S. 241, 246  
 Matsumura, Y., see Ando, H. 22  
 Matsuoka, T., see Imamura, H. 53  
 Matsuura, S., see Haneda, M. 196, 197  
 Matsuura, S., see Miki, T. 188, 190, 247, 257  
 Matsuzaki, T., see Kim, J.H. 297  
 Matsuzaki, T., see Sugi, Y. 275, 278, 297, 298  
 Matzuo, K., see Hasimoto, K. 302  
 Maugé, F. 281  
 Maunula, T. 204, 211, 213, 220  
 Maunula, T., see Valden, M. 217  
 Mavrodinova, V., see Karge, H.G. 276, 277, 285  
 Mazanec, T.J. 95  
 Mazdiyasi, K.S., see Brown, L.M. 48  
 Mazerolles, L., see Michel, D. 239  
 Mazieres, C., see Livage, J. 239  
 McCabe, R.W. 160, 166, 171  
 McCabe, R.W., see Graham, G.W. 257  
 McCabe, R.W., see Usmen, R.K. 247, 257  
 McCarty, J.G. 117  
 McCarty, J.G., see Quinlan, M.A. 115  
 McCullough, J.P., see Meisel, S.L. 298  
 McDaniel, C.V., see Maher, P.K. 286  
 McGarry, D.G., see Colvin, E.W. 328  
 McHale, A.E. 237  
 McKay, H.B., see Luengo, C.A. 22  
 Meera, V., see Sugunan, S. 146  
 Meeson, M.L., see Ife, R.J. 362  
 Mehrotra, R.C. 48  
 Meier, W.M. 270, 272, 273  
 Meisel, S.L. 298  
 Mello, N.C., see Nery, J.G. 278, 279  
 Melo, F.V., see Corma, A. 272  
 Mendelovici, L. 197, 198  
 Menon, P.G., see Zwinkels, M.F.M. 115, 125, 129  
 Mergler, Y., see deLange, M. 213  
 Mergler, Y.J. 220  
 Mergler, Y.J., see Ito, E. 303, 304

- Meriani, S. 237, 238, 240  
 Meriani, S., see Balducci, G. 239, 249  
 Meriani, S., see Fornasiero, P. 239, 241, 247, 248, 252  
 Meriani, S., see Ranga Rao, G. 172, 200, 218, 234, 239, 241, 246–248, 252, 254  
 Meriaudeau, P. 229  
 Merzhanov, A.G. 78  
 Mesmer, R.E., see Baes Jr, C.F. 316  
 Mester, Z.C., see Iyer, P.S. 278, 287  
 Meyer, E., see Lubineau, A. 317  
 Meyers, B.L., see Fleisch, T.H. 272, 276  
 Michel, D. 239  
 Michouk, M., see Mravec, D. 297  
 Mieville, R.L., see Balachandran, U. 96, 97  
 Mifsud, A., see Corma, A. 287, 291  
 Migone, R.A., see Ulla, M.A. 106, 112, 113  
 Mihara, T., see Imamura, H. 46, 58, 59, 61, 62, 65, 71  
 Mikami, K. 317, 354, 360  
 Mikhailov, B.M., see Grigos, V.I. 362  
 Miki, T. 188, 190, 247, 257  
 Mikuriya, S., see Iwamoto, M. 303  
 Miller, J.L., see Forsberg, J.H. 316  
 Miller, S.J., see Evans, D.A. 354  
 Millman, W.S., see Aparicio, L.M. 302  
 Millman, W.S., see Ulla, M.A. 278  
 Milt, V.G. 78, 123, 124, 141  
 Minachev, K.M. 291  
 Minachev, Kh.M., see Azbel, B.I. 274, 302  
 Minakata, S. 365  
 Minami, I., see Tstuji, J. 317  
 Mine, Y., see Iwamoto, M. 303  
 Minichelli, D., see Longo, V. 239  
 Miró, E.E. 98  
 Misono, M. 303  
 Misono, M., see Fujii, H. 82  
 Misono, M., see Inumaru, K. 46  
 Misono, M., see Mizuno, N. 80, 81, 141, 142  
 Misono, M., see Nakamura, T. 129  
 Misono, M., see Nishizaka, Y. 304  
 Misono, M., see Nitadori, T. 115–117, 138  
 Misono, M., see Wang, Y. 137, 138  
 Misono, M., see Yasuda, H. 136, 137, 274, 303  
 Misono, M., see Yokoyama, Ch. 303, 304  
 Mita, T., see Imamoto, T. 19, 20  
 Mitchell, P.J., see Schlatter, J.C. 221  
 Mitsuhashi, T., see Yashima, M. 237  
 Mitsuhasi, T. 239  
 Miura, N., see Shimizu, Y. 152  
 Miura, N., see Zhang, H.M. 118–120  
 Miura, Y., see Imamura, H. 70, 72  
 Miyake, H., see Ono, N. 317  
 Miyamae, N., see Matsuda, T. 149  
 Miyamoto, T., see Yasuda, H. 274, 303  
 Miyamura, H., see Ando, H. 22  
 Miyata, M., see Ishihara, K. 362  
 Miyazaki, E., see Ichimura, K. 107  
 Miyazaki, Y., see Kamegashira, N. 86  
 Miyoshi, M., see Imamura, H. 53  
 Miyoshi, N., see Matsumoto, S. 241, 246  
 Mizukami, F., see Niwa, S. 51  
 Mizumoto, M., see Matsuda, S. 83  
 Mizuno, K., see Imamura, H. 70  
 Mizuno, N. 80–82, 141, 142  
 Mizuno, N., see Fujii, H. 82  
 Mizuno, N., see Sato, S. 303  
 Mizuno, N., see Yasuda, H. 136, 137  
 Mizushima, T., see Haneda, M. 196, 197, 206  
 Moeller, T. 171  
 Moffatt, K., see Song, Ch. 298  
 Mokrushin, V.S., see Shafran, Y.M. 340  
 Molander, G.A. 316  
 Moldvan, A.G., see Wallace, W.E. 63  
 Monceaux, L., see Sri Rahayu, W. 122, 123  
 Mongin, F. 362  
 Monnier, J.R., see Gysling, H.J. 84, 85, 107–109  
 Monroe, D.R., see Summers, J.C. 163  
 Monteiro, J.L.F., see Corma, A. 291  
 Montón, J.B., see Corma, A. 283  
 Montreuil, C.N., see Su, E.C. 195–197, 201  
 Mooi, J., see Johnson, M.F.L. 177–181, 235  
 Moon, Y.H. 38, 39  
 More, K., see Hori, C.E. 250  
 Moreau, P. 297  
 Moreau, P., see Amouzegh, P. 300  
 Moreau, P., see Goux, A. 297  
 Moreau, S. 78, 82, 83  
 Mori, H. 274, 301  
 Mori, H., see Masui, T. 185, 240  
 Morikawa, A., see Otsuka, K. 172, 199, 200, 218, 222, 229  
 Morikawa, H., see Otsuka-Yao-Matsuo, S. 239  
 Morimoto, K., see Yashima, M. 237, 238  
 Morodome, M., see Yanagisawa, A. 337  
 Morris, M.A., see Cunningham, J. 232  
 Morris, M.A., see Harrison, P.G. 242  
 Morrison, T.I., see Suib, S.L. 278, 281  
 Morrissey, M.M., see Evans, D.A. 369  
 Mortier, W.J., see Costenoble, M.L. 278  
 Mortinov, E.S., see Minachev, K.M. 291

- Moser, W.R., see Tsai, C.Y. 97  
 Moss, W.D., see Fisher, R. 302  
 Mostad, H. 274, 275, 293, 294  
 Mostad, H.B., see Rørbik, T. 275, 293  
 Mostovoy, N.V., see Minachev, K.M. 291  
 Motoyama, M., see Murota, T. 239, 241, 246, 248, 252  
 Motoyama, Y., see Mikami, K. 354  
 Mouaddib-Moral, N., see Taha, R. 179  
 Moure, C., see Duran, P. 237  
 Mowthorpe, D.J., see Brown, J.M. 344  
 Mravec, D. 297  
 Mu, R., see Deng, G. 302  
 Muhammed, M., see Zhang, Y. 239, 240, 257  
 Mukai, C. 325  
 Mukaiyama, T. 317, 325, 328  
 Mukaiyama, T., see Kobayashi, S. 317, 337  
 Müller, S. 152  
 Mullins, D.R., see Overbury, S.H. 250  
 Munuera, G. 211, 232  
 Munuera, G., see Holgado, J.P. 191, 193  
 Murakami, M., see Kobayashi, S. 317, 337  
 Murakami, T., see Niwa, S. 51  
 Murakami, Y., see Niwa, M. 216, 218  
 Muraki, H., see Fujitani, Y. 241  
 Muraki, H., see Shinjoh, H. 213  
 Murase, N., see Maruoka, K. 317, 354  
 Murata, S. 317  
 Murata, S., see Noyori, R. 325  
 Murota, T. 239, 241, 246, 248, 252  
 Murrell, L.L. 201–203, 230–232  
 Murthy, Y.V.S.N. 302  
 Music, S., see Stefanic, G. 239, 243  
  
 Naakata, s., see Kim, J.H. 297  
 Naccache, C., see Meriaudeau, P. 229  
 Nagahara, H., see Fukuoka, Y. 51  
 Nagami, K., see Mukai, C. 325  
 Nagarajan, V.S. 240  
 Nagayama, S., see Kobayashi, S. 326, 329, 333, 340, 343, 347  
 Nakai, T., see Mikami, K. 317, 354, 360  
 Nakamura, E. 317  
 Nakamura, E., see Noyori, R. 317  
 Nakamura, T. 84, 129  
 Nakamura, T., see Fujitani, Y. 241  
 Nakaoka, T., see Sakai, M. 51  
 Nakashima, M., see Narasaka, K. 354  
 Nakatsugawa, K., see Ojima, I. 341  
 Nakayama, A., see Kametani, T. 370  
 Namdev, N.D., see Iyer, M.S. 344  
  
 Namy, J.L., see Kagan, H.B. 3  
 Narasaka, K. 347, 354, 358, 362, 365, 371  
 Narasaka, K., see Mukaiyama, T. 317  
 Narisano, E., see Guanti, G. 332  
 Naruta, Y., see Yamamoto, Y. 337  
 Nassar, E.J., see Rosa, I.L.V. 278  
 Nasukhanov, Kh.S.U. 278, 280, 282  
 Nasukhanov, Kh.S.-U., see Spiridonov, S.E. 274, 281, 282  
 Nayak, R.M., see Hatwar, T.K. 55  
 Neikam, W.C. 69  
 Neikam, W.C., see Vannice, M.A. 69  
 Neoh, K.G., see Lin, Y. 137  
 Neri, G., see Galvagno, S. 51  
 Nery, J.G. 278, 279  
 Nestrick, T.J., see Brieger, G. 70  
 Netzer, F. 6, 13, 22, 31  
 Netzer, F.P. 63  
 Neumann, M., see Christmann, K. 59  
 Ng, K.Y.S., see Halasz, I. 132  
 Ng, K.Y.S., see Hori, C.E. 250  
 Ng, K.Y.S., see Permana, H. 237, 251, 252  
 Nibbelke, R.H. 212, 224  
 Nicks, J.J., see Baglin, E.G. 26, 27  
 Nicks, L.J., see Atkinson, G.B. 22  
 Nicks, L.J., see Baglin, E.G. 27  
 Nicula, A. 278  
 Nieto, J.M.L., see Kremenić, G. 90, 116  
 Nieuwenhuys, B., see deLange, M. 213  
 Nieuwenhuys, B.E., see Ito, E. 303, 304  
 Nieuwenhuys, B.E., see Mergler, Y.J. 220  
 Nii, H., see Teraoka, Y. 144  
 Nijs, H., see Crespín, M. 85  
 Nilsson, A., see Andersen, J.N. 63–65  
 Nisar, M., see Tsuji, J. 317  
 Nishiyama, Y., see Shiraishi, H. 3  
 Nishizaka, Y. 304  
 Nitadori, T. 115–117, 138  
 Nitadori, T., see Yasuda, H. 136  
 Niwa, M. 216, 218  
 Niwa, S. 51  
 Nix, R.M. 11, 28, 29, 33, 41, 63–65  
 Nix, R.M., see Bryan, S.J. 7, 28  
 Nix, R.M., see Hay, C.M. 29  
 Nix, R.M., see Jennings, J.R. 31  
 Nix, R.M., see Owen, G. 26–30  
 Nix, R.M., see Walker, A.P. 31  
 Nobe, K., see Chien, M.W. 80  
 Noller, H. 132  
 Nolting, J., see Ricken, M. 172  
 Nomura, Y. 353

- Nortier, P., see Pijolat, M. 239, 241, 257  
 Nowick, A.S., see Tuller, H.L. 247, 257  
 Noyori, R. 317, 325  
 Noyori, R., see Kitamura, M. 361  
 Noyori, R., see Murata, S. 317  
 Noyori, R., see Nakamura, E. 317  
 Nozaki, T. 105  
 Nubling, C., see Enders, D. 333, 335  
 Nudel, J.N. 80, 106  
 Nukui, K., see Imamura, H. 9, 37, 38, 66  
 Nunan, J.G. 233, 234, 289  
 Nygren, M., see Skoglundh, M. 142, 143  
 Nygren, M., see Teraoka, Y. 144  
  
 O'Brien, S., see Cunningham, J. 181, 182, 229, 232  
 Öcal, M. 141  
 Occelli, M.L. 270, 272, 290  
 Odell, F., see Duwez, P. 237, 240  
 Odriscoll, J.P., see Cunningham, J. 232  
 Oelker, P., see Parvulescu, V.I. 303  
 Ogawa, T., see Miki, T. 188, 190, 247, 257  
 Ogino, Y., see Mori, H. 274, 301  
 Oguni, N. 361  
 Oh, S.H. 203, 204, 206, 207, 211–217, 219  
 Ohmura, A., see Imamura, H. 50, 52, 53  
 Ohnishi, T., see Sakamoto, E. 276, 303, 304  
 Ohno, R., see Onaka, M. 328  
 Ohno, T., see Mukaiyama, T. 325  
 Ohshiro, Y., see Minakata, S. 365  
 Ohta, T., see Hori, K. 365  
 Ohtake, K., see Yashima, M. 239  
 Oishi, M., see Maruoka, K. 317  
 Ojima, I. 328, 332, 341  
 Okada, S., see Kitamura, M. 361  
 Okado, H., see Yamamura, M. 101  
 Okikawa, S. 240  
 Okonji, Ch., see Gárdos, G. 292  
 Okuara, T., see Jin, T. 208, 209, 223  
 Okuda, K., see Otsuka-Yao-Matsuo, S. 239  
 Okumura, K., see Sasai, H. 354  
 Oldman, R.J., see Walker, A.P. 32, 34  
 Oldmann, R.J., see Shaw, E.A. 27  
 Oliva, C., see Forni, L. 142  
 Oliván, A.M.O., see Tascón, J.M.D. 84, 85  
 Ollis, D.F., see Grenoble, D.C. 221  
 Olmez, I., see Kitto, M.E. 284  
 Olsbye, U., see Slagtern, Å. 92–94  
 Olson, D.H. 278, 279  
 Olson, D.H., see Meier, W.M. 270, 272, 273  
 Omata, K., see Nozaki, T. 105  
 Omata, T., see Izu, N. 239  
 Omata, T., see Otsuka-Yao-Matsuo, S. 239  
 Omori, Y., see Harusawa, S. 343, 344  
 Onaka, M. 328  
 Onaka, M., see Kawai, M. 317  
 Onishi, T., see Arai, T. 218  
 Onishi, T., see Li, C. 187, 204, 206, 216  
 Ono, N. 317  
 Ono, Y., see Baba, T. 54, 56, 274, 278, 301  
 Ono, Y., see Tanaka, T. 55, 56, 278  
 Onsgaard, J., see Andersen, J.N. 63–65  
 Onuferko, J.H., see Foley, H.C. 108  
 Onyestyak, G., see Karge, H.G. 275–277  
 Orchillés, A.V., see Corma, A. 287  
 Orchillés, V., see Corma, A. 283  
 Orlik, S.N. 303  
 Ormerod, R.M., see Hardacre, C. 204, 206  
 Osaki, A., see Aiko, K.I. 34  
 Otamini, J., see Hansen, S. 90, 91  
 Otamiri, J.C. 131  
 Otomasu, H., see Takahashi, H. 333, 335  
 Otsuka, K. 172, 199, 200, 218, 222, 229  
 Otsuka, K., see Yamamura, M. 101  
 Otsuka, T., see Soga, K. 13  
 Otsuka-Yao-Matsuo, S. 239  
 Otsuka-Yao-Matsuo, S., see Izu, N. 239  
 Otto, K. 167, 213  
 Otto, K., see Shyu, J.Z. 230, 231  
 Oukaci, R., see Öcal, M. 141  
 Overbury, S.H. 250  
 Overman, L.E. 336  
 Owen, G. 26–30  
 Owen, G., see Bryan, S.J. 7, 28  
 Owen, G., see Hay, C.M. 29  
 Owen, G., see Jennings, J.R. 31  
 Owen, G., see Nix, R.M. 11, 28, 29, 33, 41  
 Owens, D.A., see Matier, W.L. 340  
 Oyama, S.T. 63  
 Oyamada, H. 333  
 Oyamada, H., see Kobayashi, S. 326, 333  
 Oyamada, H., see Manabe, K. 335  
 Ozawa, M. 2, 239–241, 246  
 Ozawa, M., see Matsumoto, S. 241, 246  
 Ozawa, S., see Mori, H. 274, 301  
  
 Padalia, B.D., see Hatwar, T.K. 55  
 Padalia, B.D., see Prabhawalkar, V. 55  
 Padeste, C. 177, 187, 200, 209, 216, 217, 232  
 Pajonk, G.M., see Conner Jr, W.C. 69  
 Pakkanen, T.T., see Timonen, J.T. 278  
 Pal-Borbely, G., see Beyer, H.K. 276, 278

- Pal-Borbely, G., see Karge, H.G. 276–278  
 Palan, P.R., see Davies, A.G. 344  
 Palczewska, W. 68  
 Pal'guev, S.F. 240  
 Palomares, A.E., see Corma, A. 289  
 Palomo, C. 370  
 Pan, M., see Bernal, S. 192  
 Pande, N.K. 214, 215, 217, 218  
 Pang, W.Q., see Tian, Y.G. 278  
 Papadakis, V.G. 257  
 Papadakis, V.G., see Pliangos, C. 257  
 Park, C., see Kim, J.H. 297  
 Park, J.-Y., see Kodata, I. 333, 335  
 Parker, D.G., see Chinchén, G.C. 30  
 Parker, S.C., see Sayle, T.X.T. 176, 179, 204, 232, 242  
 Parker Jr, W.O., see Flego, C. 274, 293, 295  
 Parrish, D.R., see Hajos, Z.G. 317  
 Parsons, M.E., see Ife, R.J. 362  
 Parvulescu, V.I. 303  
 Pascal, C., see Duran, P. 237  
 Pasztor, M., see Solymosi, F. 202  
 Pataskar, S.G., see Choudhary, V.R. 119  
 Patil, G., see Mai, K. 341  
 Patrick, J.M., see Harrowfield, J.M. 316  
 Paul-Boncour, V. 22, 24, 41  
 Paul-Boncour, V., see Barrault, J. 14, 15, 23, 24, 40, 41  
 Paul-Boncour, V., see Sim, K.S. 17, 18  
 Paul-Boncour, V., see Wang, Z.L. 24, 25, 41  
 Pauli, I.A., see Isupova, L.A. 128  
 Pearson, I.M., see Chien, M.W. 80  
 Pechy, L., see Gárdos, G. 292  
 Peet, W.G. 337  
 Pei, S., see Balachandran, U. 96, 97  
 Peña, J.L., see van Grieken, R. 109–111  
 Peña, M.A., see Fierro, J.L.G. 85  
 Peña, M.A., see Lago, R. 94  
 Peng, Y., see Jiang, A.R. 132  
 Peng, Y.M., see Masui, T. 185, 240  
 Penner-Hahn, J.E., see Li, P. 177  
 Perathoner, S., see Centi, G. 206  
 Percheron-Guégan, A. 8, 63  
 Percheron-Guégan, A., see Barrault, J. 14, 15, 23, 24, 36, 40, 41  
 Percheron-Guégan, A., see Paul-Boncour, V. 22, 24, 41  
 Percheron-Guégan, A., see Sim, K.S. 17, 18  
 Percheron-Guégan, A., see Wang, Z.L. 24, 25, 41  
 Pere, J., see Valden, M. 217  
 Pereyre, M. 337  
 Pereyre, M., see Daude, G. 337  
 Perez-Omil, J.A., see Bernal, S. 175, 177, 181–183, 193, 201, 202, 229, 232, 247, 257  
 Permana, H. 237, 251, 252  
 Permana, H., see Hori, C.E. 250  
 Pernet-Bolano, L., see Diaz-Mendoza, F.A. 295  
 Perot, G., see Richard, F. 299  
 Perrichon, V. 172, 175, 177, 179–181, 184, 203, 232  
 Perrichon, V., see Badri, A. 187, 255  
 Perrichon, V., see Bernal, S. 179, 182, 193, 229, 232, 257  
 Perrichon, V., see Laachir, A. 172, 174, 179, 181, 183, 185, 192, 255  
 Perrichon, V., see Rogemond, E. 184, 232  
 Perrichon, V., see Zotin, F.M.Z. 173, 177, 181, 192  
 Perricini, S.C., see Worth, D.F. 347  
 Perrone, E. 370  
 Pessa, M., see Valden, M. 217  
 Pettrini, G., see Bossi, A. 33  
 Petrov, A.A. 53  
 Petunchi, J.O. 85, 106, 107, 113  
 Petunchi, J.O., see Ulla, M.A. 106, 112, 113  
 Petzow, G., see Nakamura, T. 84  
 Phillips, B.T., see Claremon, D.A. 333, 335  
 Piagentini, R.O., see Nudel, J.N. 106  
 Pickert, P.E., see Bolton, A.P. 298  
 Pickert, P.E., see Rabo, J.A. 284, 302  
 Pietropaolo, D., see Galvagno, S. 51  
 Pijolat, M. 239, 241, 257  
 Pijolat, M., see Colon, G. 243  
 Pijolat, M., see Gruy, F. 241  
 Piken, A.G., see Gandhi, H.S. 169  
 Pikul, S., see Corey, E.J. 354  
 Pillai, C.N., see Murthy, Y.V.S.N. 302  
 Pillai, C.N., see Pillai, R.B.C. 297  
 Pillai, R.B.C. 274, 297, 302  
 Pine, L.A. 287  
 Pintado, J.M., see Bernal, S. 175, 177, 181–183, 193, 198, 201, 202, 232, 247, 254, 257, 258  
 Piotrowski, D.W., see Denmark, S.E. 333, 335  
 Pires, E.L. 302  
 Pires de Matos, A., see Ballivet-Tkatchenko, D. 38  
 Pitchon, V., see Fritz, A. 303  
 Plank, C.J. 284  
 Pleizier, G., see Amenomiya, Y. 222  
 Pliangos, C. 257

- Pliangos, C.A., see Papadakis, V.G. 257  
 Pod'yacheva, E.B., see Spiridonov, S.E. 274, 281, 282  
 Poeppel, R.B., see Balachandran, U. 96, 97  
 Pohjola, V.J., see Maunula, T. 204, 211, 213, 220  
 Poix, P., see Rehspringer, J.L. 100  
 Poldy, C.A., see Kirchmayr, H.R. 13  
 Pollert, E. 131  
 Poluboyarov, V.A., see Isupova, L.A. 128  
 Pomonis, P.J., see Ladavos, A.K. 142  
 Pomonis, P.J., see Skaribas, S.P. 78  
 Pomonis, P.J., see Trikalitis, P.N. 147  
 Popova, N.M., see Sass, A.S. 206  
 Popovic, S., see Stefanic, G. 239, 243  
 Porte, A.M., see Burgess, K. 367  
 Posner, G.H. 365  
 Poteruca, J.J., see Forsberg, J.H. 316  
 Potts, J.D., see Kirsch, F.W. 290, 292  
 Povarov, L.S. 347  
 Povarov, L.S., see Grigos, V.I. 362  
 Prabhawalkar, V. 55  
 Pradhan, A.R. 296  
 Pradhan, S.K., see Chatterjee, A. 239, 243  
 Praliaud, H., see Duplan, J.L. 201  
 Prasad, R. 114  
 Prato, M., see Borriore, E. 362  
 Prato, M., see Lucchini, V. 331, 336, 347, 351  
 Prewitt, C.T., see Shannon, R.D. 240  
 Prigent, M., see Weibel, M. 223  
 Primavera, A., see de Leitenburg, C. 257  
 Primet, M. 201  
 Primet, M., see Beguin, B. 83  
 Primet, M., see de Collongue, B. 80, 126  
 Primet, M., see Rogemond, E. 184, 232  
 Primo, J., see Algarra, F. 283  
 Primo, J., see Armengol, E. 299  
 Primo, J., see Corma, A. 299  
 Prin, M. 241  
 Prin, M., see Pijolat, M. 239, 241, 257  
 Prins, R., see Huizinga, T. 211  
 Procop, M., see Volter, J. 59  
 Przheval'skaya, L.K., see Tarasov, A.L. 206  
 Puchot, C. 361  
 Putna, E.S. 208, 211, 252  
 Putna, E.S., see Bunluesin, T. 204–209  
 Pytlewski, L.L., see Howell, K. 54  
 Pyun, Ah.-H., see Hong, S.B. 274, 278  
 Qi, M., see Chen, Y.L. 239  
 Qiu, S.L., see Tian, Y.G. 278  
 Queguiner, G., see Mongin, F. 362  
 Quemere, E., see Badri, A. 187, 255  
 Quémeré, E., see Cuif, J.P. 242, 243  
 Quémeré, E., see Laachir, A. 172, 174, 179, 181, 183, 192, 255  
 Quian, Y.T., see Carreiro, L. 84  
 Quimper, M. 354  
 Quinlan, M.A. 115  
 Quinones, A.R., see Ardito, S.C. 298  
 Quintard, J.-P., see Pereyre, M. 337  
 Raabe, G., see Enders, D. 333, 335  
 Raaen, S., see Braaten, N.A. 9  
 Rabo, J.A. 278, 281, 284, 302  
 Radha, R. 90, 91  
 Rahm, A., see Pereyre, M. 337  
 Rahmoeller, K.M., see Hori, C.E. 250  
 Rahmoeller, M., see Permana, H. 237, 251, 252  
 Rajadurai, S., see Gunasekaran, N. 123, 124, 139  
 Rajappa, S., see Reddy, T.I. 301  
 Rajaram, R.R., see Diwell, A.F. 201, 226  
 Rajaram, R.R., see Golunski, S.E. 232–234  
 Rakhely, G., see Solymosi, F. 202  
 Rama Rao, A.V., see Subba Rao, Y.V. 300  
 Ramesh, S. 131, 132  
 Ramirez, F., see Bernal, S. 192  
 Ramoa Ribeiro, F., see Lemos, F. 283, 285  
 Rane, V.H., see Choudhary, V.R. 197, 198  
 Ranga Rao, G. 172, 200, 218, 234, 239, 241, 246–248, 252, 254  
 Ranga Rao, G., see Fornasiero, P. 234, 235, 239, 241, 247, 248, 252, 256  
 Rao, B.S., see Pradhan, A.R. 296  
 Rao, C.N.R. 55, 77  
 Rao, C.N.R., see Kulkarni, G.U. 131  
 Rao, K.J., see Nagarajan, V.S. 240  
 Raphael, R.A., see Dobson, N.A. 53  
 Rauckman, B.S. 362  
 Rauckman, B.S., see Johnson, J.V. 362  
 Rault, S., see Mongin, F. 362  
 Ravet, M.F., see Le Normand, F. 35, 41  
 Rawlance, D.J., see Corma, A. 272  
 Ray, G.J., see Fleisch, T.H. 272, 276  
 Rayment, T., see Hardacre, C. 39, 204  
 Rayment, T., see Hay, C.M. 29  
 Rayment, T., see Nix, R.M. 11, 28, 29, 33  
 Rayment, T., see Shaw, E.A. 27, 29–31  
 Rayment, T., see Walker, A.P. 32–34  
 Reavill, D.R., see Ife, R.J. 362  
 Reddy, G.V., see Chakraborty, T.K. 341

- Reddy, T.I. 276, 297, 301  
 Redey, A., see Gárdos, G. 292, 293  
 Rees, L.V.C. 276  
 Rees, L.V.C., see Keir, D. 275, 282, 283  
 Rees, L.V.C., see Lai, P.P. 281  
 Rees, L.V.C., see Lee, E.F.T. 279–281  
 Reetz, M.T. 360  
 Rehspringer, J.L. 100  
 Reilly, J.J., see Johnson, J.R. 14–16, 40  
 Reller, A., see Baiker, A. 115, 117  
 Remeika, J.P., see Voorhoeve, R.J.H. 115, 129, 140  
 Rey, F., see Corma, A. 289  
 Rheingold, A.L., see Bao, J. 359, 360  
 Rhodes, A.K. 284  
 Rhodes, W.W., see Johnson Jr, D.W. 80  
 Riant, O., see Kagan, H.B. 354  
 Richard, C.J., see Sartor, D. 354  
 Richard, F. 299  
 Ricken, M. 172  
 Rideout, D.C. 345  
 Rieck, J.S., see Kubsch, J.E. 242, 247, 257  
 Riess, I., see Ricken, M. 172  
 Rigutto, M.S., see Ito, E. 275, 303, 304  
 Roberts, M.W., see Kulkarni, G.U. 131  
 Roberts, S., see Dictor, R. 201, 202  
 Robinson, N.P., see Hollis, T.K. 345  
 Robota, H.J., see Nunan, J.G. 233, 234, 289  
 Robson, H.E., see Occelli, M.L. 270, 272  
 Roche, R., see Serre, C. 190, 211  
 Rodini, D.J., see Snider, B.B. 317  
 Rodríguez-Izquierdo, J.M., see Bernal, S. 175, 179, 181–183, 192, 193, 198, 201, 202, 232, 247, 254, 257, 258  
 Rodríguez-Ramos, I. 145–148  
 Roelofsen, D.P., see Wortel, Th.M. 299  
 Roelofsen, J.W. 278, 280  
 Rogemond, E. 184, 232  
 Roger, C., see Chandler, C.D. 78  
 Rogers, B.N., see Overman, L.E. 336  
 Rohler, J. 12  
 Rojas, M.L. 109, 110  
 Rojas, M.L., see Rodríguez-Ramos, I. 145–148  
 Rojas, M.L., see van Grieken, R. 109–111  
 Rojo, J.M., see Cunningham, J. 181, 182, 193, 229, 232  
 Rojo, J.M., see Fierro, J.L.G. 172, 181, 182  
 Rokosz, M.J. 274, 305  
 Roland, E. 270  
 Romanovsky, B.V., see Ivanova, I.I. 283  
 Rooney, J.J., see Hegarty, B.F. 67  
 Root, T.W. 217  
 Rørbik, T. 275, 293  
 Rosa, I.L., see Serra, O.A. 278  
 Rosa, I.L.V. 278  
 Rosinski, E.J., see Plank, C.J. 284  
 Ross, S.D. 49  
 Rostrup-Nielsen, J.R. 92  
 Roth, B., see Johnson, J.V. 362  
 Roth, B., see Rauckman, B.S. 362  
 Rothschild, W.G., see Su, E.C. 195–198, 201  
 Rowlinson, H.C. 67  
 Rozovskii, A.Y., see Kagan, Y.B. 27  
 Rozovskii, A.Ya., see Isupova, L.A. 128  
 Rubingh, D.N., see Holland, P.M. 326  
 Ruckenstein, E., see Prasad, R. 114  
 Rumpf, P., see Blouri, B. 47  
 Ryoo, R., see Kim, J.-G. 278, 280  
 Sabatini, D.A. 326  
 Sachtler, W.M.H., see Lei, G.D. 303  
 Sachtler, W.M.H., see Weyrich, P.A. 302  
 Sachtler, W.M.H., see Yan, J.Y. 305  
 Sachtler, W.M.H., see Zhang, Z.C. 12  
 Saddawi, S., see Gunasekaran, N. 122  
 Sadykov, V.A., see Isupova, L.A. 128  
 Saffrich, J., see Sartor, D. 354  
 Saigo, K., see Shimada, S. 328  
 Saito, S., see Okikawa, S. 240  
 Saito, Y., see Fujii, T. 66  
 Sakaguchi, H., see Corré, S. 17  
 Sakaguchi, S., see Shiraiishi, H. 3  
 Sakai, M. 51  
 Sakai, S., see Fukuzawa, S. 337  
 Sakai, T., see Imamura, H. 9, 37, 38  
 Sakakibara, Y., see Sakai, M. 51  
 Sakamoto, E. 276, 303, 304  
 Sakamoto, T., see Imamura, H. 53, 72  
 Sakata, J., see Nakamura, E. 317  
 Sakata, J., see Noyori, R. 317  
 Sakata, T., see Masui, T. 185, 240  
 Sakata, Y., see Imamura, H. 46–49, 51, 53, 54, 56–65, 68, 70–72  
 Sakata, Y., see Li, C. 187, 204  
 Salmi, T., see Mannila, P. 204  
 Salmi, T., see Maunula, T. 204, 211, 213, 220  
 Salot, S. 46, 53  
 Sampathkumaran, E.V., see Hatwar, T.K. 55  
 Sampathkumaran, E.V., see Rao, C.N.R. 55  
 Samuel, O., see Puchot, C. 361  
 Sanchez-Blanco, A.I. 365  
 Sano, T., see Soga, K. 13



- Santamaria, J., see Miró, E.E. 98  
 Santoni, A., see Trovarelli, A. 177, 181, 191, 200, 218, 229, 232, 234  
 Sanz, J., see Cunningham, J. 181, 182, 193, 229, 232  
 Sanz, J., see Fierro, J.L.G. 172, 181, 182  
 Saracco, G. 80, 125, 126  
 Sarges, R. 362  
 Sarkany, J., see Lei, G.D. 303  
 Sarma, D.D., see Rao, C.N.R. 55  
 Sarode, P.R., see Rao, C.N.R. 55  
 Sartor, D. 354  
 Sasahara, A. 213  
 Sasai, H. 354  
 Sass, A.S. 206  
 Sastre, E., see Corma, A. 298  
 Sato, K., see Fukuzawa, S. 337  
 Sato, M., see Haneda, M. 196, 197  
 Sato, M., see Miki, T. 188, 190, 247, 257  
 Sato, M., see Soga, K. 13  
 Sato, S. 303  
 Sato, Y., see Haneda, M. 196, 197  
 Sauerlandt, U., see Grünert, W. 278, 281  
 Saussey, J., see Lavalley, J.C. 216  
 Sauvion, N.S., see Badri, A. 187, 255  
 Sauvion, N.S., see Laachir, A. 172, 174, 179, 181, 183, 192, 255  
 Savel'eva, G.A., see Sass, A.S. 206  
 Savimaki, A., see Valden, M. 217  
 Sayle, T.X.T. 176, 179, 204, 232, 242  
 Schabes-Retchiman, P., see Krause, K.R. 11  
 Schaper, H. 83  
 Schawarzmman, M., see Lerner, H. 300  
 Scheeren, H.W., see Seerden, J.G. 354  
 Scheeren, H.W., see Seerden, J.-P.G. 365  
 Scherzer, J. 272, 278, 282, 285, 287  
 Scherzer, J., see Hunter, F.D. 278, 279, 281  
 Scherzer, J., see Iyer, P.S. 278, 287  
 Schinzer, D. 316  
 Schlapbach, L., see Siegmman, H.C. 8, 40  
 Schlatter, J.C. 221  
 Schlatter, J.C., see Taylor, K.C. 167, 213  
 Schlögl, R., see Grünert, W. 278, 281  
 Schmid, W. 338  
 Schmid, W., see Kim, E. 338  
 Schmidt, L.D., see Chojnacki, T. 10, 11, 40  
 Schmidt, L.D., see Krause, K.R. 11  
 Schmidt, L.W., see Root, T.W. 217  
 Schmieg, S.J. 172  
 Schmieg, S.J., see Permana, H. 237, 251, 252  
 Schmitz, P.J., see Graham, G.W. 257  
 Schober, O., see Christmann, K. 59  
 Scholte op Reimer, A.W.A., see Seerden, J.-P.G. 365  
 Scholten, J.J.F., see Struijk, J. 51  
 Schomaker, V., see Rabo, J.A. 278, 281, 284  
 Schrey, F., see Gallagher, P.K. 80  
 Schrey, F., see Johnson Jr, D.W. 80  
 Schubert, H., see Enders, D. 333, 335  
 Schubert, P., see Engler, B. 206  
 Schuchardt, U., see Pires, E.L. 302  
 Schulz, H. 299  
 Schwing-Weill, M.-J., see Almasio, M.-C. 316  
 Scibilia, G., see Saracco, G. 80, 125, 126  
 Scorrano, G., see Borriore, E. 362  
 Scorrano, G., see Lucchini, V. 331, 336, 347, 351  
 Scott, W.R., see Tofield, B.C. 86  
 Sedmidubsky, D., see Pollert, E. 131  
 Seebach, D. 335, 365, 371  
 Seerden, J.G. 354  
 Seerden, J.-P.G. 365  
 Seff, K., see Yeom, Y.H. 273  
 Seidehamel, R.J., see Matier, W.L. 340  
 Seigneurin, A., see Cuif, J.P. 242, 243  
 Seiyama, T. 88, 119  
 Seiyama, T., see Arai, H. 116, 117, 121, 122  
 Sekiya, M. 370  
 Sekiya, M., see Ikeda, K. 328  
 Sell, A.T., see Herz, R.K. 223  
 Seo, G., see Kim, J.H. 297  
 Seo, J.S., see Hong, S.B. 274, 278  
 Seoane, X.L., see Martinez-Arias, A. 216, 255  
 Sergo, V. 175  
 Sergo, V., see Fornasiero, P. 174, 181, 195, 238, 239, 248, 249  
 Sermon, P.A., see Sun, Y. 240, 243  
 Serra, O.A. 278  
 Serra, O.A., see Rosa, I.L.V. 278  
 Serre, C. 185, 190, 193, 200, 211, 212  
 Seshan, K., see Brait, A. 284  
 Settu, T. 239  
 Seyama, T. 2  
 Shafran, Y.M. 340  
 Shalabi, M.A. 204  
 Shamsi, A., see Siriwardane, R.V. 101, 102  
 Shamsi, A., see Wallace, W.E. 26  
 Shangong, H., see Yiguang, T. 278  
 Shanks, B.H., see Cho, B.K. 213, 214, 219, 220  
 Shannon, M.D., see Jennings, J.R. 31  
 Shannon, R.D. 176, 240

- Shaw, E.A. 27, 29–31  
 Shaw, H.A., see Diwell, A.F. 201, 226  
 Shelef, M. 160, 163, 212, 213, 256  
 Shelef, M., see Gandhi, H.S. 169  
 Shelef, M., see Haack, L.P. 278, 280  
 Shelef, M., see Halasz, I. 132  
 Shelef, M., see Logan, A.D. 174, 247, 257, 258  
 Shelef, M., see Rokosz, M.J. 274, 305  
 Shelef, M., see Sinev, M.Y. 239, 247, 257, 258  
 Shenoy, G.K., see Suib, S.L. 278, 281  
 Sherry, A.D., see Young, S.W. 284  
 Sherry, H.S. 274–276, 281  
 Shesheniah, M., see Dyer, A. 278  
 Shi, J., see Balkus, K.J. 284  
 Shibasaki, M., see Sasai, H. 354  
 Shibata, T., see Narasaka, K. 347, 371  
 Shido, T. 222  
 Shilun, Q., see Yiguang, T. 278  
 Shimada, S. 328  
 Shimizu, M., see Nakamura, E. 317  
 Shimizu, M., see Noyori, R. 317  
 Shimizu, M., see Yi, G. 90, 91  
 Shimizu, N., see Honna, K. 302  
 Shimizu, T. 90, 91, 129  
 Shimizu, Y. 152  
 Shimizu, Y., see Zhang, H.M. 118–120  
 Shindo, T., see Makioka, Y. 347  
 Shinjoh, H. 213  
 Shinouskis, E.J., see Hertz, R.K. 170, 171  
 Shiokawa, J., see Arakawa, T. 115, 278  
 Shiomitsu, T., see Arai, H. 127, 128  
 Shiraishi, H. 3  
 Shiralkar, V.P. 279, 283  
 Shirasaki, T., see Maruoka, K. 354  
 Shu, Y.-J., see Liu, S.-B. 274, 278  
 Shvets, V.A., see Sass, A.S. 206  
 Shvets, V.A., see Tarasov, A.L. 206  
 Shyu, J.Z. 188, 190, 230, 231, 246  
 Siegmann, H.C. 8, 40  
 Silvestri, A.J., see Chang, C.D. 298  
 Sim, K.S. 17, 18  
 Simmons, G.W., see Klier, K. 110  
 Simon, M.W. 281  
 Sinev, M.Y. 239, 247, 257, 258  
 Sinfelt, J.H. 36, 66  
 Sinkewitch, R.M., see Taylor, K.C. 221  
 Siriwardane, R.V. 101, 102  
 Sisko, J. 348  
 Siwei, Z., see Schulz, H. 299  
 Skaribas, S.P. 78  
 Skoda, J., see Gaut, H. 319  
 Skoglundh, M. 142, 143  
 Skoudos, A.T., see Skaribas, S.P. 78  
 Slade, R.C.T. 278  
 Slagtern, Å. 92–94  
 Smith, D.J., see Datye, A.K. 2, 229, 232  
 Smith, J.V. 271, 273, 278, 279, 281  
 Smith, J.V., see Bennett, J.M. 278  
 Smith, P.J., see Brown, J.M. 344  
 Snider, B.B. 317  
 Snijder, E.D. 16  
 Sobukawa, H., see Fujitani, Y. 241  
 Soderholm, L., see Antonio, M.R. 278  
 Soga, K. 13, 63  
 Soga, K., see Imamura, H. 35  
 Sohler, M.P. 9, 19  
 Sohlo, J., see Mannila, P. 204  
 Sokobai, Y., see Gárdos, G. 292  
 Solberg, J., see Akporiaye, D.E. 274, 281, 300  
 Solofo, J., see Moreau, P. 297  
 Solovyova, L.P., see Isupova, L.A. 128  
 Solymosi, F. 202  
 Somiya, S., see Okikawa, S. 240  
 Somiya, S., see Tani, E. 237, 239, 240, 245  
 Somorjai, G.A., see Watson, P.R. 107, 108  
 Song, Ch. 297, 298  
 Song, I., see Antonio, M.R. 278  
 Song, S.H., see Yeom, Y.H. 273  
 Soraru, G., see Meriani, S. 240  
 Sorensen, O.T. 176  
 Soria, J. 206, 232  
 Soria, J., see Cunningham, J. 181, 182, 193, 229, 232  
 Soria, J., see Fierro, J.L.G. 172, 181, 182  
 Soria, J., see Martinez-Arias, A. 216, 223, 255, 256  
 Souma, Y., see Ando, H. 22  
 Sousa-Aguiar, E.F. 278, 282  
 Sousa-Aguiar, E.F., see Corma, A. 291  
 Sousa-Aguiar, E.F., see Serra, O.A. 278  
 Soustelle, M., see Pijolat, M. 239, 241, 257  
 Souza-Aguiar, E.F., see Nery, J.G. 278, 279  
 Spagnol, M. 299  
 Spaziano, V.T., see Forsberg, J.H. 316  
 Spencer, M.S., see Chinchén, G.C. 27, 30  
 Spencer, N.D., see Kubsch, J.E. 242, 247, 257  
 Spiridonov, S.E. 274, 281, 282  
 Spiridonov, S.E., see Nasukhanov, Kh.S.U. 278, 280, 282  
 Spretz, R., see Milt, V.G. 78, 123, 124, 141  
 Sri Rahayu, W. 122, 123  
 Srinivasan, K.R., see Choudhary, V.R. 274, 282

- Staiti, P., see Galvagno, S. 51  
 Stamires, D.N., see Rabo, J.A. 284, 302  
 Stasevich, V.P., see Orlik, S.N. 303  
 Steel, A.T., see Berry, F.J. 278  
 Stefanic, G. 239, 243  
 Steimberg, K.-H., see Winkler, H. 279  
 Steinberg, M., see Mendelovici, L. 197, 198  
 Stiles, A.B. 271  
 Stinson, S.C. 355  
 Stiranello, M., see Borriore, E. 362  
 Stöcker, M., see Akporiaye, D.E. 274, 281, 300  
 Stöcker, M., see Mostad, H. 274, 275, 293, 294  
 Stöcker, M., see Rørbik, T. 293  
 Stonecipher, D.L. 290  
 Stork, G. 317  
 Stoukides, M., see Chiang, P.H. 152, 153  
 Stoukides, M., see Eng, D. 152  
 Streitwieser, A., see Gong, L. 317  
 Striebel, J., see Müller, S. 152  
 Strömberg, D., see Lindstedt, A. 142  
 Struijk, J. 51  
 Struzhko, V.L., see Orlik, S.N. 303  
 Stubenrauch, J. 208, 209  
 Stubenrauch, J., see Cordatos, H. 194, 204, 208–210, 218, 255  
 Stucky, G.D., see Suib, S.L. 278, 281  
 Su, E.C. 195–198, 201  
 Subba Rao, Y.V. 300  
 Subrahmanyam, M., see Subba Rao, Y.V. 300  
 Suda, E., see Imamura, H. 53, 54, 56  
 Suda, E., see Konishi, T. 49, 53  
 Sudo, A., see Shimada, S. 328  
 Suga, S., see Kitamura, M. 361  
 Sugi, Y. 275, 278, 297, 298  
 Sugi, Y., see Kim, J.H. 297  
 Sugimori, J., see Narasaka, K. 354  
 Sugimoto, H., see Imamura, H. 60, 61  
 Sugimoto, M., see Honna, K. 302  
 Sugita, K., see Kobayashi, S. 333  
 Sugita, K., see Manabe, K. 335  
 Sugunan, S. 146  
 Suib, S.L. 278, 281  
 Suib, S.L., see Simon, M.W. 281  
 Sulikowski, B. 277  
 Sulikowski, G.A., see Burgess, K. 367  
 Summers, J.C. 163, 201, 204, 211, 212  
 Sun, Y. 240, 243  
 Suzuki, K., see Yi, G. 90, 91  
 Suzuki, M., see Murata, S. 317  
 Suzuki, M., see Noyori, R. 325  
 Suzuki, T., see Sasai, H. 354  
 Suzuki, Y., see Kametani, T. 347  
 Suzuki, Y., see Yashima, M. 237  
 Swamy, C.S. 137  
 Swamy, C.S., see Radha, R. 90, 91  
 Swaroop, S.H. 303  
 Taal, R., see Wortel, Th.M. 299  
 Tada, T., see Ishihara, K. 362  
 Tagawa, T. 98  
 Tagawa, T., see Imai, H. 37  
 Taha, R. 179, 193, 250, 254  
 Takada, T., see Imamura, H. 9, 37, 38, 66  
 Takahashi, H. 333, 335  
 Takahashi, H., see Ikemoto, M. 282  
 Takahashi, T., see Imamura, H. 8, 13  
 Takahori, T., see Kobayashi, S. 324, 345  
 Takai, K. 317  
 Takaki, K., see Makioka, Y. 347  
 Takakuwa, M., see Arakawa, T. 278  
 Takamoto, M., see Imamura, H. 57, 61, 62, 64  
 Takano, S., see Okikawa, S. 240  
 Takashima, H., see Yashima, M. 237  
 Takeda, H., see Kametani, T. 347  
 Takehira, K., see Yi, G. 90, 91  
 Takeshita, T. 31  
 Takeshita, T., see Coon, V.T. 22  
 Takeshita, T., see Wallace, W.E. 32  
 Takeuchi, Y., see Nomura, Y. 353  
 Tam, W., see Pect, W.G. 337  
 Tamura, H., see Sasahara, A. 213  
 Tan, K.L., see Lin, Y. 137  
 Tanaka, A., see Domen, K. 151, 152  
 Tanaka, H., see Ando, H. 22  
 Tanaka, H., see Narasaka, K. 358  
 Tanaka, H., see Yamada, K. 250  
 Tanaka, K., see Lombardo, E.A. 86, 106  
 Tanaka, K., see Sasahara, A. 213  
 Tanaka, K., see Sasai, H. 354  
 Tanaka, M. 343, 344  
 Tanaka, M., see Mizuno, N. 141, 142  
 Tanaka, T. 55, 56, 278  
 Tanaka, T., see Baba, T. 54, 56, 274, 278, 301  
 Tani, E. 237, 239, 240, 245  
 Taniguchi, Y., see Makioka, Y. 347  
 Taouk, B., see Sri Rahayu, W. 122, 123  
 Taraoka, Y., see Zhang, H.M. 80  
 Tarasov, A.L. 206  
 Tascón, J.M.D. 84, 85, 129  
 Tascón, J.M.D., see Fierro, J.L.G. 84  
 Tascón, J.M.D., see Kremenić, G. 90, 116

- Tascón, J.M.D., see Tejuca, L.G. 76, 85, 106, 140
- Tateishi, S., see Miki, T. 190, 247, 257
- Tatsuke, U., see Mitsuhasi, T. 239
- Tau, K.D., see Foley, H.C. 108
- Taube, R. 46
- Tauster, S.J. 229
- Tauster, S.J., see Murrell, L.L. 201–203, 230–232
- Taylor, B.W., see Kobylinski, T.P. 213
- Taylor, K.C. 160–163, 167, 212, 213, 221
- Tecilla, P., see Lucchini, V. 331, 336, 347, 351
- Teichner, S.J., see Conner Jr, W.C. 69
- Tejuca, L.G. 76, 85, 106, 140
- Tejuca, L.G., see Fierro, J.L.G. 84, 85
- Tejuca, L.G., see Kremenčić, G. 90, 116
- Tejuca, L.G., see Rojas, M.L. 109, 110
- Tejuca, L.G., see Tascón, J.M.D. 84, 85, 129
- Tellew, J.E., see Overman, L.E. 336
- Tempere, J.F., see Fajardie, F. 252, 256
- Teo, W.K., see Lin, Y. 137
- Terada, M., see Mikami, K. 317, 354, 360
- Terao, Y., see Sekiya, M. 370
- Teraoka, Y. 95, 132, 133, 144
- Teraoka, Y., see Yamazoe, N. 118, 123, 138
- Teraoka, Y., see Zhang, H.M. 118–120
- Terribile, D. 185, 243, 244
- Theobald, C.J., see Ife, R.J. 362
- Thite, G.A., see Choudhary, V.R. 119
- Thom, K.F. 316
- Thomas, J.M. 132
- Thomas, J.M., see Cheetham, A.K. 278, 279, 281
- Thompson, D.S. 46, 53
- Thompson, J.C. 46
- Thomsen, I., see Gothelf, K.V. 365
- Tian, Y.G. 278
- Tidwell, M.Y., see Rauckman, B.S. 362
- Timonen, J.T. 278
- Toba, M., see Niwa, S. 51
- Tofield, B.C. 86
- Tokunaga, Y., see Imamura, H. 47, 48
- Tomita, K., see Takahashi, H. 333, 335
- Tomita, M., see Fujitani, Y. 241
- Tomoda, S., see Nomura, Y. 353
- Torrsell, K.B.G. 365
- Toshihaw, T., see Arakawa, T. 278
- Touret, O., see Badri, A. 187, 255
- Touret, O., see Cuif, J.P. 2, 242, 243
- Touret, O., see El Fallah, J. 179, 181–184, 191, 195
- Touret, O., see Fajardie, F. 252, 256
- Touret, O., see Laachir, A. 172, 174, 179, 181, 183, 192, 255
- Touret, O., see Perrichon, V. 172, 175, 177, 179–181, 184, 203, 232
- Touret, O., see Pijolat, M. 239, 241, 257
- Tournayan, L. 174
- Tournayan, L., see Perrichon, V. 172, 175, 177, 179–181, 184
- Tournayan, L., see Zotin, F.M.Z. 173, 177, 181, 192
- Tournoux, M., see Barrault, J. 77
- Touroude, R., see Sim, K.S. 17, 18
- Townsend, R.P. 275
- Toyoshima, I., see Lombardo, E.A. 86, 106
- Treacy, M.M. 270, 272
- Trecourt, F., see Mongin, F. 362
- Trenkle, W.C., see Overman, L.E. 336
- Tretyakov, V.F., see Isupova, L.A. 128
- Treviño, H., see Weyrich, P.A. 302
- Trif, E., see Nicula, A. 278
- Trikalitis, P.N. 147
- Trimble, L.E., see Voorhoeve, R.J.H. 129, 140
- Trimm, D.L., see Dumpelmann, R. 213
- Trimm, D.L., see Padeste, C. 177, 187, 200, 209, 216, 217, 232
- Trimm, D.L., see Whittington, B.J. 226, 227
- Trovarelli, A. 169, 177, 181, 186, 189–191, 193, 194, 197, 200, 216, 218, 229, 230, 232, 234, 242, 252
- Trovarelli, A., see de Leitenburg, C. 90, 91, 174, 179, 216, 229, 232, 235, 239, 240, 247–249, 257
- Trovarelli, A., see Fornasiero, P. 239, 241, 247, 248
- Trovarelli, A., see Kašpar, J. 213, 214, 217, 225, 256
- Trovarelli, A., see Terribile, D. 185, 243, 244
- Trovarelli, A., see Zamar, F. 174, 243, 247, 252, 257
- Truex, T.J., see Diwell, A.F. 201, 226
- Truex, T.J., see Golunski, S.E. 232–234
- Truhlar, D.G., see Cramer, C.J. 326
- Tsai, C.Y. 97
- Tschope, A. 204
- Tsuchiya, S., see Arakawa, T. 115
- Tsuchiya, S., see Imamura, H. 8, 9, 13, 34, 37, 38, 46–54, 56–66, 68, 70–72
- Tsujii, J. 317
- Tsutsumi, K., see Ikemoto, M. 282
- Tsuzuki, N., see Yamamura, M. 101

- Tu, X., see Kim, J.H. 297  
 Tu, X., see Sugi, Y. 275, 278, 297, 298  
 Tufariello, J.J. 365  
 Tull, R., see Weinstock, L.M. 340  
 Tuller, H.L. 247, 257  
 Turner, T.W., see Bruce, L.A. 174, 179–181, 183  
 Tuxworth, R.H., see Burwell Jr, R.L. 67  
 Tuxworth, R.H., see Rowlinson, H.C. 67
- Uamada, K., see Imamura, H. 37  
 Uchijima, T., see Hishida, T. 66  
 Uchino, N., see Sakai, M. 51  
 Udovich, C.A., see Balachandran, U. 96, 97  
 Ueda, M., see Niwa, S. 51  
 Uemura, F., see Iwamoto, M. 303  
 Uemura, K., see Shimizu, Y. 152  
 Ueno, A., see Haneda, M. 196, 197  
 Ueno, A., see Miki, T. 188, 190, 247, 257  
 Ueno, M., see Kobayashi, S. 333, 341  
 Uh, Y.S., see Hong, S.B. 274, 278  
 Ulla, M.A. 106, 112, 113, 278  
 Ulla, M.A., see Aparicio, L.M. 302  
 Ulla, M.A., see Milt, V.G. 78, 123, 124, 141  
 Ulla, M.A., see Petunchi, J.O. 106, 107, 113  
 Umansky, B.S., see Nudel, J.N. 80, 106  
 Uphade, B.S., see Choudhary, V.R. 92–96, 119  
 Upreti, M.C., see Das, D. 276  
 Usmen, R.K. 247, 257  
 Usmen, R.K., see Graham, G.W. 257  
 Uytterhoeven, J.B., see Costenoble, M.L. 278  
 Uytterhoeven, J.B., see Jacobs, P.A. 278
- Vaillancourt, J., see Kirchnerova, J. 123  
 Valden, M. 217  
 Valdivieso, F., see Colon, G. 243  
 van Bekkum, H. 270  
 Van Bekkum, H., see Floor, M. 299  
 van Bekkum, H., see Hölderich, W.F. 299, 301  
 van Bekkum, H., see Ito, E. 275, 303, 304  
 van Bekkum, H., see Wortel, Th.M. 299  
 van Damme, H. 151  
 van den Bleek, C.M., see Hultermans, R.J. 305  
 van den Bleek, C.M., see Ito, E. 275, 303, 304  
 van der Kerk, G.J.M., see Luijten, J.G.A. 343, 344  
 van der Veen, A.M.H., see Hazenkamp, M.F. 275, 278  
 van Grieken, R. 109–111  
 van Grondelle, J., see Huizinga, T. 211
- Van Minnen-Pathuis, G., see Wortel, Th.M. 299  
 Van Reijen, L.L., see Schaper, H. 83  
 Van Swaaij, W.P.M., see Snijder, E.D. 16  
 van Vucht, J.H.N. 63  
 van Woerkom, P.C.M., see Roelofsen, J.W. 278, 280  
 Vannice, M.A. 69  
 Vannice, M.A., see Neikam, W.C. 69  
 Vansant, E.F., see Voort, P.V.D. 48  
 Varloud, J., see Zotin, F.M.Z. 173, 177, 181, 192  
 Varma, R.S., see Reddy, T.I. 276, 297, 301  
 Varo, A., see Bernal, S. 202, 232  
 Vasek, P., see Pollert, E. 131  
 Vasishta, S.C., see Davies, A.G. 344  
 Vatti, F.P., see Forni, L. 142  
 Vayenas, C.G., see Papadakis, V.G. 257  
 Vayenas, C.G., see Pliangos, C. 257  
 Venuto, P.B. 270, 276, 284, 295, 296, 298, 299, 301  
 Venuto, P.B., see Landis, P.S. 284  
 Veron, J., see Breysse, M. 204, 205, 257  
 Versteeg, G.F., see Snijder, E.D. 16  
 Verykios, X.E., see Ioannides, T. 257  
 Verykios, X.E., see Papadakis, V.G. 257  
 Verykios, X.E., see Pliangos, C. 257  
 Vidal, H., see Bernal, S. 257, 258  
 Vidal, H., see Colon, G. 243  
 Vidal, H., see Daturi, M. 181  
 Vidmar, P. 239, 249–251, 257, 259  
 Vidyasagar, J.K., see Rao, C.N.R. 77  
 Vijayaraghavan, R., see Hatwar, T.K. 55  
 Vijayaraghavan, R., see Rao, C.N.R. 55  
 Villadsen, J., see Gordes, P. 78  
 Villain, F., see El Fallah, J. 179, 181–184, 191, 195  
 Villarubia, J.S. 217  
 Vinek, H., see Noller, H. 132  
 Virkar, A.V., see Hong, S.J. 240  
 Vishniakov, A.V., see Forni, L. 142  
 Viswanathan, B. 129  
 Vlaic, G. 248  
 Vlaic, G., see Ranga Rao, G. 172, 200, 234, 252, 254  
 Vogel, E.M. 84, 85  
 Vogel, E.M., see Johnson Jr, D.W. 122  
 Vohs, J.M., see Cordatos, H. 194, 204, 208–210, 218, 255  
 Vohs, J.M., see Putna, E.S. 208, 211, 252  
 Vohs, J.M., see Stubenrauch, J. 208, 209

- Volchenkova, Z.S., see Pal'guev, S.F. 240  
 Volter, J. 59  
 Von Ballmoos, R., see Treacy, M.M. 270, 272  
 von Ballmoos, R.A. 290  
 Voorhoeve, R.J.H. 115, 129, 140  
 Voort, P.V.D. 48  
 Vougioukas, A.E. 317  
 Vrieland, E.G. 122  
 Vvedensky, D.D. 12  
  
 Wachowski, L. 84  
 Wade, L.E., see Brousard, J.A. 109  
 Wakabayashi, T., see Kobayashi, S. 326  
 Wakatsuki, T., see Yamamura, M. 101  
 Waldmann, H. 362  
 Walker, A.P. 9, 31–34  
 Walker, A.P., see Shaw, E.A. 27, 29–31  
 Wallace, D.N. 1  
 Wallace, W.E. 16, 26, 32, 63, 64  
 Wallace, W.E., see Coon, V.T. 22  
 Wallace, W.E., see Elattar, A. 22  
 Wallace, W.E., see France, J.E. 13, 24, 26, 41  
 Wallace, W.E., see Imamura, H. 13, 35  
 Wallace, W.E., see Takeshita, T. 31  
 Wallau, M., see Pires, E.L. 302  
 Wang, G. 299  
 Wang, Q., see Zhu, G. 17  
 Wang, W. 104  
 Wang, X., see Wang, G. 299  
 Wang, Y. 137, 138  
 Wang, Z.L. 24, 25, 41  
 Ward, D., see Enders, D. 333, 335  
 Ward, J.W. 276, 278, 282  
 Warf, J.C. 48  
 Warf, J.C., see Salot, S. 46, 53  
 Warren, J.P. 9, 39  
 Watcher, W.A., see Pine, L.A. 287  
 Waterman, E.M., see Farrauto, R.J. 231  
 Watkins, W.L.H., see Shyu, J.Z. 230, 231  
 Watkins, W.L.H., see Usmen, R.K. 247, 257  
 Watson, P.R. 107, 108  
 Waugh, J.S., see Thompson, D.S. 46, 53  
 Waugh, K.C., see Chinchin, G.C. 27, 30  
 Waugh, K.C., see Harrison, P.G. 242  
 Weber, T., see Denmark, S.E. 333, 335  
 Weber, W.H., see Shyu, J.Z. 188, 190, 246  
 Wee, A.T.S., see Lin, Y. 137  
 Wehrer, P., see Dauscher, A. 257  
 Wei, Q., see Li, R.-S. 278  
 Weibel, M. 223  
 Weihe, M., see Weiß, U. 274, 283  
 Weinreb, S.M. 347, 362  
 Weinreb, S.M., see Boger, D.L. 347, 362  
 Weinreb, S.M., see Sisko, J. 348  
 Weinstock, L.M. 340  
 Weiqi, Lu 9, 13, 36, 40  
 Weisz, P.B., see Meisel, S.L. 298  
 Weitkamp, J. 292, 302  
 Weitkamp, J., see Hunger, M. 278  
 Weitkamp, J., see Weiß, U. 274, 283  
 Weits, H.H., see Fisher, R. 302  
 Weiß, U. 274, 283  
 Wells, A.F. 77  
 Welter, J.M., see Percheron-Guégan, A. 8  
 Welter, J.-M., see Percheron-Guégan, A. 63  
 Wemple, J., see Lucast, D.H. 317  
 Wen, R.-W., see Li, R.-S. 278  
 Weng, H.S., see Liang, J.J. 146, 149  
 Weng, H.S., see Yao, C.S. 303  
 Wenqin, P., see Yiguang, T. 278  
 Wertheim, G.K., see Johnson Jr, D.W. 122  
 Weyrich, P.A. 302  
 Whan, D.A., see Chinchin, G.C. 27, 30  
 White, A.H., see Harrowfield, J.M. 316  
 White, J.M., see Campbell, C.T. 217  
 White, J.M., see Jin, T. 208, 209, 223  
 White, W.B., see Keramidas, V.G. 239  
 Whitesides, G.M., see Kim, E. 338  
 Whitesides, G.M., see Schmid, W. 338  
 Whittington, B.J. 226, 227  
 Wiggall, K.J., see Ife, R.J. 362  
 Wilby, A.H., see Johnstone, R.A.W. 70  
 Wilkinson, G., see Cotton, F.A. 354, 356, 359  
 Willis, R.G., see Dobson, N.A. 53  
 Willson, P.J., see Church, M.L. 162, 163  
 Winkler, H. 279  
 Wise, H., see McCarty, J.G. 117  
 Wise, H., see Quinlan, M.A. 115  
 Wise, J.J., see Venuto, P.B. 276, 284, 295, 296, 298  
 Wittstock, K., see Lintz, H.G. 118  
 Wokaun, A., see Kritzenberger, J. 49  
 Wolcyrz, M., see Kepinski, L. 201–203, 232  
 Wold, A., see Carreiro, L. 84  
 Wolf, E.E., see Miró, E.E. 98  
 Wolfendale, B.A., see Harrison, P.G. 242  
 Wortel, Th.M. 299  
 Worth, D.F. 347  
 Wrobel, G., see Lamonier, C. 177  
 Wrobel, G., see Sohler, M.P. 9, 19  
 Wu, K.H., see Chen, Y.L. 239  
 Wu, Y., see Liu, Ch. 146, 150

- Wu, Y., see Yu, Z. 148  
 Wu, Y., see Zhao, Z. 88, 133–135, 137  
 Wulff, W.D., see Bao, J. 359, 360  
 Wurisika, R.R., see Swaroop, S.H. 303  
 Wykypiel, W., see Seebach, D. 335, 371
- Xiang, N., see Valden, M. 217  
 Xiang, Y.B., see Corey, E.J. 354  
 Xiangsheng, W. 297  
 Xingqun, Zhang, see Jianhui, Li 9, 13, 36  
 Xiong, J., see Li, Q. 278, 280  
 Xu, X. 218  
 Xue, Z., see Li, Q. 278, 280
- Yahiro, H., see Sato, S. 303  
 Yamada, K. 250  
 Yamada, K., see Funabiki, T. 257  
 Yamada, K., see Imamura, H. 8, 9, 13, 37, 38, 66  
 Yamada, T., see Arai, H. 116, 117, 121, 122  
 Yamada, T., see Narasaka, K. 354  
 Yamaguchi, O., see Kawabata, A. 239  
 Yamamoto, H., see Hattori, K. 328, 359  
 Yamamoto, H., see Ishihara, K. 354, 362  
 Yamamoto, H., see Kamegashira, N. 86  
 Yamamoto, H., see Maruoka, K. 317, 354, 359, 362, 365  
 Yamamoto, H., see Yanagisawa, A. 337  
 Yamamoto, M., see Yamada, K. 250  
 Yamamoto, Y. 337, 340  
 Yamamoto, Y., see Kodata, I. 333, 335  
 Yamamura, M. 101  
 Yamanoi, Y., see Kobayashi, S. 320  
 Yamashita, H., see Kato, A. 83  
 Yamashita, H., see Matsuda, S. 83  
 Yamazaki, O., see Nozaki, T. 105  
 Yamazaki, T., see Mori, H. 274, 301  
 Yamazoe, N. 118, 123, 138  
 Yamazoe, N., see Seiyama, T. 88  
 Yamazoe, N., see Shimizu, Y. 152  
 Yamazoe, N., see Teraoka, Y. 95  
 Yamazoe, N., see Zhang, H.M. 80, 118–120  
 Yamplo-Skii, Yu.Yu., see Azbel, B.I. 274, 302  
 Yan, J.Y. 305  
 Yan, Q., see Zhong, Z. 124, 125  
 Yanagisawa, A. 337  
 Yanagiya, N., see Onaka, M. 328  
 Yang, D.Z., see Chen, Y.L. 239  
 Yang, M. 3  
 Yang, S.-J. 290  
 Yang, X., see Liu, Ch. 146, 150
- Yang, X., see Zhao, Z. 88, 133–135, 137  
 Yang, X., see Zhu, G. 17  
 Yao, C.S. 303  
 Yao, H.C. 1, 173, 174, 177, 188–191, 194–197, 235  
 Yao, H.C., see Otto, K. 167, 213  
 Yao, M.H. 240, 244, 245  
 Yao, M.H., see Datye, A.K. 2, 229, 232  
 Yao, Y.F., see Yao, H.C. 1  
 Yashima, M. 237–240  
 Yashima, M., see Du, Y. 237  
 Yasuda, H. 46, 136, 137, 274, 303  
 Yasuda, H., see Wang, Y. 137, 138  
 Yasuda, M., see Kobayashi, S. 330  
 Yasumori, I., see Ichimura, K. 106, 107  
 Yatagai, H., see Yamamoto, Y. 337  
 Yates, D. 345  
 Ye, X., see Liu, Ch. 146, 150  
 Yeh, L.-A., see Sarges, R. 362  
 Yentekakis, I.V., see Papadakis, V.G. 257  
 Yentekakis, I.V., see Pliangos, C. 257  
 Yeom, Y.H. 273  
 Yi, G. 90, 91  
 Yiguang, T. 278  
 Ying, J.Y., see Tschope, A. 204  
 Ying, M., see Wang, G. 299  
 Yokota, K., see Fujitani, Y. 241  
 Yokoyama, Ch. 303, 304  
 Yokoyama, K., see Nakamura, E. 317  
 Yokoyama, K., see Noyori, R. 317  
 Yokoyama, M., see Imamoto, T. 19, 20  
 Yokoyama, T. 12  
 Yoldas, B.E. 239  
 Yoneda, R., see Harusawa, S. 343, 344  
 Yoneda, Y., see Hishida, T. 66  
 Yoneda, Y., see Nakamura, T. 129  
 York, A.P.E., see Yi, G. 90, 91  
 Yoshida, K., see Ojima, I. 328, 332  
 Yoshida, S., see Baba, T. 54, 56, 274, 278, 301  
 Yoshida, S., see Tanaka, T. 55, 56, 278  
 Yoshida, T., see Baba, T. 54, 56, 274, 301  
 Yoshida, T., see Tanaka, T. 56, 278  
 Yoshimochi, H., see Imamura, H. 46  
 Yoshimura, K., see Imamura, H. 57, 59–62, 64, 71  
 Yoshimura, M., see Du, Y. 237  
 Yoshimura, M., see Tani, E. 237, 239, 240, 245  
 Yoshimura, M., see Yashima, M. 237–240  
 Yoshinaka, M., see Kawabata, A. 239  
 Yoshinobu, M., see Imamura, H. 46, 58, 59, 61, 62, 65, 71

- Young, J.R., see Matier, W.L. 340  
Young, S.W. 284  
Yu, Z. 148  
Yu-u, Y., see Sato, S. 303  
Yu Yao, Y.F. 203, 205, 206, 212  
Yu Yao, Y.F., see Yao, H.C. 173, 174, 177, 188–191, 194–197, 235  
Yuan, H.Q., see Jiang, A.R. 132  
Yuan, S., see Yu, Z. 148  
Yukawa, K., see Fujii, T. 66  
  
Zadeh, J.A., see Blouri, B. 47  
Zafiris, G.S. 194, 204, 206–209, 211, 218, 223  
Zamar, F. 174, 243, 247, 252, 257  
Zamar, F., see de Leitenburg, C. 239, 240, 247–249  
Zdansky, E., see Andersen, J.N. 63–65  
Zen'kovski, S.M., see Minachev, K.M. 291  
Zerger, R.P., see Suib, S.L. 278, 281  
Zhang, H.M. 80, 118–120  
Zhang, H.M., see Teraoka, Y. 95  
Zhang, H.Y., see Corey, E.J. 354  
Zhang, J., see Kang, Z.C. 176, 177  
Zhang, T., see Amiridis, M.D. 303  
Zhang, T.J., see Amiridis, M.D. 160  
Zhang, W.-Y., see Li, R.-S. 278  
  
Zhang, X. 206  
Zhang, X., see Warren, J.P. 9, 39  
Zhang, Y. 239, 240, 257, 274, 276, 278, 303  
Zhang, Z. 100  
Zhang, Z.C. 12  
Zhao, S., see Puchot, C. 361  
Zhao, Z. 88, 133–135, 137  
Zhao, Z., see Liu, Ch. 146, 150  
Zhao, Z.L. 197  
Zhdanov, V.P. 213  
Zheng, Z., see Karge, H.G. 276, 277, 285  
Zhon, Q.W., see Jiang, A.R. 132  
Zhong, Z. 124, 125  
Zhou, F.Q., see Tian, Y.G. 278  
Zhu, G. 17  
Zhu, L., see Li, Q. 278, 280  
Zhuravlev, L.T. 48  
Zielinski, S., see Wachowski, L. 84  
Zierke, T., see Reetz, M.T. 360  
Zinner, K., see Zinner, L.B. 274, 296  
Zinner, L.B. 274, 282, 296  
Zotin, F.M.Z. 173, 177, 181, 192  
Zotin, F.M.Z., see Sousa-Aguiar, E.F. 278, 282  
Zundel, G., see Fritsch, J. 359, 369  
Zuyi, T., see Rees, L.V.C. 276  
Zwinkels, M.F.M. 115, 125, 129



## SUBJECT INDEX

- AES (Auger electron spectroscopy) 25
- A/F ratio 161–163, 165, 166, 169, 170, 173, 185, 213
- acidic zeolite catalysts 281
- acylations on R-containing zeolites 299
- acylhydrazones 333–336
- Ag/ThO<sub>2</sub> 30
- Al<sub>2</sub>O<sub>3</sub> 163, 166, 168, 169, 179, 188–190, 197, 198, 203, 212, 218, 219, 222, 225, 226, 229, 240, 242, 244, 246, 251, 253
- aldol reactions 317–327
  - in aqueous media 317–322
  - micellar systems 326, 328
- alkylation
  - of aromatics on R-containing zeolites 295
  - of benzene with ethylene 296
  - of isobutane/butene
    - on Ce-exchanged zeolites 292
    - on La-exchanged zeolites 294
    - on R-containing zeolites 290
  - of naphthalene 297
  - of phenol or aniline on R-containing zeolites 297
  - reaction of Ce-Y zeolite compared with Nafion-H 293
- alkylthiolation of phenol on R-containing zeolites 297
- alloys
  - Ce<sub>3</sub>Rh<sub>2</sub> 39
  - Cu–Ce–Al 31
- allylation 337–340
  - of aldehydes and ketones 337–340
  - of imines 340
- aluminum halides 35
- amorphous alloys 7
  - Cu–Ce–Al 28
  - Cu–MM–Al 28
- aromatization
  - cyclohexane 36
  - 3-methylhexane 35
  - *n*-pentane 36
- asymmetric reactions
  - 1,3-dipolar cycloadditions 365–370
  - aza Diels–Alder 362–365
  - Diels–Alder 354–362
- Au/ThO<sub>2</sub> 30
- aza Diels–Alder reactions 347–354
- bastnaesite 285
  - rare-earth content of 285
- β-amino esters
  - one-pot synthesis 330–332
- β hydride phase 14
- bimetallic alloy Nd–Ni 39
- bimetallic catalysts 40
- bimetallic compounds 56
- Brønsted acid sites
  - in R-containing zeolites 282
  - on La-containing materials 282
- CCC, *see* close-coupled catalyst
- C<sub>6</sub>H<sub>12</sub>–D<sub>2</sub> exchange reaction 47, 67, 71
- C<sub>2</sub>H<sub>5</sub>Br 8
- CO 17, 161–167, 169, 170, 173, 174, 185, 186, 194–196, 198, 201, 202, 204–207, 209–213, 215, 216, 218, 220–227, 229–234, 236, 237, 250–252, 255
- CO<sub>x</sub>, CO<sub>2</sub> + H<sub>2</sub> 112
- CO<sub>x</sub> hydrogenation 107–114
  - LaMn<sub>1–x</sub>Cu<sub>x</sub>O<sub>3–λ</sub> 111
- CO/NO reaction 213–216, 252
- CO/O<sub>2</sub>/NO reaction 214, 252
- CO oxidation 162, 185, 194, 203–212, 214, 220, 224, 226, 252, 255, 257
  - kinetics 207–210, 212
- CRY (calcined rare earth Y), production process 286
- catalysis of R–Co and R–Ni 56
- catalysis of R–Pd/SiO<sub>2</sub> with hydrogen uptake 68–70
- catalysis of rare earths 47
  - Eu/SiO<sub>2</sub> 49

catalysis of rare earths (*cont'd*)

- R/C 53, 54
- – hydrogenation activity for ethene 53
- R/SiO<sub>2</sub> 47–53
- – high loading 51
- – low loading 49
- – turnover frequencies (TOF) 50
- R/zeolite 54–56
- – europium and ytterbium (R/zeolite) introduced into K<sup>+</sup>-exchanged Y-zeolite 54
- selective hydrogenation 49
- Yb/SiO<sub>2</sub> 49
- catalytic converters 167, 168
- catalytic cracking on R-containing zeolites 284
- catalytic properties for hydrogenolysis 47
- catalytic properties of rare earths 46
- catalytic transfer hydrogenation with ammonia 70, 71
- CeAlO<sub>3</sub> 190, 246
- Ce<sup>4+</sup>/Ce<sup>3+</sup> redox couple 171, 173, 197, 198, 200, 246, 254
- CeCu<sub>2</sub> 27
- CeH<sub>2-x</sub>/Co catalyst 33
- CeH<sub>2-x</sub>/Fe catalyst 33
- CeH<sub>2-x</sub>/Ru catalyst 33
- CeN 33
- CeO<sub>2-x</sub> 172–175, 185, 190, 204, 216, 218, 221
- CeO<sub>2</sub> 38, 39, 160, 166–169, 171, 174–180, 182, 183, 185, 189, 191, 194, 196–199, 201–207, 209, 210, 212–214, 216, 217, 219, 220, 222, 224–230, 232–235, 237, 239, 242, 246, 247, 249, 250, 258
- α-phase 175, 177, 178
- CO oxidation 205, 206, 209, 210
- CO-TPR 185–188, 190, 196, 204, 209
- doped systems 241, 242, 247, 257
- dynamic-OSC 173, 174, 194–197
- H<sub>2</sub> adsorption 190
- H<sub>2</sub> chemisorption 181
- H<sub>2</sub>-TPR 178, 187, 188, 235, 236
- hydrogen bronzes 181–183
- lattice oxygen 186, 187, 204, 206, 208, 209, 221
- lattice parameters 177
- oxidation 199, 216
- oxidation catalyst 204
- oxygen diffusion 184, 194, 257
- oxygen storage capacity 169, 171, 173, 199, 219, 223, 247

- phase diagram 172, 175
- reduction behaviour 185, 188, 193, 194, 200
- reduction kinetics 181, 182, 184, 187, 199, 200
- reduction mechanism 181–183, 185
- reduction of surface 192–194
- σ-phase 175
- structural doping 247
- surface area 179–181, 183, 184, 187, 188, 192, 193, 203, 232, 237, 242
- surface sites 180, 194, 201, 204, 232, 255
- synthesis 185
- thermal stability 241, 242, 252, 257
- total-OSC 173, 174, 194, 195, 197
- water gas shift 169, 185, 208
- Ce<sub>2</sub>O<sub>3</sub> 172, 175, 176, 206, 222, 239
- Ce<sub>2</sub>O<sub>3</sub>-containing Cu–Mg hydrotalcite for reduction of SO<sub>x</sub> and NO<sub>x</sub> emissions 289
- CeO<sub>2</sub>–ZrO<sub>2</sub> 161, 167, 235
- phase diagram
- – c phase 237
- – κ-phase 239
- – m phase 237
- – t phase 237
- – t' phase 237
- – t'' phase 237, 239
- – t\*-phase 239
- thermal stability 243
- CeO<sub>2</sub>–ZrO<sub>2</sub>/Al<sub>2</sub>O<sub>3</sub>
- thermal stability 245, 246
- CeO<sub>2</sub>–ZrO<sub>2</sub> mixed oxides 235–256, 258
- catalytic reactions 252–256
- doped systems 239, 250, 254, 257
- dynamic-OSC 243
- H<sub>2</sub>-TPR 249
- homogeneity of solid solution 240, 243
- lattice parameters 240, 244
- m-phase 238
- particle size 244
- phase diagram 237–239
- redox behaviour 241, 246–251
- solid solutions 240, 244
- structural properties 248
- synthesis 239, 240, 243
- thermal stability 241–246, 251
- total-OSC 251
- t''-phase 238
- t'-phase 238
- t-phase 238

- $\text{CeO}_2/\text{Al}_2\text{O}_3$  174, 185, 188–190, 195, 197, 217,  
 224, 234, 244, 246, 257  
 – CO oxidation 207  
 – CO-TPR 188, 190, 193  
 – dynamic-OSC 195–197  
 –  $\text{H}_2$ -TPR 188, 190, 193  
 –  $\text{O}_2$  uptake 189  
 $\text{CeO}_2$ -based electrolytes 247  
 $\text{CeO}_2/\text{SiO}_2$  190  
 $\text{CePd}_3$  35  
 $\text{Ce}_2\text{Si}_2\text{O}_7$  11  
 $\text{Ce}_{0.5}\text{Zr}_{0.5}\text{O}_2$  239, 248–250, 253, 255  
 –  $\text{H}_2$ -TPR 251  
 – reduction mechanism 250  
 $\text{Ce}_2\text{Zr}_2\text{O}_7$  239  
 $\text{Ce}_3\text{ZrO}_8$  239  
 chiral rare-earth metal triflates 359, 360  
 close-coupled catalyst 164, 165, 167, 230, 235,  
 258  
 $\text{Co}/\text{Al}_2\text{O}_3$  catalyst 24  
 $\text{Co}/\text{CeO}_2$  24  
 $\text{Co}/\text{CeO}_2$  catalyst 24  
 $\text{Co}/\text{La}_2\text{O}_3$  23  
 $\text{Co}/\text{La}_2\text{O}_3$  catalyst 24  
 $\text{Co}/\text{SiO}_2$  catalyst 24  
 combustion  
 – of diesel soot 122, 123  
 – of methane 115, 117, 119, 120, 123, 124  
 – – kinetic rate 121, 122  
 – of VOCs 118  
 condensation of carbonyl compounds on  
 R-containing zeolites 301  
 cracking reactions 34  
 $\text{Cu}/\text{CeO}_2$  33  
 $\text{CuO}$  38, 150  
 $\text{CuO}-\text{La}_2\text{O}_3-\text{SrO}$  150  
 $\text{Cu}/\text{ZnO}/\text{Al}_2\text{O}_3$  27  
 $\text{Cu}/\text{ZnO}/\text{Al}_2\text{O}_3$  catalyst 26  
 cyclization 71  
 $c\text{-ZrO}_2$  239  
  
 $\text{D}_2$  84  
 decomposition of water 152  
 dehydrogenation 47, 71  
 – alcohols 9, 37  
 – alkanes 37  
 – alkenes 37  
 – cyclohexane 65–67  
 – – kinetics 66  
 – cyclohexene 37  
 – hydrocarbon 37  
 – methanol 37, 145, 147  
 – *n*-heptane 37  
 – propan-2-ol 37  
 – 2-propanol 14  
 diamide 46  
 dibromoethane 8  
 Diels–Alder reactions 345–347  
 – on R-containing zeolites 302  
 diffusion coefficients of hydrocarbons in Me-X  
 zeolites 283  
 – 1-butene 283  
 – isobutane 283  
 – *n*-butane 283  
 1,2-diiodoethane 8  
 disproportionation 71  
 – of cyclohexa-1,3-diene 51  
 – of ethylbenzene 277  
 – of toluene 146, 149  
 $\text{Dy}(\text{OTf})_3$  319  
 dynamic-OSC 194, 198, 201  
  
 EXAFS (extended X-ray absorption spectroscopy)  
 23, 27  
 electrochemical reactors 152  
 electrodes 152  
 $\text{Er}(\text{OTf})_3$  319  
 ethylation of ethylbenzene 297  
 ethylbenzene disproportionation on R-containing  
 zeolites 283  
 $\text{Eu}-\text{Co}$  58, 59, 63  
 $\text{Eu}-\text{Co}$  catalyst 64  
 $\text{Eu}-\text{Ni}$  57–59, 63  
 $\text{Eu}-\text{Ni}$  catalyst 64, 67  
 $\text{Eu}$ -exchanged zeolites, tetrahedral  $[\text{Eu}_4\text{O}]^{10+}$   
 complex 281  
 $\text{EuN}$  54, 56  
 $\text{EuNH}$  56  
 $\text{Eu}(\text{NH}_2)_2$  54  
 $\text{Eu}(\text{NH}_2)_3$  56  
 $\text{Eu}(\text{OTf})_3$  319  
 $\text{Eu}/\text{PVA}$  catalyst 51  
 $\text{Eu}/\text{SiO}_2$  catalyst 50, 52  
 $\text{Eu}/\text{zeolite}$  55, 56  
 europium 46  
  
 FCC catalysts 284  
 – preparation 285, 286  
 faujasite  
 – structure 273

- faujasite (*cont'd*)  
 – topology 271, 273  
 fluorite-type oxides 175–177  
 formaldehyde 317, 318  
 fraction of  $R^{2+}$  and  $R^{3+}$  evaluated from XANES of  
   R/zeolite 55  
  
 gadolinium triflate, *see* Gd(OTf)<sub>3</sub>  
 GdMnO<sub>3</sub> 101  
 Gd(OTf)<sub>3</sub> 319  
 Gd<sub>1-x</sub>Sr<sub>x</sub>CoO<sub>3</sub> 118  
 global catalyst FCC, preparation procedure 288  
 grafting of zeolites 272  
  
 H<sub>2</sub> + hydrocarbons 106, 107  
 – C<sub>2</sub>–C<sub>4</sub> hydrocarbons 106  
 – C<sub>2</sub>–C<sub>5</sub> hydrocarbons 107  
 – ethene hydrogenation 107  
 H<sub>2</sub>(10%)/N<sub>2</sub> 84  
 H<sub>2</sub>–D<sub>2</sub> exchange 47, 71  
 H<sub>2</sub>–D<sub>2</sub> isotopic exchange 59  
 H<sub>2</sub> adsorption 59  
 H<sub>2</sub> chemisorption by R–Co and R–Ni 59  
 HREM 23, 175, 179, 201, 203, 232, 245  
 HTR (high-temperature reduction) 202, 232,  
   234  
 hetero-chiral Yb(III) catalyst 369  
 Ho(OTf)<sub>3</sub> 319  
 hydrides 7, 40  
 – CeH<sub>2.4x</sub> 32  
 – CeRu<sub>2</sub>H<sub>x</sub> 32  
 – LaNi<sub>5</sub> 17, 19  
 – LaNi<sub>4.5</sub>Al<sub>0.5</sub> 19  
 – LaNi<sub>5</sub>H<sub>6</sub> 20–22  
 – Nd<sub>2</sub>Co<sub>7</sub>H<sub>0.1</sub> 37  
 – Nd<sub>2</sub>Co<sub>7</sub>H<sub>2.7</sub> 37  
 – Nd<sub>2</sub>Co<sub>7</sub>H<sub>5.1</sub> 37  
 hydrocarbons (HC) 161–167, 173, 195, 198, 212,  
   227, 234, 236, 237, 251  
 hydrodesulfurization 38  
 – thiophene 38  
 hydroformylation of ethylene 107, 108  
 hydrogenation 47, 71  
 – aldehydes 19  
 – alkenes 57  
 – alkynes 17, 19, 52  
 – benzene 19  
   – – partial 51  
 – but-1-ene 17  
 – but-1-yne 17  
   – buta-1,3-diene 17, 58  
 – butadiene 49  
 – butene 49  
 – CO 24, 31  
 – carbon monoxide 22–31  
 – cyclohexene 16  
 – dienes 17  
 – ethene 49, 60  
 – ethylene 14  
 – imines 19  
 – isoprene 19  
 – naphthalene 19  
 – nitrocompounds 19  
 – 1-octene 17  
 – olefins 13, 19  
 – oleic acid 17  
 – organic functional groups 20–22  
 – propene 14, 15, 58  
 – 1-undecene 14  
 – unsaturated carboxylic acids 19  
 hydrogenolysis 71  
 – alkanes 56  
 – cyclohexane 57  
 – ethane 36, 57  
 – methylcyclopentane 35  
 hydroxide  
 – lanthanum oxide 17  
 – nickel particles 17  
 hydroxylation of phenol 146, 150  
 hydroxymethylation 317  
  
 IR spectra  
 – of adsorbed CO 59  
 – of mixed rare-earth-exchanged Y zeolite 282  
 – of R/(PVA)polyvinyl alcohol 48  
 – of 15 wt.% Yb/SiO<sub>2</sub> 47  
 imide 46  
 imines, reactions with silyl enolates 327  
 intermetallic compounds 7, 13, 40  
 – Ag–Ce 30  
 – Ag–Cu–Ce 30  
 – CeAg<sub>2</sub> 27  
 – CeAl<sub>2</sub> 34, 35  
 – CeAu<sub>2</sub> 31  
 – CeCo<sub>2</sub> 32  
 – CeCo<sub>5</sub> 13  
 – CeCu<sub>2</sub> 26, 27, 29, 38  
 – CeCu<sub>6</sub> 29  
 – CeFe<sub>2</sub> 32  
 – CeIn<sub>3</sub> 35

- CeNi<sub>5</sub> 13
- CeNi<sub>5-x</sub>Co<sub>x</sub> 13, 24
- CeRu<sub>2</sub> 32
- CeTi<sub>3</sub> 35
- Cu-Ce 31
- DyCu<sub>2</sub> 27
- ErAl<sub>2</sub> 34, 35
- Gd-Ti-Cu 30
- GdCu<sub>0.5</sub> 27
- GdCu 27
- GdCu<sub>1.5</sub> 27
- GdCu<sub>2</sub> 27
- LaAl<sub>2</sub> 34, 35
- LaCo<sub>5</sub> 23, 24
- LaCu<sub>2.2</sub> 27
- LaNi 14, 36
- LaNi<sub>5</sub> 13, 15, 16, 22, 36
- La<sub>3</sub>Ni 36
- LaNi<sub>4</sub>Al 15
- LaNi<sub>4.7</sub>Al<sub>0.3</sub> 37
- LaNi<sub>4.8</sub>Al<sub>0.2</sub> 16
- LaNi<sub>4.9</sub>Al<sub>0.1</sub> 16
- LaNi<sub>4</sub>Co 15
- LaNi<sub>4</sub>Fe 14, 15, 24
- LaNi<sub>4.8</sub>Fe<sub>0.2</sub> 17
- LaNi<sub>4</sub>Mn 14, 15, 23, 36
- LaNi<sub>4</sub>X (X = Ni, Cr, Al and Cu) 22
- LnNi<sub>5</sub> 22
- MM-Cu(1:1) 27
- MMNi<sub>5</sub> 36
- - CeCo<sub>2</sub> 22
- - CeNi<sub>2</sub> 22
- Nd<sub>2</sub>Co<sub>7</sub> 38
- NdCu 28
- NdCu<sub>2</sub> 27, 28
- NdCu<sub>5</sub> 28
- PrAl<sub>2</sub> 34, 35
- PrCo<sub>5</sub> 13
- Pr<sub>2</sub>Co<sub>7</sub> 38
- PrCu<sub>2</sub> 27
- PrGa<sub>2</sub> 35
- PtCe<sub>2</sub> 39
- Pt<sub>3</sub>Ce<sub>7</sub> 39
- RCo<sub>3</sub> 32
- R<sub>2</sub>Co<sub>7</sub> 37
- RCu<sub>x</sub> 26
- RCu<sub>2</sub> 38
- RFe<sub>2</sub> 37
- RM<sub>x</sub> (M = Ni, Cu and Co) 19
- RPd<sub>3</sub> (R = La, Ce, Pr, Nd, Sm) 17
- SmCo<sub>2</sub> 14
- SmCo<sub>5</sub> 13
- Sm<sub>2</sub>Co<sub>7</sub> 38
- ThAl<sub>2</sub> 34, 35
- ThCo<sub>5</sub> 13
- ThCu<sub>2</sub> 26
- ThCu<sub>6</sub> 27
- ThGa<sub>2</sub> 35
- ThNi<sub>5</sub> 13
- TiCu<sub>2</sub> 27, 29
- ZrCu<sub>2</sub> 27, 29
- Zr<sub>2</sub>Ni 37
- Zr<sub>0.7</sub>Ru<sub>0.3</sub>Cu<sub>0.2</sub> 30
- intermetallic surface compound 65
- ion exchange of zeolites 275
- isobutane/2-butene alkylation
  - on La-exchanged zeolites 294
  - product compositions 291
- isomerization 34
  - but-1-ene 18
  - but-2-ene 18
  - C<sub>8</sub> alkylaromatics on R-containing zeolites 298
  - 2-methylpentane 35
  - *n*-pentane 35
- isomerization and hydrocracking of paraffins and cycloalkanes on R-containing zeolites 302
- isomorphous substitution of zeolites 272
- isopropylation
  - biphenyl 298
  - naphthalene 297
- isotopic exchange 66
- K<sub>1-x</sub>La<sub>x</sub>Ca<sub>2-x</sub>Nb<sub>3</sub>O<sub>10</sub> 151, 152
- (La<sub>0.82</sub>Sr<sub>0.18</sub>)<sub>2</sub>Co<sub>0.46</sub>Cu<sub>0.51</sub>Ru<sub>0.03</sub>O<sub>4</sub> 144
- La-(Rh, Ni)-O 93
- La-Rh-O 93
- La<sub>0.7</sub>Ag<sub>0.3</sub>CoO<sub>3</sub> 119
- La<sub>1-x</sub>Ag<sub>x</sub>CoO<sub>3</sub> 119
- La<sub>1-x</sub>Ag<sub>x</sub>MnO<sub>3</sub> 119
- La<sub>1-x</sub>Ag<sub>x</sub>NiO<sub>3</sub> 119
- LaAlO<sub>3</sub> 82, 83, 98
- LaAl<sub>11</sub>O<sub>18</sub> 82
- La<sub>0.95</sub>Ba<sub>0.05</sub>CoO<sub>3</sub> 124
- LaBa<sub>2</sub>Cu<sub>2</sub>CoO<sub>7-γ</sub> 131
- LaBa<sub>2</sub>Cu<sub>3</sub>O<sub>7-γ</sub> 131
- La<sub>0.95</sub>Ba<sub>0.05</sub>FeO<sub>3</sub> 124
- La<sub>0.95</sub>Ba<sub>0.05</sub>MnO<sub>3</sub> 124
- La(CO<sub>3</sub>)(OH) 23

- $\text{La}_{0.6}\text{Ca}_{0.4}\text{CoO}_3$  152  
 $\text{LaCaMnCoO}_6$  103  
 $\text{La}_{0.8}\text{Ca}_{0.2}\text{NiO}_3$  93, 94  
 $\text{La}_{1-x}\text{Ce}_x\text{CoO}_3 + \delta$  142  
 $\text{LaCo}_5$  8  
 $\text{LaCo}_{0.4}\text{Fe}_{0.6}\text{O}_3$  119  
 $\text{LaCoO}_3$  78, 82, 84, 93, 94, 106, 119, 123, 124, 141, 142  
 $\text{La}_2\text{CoO}_4$  142  
 $\text{LaCrO}_3$  84, 93, 125, 141  
 $\text{LaCuO}_3$  143  
 $\text{LaCu}_{0.8}\text{Ru}_{0.2}\text{O}_3$  143  
 $\text{LaCu}_{0.9}\text{Ru}_{0.1}\text{O}_3$  143  
 $\text{La}_2\text{CuO}_4$  78, 143, 150  
 $\text{LaFe}_{0.8}\text{Nd}_{0.2}\text{O}_3 - \delta$  99  
 $\text{LaFeO}_3$  84, 123, 124, 141  
 $\text{LaMn}_{0.4}\text{Cu}_{0.6}\text{O}_3$  147  
 $\text{LaMn}_{0.5}\text{Cu}_{0.5}\text{O}_3$  145, 147  
 $\text{LaMn}_{0.6}\text{Cu}_{0.4}\text{O}_3$  147  
 $\text{LaMn}_{0.8}\text{Cu}_{0.2}\text{O}_3$  147  
 $\text{LaMn}_{1-x}\text{Cu}_x\text{O}_3 + y$  109  
 $\text{LaMnO}_3$  84, 119, 124, 141, 147  
 $\text{LaNb}_2\text{O}_7$  149  
 $\text{LaNi}$  8  
 $\text{LaNi}_5$  8  
 $-\alpha$  phase 14  
 $\text{LaNi}_{0.2}\text{Co}_{0.8}\text{O}_3$  94  
 $\text{LaNi}_{0.4}\text{Co}_{0.6}\text{O}_3$  94  
 $\text{LaNi}_{0.6}\text{Co}_{0.4}\text{O}_3$  94  
 $\text{LaNi}_{0.8}\text{Co}_{0.2}\text{O}_3$  94  
 $\text{LaNi}_{1-x}\text{Co}_x\text{O}_3$  93  
 $\text{LaNiO}_3 - \delta$  154  
 $\text{LaNiO}_3$  78, 84, 93, 94, 107, 133, 135, 141  
 $\text{La}_2\text{NiO}_4$  133, 135, 142  
 $\text{La}_2\text{O}_3$  14, 124, 150  
 $\text{La}_2\text{O}_2\text{CO}_3$  124  
 $\text{La}(\text{OH})_3$  14, 23  
 $(\text{La}(\text{OTf}))_3$  319  
 $\text{La}(\text{OTf})_3$  319  
 $\text{LaRhO}_3$  84, 85, 107, 108  
 $-\text{Rh}3d_{5/2}$  signal 108  
 $\text{La}_{0.8}\text{Sr}_{0.2}\text{BO}_3 - \delta$  99  
 $\text{La}_{0.8}\text{Sr}_{0.2}\text{Co}_{1-2y}\text{Cu}_y\text{Ru}_y\text{O}_3$  144  
 $\text{La}_{0.2}\text{Sr}_{0.8}\text{Co}_{1-y}\text{Fe}_y\text{O}_3$  120  
 $\text{La}_{0.6}\text{Sr}_{0.4}\text{Co}_{0.4}\text{Fe}_{0.6}\text{O}_3$  119  
 $\text{La}_{1-x}\text{Sr}_x\text{Co}_{0.4}\text{Fe}_{0.6}\text{O}_3$  118, 133  
 $\text{La}_{1-x}\text{Sr}_x\text{Co}_{1-y}\text{Fe}_y\text{O}_3$  120  
 $\text{La}_{0.6}\text{Sr}_{0.4}\text{Co}_{0.94}\text{Pt}_{0.03}\text{Ru}_{0.03}\text{O}_3$  140  
 $\text{La}_{0.6}\text{Sr}_{0.4}\text{CoO}_3$  85, 119, 141  
 $\text{La}_{0.8}\text{Sr}_{0.2}\text{CoO}_3$  133, 137  
 $\text{La}_{1-x}\text{Sr}_x\text{CoO}_3 - y$  85  
 $\text{La}_{1-x}\text{Sr}_x\text{CoO}_3 - \delta$  153  
 $\text{La}_{1-x}\text{Sr}_x\text{CoO}_3$  118, 119, 129, 133  
 $\text{LaSrCuO}_4$  150  
 $\text{La}_{0.8}\text{Sr}_{0.2}\text{Cu}_{0.8}\text{Ru}_{0.2}\text{O}_3$  143  
 $\text{La}_{0.8}\text{Sr}_{0.2}\text{Cu}_{0.9}\text{Ru}_{0.1}\text{O}_3$  143  
 $\text{La}_{0.9}\text{Sr}_{0.1}\text{Cu}_{0.8}\text{Ru}_{0.2}\text{O}_3$  143  
 $\text{La}_{0.9}\text{Sr}_{0.1}\text{Cu}_{0.9}\text{Ru}_{0.1}\text{O}_3$  143  
 $\text{La}_{0.8}\text{Sr}_{0.2}\text{CuO}_3$  143  
 $\text{La}_{1.3}\text{Sr}_{0.7}\text{CuO}_4$  150  
 $\text{La}_{1.8}\text{Sr}_{0.2}\text{CuO}_4 - \delta$  139  
 $\text{La}_{1.9}\text{Sr}_{0.1}\text{CuO}_4$  150  
 $\text{La}_2 - x\text{Sr}_x\text{CuO}_3 - \delta$  99  
 $\text{La}_2 - x\text{Sr}_x\text{CuO}_4$  137  
 $\text{La}_2 - x\text{Sr}_x\text{CuO}_4 \pm \lambda$  146  
 $\text{La}_{0.9}\text{Sr}_{0.1}\text{CuO}_3$  143  
 $\text{La}_{0.4}\text{Sr}_{0.6}\text{Fe}_{0.4}\text{Co}_{0.6}\text{O}_3$  123  
 $\text{La}_{0.2}\text{Sr}_{0.8}\text{FeO}_3$  120  
 $\text{La}_{0.2}\text{Sr}_{0.8}\text{Mn}_{0.999}\text{Pd}_{0.001}\text{O}_3 + \lambda$  122  
 $\text{La}_{0.8}\text{Sr}_{0.2}\text{Mn}_{0.999}\text{Pt}_{0.001}\text{O}_3 + \lambda$  123  
 $\text{La}_{0.6}\text{Sr}_{0.4}\text{MnO}_3$  119  
 $\text{La}_{0.8}\text{Sr}_{0.2}\text{MnO}_3$  118  
 $\text{La}_{1-x}\text{Sr}_x\text{MnO}_3$  118, 119, 133  
 $\text{La}_{0.66}\text{Sr}_{0.34}\text{Ni}_{0.3}\text{Co}_{0.7}\text{O}_3$  123  
 $\text{LaSrNiO}_4$  88, 133, 135  
 $\text{La}_{0.1}\text{Sr}_{0.9}\text{NiO}_3$  133  
 $\text{La}_{0.3}\text{Sr}_{0.7}\text{NiO}_3$  149  
 $\text{La}_{0.5}\text{Sr}_{0.5}\text{NiO}_3$  149  
 $\text{La}_{0.7}\text{Sr}_{0.3}\text{NiO}_3$  149  
 $\text{La}_{0.8}\text{Sr}_{0.2}\text{NiO}_3$  93, 94  
 $\text{La}_{1-x}\text{Sr}_x\text{NiO}_3 - \lambda$  148  
 $\text{La}_{1-x}\text{Sr}_x\text{NiO}_3$  146  
 $\text{La}_{1-x}\text{Sr}_x\text{VO}_3$  147  
 $\text{La}_{0.8}\text{Sr}_{0.2}\text{YO}_{2.9}$  99  
 $\text{La}_{0.8}\text{Th}_{0.2}\text{CoO}_3$  85, 113  
 $\text{La}_{1-1.33x}\text{Th}_x\text{NiO}_3 - \lambda$  148  
 $\text{LaTi}_{0.2}\text{Cu}_{0.8}\text{O}_3$  147  
 $\text{LaTi}_{0.7}\text{Cu}_{0.3}\text{O}_3$  147  
 $\text{LaTi}_{1-x}\text{Cu}_x\text{O}_3$  109  
 $\text{LaTi}_{1-x}\text{Cu}_x\text{O}_3$  ( $0 \leq x \leq 1$ ) 110  
 $\text{LaTiO}_3$  147  
 $\text{LaVO}_3$  84, 148  
 $\text{LaYO}_3$  99  
 $\text{La}_2\text{Zr}_2\text{O}_7$  80  
 $\lambda$  equivalence ratio 161, 233  
 $\lambda$  sensor 163, 165, 169  
lanthanum triflate, *see*  $(\text{La}(\text{OTf}))_3$   
light-off temperature 164, 168, 204, 220, 224, 225  
Lindlar catalyst 17

- liquid ammonia 46, 47  
 liquid ammonia solutions of Eu and Yb metals 46  
 $\text{Ln}(\text{OTf})_3$   
 – recovery and reuse 323, 324  
 $\text{Lu}(\text{OTf})_3$  319  
 lutetium triflate, *see*  $\text{Lu}(\text{OTf})_3$
- magnetic measurements 12  
 magnetic susceptibility 36  
 Mannich-type reactions 327–336  
 membranes 95–97, 104–106, 150  
 – composition 105  
 – dense ceramic 95  
 –  $\text{La}_{0.2}\text{Ba}_{0.8}\text{Fe}_{0.8}\text{Co}_{0.2}\text{O}_{3-y}$  97  
 –  $\text{La}_{0.2}\text{Sr}_{0.8}\text{Fe}_{0.2}\text{Co}_{0.8}\text{O}_{3\pm x}$  96  
 – oxygen permeation rates 97  
 – reactors 95, 104  
 –  $\text{SrCe}_{0.95}\text{Yb}_{0.05}\text{O}_3$  106  
 –  $\text{SrCo}_{0.5}\text{FeO}_x$  96  
 – structural stability 97  
 methanation reaction 22  
 methanol  
 – conversion on zeolites 298  
 – from syngas 111  
 – synthesis 26–31  
 methylcyclopentane reaction 35  
 monazite 285  
 – rare-earth content 285  
 Mössbauer spectroscopy 24  
 $m\text{-ZrO}_2$  239, 243
- $\text{NH}_3$  46  
 $\text{NM}/\text{Al}_2\text{O}_3$  195, 207, 208, 215–217, 224, 231  
 – WGS reaction 226  
 $\text{NM}/\text{CeO}_2$  169, 190, 193, 194, 200, 203, 205, 208, 209, 211, 215, 216, 218, 231, 232, 250, 255, 256  
 – CO oxidation 205, 208  
 – CO-TPR 185  
 – dynamic-OSC 194, 195  
 –  $\text{H}_2$ -TPR 191, 209  
 – metal-support interactions 229–231  
 – NM encapsulation 203  
 – reduction behaviour 190, 191  
 – total-OSC 195  
 $\text{NM}/\text{CeO}_2\text{-ZrO}_2$  252  
 –  $\text{H}_2$ -TPR 249  
 $\text{NM}/\text{CeO}_2\text{-ZrO}_2/\text{Al}_2\text{O}_3$  251  
 $\text{NM}/\text{CeO}_2/\text{Al}_2\text{O}_3$  173, 190, 217, 218, 224, 227, 229, 231, 233, 234, 251  
 – CO oxidation 205–207, 224  
 – CO-TPR 193  
 – dynamic-OSC 195, 196  
 – steam reforming 228  
 – WGS reaction 221, 223, 225, 226  
 $\text{NM}/\text{CeO}_2$  interactions 229, 235  
 $\text{NO}_x$  161–163, 165, 166, 170, 173, 212, 236, 237, 251, 259  
 NO and  $\text{N}_2\text{O}$  decomposition 132, 133  
 NO/CO reaction 219, 225, 234  
 NO decomposition 212, 216, 219, 220  
 NO dissociation 200, 213, 214, 216–219, 221  
 $\text{NO}_x$  elimination on R-containing zeolites 303  
 – direct catalytic decomposition 303  
 – selective catalytic reduction (SCR) 303  
 NO/ $\text{H}_2$  reaction 213, 220  
 NO reduction 167, 212, 213, 219, 252, 254, 255, 289  
 $n$ -pentane reaction 35  
 $\text{Nd-Co-O}$  94  
 $\text{NdCoO}_3$  95  
 $(\text{Nd}(\text{OTf})_3)_3$  319  
 $\text{Nd}(\text{OTf})_3$  319  
 $\text{Nd}_{1-x}\text{Sr}_x\text{CoO}_{3-y}$  130  
 neodymium triflate, *see*  $(\text{Nd}(\text{OTf})_3)_3$   
 $\text{Ni-SiO}_2$  (19) 36  
 $\text{Ni}/\text{Al}_2\text{O}_3$  23  
 $\text{Ni}/\text{CeO}_2$  19  
 $\text{Ni}_{5-x}\text{Co}_x$  particles 24  
 $\text{Ni}_x\text{Fe}$  particles 24  
 $\text{NiMg}_2$  8, 13  
 $\text{Ni}$  particles 14  
 nitrides 46
- oil refining for gasoline production on R-containing zeolites 284  
 oxidation  
 – of ammonia 148  
 – of CO 129  
 – of carbon monoxide 39  
 – of hydrocarbons 114–123  
 – –  $n$ -butane 119  
 – – propane 115  
 – – propene 116  
 – on R-containing zeolites 302  
 oxidative coupling of methane 97–106  
 – alkali halides 101  
 – –  $\text{BaPrO}_3$  101

oxidative coupling of methane – alkali halides  
(*cont'd*)

- – KNbO<sub>3</sub> 101
- – NaCl/BaPrO<sub>3</sub> 101
- – NaCl/KNbO<sub>3</sub> 101
- – NaCl/LiNbO<sub>3</sub> 101
- – NaCl/NaNbO<sub>3</sub> 101
- – NaNbO<sub>3</sub> 101
- alkali promotion 101, 102
- – GdMnO<sub>3</sub> 102
- – Gd<sub>2</sub>O<sub>3</sub> 102
- – Gd<sub>2</sub>O<sub>3</sub>–Mn<sub>3</sub>O<sub>4</sub> 102
- – Mn<sub>3</sub>O<sub>4</sub> 102
- – Na<sub>2</sub>CO<sub>3</sub>/GdMnO<sub>3</sub> 102
- – Na<sub>4</sub>P<sub>2</sub>O<sub>7</sub>/Gd<sub>2</sub>O<sub>3</sub> 102
- – Na<sub>4</sub>P<sub>2</sub>O<sub>7</sub>/Gd<sub>2</sub>O<sub>3</sub>–Mn<sub>3</sub>O<sub>4</sub> 102
- – Na<sub>4</sub>P<sub>2</sub>O<sub>7</sub>/GdMnO<sub>3</sub> 102
- – Na<sub>4</sub>P<sub>2</sub>O<sub>7</sub>/Mn<sub>3</sub>O<sub>4</sub> 102
- CaO–CeO<sub>2</sub> 100
- LaFe<sub>0.8</sub>Nb<sub>0.2</sub>O<sub>3–δ</sub> 99
- La<sub>0.8</sub>Sr<sub>0.2</sub>MnO<sub>3–δ</sub> 99
- La<sub>0.8</sub>Sr<sub>0.2</sub>YO<sub>2.9</sub> 99
- LaYO<sub>3</sub> 99
- LaYO<sub>3</sub> bixbyite 100
- LaYO<sub>3</sub> mixed oxides 100
- LaYO<sub>3</sub> perovskite 100
- layered perovskites 102, 103
- membrane reactors 104–106
- methane activation 97
- transient studies 98
- oxycerium complex in Ce–Y zeolite 281
- oxygen buffering capacity (OBC) 199
- oxygen storage and release capacity (OSC), *see*  
oxygen buffering capacity
- PVA-grafted rare earth 49
- Pd/Al<sub>2</sub>O<sub>3</sub> 219, 231
- Pd/Al<sub>2</sub>O<sub>3</sub> catalyst 35
- Pd/CeO<sub>2</sub> 205, 209, 218, 219, 231, 232
- Pd/CeO<sub>2</sub> catalyst 35
- Pd/Ce<sub>0.6</sub>Zr<sub>0.4</sub>O<sub>2</sub>/Al<sub>2</sub>O<sub>3</sub> 256
- Pd/La<sub>2</sub>O<sub>3</sub> 19
- Pd/SiO<sub>2</sub> catalyst 35
- perovskites (ABO<sub>3</sub>) 76–78
  - ion vacancies 77
  - oxygen sorption 86–90, 98, 119–121, 134, 135, 140
    - – α, α', β oxygen 88
    - – LaMnO<sub>3.12</sub> 86
    - – La<sub>1–x</sub>Sr<sub>x</sub>MO<sub>3–δ</sub> 87

- – TPD of oxygen 89
- oxygen vacancies 86
- preparation of massive perovskites 78, 79
  - – direct pyrolysis 78
  - – explosion method 78
  - – freeze-drying 78
  - – sol–gel technique 78
- structure 76
- surface composition 122, 123
- tolerance factor 76, 129
- Pr–Co–O 94
- PrBa<sub>2</sub>Cu<sub>3</sub>O<sub>6+γ</sub> 131
- PrCoO<sub>3</sub> 85
- PrO<sub>x</sub>–CeO<sub>2</sub> 258
- (Pr(OTf)<sub>3</sub>)<sub>3</sub> 319
- Pr(OTf)<sub>3</sub> 319
- praseodymium triflate, *see* (Pr(OTf)<sub>3</sub>)<sub>3</sub>
- preparation procedures
  - CRY (calcined rare earth Y) 286
  - global catalyst FCC 288
  - R-USY zeolite for FCC catalysts 286
  - rare-earth zeolites by ion exchange 274
  - R-exchanged zeolites 275
- production of chemicals and fine chemicals on  
zeolites 299
- Pt–Ce alloys 39
- Pt–R (R = Gd, Tb, Dy, Ho and Tm)/Al<sub>2</sub>O<sub>3</sub> 36
- Pt/Al<sub>2</sub>O<sub>3</sub> 37, 201, 206, 210–212, 220, 225, 226, 230, 231
  - CO oxidation 224
  - steam reforming 228
- Pt/CeO<sub>2</sub> 201, 205, 207, 209, 223, 225, 231, 232, 234
  - steam reforming 228
- Pt/CeO<sub>2</sub>–ZrO<sub>2</sub> 250
- Pt/CeO<sub>2</sub>/Al<sub>2</sub>O<sub>3</sub> 201, 210, 212, 221, 223, 226, 230
  - CO oxidation 211, 212
  - steam reforming 228
- Pt/CeO<sub>2</sub>/Al<sub>3</sub>O<sub>3</sub> 210, 211
- R–Ag 71
- R–Ag/ZrO<sub>2</sub> 70
- R–Co 57, 71
- R–Cu 71
- R–Cu/SiO<sub>2</sub> 70
- R–M binary catalysts 71
- R–Ni 57, 71
- R–Ni/SiO<sub>2</sub> 70
- R–Pd 71



- R–Ru/C 70
- RCO<sub>3</sub> 115
- RCrO<sub>3</sub> 115
- RCu<sub>2</sub>O<sub>x</sub> 38
- R<sub>2</sub>CuO<sub>4</sub> (R = La, Pr, Nd) 38
- RFeO<sub>3</sub> 115
- RMnO<sub>3</sub> 115
- RN 46
- RNH 46
- R(NH<sub>2</sub>)<sub>2</sub> 46
- R(NH<sub>2</sub>)<sub>3</sub> 46
- RNiO<sub>3</sub> 115
- R/SiO<sub>2</sub>
  - hydrogenation of acetylene 52
  - hydrogenation of propyne 52
- R-USY zeolite for FCC catalysts, preparation 286
- Raney catalysts 8, 13
- rare-earth catalysts 46
  - immobilized on SiO<sub>2</sub> 49
- rare-earth-containing bimetallic compounds 46
- rare-earth-containing zeolites 269–305
  - as catalysts 284–305
  - physico-chemical characterization 278–284
  - preparation by ion exchange 274
- rare-earth halides 35
- rare-earth metal catalysts prepared by metal vaporization 53
- rare-earth metal overlayers 46, 56
- rare-earth metals and alloys from ammonia solutions in catalysis 45–72
- rare earths
  - (Eu, Yb) introduced onto active carbon (C) 53
  - in FCC catalysts 284
  - in SO<sub>x</sub> and NO<sub>x</sub> abatement additives for FCC 288
- reducibility of perovskites 83–86
  - bulk 83
  - extent of reduction 84
  - model 113
  - stability 85
  - surface composition 86
  - surface reduction 85
- Rh–Ce 39
- Rh/Al<sub>2</sub>O<sub>3</sub> 203, 207, 209, 211, 214, 215, 217–220, 225, 226, 253
  - CO/NO reaction 214
  - CO oxidation 207
  - dynamic-OSC 196
  - steam reforming 228
  - WGS reaction 223
- Rh/CeO<sub>2</sub> 39, 182, 191, 193, 201, 205, 209, 211, 215, 216, 219, 220, 224, 232, 247, 255
  - CO desorption 194
  - H<sub>2</sub> adsorption 193
  - H<sub>2</sub>-TPR 191, 192, 236
  - NO/CO reaction 219
  - surface area 193
  - WGS reaction 222, 223
- Rh/CeO<sub>2</sub>–ZrO<sub>2</sub> 254
  - H<sub>2</sub>-TPR 246–248
  - NO adsorption 256
  - NO/CO reaction 252–256
  - reduction 250
- Rh/CeO<sub>2</sub>–ZrO<sub>2</sub> mixed oxides
  - NO/CO reaction 253
- Rh/CeO<sub>2</sub>/Al<sub>2</sub>O<sub>3</sub> 197, 202, 215, 219, 225, 226, 237, 255
  - CO/NO reaction 214, 215
  - CO oxidation 207
  - dynamic-OSC 196
  - NO/H<sub>2</sub> reaction 220
  - steam reforming 228
  - WGS reaction 223
- Rh/CeO<sub>2</sub> interactions 232
- Rh/CeO<sub>2</sub>/SiO<sub>2</sub> 215
- Rh/Ce<sub>0.5</sub>Zr<sub>0.5</sub>O<sub>2</sub> 255
- RhCl<sub>3</sub> 38
- Rh reductive agglomeration/oxidative disruption 202
- Rh/TiO<sub>2</sub> 215, 218
- Ru/Al<sub>2</sub>O<sub>3</sub> 33
- Ru/MgO 33
- Ru/SiO<sub>2</sub> 33
- SMSI effect 203, 229, 232, 234, 235
- SO<sub>2</sub> 17
- SO<sub>x</sub> emission, abatement of, in FCC units 289
- saturated hydrocarbons
  - reactions 34
  - skeletal rearrangements 35
- Sc(OTf)<sub>3</sub> 325, 333, 337, 343, 358
- scandium triflate, *see* Sc(OTf)<sub>3</sub>
- selective cyclic dimerization and trimerization of propyne and ethyne 54
- selective oxidation 90, 91
  - 2-propanol to acetone 91
  - ammoxidation of toluene 91
  - Ce<sub>0.8</sub>Zr<sub>0.2</sub>O<sub>2</sub> 90

- selective oxidation (*cont'd*)
- ethanol to acetaldehyde 91
  - $i\text{-C}_4\text{H}_8$  to methacrolein 91
  - $\text{LaCoO}_3$  90
  - $\text{LaMO}_3$  ( $M = \text{Co, Cr, Mn, Fe, Ni}$ ) 90
  - $\text{La}_2\text{MnMO}_6$  ( $M = \text{Co, Ni, Cu}$ ) 90
  - $\text{La}_{1-x}\text{Sr}_x\text{FeO}_3$  90
  - oxidative dehydrogenation 91
  - toluene to benzaldehyde 91
  - $\text{YBa}_2\text{Cu}_3\text{O}_{6+x}$  90
- silyl enol ethers 317, 318
- $\text{Sm-Co-O}$  94
- $\text{Sm}$  catalyst 50
- $\text{SmCo}_2$  8
- $\text{SmCo}_5$  8
- $\text{Sm}_2\text{Co}_7$  8
- $\text{SmMg}_3$  8, 13
- $\text{Sm}(\text{OTf})_3$  319
- sodalite ( $\beta$ -cage) unit 271, 273
- sodium dodecyl sulfate (SDS) 326
- solid electrolytes 152
- spillover 69, 193, 194, 210, 218, 232, 254, 255
- $\text{SrCe}_{0.95}\text{Yb}_{0.05}\text{O}_3 - \alpha$  152
- $\text{Sr}_{0.8}\text{La}_{0.2}\text{MnAl}_{11}\text{O}_{19 - \alpha}$  128
- $\text{Sr}_{1-x}\text{La}_x\text{MnAl}_{11}\text{O}_{19 - \alpha}$  127
- $\text{SrNiO}_3$  149
- $\text{SrO}$  150
- steam reforming 162, 169, 226–229
- Strecker-type reactions 340–345
- structural characteristics of zeolites 272
- supported bimetallic alloys 9
- $\text{Ni/CeO}_2$  catalyst 9
  - $\text{Pt-R}/\gamma\text{-Al}_2\text{O}_3$  catalysts 9
- supported mixed oxides 78–83, 151
- $\text{LaCoO}_3$  80
  - $\text{LaCr}_{1-x}\text{Mg}_x\text{O}_3$  80, 125
  - $\text{LaCrO}_3$  126
  - $\text{LaNiO}_3$  142
  - $\text{La}_{0.6}\text{Sr}_{0.4}\text{MnO}_3$  126
  - $\text{La}_{0.8}\text{Sr}_{0.2}\text{MnO}_{3+x}$  82
  - monolithic honeycomb 128
  - preparation 80
  - support stabilization 83
- surface intermetallic phases 63
- surfactants 326, 327
- synergetic effects 58
- syngas from methane 92–97
- coke formation 92
  - $\text{Gd-Co-O}$  system 94
  - membrane reactors 96
  - metal particles 93
  - XRD analysis of catalysts 93
- synthesis
- ammonia 9, 31–34
  - isopentane 35
  - methane 9
  - methanol 9, 26–31
  - stearic acid 17
- TOF 61
- TPD (temperature-programmed desorption) 55, 59, 206, 207, 209–211, 215, 217–219, 223
- TWC (three-way catalyst) 159–259
- $\text{TbO}_x\text{-CeO}_2$  258
- thermal stability 165–167, 169, 206, 216, 244, 258
- thin films 9–11
- $\text{Al/Ce}$  9
  - $\text{Ce/Al}_2\text{O}_3$  11
  - $\text{Ce/Rh}$  39
  - $\text{Ce/SiO}_2$  11
  - $\text{Pt-Ce/SiO}_2$  11
  - $\text{Rh-Ce/SiO}_2$  11
  - $\text{Ru}(0001)\text{-Ce-H}_2$  9, 34
  - $\text{Ta/Ce}$  9
- three-way catalyst, *see* TWC
- thulium triflate, *see*  $\text{Tm}(\text{OTf})_3$
- $\text{Tm}(\text{OTf})_3$  319
- topology of Linde type A zeolites 273
- total-OSC 194, 247
- transfer hydrogenation 47, 71
- triamide 46
- triflates 315–370
- $t\text{-ZrO}_2$  239
- ultrastable Y zeolites 287
- WGS reaction 162, 169, 185, 221–226, 229, 234
- washcoat 168
- water–gas shift reaction, *see* WGS reaction
- XAFS (X-ray absorption fine structure) 55
- XAS (X-ray absorption spectroscopy) 34
- XPS (X-ray photoelectron spectroscopy) 18, 36
- XRD 11, 18, 22, 24, 26, 31
- X-ray absorption 12
- $\text{YBa}_2\text{Cu}_2\text{CoO}_{7-\gamma}$  131
- $\text{YBa}_2\text{Cu}_3\text{O}_{7-\gamma}$  131, 132

- $\text{YBa}_2\text{Cu}_3\text{O}_7$  137  
 $\text{Y}_2\text{BaCuO}_5$  132  
 $\text{YFeO}_3$  84  
 $\text{Y}(\text{OTf})_3$  325  
 $\text{Yb-Co}$  58, 59  
 $\text{Yb-Ni}$  58, 59  
 $\text{Yb-Ni}$  catalyst 67  
 $\text{Yb-Pd/SiO}_2$  68  
 $\text{Yb}$  catalyst 50  
 $\text{YbCl}_3$  320  
 $\text{Yb}(\text{ClO})_3$  320  
 $\text{Yb}(\text{ClO})_4$  320  
 $\text{Yb(II)}$  amide 54  
 $\text{Yb(III)}$  amide 54  
 $\text{Yb}$  imide 54  
 $\text{YbN}$  54  
 $\text{YbNH}$  54, 56  
 $\text{Yb}(\text{NH}_2)_2$  56  
 $\text{Yb}(\text{NH}_2)_3$  56  
 $\text{Yb}(\text{NH}_2)_2$ ,  $\text{Yb}(\text{NH}_2)_3$  54  
 $\text{Yb}(\text{NH}_2)_2$  and/or  $\text{Yb}(\text{NH}_2)_3$  56  
 $\text{Yb}(\text{NO}_3)_3 \cdot 5\text{H}_2\text{O}$  320  
 $\text{Yb}(\text{OAc})_3 \cdot 8\text{H}_2\text{O}$  320  
 $\text{Yb}(\text{OTf})_3$  319, 320, 325, 330, 341, 345, 347, 354, 362, 365  
 $\text{Yb/PVA}$  catalyst 51  
 $\text{Yb}(\text{SO}_4)_3 \cdot 5\text{H}_2\text{O}$  320  
 $\text{Yb}_2(\text{SO}_4)_3 \cdot 5\text{H}_2\text{O}$  320  
 $\text{Yb/SiO}_2$  catalyst 50–52  
 $\text{Yb/zeolite}$  55  
ytterbium 46  
ytterbium triflate, *see*  $\text{Yb}(\text{OTf})_3$   
yttria-stabilized zirconia (YSZ) 152  
yttrium triflate, *see*  $\text{Y}(\text{OTf})_3$
- zeolites  
– characteristics and main commercial uses 270–273  
– EPR 278  
– EXAFS–XANES 278  
– effect of R exchange on stability and acidity 280–284  
– grafting 272  
– infrared spectroscopy 278  
– ion exchange 275  
– in solid state 276  
– ionic conductivity 278  
– isomorphous substitution 272  
– luminescence spectroscopy 278  
– modification with rare earths 273–284  
– neutron diffraction 278  
– preparation of, by ion exchange  
– – A 275  
– – Beta 274  
– – EMT 275  
– – H-ZSM-5 274  
– – MCM-22 274  
– – Mordenite 275  
– – X 274  
– – Y 274  
– rare-earth-exchanged  
– – sorption capacity 283  
– – X-ray diffraction 278  
– solid-state NMR spectroscopy 278  
– structural characteristics 272  
– – Beta 272  
– – Chabazite 272  
– – Erionite 272  
– – Faujasite (Y, X) 272  
– – Ferrierite 272  
– – Heulandite 272  
– – Linde Type A 272  
– – Linde type L 272  
– – Mordenite 272  
– – NV-87 272  
– – Offretite 272  
– – Rho 272  
– – VPI-5 272  
– – ZSM-4/Omega 272  
– – ZSM-5 272  
– – ZSM-11 272  
– – ZSM-18 272  
– – ZSM-22/Theta-1 272  
– – ZSM-23 272  
– structures 271  
– US demand 270  
– XPS 278  
– zeolite A 271  
– zeolite X 271  
– zeolite Y 271
- $\text{ZrO}_2$  168, 177, 209, 231, 235, 237, 239, 241–243, 246–248